

*File copy*  
**NASA CR-183424**

CSC/TM- 80/6234

**ONBOARD ORBIT DETERMINATION WITH  
TRACKING AND DATA RELAY SATELLITE SYSTEM  
(TDRSS) DATA**

**VOLUME II. SLIDING BATCH DIFFERENTIAL CORRECTOR  
(SBDC) EVALUATION**

**Prepared For  
NATIONAL AERONAUTICS AND SPACE ADMINISTRATION  
Goddard Space Flight Center  
Greenbelt, Maryland**

**CONTRACT NAS 5-24300  
Task Assignment 992**

**DECEMBER 1980**

**CSC**

**COMPUTER SCIENCES CORPORATION**

**(NASA-CR-183424) ONBOARD ORBIT  
DETERMINATION WITH TRACKING AND DATA RELAY  
SATELLITE SYSTEM (TDRSS) DATA. VOLUME 2:  
SLIDING BATCH DIFFERENTIAL CORRECTOR (SBDC)  
EVALUATION (Computer Sciences Corp.)**

**N89-71305**

**Unclass**

**316 p 00/18 0205411**

ONBOARD ORBIT DETERMINATION WITH TRACKING AND  
DATA RELAY SATELLITE SYSTEM (TDRSS) DATA  
VOLUME II. SLIDING BATCH DIFFERENTIAL  
CORRECTOR (SBDC) EVALUATION

Prepared for  
GODDARD SPACE FLIGHT CENTER

By  
COMPUTER SCIENCES CORPORATION

Under  
Contract NAS 5-24300  
Task Assignment 992

Prepared by:

Kirk A. Preiss 12/12/80  
K. A. Preiss Date

J. B. Dunnam 12/12/80  
J. B. Dunnam Date

Reviewed by:

Anne C. Long 12/12/80  
A. C. Long Date  
Technical Reviewer

Approved by:

R. D. Headrick 12/14/80  
R. D. Headrick Date  
Department Manager

## PREFACE

Three orbit determination algorithms have been studied to determine their suitability for onboard use with Tracking and Data Relay Satellite System (TDRSS) data: the extended Kalman filter (EKF), the sliding batch differential corrector (SBDC), and the consider filters (consider Kalman filter (CKF) and consider extended Kalman filter (CEKF)). This volume of Onboard Orbit Determination With Tracking and Data Relay Satellite System (TDRSS) Data presents the results of the SBDC study. The EKF and CKF/CEKF study results are described in Volumes I and III, respectively.

### ABSTRACT

This document presents the results of an evaluation of Landsat-D and Gamma Ray Observatory (GRO) orbit determination accuracies achievable using Tracking and Data Relay Satellite System (TDRSS) data in the sliding batch differential corrector (SBDC). The evaluation used the Research and Development Goddard Trajectory Determination System (R&D GTDS) to analyze the effects of parameters such as data contact frequency, data type, and data simulation errors. The result is a recommendation on the feasibility of using the SBDC as an onboard orbit estimator in future spaceflight missions.

## TABLE OF CONTENTS

<u>Section 1 - Introduction</u> . . . . .	1-1
<u>Section 2 - Measurement Models for TDRSS Data</u> . . . . .	2-1
2.1 Range and Delta-Range Measurements . . . . .	2-2
2.2 TDRSS Tracking Schedules . . . . .	2-2
<u>Section 3 - Sliding Batch Differential Corrector and Associated Software</u> . . . . .	3-1
3.1 SBDC Description and Use . . . . .	3-1
3.2 Convergence and Editing Criteria . . . . .	3-2
3.3 Observation Data Set Merge Routine . . . . .	3-5
3.4 Observation Data Set Error Plotting Program . . . . .	3-6
<u>Section 4 - Evaluation Procedure</u> . . . . .	4-1
4.1 Test Cases . . . . .	4-4
4.2 Measurement Error Model . . . . .	4-9
4.2.1 TDRS Ephemeris Errors . . . . .	4-9
4.2.2 User-Clock Errors . . . . .	4-12
4.2.3 Range Measurement Bias . . . . .	4-15
4.2.4 Range and Delta-Range Observation Random Errors . . . . .	4-16
4.3 Dynamic Error Model . . . . .	4-16
4.3.1 Geopotential . . . . .	4-16
4.3.2 Drag Parameters . . . . .	4-17
4.3.3 Solar Radiation Parameters . . . . .	4-17
4.3.4 Third-Body Parameters . . . . .	4-17
4.4 Convergence and Data Editing Criteria . . . . .	4-17
<u>Section 5 - Evaluation Results for Landsat-D</u> . . . . .	5-1
5.1 Two-Way Data . . . . .	5-1
5.1.1 Baseline Data Runs . . . . .	5-3
5.1.2 Variation of Contact Frequency . . . . .	5-4
5.1.3 Variation of TDRS Ephemeris Errors . . . . .	5-5
5.1.4 Effects of TDRS Ephemeris Update . . . . .	5-6

## TABLE OF CONTENTS (Cont'd)

### Section 5 (Cont'd)

5.2	Two-Way Data With a Bad Pass . . . . .	5-6
5.3	One-Way Data . . . . .	5-10
5.3.1	Accurate Clock. . . . .	5-12
5.3.2	NASA Standard Transponder . . . . .	5-12
5.3.3	Variable Data Spacing . . . . .	5-13

### Section 6 - Evaluation Results for GRO. . . . .

6-1

6.1	Two-Way Data . . . . .	6-1
6.1.1	Baseline Run. . . . .	6-2
6.1.2	Variation of Contact Frequency. . . . .	6-2
6.1.3	Variation of TDRS Ephemeris Errors. . . . .	6-2
6.1.4	Effects of TDRS Ephemeris Updates . . . . .	6-4
6.2	Two-Way Data With a Bad Pass . . . . .	6-5
6.3	One-Way Data . . . . .	6-9
6.3.1	Accurate Clock. . . . .	6-9
6.3.2	NASA Standard Transponder . . . . .	6-9
6.3.3	Sinusoidal Clock Errors . . . . .	6-11
6.3.4	Variable Data Spacing . . . . .	6-11

### Section 7 - Conclusions and Recommendations . . . . .

7-1

#### Appendix A - Estimator Error Plots

#### Appendix B - Accuracy of SBDC Force Model

#### Appendix C - Psuedo-TDRSS Observations File Description

#### Appendix D - Sample SBDC Deck Setups

#### Appendix E - R&D GTDS SBDC Updates

#### Appendix F - Merge Routine Source Code

#### References

## LIST OF ILLUSTRATIONS

### Figure

2-1	Visibility of TDRS-E and TDRS-W for Landsat-D. . . . .	2-3
2-2	Visibility of TDRS-E and TDRS-W for GRO. . . . .	2-4
3-1	SBDC Flow. . . . .	3-3
4-1	Evaluation Procedure for TDRSS Study . . . . .	4-2
4-2	Landsat-D Example of SBDC Testing Procedure. . . . .	4-3
4-3	Baseline TDRS-E Ephemeris Errors Over 24 Hours . . . . .	4-10
4-4	Baseline TDRS-E Ephemeris Errors With Update at 14 Hours . . . . .	4-11

## LIST OF TABLES

### Table

2-1	TDRS-E and TDRS-W Orbital Elements . . . . .	2-5
4-1	Landsat-D and GRO Orbital Elements, Area, and Mass . . . . .	4-5
4-2	Baseline Data Simulation TDRS Ephemeris Error Model. . . . .	4-6
4-3	Baseline Data Simulation Quadratic User-Clock Error Model . . . . .	4-6
4-4	Baseline Data Simulation Measurement Errors. . . . .	4-6
4-5	A Priori Values and Measurement Standard Deviations in SBDC . . . . .	4-7
4-6	Options Used in SBDC . . . . .	4-7
4-7	Dynamic Models . . . . .	4-8
4-8	Position and Velocity Modeling Errors Over 24 Hours. . . . .	4-16
5-1	Two-Way Observation Data Results for Landsat-D. . . . .	5-2
5-2	Two-Way Bad Pass Results for Landsat-D . . . . .	5-7
5-3	Anomalous Data Sets for Landsat-D. . . . .	5-8
5-4	One-Way Observation Data Results for Landsat-D. . . . .	5-11
6-1	Two-Way Observation Data Results for GRO . . . . .	6-2
6-2	Two-Way Bad Pass Results for GRO . . . . .	6-6
6-3	Anomalous Data Sets for GRO. . . . .	6-7
6-4	One-Way Observation Data Results for GRO . . . . .	6-10

## SECTION 1 - INTRODUCTION

The National Aeronautics and Space Administration's Goddard Space Flight Center (NASA/GSFC) is currently investigating the feasibility of autonomous spacecraft navigation. For this application, an onboard orbit determination algorithm must be selected that will provide both reliability and accuracy. Several ongoing studies are evaluating the use of sequential estimation for real-time processing in the Tracking and Data Relay Satellite (TDRS) System (TDRSS) environment. An automated batch differential correction estimator is expected to be more reliable than a sequential estimator under the various errors associated with TDRSS data.

This document presents the results of a study evaluating the performance of an automated batch differential correction estimator in determining a user-satellite orbit state from TDRSS tracking data. The types of TDRSS tracking data used were one-way Doppler and two-way range and Doppler measurements. Two categories of orbits were considered: (1) a heavily drag-perturbed orbit (Gamma Ray Observatory (GRO)) and (2) an orbit of higher altitude in which drag was not a predominant factor (Landsat-D).

Tests were run and evaluated on TDRSS observation data sets containing TDRSS data problems, user-clock frequency errors (one-way), dynamic errors affecting the spacecraft, and TDRS ephemeris updates during a data arc.

To maintain testing uniformity, the TDRSS configurations used were the same as those used in testing the extended Kalman filter (EKF) (Reference 1). In this study data pass time intervals were fixed at 10 minutes (30 range and 30 delta-range observations), and all data arcs were approximately 12 hours.

The research described herein was carried out using a modified version of the current Research and Development Goddard Trajectory Determination System (R&D GTDS) Differential Correction (DC) program (References 2 and 3). A TDRSS observation data set merging routine and an observation error plotting program were also used in the research.

Section 2 of this document discusses the TDRSS measurement models used in the evaluation. Section 3 describes the automated batch strategy and the modifications made to R&D GTDS. Section 4 discusses the evaluation procedure and describes the baseline parameters used in testing. Section 5 analyzes the orbit prediction accuracies for Landsat-D using TDRSS data and the automated batch. Section 6 discusses a parallel analysis performed on GRO. Section 7 provides conclusions and recommendations concerning the use of an automated batch estimator for onboard orbit determination.

## SECTION 2 - MEASUREMENT MODELS FOR TDRSS DATA

TDRSS is a system of three tracking and data relay satellites to be maintained in circular, near-equatorial, geosynchronous orbits. Two operational satellites, TDRS East (TDRS-E) and TDRS West (TDRS-W), will be spaced approximately 130 degrees apart at 41 degrees and 171 degrees west longitude, respectively. The third, TDRS Spare, to be situated between the other two, will be used primarily in the event of a failure in one of the operational satellites. TDRSS is discussed in detail in Reference 4.

In the current study, two types of TDRSS tracking data were investigated for use in onboard orbit determination. The first, referred to as one-way, is a Doppler measurement that is extracted on board the user satellite from tracking signals originating on the ground, relayed through a TDRS, and received by the user spacecraft. The second data type, referred to as two-way, is extracted on the ground from a round-trip propagation of the tracking signals; the resulting range and/or Doppler measurements are relayed back to the user spacecraft.

The accuracy of the one-way measurements is degraded by any timing errors in the onboard user clock that is used to extract the tracking signals. On the other hand, the two-way measurements can be regarded as having been determined with a perfect clock. For the purposes of this study, three separate data-type cases were considered: one-way Doppler data, two-way Doppler data, and two-way range and Doppler data. The Doppler measurement was simulated as a delta-range measurement so that existing R&D GTDS capabilities could be used.

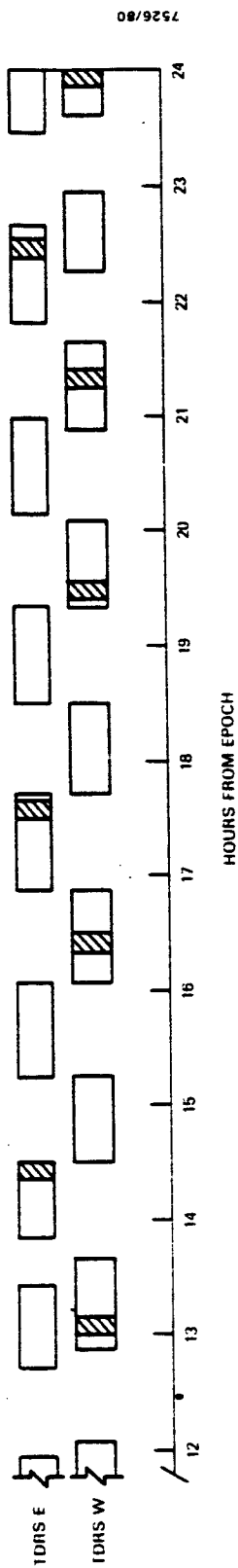
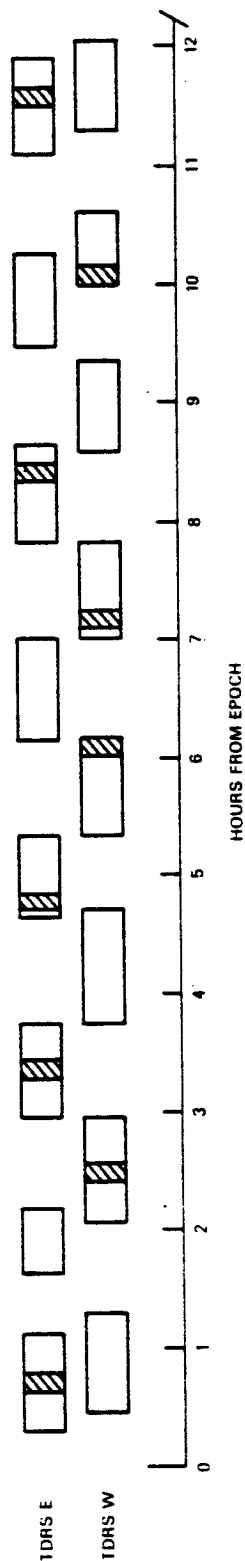
## 2.1 RANGE AND DELTA-RANGE MEASUREMENTS

The range and delta-range measurements were simulated using the pseudo-TDRSS data capabilities in the Data Simulation (DATASIM) program of R&D GTDS. A discussion of these measurements can be found in Reference 1. A set of range and/or delta-range measurements constitutes a pass of data. In all cases, the user satellite was assumed to be in contact with a single TDRS for 10 minutes for each pass of data. The time between range and delta-range measurements and the delta-range computation interval were set at 10 seconds, which yields 60 measurements for every complete pass of data (30 range and 30 delta-range measurements).

## 2.2 TDRSS TRACKING SCHEDULES

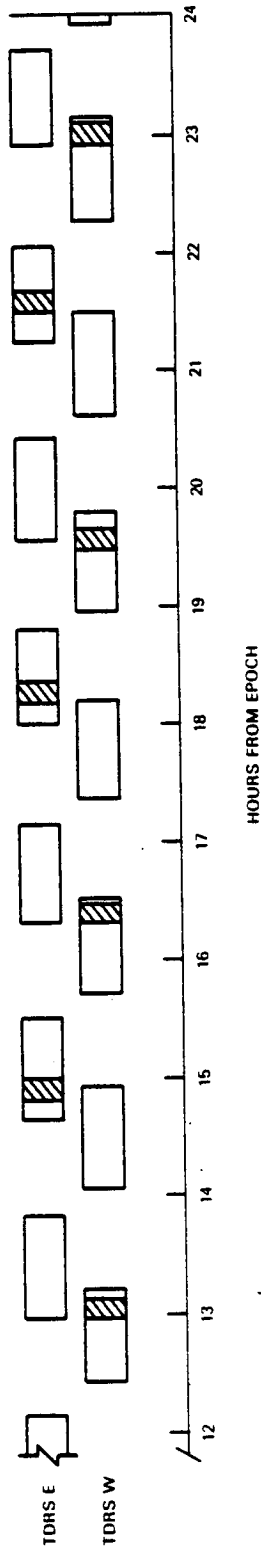
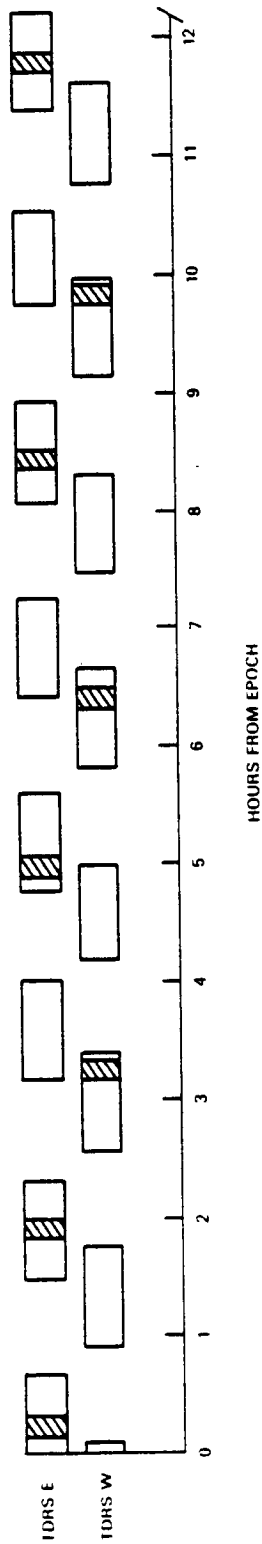
All runs used a tracking schedule of 10 minutes every N revolutions of the user satellite. In cases in which the satellite had contact every revolution, the observations were alternated between the two TDRSSs. Figures 2-1 and 2-2 show the periods of visibility of TDRS-E and TDRS-W and the associated tracking contacts for Landsat-D and GRO, respectively, for 24 hours from the time of epoch (October 1, 1980).

Table 2-1 specifies the TDRS orbital elements. The TDRS ephemerides are computed as two-body orbits with the errors from Table 4-2 added.



- NOTES:
1. EPOCH OCTOBER 1, 1980.
  2. SHADED AREAS CORRESPOND TO ONE PASS PER REVOLUTION DATA SET.

Figure 2-1. Visibility of TDRS-E and TDRS-W for Landsat-D



NOTES: 1. EPOCH OCTOBER 1, 1980.

2. SHADED AREAS CORRESPOND TO ONE PASS PER REVOLUTION DATA SET.

Figure 2-2. Visibility of TDRS-E and TDRS-W for GRO

Table 2-1. TDRS-E and TDRS-W Orbital Elements

PARAMETER	TDRS-E	TDRS-W
EPOCH	OCTOBER 1, 1980	OCTOBER 1, 1980
COORDINATE SYSTEM	TRUE OF DATE	TRUE OF DATE
SEMIMAJOR AXIS (km)	42,166.75	42,163.75
ECCENTRICITY	0.0004	0.0004
INCLINATION (deg)	5.0	5.0

7651/80

### SECTION 3 - SLIDING BATCH DIFFERENTIAL CORRECTOR AND ASSOCIATED SOFTWARE

The R&D GTDS DC program was modified to accommodate an automated batch. This required updates to the main routine (ODSEEXEC) and subroutine SETDC. Appendix E contains a listing of the R&D GTDS temporary updates required to run the sliding batch differential corrector (SBDC). The external software that was developed was used to merge observation data sets and plot errors occurring in generated observation data sets.

#### 3.1 SBDC DESCRIPTION AND USE

The SBDC moves in discrete steps along TDRSS observation data, performing a least-squares state estimation at each step. The output solve-for state for each batch becomes the a priori input state for the following batch. The length of the observation data span and the length of each step are determined by user input. Input for the SBDC is the same as for the DC program with the following additions:

- TDRS schedule (TDRSSCH) cards--These cards must be put in the DCOPT subdeck and should correspond to the schedule cards used in the R&D GTDS Error Analysis (ANALYSIS) or DATASIM program that created the observation data set.
- DCSLIDE card--This card must be put in the DCOPT subdeck and must be in the following form:

Col.				
1-8	9-11	12-14	15-17	18-38
↓	↓	↓	↓	↓
DCSLIDE	I1	I2	I3	R1

where I1 = number of batches in the run

I2 = number of observation pass intervals to  
slide each time

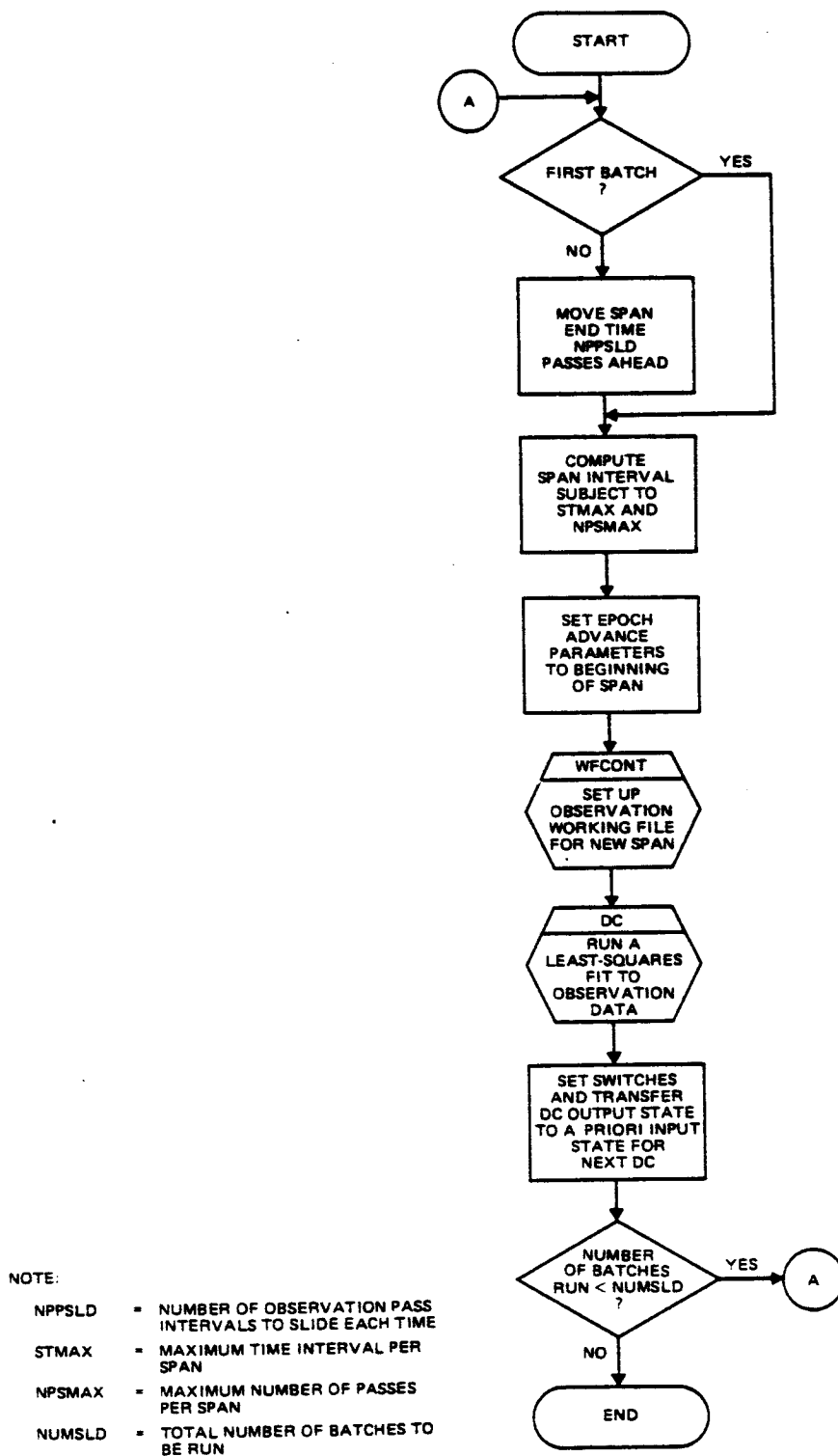
I3 = maximum number of passes per span  
R1 = maximum time interval allowed

Appendix D provides a sample SBDC deck setup.

The SBDC first advances the epoch state to the beginning of the first pass of observation data. It then executes a DC on the largest span of observation data subject to the restrictions imposed in locations I3 and R1 of the DCSLIDE keyword card. The SBDC next slides the end of the data span interval down the number of passes specified in location I2 on the DCSLIDE keyword card. It chooses the beginning of the new span to meet the span restrictions imposed in locations I3 and R1 of the DCSLIDE keyword card. This process continues until the SBDC has performed the number of batches specified in location I1 of the DCSLIDE keyword card. Figure 3-1 is a flow diagram of this process.

### 3.2 CONVERGENCE AND EDITING CRITERIA

The convergence criteria in the R&D GTDS DC program are based on two tests: (1) comparison of the root mean square (rms) of the observation residuals from iteration to iteration and (2) comparison of the predicted rms against the smallest rms found from the iterations processed. When the ratio of the difference between the smallest rms and the predicted rms to the smallest rms is less than a preset value, the DC is considered to have converged to a solution, and the estimation stops. Data are edited during the observation processing by using the rms from the previous iteration to compute a predicted residual and then testing the residual against this expected deviation. If the residual is larger than the expected deviation, the observation is rejected.



08/15/80

Figure 3-1. SBDC Flow

For the SBDC, the rms, RMS, is computed as

$$RMS = \left[ \frac{1}{n} \sum_{i=1}^n (y_i)^2 w_i \right]^{1/2}$$

where  $n$  = number of observations

$y_i$  =  $i$ th observation residual

$w_i$  = weight for the  $i$ th observation

=  $1/\sigma_i^2$ , where  $\sigma_i^2$  is the measurement noise variance for the  $i$ th observation

The predicted rms, PRMS, is computed as

$$PRMS = \left[ \frac{1}{n} \sum_{i=1}^n (y_i - F_i \Delta \hat{x})^2 w_i \right]^{1/2}$$

where  $F_i$  = matrix of partial derivatives of the  $i$ th observation with respect to the state parameters

$\Delta \hat{x}$  = state update from the iteration just completed

PRMS is the rms that would be obtained from the next iteration with the new state estimate in a linear problem. The PRMS values are stored from one iteration to the next, and the smallest value achieved, MRMS, is compared to PRMS to determine whether the DC has converged to a solution. If

$$\left| \frac{MRMS - PRMS}{MRMS} \right| < e$$

where  $e$  is an input value, the DC is considered to have converged. At the end of each iteration, the rms is compared with the previous iteration's rms to determine whether it is larger than the previous rms, which would indicate that the DC is diverging. If for four consecutive iterations the rms has increased, the DC is halted for diverging.

The data editing criterion is that

$$\frac{(w_i y_i^2)^{1/2}}{\text{RMS}} < N$$

where N is an input value, and RMS is the rms observation residual from the previous iteration.

The SBDC does not record whether data were edited in a previous iteration or in a previous slide. That is, at each iteration, each observation is processed again to determine whether it passes or fails the editing test. Also, no data editing occurs in the first iteration with a batch of data. The processing of each slide of data in the SBDC is done independently of the processing of the previous slide.

### 3.3 OBSERVATION DATA SET MERGE ROUTINE

The observation data set merge routine, MERGE, requires as input two TDRSS observations data files and the start and end times (in seconds from epoch) of the merged portion. Since this routine simply merges records sequentially, assuming a one-to-one correspondence between the records in the two files, the paired observations must have the same time tag. To ensure this, both observation files must have been created by the ANALYSIS or DATASIM program using the same epoch time and TDRS schedule cards. Appendix C contains the pseudo-TDRSS observation file description, and Appendix F provides a source listing of MERGE.

The base observation data set is entered on FORTRAN unit 1, and the observation data set to be merged into the base set is entered on FORTRAN unit 2. Merge interval times may be entered as data cards through unit 5. MERGE has proved useful in studies of non-nominal data such as a pass with an unusually large bias.

### 3.4 OBSERVATION DATA SET ERROR PLOTTING PROGRAM

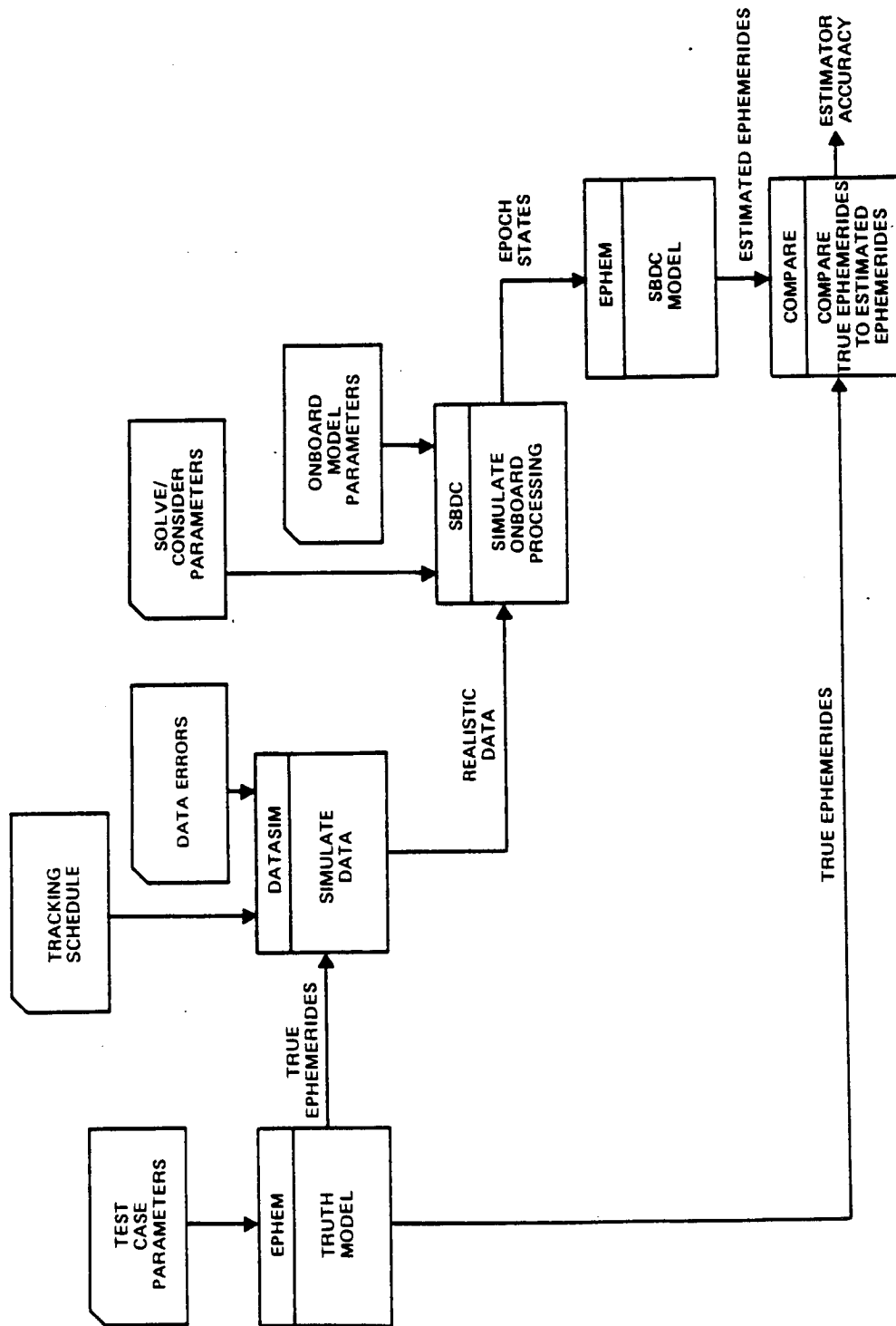
The Observation Data Set Error Plotting program plots the errors in observation data and TDRS ephemerides that are artificially imposed on the observation data by the DATASIM or ANALYSIS program. The only input required for this program is the observation data set that the user wants to test on unit 2. This program has been helpful in understanding the various magnitudes of errors imposed on observation data sets used in testing.

#### SECTION 4 - EVALUATION PROCEDURE

Several programs available in R&D GTDS were used in the evaluation of SBDC orbit determination accuracy. Figure 4-1 illustrates the evaluation procedure by which the ephemerides of a "truth" model for the user satellite were compared with the ephemerides produced via SBDC estimation. Deviations between the two ephemerides provide a measurement of the accuracy obtained by the SBDC for a particular test case. The simulated data used by the SBDC are supplied by the DATASIM program, which has the capability to corrupt the range and delta-range measurements with measurement errors and random measurement noise. If data containing a bad pass are to be simulated, the MERGE routine is used to merge observation data sets that were previously created by the DATASIM program.

The SBDC generates estimated orbital states for the beginning of each data span in the run. The estimated elements from each span are then used to generate ephemerides that are compared with the truth model ephemerides. These determine the solution accuracy over the data span (definitive arc statistics) and for several hours beyond the end of the data span (predicted arc solution). The differences in the two ephemerides are plotted in along-track, cross-track, and radial components. Also available from each comparison is a statistical report giving the rms of the differences and the minimum and maximum differences in the position component. Figure 4-2 provides an illustrated example of the testing procedure.

The analysis procedure used in comparing the ephemerides involved examining (1) the solve-for parameter report, (2) the rms and the maximum deviations of the position and velocity errors, and (3) the radial, along-track, and



7651/80

Figure 4-1. Evaluation Procedure for TDRSS Study

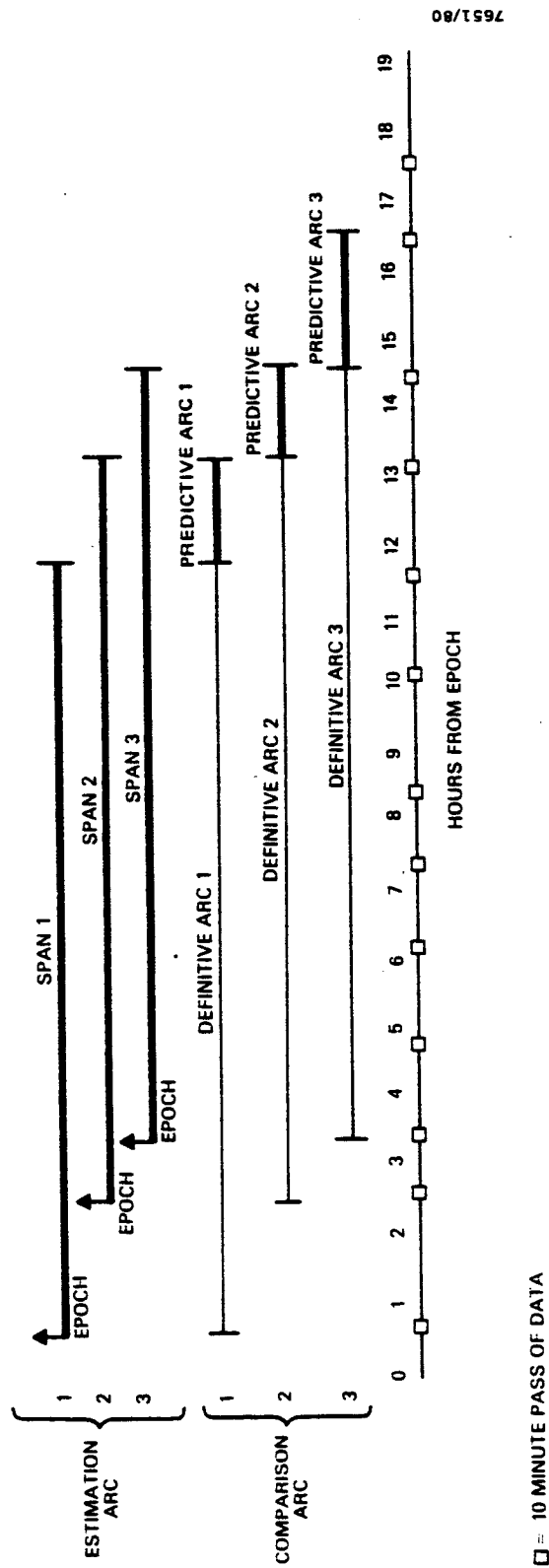


Figure 4-2. Landsat-D Example of SBDC Testing Procedure

cross-track ephemeris comparison plots of the position and velocity errors. These statistics were recorded for each data span along with the span interval number, DC convergence information, and applied measurement and modeling errors.

#### 4.1 TEST CASES

As described in Reference 1, Landsat-D and GRO were selected as the sample test cases for onboard orbit estimation. Landsat-D has a near-polar inclination and a medium altitude. GRO has a lower altitude and a less-inclined orbit, resulting in an orbit estimation far more influenced by drag.

For each satellite, baseline runs were generated representing each of the three data types (one-way Doppler data, two-way Doppler data, and two-way range and Doppler data). Table 4-1 lists the Landsat-D and GRO orbital elements and spacecraft parameters. Tables 4-2 through 4-4 describe the TDRS ephemeris error model, the user-clock error model, and the random errors applied to the measurements in the data simulation, respectively. Table 4-5 specifies the a priori values and the standard deviation of the measurement errors for the data used in the SBDC. Table 4-6 lists the solve-for parameters used in the SBDC. Table 4-7 lists the values used for the dynamic errors.

A comparison of these tables with Tables 3-1 through 3-7 of Reference 1 shows that all tables except Tables 4-5 and 4-7 are identical in both studies. The a priori values and standard deviations (Table 4-5) are not the same for the EKF and the SBDC due to the differing requirements of the two estimators. Also, as seen in Table 4-7, the integrator used in the SBDC was the Cowell 12th-order rather than the

Table 4-1. Landsat-D and GRO Orbital Elements, Area, and Mass

PARAMETER	LANDSAT-D	GRO
EPOCH	OCTOBER 1, 1980	OCTOBER 1, 1980
COORDINATE SYSTEM	TRUE OF DATE	TRUE OF DATE
SEMIMAJOR AXIS (km)	7086.901	6778.140
ECCENTRICITY	0.001	0.0017
INCLINATION (deg)	98.181	28.0
LONGITUDE OF ASCENDING NODE (deg)	354.878	0.0
ARGUMENT OF PERIGEE (deg)	180.0	0.0
MEAN ANOMALY (deg)	0.0	0.0
PERIOD (min)	98.956	92.56
AREA (m <sup>2</sup> )	20.0	20.0
MASS (kg)	1700.0	1700.0

7657/80

Table 4-2. Baseline Data Simulation TDRS Ephemeris Error Model

PARAMETER	VALUE
PERIOD OF SINUSOID <sup>1</sup> (hr)	24
RADIAL AMPLITUDE (H) (m)	35
CROSS-TRACK AMPLITUDE (C) (m)	35
ALONG-TRACK AMPLITUDE (L) (m)	80
ALONG-TRACK GROWTH RATE ( $\dot{L}$ ) (m/day)	250

7651/80

<sup>1</sup>SINUSOIDAL PERIOD FOR RADIAL, CROSS-TRACK, AND ALONG-TRACK TDRS EPHEMERIS ERRORS.

Table 4-3. Baseline Data Simulation Quadratic User-Clock Error Model

COEFFICIENT	ONE-WAY DATA		TWO-WAY DATA
	NASA STANDARD TRANSPONDER	ACCURATE ONBOARD CLOCK	PERFECT CLOCK
USER-CLOCK BIAS (b) (sec)	0	0	0
USER-CLOCK DRIFT ( $\dot{b}$ ) (sec/sec)	$1 \times 10^{-6}$	$2 \times 10^{-7}$	0
USER-CLOCK DRIFT RATE ( $\ddot{b}$ ) (sec/sec/day)	$2 \times 10^{-7}$	$2 \times 10^{-9}$	0
USER-CLOCK SINUSOIDAL BIAS AMPLITUDE (sec)	0	0	0

7651/80

Table 4-4. Baseline Data Simulation Measurement Errors

PARAMETER	BASELINE STANDARD DEVIATION	
	ONE-WAY DATA	TWO-WAY DATA
RANDOM RANGE ERROR (m)	—	1
RANDOM DELTA-RANGE ERROR (cm)	10	1
RANGE MEASUREMENT BIAS (m)	—	7
DELTA-RANGE MEASUREMENT BIAS (m)	EQUATION (4-4)	—

7651/80

Table 4-5. A Priori Values and Measurement Standard Deviations in SBDC

PARAMETER	BASELINE INPUT VALUE	
	ONE-WAY DATA	TWO-WAY DATA
<b>A PRIORI STATE OFFSETS</b>		
$x, y, z$	100 m	100 m
$\dot{x}, \dot{y}, \dot{z}$	30 cm/sec	30 cm/sec
<b>A PRIORI USER CLOCK PARAMETERS</b>		
$b$ (BIAS)	0 sec	—
$\dot{b}$ (DRIFT)		
NASA STANDARD TRANSPONDER	$1.1 \times 10^{-6}$ sec/sec	—
ACCURATE ONBOARD CLOCK	$2.2 \times 10^{-7}$ sec/sec	—
$\ddot{b}$ (DRIFT RATE)	0 sec/sec/day	—
A PRIORI $\rho_1$	0.0	0.0
<b>A PRIORI COVARIANCES</b>		
$x, y, z$	$\infty$	$\infty$
$\dot{x}, \dot{y}, \dot{z}$	$\infty \text{ m}^2/\text{sec}^2$	$\infty \text{ m}^2/\text{sec}^2$
$b$	$\infty \text{ sec/sec}$	—
$\rho_1$ (GRO ONLY)	$\infty$	$\infty$
<b>STANDARD DEVIATION OF MEASUREMENT ERROR</b>		
RANGE	—	40 m
DELTA-RANGE	10 cm	1 cm

7651/80

Table 4-6. Options Used in SBDC

OPTION	ONE-WAY DATA	TWO-WAY DATA
<b>ESTIMATED PARAMETERS</b>		
LANDSAT-D	$x, y, z, \dot{x}, \dot{y}, \dot{z}, \ddot{x}, \ddot{y}, \ddot{z}, \ddot{b}$	$x, y, z, \dot{x}, \dot{y}, \dot{z}, \ddot{x}, \ddot{y}, \ddot{z}, \ddot{b}$
GRO	$x, y, z, \dot{x}, \dot{y}, \dot{z}, \ddot{x}, \ddot{y}, \ddot{z}, \ddot{b}, \rho_1$	$x, y, z, \dot{x}, \dot{y}, \dot{z}, \ddot{x}, \ddot{y}, \ddot{z}, \ddot{b}, \rho_1$

7651/80

Table 4-7. Dynamic Models

PARAMETER	DATA SIMULATION VALUE	BATCH VALUE
GEOPOTENTIAL	15 x 15, GEM-9 <sup>a</sup>	8 x 8, GEM-7
SOLAR FLUX	$150 \times 10^{-22}$ watt/m <sup>2</sup> /Hz	$200 \times 10^{-22}$ watt/m <sup>2</sup> /Hz
AERODYNAMIC DRAG COEFFICIENT	2.0	2.2
SUN AND MOON	YES	NO
SOLAR RADIATION PRESSURE	NO	NO
INTEGRATOR	COWELL 12TH-ORDER	COWELL 12TH-ORDER
RESONANCE (GRO ONLY)	YES	NO

7657/80

<sup>a</sup>GEM = GODDARD EARTH MODEL.

Runge-Kutta 3(4+) required by the EKF. The error modeling is described further in Section 3.2 of Reference 1.

#### 4.2 MEASUREMENT ERROR MODEL

Measurement errors are passed to the SBDC through observation data. Each observation record contains a time tag, a range or delta-range observation measurement, and a TDRS position vector. (Appendix C specifies the format of the TDRS observation file.) Measurement errors imposed on the observation data by the DATASIM program affect the accuracy of the passed information in different ways. The remainder of this section describes the different types of measurement errors modeled in the DATASIM program and specifies their effect on the observation data.

##### 4.2.1 TDRS EPHEMERIS ERRORS

TDRS ephemeris errors affect the TDRS position vector. They have no effect on the simulated range or delta-range observations. In a DC batch run, the TDRS ephemeris errors are manifested in the computed values rather than in the observed values.

The TDRS ephemeris errors were modeled as a sinusoidal term for the radial (H), cross-track (C), and along-track (L) errors with an additional linear along-track rate included. The sinusoidal errors H, C, and L are all in phase, starting with a value of zero at epoch for TDRS-E. The TDRS-W errors are 180 degrees out of phase with the TDRS-E errors. The period is equal to the period of the TDRS, i.e., 24 hours. The nominal amplitude for H and C is 35 meters; for L, 80 meters. The nominal along-track rate is 250 meters per day. Figure 4-3 is a plot of the error in time after epoch. Figure 4-4 is a plot of the error imposed when simulating a TDRSS ephemeris update at 14 hours.

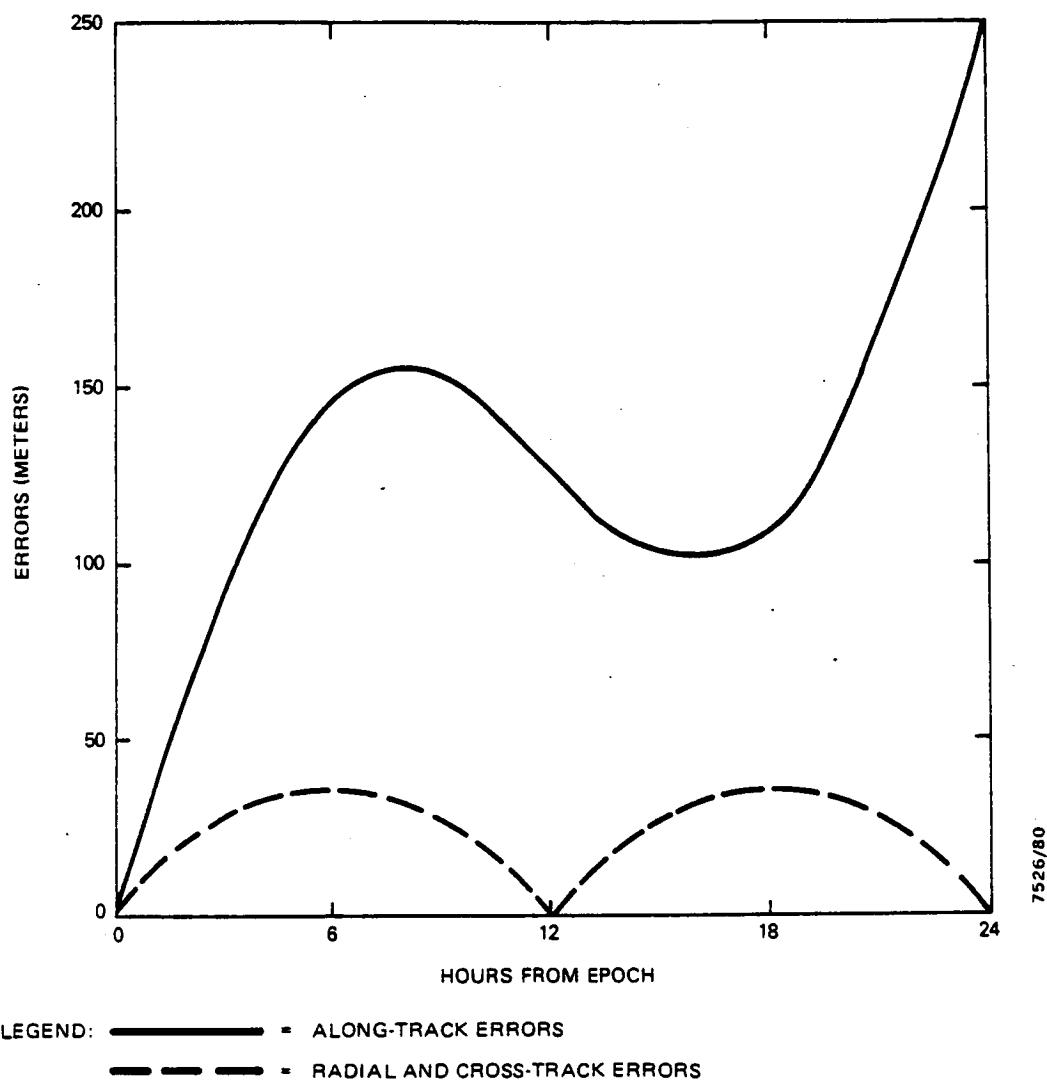
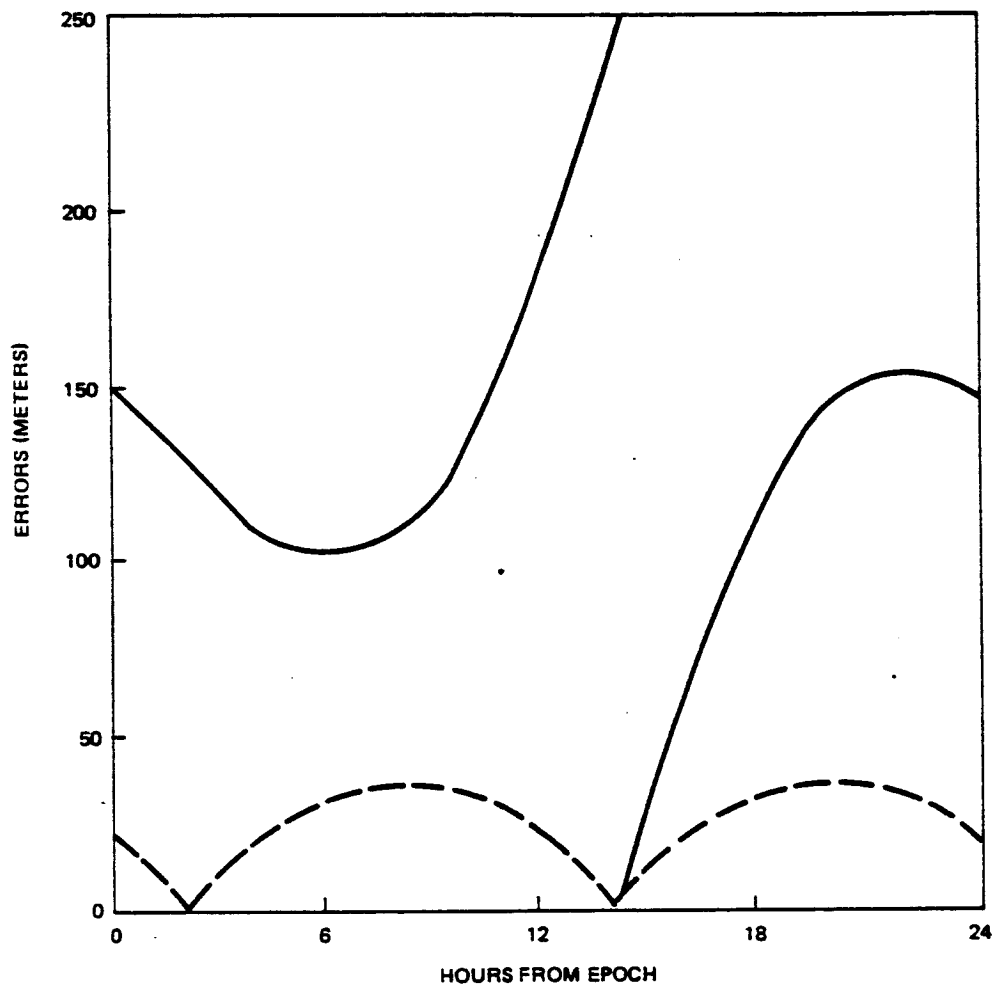


Figure 4-3. Baseline TDRS-E Ephemeris Errors Over 24 Hours



7651/80

LEGEND:

- = ALONG-TRACK ERRORS
- - - = RADIAL AND CROSS-TRACK ERRORS

Figure 4-4. Baseline TDRS-E Ephemeris Errors With Update at 14 Hours

Changes in the TDRS ephemeris errors were made to determine their influence on prediction accuracy. In some cases the errors were increased by nearly an order of magnitude over their initial baseline values.

#### 4.2.2 USER-CLOCK ERRORS

Although user-clock errors affect all three components of the observation data, their primary effect is as a bias on the range and delta-range observations. In this study, only delta-range data were used.

The onboard user-clock errors were simulated with two sets of values using a quadratic clock model with a sinusoidal term as given by the following equation:

$$T_u(t) = b + \dot{b}(t - t_0) + \frac{1}{2} \ddot{b}(t - t_0)^2 + A \sin \left[ \frac{2\pi}{T}(t - t_0) + \theta \right] \quad (4-1)$$

where  $T_u(t)$  = instantaneous user-clock bias timing error at time  $t$

$b$  = user-clock bias

$\dot{b}$  = drift

$\ddot{b}$  = drift rate

$t$  = time of observation

$t_0$  = time of epoch

$A$  = amplitude of the sinusoidal bias

$T$  = period of the sinusoidal bias

$\theta$  = phase angle

The values of the coefficients for user-clock bias ( $b$ ), drift ( $\dot{b}$ ), and drift rate ( $\ddot{b}$ ) were based on (1) the NASA standard transponder and (2) an "accurate" onboard clock. These values, listed in Table 4-3, were used only in the simulation and processing of one-way data. Two-way signals are transmitted and received on the ground using the same

clock and therefore have no significant timing error associated with them. For the case of one-way data with a quadratic clock model, the user-clock drift ( $\dot{b}$ ) and drift rate ( $\ddot{b}$ ) were additional solve-for parameters in the SBDC.

#### 4.2.2.1 Input

Input for the user-clock bias timing error simulation is through the GPSSIM4 keyword cards in the DATASIM program. These cards must reside in the DCOPT subdeck and must be in the following form:

Col.						
1-8	9-11	12-14	15-17	18-38	39-59	60-80
↓		↓		↓	↓	↓
GPSSIM4		1		b	$\dot{b}$	$\ddot{b}$
GPSSIM4		2		$a_1$	$a_2$	T

where  $b$  = user-clock bias ( $\times 10^{-9}$ ) (seconds)  
 $\dot{b}$  = user-clock drift ( $\times 10^{-12}$ ) (seconds per second)  
 $\ddot{b}$  = user-clock drift rate ( $\times 10^{-8}$ ) (seconds per second per day)  
 $= 1.15 \times 10^{13}$  seconds per second squared  
 $a_1 = A \cos \theta$  ( $\times 10^{-9}$ ) (seconds)  
 $a_2 = A \sin \theta$  ( $\times 10^{-9}$ ) (seconds)  
 $T$  = period (seconds)

#### 4.2.2.2 Effect of User-Clock Errors on Delta-Range Observational Data

The delta-range bias imposed by the user-clock bias,  $\Delta \rho_{t_{BIAS}}$ , is computed as follows:

$$\Delta \rho_{t_{BIAS}} = cT_u(t + \Delta t) - cT_u(t) \quad (4-2)$$

where  $c$  = speed of light ( $3 \times 10^{10}$  centimeters per second)

$T_u(t)$  = instantaneous user-clock bias

$\Delta t$  = delta-range integration time

Using Equations (4-1) and (4-2),  $\Delta\rho_{t_{\text{BIAS}}}$  can be calculated as follows:

$$\Delta\rho_{t_{\text{BIAS}}} = c \left\{ \dot{b}\Delta t + \ddot{b}(t - t_0)\Delta t + \frac{1}{2}\ddot{b}\Delta t^2 + 2A \cos \left[ \frac{2\pi(t - t_0)}{T} + \frac{\Delta t}{2T} + \theta \right] \sin \left( \frac{\pi\Delta t}{T} \right) \right\} \quad (4-3)$$

In all cases presented in this study,  $\Delta t \ll T$  and  $\Delta t \ll t - t_0$ . Therefore,  $\Delta\rho_{t_{\text{BIAS}}}$  may be reasonably estimated by the following equation:

$$\Delta\rho_{t_{\text{BIAS}}} \approx c\Delta t \left\{ \dot{b} + \ddot{b}(t - t_0) + \frac{2\pi A}{T} \left[ \cos \frac{2\pi(t - t_0)}{T} + \theta \right] \right\} \quad (4-4)$$

Using the information from Table 4-3 along with Equation (4-4), the effects of the user-clock errors on delta-range measurements can be calculated as specified below.

For all cases:

$\Delta t = 10$  seconds

$T =$  period of the satellite

$= 5937$  seconds for Landsat-D

$= 5554$  seconds for GRO

$t' = t - t_0$

$=$  time in seconds from epoch

Accurate onboard clock:

$$\begin{aligned}\dot{b} &= 2 \times 10^{-7} \text{ seconds per second} \\ \ddot{b} &= 2 \times 10^{-9} \text{ seconds per second per day} \\ &= 2.31 \times 10^{-14} \text{ seconds per second squared} \\ A &= 0 \text{ (no sinusoidal term)}\end{aligned}$$

$$\Delta\rho_{t_{\text{BIAS}}} \approx 60000 + 0.00694t' \text{ centimeters}$$

NASA Standard transponder:

$$\begin{aligned}\dot{b} &= 1 \times 10^{-6} \text{ seconds per second} \\ \ddot{b} &= 2 \times 10^{-7} \text{ seconds per second per day} \\ &= 2.31 \times 10^{-12} \text{ seconds per second squared} \\ A &= 0 \text{ (no sinusoidal term)}\end{aligned}$$

$$\Delta\rho_{t_{\text{BIAS}}} \approx 300000. + 0.694t' \text{ centimeters}$$

Accurate onboard clock with sinusoidal model:

$$\begin{aligned}\dot{b} &= 2 \times 10^{-7} \text{ seconds per second} \\ \ddot{b} &= 2 \times 10^{-9} \text{ seconds per second per day} \\ &= 2.31 \times 10^{-14} \text{ seconds per second squared} \\ A &= 2.0 \times 10^{-8} \text{ seconds} \\ \theta &= 0 \text{ degrees} \\ T &\approx 5400 \text{ seconds}\end{aligned}$$

$$\Delta\rho_{t_{\text{BIAS}}} \approx 60000 + 0.00694t' + 6.98 \cos\left(\frac{2\pi t'}{T}\right) \text{ centimeters}$$

#### 4.2.3 RANGE MEASUREMENT BIAS

The range measurement bias is a fixed bias that is added to all range observation data. It has no effect on delta-range data or any other component of the observation data.

The standard deviation of the range measurement bias used in all runs was 7 meters. In the DATASIM runs, the range measurement bias for TDRS-E and TDRS-W was -13 meters and -2 meters, respectively.

#### 4.2.4 RANGE AND DELTA-RANGE OBSERVATION RANDOM ERRORS

Random noise was added to the range and delta-range observation data. The standard deviation for these random errors was 1 meter for range observations and 1 centimeter for delta-range observations for two-way data and 10 centimeters for one-way delta-range data. To maintain the integrity of the testing results, the random-number generator used the same seed for all test runs. Therefore, the observation "random" noise was held fixed throughout the study.

#### 4.3 DYNAMIC ERROR MODEL

To simulate dynamic mismodeling, a different force model was used in data simulation than was used in SBDC estimation (see Table 4-7). Table 4-8 lists the propagation errors resulting from the use of different force models on Landsat-D and GRO. Appendix B contains radial, along-track, and cross-track error plots showing the error growth due to dynamic mismodeling.

Table 4-8. Position and Velocity Modeling Errors Over 24 Hours

SATELLITE	POSITION rms (m)	VELOCITY rms (cm/sec)	MAXIMUM POSITION DIFFERENCE (m)
LANDSAT-D	680.1	71.9	1,235.2
GRO	11,940.0	1,354.5	26,575.9

7651/80

##### 4.3.1 GEOPOTENTIAL

A 15-by-15 Goddard Earth Model-9 (GEM-9) geopotential was used in the DATASIM program, and an 8-by-8 GEM-7 geopotential was used in the SBDC. The purpose of this mismatch was to simulate errors in the current knowledge of the Earth's geopotential field when using the SBDC. Higher order

resonant terms were included for GRO in the DATASIM program but were not used in the SBDC.

#### 4.3.2 DRAG PARAMETERS

The aerodynamic drag coefficient,  $C_D$ , was taken to be a constant of 2.0 in the DATASIM program and 2.2 in the SBDC. Additional drag modeling errors were simulated by using a solar flux having a value of  $150 \times 10^{-22}$  watts per square meter per hertz in the DATASIM program and  $200 \times 10^{-22}$  watts per square meter per hertz in the SBDC.

#### 4.3.3 SOLAR RADIATION PARAMETERS

Solar radiation pressure was not included in either the data simulation phase or the estimation phase of the model.

#### 4.3.4 THIRD-BODY PARAMETERS

The Sun and the Moon were included in the DATASIM program but not in the SBDC. They were included in the EKF (Reference 1), but their effects on the overall solution were minimal.

#### 4.4 CONVERGENCE AND DATA EDITING CRITERIA

Several runs were made using the default iteration convergence criterion (0.0001) (e in Section 3.2) and allowing the DC 10 iterations in which to converge. Runs with reasonable errors (up to eight times the baseline errors) converged within three iterations. More difficult cases often required 10 or more iterations to converge. Runs requiring more than four iterations rarely improved their accuracy by continuing. In many instances they began to diverge, and in some cases they edited good data. For these reasons, and in light of the onboard processor time constraints, it was decided to loosen the iteration convergence criterion to 0.01 and allow a maximum of four iterations for convergence. Therefore, all cases documented herein use a 0.01 iteration convergence criterion and a maximum of four iterations for

convergence. Not all runs satisfied the iteration convergence criterion in four iterations, although all runs were converging. (No run presented here diverged.)

The data editing criterion used in all of the two-way runs was that the weighted residual be no more than three times its expected value (three-sigma edit, in which  $N$  of Section 3.2 is equal to three). The test results on anomalous data improved significantly using a three-sigma editing procedure in conjunction with the new convergence criteria. Some difficulties were experienced using the three-sigma edit with one-way data, and it was not used for the results presented in this document. Lack of time prevented further investigation of data editing when processing one-way data. This question should be addressed in any continuation of this study.

## SECTION 5 - EVALUATION RESULTS FOR LANDSAT-D

As specified in Section 2, all baseline runs and their variations used a tracking schedule of 10 minutes every one, two, or three revolutions of the user satellite. The visibility of the TDRSS satellites from the Landsat-D orbit is given in Figure 2-1. The shaded areas in that figure correspond to the tracking times for the one-pass-per-revolution data set. The tracking times for the data sets with tracking every other or third revolution were selected by deleting every other or third pass from the one-revolution data set. The following subsections present the SBDC evaluation results for Landsat-D, including a tabular summary of the performance statistics. Appendix A contains radial, cross-track, and along-track plots of the position differences for several representative runs.

### 5.1 TWO-WAY DATA

This section presents the evaluation results for SBDC performance using two-way data. Table 5-1, which summarizes the performance statistics, includes the following information:

- Run identification number
- Contact frequency
- Observation data type(s) used in differential correction--o indicates range data;  $\Delta$ o indicates delta-range data. If only delta-range data are used, 30 observations are made per pass. A run with a contact frequency of 2 revolutions using delta-range data gives the DC program 120 data points, whereas a run with a contact frequency of 1 revolution using range and delta-range data gives the DC program 540 data points. This difference can affect

Table 5-1. Two-Way Observation Data Results for Landsat-D

RUN	CONTACT FREQUENCY	DATA STYLE	TURNS EPIMERIS ERRORS	$\sigma_{\rho}$ (m)	$\sigma_{\phi}$ (m)	rms/MAXIMUM DEFINITIVE POSITION DIFFERENCES (m) <sup>a</sup>					rms/MAXIMUM PREDICTED POSITION DIFFERENCES (m) <sup>b</sup>					FIGURE NUMBERS (A)	SPANS PLOTTED
						1	2	3	4	5	1	2	3	4	5		
L01	1 REV	$\rho$	BASE LINE		1	56/111	78/139	41/127	43/92	50/112	128/193	81/124	39/65	51/87	57/81	1, 2, 3	3
L02		$\rho + \Delta\rho$	BASE LINE	40	1	56/111	78/139	41/127	43/92	55/124 <sup>c</sup>	128/193	81/124	39/65	50/85	65/106 <sup>c</sup>		
L03		$\Delta\rho$	8H, 8C		1	77/179	84/154	69/118	91/108	98/195	147/206	78/123	51/82	93/159	99/170	4, 5, 6	3
L04		$\rho + \Delta\rho$	8H, 8C	200	1	77/179	85/154	69/118	91/108	98/195	147/205	78/123	51/81	93/159	99/170		
S06		$\rho + \Delta\rho$	8H, 8C	2	12	35/513	339/608	295/471	284/457	300/505	342/459	426/701	328/545	346/513	363/644		
L05		$\rho + \Delta\rho$	4L	40	1	75/170	81/112	53/116	39/98	74/122 <sup>c</sup>	191/245	62/115	34/99	47/84	107/182 <sup>c</sup>	7, 8, 9	3
L06		$\Delta\rho$	4L		1	44/170	94/159	86/125	91/145	100/165	54/84	104/144	92/134	83/128	96/150	10, 11, 12	3
L07		$\rho + \Delta\rho$	4L	65	1	74/123	94/159	92/134	91/145	101/169	107/182	103/144	86/124	83/128	97/152		
L15		$\Delta\rho$	8H, 8C, 4L, 4L (UPDATE 14 00)		1	166/278	178/285	106/235	105/171	99/153	187/262	202/304	127/189	141/191	139/190	13, 14, 15, 16, 17, 18	2, 5
L16		$\rho + \Delta\rho$	8H, 8C, 4L, 4L (UPDATE 14 00)	200	1	167/278	178/285	106/235	105/171	100/153	187/262	202/304	127/189	141/191	140/190		
L11	2 REVS	$\Delta\rho$	BASE LINE		1	115/272	65/115	97/198			349/464	96/116	137/274			19, 20, 21	1
L12		$\rho + \Delta\rho$	BASE LINE	40	1	114/271	64/115	96/196			347/465	95/155	137/274				
L13		$\Delta\rho$	8H, 8C		1	95/176	88/157	109/233			210/305	120/174	91/204			22, 23, 24	2
L14		$\rho + \Delta\rho$	8H, 8C	200	1	96/176	88/157	108/233			210/305	120/174	90/203				
S08		$\rho + \Delta\rho$	8H, 8C	2	12	35/4516	292/471	300/504			340/445	399/631	348/567				
L23	3 REVS	$\Delta\rho$	BASE LINE		1	222/412	40/81 <sup>c</sup>	53/90			447/694	51/72 <sup>c</sup>	122/257			25, 26, 27	1
L26		$\rho + \Delta\rho$	BASE LINE	40	1	234/434	38/81	54/93			475/736	55/76	123/259				

<sup>a</sup>PREDICTIVE TIME SPANS

ONE CONTACT EVERY REVOLUTION

1 - 11 40 14 40  
2 - 13 10 15 10  
3 - 14 30 17 30  
4 - 16 30 19 30  
5 - 17 40 20 40

ONE CONTACT EVERY TWO REVOLUTIONS

1 - 11 40 17 40  
2 - 14 30 20 30  
3 - 17 40 23 40

ONE CONTACT EVERY THREE REVOLUTIONS

1 - 11 40 19 20  
2 - 16 30 24 00  
3 - 21 25 28 50

<sup>b</sup>DEFINITIVE TIME SPANS

ONE CONTACT EVERY REVOLUTION

1 - 0 40 11 40  
2 - 2 25 13 10  
3 - 3 20 14 30  
4 - 4 45 16 30  
5 - 6 00 17 40

ONE CONTACT EVERY TWO REVOLUTIONS

1 - 0 40 11 40  
2 - 3 20 14 30  
3 - 6 00 17 40

ONE CONTACT EVERY THREE REVOLUTIONS

1 - 0 40 11 40  
2 - 4 45 16 30  
3 - 8 18 21 25

<sup>c</sup>LOC FAILED TO CONVERGE IN FOUR ITERATIONS TO A TOLERANCE OF 0.01

08/1592

the DC program's performance, especially in cases involving anomalous data.

- TDRS ephemeris error coefficients--The baseline values are specified in Table 4-2. H, C, and L indicate radial, cross-track, and along-track errors, respectively. A notation such as 8H signifies eight times the baseline radial error.
- Range ( $\sigma_\rho$ ) and delta-range ( $\sigma_{\Delta\rho}$ ) standard deviations input to the SBDC--All other input values are as described in Section 3.
- Root-mean-square and maximum position vector differences--The rms and maximum position differences were obtained by comparison with the "true" ephemeris over the time intervals specified in the table footnotes; the time intervals include the definitive and predictive arcs for each batch. The information for the predictive arcs is of more interest, since it is from this time frame that information would be extracted for annotation.
- Reference figure numbers--The numbers of the appropriate position difference plots in Appendix A are specified.
- Spans plotted--The spans plotted in the referenced Appendix A figures are specified.

#### 5.1.1 BASELINE DATA RUNS

Runs L01 and L02 are examples of the behavior of the SBDC with 10 minutes of nominal data in each revolution. The errors in both runs are relatively constant over all five data spans, as would be expected. Run L02, with both range and delta-range data, has twice as much data as run L01, yet the two obtain nearly identical results. Clearly, the delta-range data dominate the solution in run L02. The

range data have been specified to have a larger measurement standard deviation and consequently a smaller weight than the delta-range data to account for the effects of the TDRS ephemeris errors. These TDRS errors have little effect on the delta-range data accuracy.

In Table 5-1, the letter c indicates cases in which the DC solution failed to pass the convergence test in four iterations. The solutions were still quite good, indicating that the tolerance used in the convergence criteria can be relaxed.

The errors of the definitive and predicted areas of the third span of run L01 are plotted in Figures A-1 through A-3 (Appendix A). These are plots of the radial (H), cross-track (C), and along-track (L) differences between the truth model ephemeris and the estimated ephemeris. These plots are typical of all the solution error plots. Plots of all the runs discussed in this document are available for further reference (Reference 5) but are not included in this document because of their bulk.

#### 5.1.2 VARIATION OF CONTACT FREQUENCY

The SBDC was run with data simulated with the baseline error models at contact frequencies of every two (runs L11, L12) or every three (runs L23, L25) revolutions. Here, the effect of less data is an increase in both the definitive and predicted solution errors. For the two-revolution case, the errors in runs L11 and L12 are about twice as large as those in runs L01 and L02. There are 270 observations in run L12, as opposed to 540 in run L02 and 270 in run L01. The delta-range data still dominate the solution. Very little difference exists between the L11 and L12 solutions. The error in the first span of run L11 is plotted in Figures A-19 through A-21 (Appendix A).

### 5.1.3 VARIATION OF TDRS EPHEMERIS ERRORS

Runs were made in which the TDRS ephemeris error levels were increased to find the point at which these errors begin to affect the estimation accuracy. Runs L03 and L04 show the effects of eight times the baseline error, or 280 meters, in the H and C directions of the TDRS orbits. At this level, the solutions are slightly degraded from the solutions of the baseline cases L01 and L02. Here, also, the estimation accuracy of run L04, with range and delta-range observations, is virtually identical to that of run L03, with delta-range data only, because the range data have been de-weighted to reflect the contribution of the TDRS ephemeris errors. The delta-range data are much less affected by the increase in the TDRS ephemeris errors than are the range data, and thus proper weighting of the range data effects no change in the solution accuracies. However, as demonstrated in run S05, improper weighting produces a severe degradation of the estimation accuracy.

Run L05 shows a small increase in the estimation errors over certain spans with data containing four times the baseline L error, or 320 meters, whereas runs L06 and L07 show an increase of between 20 and 100 percent for four times the L error, or 1000 meters per day. Plots of the H, C, and L errors of the definitive arc solutions are given for the third span of runs L03, L05, and L06 in Figures A-4 through A-12 (Appendix A).

Comparison of run L13 to run L03 and of run L14 to run L04 shows a decrease in the estimation accuracy from using less data, but the estimation using range and delta-range data achieves results almost identical to those obtained when delta-range data only are used. Run S06 is another run made with the range data improperly weighted with respect to the delta-range data. The accuracy of the estimation is

seriously affected here as well. The errors of the second span of run L13 are plotted in Figures A-22 through A-24 (Appendix A).

#### 5.1.4 EFFECTS OF TDRS EPHEMERIS UPDATE

The TDRS ephemeris error modeling capability in the R&D GTDS DATASIM program assumes that the TDRS ephemeris is updated once every 24 hours. For most of the study, the ephemeris update was assumed to be at 0 hours of the data set. To test the effect of this update, two runs (L15 and L16) were made in which the TDRS ephemeris errors were simulated with an update at 14 hours. This would be at the end of the third span for the case with data every revolution. To increase the effect, the runs were made using 280 meters, 280 meters, 320 meters, and 1000 meters per day for the H, C, L, and I errors, respectively. The errors in the second span, just before the update, are the largest for both runs. Plots of the errors of spans 2 and 5 are given in Figures A-13 through A-18 (Appendix A).

#### 5.2 TWO-WAY DATA WITH A BAD PASS

This section presents the evaluation results for SBDC performance using two-way data containing a bad pass. Table 5-2, which summarizes the performance statistics, includes the following information:

- Run identification number
- Contact frequency
- Observation data type(s) used in differential correction--p indicates range data;  $\Delta p$  indicates delta-range data.
- Contents of the bad pass, as defined in Table 5-3
- Root-mean-square and maximum position vector differences over the definitive and predicted spans

Table 5-2. Two-Way Bad Pass Results for Landsat-D

RUN	CONTACT FREQUENCY	DATA STYLE	BAD PASS	rms/MAXIMUM DEFINITIVE POSITION DIFFERENCES (m) <sup>a</sup>					rms/MAXIMUM PREDICTED POSITION DIFFERENCES (m) <sup>b</sup>					FIGURE NUMBERS (A. )	SPAN PLOTTED
				1	2	3	4	5	1	2	3	4	5		
L17	1 HEV	$\mu + \Delta\mu$	DATA SET 1	59/110 <sup>c</sup>	76/144	46/111	48/103	55/124 <sup>c</sup>	124/196 <sup>c</sup>	75/117	36/65	56/101	66/108 <sup>c</sup>	28, 29, 30 31, 32, 33 34, 35, 36 37, 38, 39	4 4 1 2
L18	$\Delta\mu$	$\Delta\mu$	DATA SET 1	58/103 <sup>c</sup>	76/145 <sup>c</sup>	46/107	68/137 <sup>c</sup>	50/112	51/88 <sup>c</sup>	76/120 <sup>c</sup>	36/64	136/215 <sup>c</sup>	57/92		
L19	$\Delta\mu$	$\Delta\mu$	DATA SET 2	56/112	129/254 <sup>c</sup>	115/244 <sup>c</sup>	132/235	65/132 <sup>c</sup>	128/193	308/345 <sup>c</sup>	275/350 <sup>c</sup>	187/278	70/94 <sup>c</sup>		
L20	2 HEVs	$\mu + \Delta\mu$	DATA SET 1	2094/ 4174	1975/ 2598	98/196	X		4422/ 7042	1948/ 2881	135/271	X		34, 35, 36	1
L21	$\Delta\mu$	$\Delta\mu$	DATA SET 2	114/272	197/308	1703/ 3034			349/464	397/621	3859/ 4700			37, 38, 39	2

<sup>a</sup>NET INITIAL TIME SPANS

ONE CONTACT EVERY REVOLUTION

- 1 - 0.40 11.40
- 2 - 2.26 13.10
- 3 - 3.20 14.30
- 4 - 4.45 16.30
- 5 - 6.00 17.40

ONE CONTACT EVERY TWO REVOLUTIONS

- 1 - 0.40 11.40
- 2 - 3.20 14.30
- 3 - 6.00 17.40

<sup>b</sup>PREDICTIVE TIME SPANS

ONE CONTACT EVERY REVOLUTION

- 1 - 11.40 14.40
- 2 - 13.10 15.10
- 3 - 14.30 17.30
- 4 - 16.30 19.30
- 5 - 17.40 20.40

ONE CONTACT EVERY TWO REVOLUTIONS

- 1 - 11.40 17.40
- 2 - 14.30 20.30
- 3 - 17.40 23.40

<sup>c</sup>DC FAILED TO CONVERGE IN FOUR ITERATIONS TO A TOLERANCE OF 0.01

Table 5-3. Anomalous Data Sets for Landsat-D

PARAMETER	VALUE	
	DATA SET 1	DATA SET 2
TIME OF ANOMALOUS DATA	4 <sup>h</sup> 45 <sup>m</sup> - 4 <sup>h</sup> 55 <sup>m</sup>	13 <sup>h</sup> 0 <sup>m</sup> - 13 <sup>h</sup> 10 <sup>m</sup>
TDRS EPHEMERIS ERRORS		
H	6.6 km	180 m
C	6.6 km	180 m
L	25.6 km	3.12 km
RANGE BIAS (m)		
TDRS-E	-360	
TDRS-W		-60
DELTA-RANGE BIAS (cm)	0	200
RANDOM RANGE ERROR (m)	10	10
RANDOM DELTA-RANGE ERROR (cm)	10	10

7651/80

- Reference figure numbers
- Span plotted

Runs L17 and L18 are runs using data every revolution in which the fourth pass of data, at 4 hours and 45 minutes after epoch, has very large errors. These errors produce errors of approximately 7 kilometers in the range observations and 300 centimeters in the delta-range observations. In the first span of run L17, the DC did not detect that the bad pass range data had errors but deleted nearly all of the bad pass delta-range observations. Run L18 also deleted nearly all of the bad pass delta-range observations. The ability of the editing criteria to detect the anomalous data in these runs produces results similar to those of baseline runs L01 and L02. The bad pass data are present in all spans except the fifth. In the second, third, and fourth spans of runs L17 and L18, all but one or two observations from the middle of the bad pass data are edited. Run L19 includes a bad pass of data (at 13 hours) that produces a delta-range observation error of approximately 200 centimeters. The bad pass of data, the ninth pass in the 24-hour data set, is not encountered until the second span and is present through the fifth span. In this set, in which the bad pass delta-range data error is less than that in the previous data set, not as many of the bad pass observations are deleted, and the solution accuracy is slightly less. The H, C, and L errors from the fourth span of runs L18 and L19 are plotted in Figure A-28 through A-33 (Appendix A).

The DC estimator did not do as well with the same bad data passes with data every other revolution. The estimator was unable to discern which of the observations were bad and accepted virtually all of them. Run L20 deleted a few of the anomalous observations but also deleted a few good ones from another pass. Run L21 did a least-squares fit through

all of the data and deleted none of them. The estimator errors are plotted for the first span of run L20 and the second span of run L21 in Figures A-34 through A-39 (Appendix A).

### 5.3 ONE-WAY DATA

This section presents the evaluation results for SBDC performance using one-way delta-range data. One-way delta-range data differs from two-way delta-range data because of the additional errors introduced by the onboard clock timing and frequency errors (see Table 4-3) and the higher random measurement noise level (10 times the default value). Runs made thus included the clock drift and drift rate as solve-for parameters. Since TDRS ephemeris errors seem to have little effect on delta-range observations, all one-way testing was done using the baseline TDRS ephemeris errors (see Table 4-2) and data errors (see Table 4-4). A standard deviation of 12 centimeters was used for the delta-range observations.

Table 5-4, which summarizes the performance statistics, includes the following information:

- Run identification number
- Contact frequency
- Standard deviation for the errors imposed on the delta-range observations
- Clock model identification, as given in Table 4-3
- Error in the clock solve-for parameter values for each batch
- Root-mean-square and maximum position vector differences

Table 5-4. One-Way Observation Data Results for Landsat-D

RUN	CONTACT FREQUENCY	$\sigma_{\text{sp}}$ (cm)	CLOCK MODEL	ERROR IN $b_1$ (x 10 <sup>-9</sup> ) ERROR IN $b_2$ (x 10 <sup>-9</sup> )					MAXIMUM ULTIMATIVE POSITION DIFFERENCES (m) <sup>a</sup>					MIN/MAXIMUM PREDICTED POSITION DIFFERENCES (m) <sup>b</sup>					FIGURE NUMBERS (A)	SPANS PLOTTED
				1	2	3	4	5	1	2	3	4	5	1	2	3	4	5		
L08	1 REV	10	ACCURATE ONBOARD CLOCK	05	05	04	04	03	278/ 581	131/ 236	184/ 358	102/ 179	101/ 230	585/ 882	289/ 344	345/ 531	183/ 294	185/ 295	40, 41, 42	2
L09		10	NASA STANDARD TRANSITION H	58.1	47.2	40.7	43.4	32.5	24138/ 48219	16367/ 31814	19586/ 41398	10604/ 19339	11749/ 2536	47989/ 86204	33892/ 45827	39718/ 54085	21821/ 28056	21821/ 28110	43, 44, 45	2
L10		10	NASA STANDARD TRANSITION H	02/ 20	21/ 53	03/ 06	13/ 17	03/ 14	102/ 280	585/ 1107	151/ 282	230/ 518	193/ 285	222/ 354	1083/ 1581	289/ 328	488/ 683	177/ 249	40, 47, 48	1
L22	VARIABLE (12 REV)	10	NASA STANDARD TRANSITION H	01/ 21	33/ 93	03/ 11	10/ 515	X	131/ 288	1514/ 3126	206/ 293	17922/ 29551	X	348/ 550	3177/ 5014	318/ 287	16927/ 28011	X	49, 50, 51, 52, 53, 54, 55, 56, 57, 58, 59, 60	ALL

<sup>a</sup>DEFINITIVE TIME SPANS.

ONE CONTACT EVERY REVOLUTION

1 0.40 11.40  
2 2.25 13.10  
3 3.20 14.30  
4 4.45 16.30  
5 6.00 17.40

ONE CONTACT EVERY TWO REVOLUTIONS

1 0.40 11.40  
2 3.20 14.30  
3 6.00 17.40  
4 8.18 21.25

<sup>b</sup>PREDICTIVE TIME SPANS.

ONE CONTACT EVERY REVOLUTION

1 11.40 14.40  
2 13.10 15.10  
3 14.30 17.30  
4 16.30 19.30  
5 17.40 20.40

ONE CONTACT EVERY TWO REVOLUTIONS

1 11.40 17.40  
2 14.30 20.30  
3 17.40 23.40  
4 21.25 27.25

7651/BC

- Reference figure numbers
- Span plotted

### 5.3.1. ACCURATE CLOCK

For the run made with the accurate clock, L08, the frequency bias was estimated as a constant. The error made in this estimation model is that the frequency bias is really a linearly increasing quantity that increases  $1 \times 10^{-9}$  seconds per second in a 12-hour data span. The attempt to estimate the bias as a constant gives an answer for  $\dot{b}$  that is an average over the span. The error found in the  $\dot{b}$  estimate of approximately  $0.5 \times 10^{-9}$  seconds per second for each of the spans of run L08 is then as would be expected for the SBDC estimator. The errors in the position estimation are increased over those found for the two-way data due to the increased error from the clock and to the larger measurement noise in the one-way data. Of additional interest is the changed character of the errors as plotted in the H, C, and L coordinates. The second span of run L08 is plotted in Figures A-40 to A-42 (Appendix A). These figures, as compared to the two-way data cases that are plotted, show the influence of the clock frequency drift, especially in the along-track (L) plot.

### 5.3.2 NASA STANDARD TRANSPONDER

Two runs presented, L09 and L10, use the NASA standard transponder in place of the accurate onboard clock. In run L09, the frequency bias ( $\dot{b}$ ) is estimated as a constant. Here, the errors are large and the solution accuracy is significantly degraded. In run L10, both the frequency bias ( $\dot{b}$ ) and the frequency drift ( $\ddot{b}$ ) are estimated. The results with this clock model in the estimator are considerably better. In this case, however, the estimator is using a model identical to that used in the data simulation. The purpose of showing such results is to demonstrate the

correctness of the data modeling, not to show a proposed onboard model.

### 5.3.3 VARIABLE DATA SPACING

A run was made with data at less-frequent intervals than one pass per revolution to test the effect on the estimator of using sparse one-way data. The data set used in the first span of run L22 is identical to that used in the first span of run L10, with one pass of data missing--the second to the last in the data set. The data following the last pass are spaced every other revolution. Therefore, as the SBDC goes from one span to the next, it drops two spans of data but picks up only one. That is, the first span has eight passes of data, the record span has seven, the third span has six, and the fourth span, with five passes, has data spaced every other revolution. So, from run L10, with data every revolution, to the fourth span of run L22 is a clear progression. The accuracy of the solution can be seen to degrade as the SBDC attempts the estimation with less and less data. The errors from all of the spans are plotted in Figures A-49 through A-60 (Appendix A).

## SECTION 6 - EVALUATION RESULTS FOR GRO

GRO evaluation runs were made using the same observation error cases as were used for Landsat-D. The major distinction was that the GRO runs included drag as a solve-for parameter. (A detailed comparison of the Landsat-D and GRO TDRS visibilities and dynamic parameters is provided in Sections 2 and 4.) The following subsections present the SBDC evaluation results for GRO, including a tabular summary of the performance statistics. Appendix A contains radial, cross-track, and along-track plots of the position differences for several representative runs.

### 6.1 TWO-WAY DATA

This section presents the evaluation results for SBDC performance using two-way data. Table 6-1 summarizes the performance statistics. The format of the table is similar to that of Table 5-1 (Section 5.1), with the addition of the estimated value for  $\rho_1$ .

The GRO orbit, at an altitude of 400 kilometers, is strongly perturbed by the atmospheric drag effects. The atmospheric density modeling errors are simulated by a mismatch of the atmospheric drag coefficients and the density models, as discussed in Section 4. This mismodeling produces large prediction errors, as shown in Table 4-8. The drag parameter,  $\rho_1$ , of the Harris-Preister density model is estimated in an attempt to reduce these modeling errors. The modeling errors cannot be corrected exactly through estimation of a constant  $\rho_1$ . However, a value from -0.43 to -0.55 produces an acceleration of approximately the same size as that produced by the truth model values at an altitude of 400 kilometers.

Table 6-1. Two-Way Observation Data Results for GRO

RUN	CONTACT FREQUENCY	DATA STYLE	TURNS EPHMERIS EPOCHS	$\sigma_p$ (m)	$\sigma_{\Delta p}$ (m)	mm MAXIMUM DEFINITIVE POSITION DIFFERENCES/ ESTIMATED $\sigma_p$ (m) <sup>a</sup>						mm MAXIMUM PREDICTED POSITION DIFFERENCES (m) <sup>b</sup>					FIGURE NUMBERS (A - I)	SPANS PLOTTED
						1	2	3	4	5		1	2	3	4	5		
G01	1 REV	$\Delta p$	BAS. LINE		1	103/248/ 0.517	113/227/ 0.506	108/248/ 0.495	108/187/ -0.416	111/233/ -0.430		236/374	217/408	303/467	187/352	252/420	61, 52, 63	2
G02		$p + \Delta p$	BAS. LINE	40	1	103/248/ 0.517	114/322/ 0.506	108/248/ 0.495	108/187/ -0.418	111/233/ -0.430		236/374	217/408	303/467	187/352	252/420		
G03		$\Delta p$	811 BC		1	105/256/ -0.512	121/232/ 0.506	127/211/ 0.482	110/210/ -0.444	110/198/ 0.458		190/283	243/434	317/446	159/226	200/343		
G04		$p + \Delta p$	811 BC	200	1	112/284/ 0.517 <sup>c</sup>	118/324/ 0.505	121/243/ 0.485	127/226/ -0.423	132/260/ -0.437		190/283 <sup>c</sup>	220/402	286/410	183/307	217/364	64, 65, 66	2
G05		$p + \Delta p$	41	40	1	131/230/ 0.536 <sup>c</sup>	107/272/ 0.501	107/207/ 0.468	121/234/ -0.437	125/210/ 0.444		268/444 <sup>c</sup>	288/493	364/532	152/242	178/314	67, 68, 69	2
G06		$\Delta p$	41		1	106/250/ -0.516	116/311/ 0.500	110/223/ 0.494	115/201/ -0.419	116/206/ -0.431		196/295	182/347	245/380	223/432	323/507	70, 71, 72	2
G07		$p + \Delta p$	41	66	1	106/250/ 0.516	116/317/ 0.506	110/224/ 0.494	115/201/ -0.419	116/206/ -0.431		196/295	182/347	245/380	223/432	323/507		
G15		$\Delta p$	811 BC, 41, 41, UPDATE 14 00		1	145/268/ -0.511	178/378/ 0.504	186/311/ -0.527	144/236/ -0.437	142/236/ -0.438		174/249	192/344	332/558	146/209	262/349	73, 74, 75, 76, 77, 78	2, 5
G16		$p + \Delta p$	811 BC, 41, 41, UPDATE 14 00	200	1	139/250/ 0.517	177/378/ -0.504	186/311/ 0.523	144/236/ 0.458	130/213/ 0.438 <sup>c</sup>		186/275 <sup>c</sup>	192/344	331/556	146/209	240/348 <sup>c</sup>		
G11	2 REV	$\Delta p$	BAS. LINE		1	161/477/ 0.463	198/310/ 0.424	180/265/ 0.449				244/393	404/636	345/426			79, 80, 81	
G12		$p + \Delta p$	BAS. LINE	40	1	161/477/ 0.463	197/308/ 0.425	179/265/ 0.446				241/396	397/621	374/466				
G13		$\Delta p$	811 BC		1	174/445/ 0.458	223/334/ 0.421	195/291/ 0.441				258/409	438/636	418/528				
G14		$p + \Delta p$	811 BC	200	1	174/445/ 0.458	223/335/ 0.420	195/291/ 0.441				258/409	425/657	419/530			82, 83, 84	2
G23	3 REV	$\Delta p$	BAS. LINE		1	137/214/ 0.454	432/652/ 0.434	391/378/ 0.516				371/659	397/644 <sup>c</sup>	276/472				
G25		$p + \Delta p$	BAS. LINE	40	1	140/228/ 0.486	301/658/ -0.438	121/237/ 0.530				394/703	886/1387	412/680				

DEFINITIVE TIME SPANS		PREDICTIVE TIME SPANS	
ONE CONTACT EVERY REVOLUTION		ONE CONTACT EVERY REVOLUTION	
1 0 10 11 50		1 11 50 14 50	
2 1 50 13 10		2 13 10 16 10	
3 3 10 15 00		3 15 00 18 00	
4 4 55 16 30		4 16 30 19 30	
5 6 20 18 10		5 18 10 21 10	
ONE CONTACT EVERY TWO REVOLUTIONS		ONE CONTACT EVERY TWO REVOLUTIONS	
1 0 10 11 50		1 11 50 17 50	
2 3 10 15 00		2 15 00 21 00	
3 6 20 18 10		3 18 10 24 00	
ONE CONTACT EVERY THREE REVOLUTIONS		ONE CONTACT EVERY THREE REVOLUTIONS	
1 0 10 11 50		1 11 50 19 20	
2 4 25 16 20		2 16 20 24 00	
3 9 40 21 40		3 21 40 29 10	

<sup>a</sup>OR FAILED TO CONVERGE IN ITERATIONS TO A TOLERANCE OF 0.01

08/10/80

#### 6.1.1 BASELINE RUN

SBDC runs G01 and G02 were made with data once per revolution with the baseline error models. Run G01, made with delta-range data only, and run G02, made with both range and delta-range data, achieve virtually identical results, indicating that the delta-range data dominate the solution. This result is the same as that obtained with the Landsat-D data sets; i.e., properly weighted range data have very little effect on the solution.

The effects of the drag errors are quite noticeable. The estimation errors are about twice as large as those found for the comparable Landsat-D cases (runs L01 and L02). Also, the character of the error plots has changed somewhat, as can be seen in the plots of the second span of run G01 given in Figures A-61 through A-63 (Appendix A).

#### 6.1.2 VARIATION OF CONTACT FREQUENCY

The SBDC was run with data every other revolution and every two revolutions with the baseline data error models. Run G11, made with data every revolution using only delta-range data, gave results nearly identical to those obtained from run G12, which was made using range and delta-range data. The solution accuracy is definitely lessened compared to that obtained using data every revolution. The errors in the estimated orbit are plotted for the second span of run G11 in Figures A-79 through A-81 (Appendix A).

#### 6.1.3 VARIATION OF TDRS EPHEMERIS ERRORS

The results of several runs made with increased levels of TDRS ephemeris errors are included in Table 6-1. Runs G03 and G04 used a data set with the amplitudes of the TDRS H and C ephemeris errors increased to 280 meters. Run G05 used a data set with the amplitude of the TDRS L error increased to 320 meters, and runs G05 and G06 used data sets

with the  $\dot{L}$  error increased to 1000 meters per day. The runs with delta-range data only (G03 and G06) produced results very close to those obtained from runs with both range and delta-range data (G04 and G07). The results from all of the runs with the increased TDRS ephemeris errors show only a slight decrease in the solution accuracy as compared to the baseline data cases (runs G01 and G02). The errors in the H, C, and L components of the GRO estimated ephemeris for the second span of runs G04, G05, and G06 are plotted in Figures A-64 through A-72 (Appendix A).

Runs G13 and G14 show the results of estimation with the TDRS H and C ephemeris errors increased to 280 meters when using data every other revolution. Here, again, the estimation accuracy with these data is degraded by the additional errors. An increase in the level of the TDRS ephemeris errors beyond this point would have a greater effect on the accuracy. The second span of run G14 is plotted in Figures A-82 through A-84 (Appendix A).

#### 6.1.4 EFFECTS OF TDRS EPHEMERIS UPDATES

The data set used for runs G15 and G16 was one in which the TDRS ephemeris error model was updated at 14 hours instead of at 0 hours, as was the case for the other runs. This data set was created with the amplitudes of the H, C, and L components of the TDRS ephemeris error model increased to 280 meters, 280 meters, and 320 meters, respectively, and the  $\dot{L}$  error increased to 1000 meters per day. In these runs, the second span, just before the update, was most affected by the TDRS ephemeris errors, and the fifth span was least affected. The errors from the second and fifth spans are plotted in Figures A-73 through A-78 (Appendix A).

## 6.2 TWO-WAY DATA WITH A BAD PASS

This section presents the evaluation results for SBDC performance using two-way data containing a bad pass.

Table 6-2 summarizes the performance statistics. The format of the table is similar to that of Table 5-2 (Section 5.2), with the addition of the estimated  $\rho_1$  values for each span. The anomalous data sets are defined in Table 6-3.

The SBDC had more difficulty with the GRO data sets including a bad pass of data than with the Landsat-D data sets including a bad pass of data. The estimator was unable to edit the bad observations out of the GRO data sets as readily as with the Landsat-D data sets. Runs G17 and G18 use a data set with one pass (at 4 hours, 45 minutes) with TDRS ephemeris errors that produce errors of approximately 7 kilometers in the range observation and 300 centimeters in the delta-range observations. In the first and second spans of run G17, the SBDC deletes about a third of the bad delta-range observations, and it deletes five of the good delta-range observations in the next data pass. It deletes none of the range data. In the third span, it deletes nearly all of the bad delta-range observations but no good ones and no range data. The third span is one in which the convergence criteria were not satisfied within four iterations; however, the convergence process was continuing, and the criteria might have been satisfied within one or two more iterations. In the fourth span, the SBDC deleted a few bad delta-range observations and a few more good ones, and the convergence criteria were met within three iterations.

The SBDC behaved slightly differently in run G18, when using delta-range data only. In the first span, only a few of the bad data points were deleted; in the second, only four were

Table 6-2. Two-Way Bad Pass Results for GRO

RUN	CONTACT FREQUENCY	DATA STYLE	BAD PASS	rms/MAXIMUM DEFINITIVE POSITION DIFFERENCES/ESTIMATED $\rho_1$ (m) <sup>a</sup>					rms/MAXIMUM PREDICTED POSITION DIFFERENCES (m) <sup>b</sup>					FIGURE NUMBERS (A-1)	SPAN PLOTTED
				1	2	3	4	5	1	2	3	4	5		
G17	1 REV	$\rho + \Delta\rho$	DATA SET 1	2055/ 3323/ -0.741	2191/ 3430/ -0.790	206/ 393/ -0.476 <sup>c</sup>	1491/ 2691/ +0.147	111/ 233/ -0.430	2060/ 2986	2151/ 3187	376/ 605 <sup>c</sup>	1848/ 3004	251/ 420	85, 86, 87	2
G18		$\Delta\rho$	DATA SET 1	2020/ 3317/ -0.742	2188/ 3427/ -0.790	5482/ 8644/ -0.236	1486/ 2694/ +0.146	111/ 233/ -0.430	2533/ 4464	2159/ 3171	10408/ 11986	1849/ 3011	251/ 420		
G19		$\Delta\rho$	DATA SET 2	103/ 249/ -0.517	346/ 553/ -0.426	571/ 1078/ -0.488	420/ 653/ -0.521	346/ 531/ -0.512	236/ 374	693/ 896	647/ 1030	377/ 556	387/ 438	88, 89, 90	2
G20	2 REV <sub>1</sub>	$\rho + \Delta\rho$	DATA SET 3	161/ 417/ -0.463	3672/ 9039/ +0.916	9855/ 16100/ -0.532	X		246/ 396	17492/ 26896	100708/ 15863	X		91, 92, 93	2
G21		$\Delta\rho$	DATA SET 2	161/ 417/ -0.463	9497/ 16111/ -0.301 <sup>c</sup>	393/ 614/ -0.587 <sup>c</sup>			244/ 393	19273/ 22116 <sup>c</sup>	950/ 1587 <sup>c</sup>	X			

<sup>a</sup>DEFINITIVE TIME SPANS:

ONE CONTACT EVERY REVOLUTION

- 1 - 0:10 - 11:50
- 2 - 1:50 - 13:10
- 3 - 3:10 - 15:00
- 4 - 4:55 - 16:30
- 5 - 6:20 - 18:10

ONE CONTACT EVERY TWO REVOLUTIONS

- 1 - 0:10 - 11:50
- 2 - 3:10 - 15:00
- 3 - 6:20 - 18:10

<sup>b</sup>PREDICTIVE TIME SPANS:

ONE CONTACT EVERY REVOLUTION

- 1 - 11:50 - 14:50
- 2 - 13:10 - 16:10
- 3 - 15:00 - 18:00
- 4 - 16:30 - 19:30
- 5 - 18:10 - 21:10

ONE CONTACT EVERY TWO REVOLUTIONS

- 1 - 11:50 - 17:50
- 2 - 15:00 - 21:00
- 3 - 18:10 - 24:00

<sup>c</sup>DC FAILED TO CONVERGE IN FOUR ITERATIONS TO A TOLERANCE OF 0.01.

Table 6-3. Anomalous Data Sets for GRO

PARAMETER	VALUE		
	DATA SET 1	DATA SET 2	DATA SET 3
TIME OF DATA	4 <sup>h</sup> 45 <sup>m</sup> - 4 <sup>h</sup> 55 <sup>m</sup>	13 <sup>h</sup> - 13 <sup>h</sup> 10 <sup>m</sup>	13 <sup>h</sup> - 13 <sup>h</sup> 10 <sup>m</sup>
TDRS EPHEMERIS ERRORS			
H	6.6 km	180 m	1.8 km
C	6.6 km	180 m	1.8 km
L	25.6 km	3.12 km	31.2 km
RANGE BIAS (m)			
TDRS-E	-360		
TDRS-W		-60	-40
DELTA-RANGE BIAS (cm)		200	0
RANDOM RANGE ERROR (m)	10	10	10
RANDOM DELTA-RANGE ERROR (cm)	10	10	10

7526/80

deleted; in the third, only three; and in the fourth, none of the bad data points was deleted. The differences in the G17 and G18 solutions are caused by the acceptance of the bad range observations in run G17, which are not present in run G18. Plots of the second span of run G17 are given in Figures A-85 through A-87 (Appendix A). Run G19 was made using a data set with a delta-range observation error of approximately 50 centimeters (arising from large TDRS ephemeris errors at 13 hours) and a delta-range bias of 200 centimeters. In this run, none of the bad data was edited. The inclusion of the bad data affected the solution accuracy, increasing the error by two to three times from the first span, with no bad data, to the second. The errors from the second span are plotted in Figures A-88 through A-90 (Appendix A).

Runs were made with data every other revolution with two different levels of observation error at 13 hours. Run G21 has the same error in the delta-range observation as does run G19, i.e., about 250 centimeters. Most of the anomalous data points were detected and deleted in the second span, and many of them were deleted from the third span.

The data set used in run G20 includes anomalous data at 13 hours with TDRS ephemeris errors that produce range errors of approximately 5 kilometers and delta-range errors of approximately 500 centimeters. The first span of run G20 contains no anomalous data. In the second span, a few observations are deleted, but none is from the anomalous data pass, and the solution accuracy reflects the resulting errors. In the third span, three anomalous delta-range observations are rejected, but so is one from another pass. The solution accuracy is still not good. The errors in the second span of run G20 are plotted in Figures A-91 through A-93 (Appendix A).

### 6.3 ONE-WAY DATA

This section presents the evaluation results for SBDC performance using one-way data. Table 6-4 summarizes the performance statistics. The format of the table is similar to that of Table 5-4 (Section 5.3), with the addition of the estimated  $\rho_1$ .

#### 6.3.1 ACCURATE CLOCK

The SBDC is able to estimate the ephemeris of GRO reasonably well with one-way data when the onboard clock is simulated using the accurate clock error model. Run G08 shows that the estimation error increases due to the additional error from the clock model and the increased measurement error in the delta-range observation. The estimate of a constant for the frequency bias,  $\dot{b}$ , when the term is really linear produces an error in the  $\dot{b}$  estimate of about  $0.5 \times 10^{-9}$  seconds per second, just as occurs in the same case with Landsat-D data. The errors in the ephemeris, as plotted for the second span in Appendix A, also show the effect of estimating the  $b$  with a linear term.

#### 6.3.2 NASA STANDARD TRANSPONDER

Run G09 is a repetition of run G08 using the less-accurate NASA transponder for the frequency standard. Here, the error made in estimating the frequency bias as a constant is about  $50 \times 10^{-9}$  seconds per second. This produces an error in the delta-range observations of 150 meters and a very poor estimate of the GRO ephemeris. When run G10 is made with the same data but with estimated frequency bias and drift, the solution accuracy is comparable to that found with the accurate clock. This is merely a demonstration that the estimation model is accurate, since the simulation is also done with the same quadratic clock model. The errors in the second span of runs G09 and G10 are plotted in Figures A-97 to A-102 (Appendix A).

Table 6-4. One-Way Observation Data Results for GRO

RUN	CONTACT FREQUENCY	$\sigma_{\Delta\phi}$ (cm)	CLOCK MODEL	ERROR IN $\dot{b}$ (x $10^{-9}$ ) (sec/sec)/ ERROR IN $\dot{b}$ (x $10^{-9}$ ) (parts/day)						rms/MAXIMUM DEFINITIVE POSITION DIFFERENCES/ESTIMATED $\rho_1$ (m) <sup>a</sup>						rms/MAXIMUM PREDICTED POSITION DIFFERENCES (m) <sup>b</sup>						FIGURE NUMBERS (A. )	SPANS PLOTTED
				1	2	3	4	5	6	1	2	3	4	5	6	1	2	3	4	5	6		
G08	1 REV	10	ACCURATE ONBOARD CLOCK	-0.3	-0.1	-0.5	-0.6	-0.5	-0.5	164/ 392/ -0.520	200/ 360/ -0.616	184/ 356/ -0.518	189/ 371/ -0.435	172/ 397/ -0.464		211/ 285	254/ 368	246/ 631	181/ 358	308/ 461		94, 95, 96	2
G09		10	NASA STANDARD TRANSPONDER	-43.6	-28.7	-65.6	-66.2	-61.2		9595/ 17447/ -0.983	13251/ 23582/ -1.21	18832/ 42454/ -2.94	13635/ 28340/ -2.03	13560/ 23754/ -2.37		15347/ 20694	20294/ 27053	20772/ 28404	12661/ 15187	18683/ 23312		97, 98, 99	2
G10		10	NASA STANDARD TRANSPONDER	-0.1/ 1.1	1.0/ -0.8	0.5/ 0.7	1.5/ -2.0	0.8/ 0.6		136/ 311/ -0.515	160/ 326/ -0.604	370/ 697/ -0.481	302/ 517/ -0.425	272/ 311/ -0.437		278/ 363	284/ 518	593/ 788	528/ 627	184/ 300		100, 101, 102	2
G26		10	ACCURATE ONBOARD CLOCK SINUSOIDAL ERRORS (0.01% AMPLITUDE)	-0.3	-0.2	-0.2	-0.6	-0.75		151/ 331/ -0.517	190/ 381/ -0.513	176/ 322/ -0.490	178/ 326/ -0.452	236/ 419/ -0.428		206/ 288	249/ 370	196/ 296	170/ 310	365/ 576			
G22	VARIABLE (12 REV)	10	NASA STANDARD TRANSPONDER	0.1/ -2.6	0.1/ -0.6	1.1/ -0.9	3.5/ 9.2			208/ 582/ -0.520	205/ 389/ -0.468	216/ 339/ -0.43	2884/ 4123/ -1.114		893/ 1514	591/ 765	173/ 315	4288/ 7145				103, 104, 105, 106, 107, 108, 109, 110, 111, 112, 113, 114	ALL

<sup>a</sup>DEFINITIVE TIME SPANS:  
ONE CONTACT EVERY REVOLUTION  
1 = 0.10 - 11.50  
2 = 1.50 - 13.10  
3 = 3.10 - 15.00  
4 = 4.55 - 16.30  
5 = 6.20 - 18.10

<sup>b</sup>PREDICTIVE TIME SPANS:  
ONE CONTACT EVERY REVOLUTION  
1 = 11.50 - 14.50  
2 = 13.10 - 16.10  
3 = 15.00 - 18.00  
4 = 16.30 - 19.30  
5 = 18.10 - 21.10

ONE CONTACT EVERY TWO REVOLUTIONS  
1 = 0.10 - 11.50  
2 = 3.10 - 15.00  
3 = 6.20 - 18.10

ONE CONTACT EVERY TWO REVOLUTIONS  
1 = 11.50 - 17.50  
2 = 15.00 - 21.00  
3 = 18.10 - 24.00

08/1592

### 6.3.3 SINUSOIDAL CLOCK ERRORS

In an effort to model the orbital effects on the accuracy of an onboard clock, sinusoidal terms were added to the clock error model. In run G26 a sinusoidal clock model was used with a 90-minute period and an amplitude equal to 0.01 percent of the original clock drift (for an accurate onboard clock). These sinusoidal errors appear to have very little effect on the accuracy of the SBDC estimator. The SBDC is apparently able to treat the effects as though they were random noise and therefore fits the middle of the curve accurately, provided the sinusoidal period is considerably smaller than the SBDC data span.

### 6.3.4 VARIABLE DATA SPACING

The data set used in run G22 is similar to that used in run L22. In this data set, the first span uses data every revolution with one data set missing. As the SBDC advances through the data, the new data sets are spaced so that for each new set added, two are lost; this continues until the fourth span, when the data are spaced every other revolution. At the four span, the solution accuracy is clearly less than that obtained in the earlier spans. The SBDC does not have enough data in this case to perform reliably.

## SECTION 7 - CONCLUSIONS AND RECOMMENDATIONS

This section specifies conclusions drawn from comparison of the SBDC's performance when processing two-way range and delta-range data, two-way delta-range data, and one-way delta-range data. Comparisons are made with respect to (1) accuracy in the baseline case with data every revolution, (2) effect of varying contact frequency, (3) effect of increased TDRS ephemeris errors, and (4) accuracy in the presence of anomalous data sets. These comparisons lead to the following general conclusions:

- Baseline performance--For the baseline data sets with a pass of data every revolution, the two-way estimation gives comparable results whether range and delta-range data or delta-range data only are used. The Landsat-D results were more accurate than those obtained for GRO, since the acceleration from atmospheric drag is larger in the case of GRO. Using the one-way data sets simulated with the accurate clock model increased the estimation errors by a factor of two to three as compared to the two-way results, which have no clock errors.

- Performance with reduced tracking for two-way data--Comparison of the data contact cases of contact every other revolution and every third revolution with the case of contact every revolution shows that as the data frequency is decreased, the accuracy also decreases. Again, however, the SBDC does as well with two-way delta-range data only as with range and delta-range data.

- TDRS ephemeris errors--Examination of the cases with increased TDRS ephemeris errors shows that the amplitudes of the cross-track and radial components must increase to eight times the baseline values (i.e., 280 meters versus

35 meters) to affect the solution. The along-track amplitude and rate must increase by four times the baseline values (i.e., 320 meters versus 80 meters and 1000 meters per day versus 250 meters per day, respectively) before their effects are noticed. These statements are true only if the weight of the range observation is decreased as the TDRS ephemeris errors increase. If this is not done, the increased error in the range observations from the TDRS ephemeris errors seriously degrades the solution accuracy. The discontinuity in the TDRS ephemeris errors caused by updating the TDRS ephemeris did not affect the estimation process.

- Anomalous data--The presence of undetected anomalous data degrades the solution accuracy. If the data errors are large, the data editing facility deletes the anomalous data, and estimation proceeds as in the baseline cases. The level of errors chosen for the anomalous data was, however, at the borderline of the editing capability. A level of error that could be detected when using Landsat-D data was not detectable when repeated with GRO data. The addition of another solve-for parameter,  $\rho_1$ , and the additional estimation errors caused by the drag mismodeling increased all the observation residuals such that the anomalous residuals were no longer more than three times their expected value.

- User clock errors--The results obtained from simulations using the NASA standard transponder as compared to those using the accurate clock show a tenfold or greater increase in the estimation errors. If both frequency drift and bias are estimated when the NASA standard transponder is used as the simulation clock, the errors drop to the level found with the accurate clock. The clock model used in the data simulation is a simple one, however, and it should be verified by a comparison with real data from a frequency

standard under consideration for onboard use before a firm conclusion is drawn as to the specific clock parameters that must be estimated.

- Reduced tracking with one-way data--The reliability of the SBDC is severely impacted if the data frequency is decreased from the baseline tracking schedule of one pass per revolution. The solution errors were increased tenfold when the data were presented to the estimator at a rate of one pass every other revolution. Estimation was performed reliably for data contacts between the one and two-revolution contact frequencies. Therefore, it can be concluded that losing some passes from a one-revolution data set would not affect the reliability.

- Data editing--The data editing criteria worked well with the two-way data sets in which the unmodeled data errors were random. With the one-way data, however, the unmodeled errors, especially when using the NASA standard transponder, were no longer random, and the data editing criteria had to be adjusted carefully. If the three-sigma editing test was used, the SBDC deleted data to the point that it could not invert the normal matrix.

The data editing and estimation convergence testing schemes used in this study start again with each new batch for the SBDC. In the first iteration, all data are accepted, and no memory exists of the final rms observation residual obtained in the previous DC. While this caused no problem in this study, it does mean that at least two iterations are required to determine convergence and that data that might be immediately detectable as erroneous are used for at least one iteration. In an onboard system, this may not be desirable. Future investigation of this problem could include the design and study of schemes in which the rms from a previous batch estimation is used to predict an rms for the

first iteration of the next batch estimation for use in data editing and convergence testing. This activity may need to be combined with a test to determine whether the estimation process should be restarted in the event that too much of the data is edited.

## APPENDIX A - ESTIMATOR ERROR PLOTS

This appendix contains plots of the radial, cross-track, and along-track position differences that were obtained by differencing the "truth" and SBDC estimated ephemerides.

Table A-1 is an index to this appendix; the run identification numbers are identical to those defined in Sections 5 and 6 in the tables listed.

Table A-1. Appendix A Index

RUN NUMBER	TABLE REFER- ENCE	SPAN PLOTTED	DEFINITIVE INTERVAL	PREDICTED INTERVAL	FIGURE NUMBERS (A- )
L01	5-1	3	3:20-14:30	14:30-17:30	1, 2, 3
L04	5-1	3	3:20-14:30	14:30-17:30	4, 5, 6
L05	5-1	3	3:20-14:30	14:30-17:30	7, 8, 9
L06	5-1	3	3:20-14:30	14:30-17:30	10, 11, 12
L15	5-1	2	2:25-13:10	13:10-16:30	13, 14, 15
L15	5-1	5	6:00-17:40	17:40-20:40	16, 17, 18
L11	5-1	1	0:40-11:40	11:40-17:40	19, 20, 21
L13	5-1	2	3:20-14:30	14:30-20:30	22, 23, 24
L23	5-1	1	0:40-11:40	11:40-19:10	25, 26, 27
L18	5-2	4	4:45-16:30	16:30-19:30	28, 29, 30
L19	5-2	4	4:45-16:30	16:30-19:30	31, 32, 33
L20	5-2	1	0:40-11:40	11:40-17:40	34, 35, 36
L21	5-2	2	3:20-14:30	14:30-20:30	37, 38, 39
L08	5-3	2	2:25-13:10	13:10-16:10	40, 41, 42
L09	5-3	2	2:25-13:10	13:10-16:10	43, 44, 45
L10	5-3	1	0:40-11:40	11:40-14:40	46, 47, 48
L22	5-3	1	0:40-11:40	11:40-17:40	49, 50, 51
L22	5-3	2	3:20-14:30	14:30-20:30	52, 53, 54
L22	5-3	3	6:00-17:40	17:40-23:40	55, 56, 57
L22	5-3	4	8:18-21:25	21:25-27:25	58, 59, 60
G01	6-1	2	1:50-13:10	13:10-16:10	61, 62, 63
G04	6-1	2	1:50-13:10	13:10-16:10	64, 65, 66
G05	6-1	2	1:50-13:10	13:10-16:10	67, 68, 69
G06	6-1	2	1:50-13:10	13:10-16:10	70, 71, 72
G15	6-1	2	1:50-13:10	13:10-16:10	73, 74, 75
G15	6-1	5	6:20-18:10	18:10-21:10	76, 77, 78
G11	6-1	2	3:10-15:00	15:00-21:00	79, 80, 81
G14	6-1	2	3:10-15:00	15:00-21:00	82, 83, 84
G17	6-2	2	1:50-13:10	13:10-16:10	85, 86, 87
G19	6-2	2	1:50-13:10	13:10-16:10	88, 89, 90
G20	6-2	2	3:10-15:00	15:00-21:10	91, 92, 93
G08	6-3	2	1:50-13:10	13:10-16:10	94, 95, 96
G09	6-3	2	1:50-13:10	13:10-16:10	97, 98, 99
G10	6-3	2	1:50-13:10	13:10-16:10	100, 101, 102
G22	6-3	1	0:10-11:50	11:50-17:50	103, 104, 105
G22	6-3	2	3:10-15:00	15:00-21:00	106, 107, 108
G22	6-3	3	6:20-18:10	18:10-24:10	109, 110, 111
G22	6-3	4	9:43-21:40	21:40-27:10	112, 113, 114

7651/80

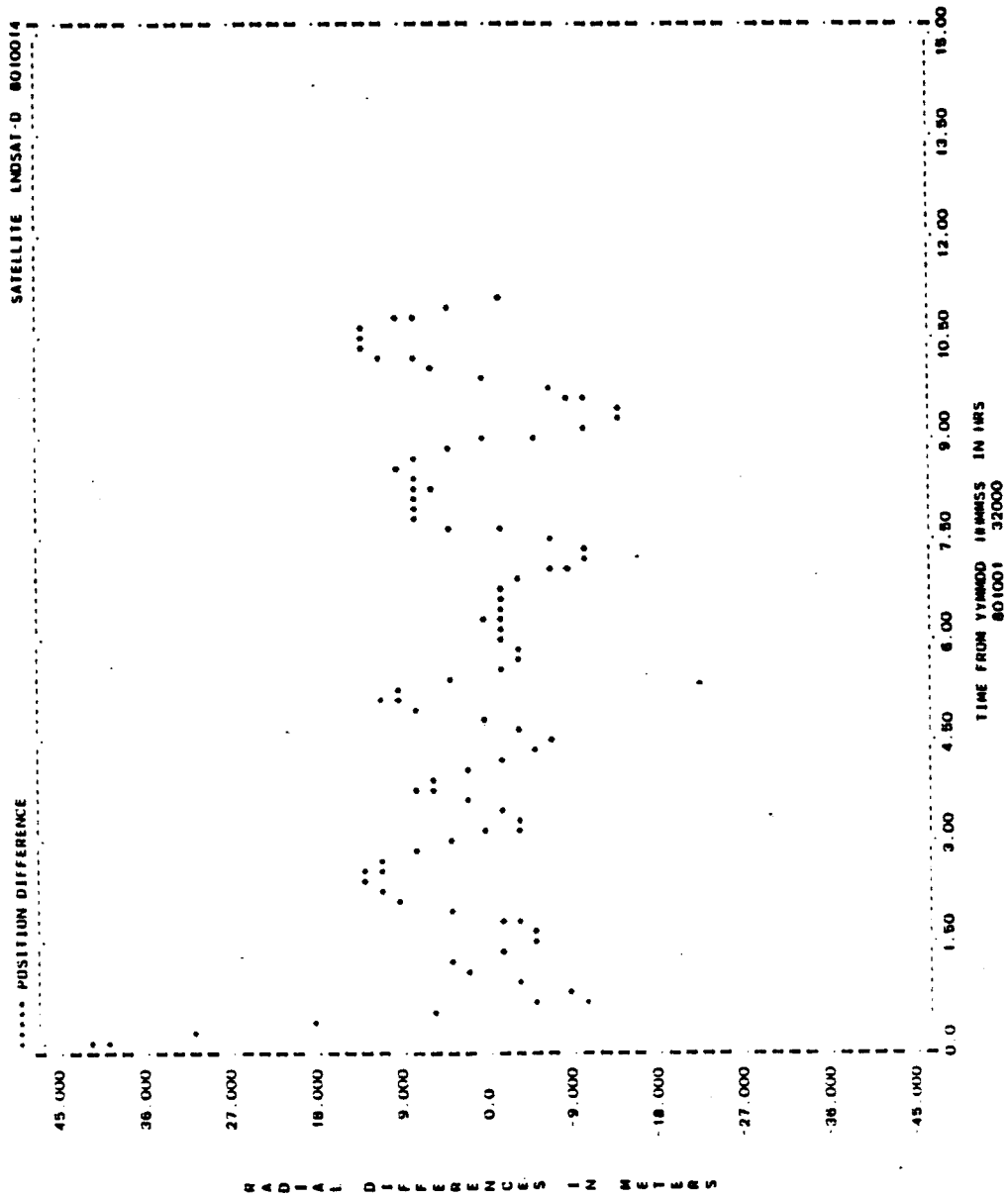


Figure A-1. Radial Differences for Run L01 (1 of 2)

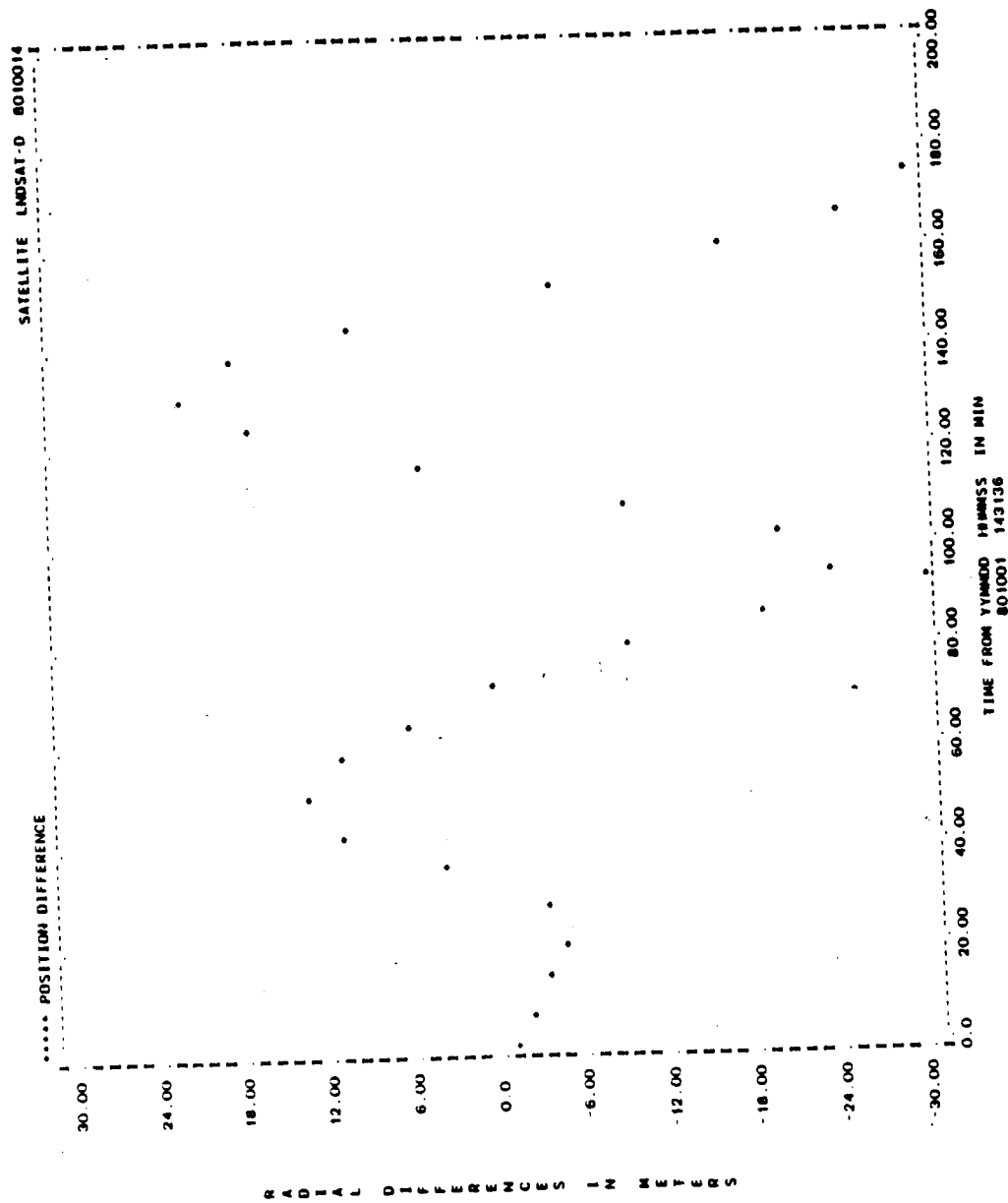


Figure A-1. Radial Differences for Run L01 (2 of 2)

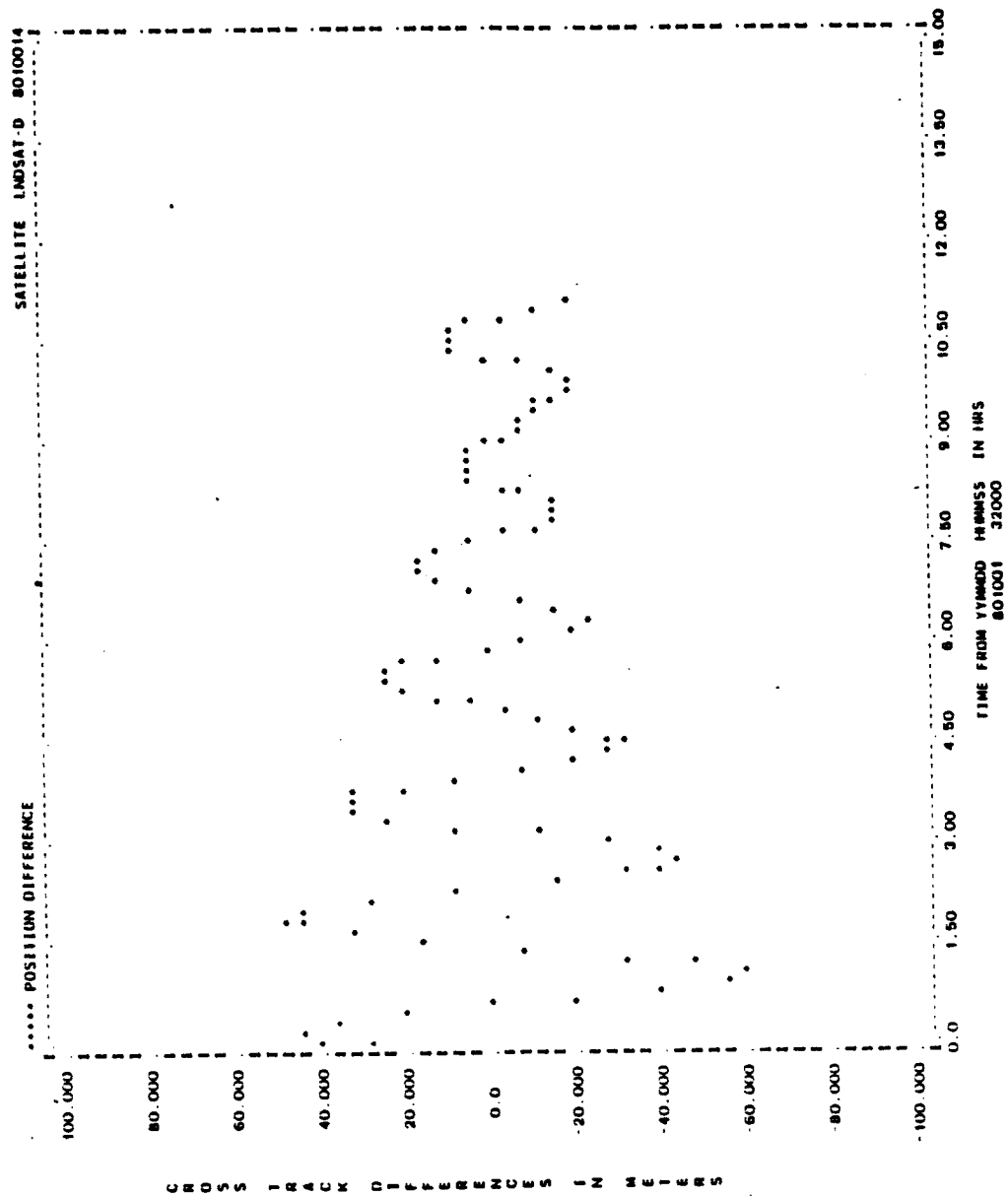


Figure A-2. Cross-Track Differences for Run L01 (1 of 2)

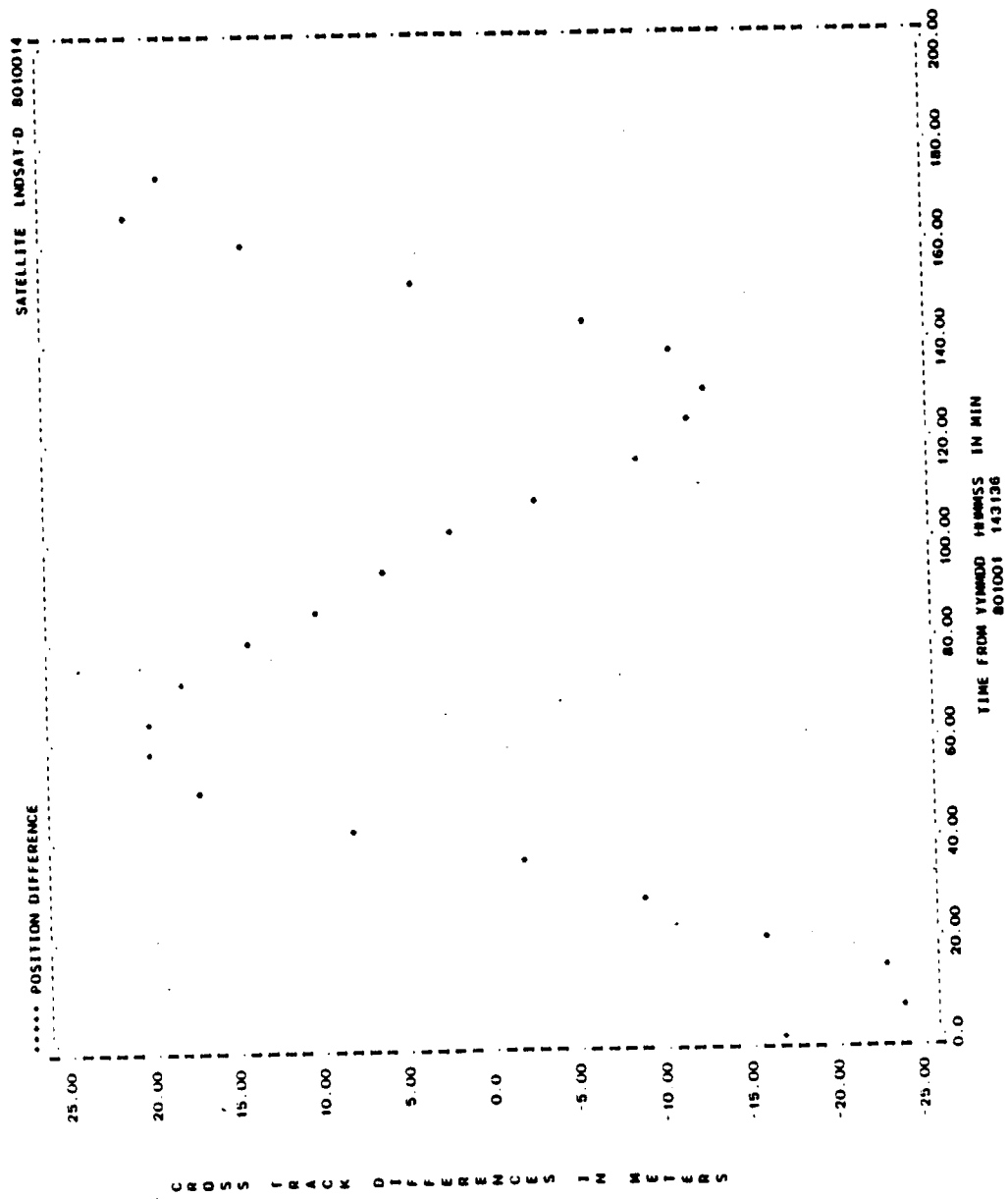


Figure A-2. Cross-Track Differences for Run L01 (2 of 2)

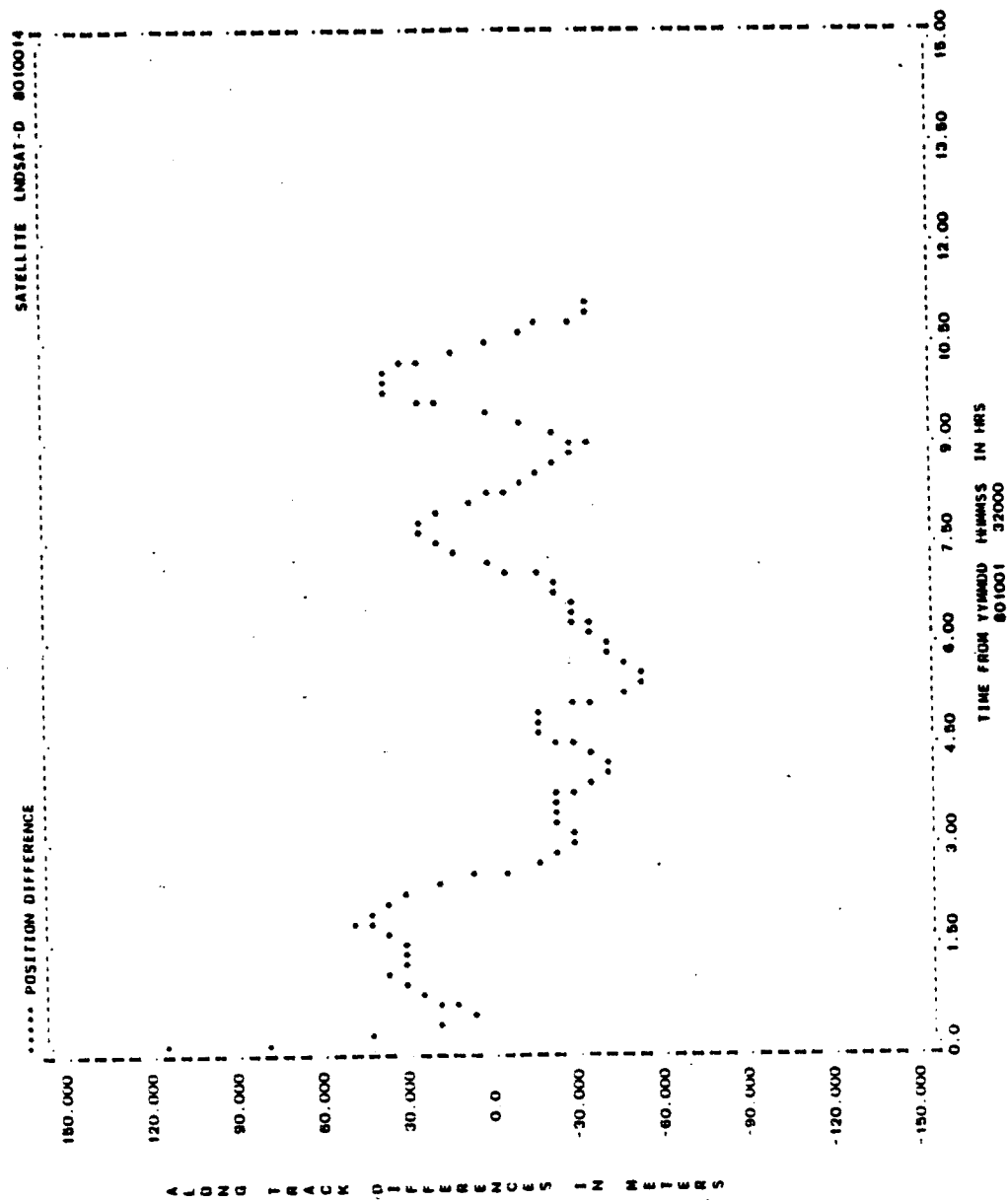


Figure A-3. Along-Track Differences for Run L01 (1 of 2)

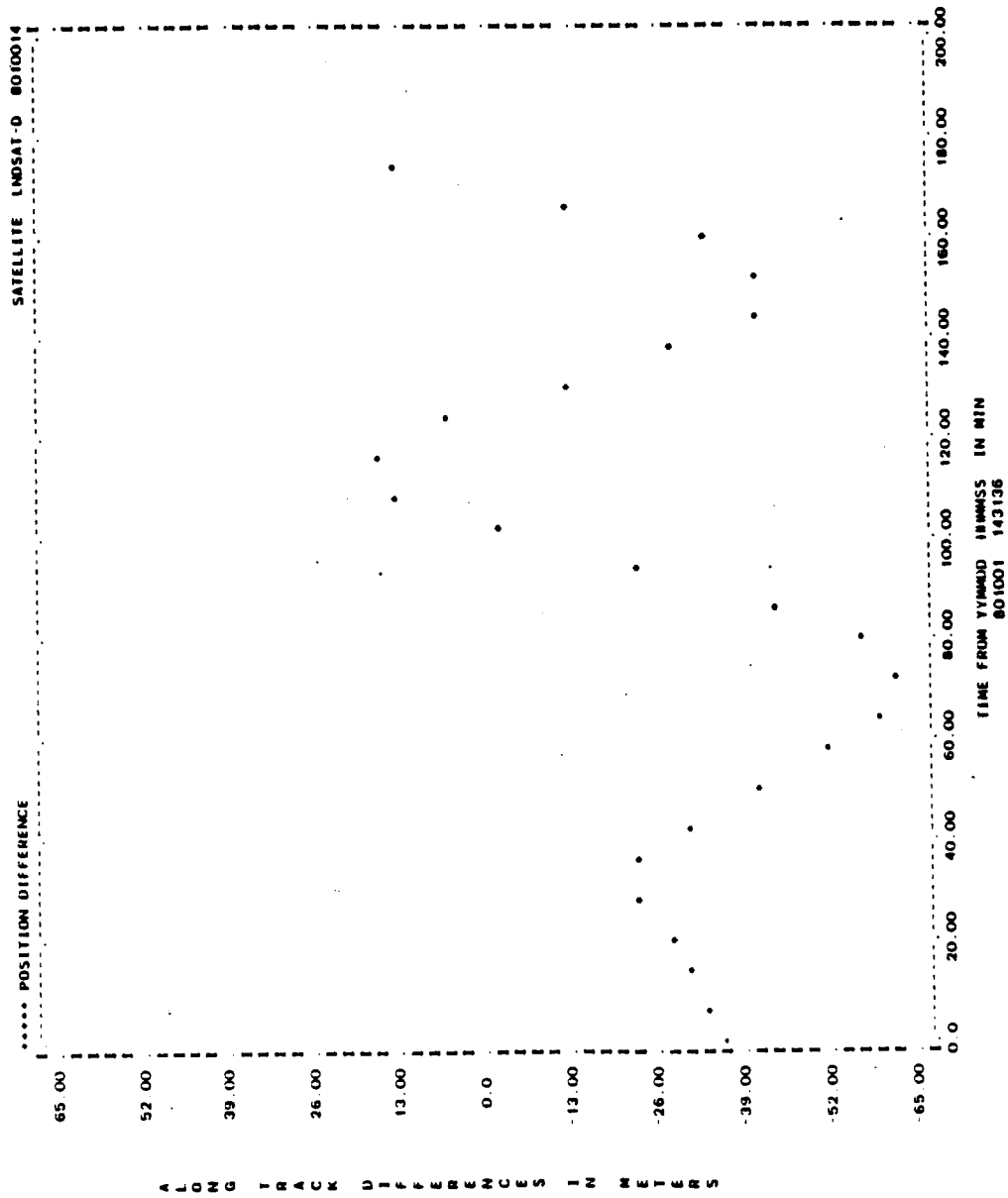


Figure A-3. Along-Track Differences for Run L01 (2 of 2)

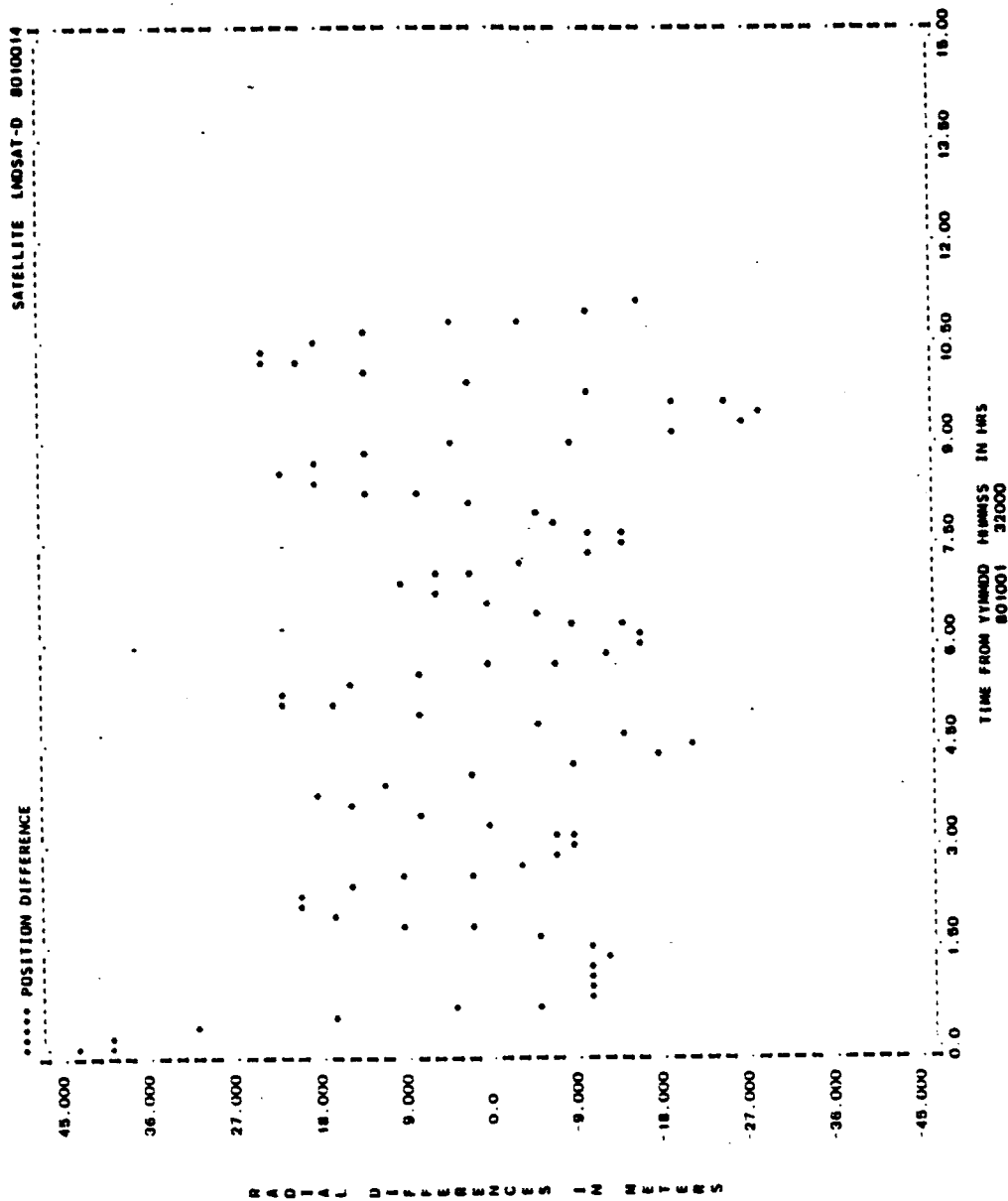


Figure A-4. Radial Differences for Run L04 (1 of 2)

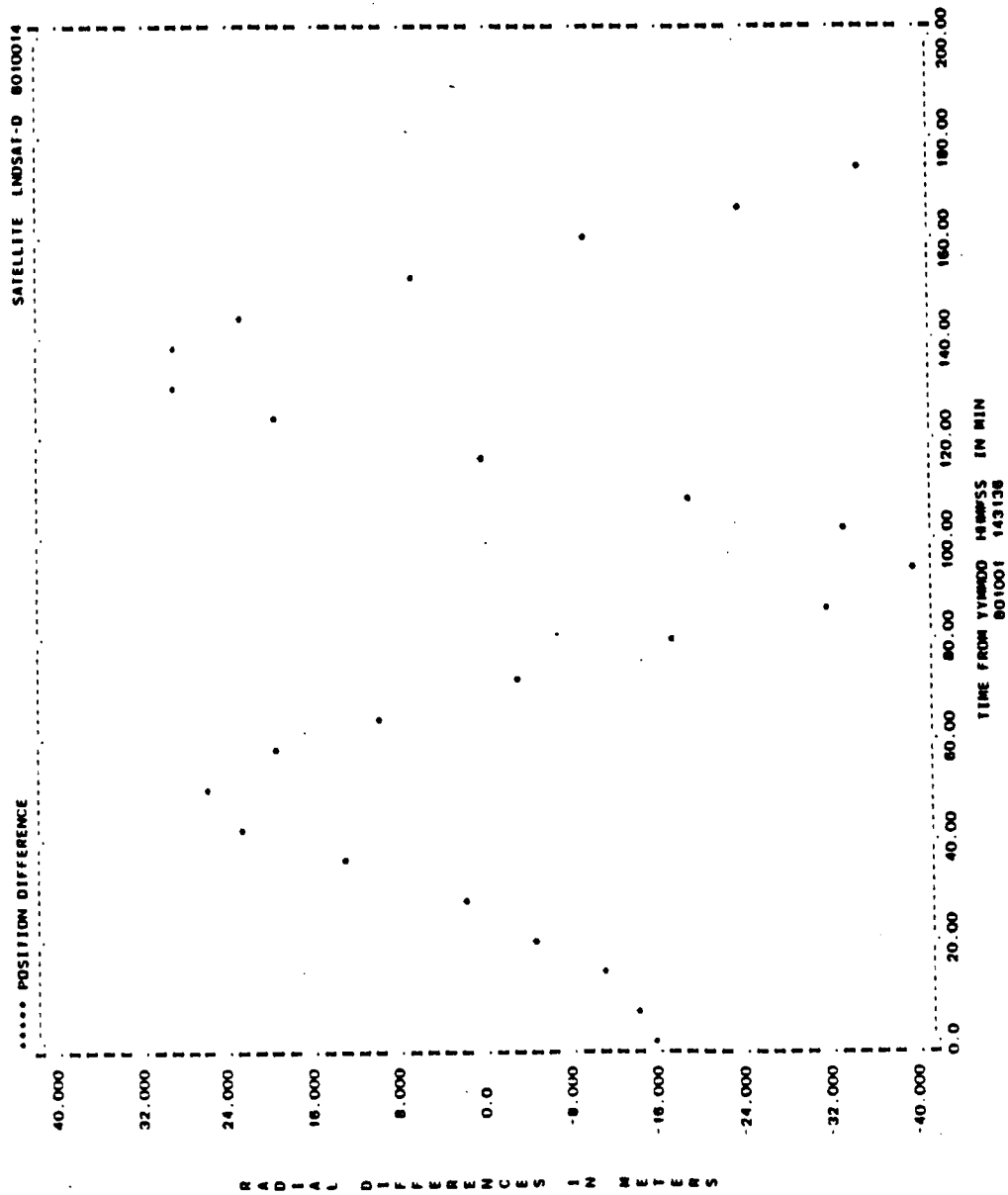


Figure A-4. Radial Differences for Run L04 (2 of 2)

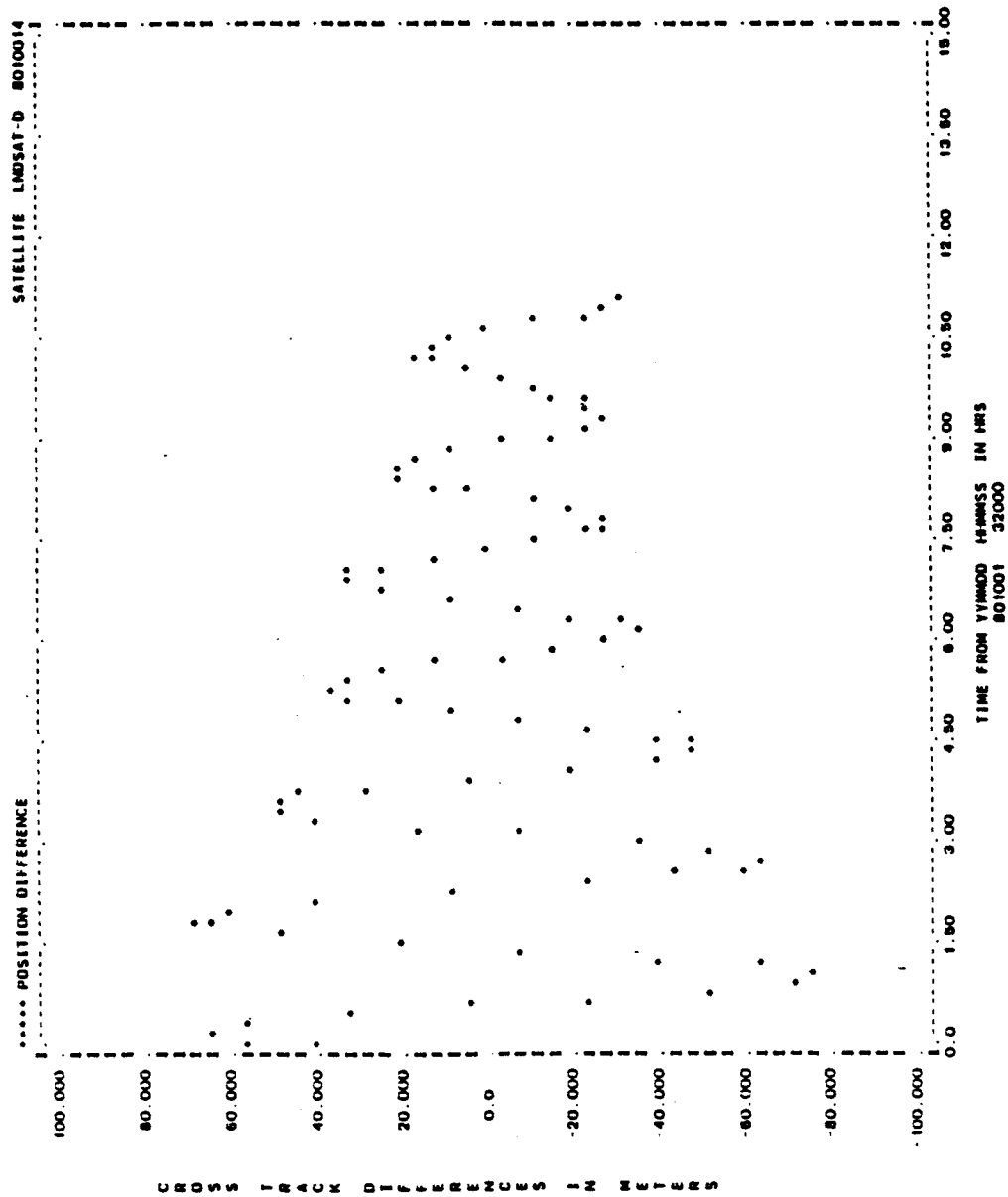


Figure A-5. Cross-Track Differences for Run L04 (1 of 2)

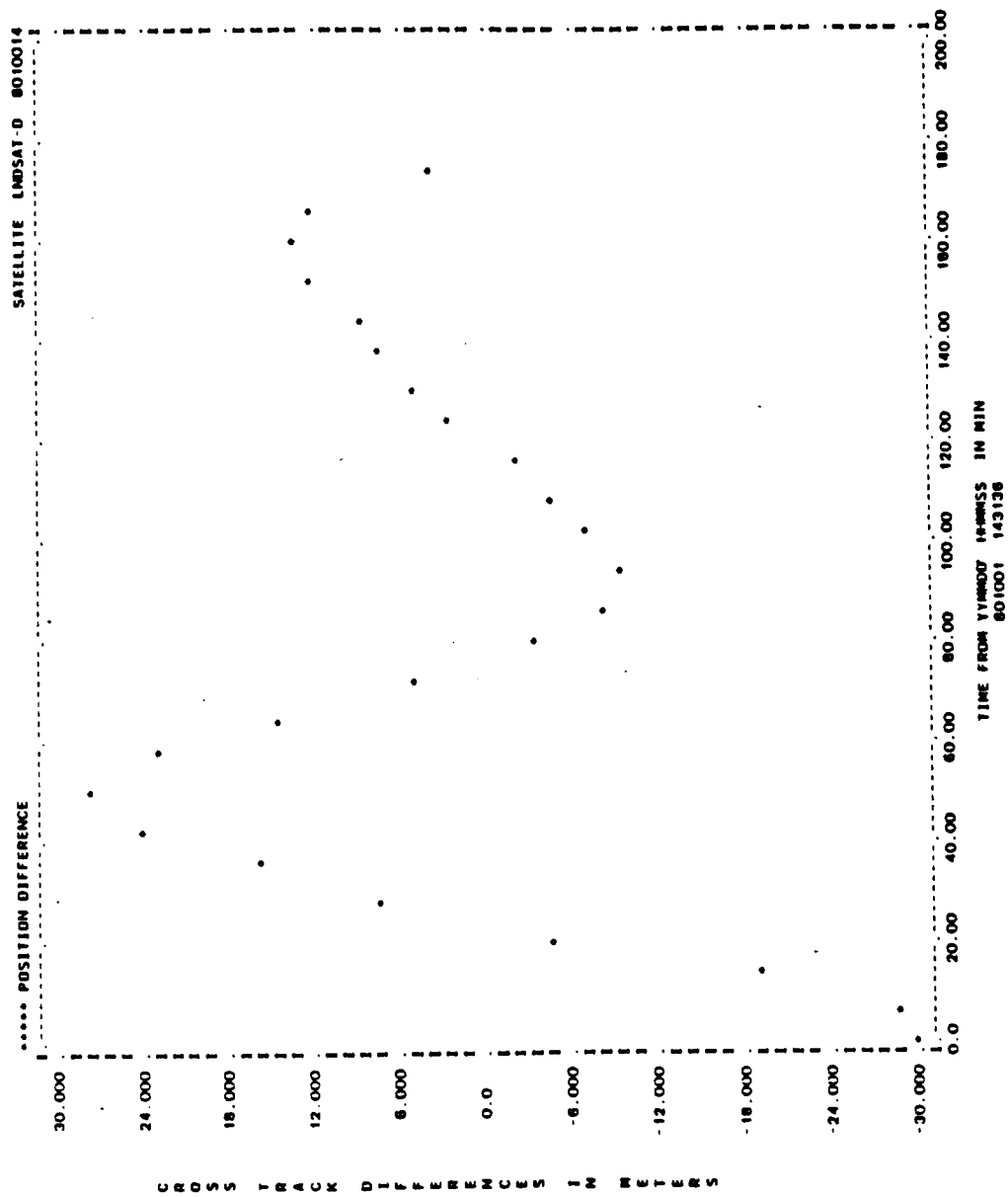


Figure A-5. Cross-Track Differences for Run L04 (2 of 2)

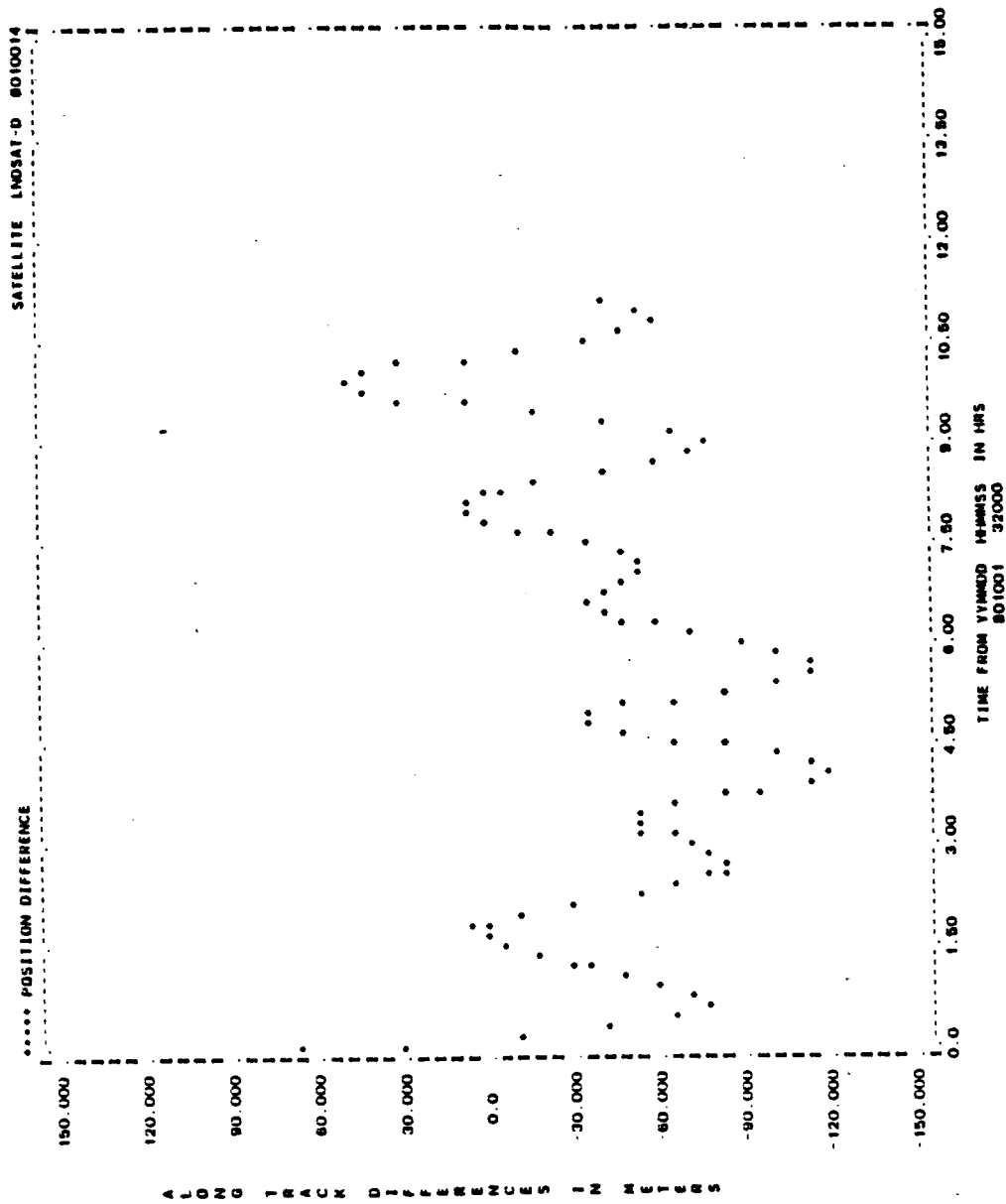


Figure A-6. Along-Track Differences for Run L04 (1 of 2)

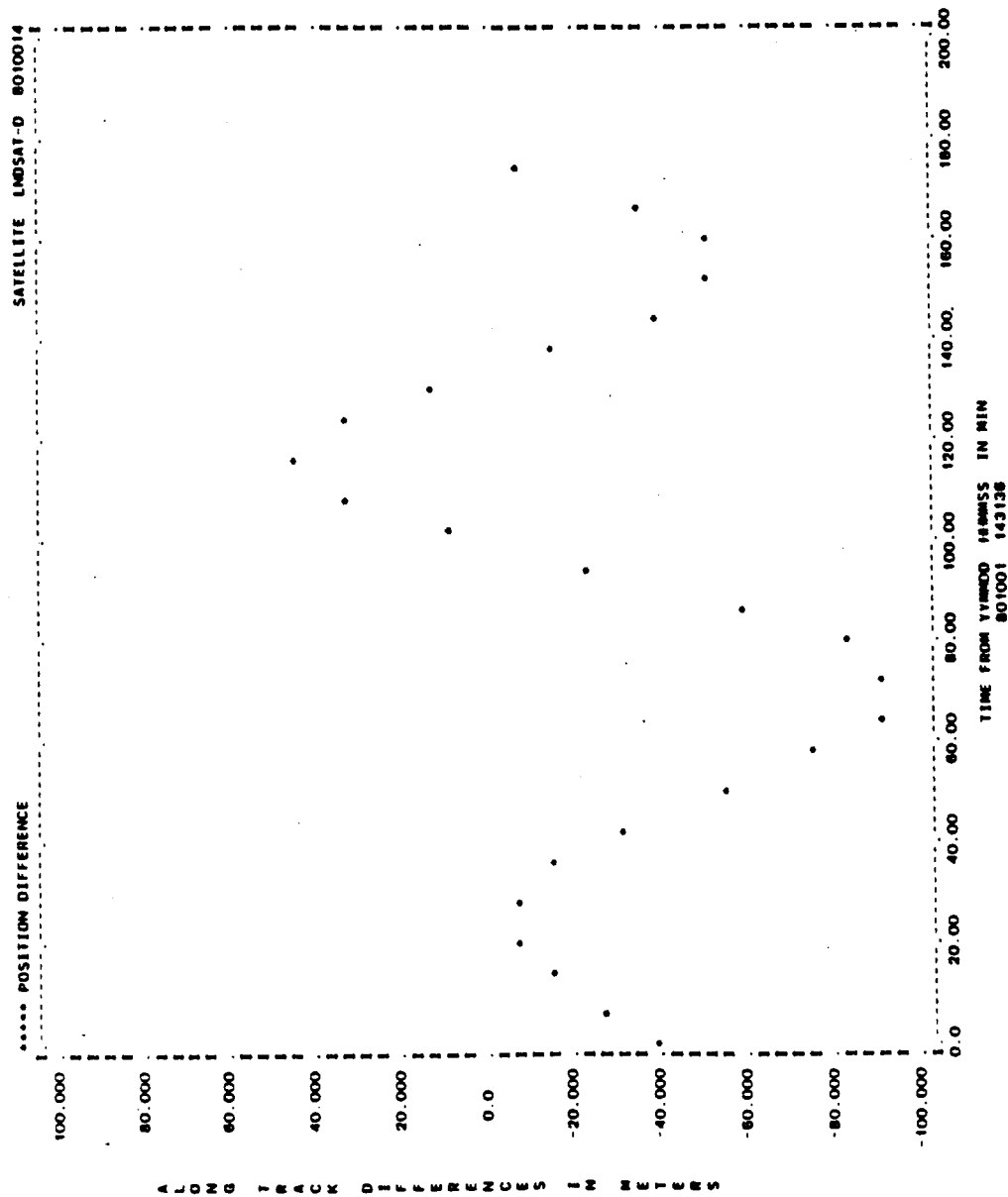


Figure A-6. Along-Track Differences for Run L04 (2 of 2)

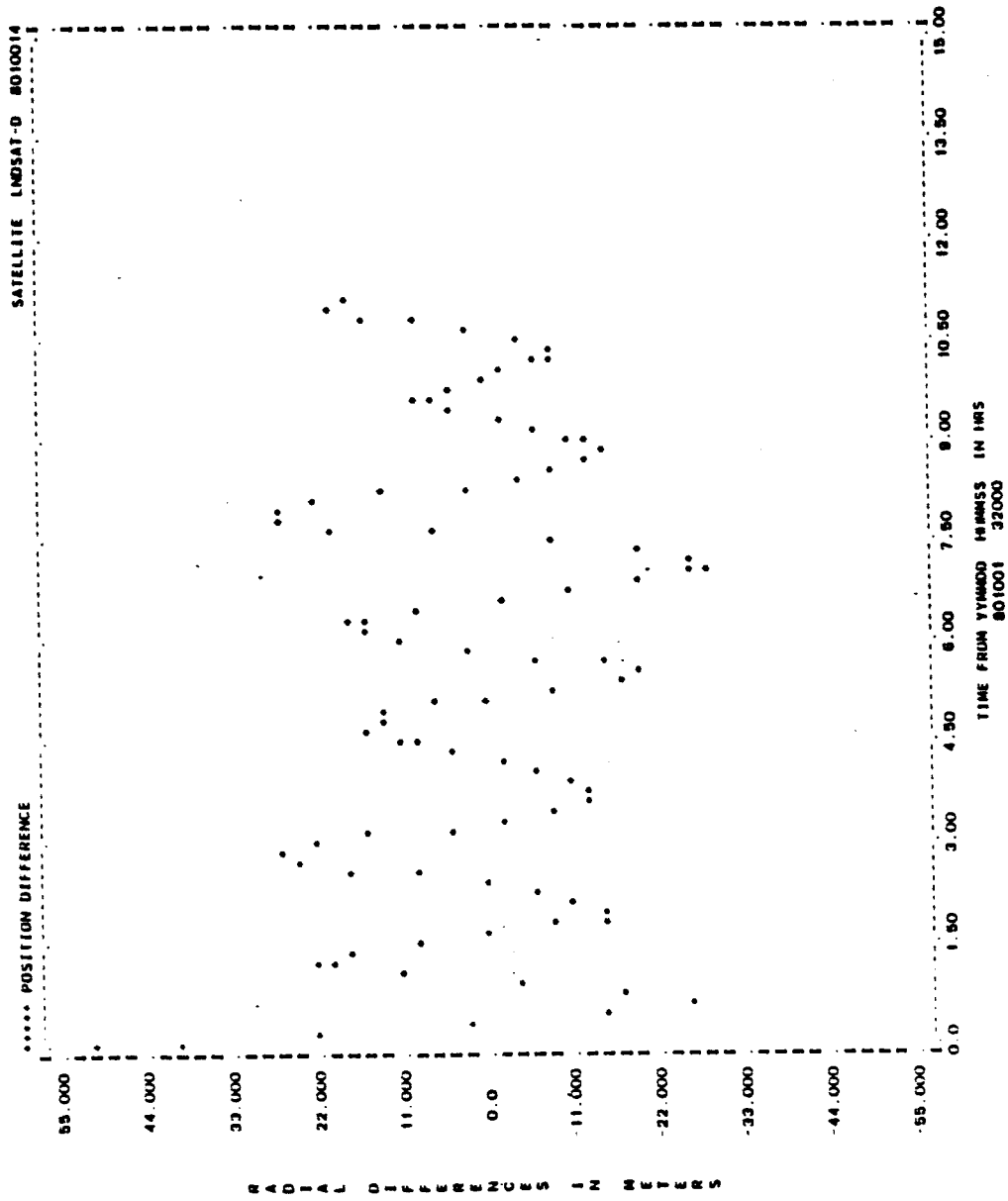


Figure A-7. Radial Differences for Run L05 (1 of 2)

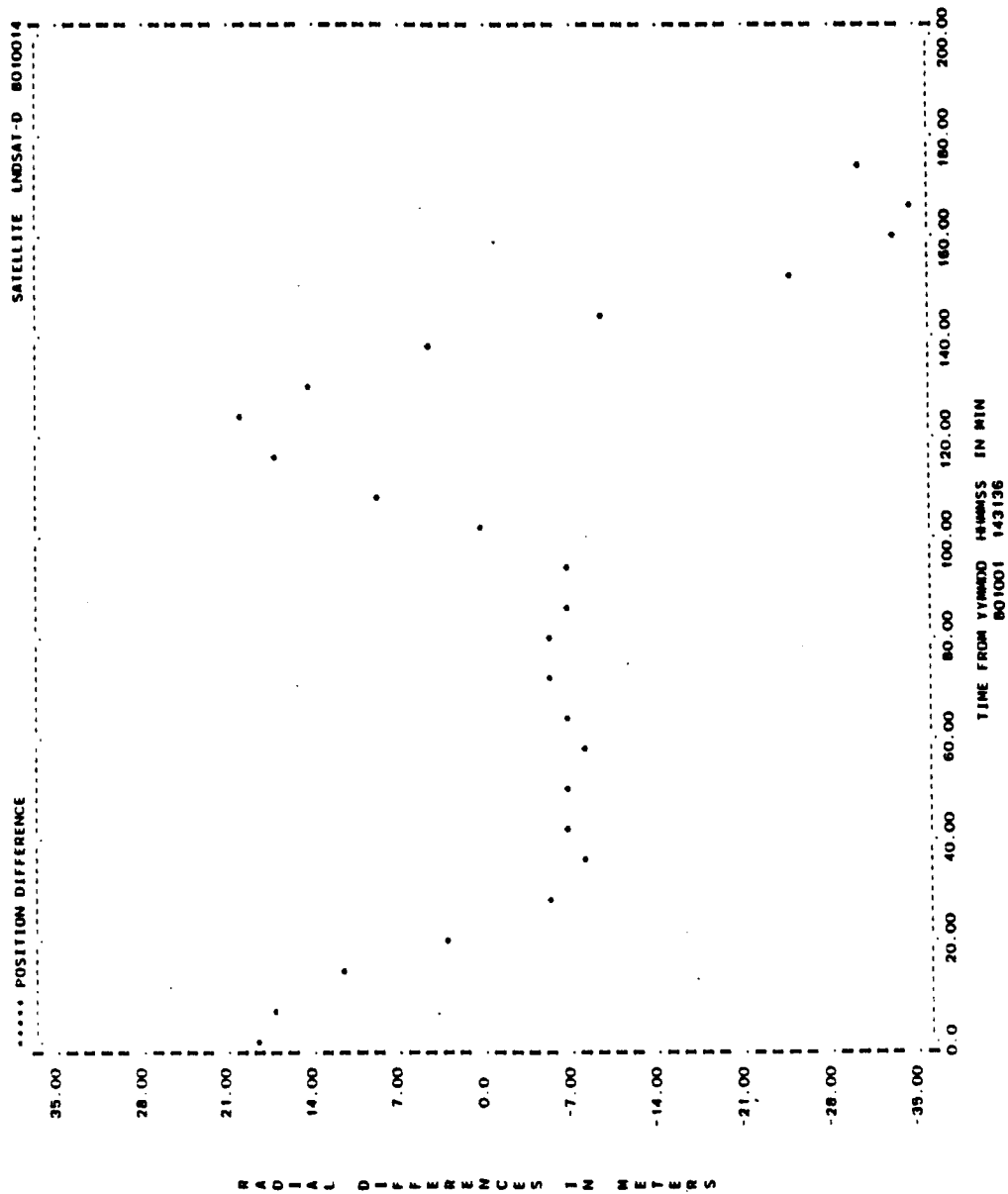


Figure A-7. Radial Differences for Run L05 (2 of 2)

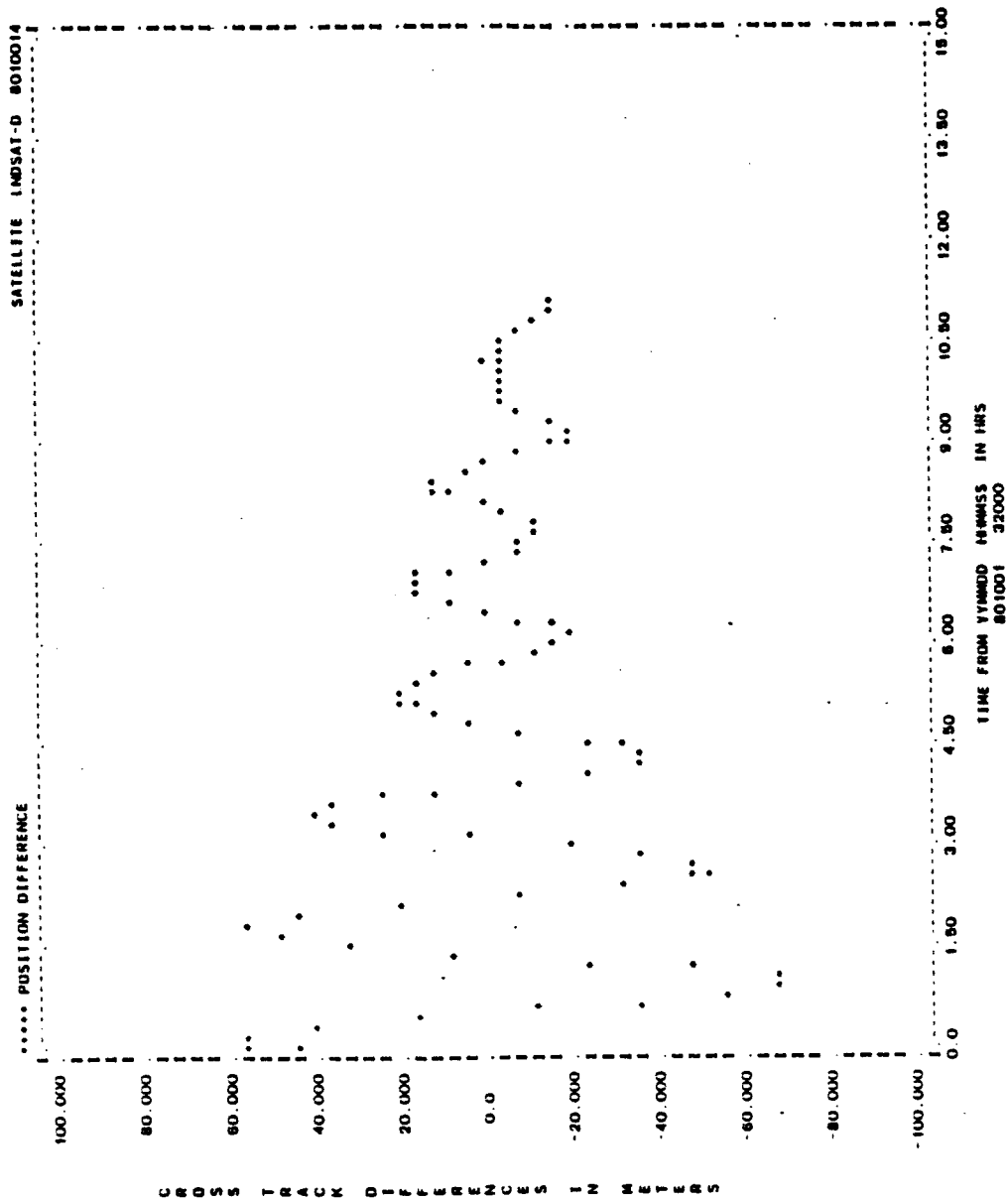


Figure A-8. Cross-Track Differences for Run L05 (1 of 2)

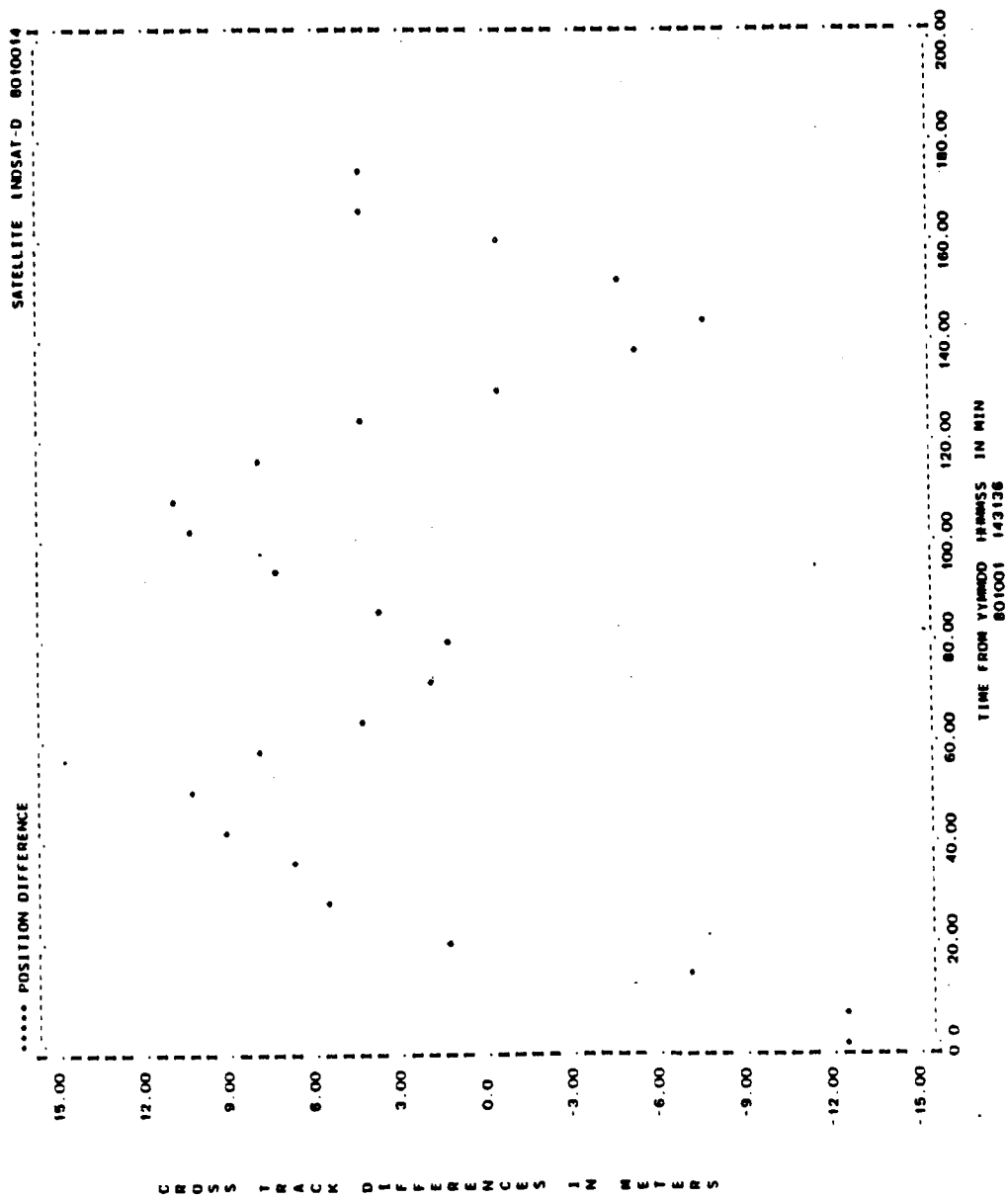


Figure A-8. Cross-Track Differences for Run L05 (2 of 2)

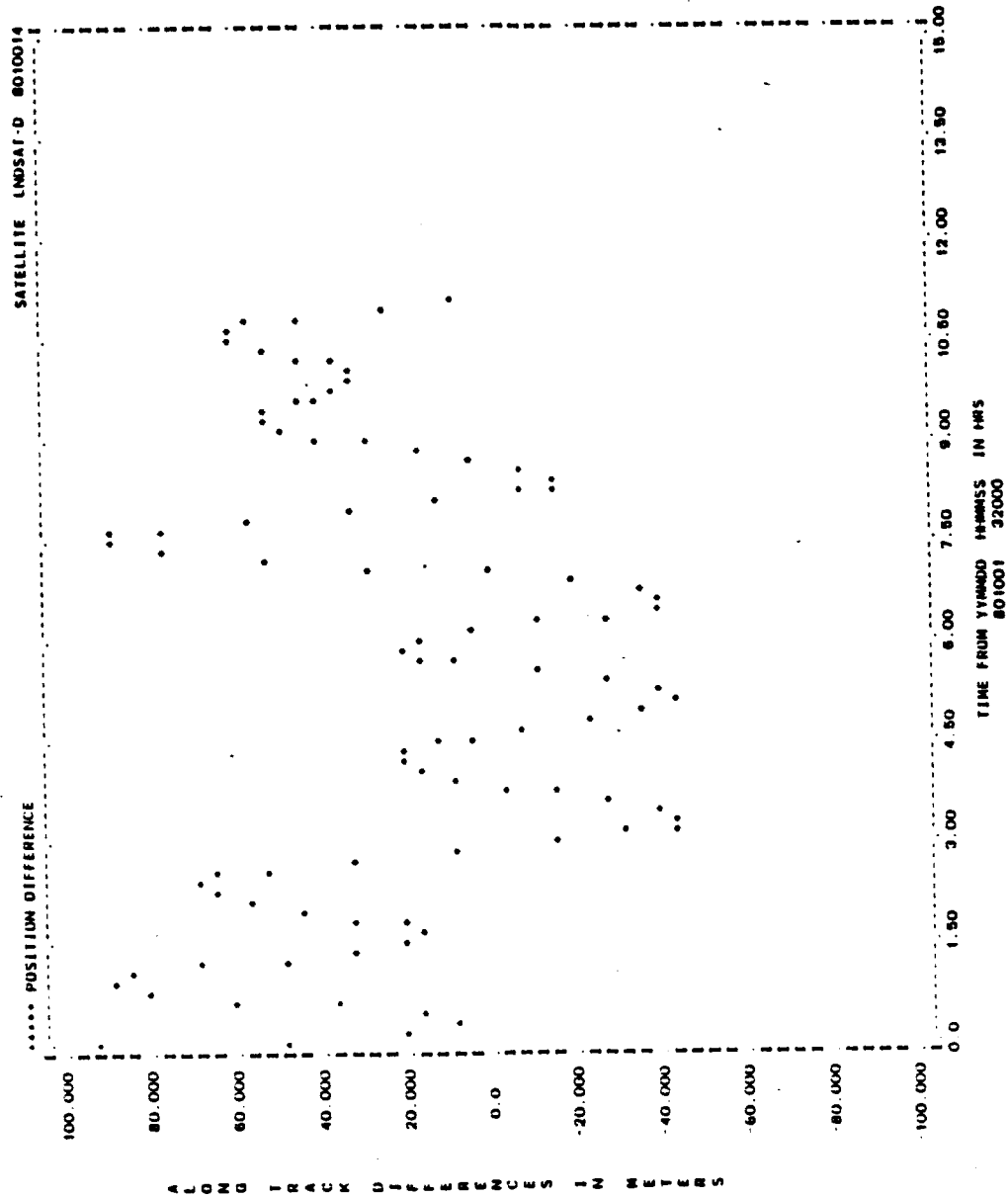


Figure A-9. Along-Track Differences for Run L05 (1 of 2)

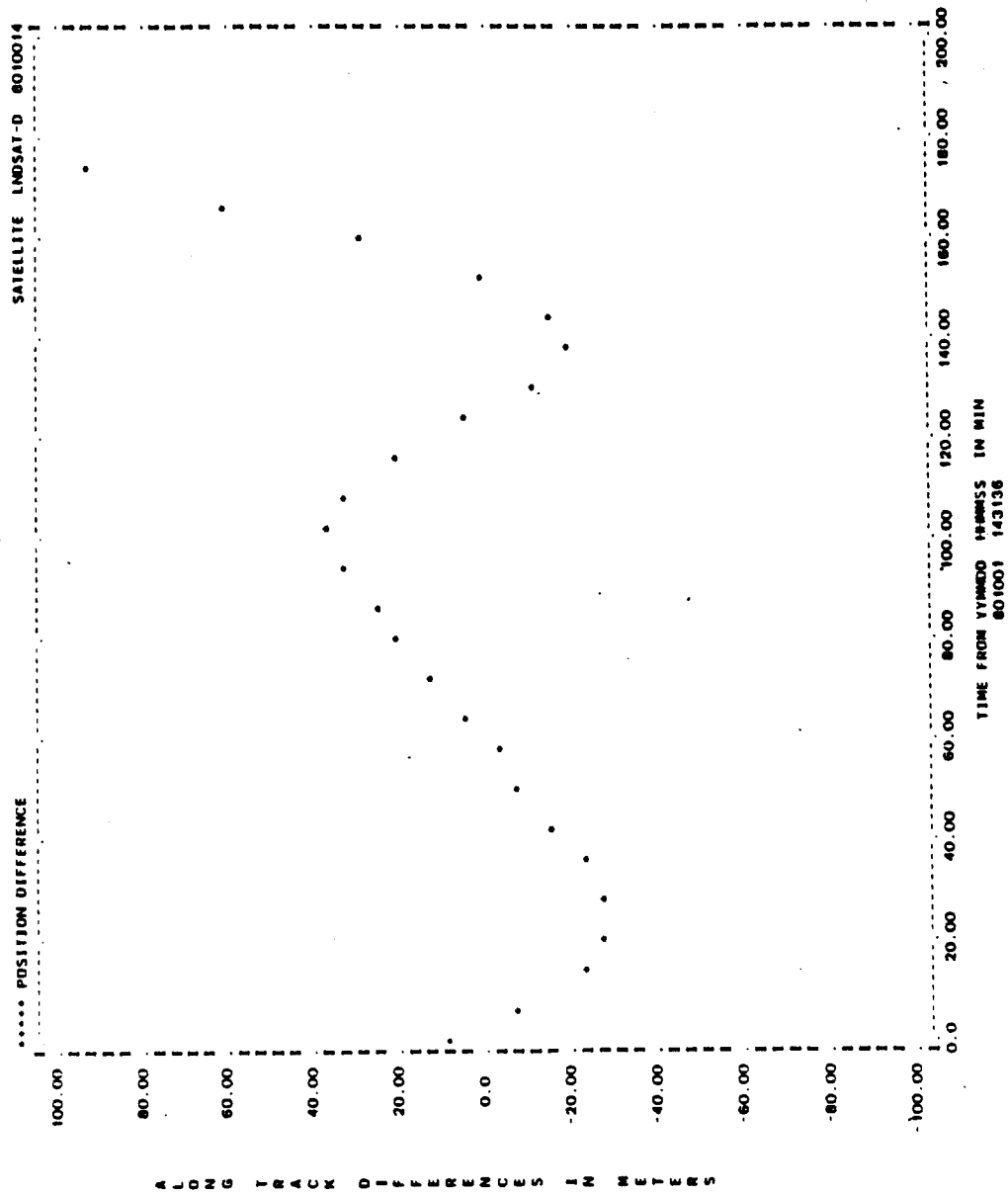


Figure A-9. Along-Track Differences for Run L05 (2 of 2)

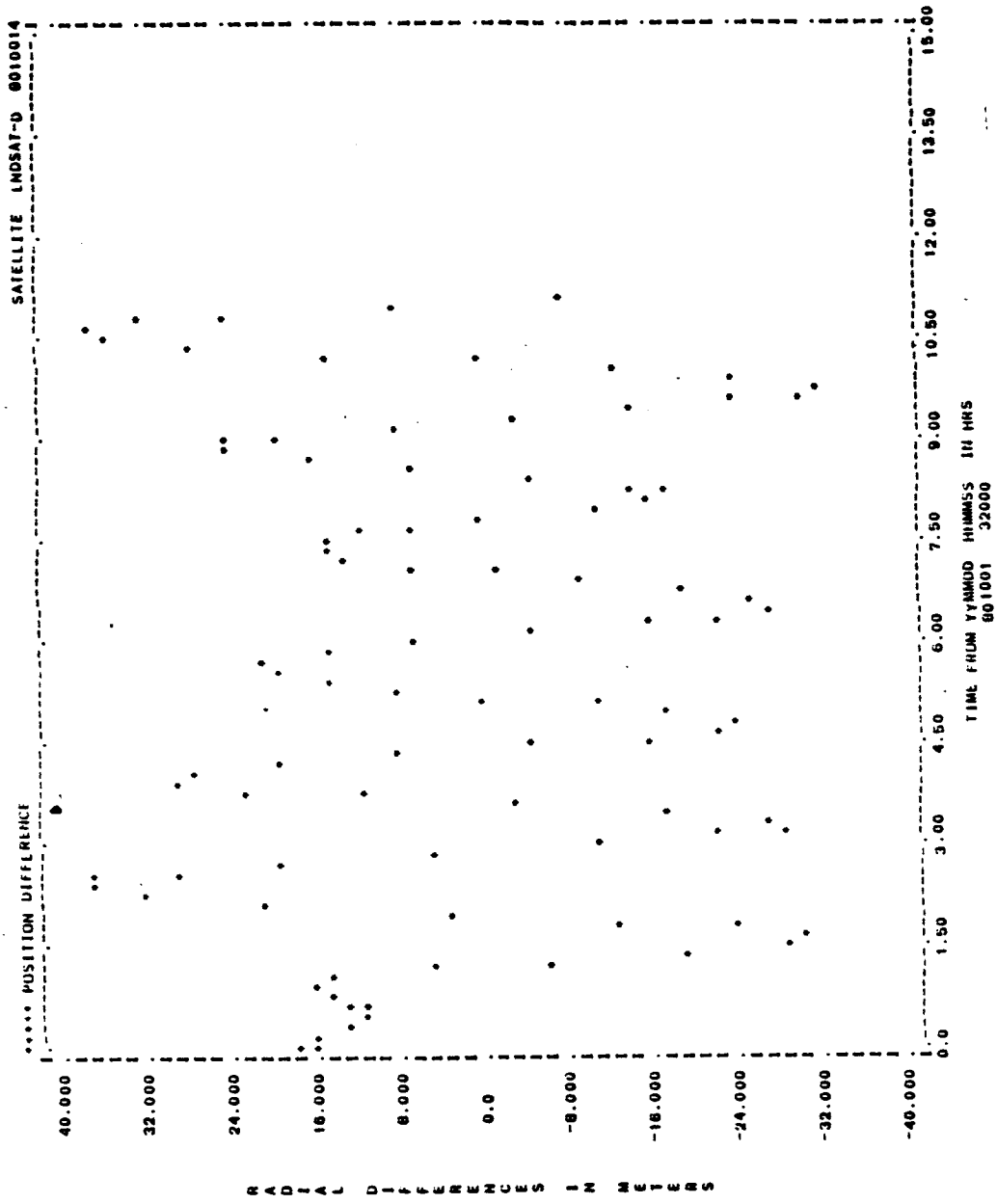


Figure A-10. Radial Differences for Run L06 (1 of 2)

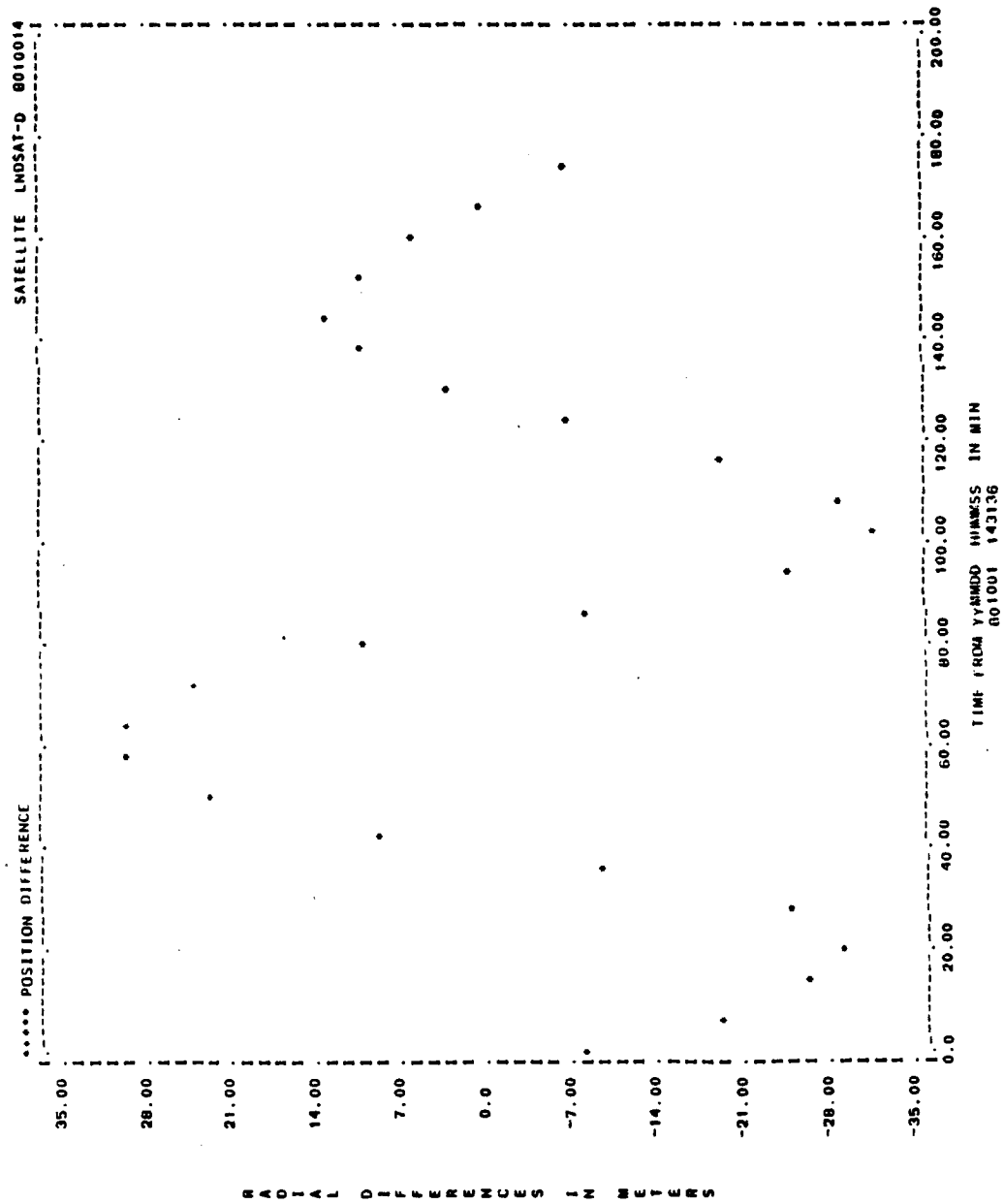


Figure A-10. Radial Differences for Run L06 (2 of 2)

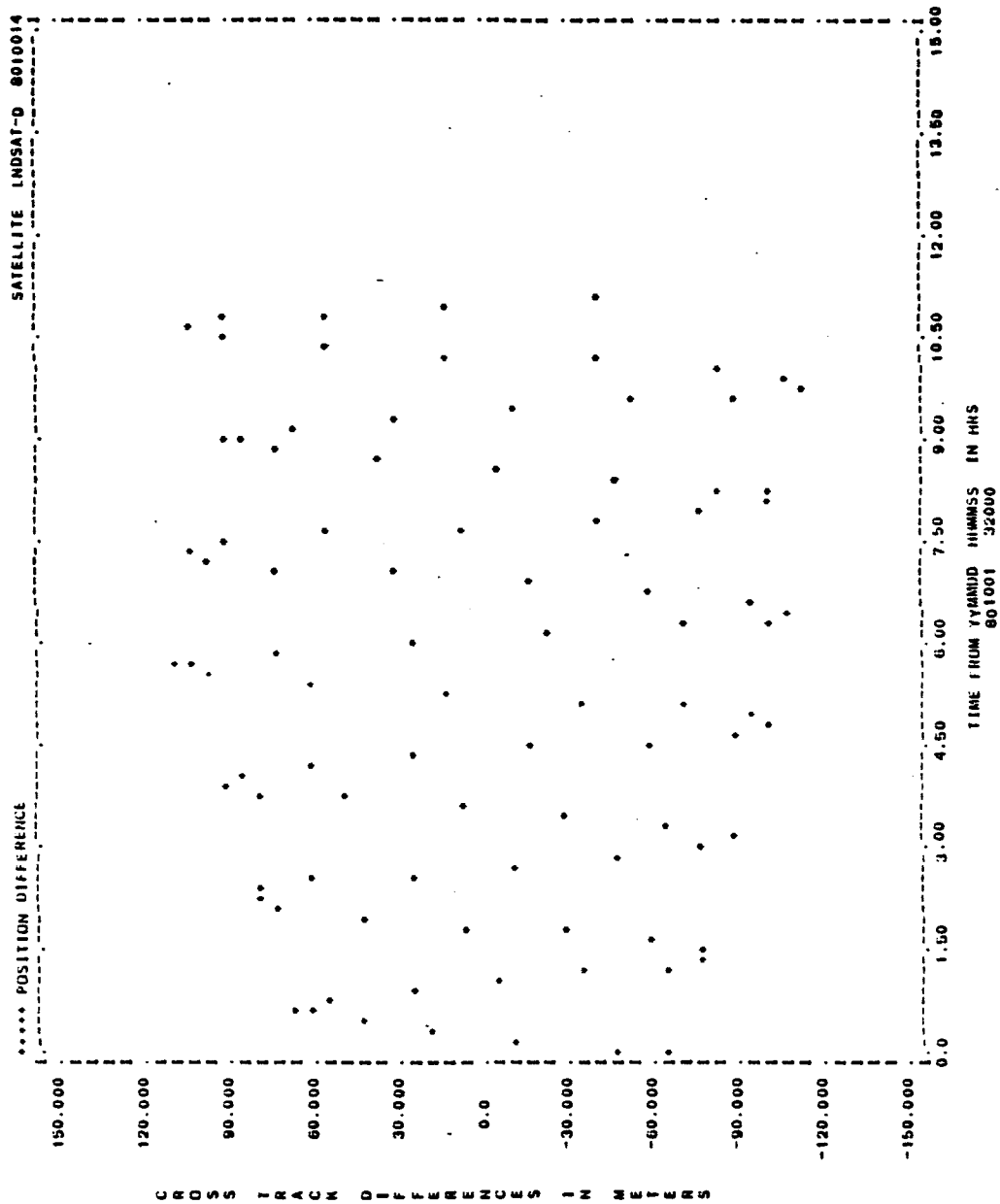


Figure A-11. Cross-Track Differences for Run L06 (1 of 2)

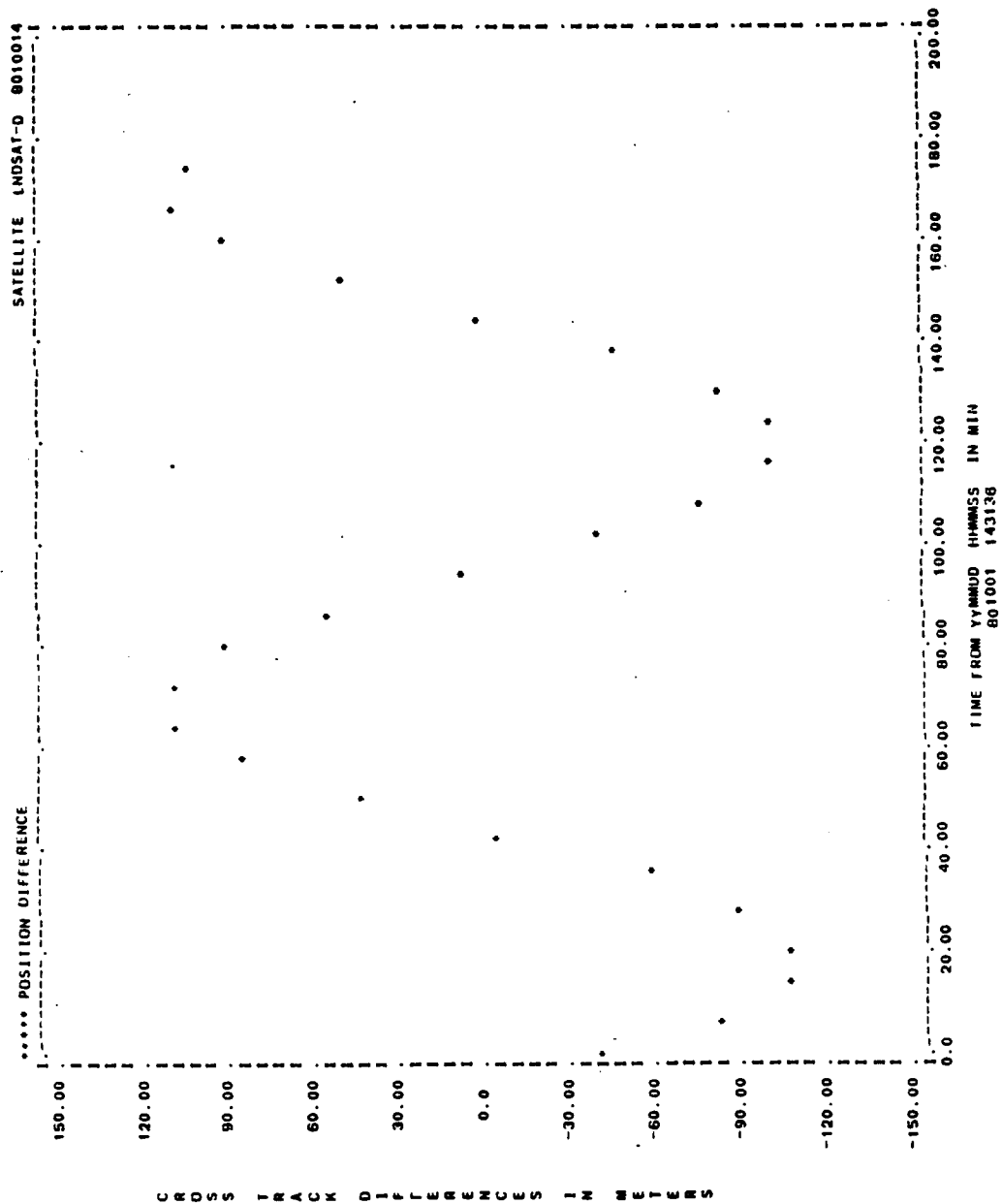


Figure A-11. Cross-Track Differences for Run L06 (2 of 2)

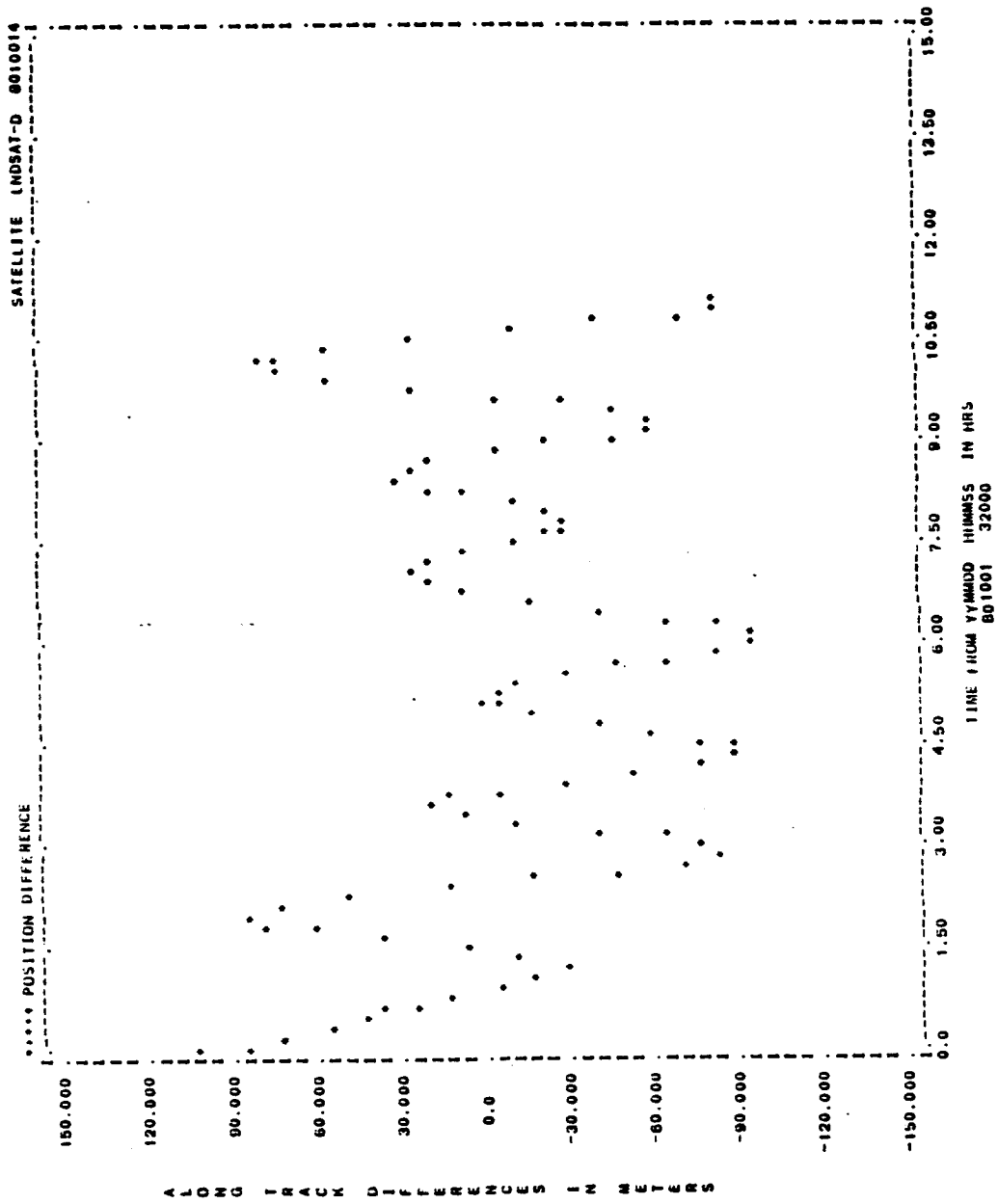


Figure A-12. Along-Track Differences for Run L06 (1 of 2)

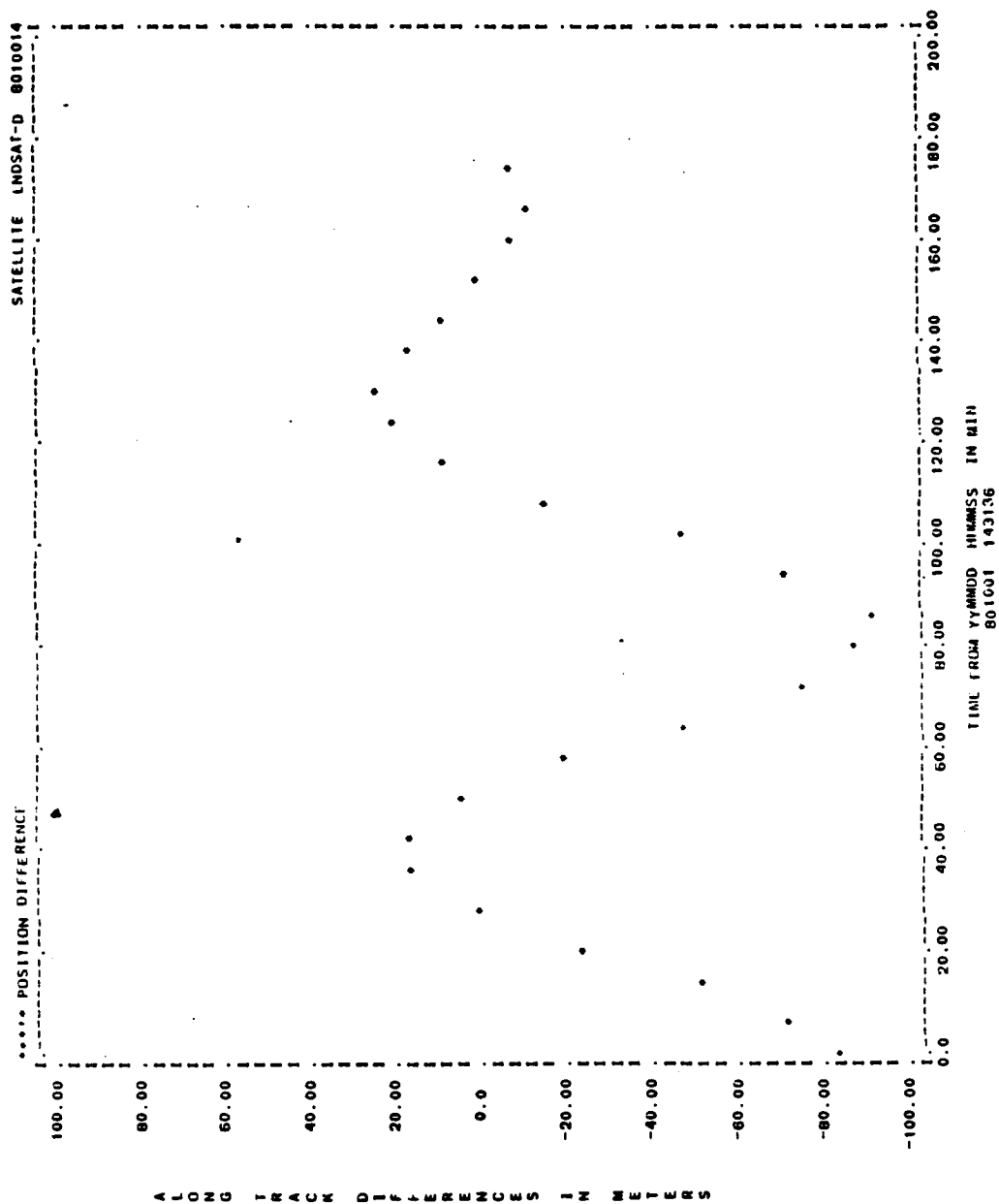


Figure A-12. Along-Track Differences for Run L06 (2 of 2)

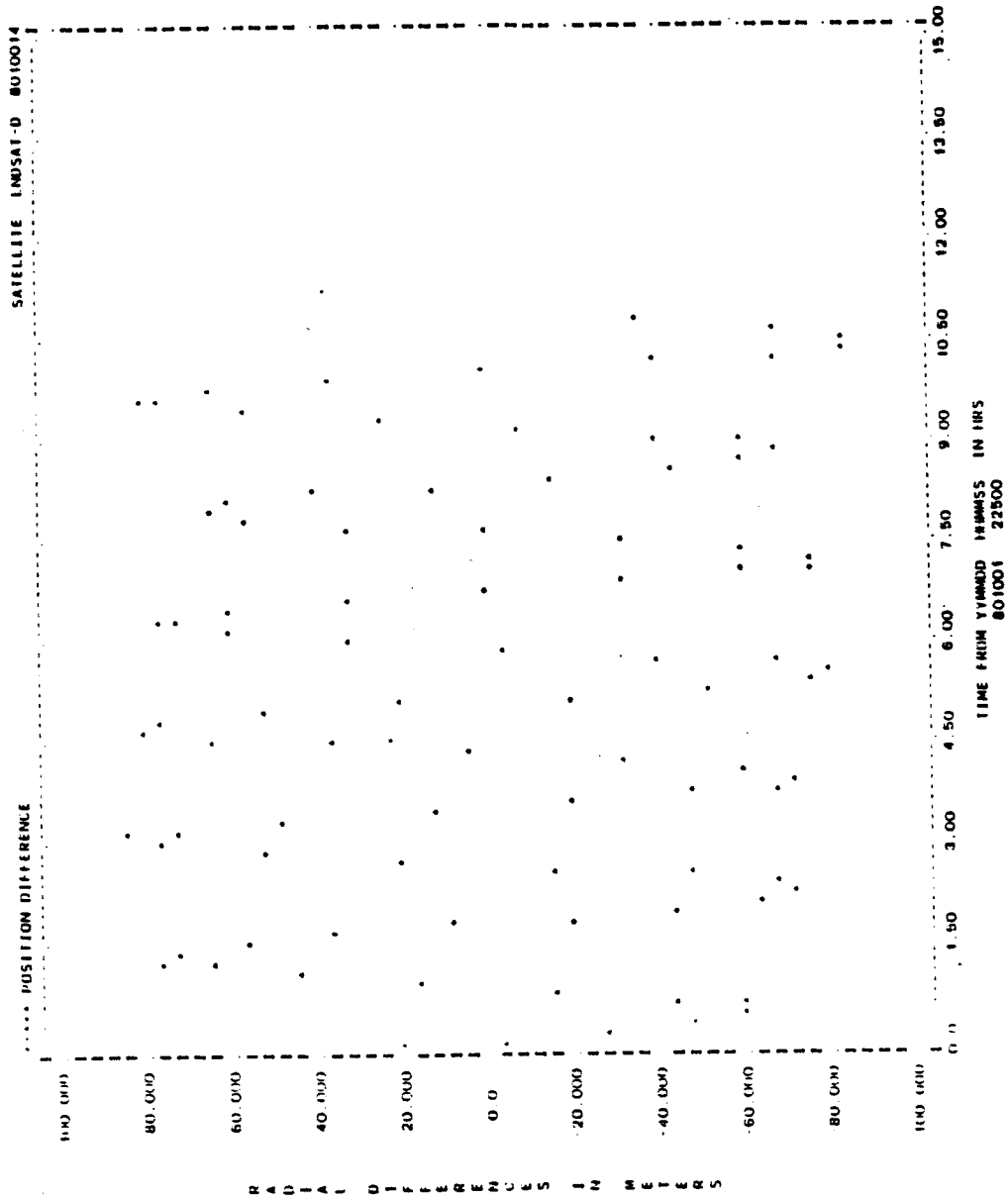


Figure A-13. Radial Differences for Run L15 (1 of 2)

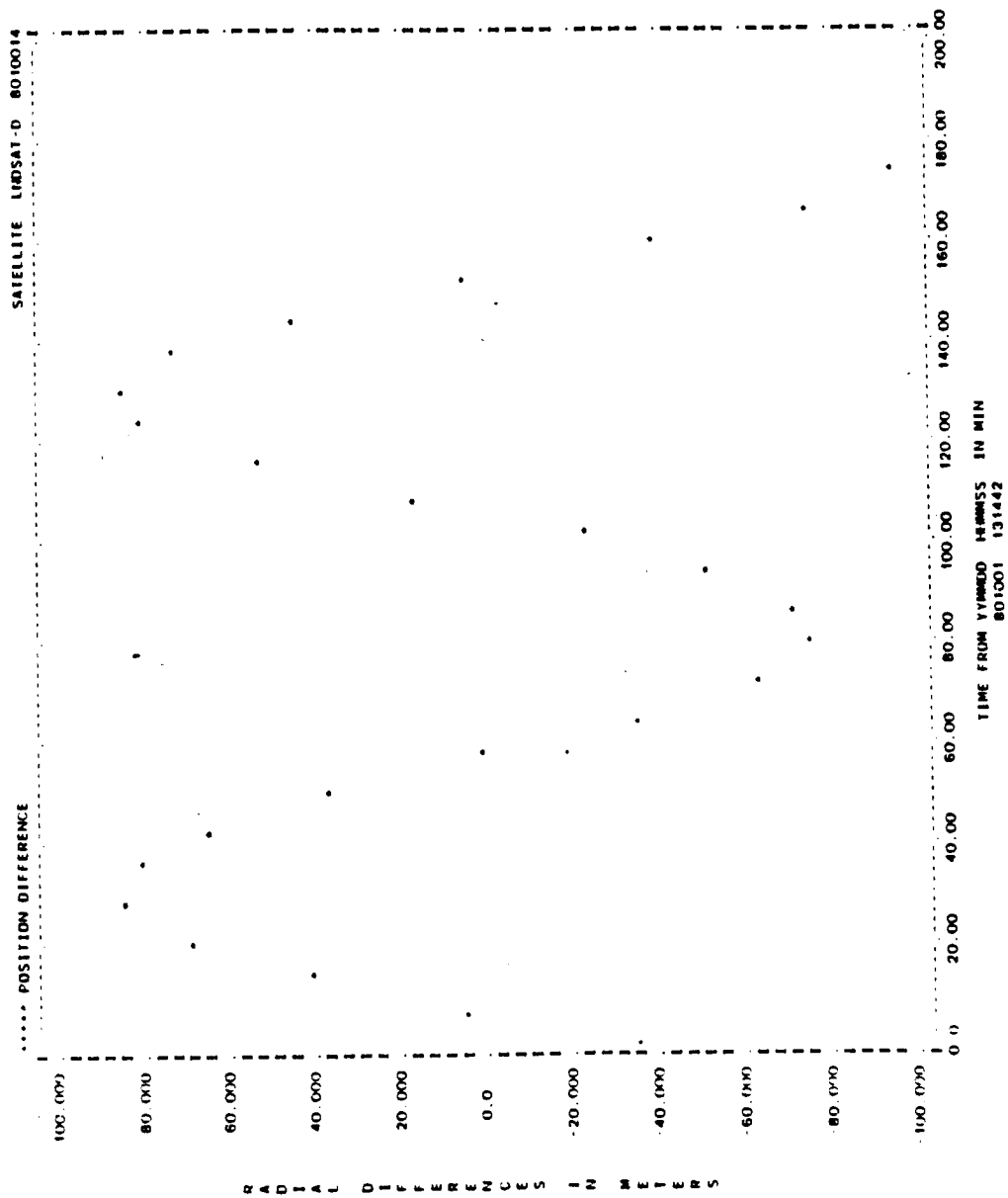


Figure A-13. Radial Differences for Run L15 (2 of 2)

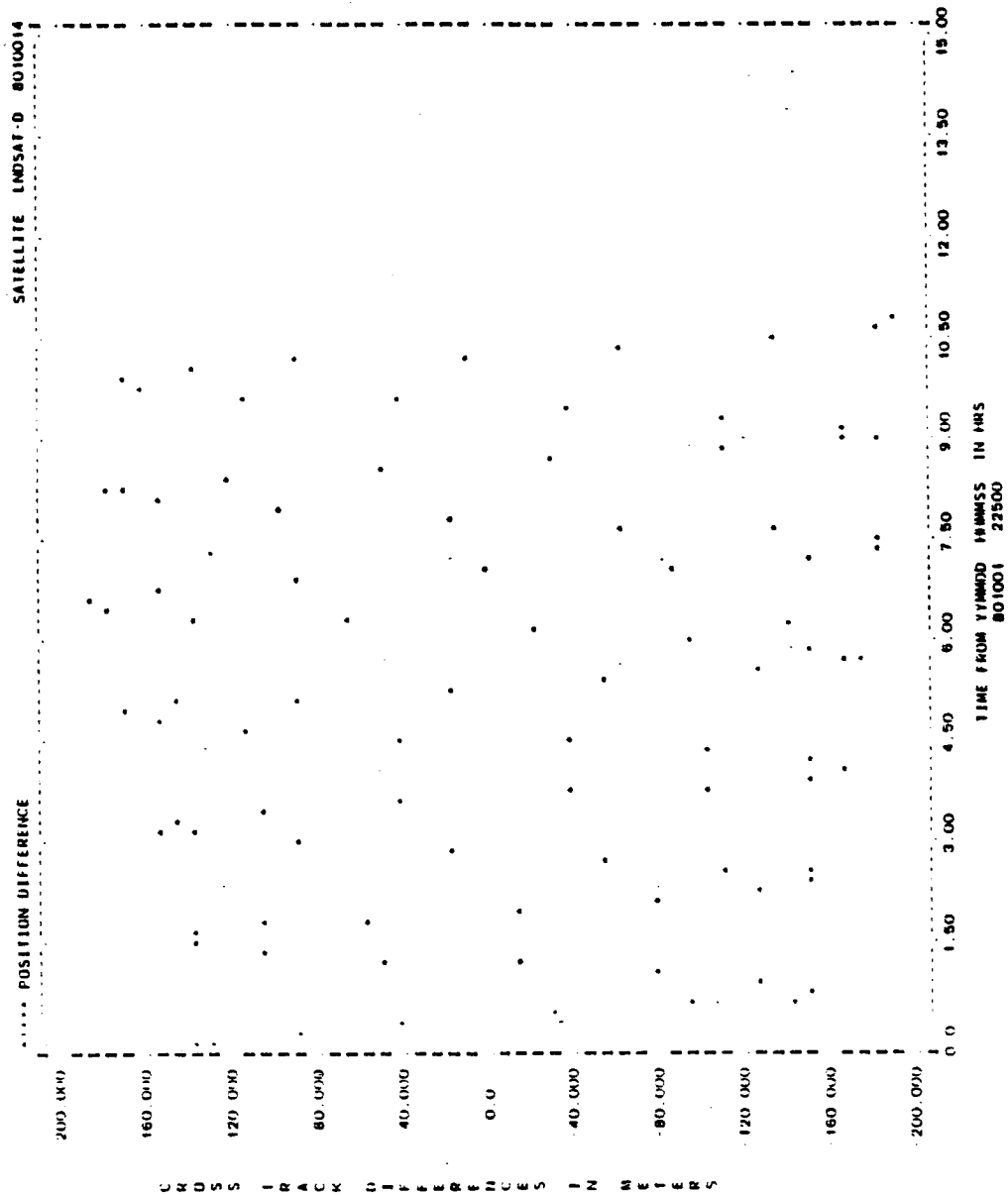


Figure A-14. Cross-Track Differences for Run L15 (1 of 2)

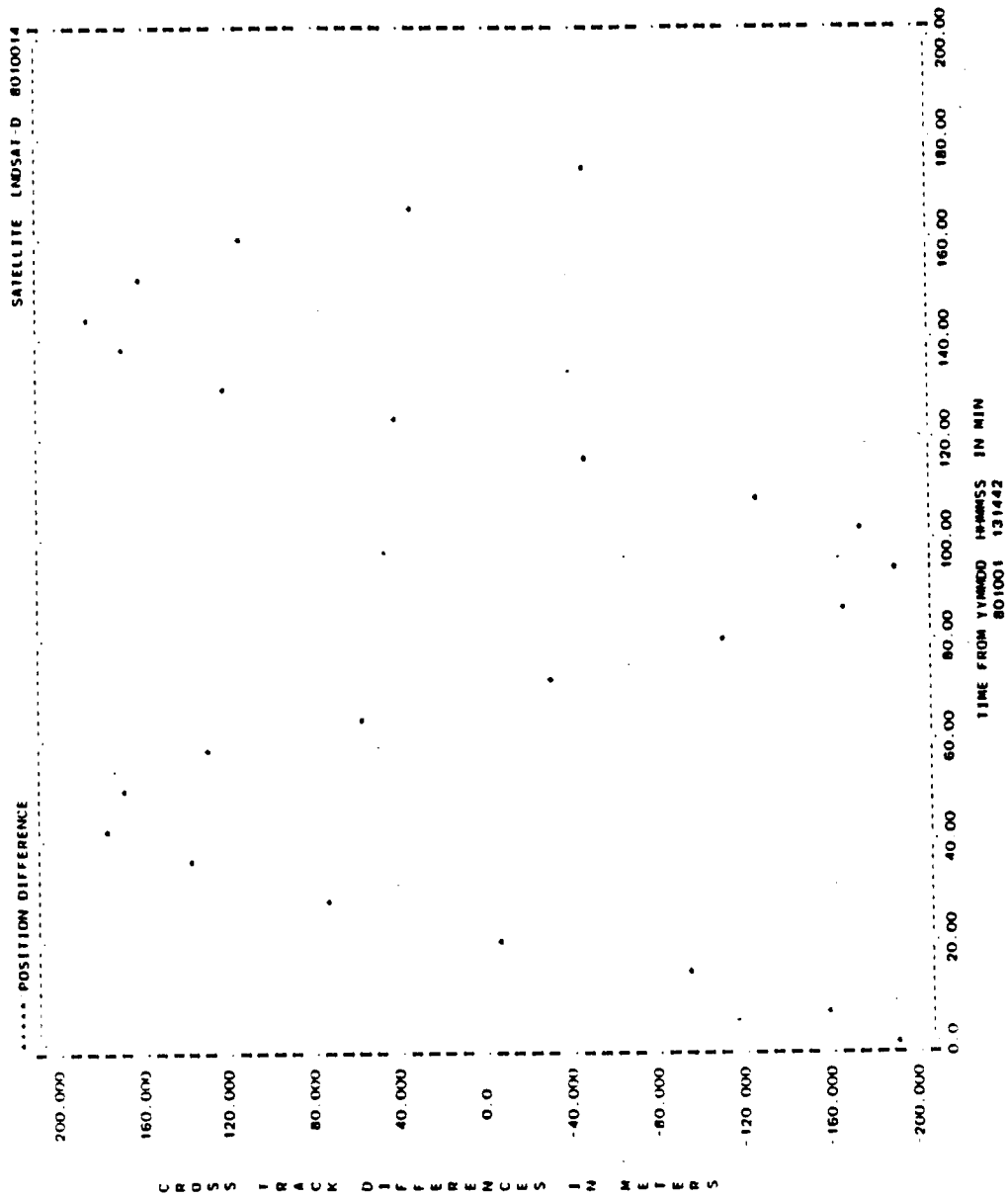


Figure A-14. Cross-Track Differences for Run L15 (2 of 2)

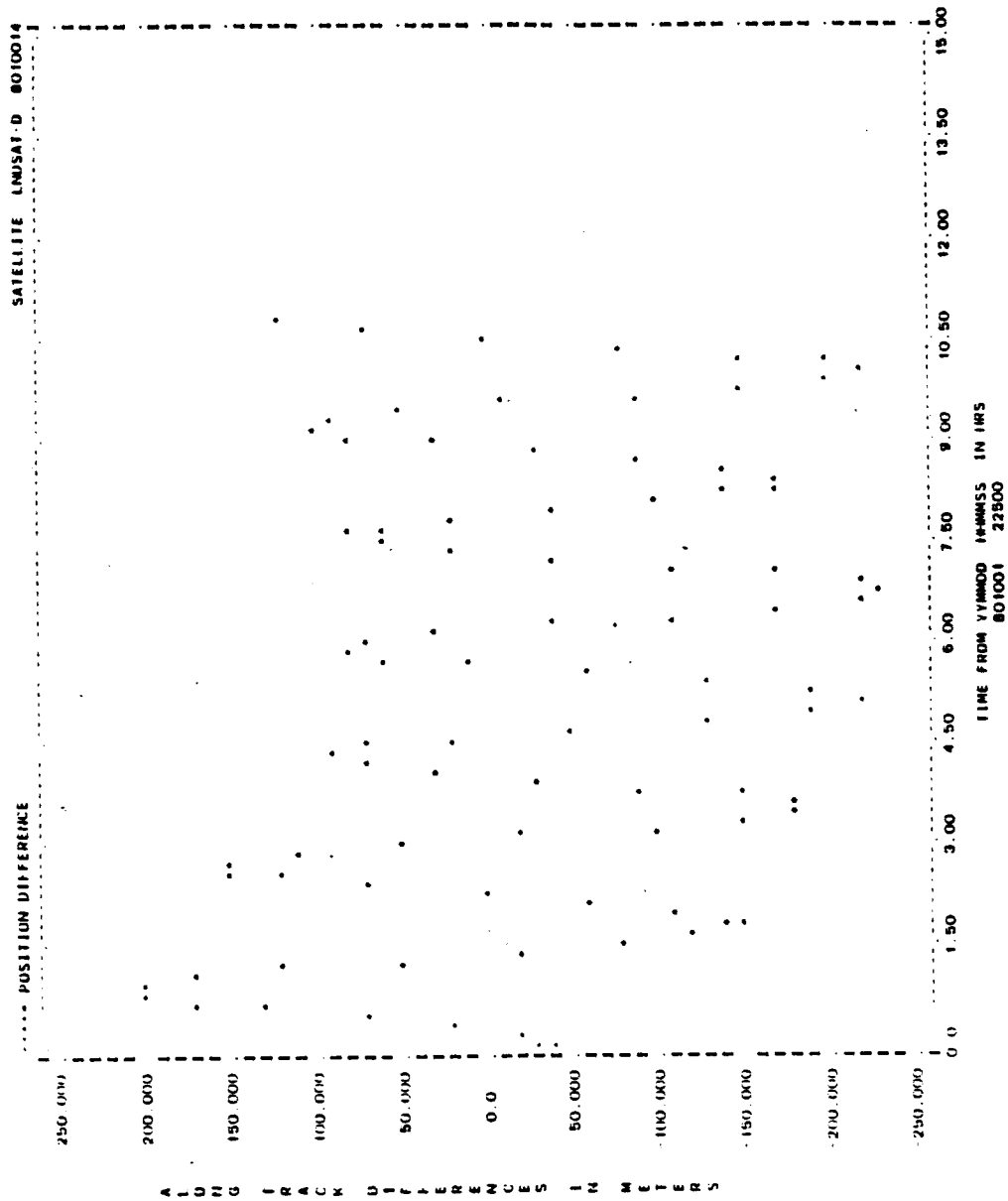


Figure A-15. Along-Track Differences for Run L15 (1 of 2)

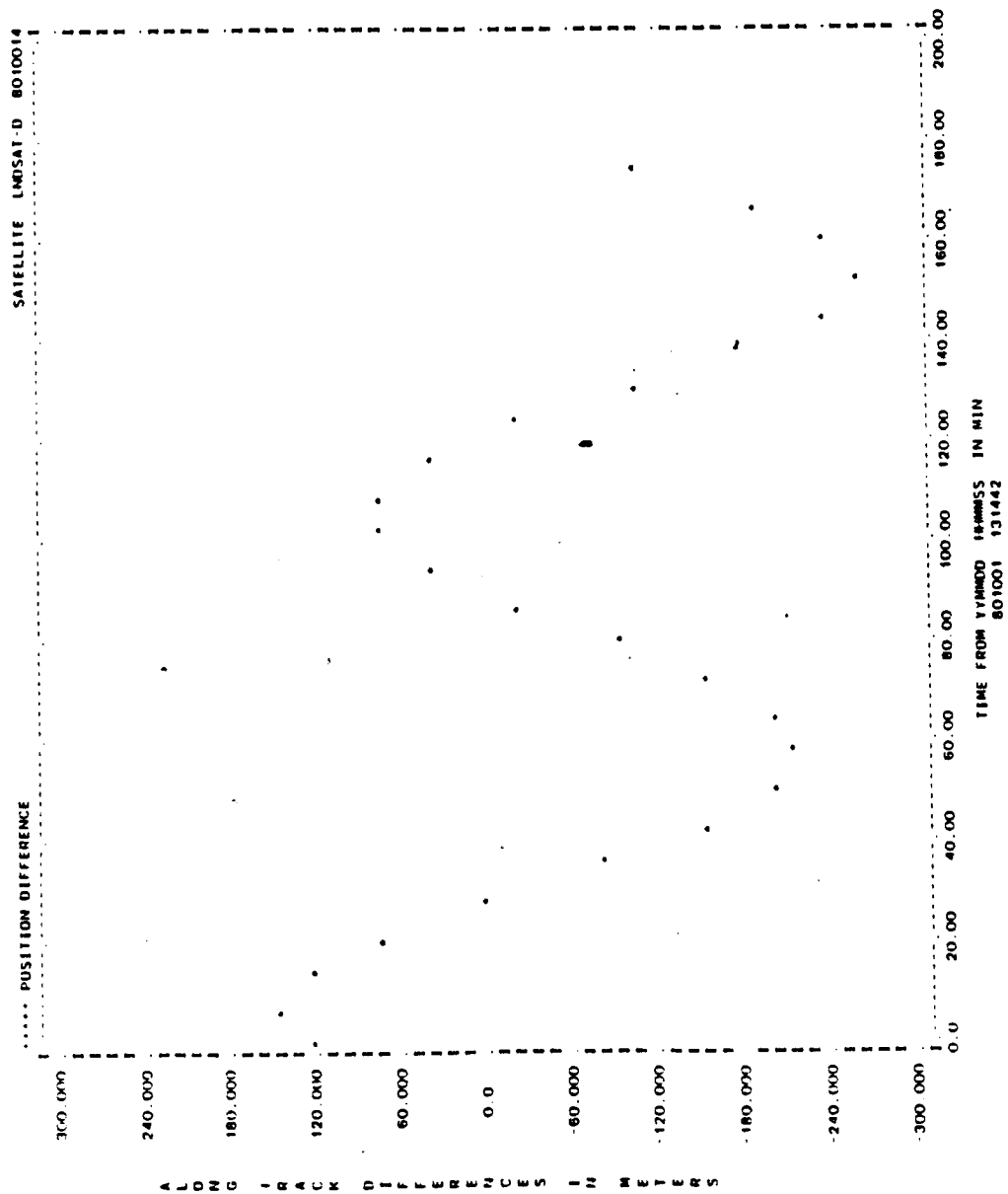


Figure A-15. Along-Track Differences for Run L15 (2 of 2)

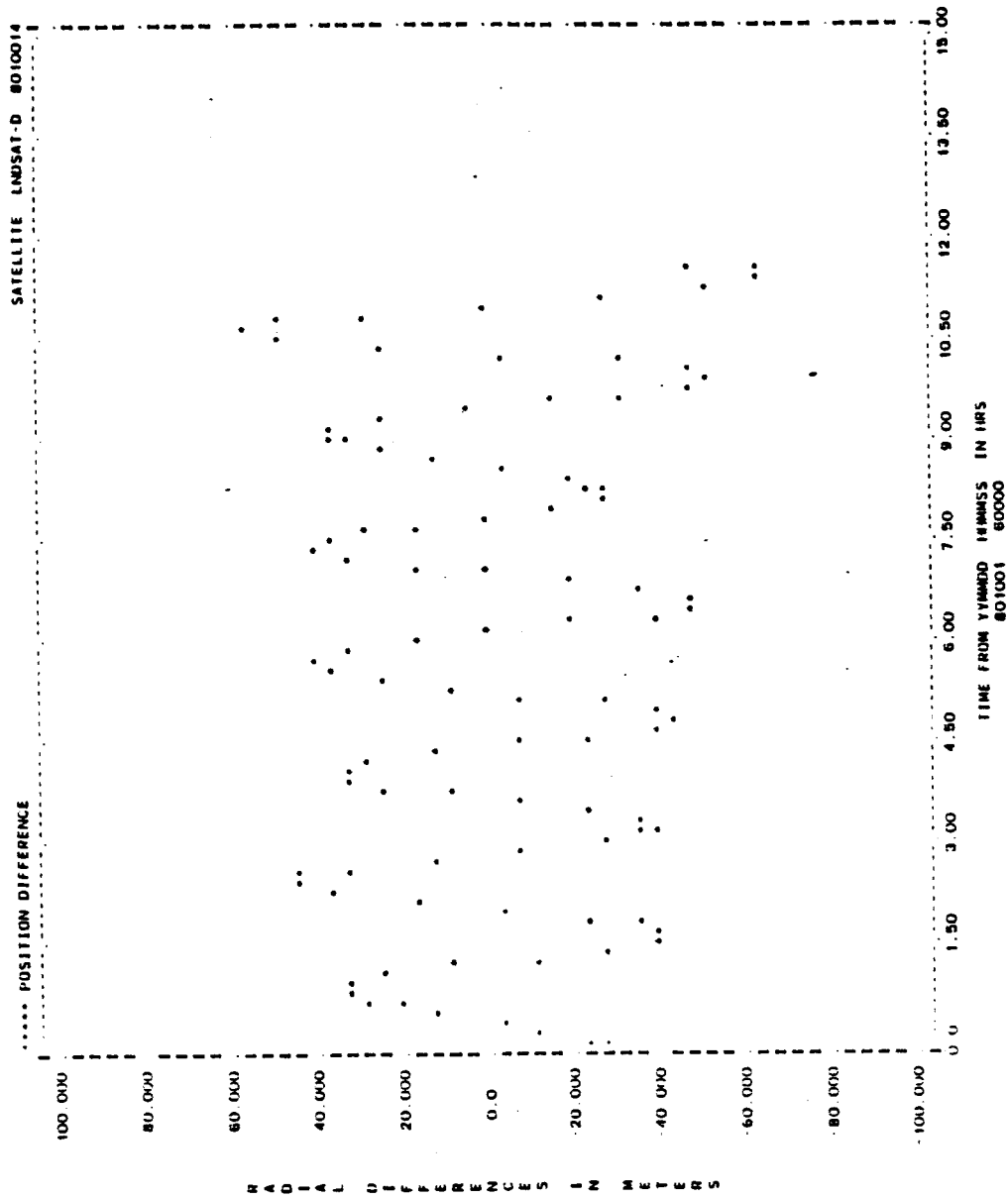


Figure A-16. Radial Differences for Run L15 (1 of 2)

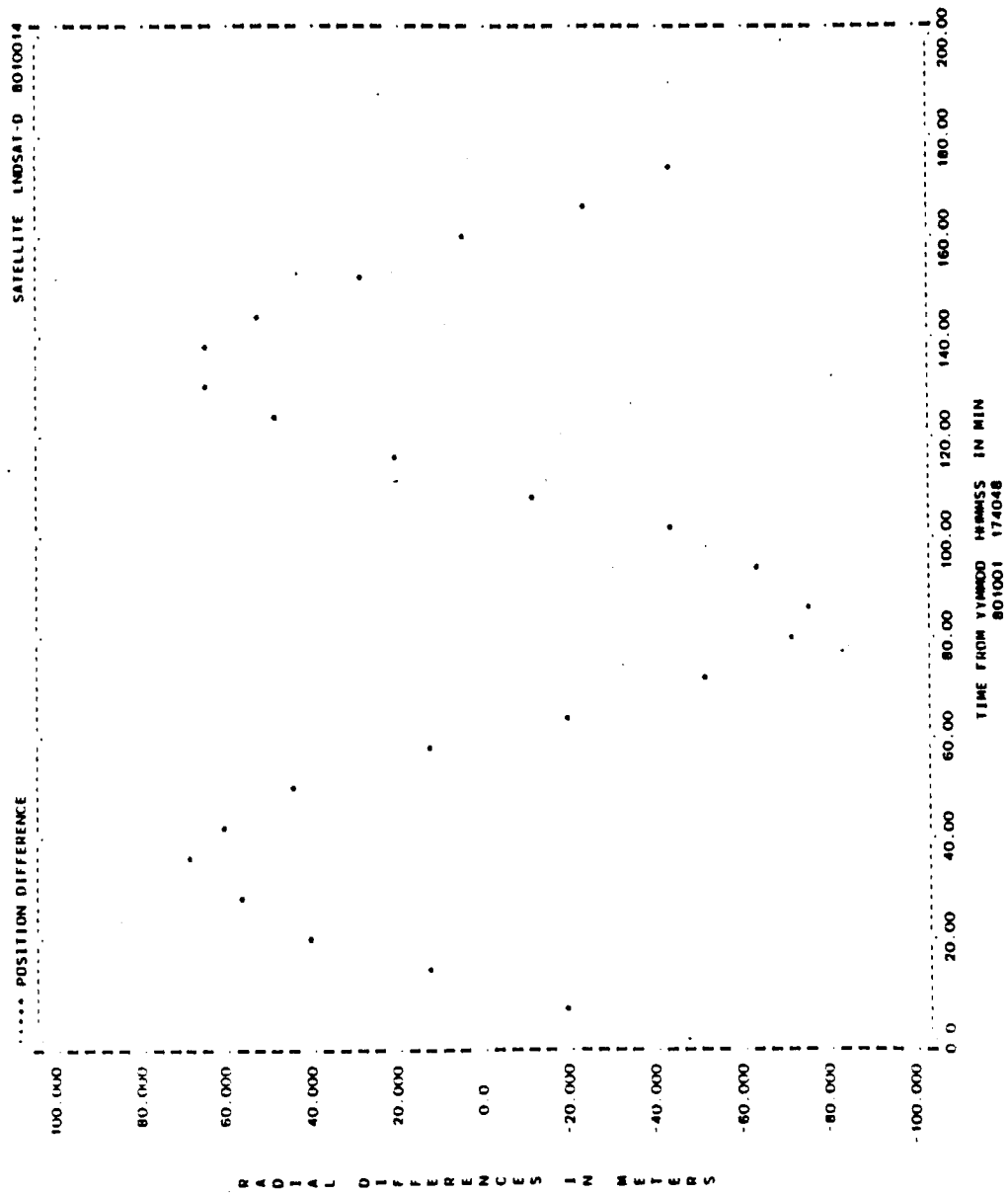


Figure A-16. Radial Differences for Run L15 (2 of 2)

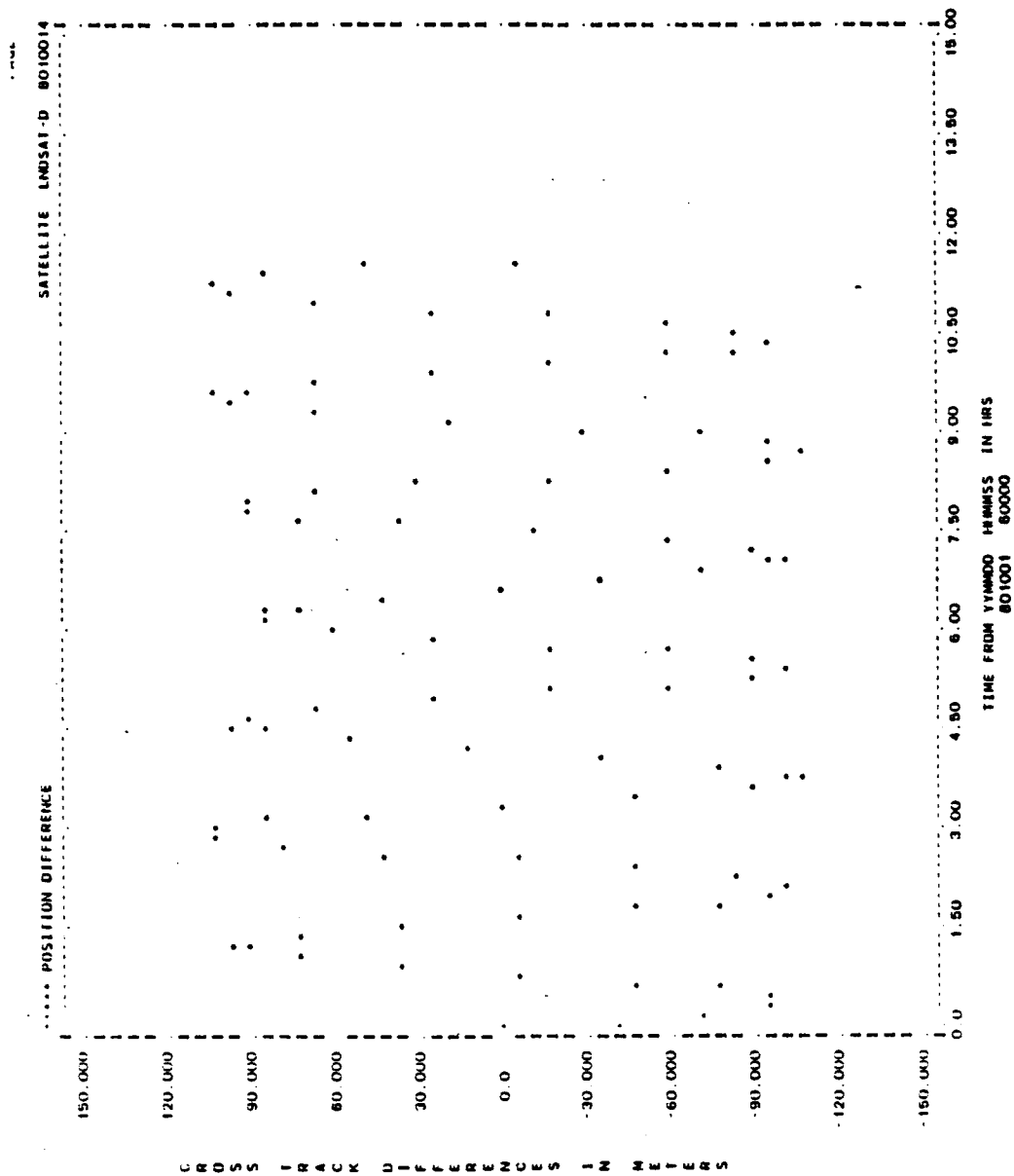


Figure A-17. Cross-Track Differences for Run L15 (1 of 2)

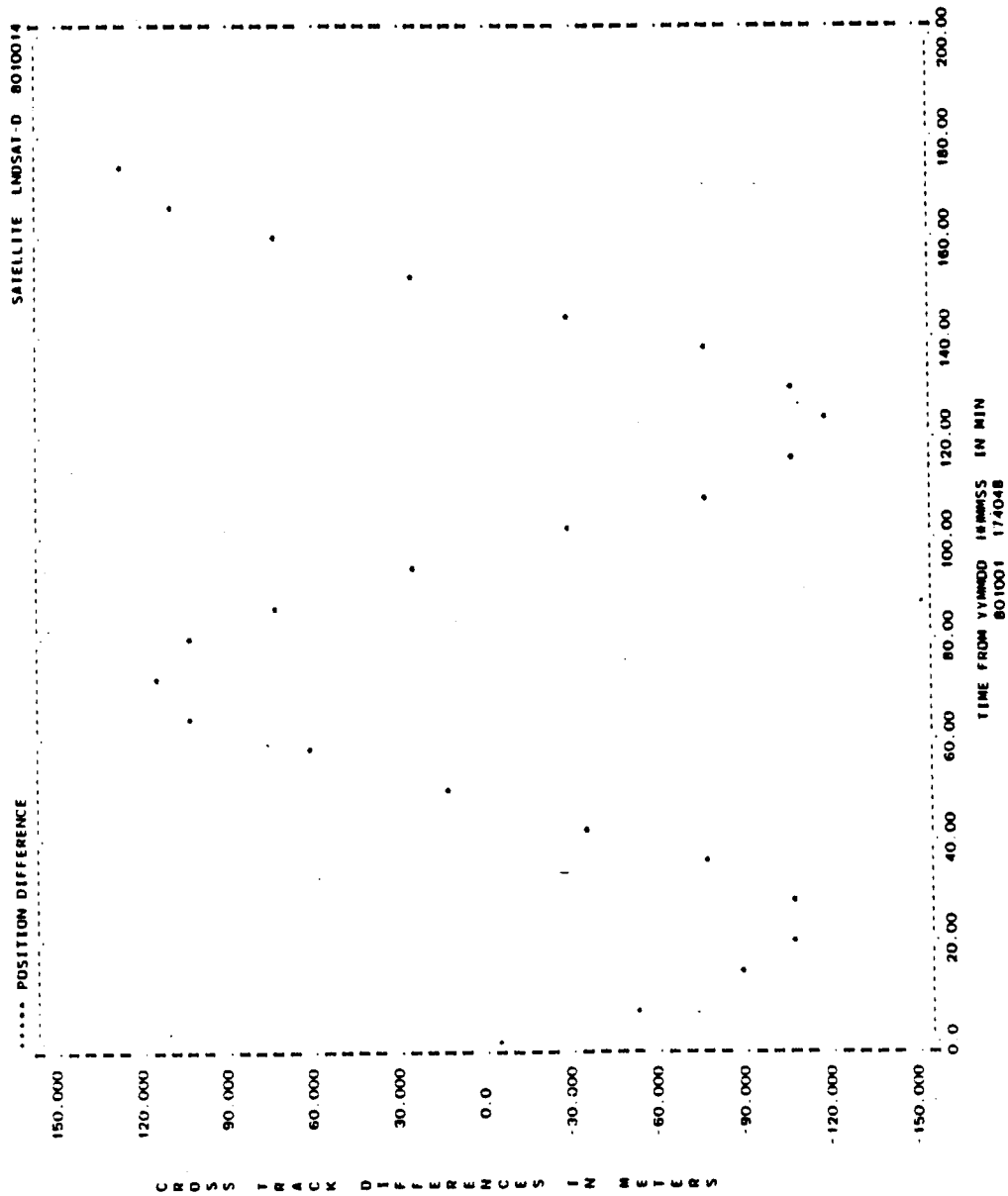


Figure A-17. Cross-Track Differences for Run L15 (2 of 2)

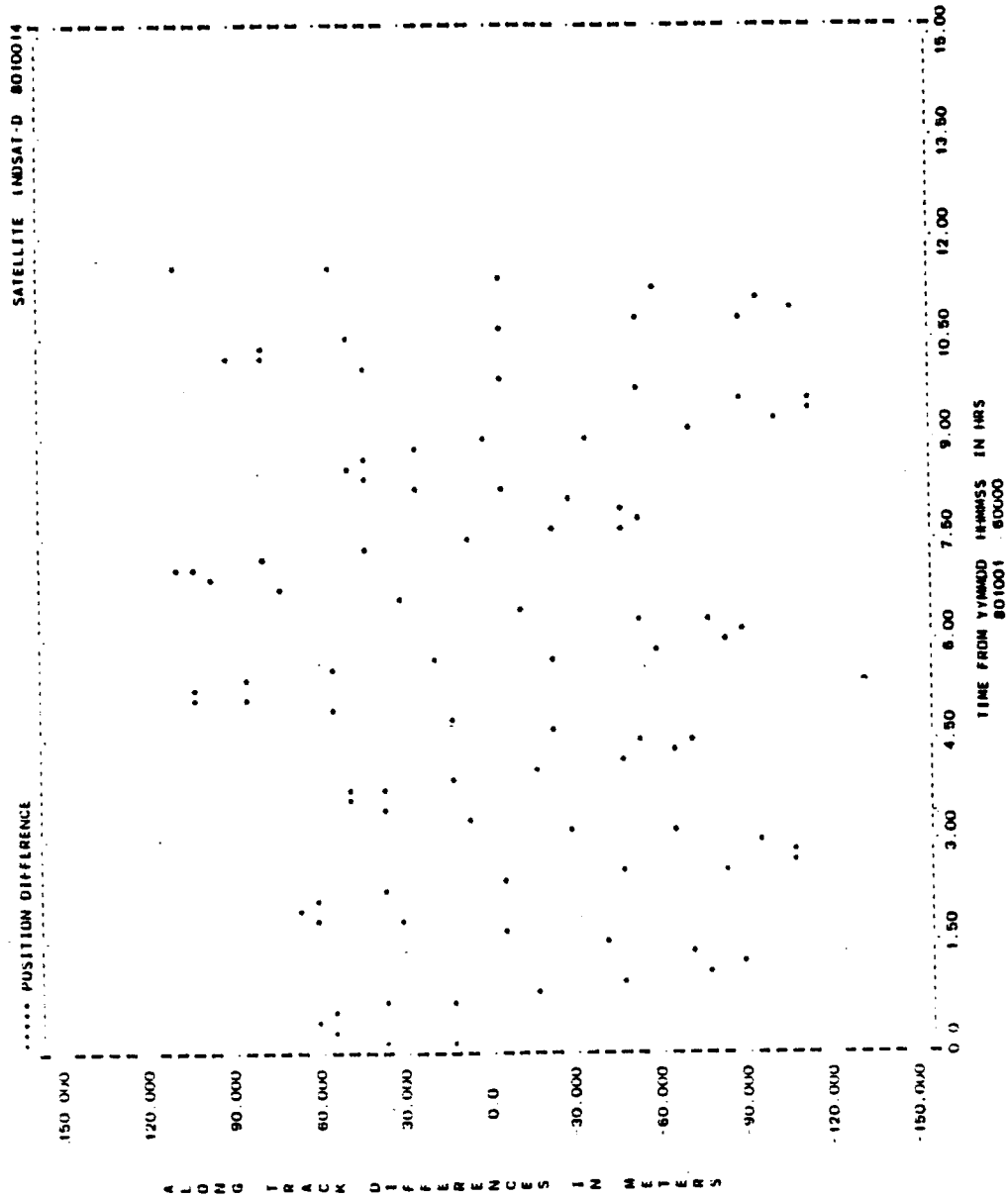


Figure A-18. Along-Track Differences for Run L15 (1 of 2)

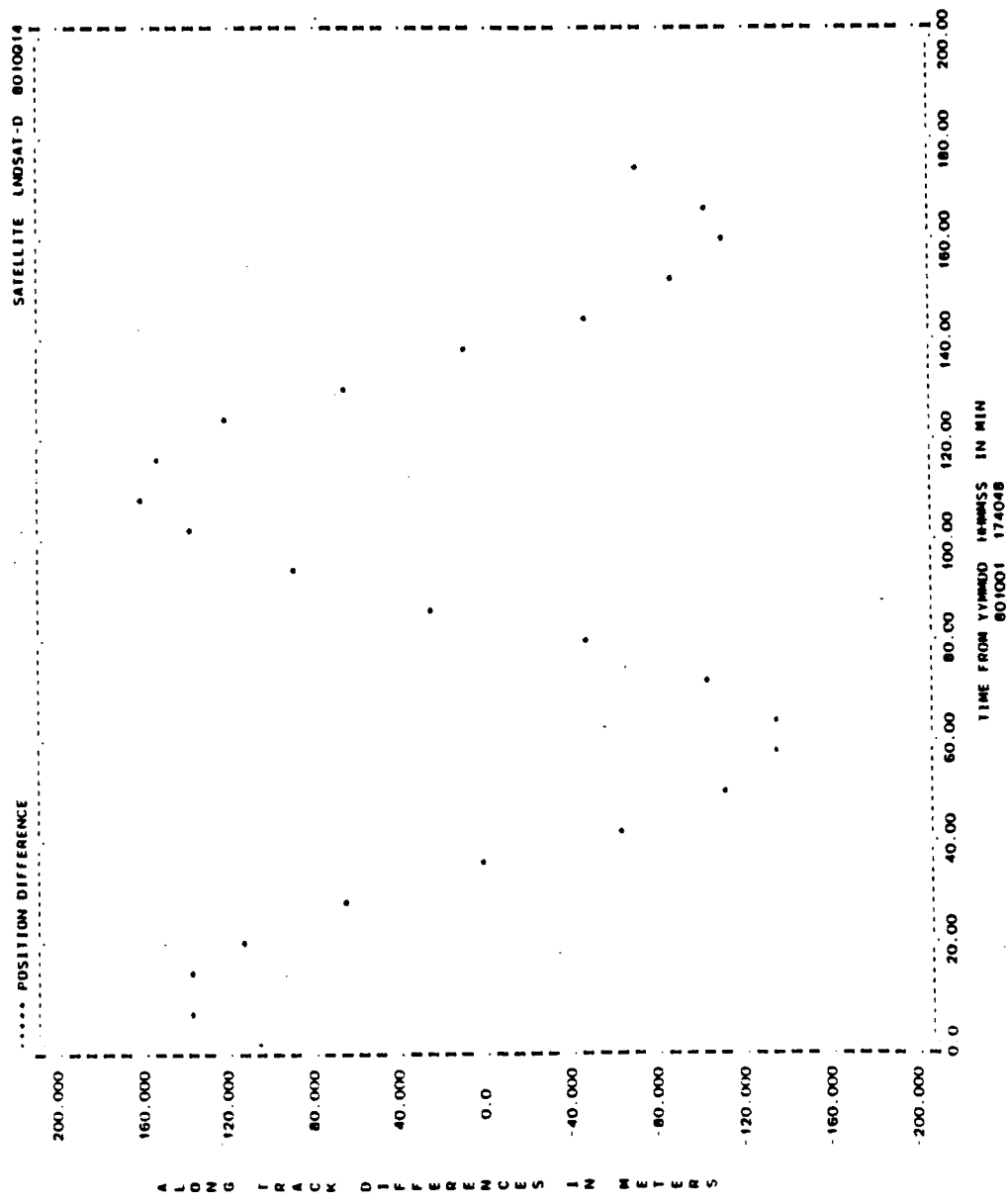


Figure A-18. Along-Track Differences for Run L15 (2 of 2)

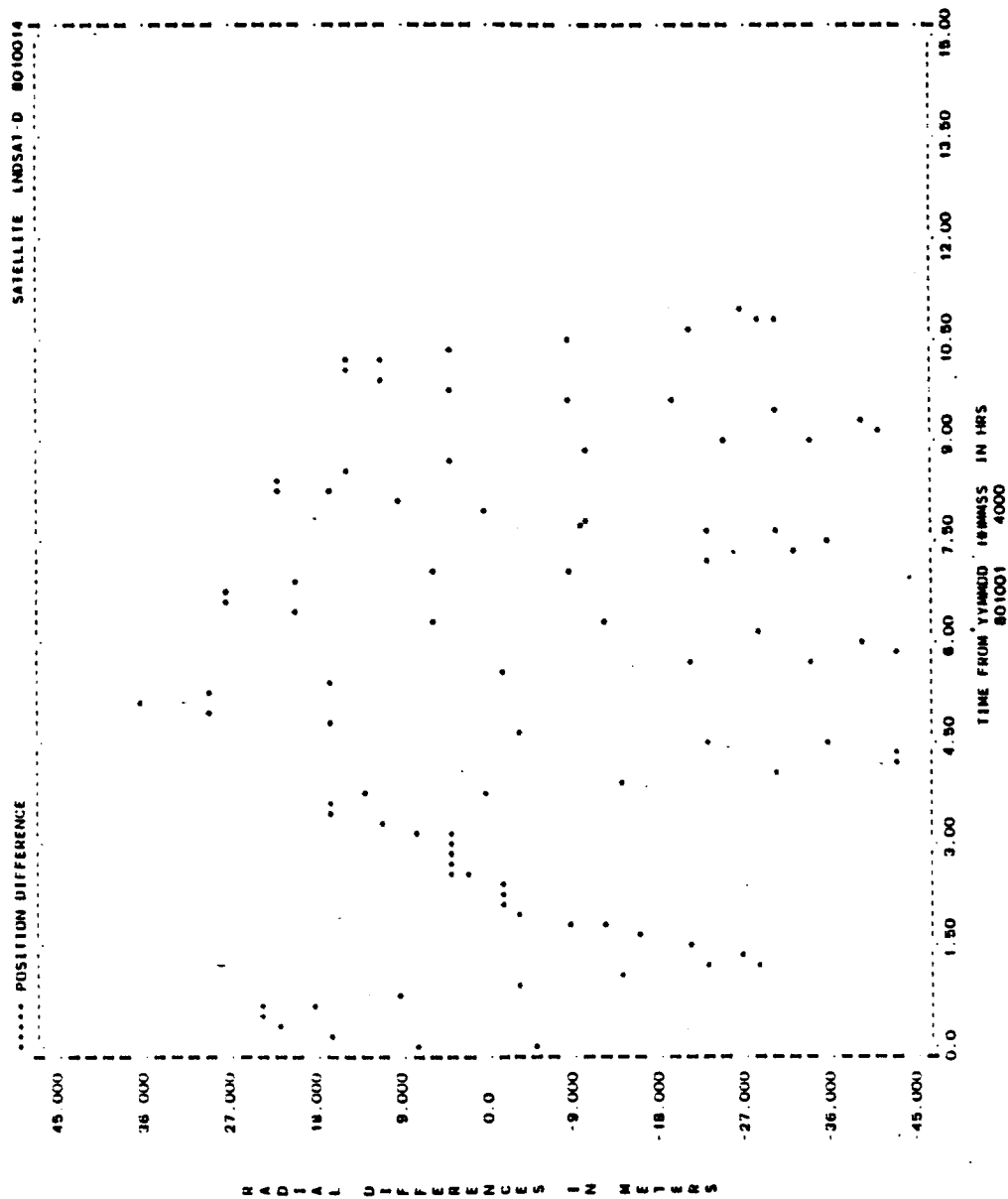


Figure A-19. Radial Differences for Run L11 (1 of 2)

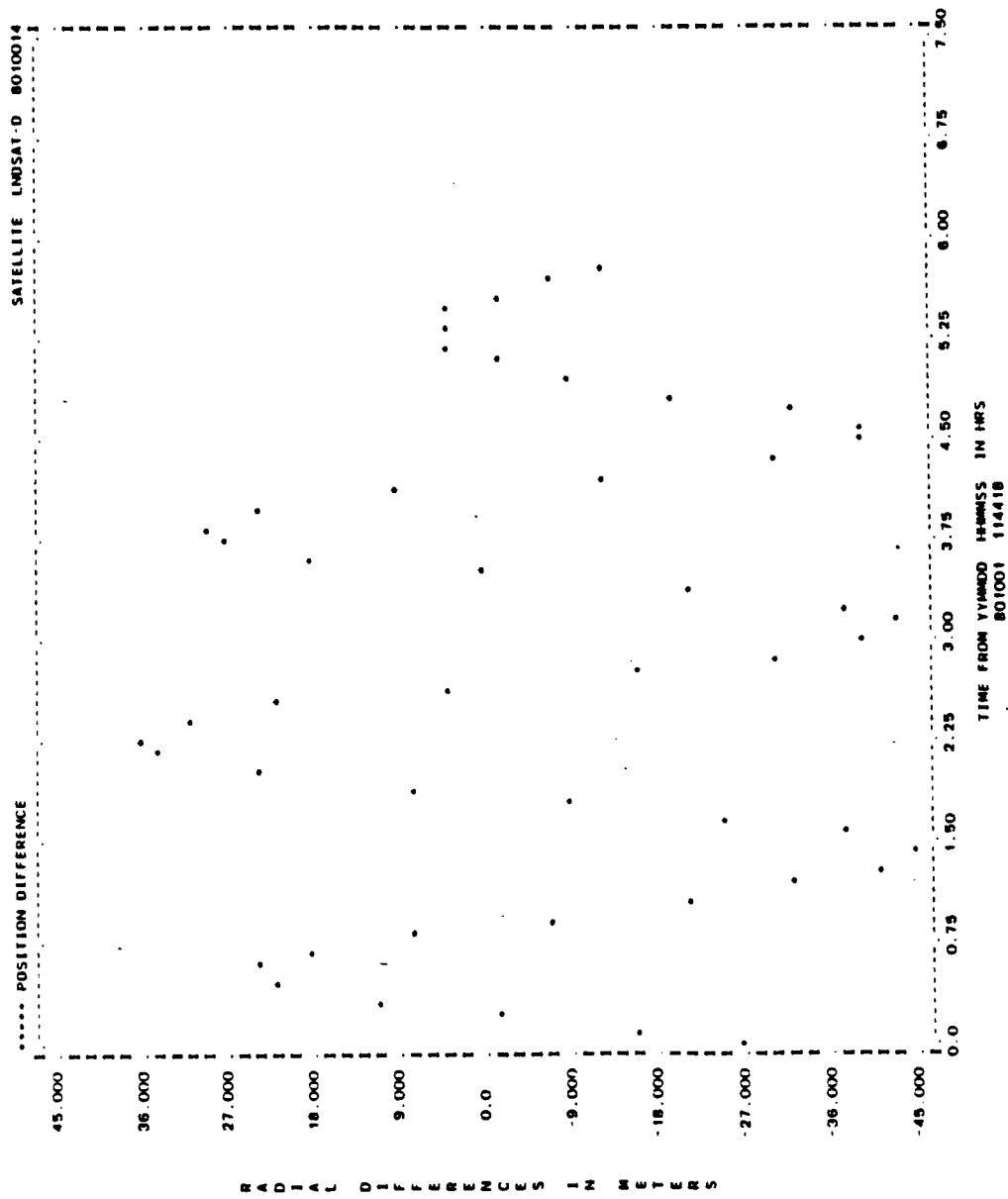


Figure A-19. Radial Differences for Run I.11 (2 of 2)

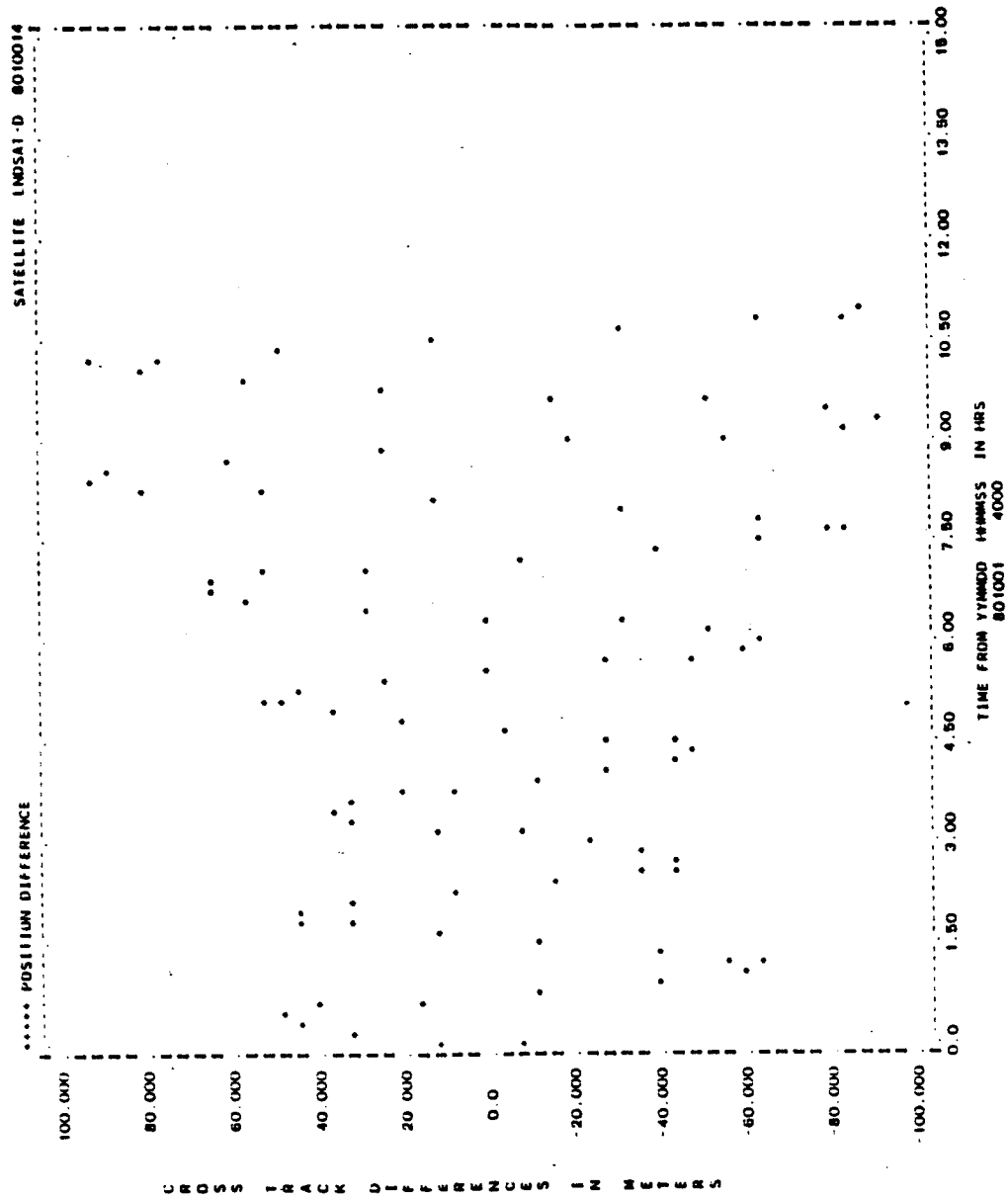


Figure A-20. Cross-Track Differences for Run L11 (1 of 2)

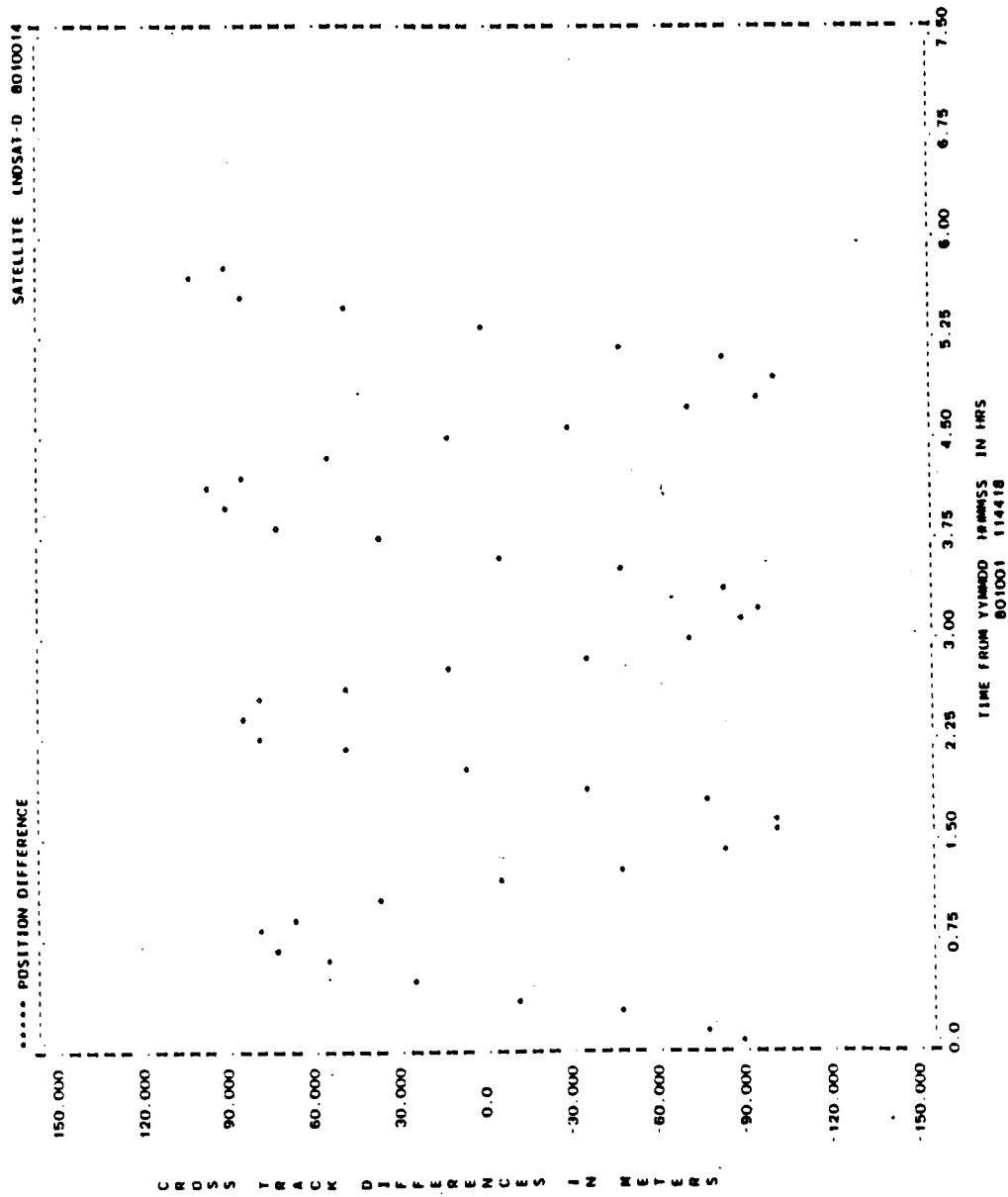


Figure A-20. Cross-Track Differences for Run L11 (2 of 2)

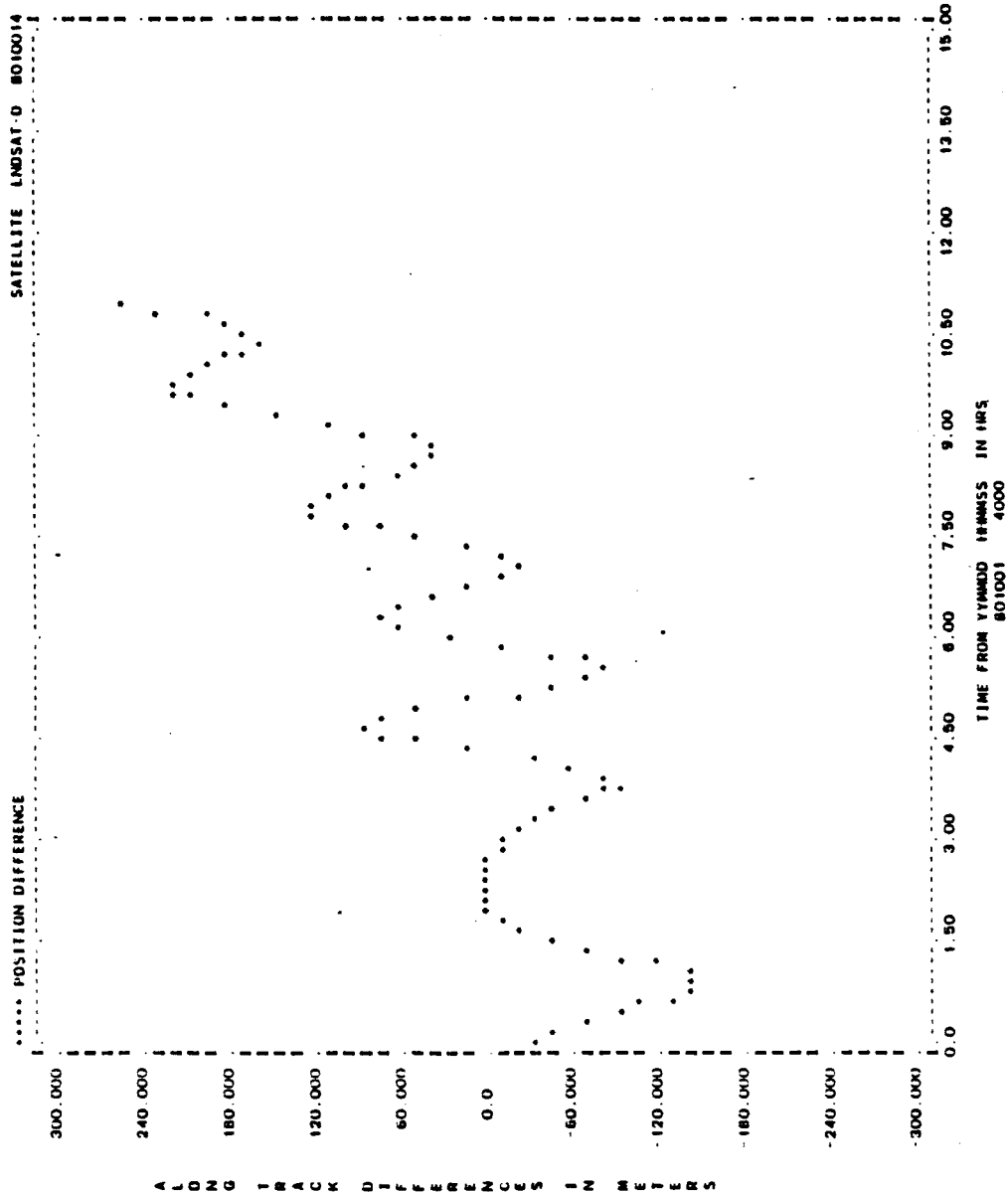


Figure A-21. Along-Track Differences for Run L11 (1 of 2)

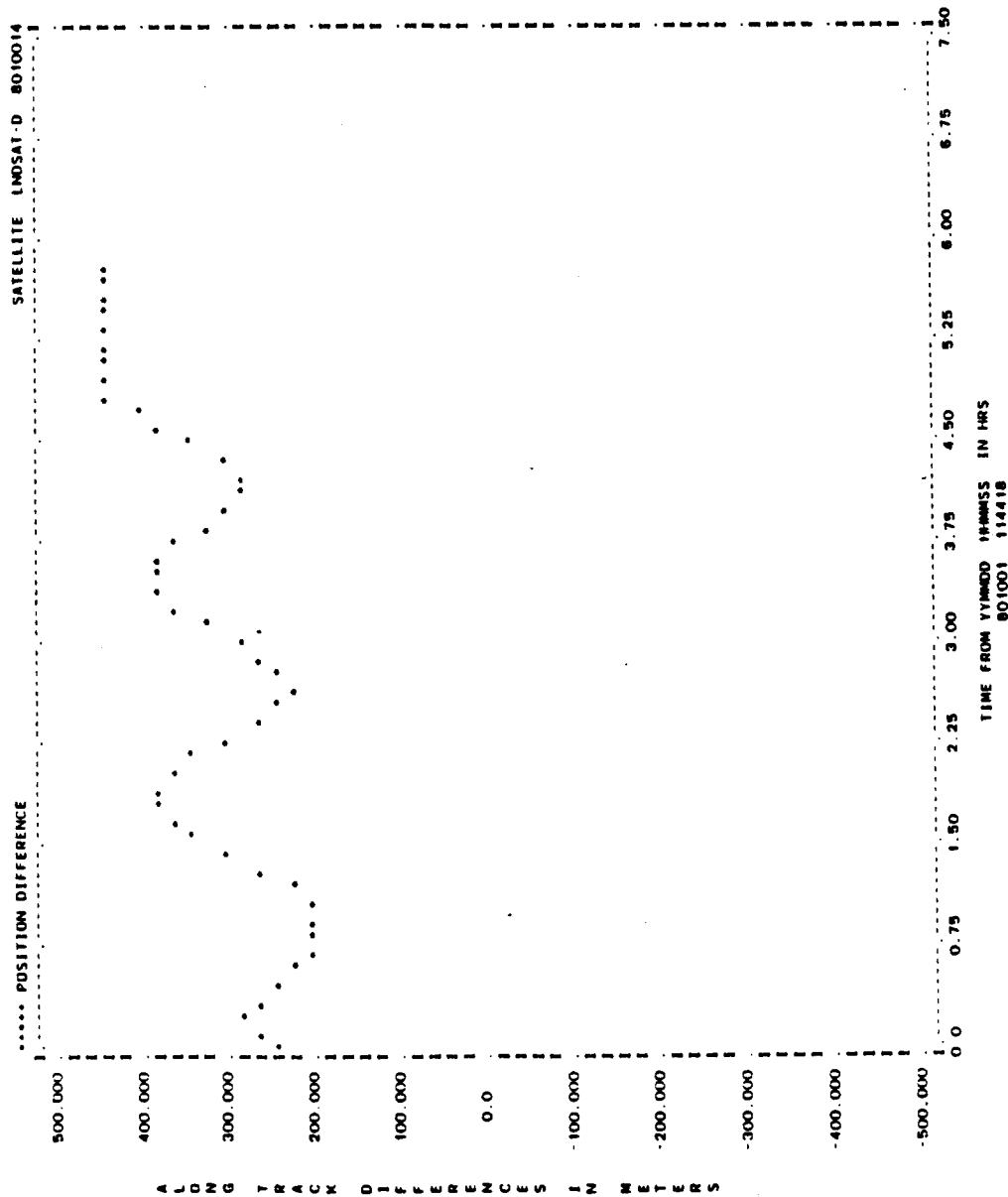


Figure A-21. Along-Track Differences for Run L11 (2 of 2)

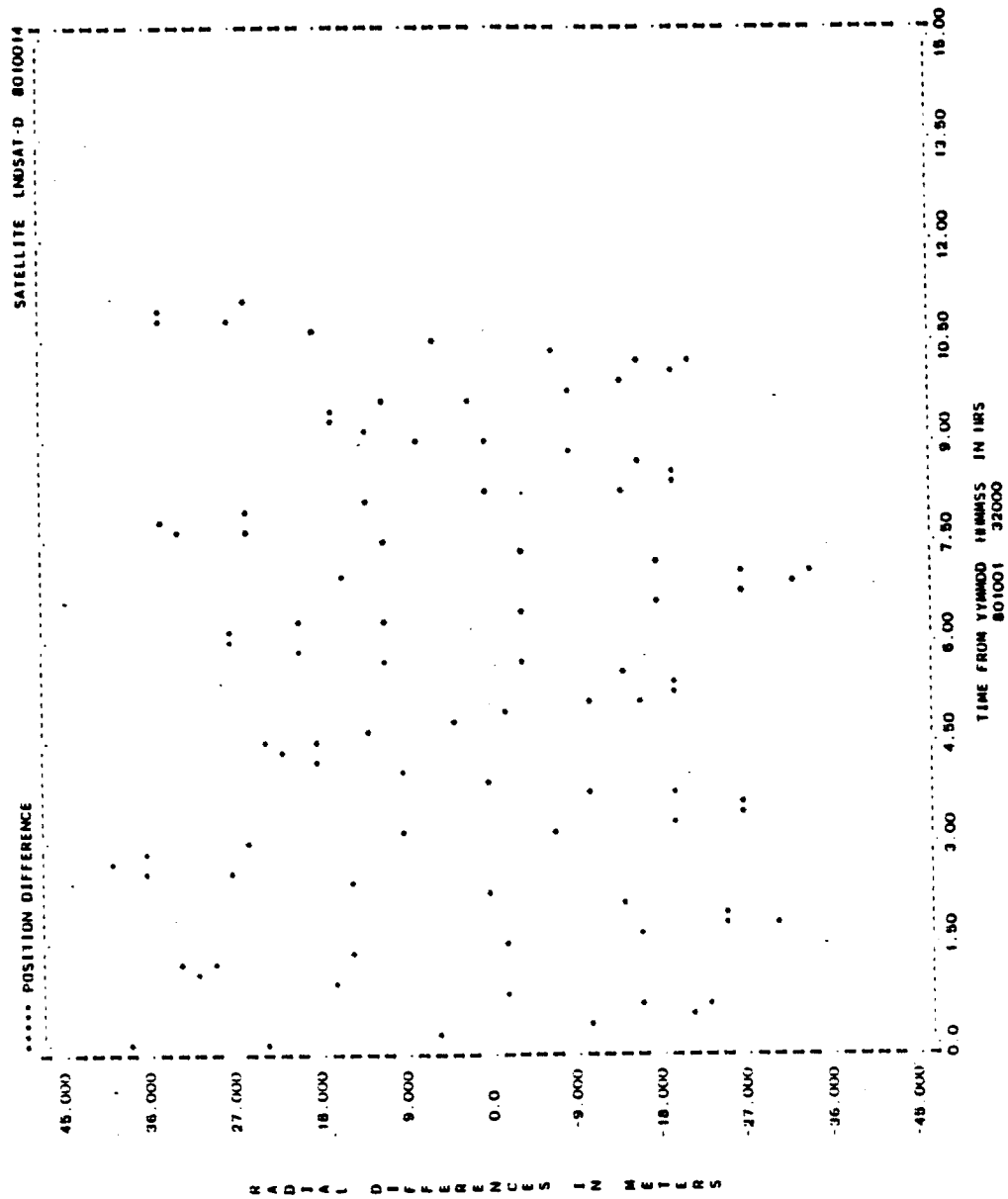


Figure 'A-22. Radial Differences for Run L13 (1 of 2)



TIME FROM VMMDD 140001 143136 IN HRS

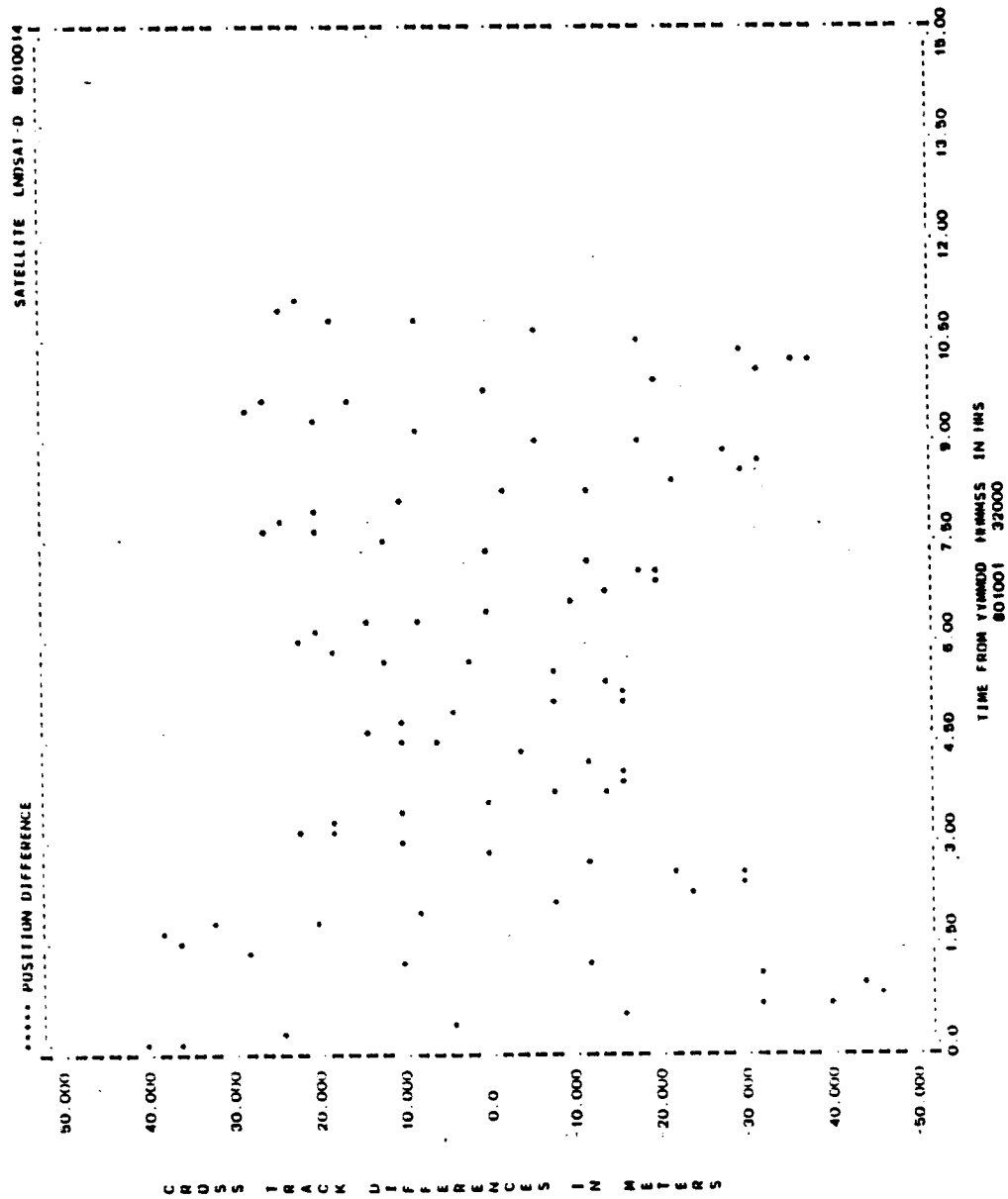


Figure A-23. Cross-Track Differences for Run L13 (1 of 2)

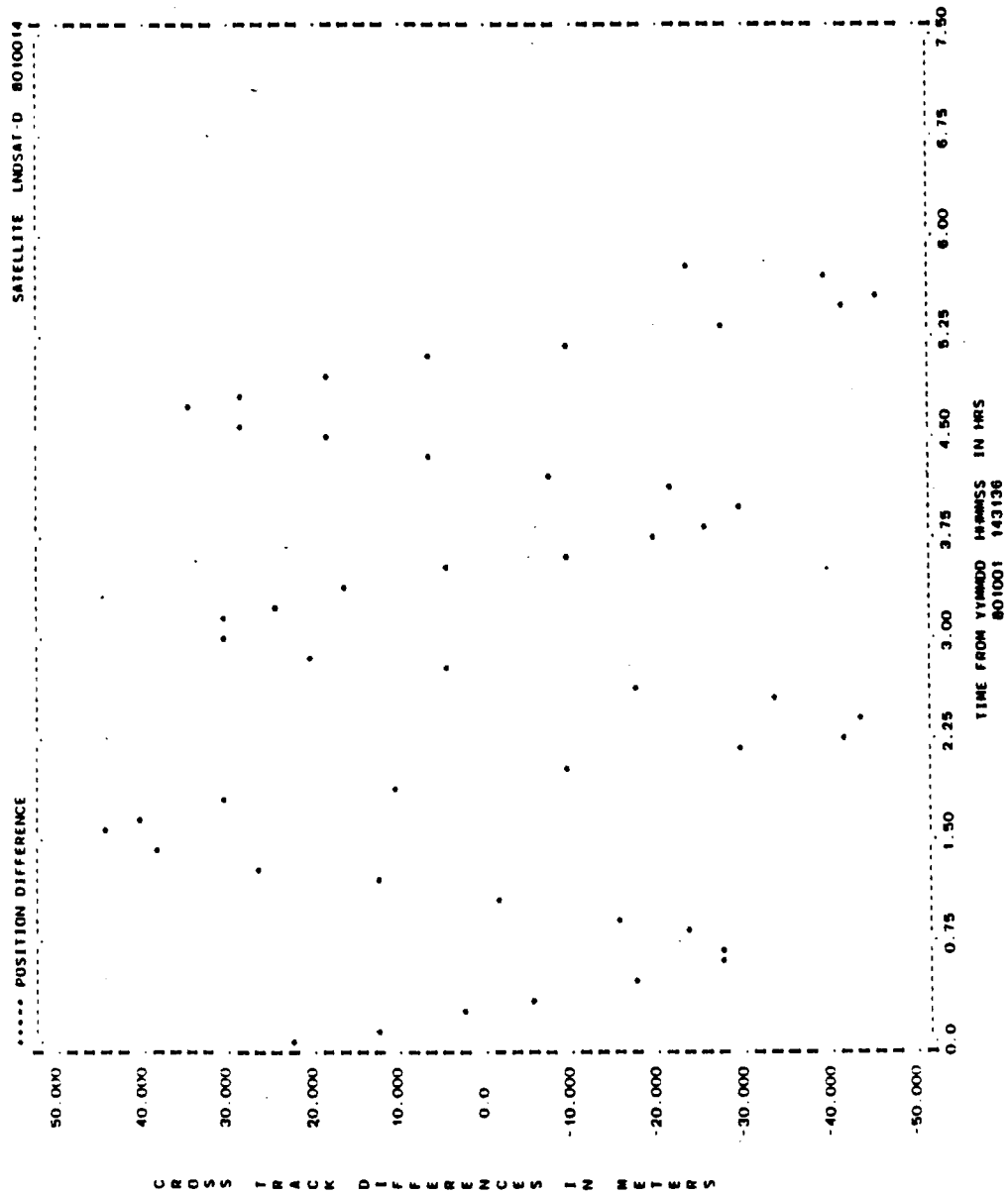


Figure A-23. Cross-Track Differences for Run L13 (2 of 2)

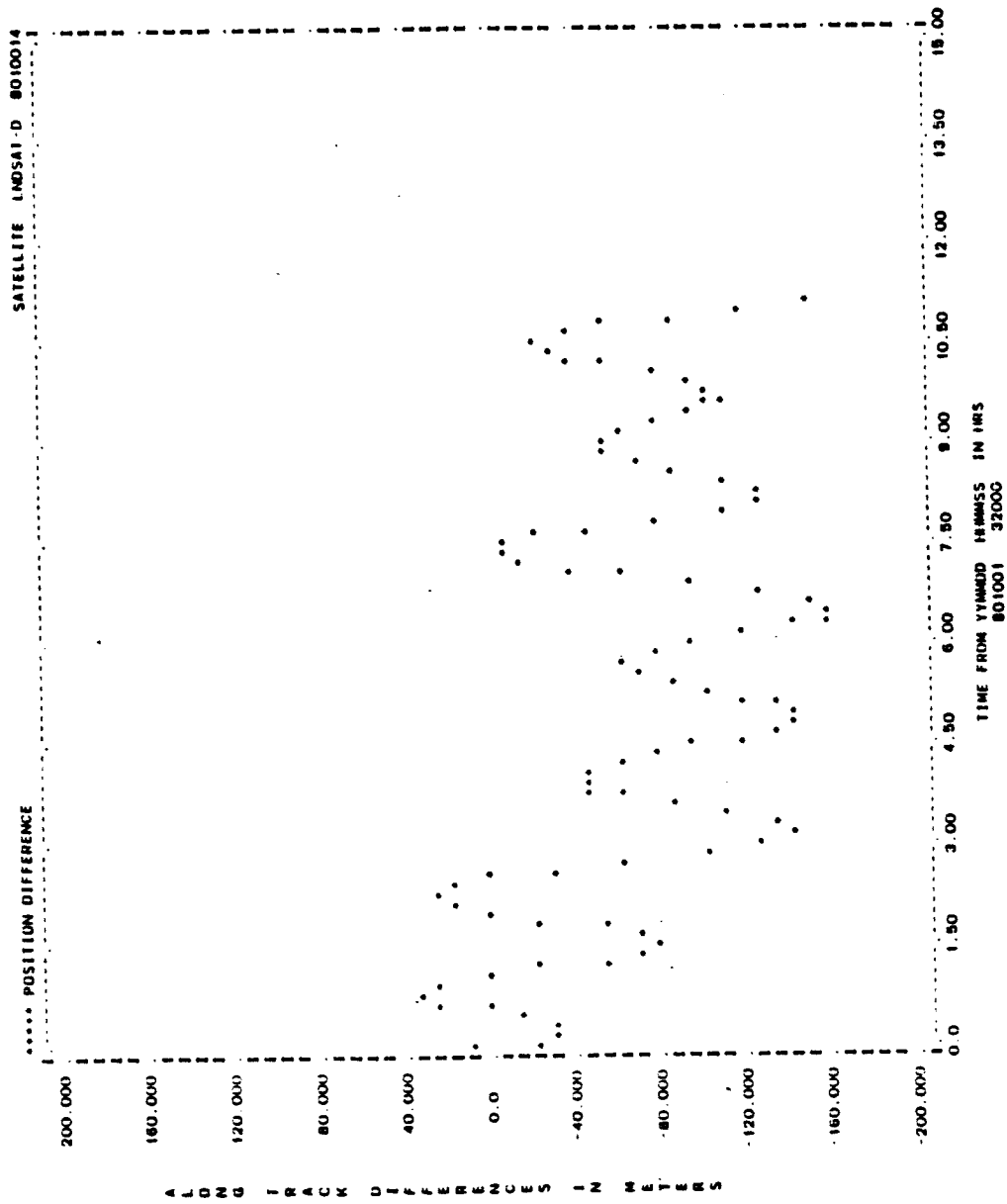


Figure A-24. Along-Track Differences for Run L13 (1 of 2)

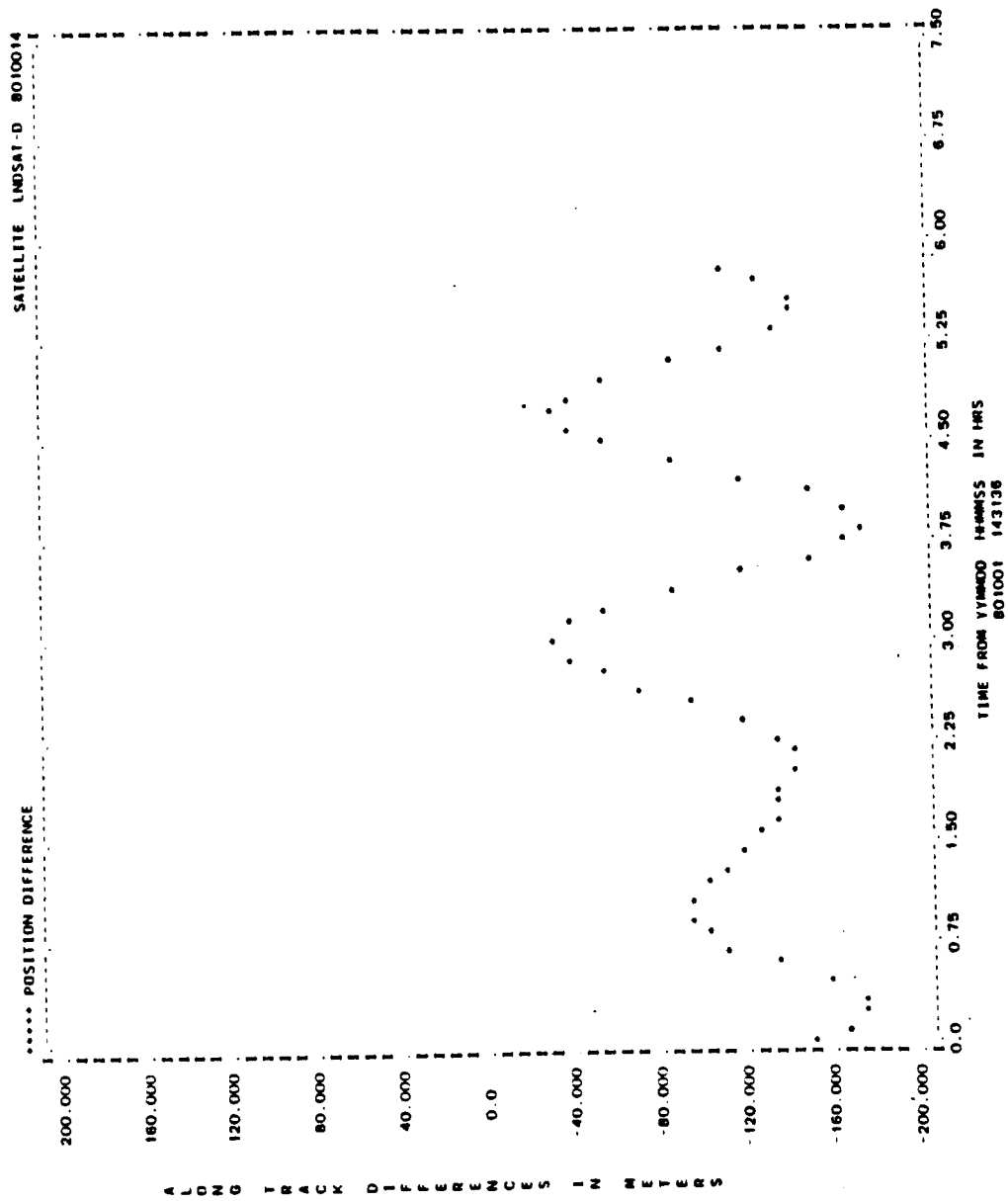


Figure A-24. Along-Track Differences for Run L13 (2 of 2)

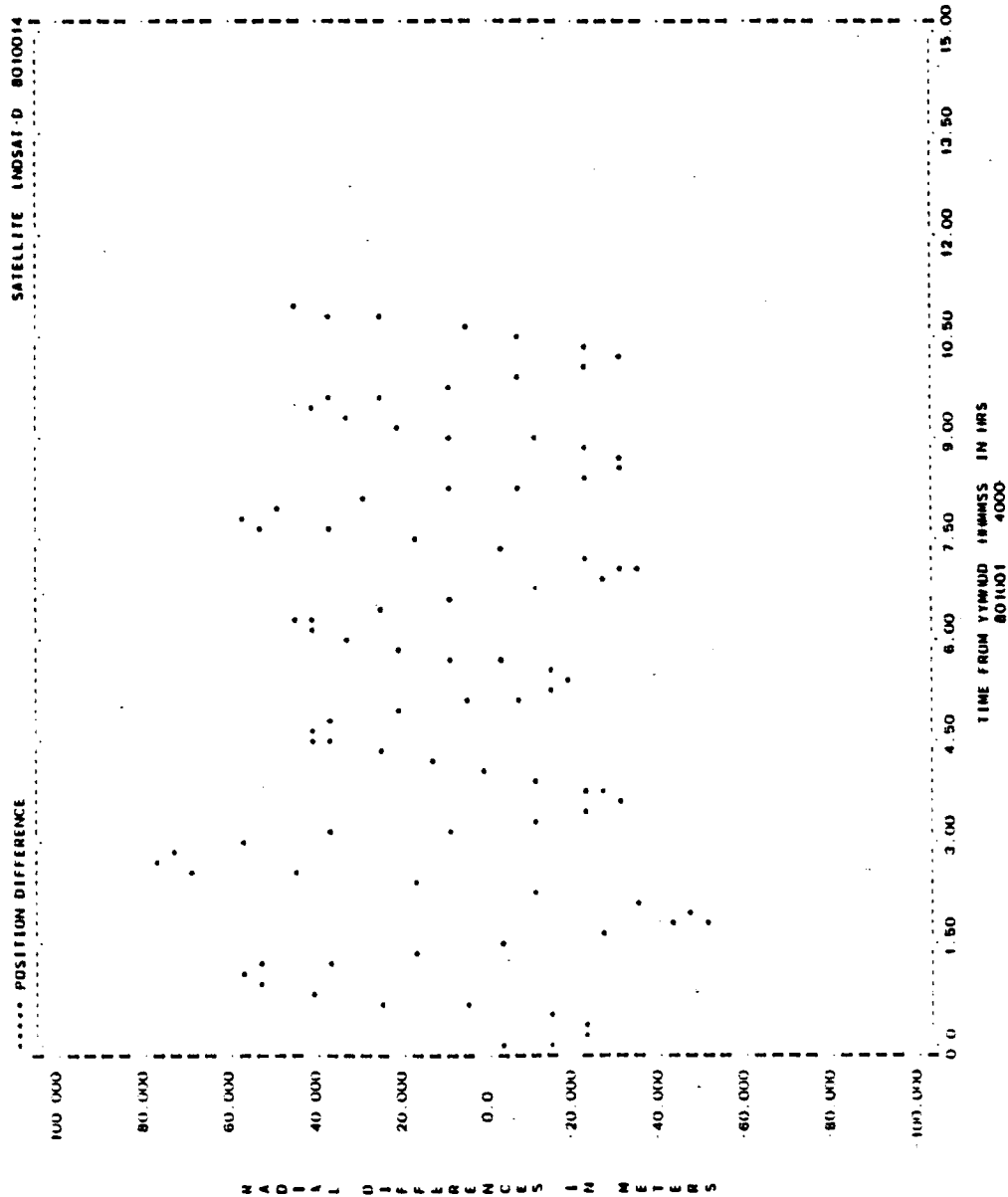


Figure A-25. Radial Differences for Run L23 (1 of 2)

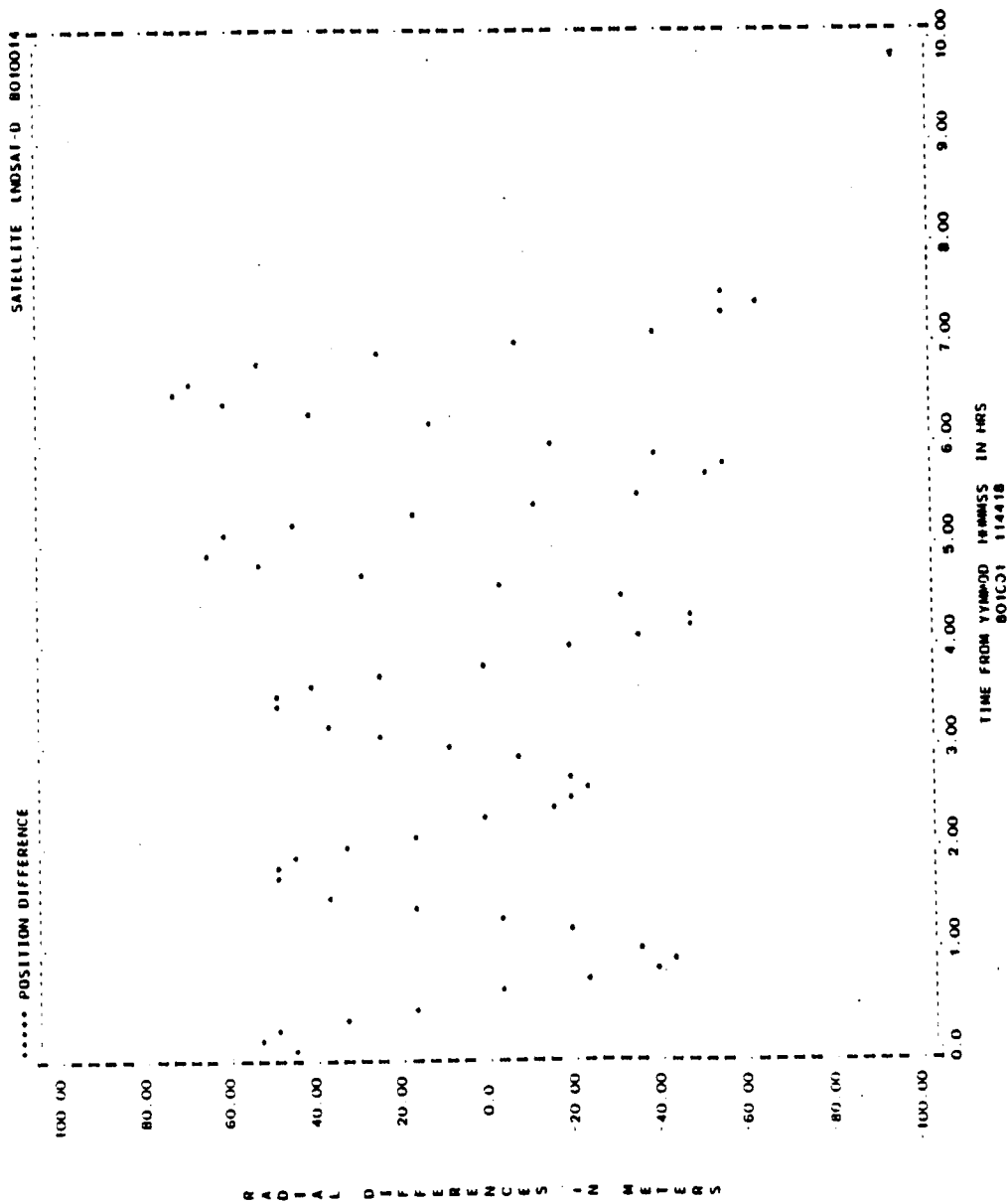


Figure A-25. Radial Differences for Run L23 (2 of 2)

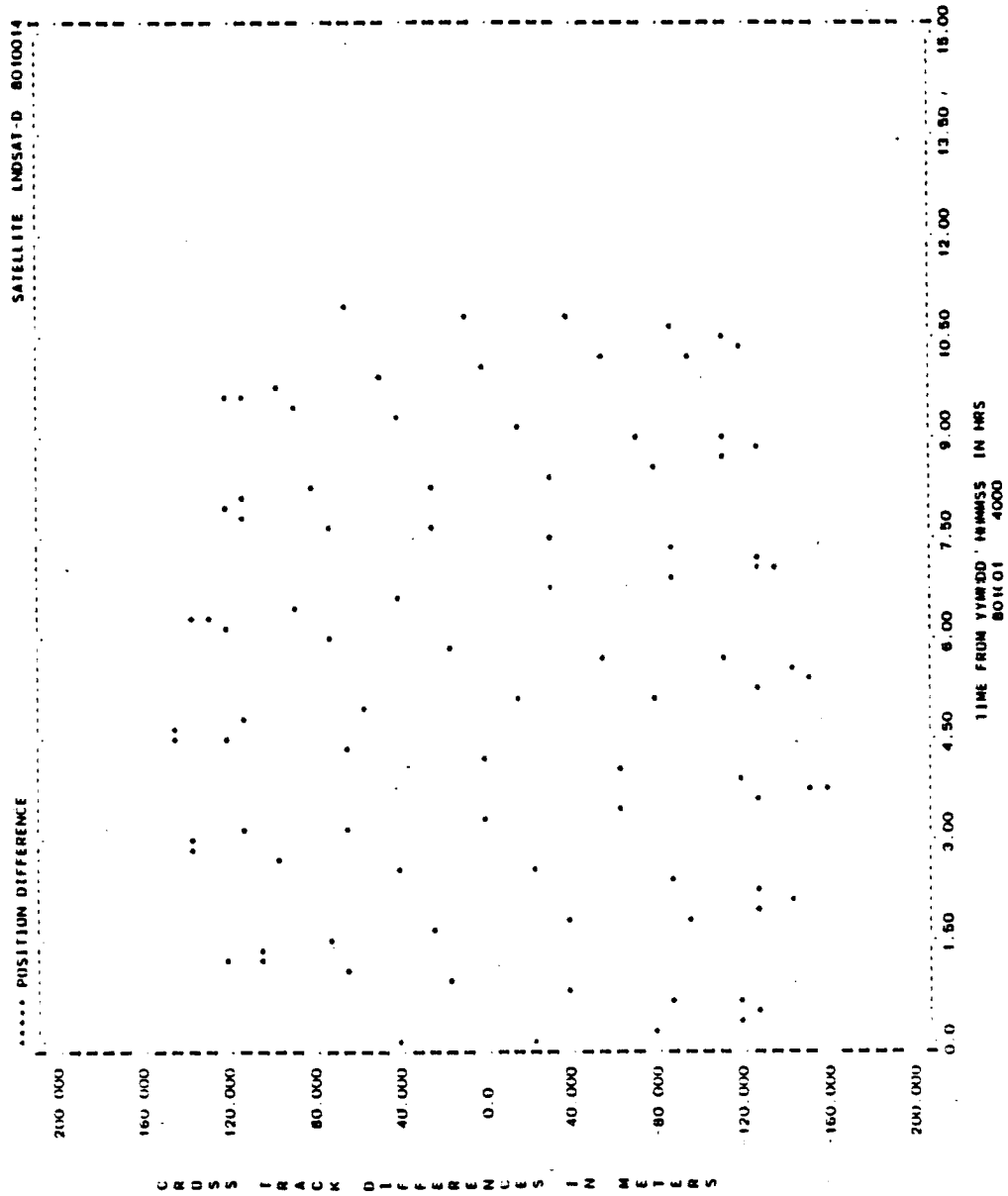


Figure A-26. Cross-Track Differences for Run L23 (1 of 2)

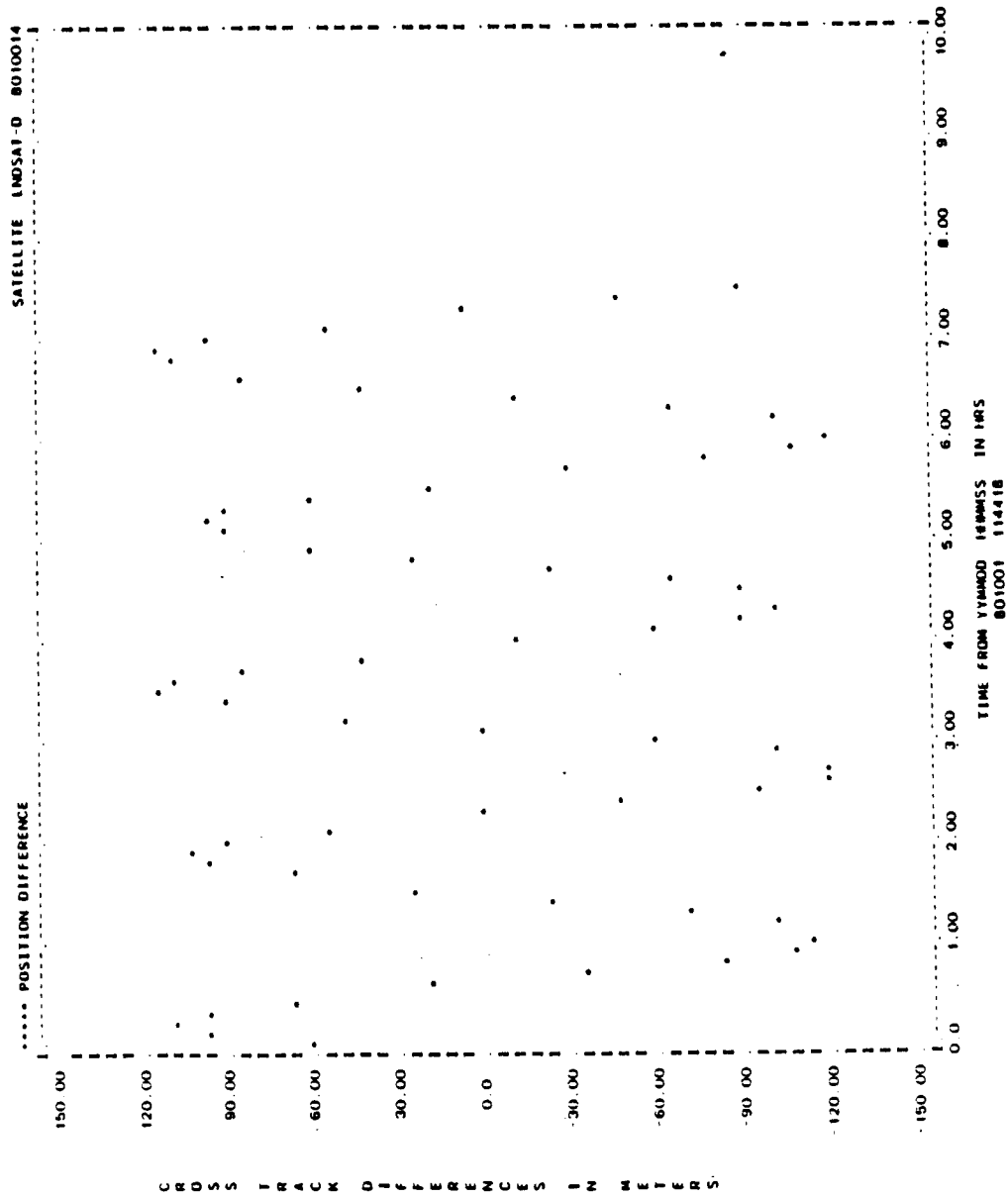


Figure A-26. Cross-Track Differences for Run L23 (2 of 2)

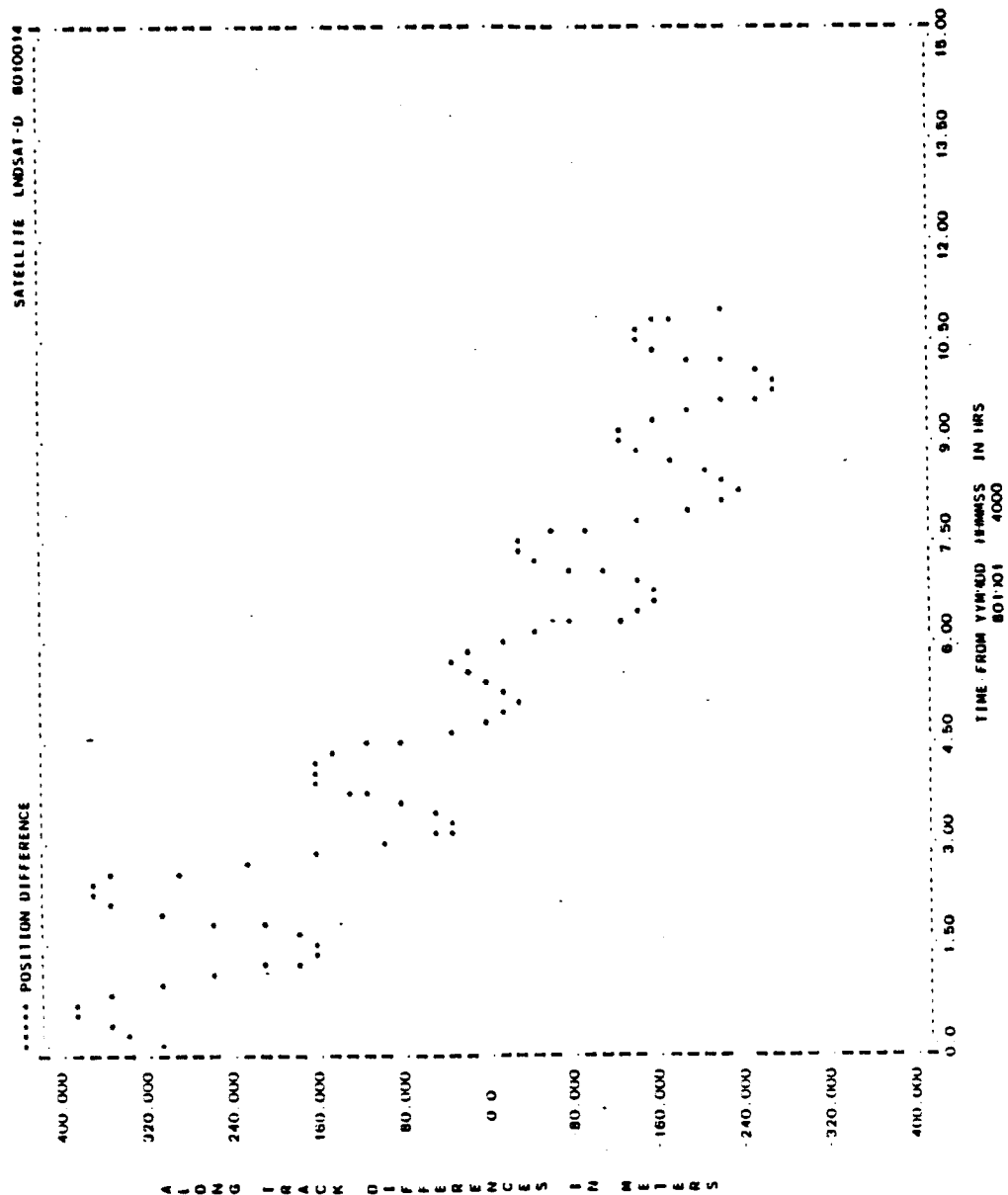


Figure A-27. Along-Track Differences for Run L23 (1 of 2)

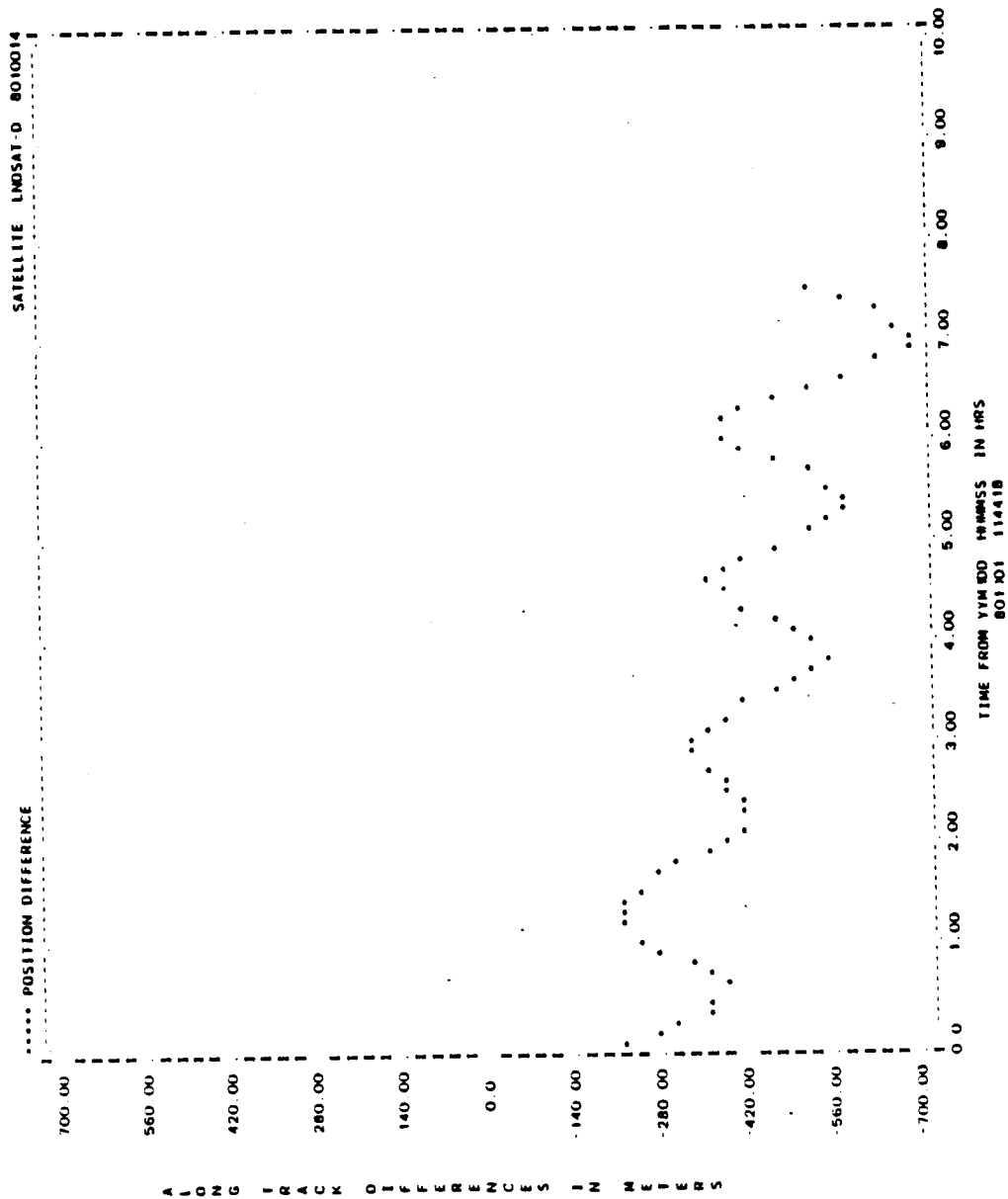


Figure A-27. Along-Track Differences for Run L23 (2 of 2)

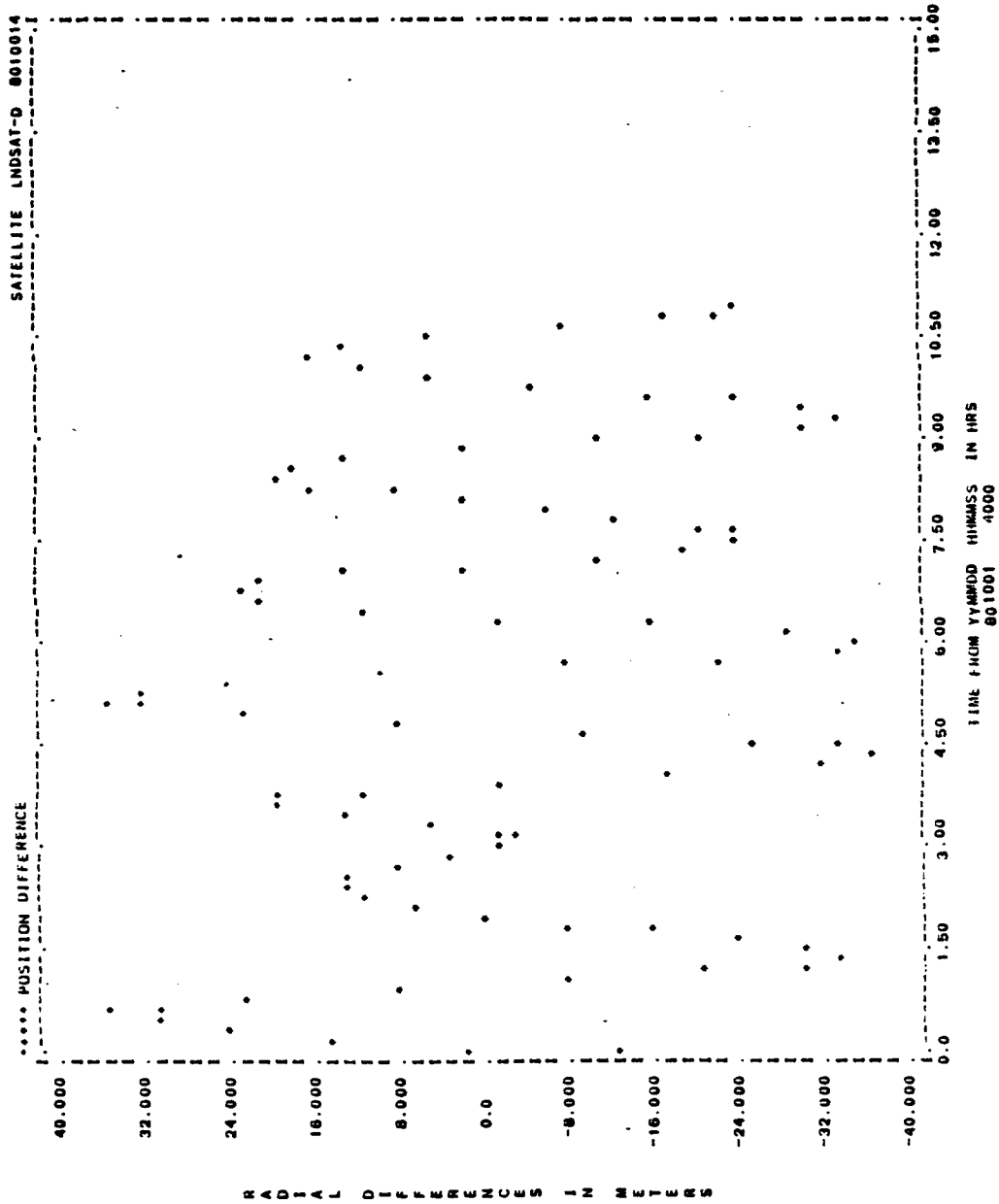


Figure A-28. Radial Differences for Run L18 (1 of 2)

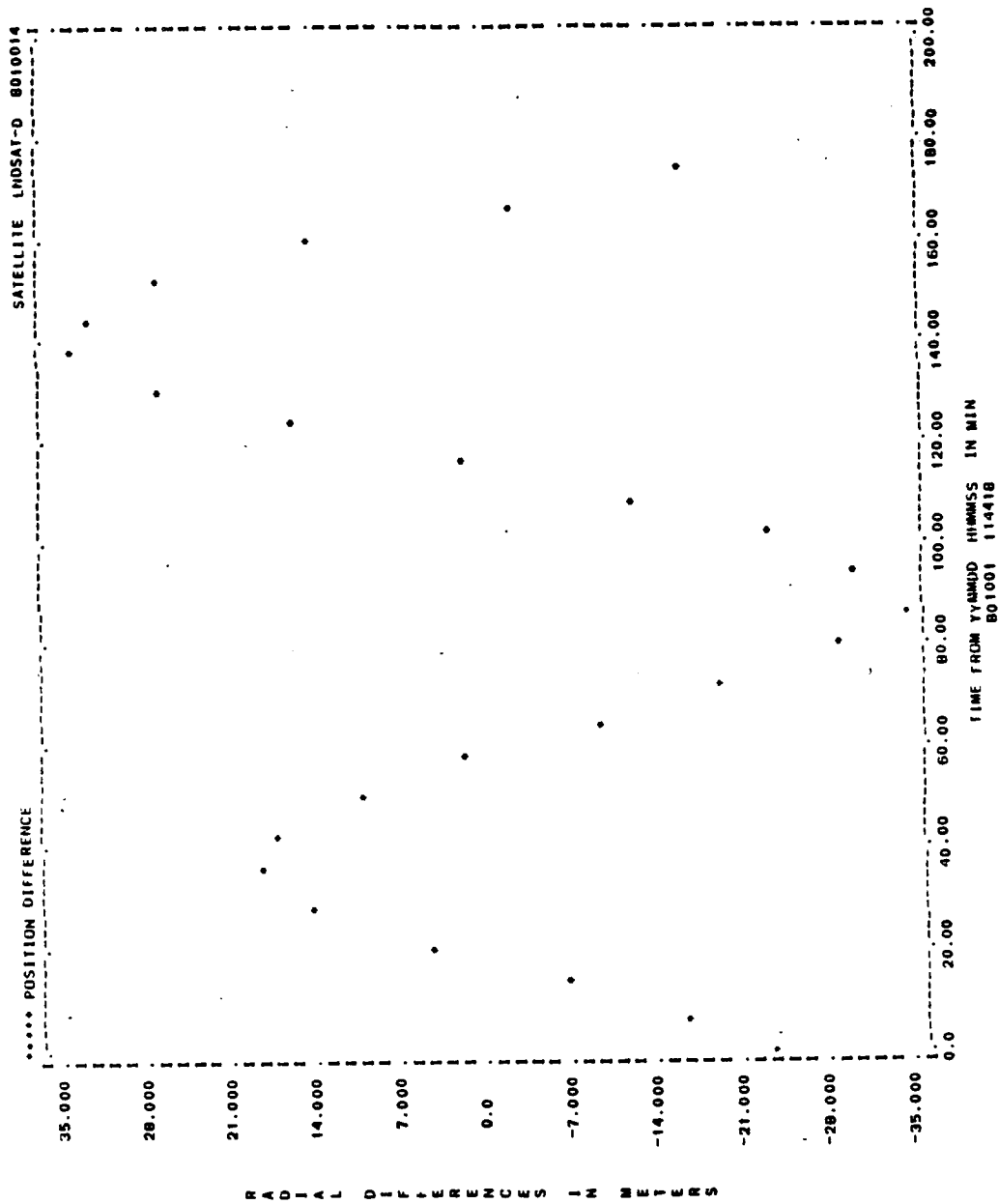


Figure A-28. Radial Differences for Run L18 (2 of 2)

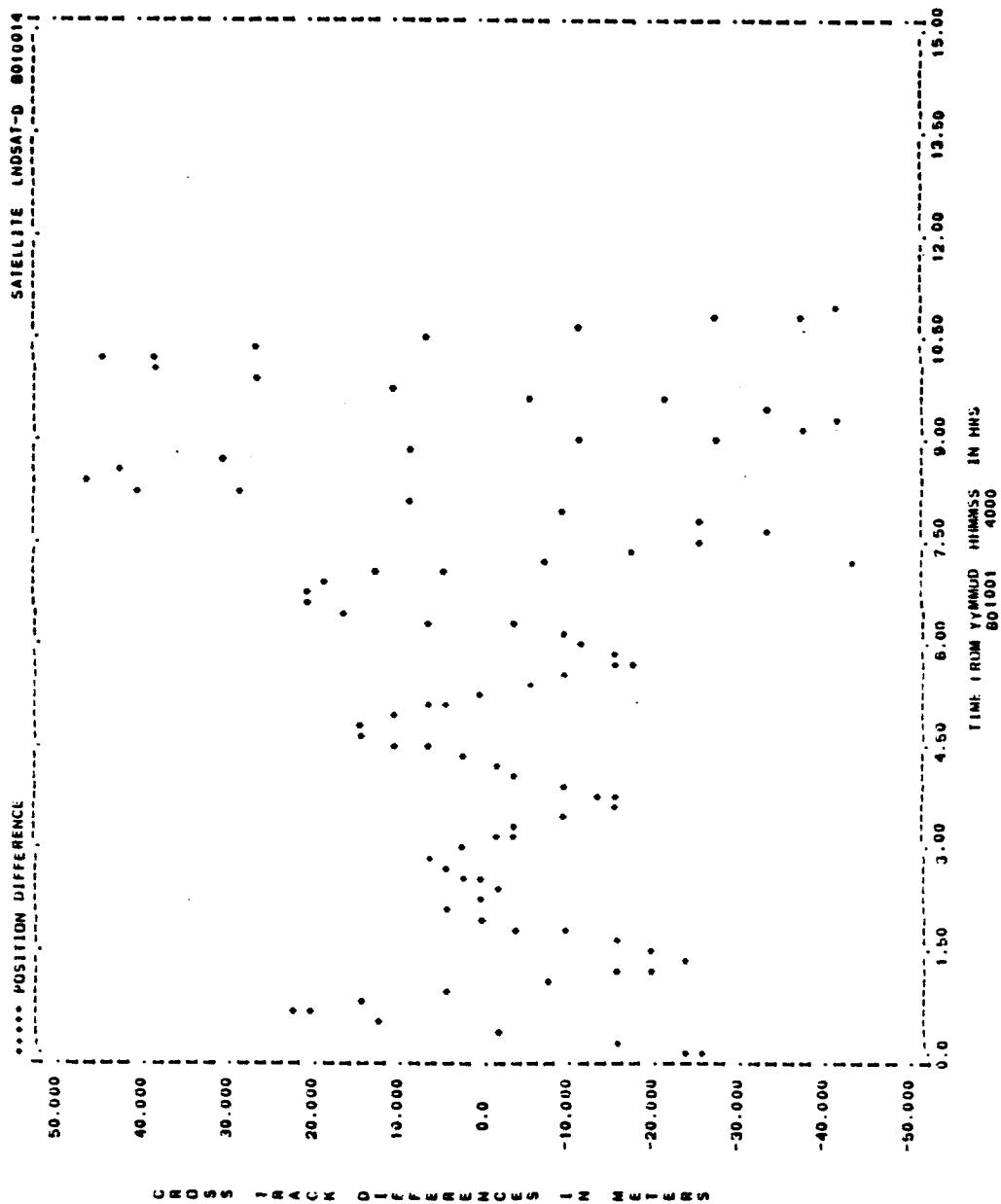


Figure A-29. Cross-Track Differences for Run L18 (1 of 2)

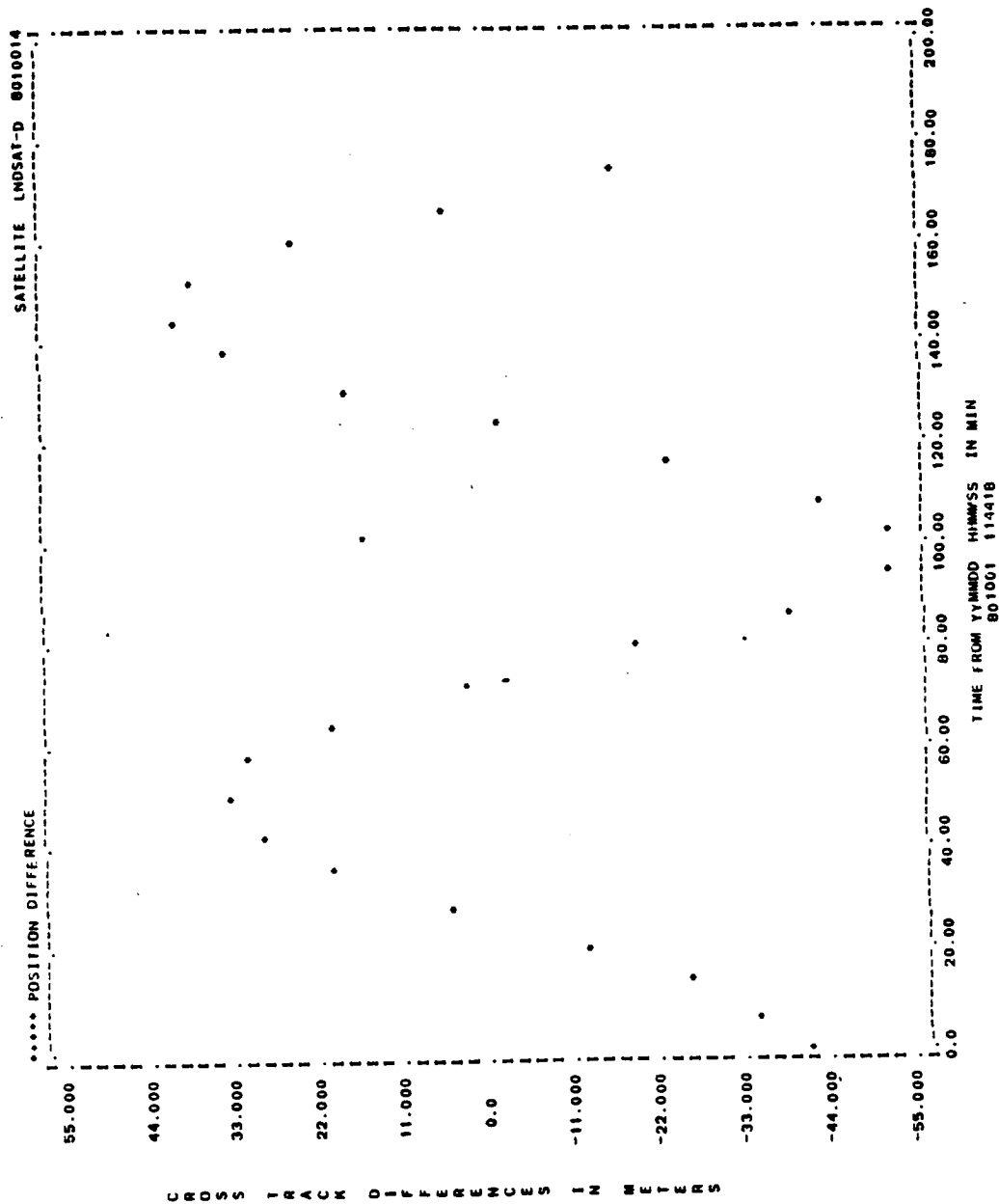


Figure A-29. Cross-Track Differences for Run L18 (2 of 2)

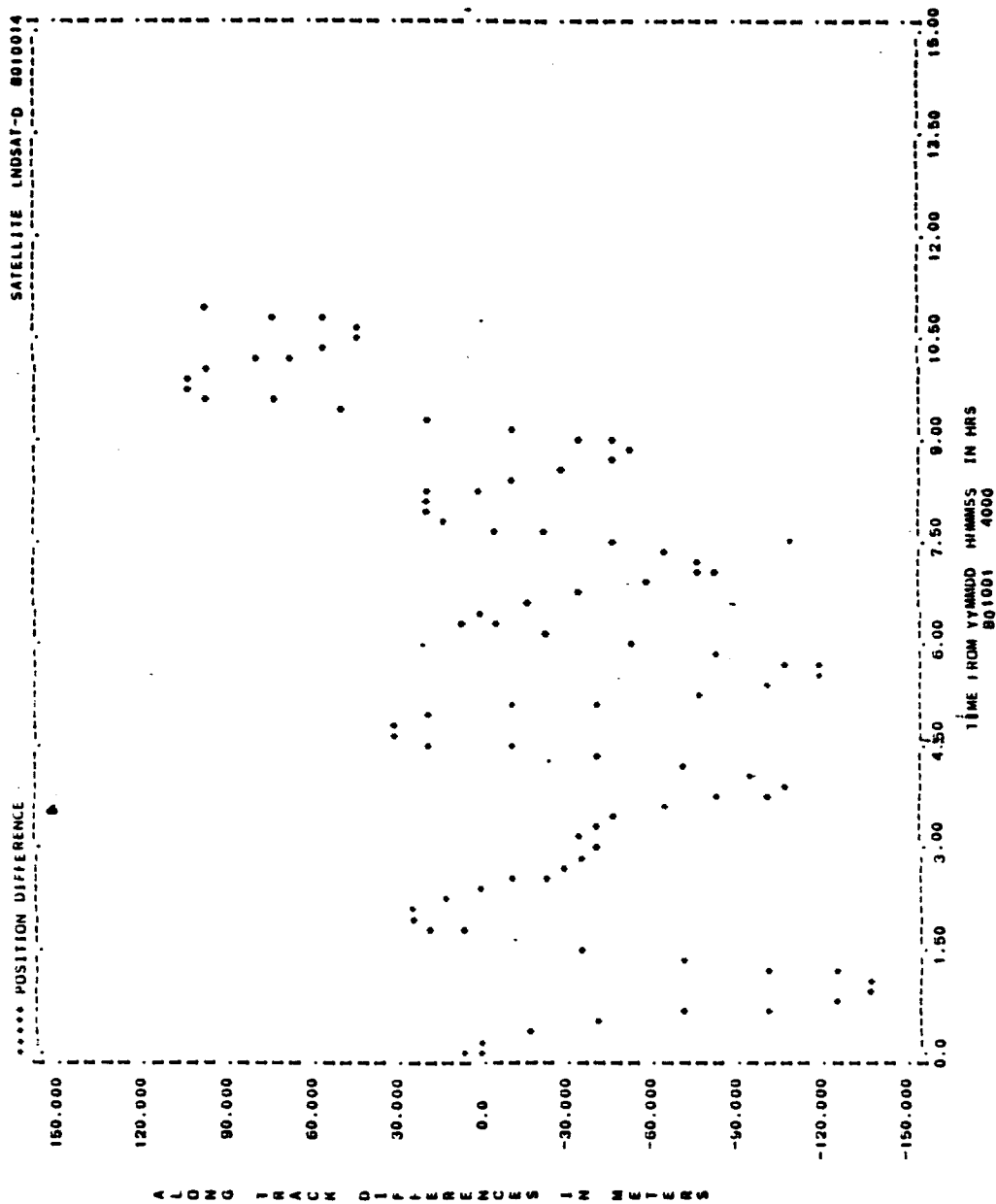


Figure A-30. Along-Track Differences for Run L18 (1 of 2)

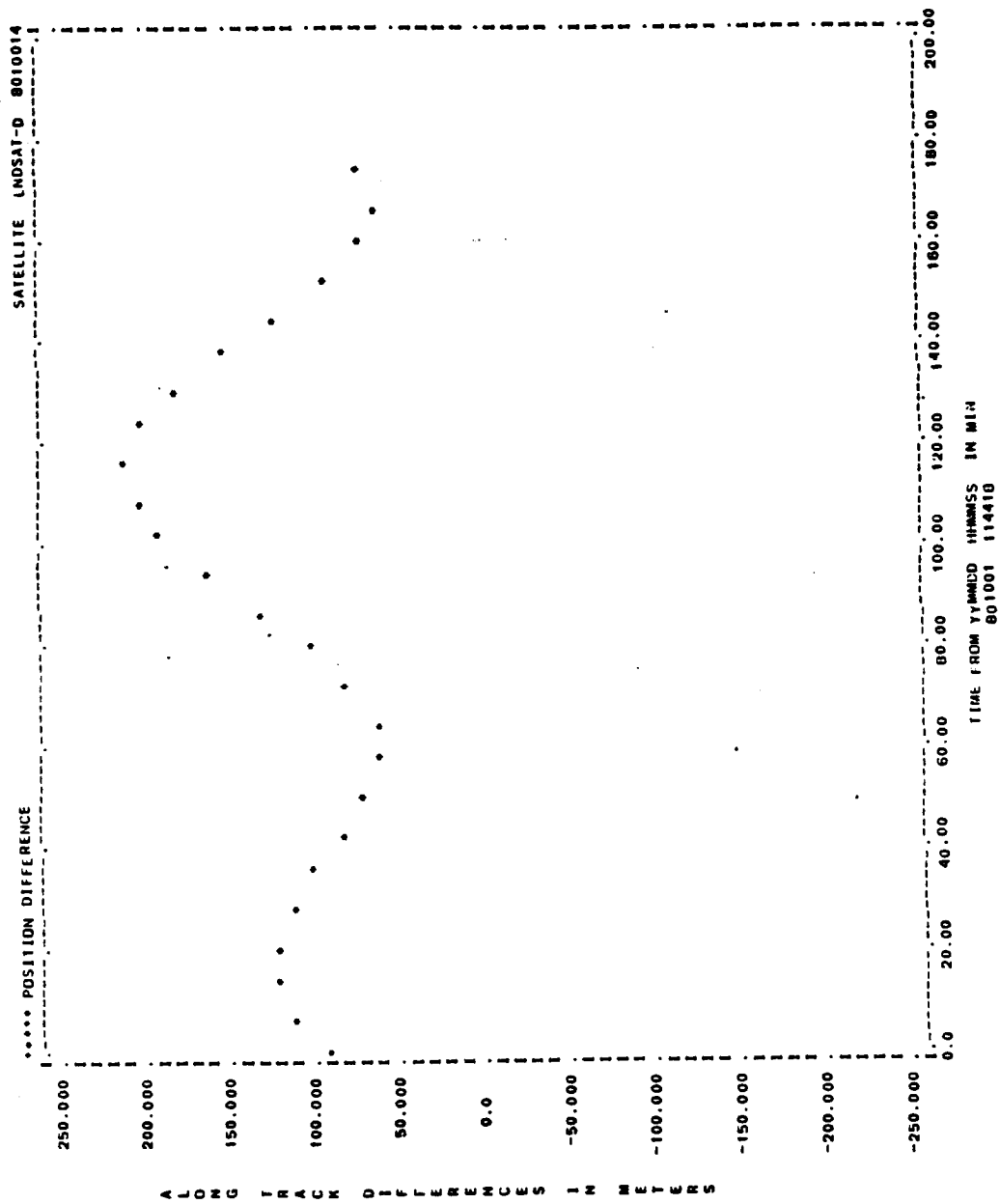


Figure A-30. Along-Track Differences for Run L18 (2 of 2)

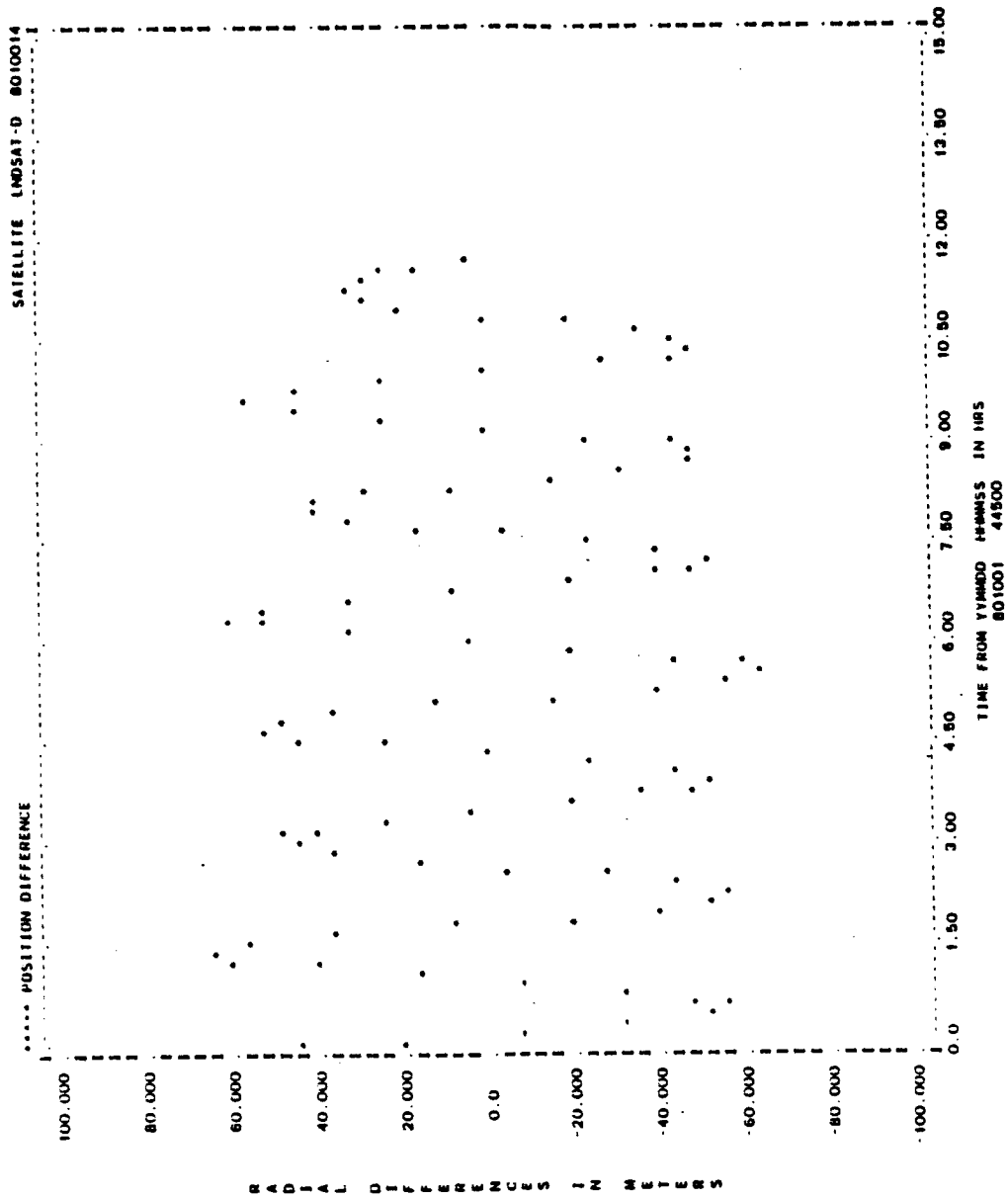


Figure A-31. Radial Differences for Run L19 (1 of 2)

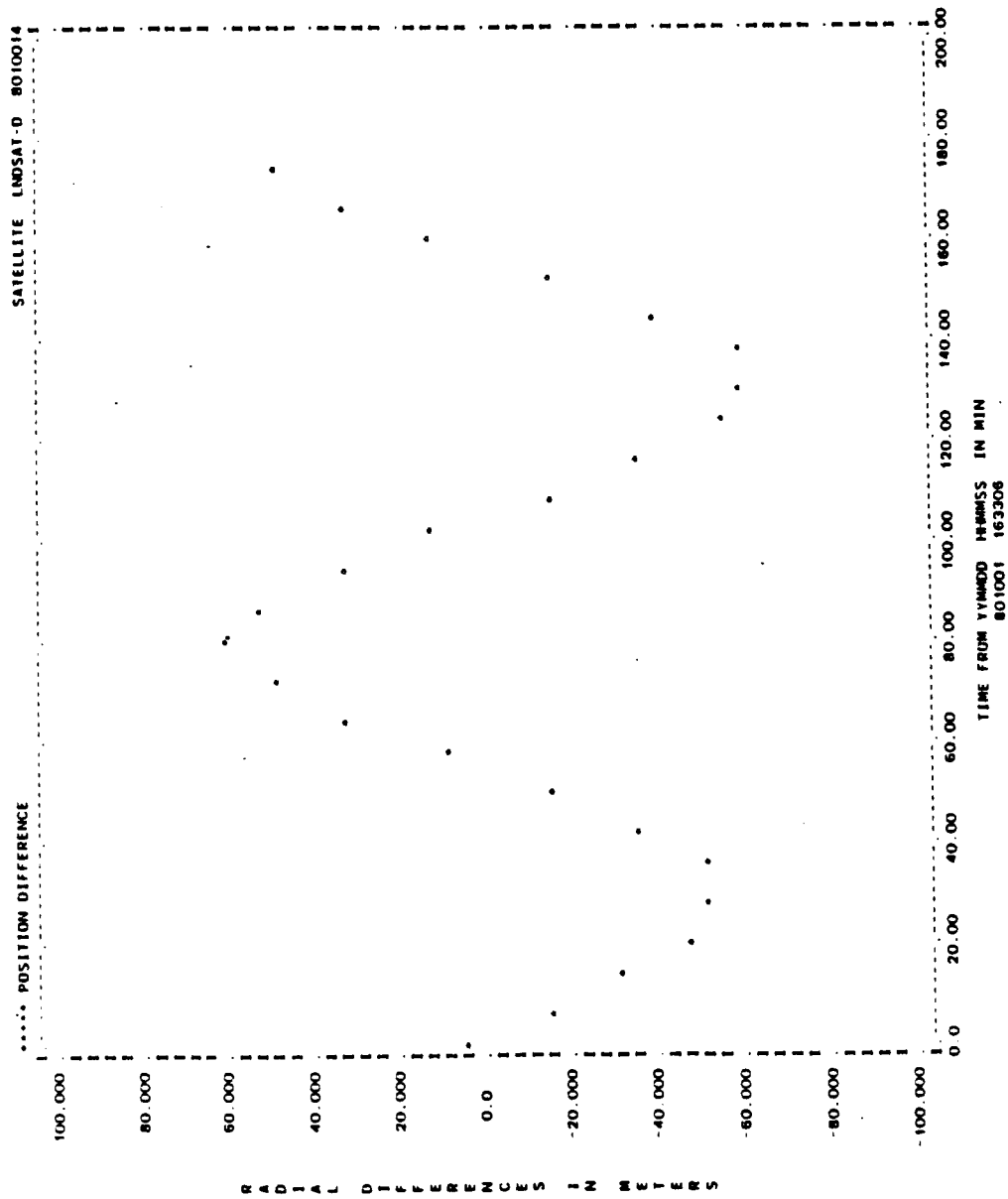


Figure A-31. Radial Differences for Run L19 (2 of 2)

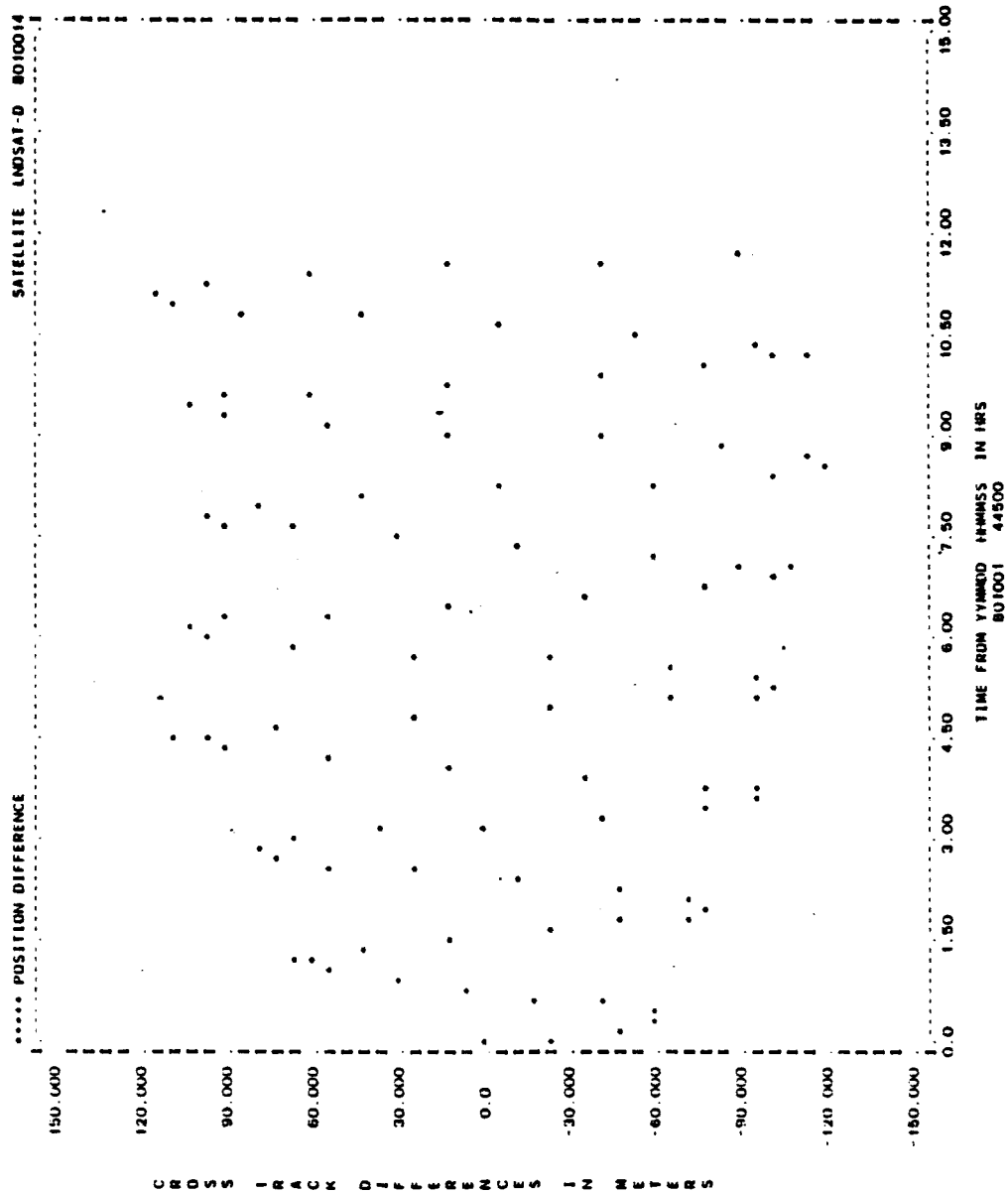


Figure A-32. Cross-Track Differences for Run L19 (1 of 2)

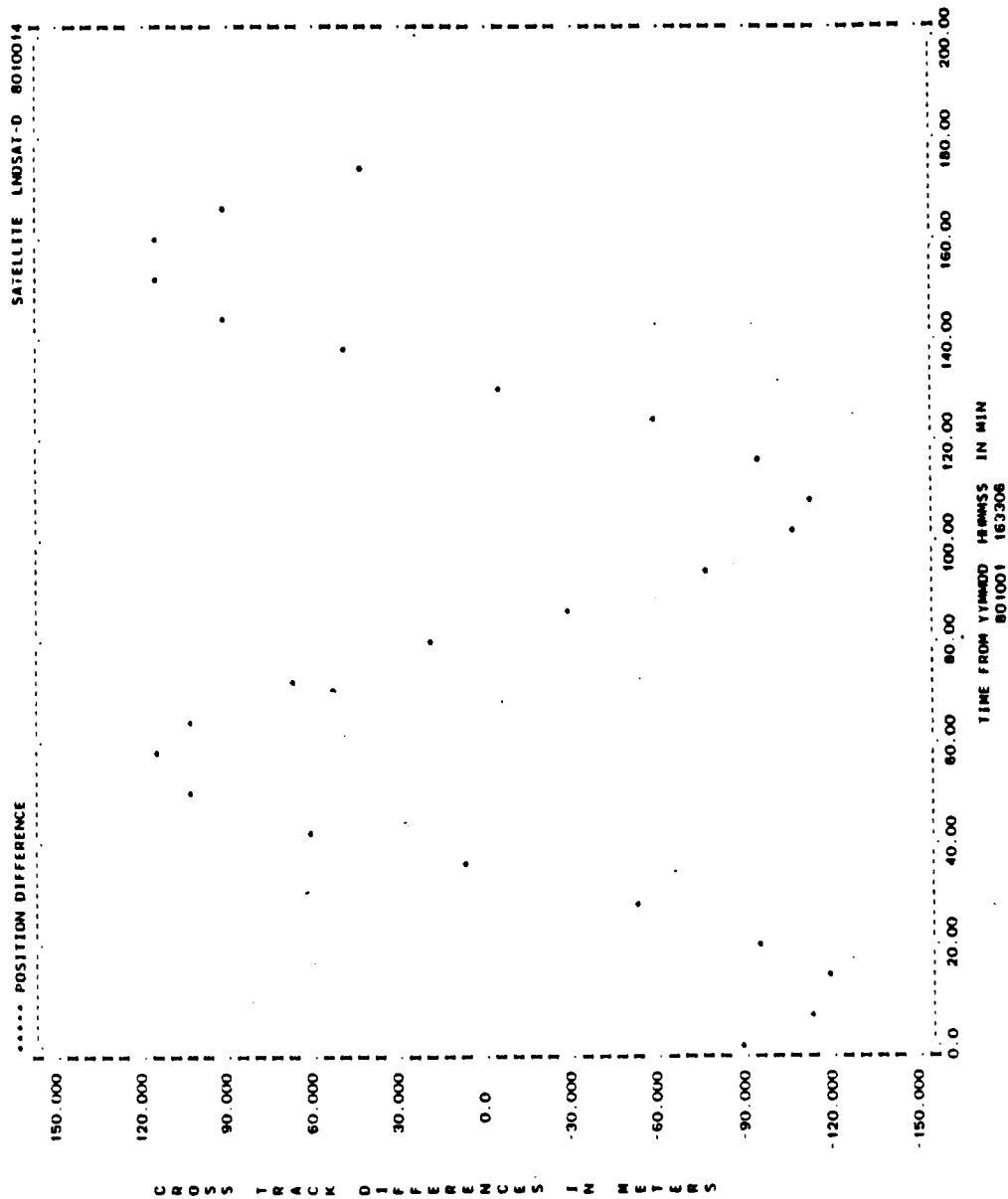


Figure A-32. Cross-Track Differences for Run L19 (2 of 2)

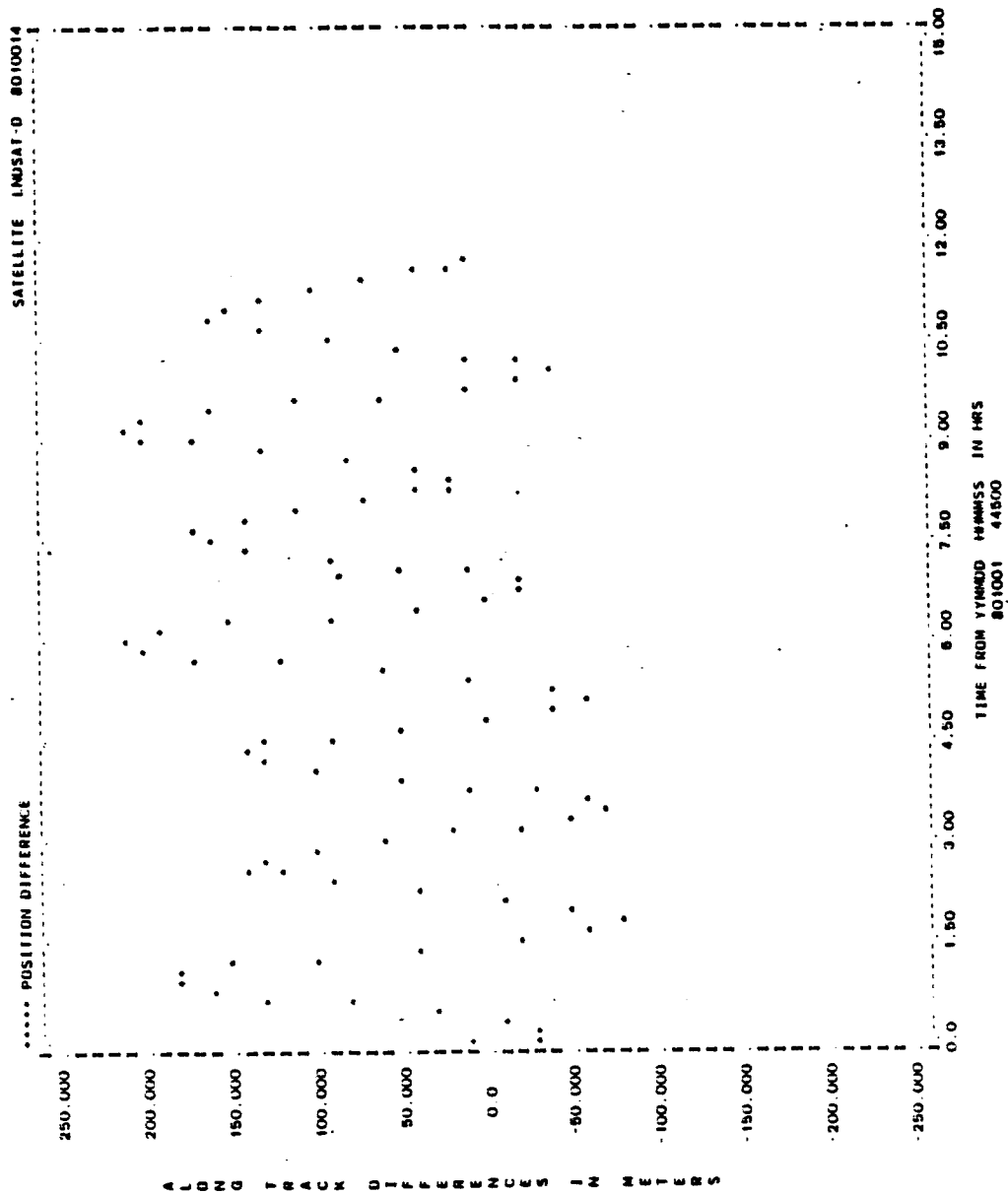


Figure A-33. Along-Track Differences for Run L19 (1 of 2)

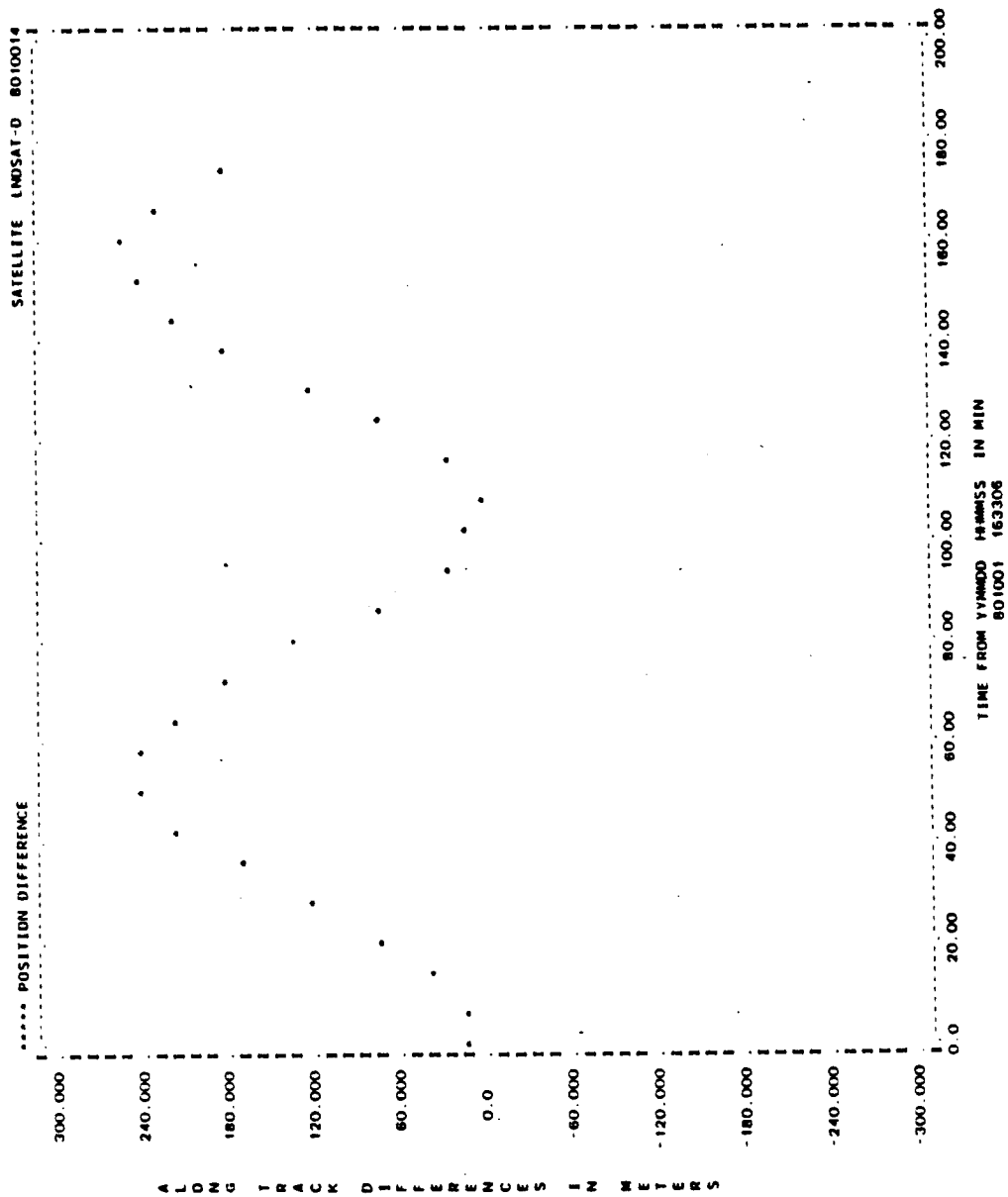


Figure A-33. Along-Track Differences for Run L19 (2 of 2)

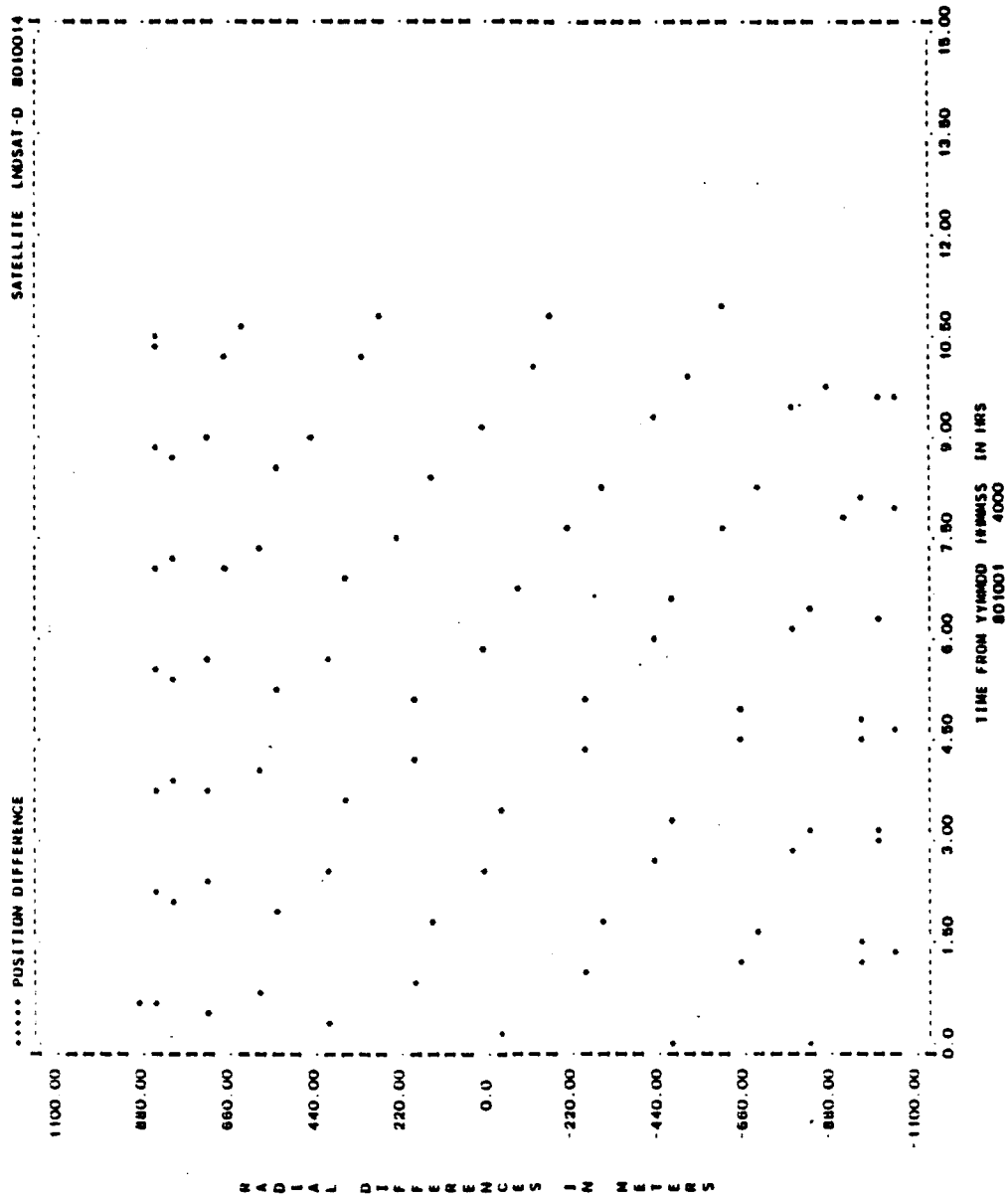


Figure A-34. Radial Differences for Run L20 (1 of 2)

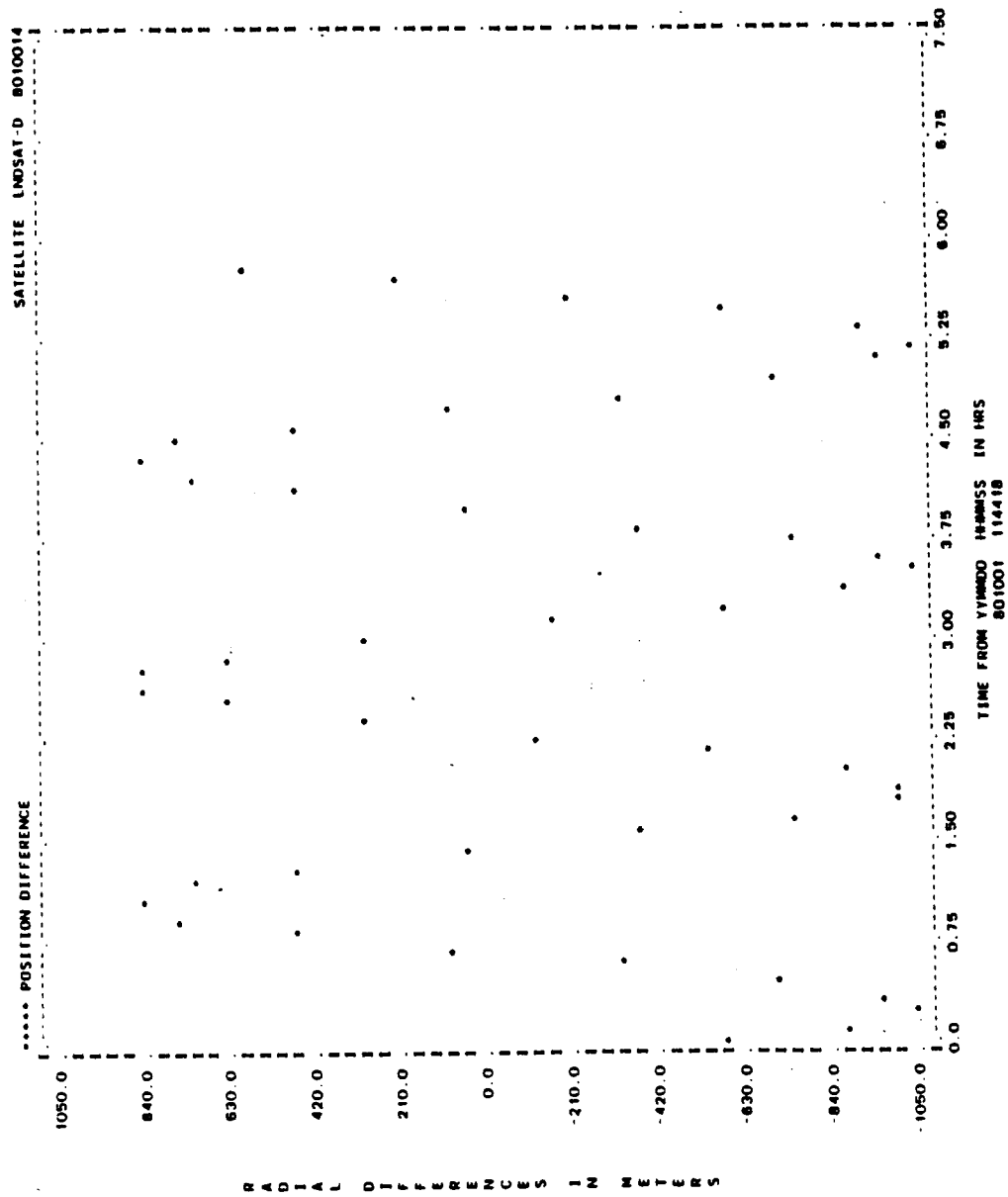


Figure A-34. Radial Differences for Run L20 (2 of 2)

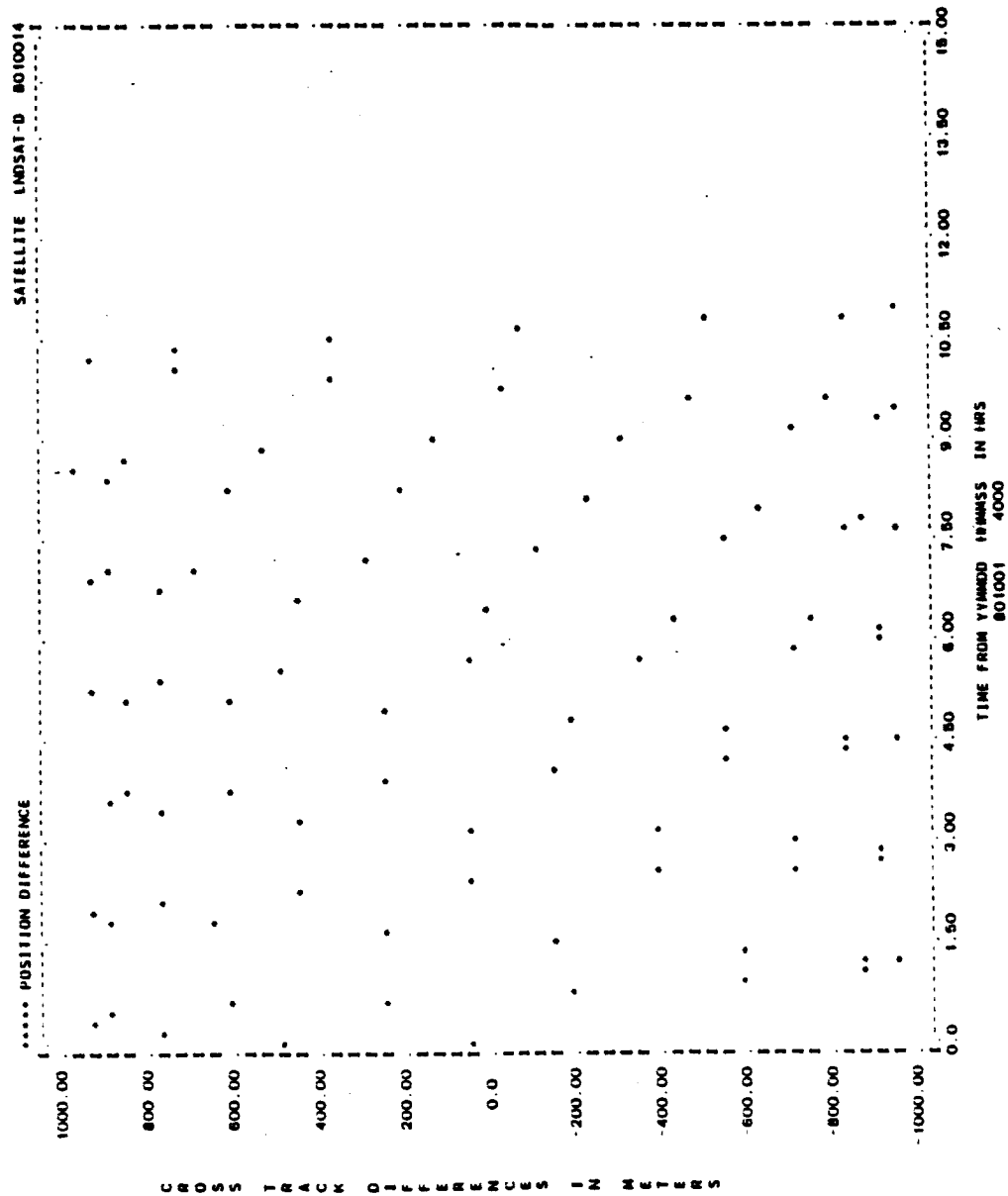


Figure A-35. Cross-Track Differences for Run L20 (1 of 2)

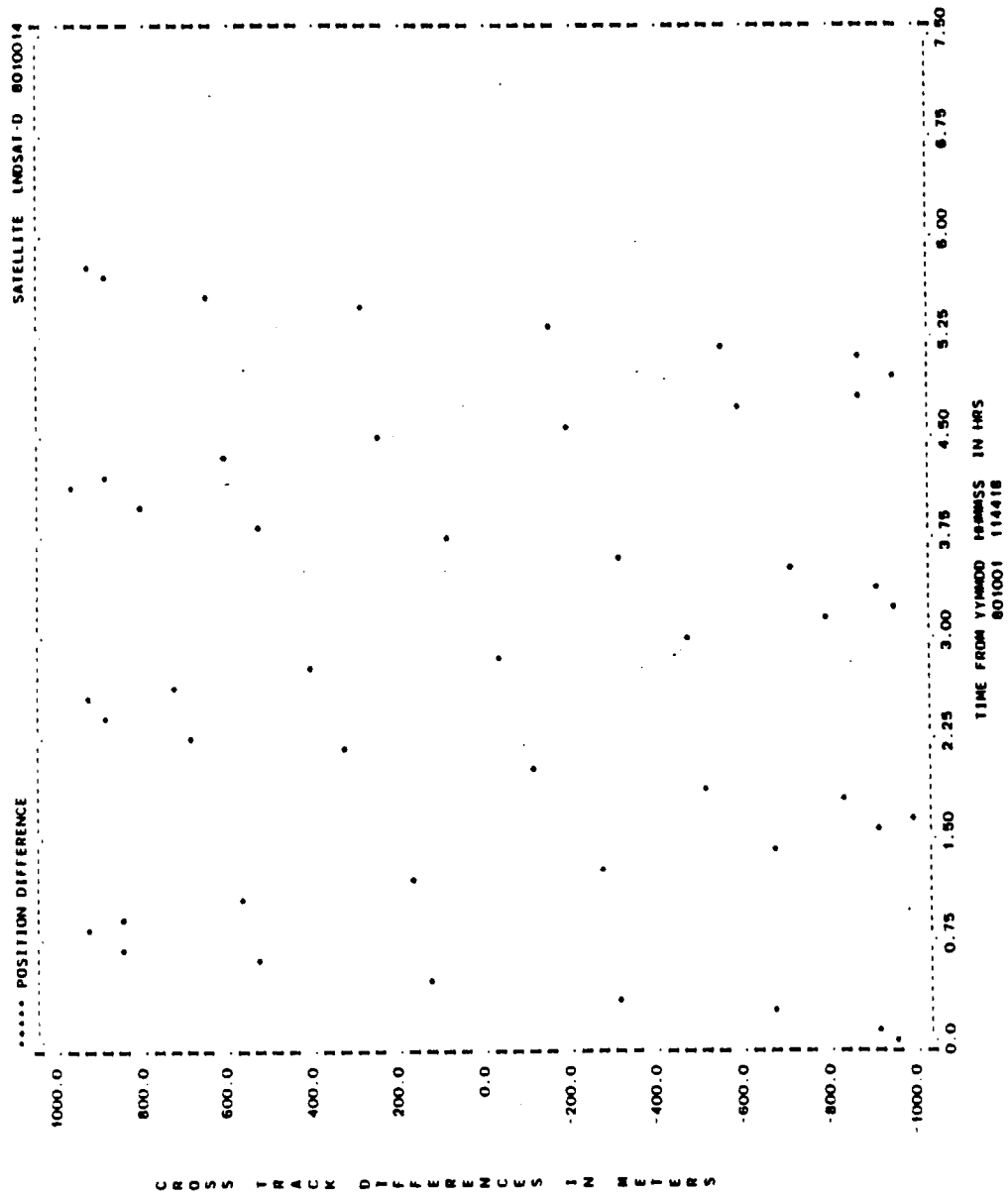


Figure A-35. Cross-Track Differences for Run L20 (2 of 2)

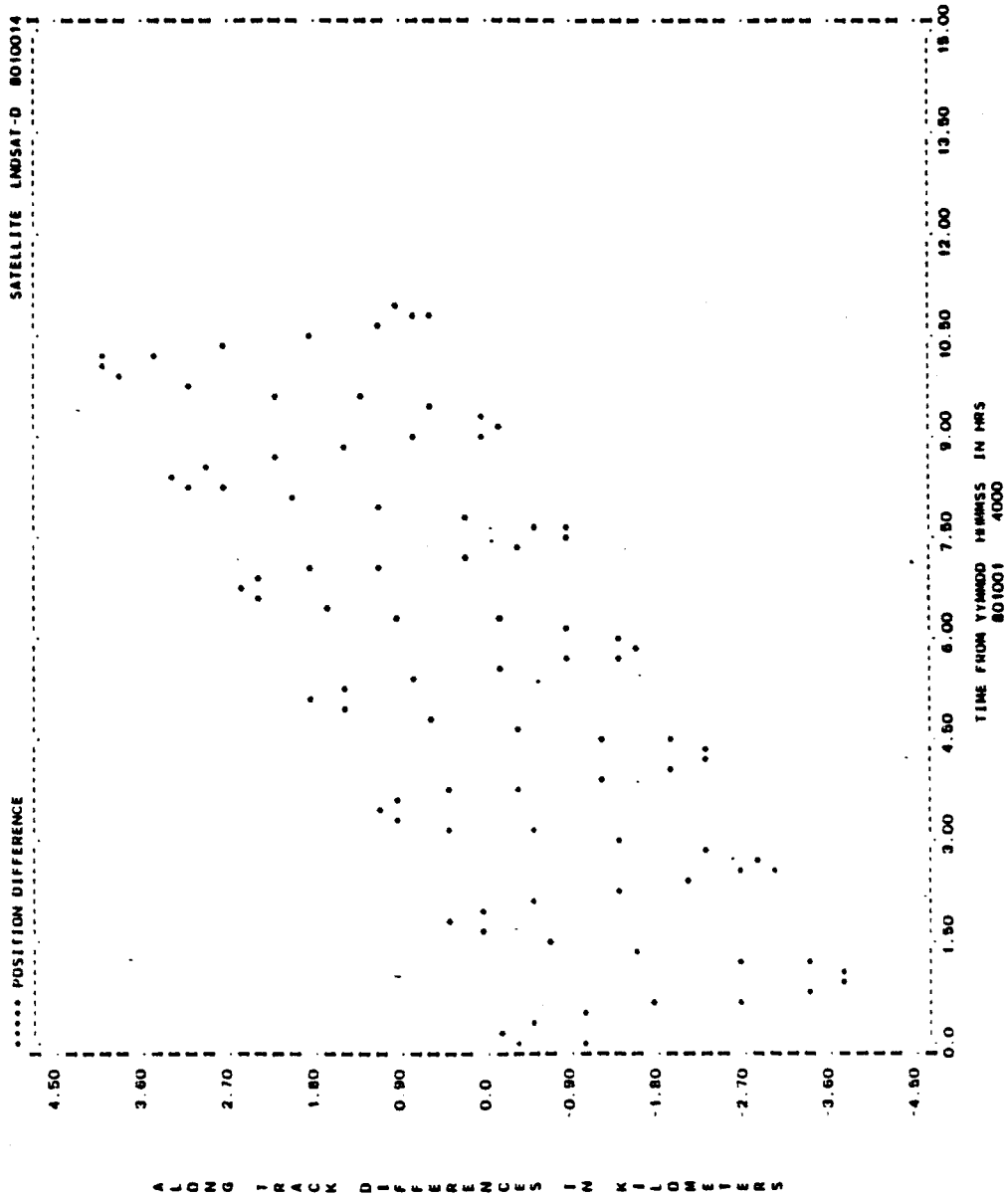


Figure A-36. Along-Track Differences for Run L20 (1 of 2)

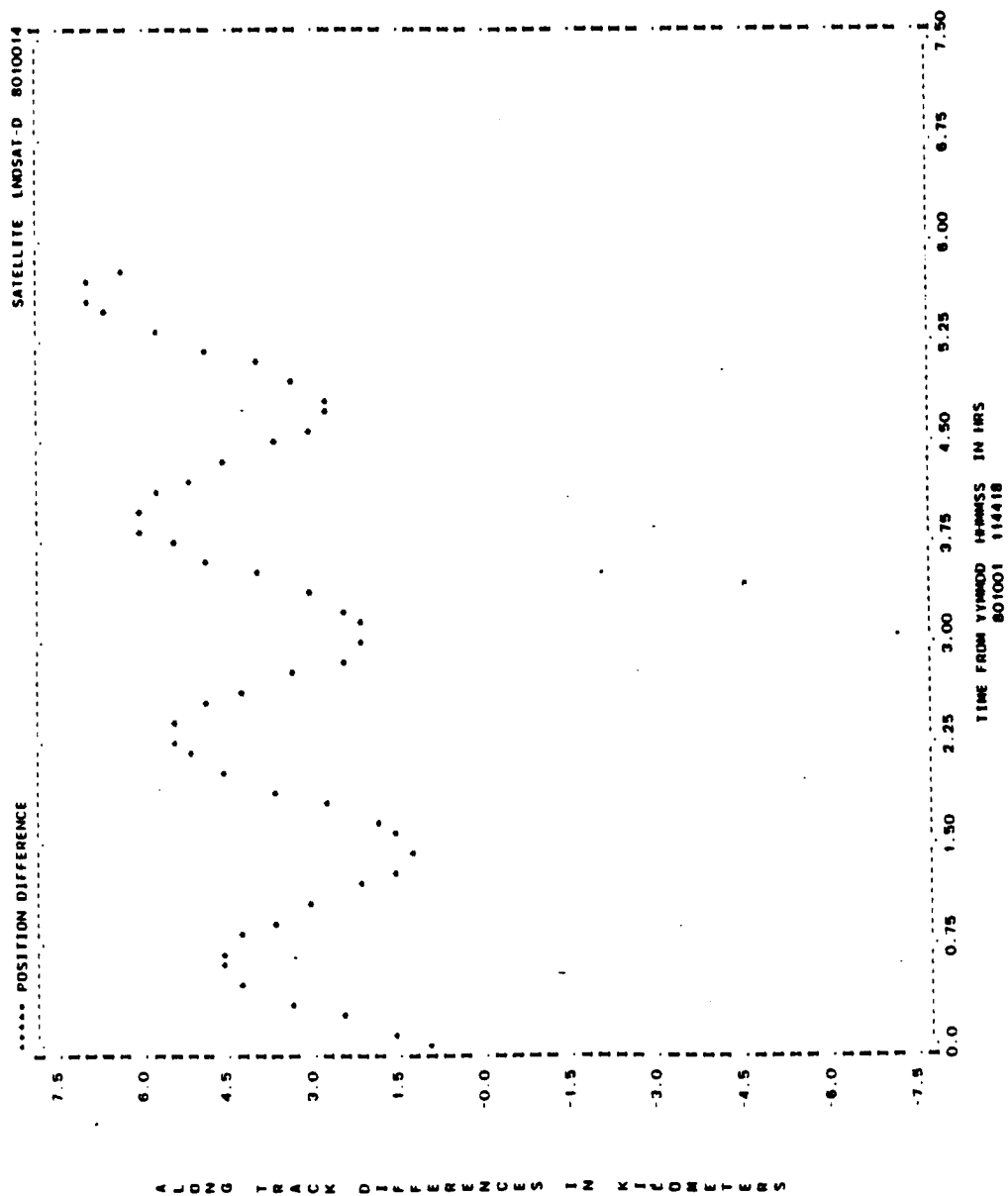


Figure A-36. Along-Track Differences for Run L20 (2 of 2)

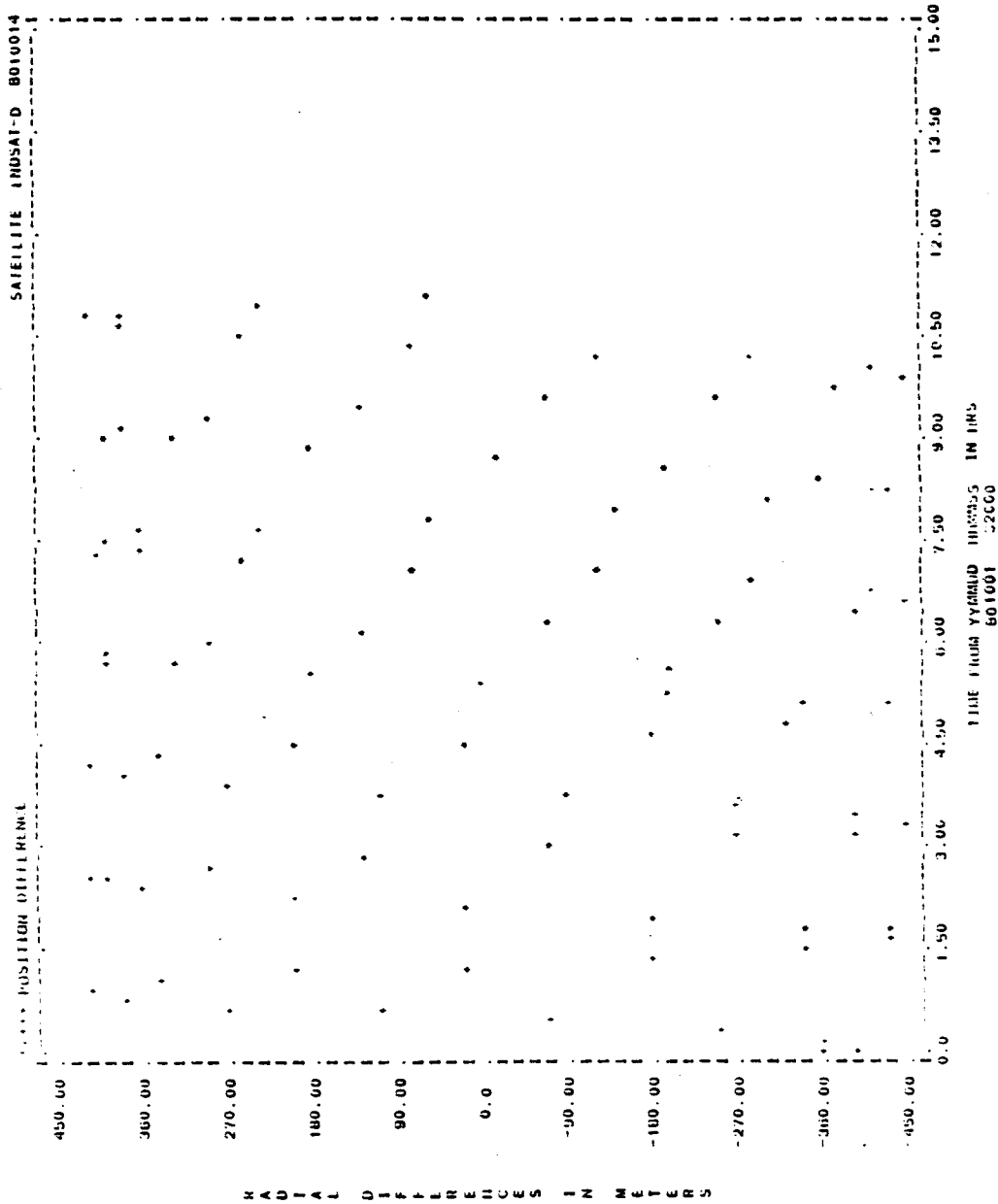


Figure A-37. Radial Differences for Run L21 (1 of 2)

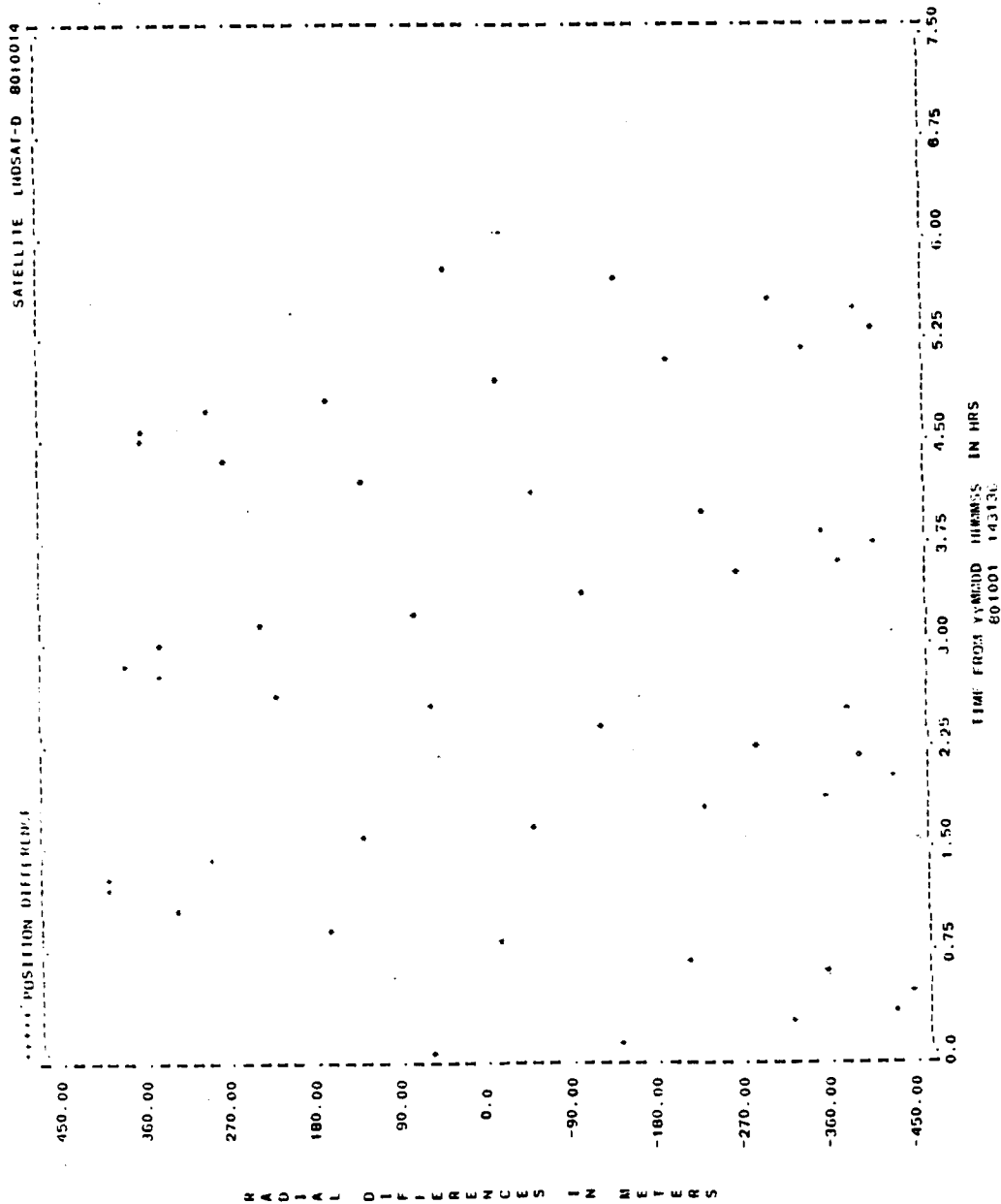


Figure A-37. Radial Differences for Run L21 (2 of 2)

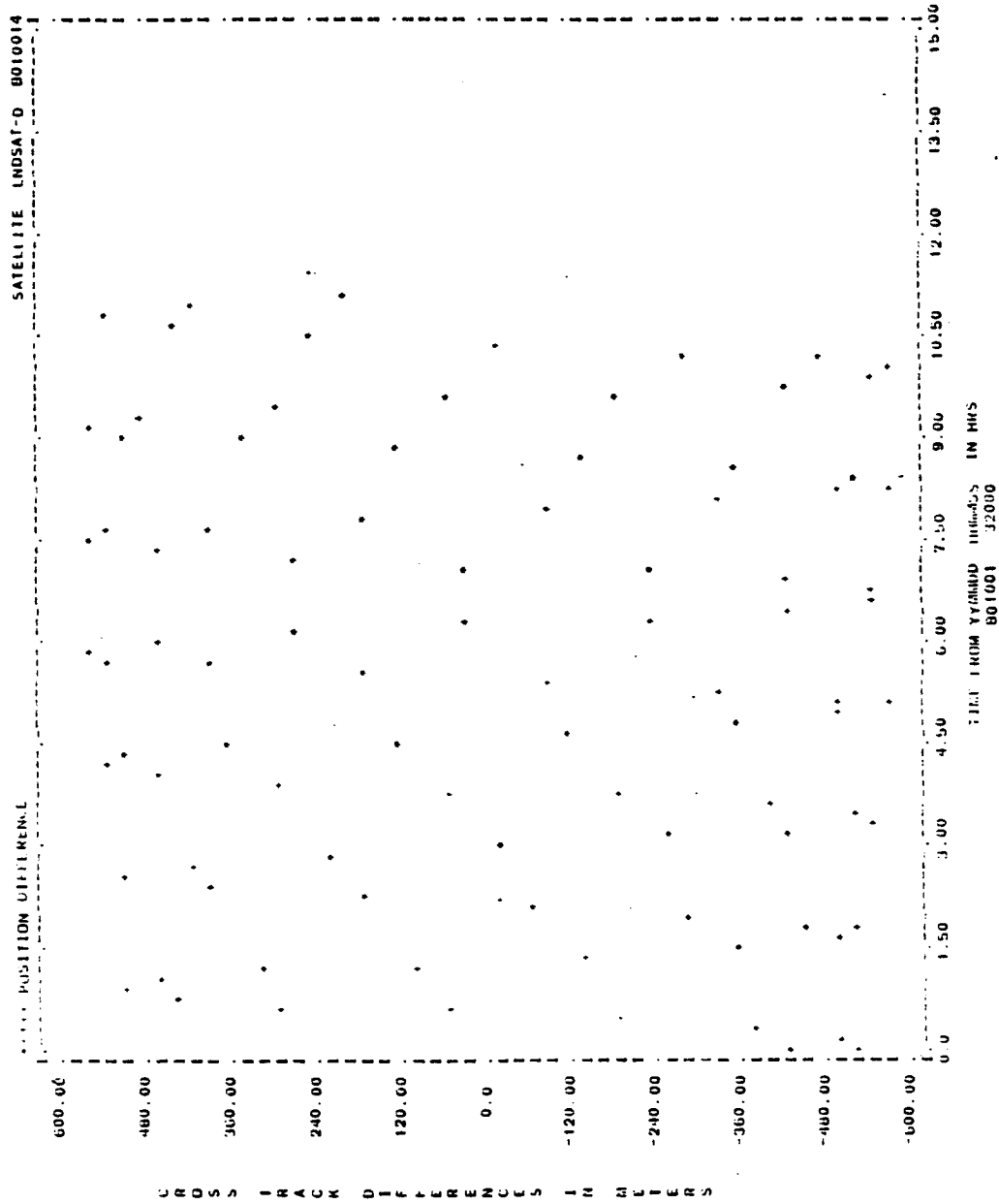


Figure A-38. Cross-Track Differences for Run L21 (1 of 2)

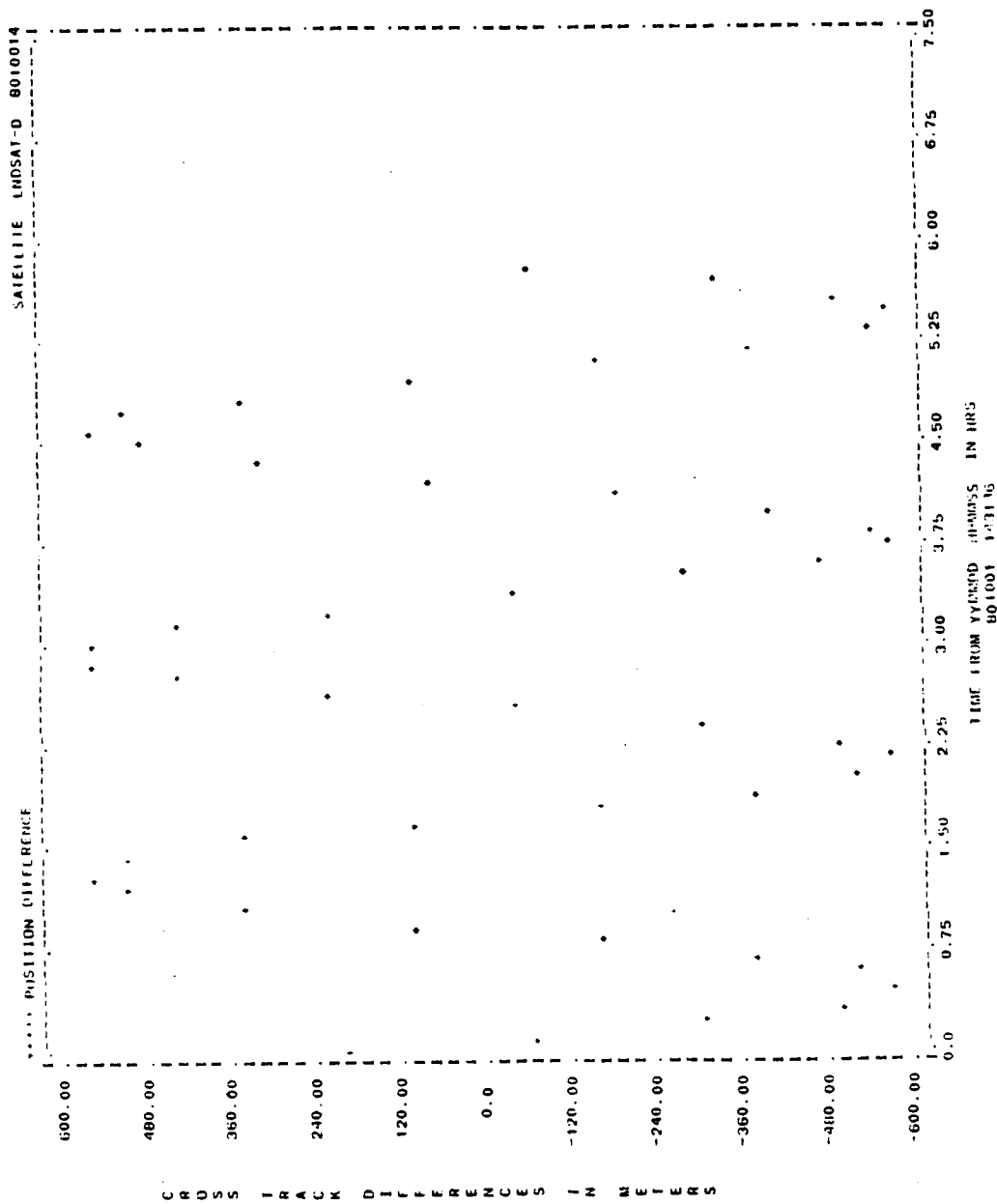


Figure A-38. Cross-Track Differences for Run L21 (2 of 2)

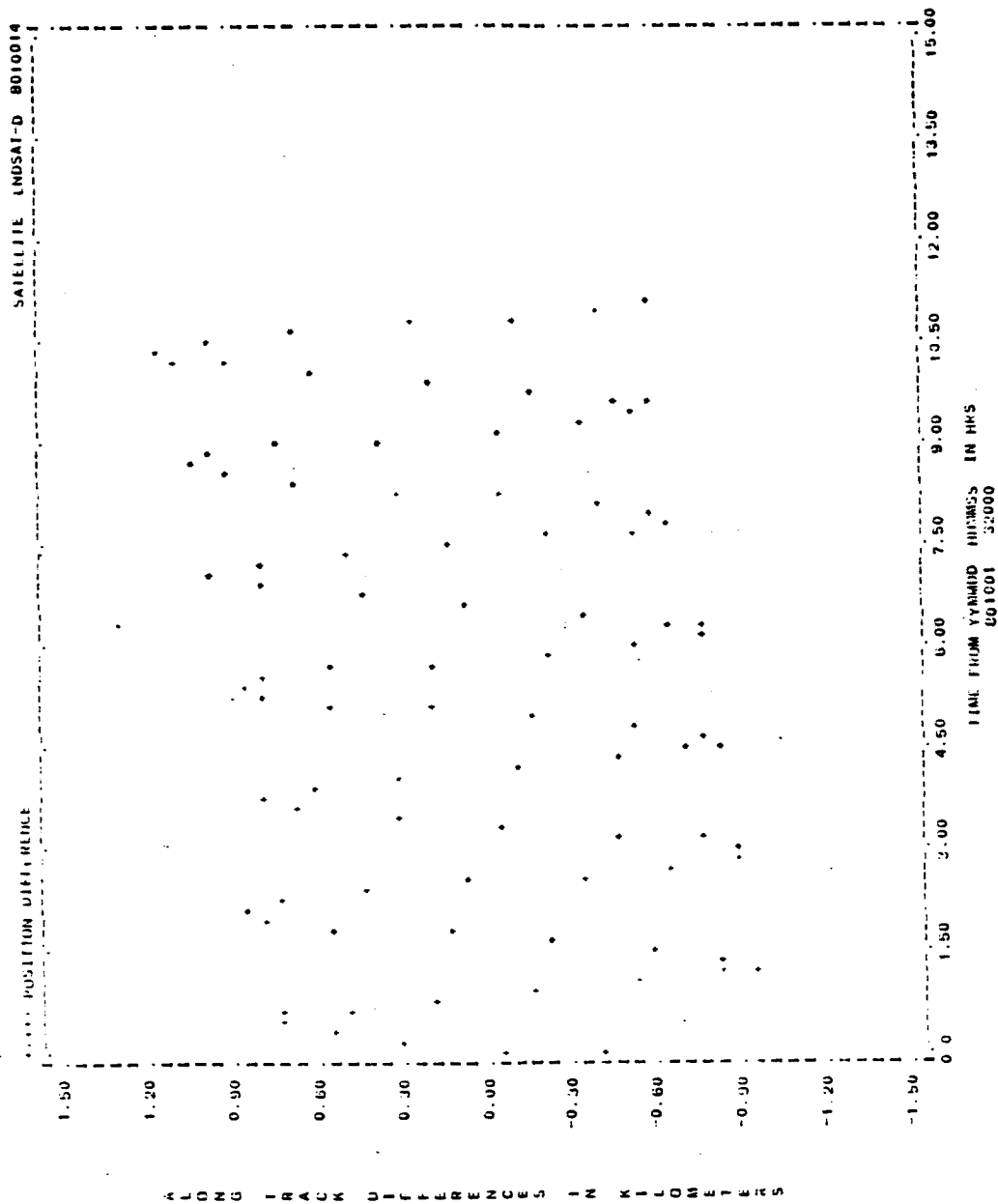
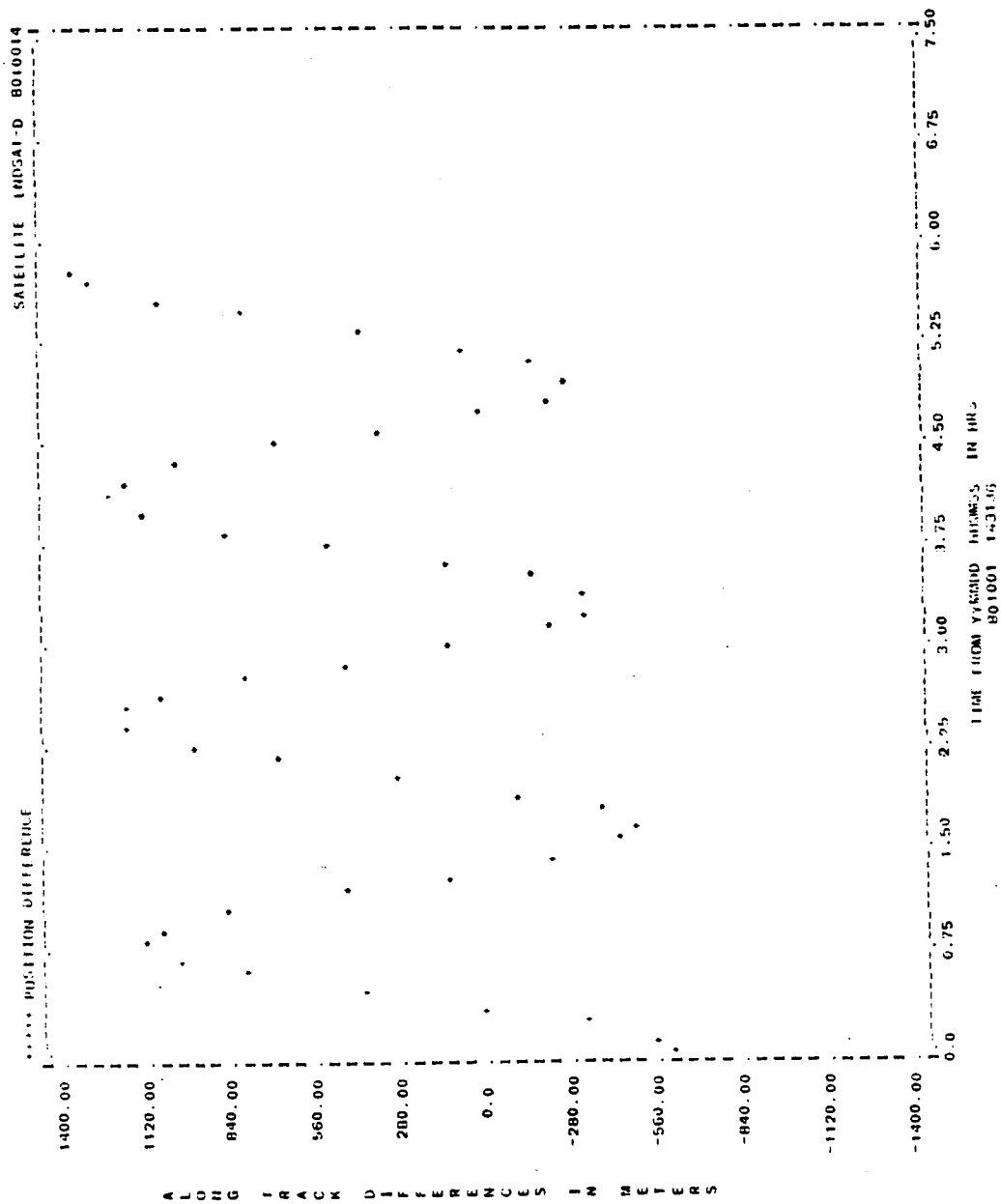


Figure A-39. Along-Track Differences for Run L21 (1 of 2)



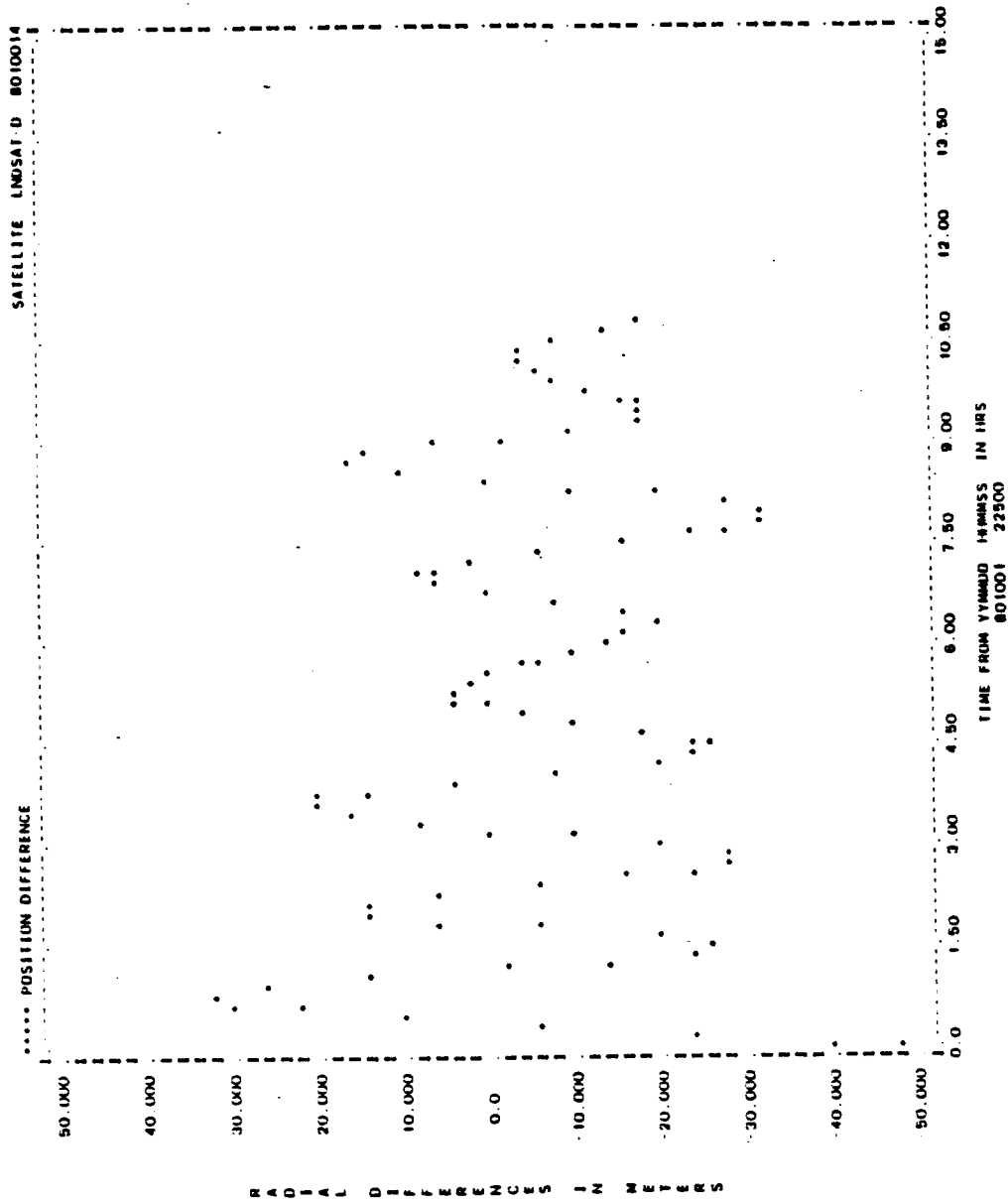


Figure A-40. Radial Differences for Run L08 (1 of 2)

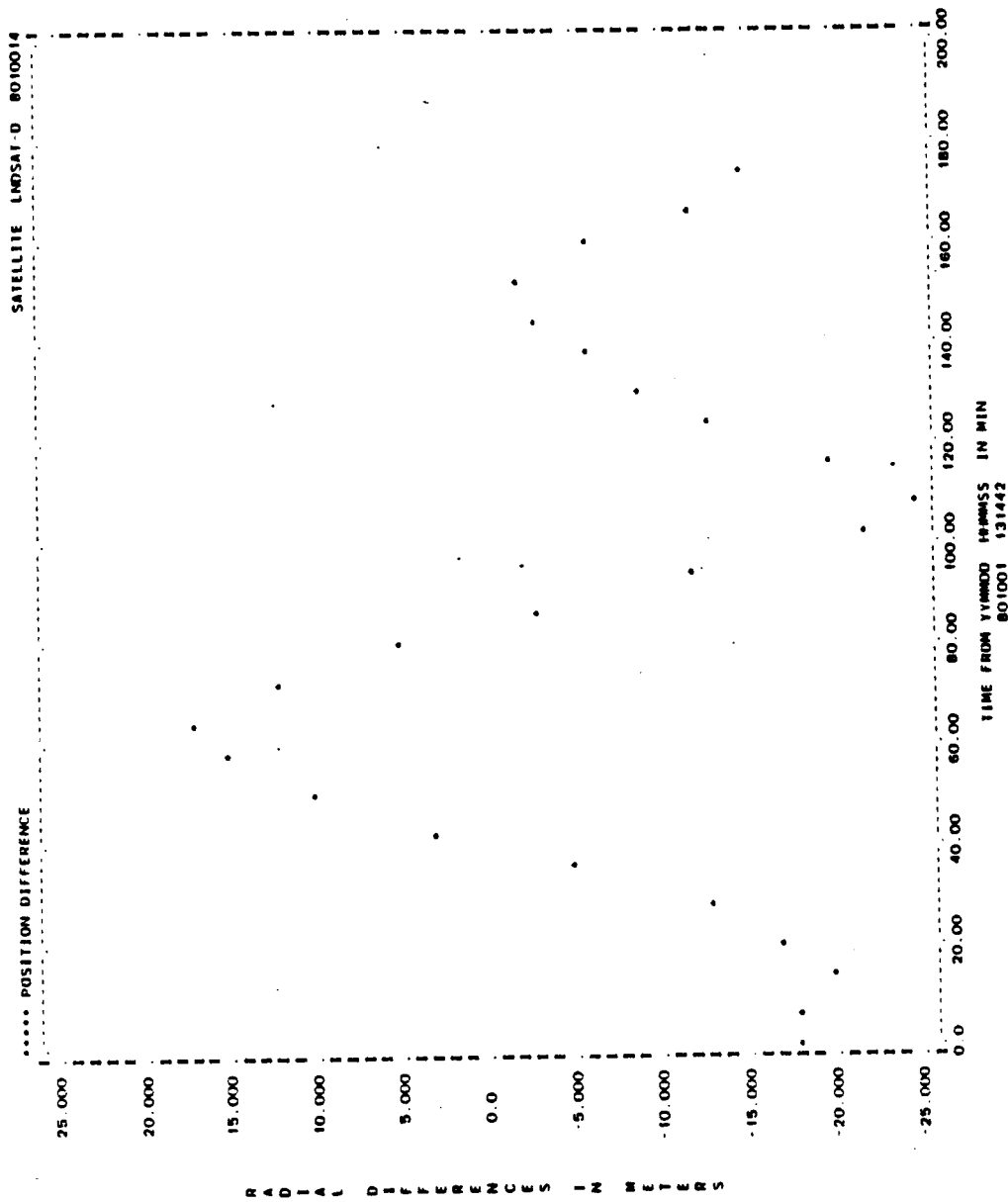


Figure A-40. Radial Differences for Run L08 (2 of 2)

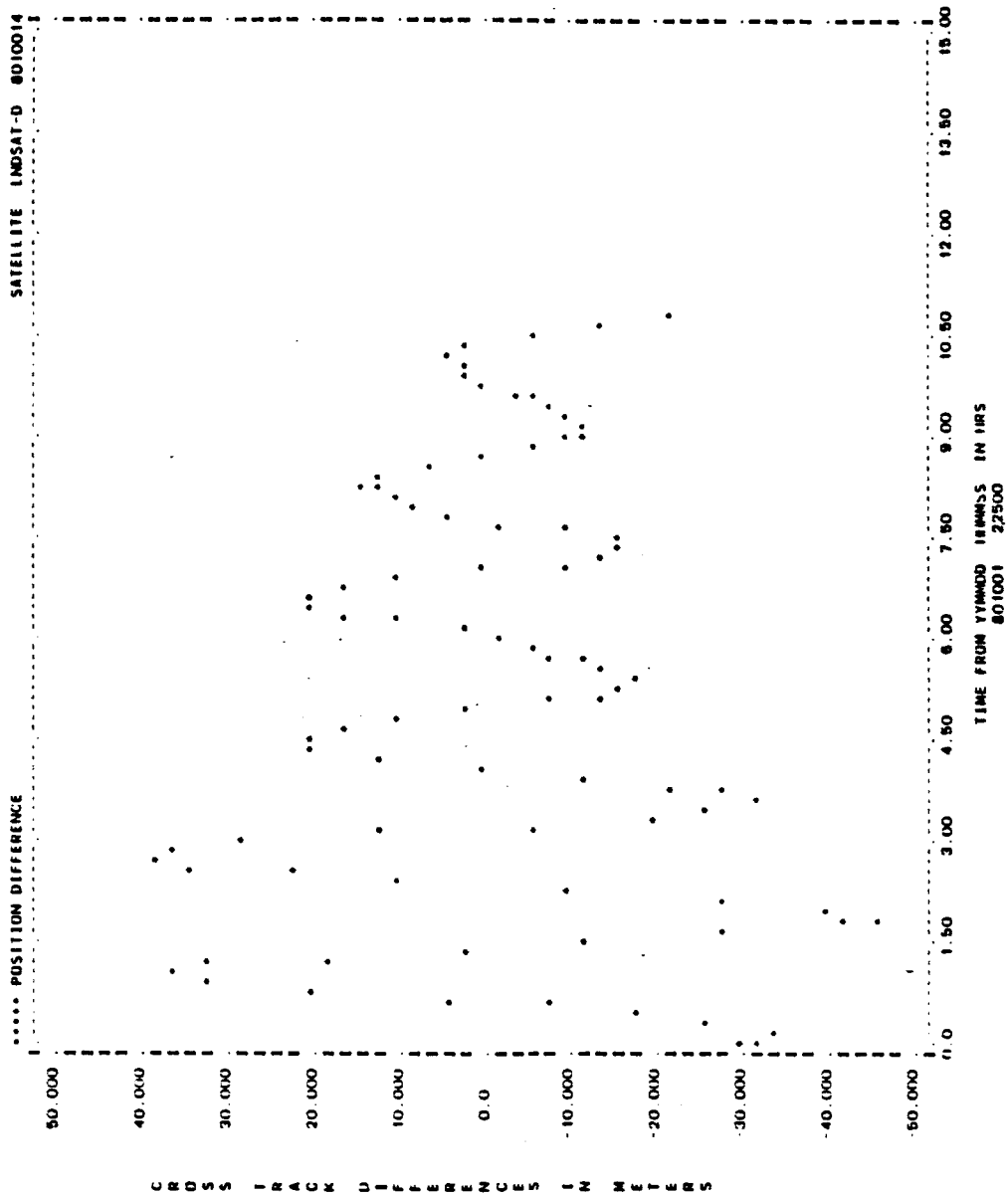


Figure A-41. Cross-Track Differences for Run L08 (1 of 2)

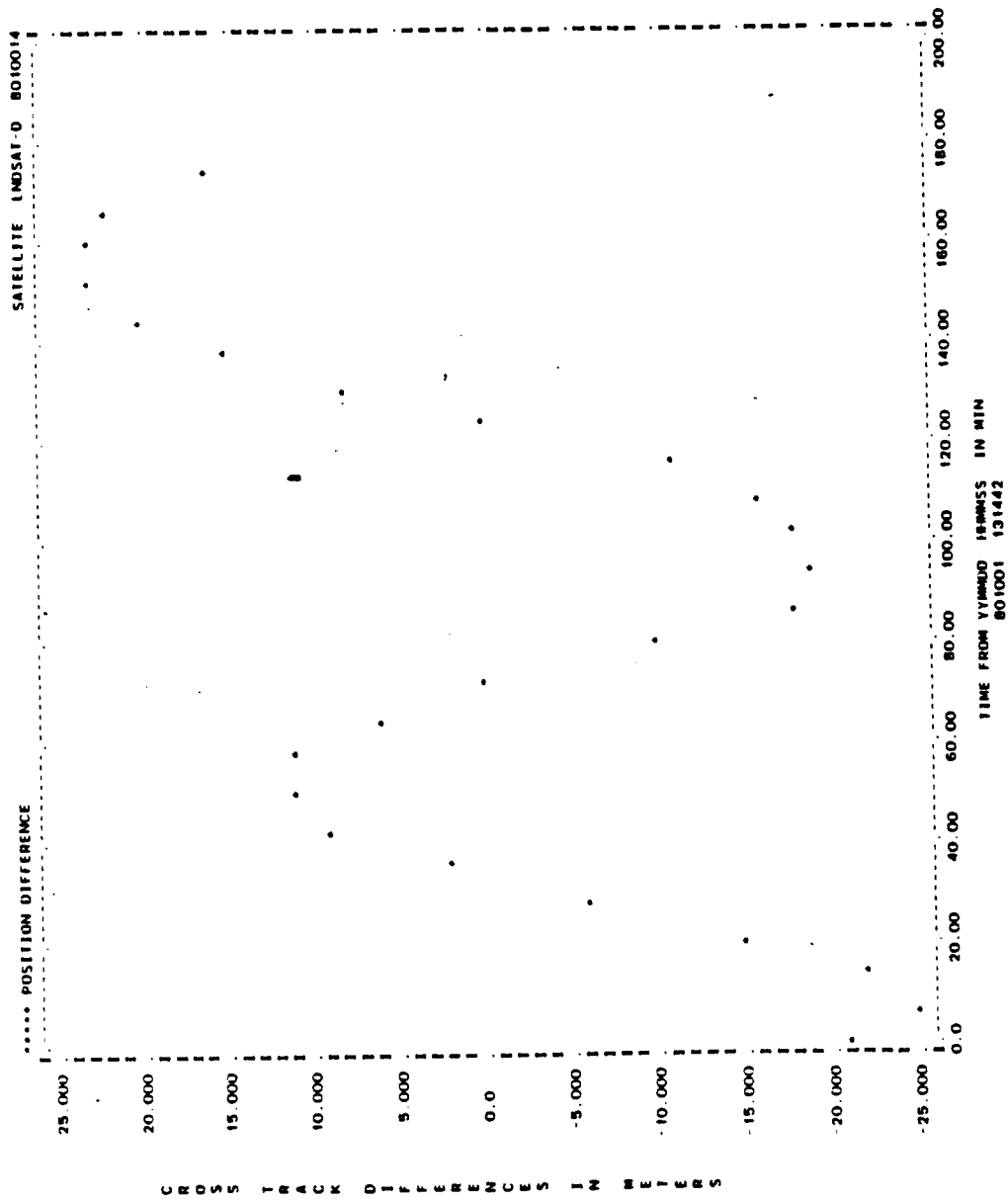


Figure A-41. Cross-Track Differences for Run L08 (2 of 2)

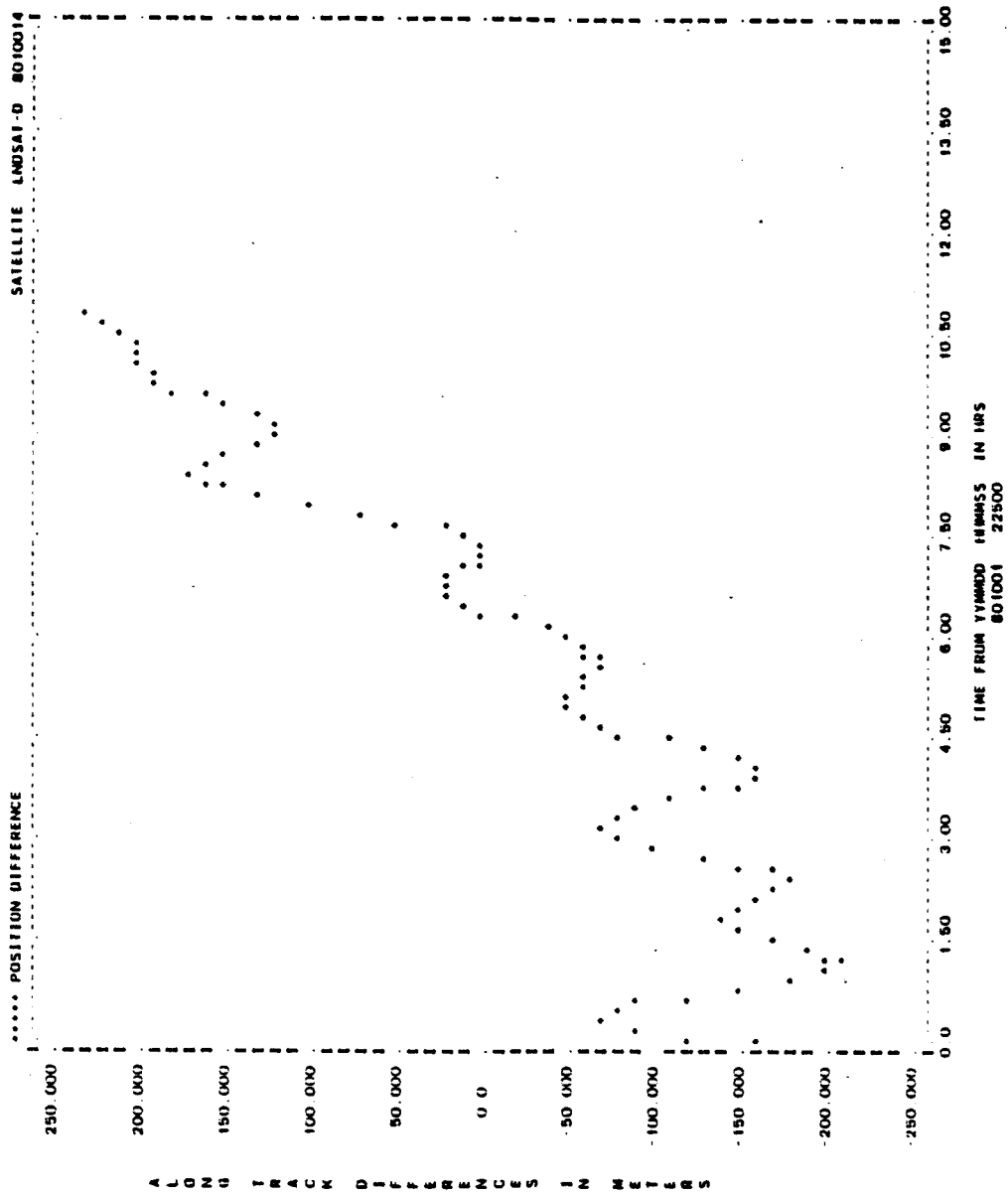


Figure A-42. Along-Track Differences for Run L08 (1 of 2)

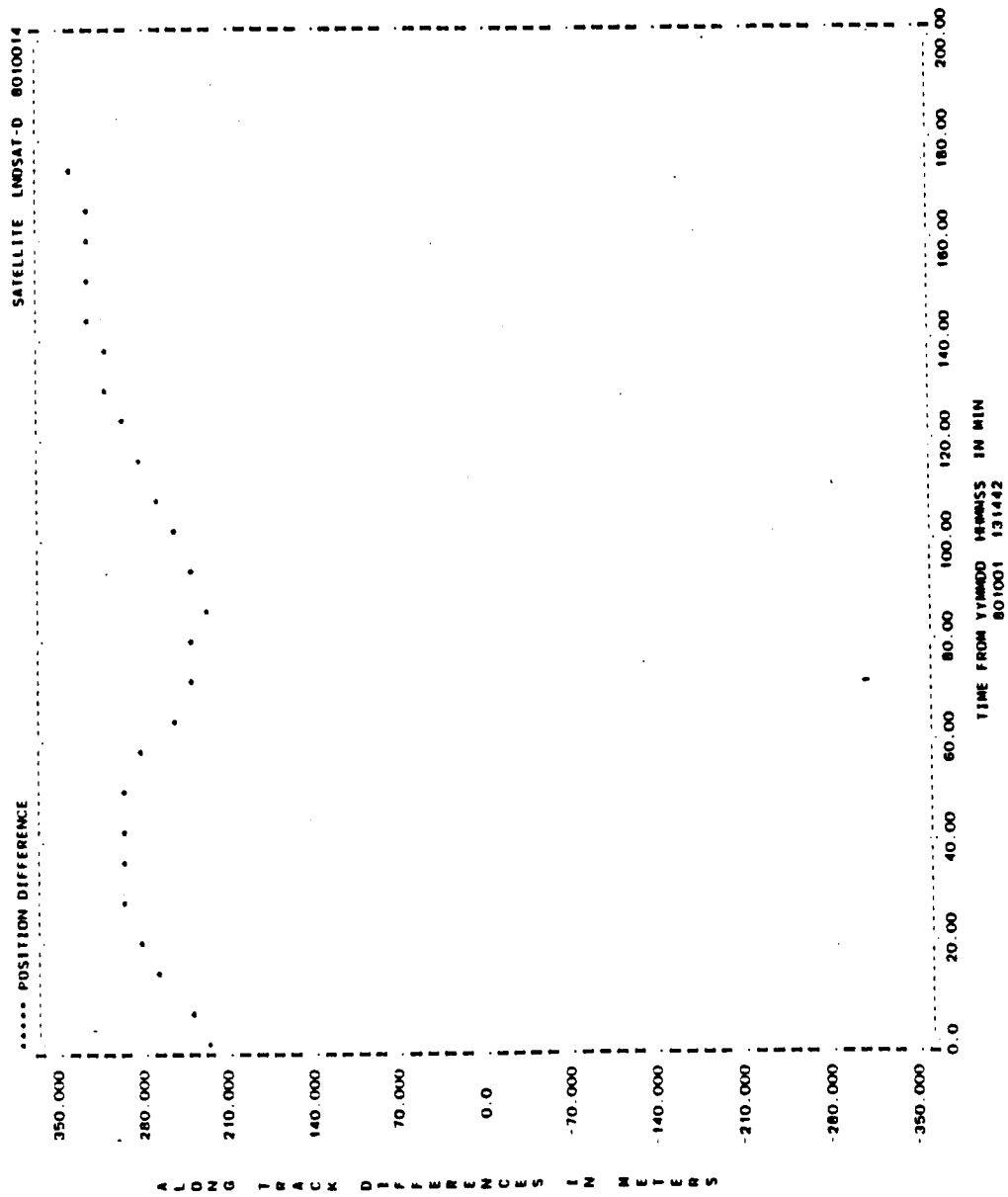


Figure A-42. Along-Track Differences for Run L08 (2 of 2)

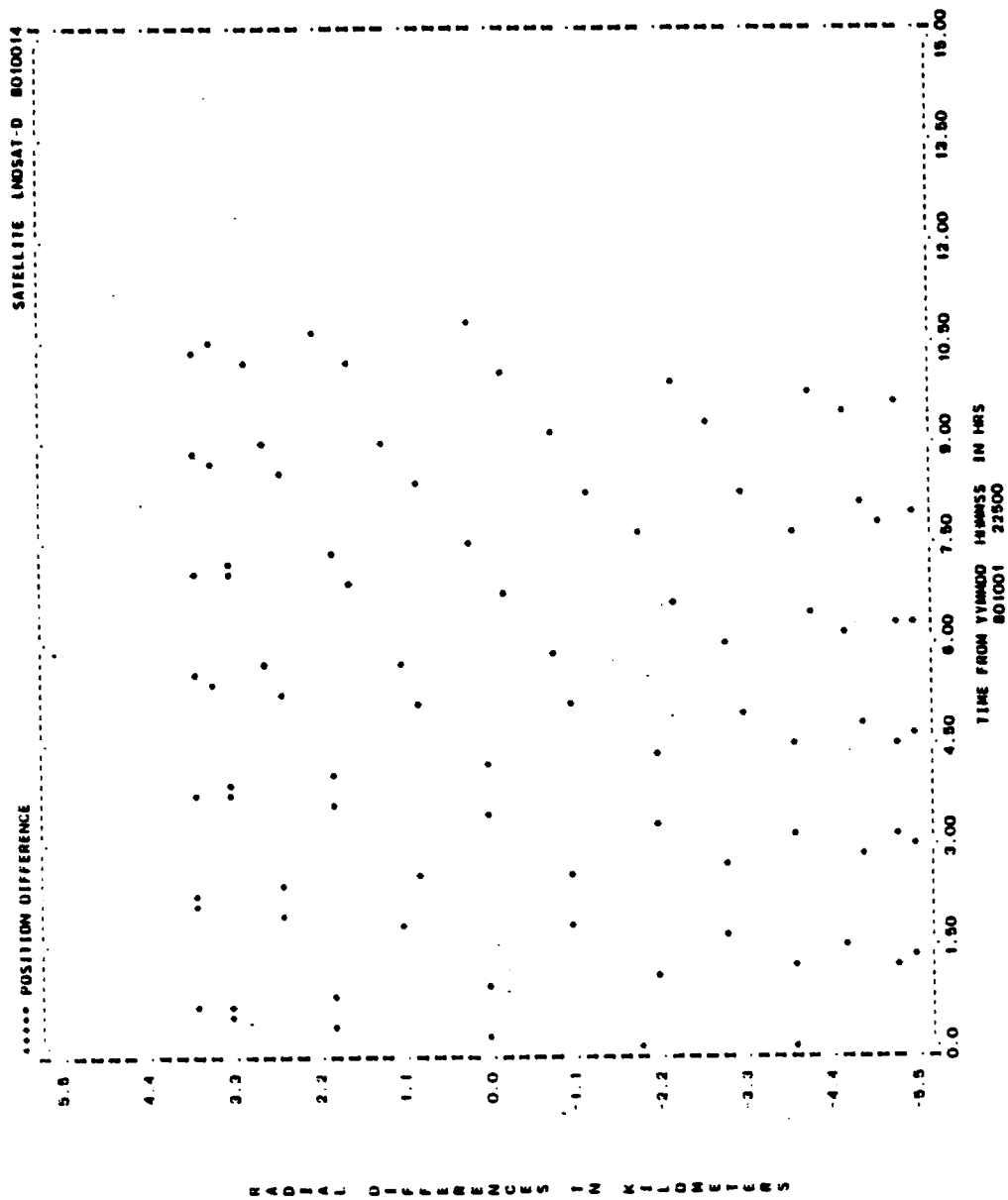


Figure A-43. Radial Differences for Run L09 (1 of 2)

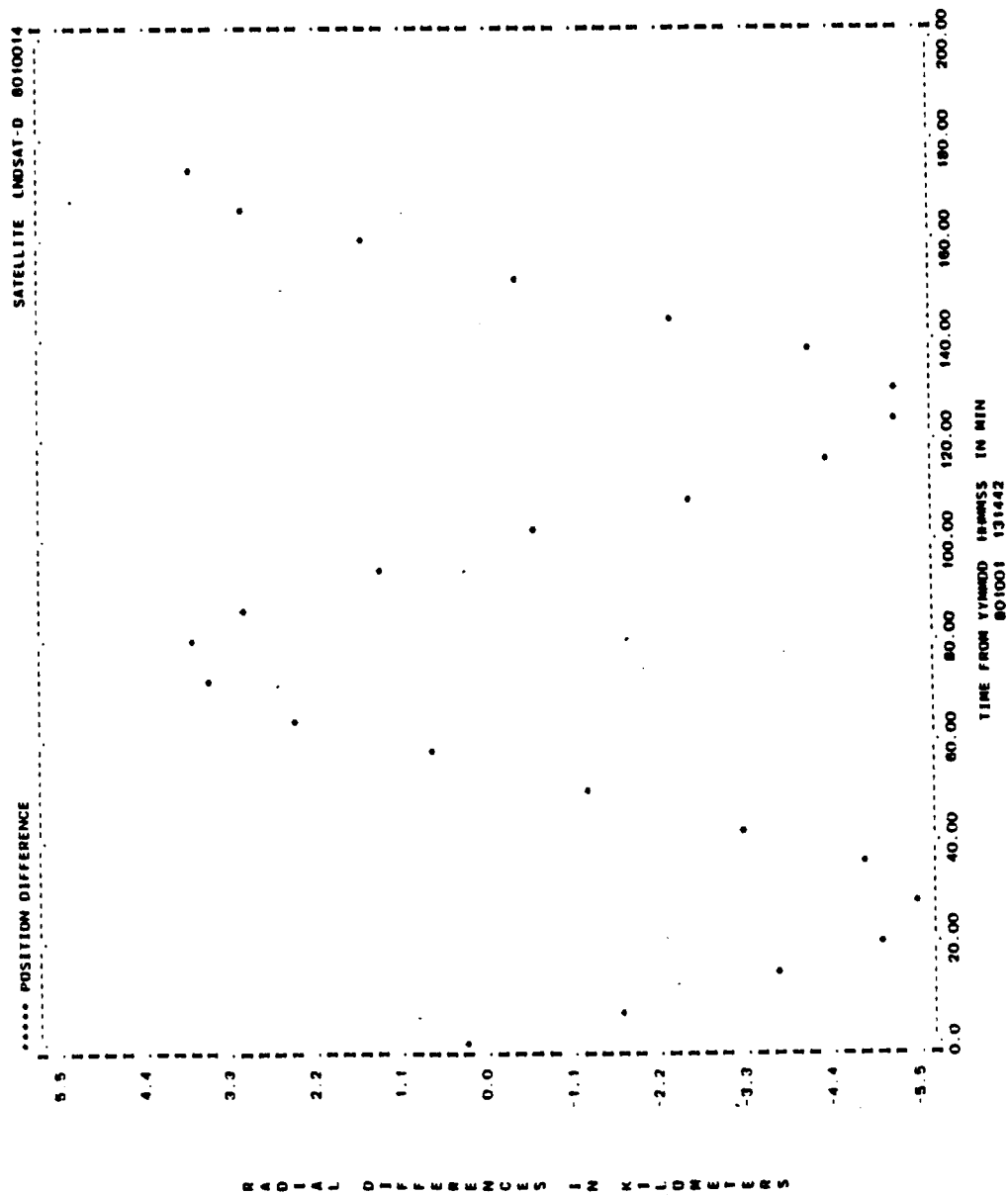


Figure A-43. Radial Differences for Run L09 (2 of 2)

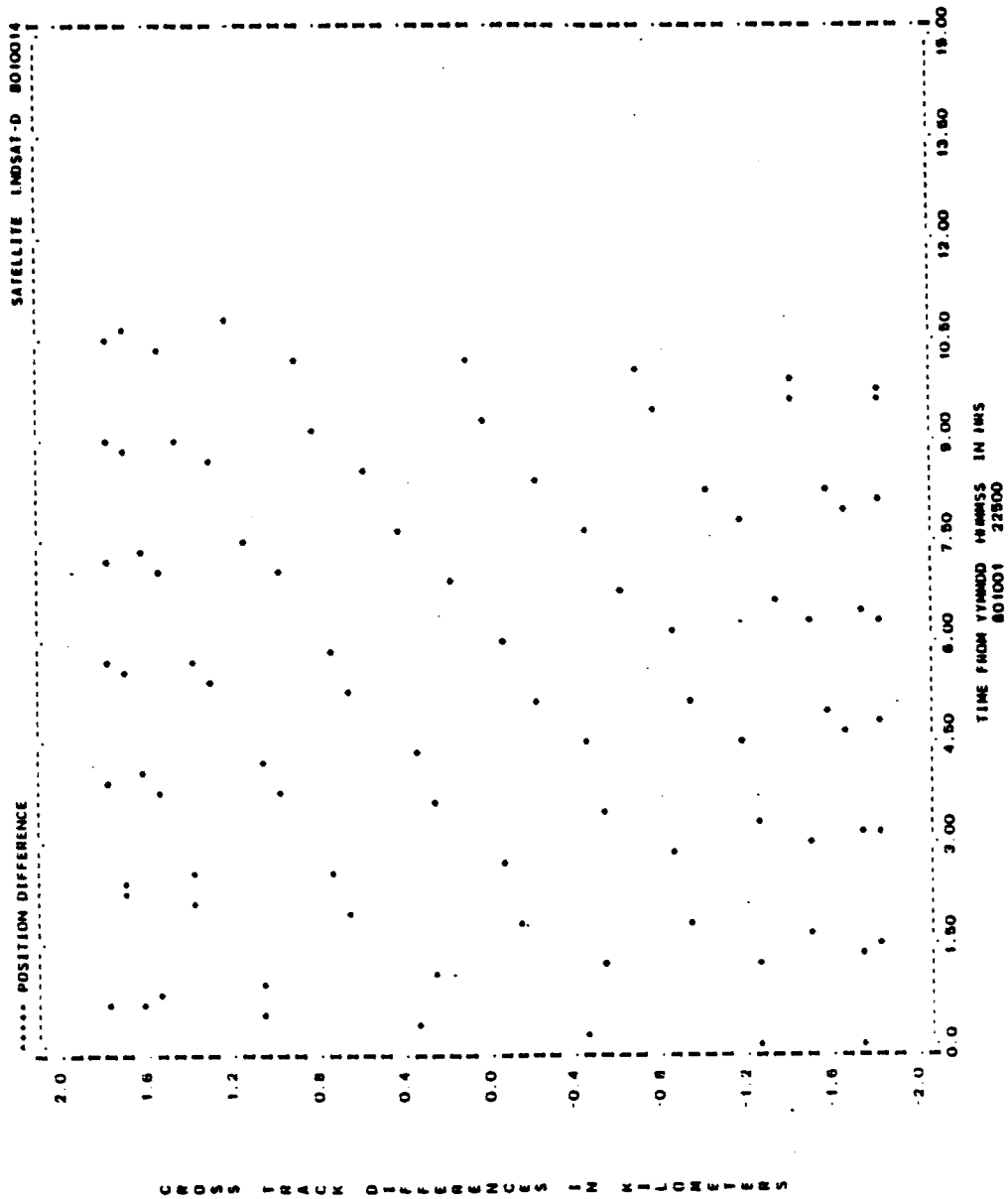


Figure A-44. Cross-Track Differences for Run L09 (1 of 2)

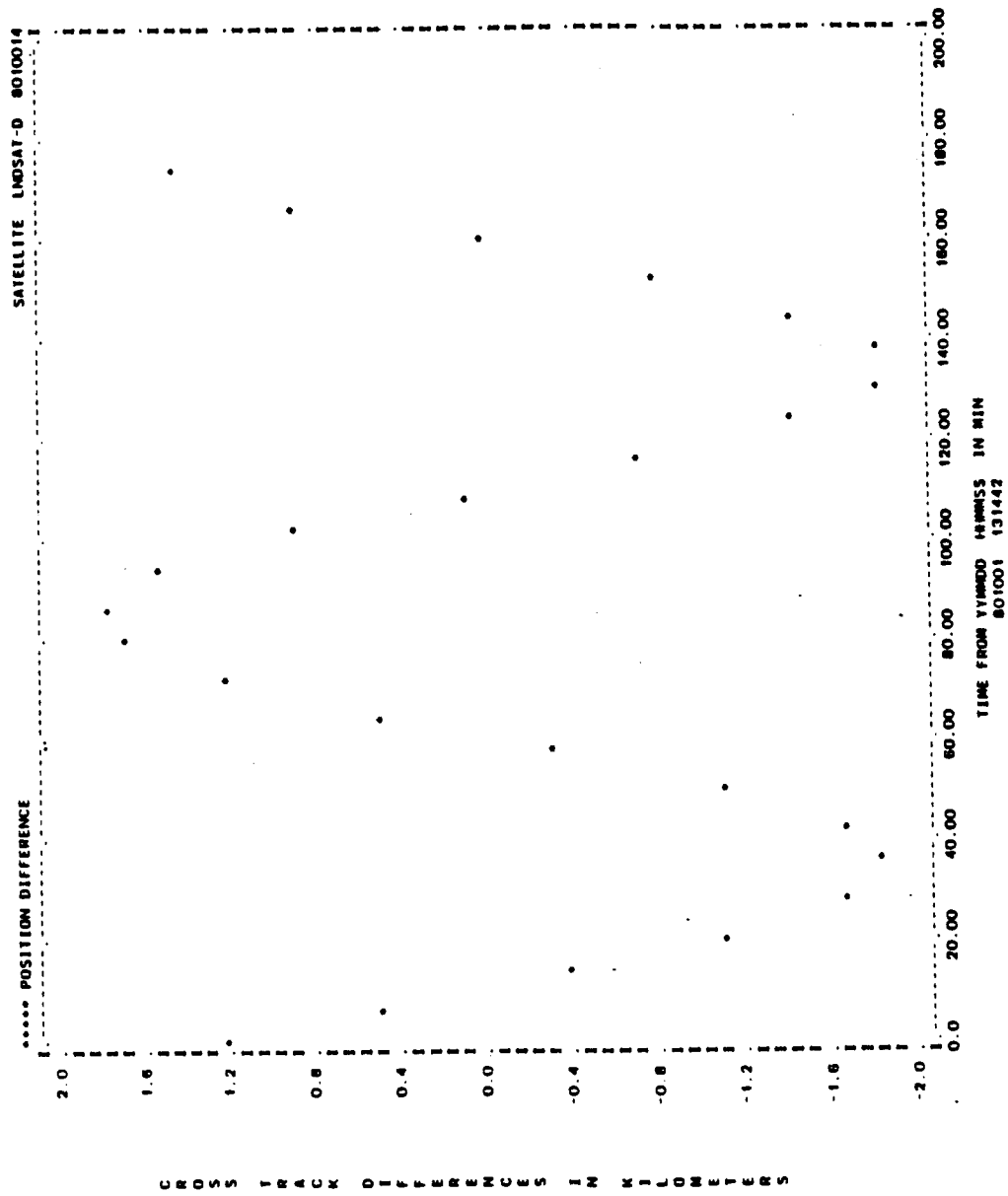


Figure A-44. Cross-Track Differences for Run L09 (2 of 2)

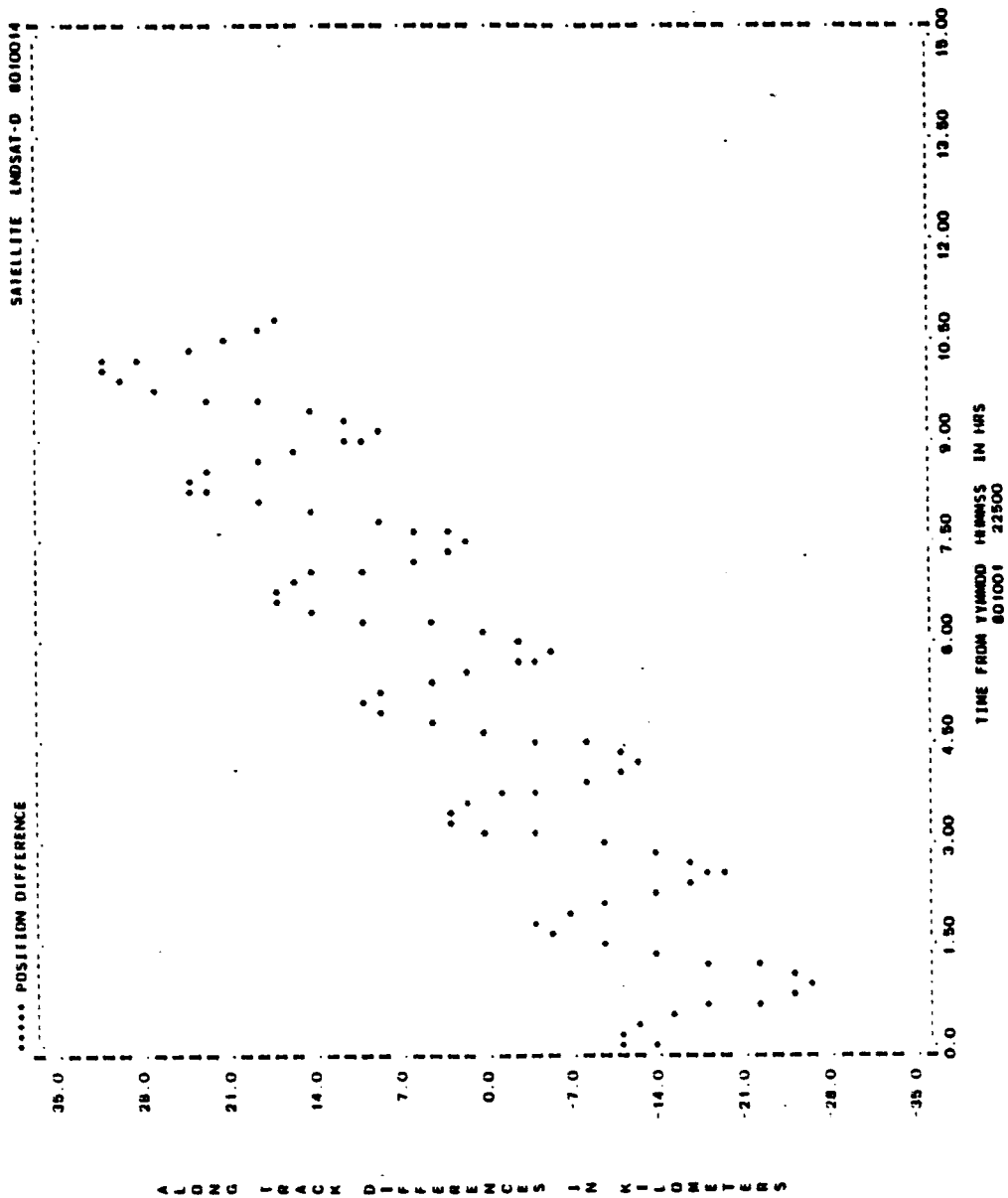


Figure A-45. Along-Track Differences for Run L09 (1 of 2)

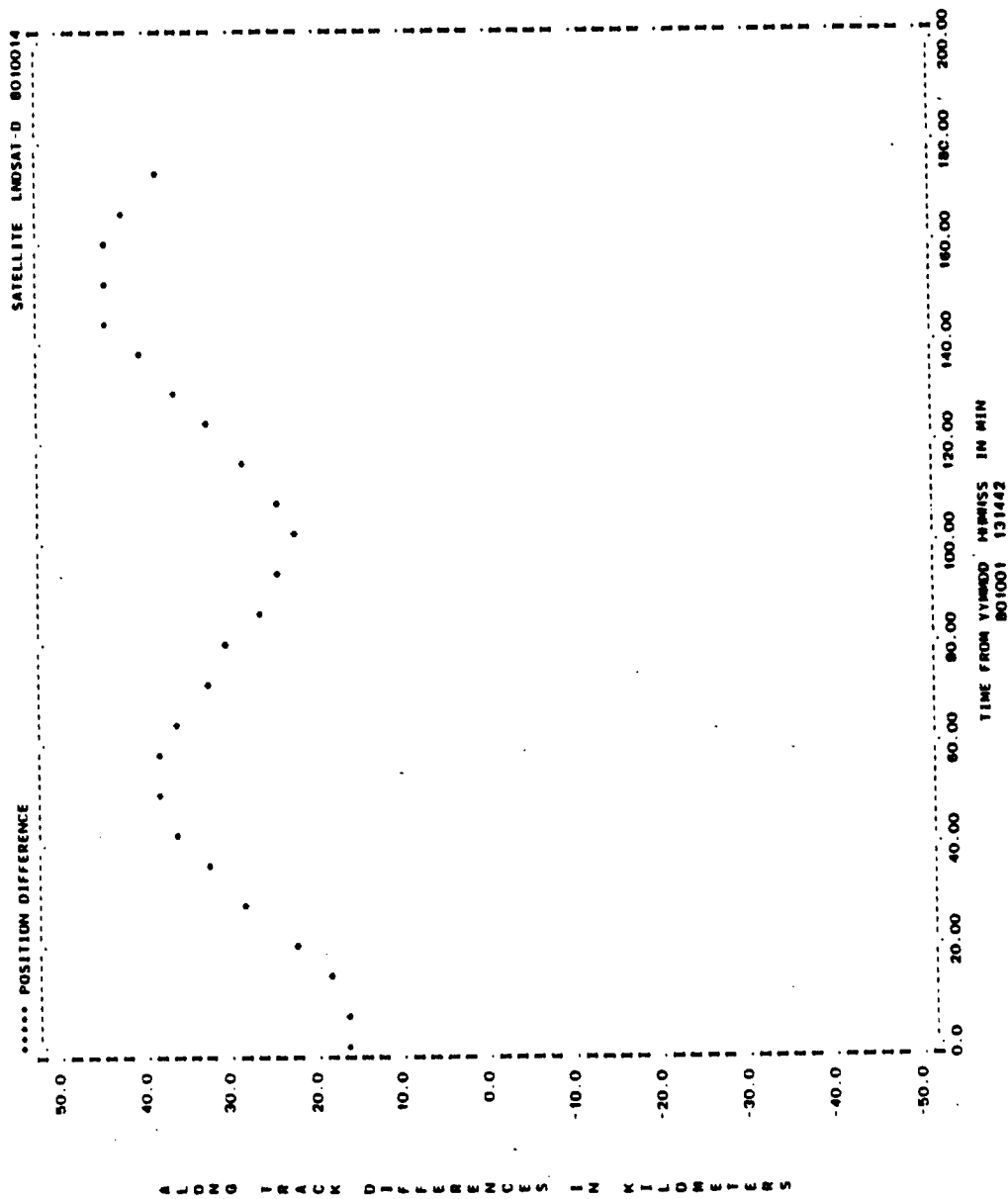


Figure A-45. Along-Track Differences for Run L09 (2 of 2)

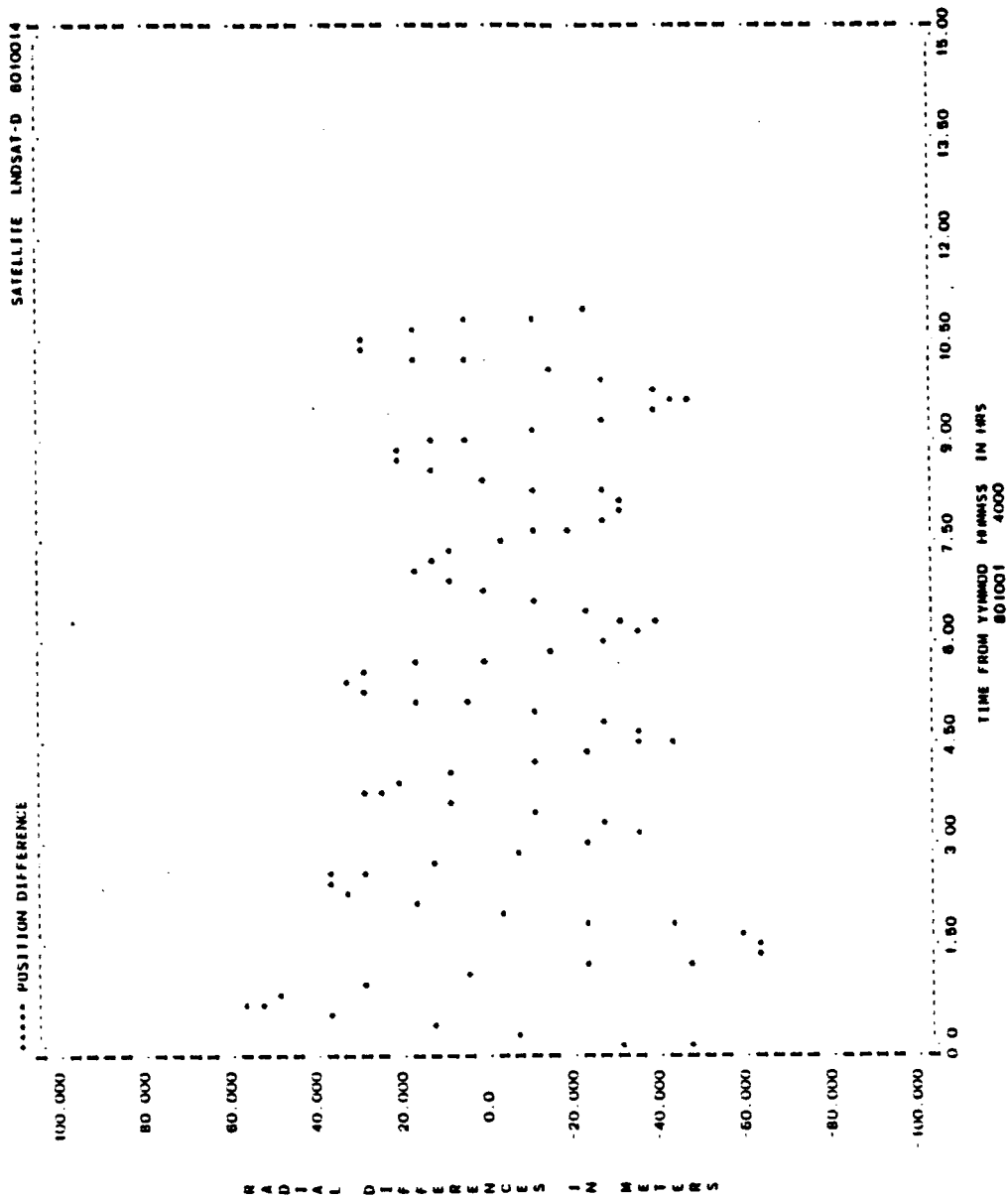


Figure A-46. Radial Differences for Run L10 (1 of 2)

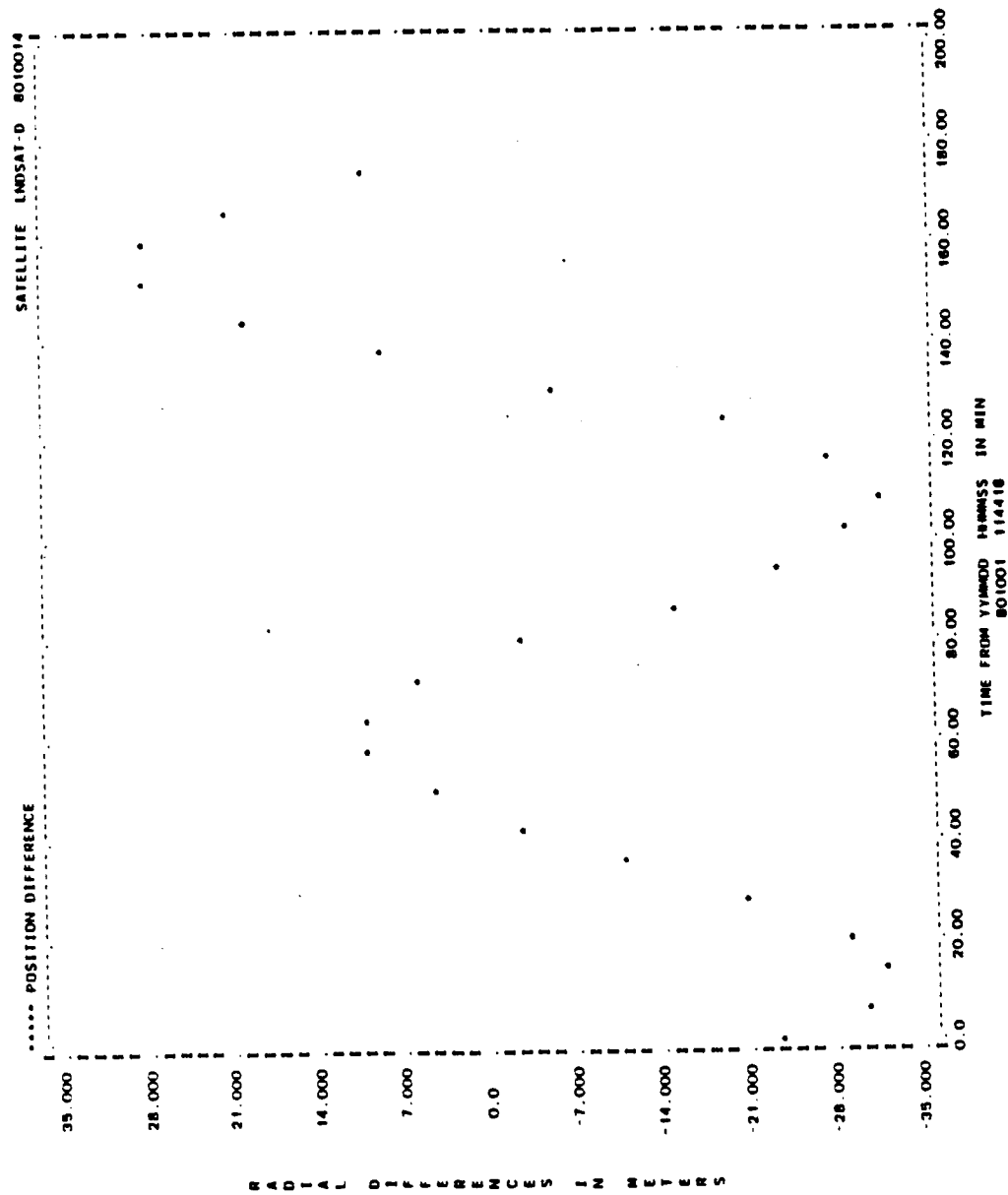


Figure A-46. Radial Differences for Run L10 (2 of 2)

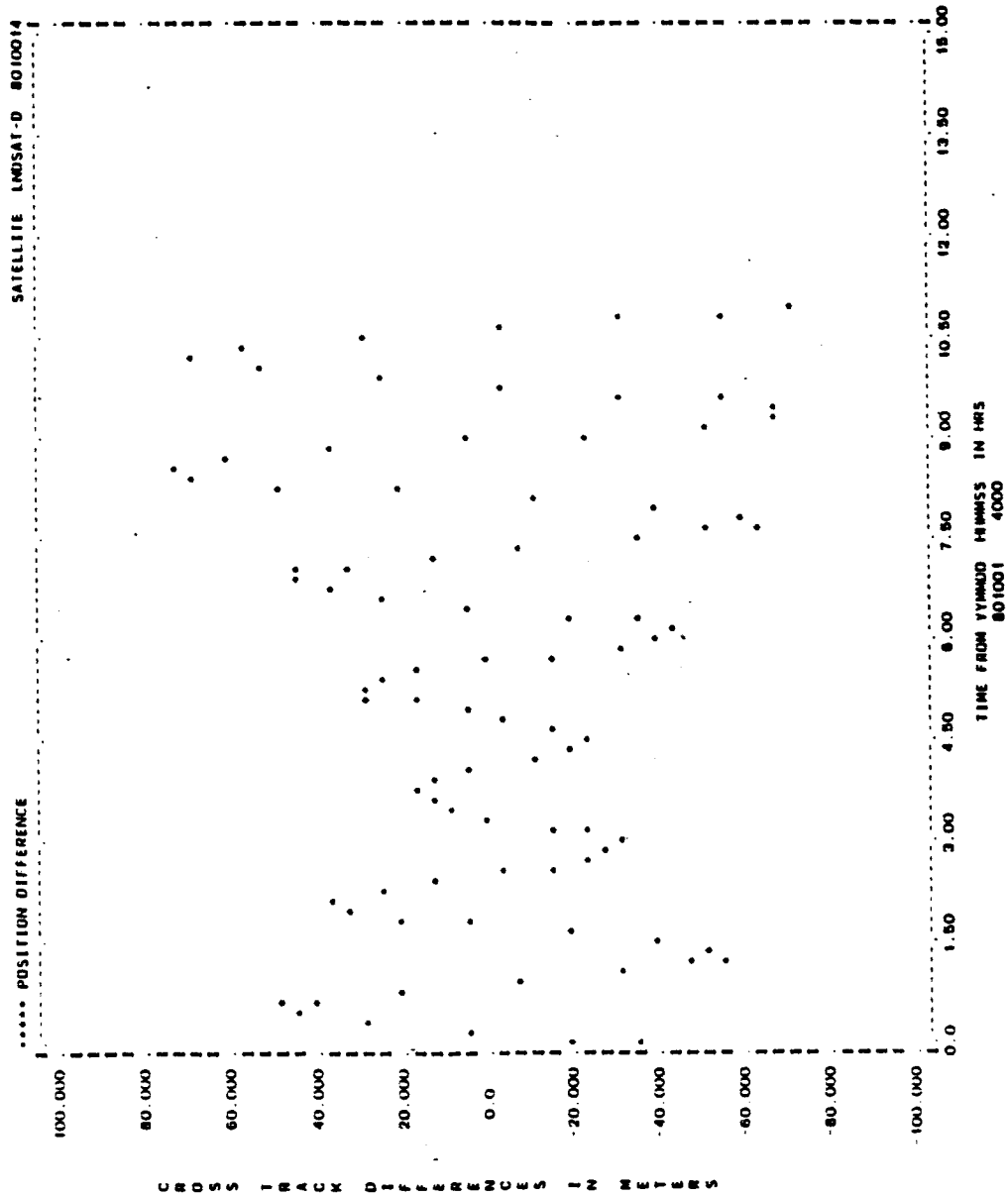


Figure A-47. Cross-Track Differences for Run L10 (1 of 2)

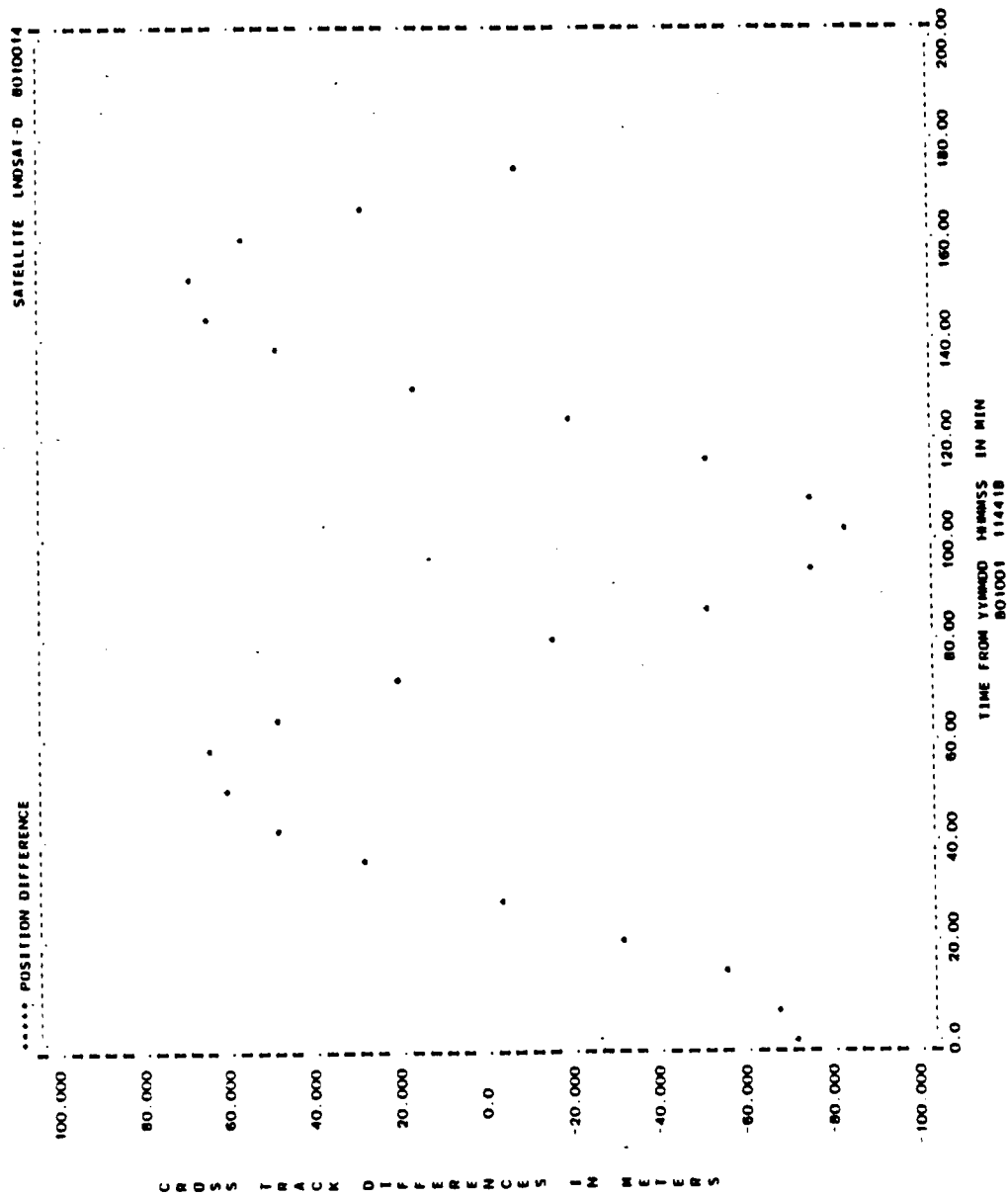


Figure A-47. Cross-Track Differences for Run L10 (2 of 2)

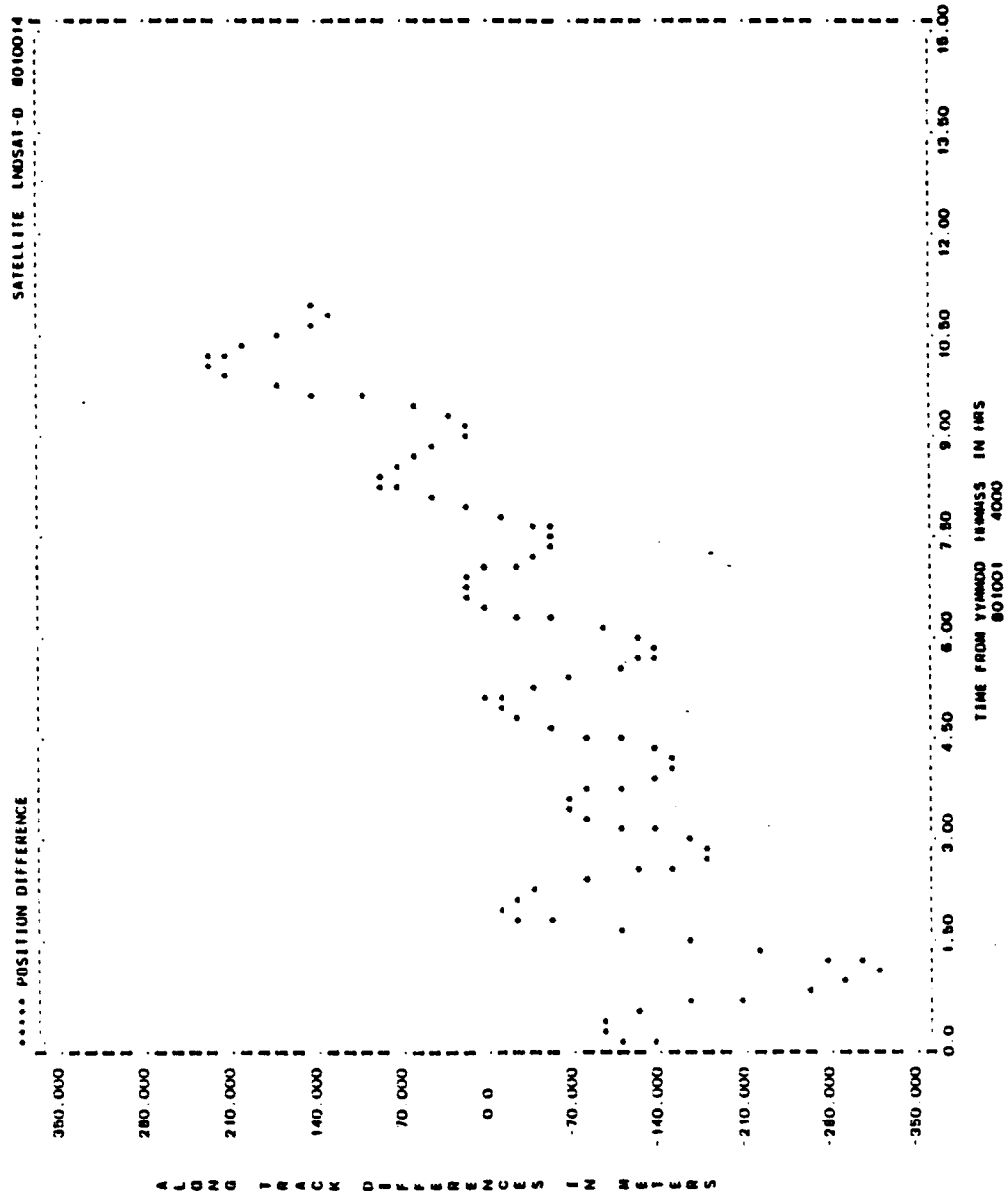


Figure A-48. Along-Track Differences for Run L10 (1 of 2)

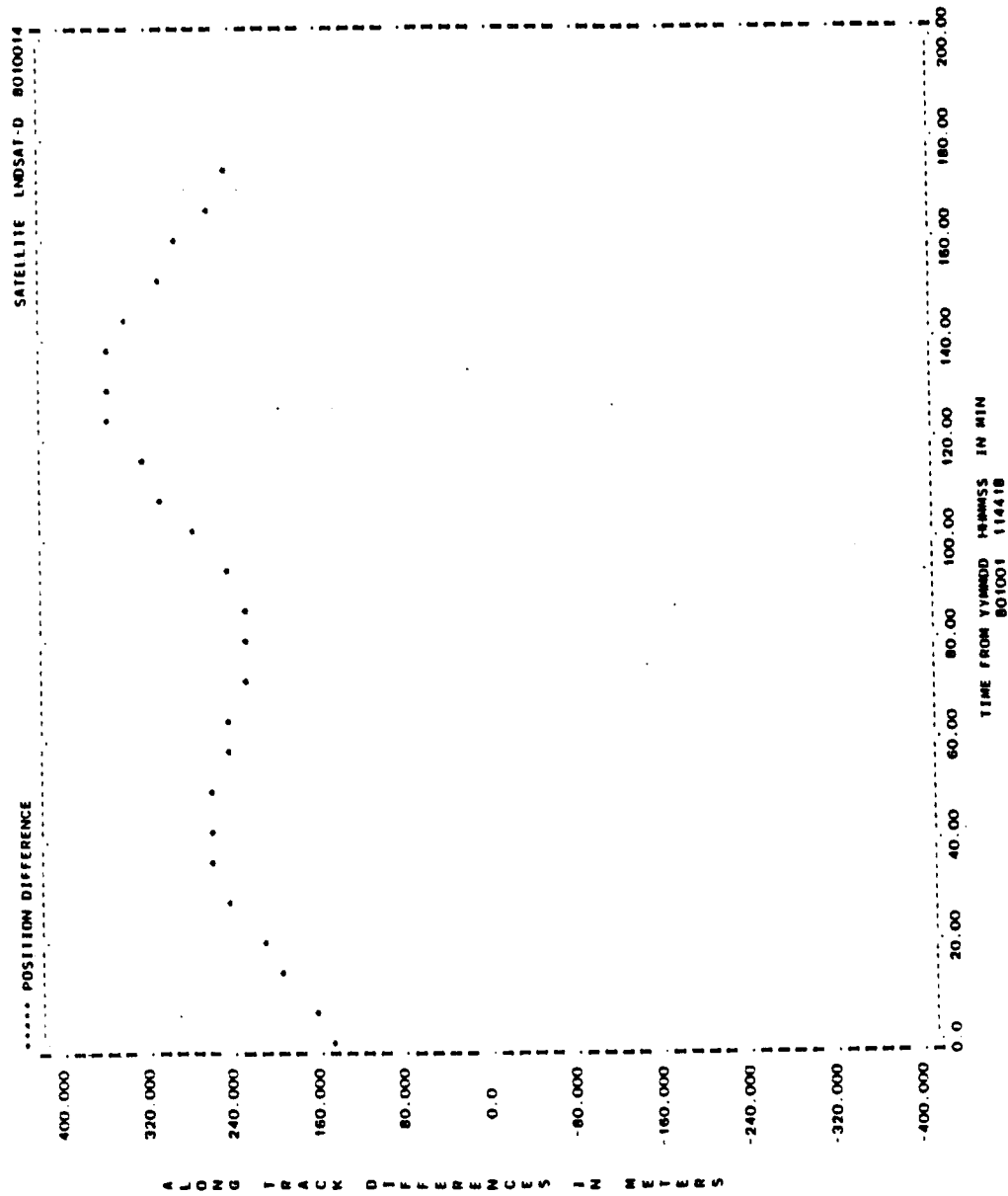


Figure A-48. Along-Track Differences for Run L10 (2 of 2)

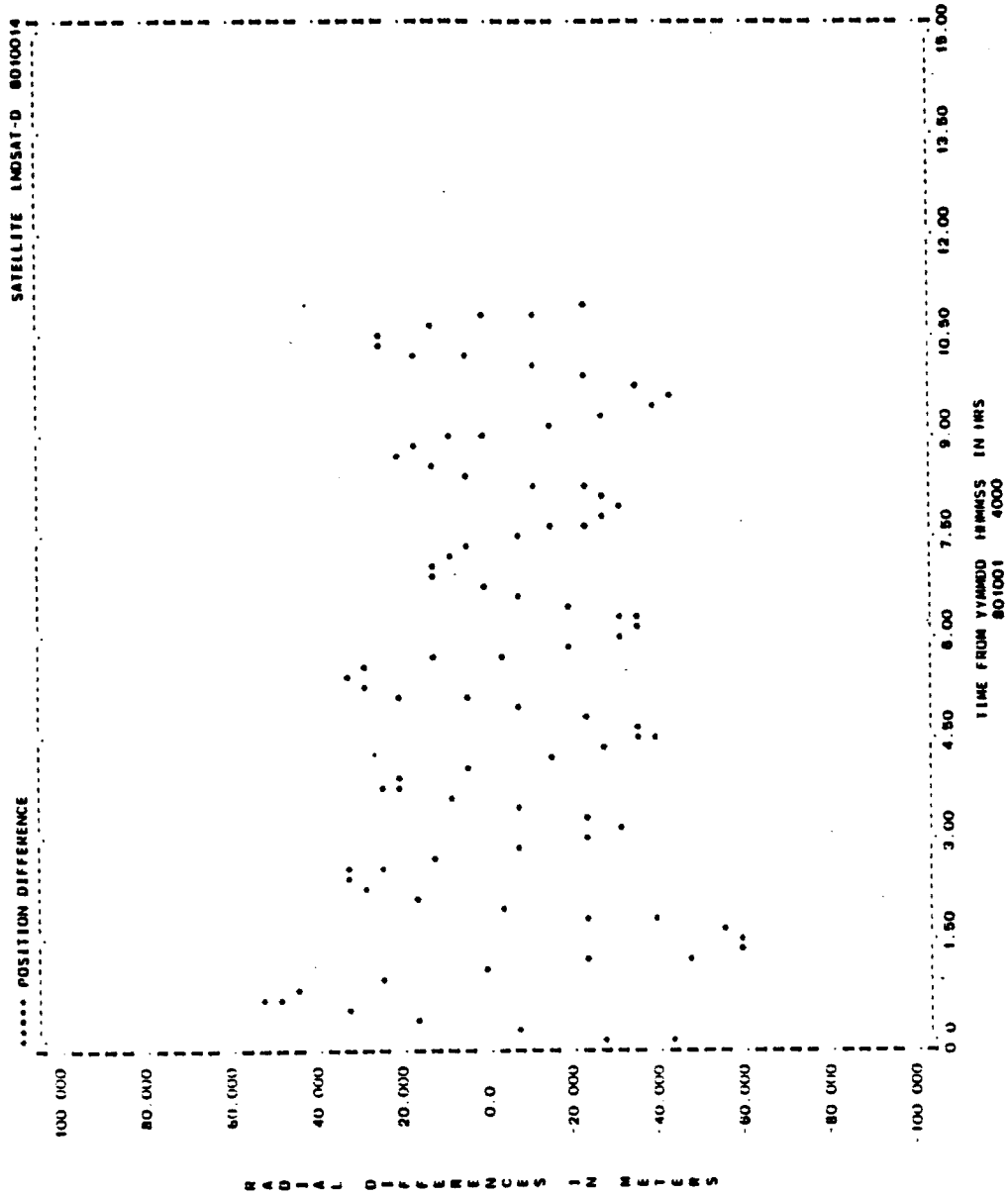


Figure A-49. Radial Differences for Run L22 (1 of 2)

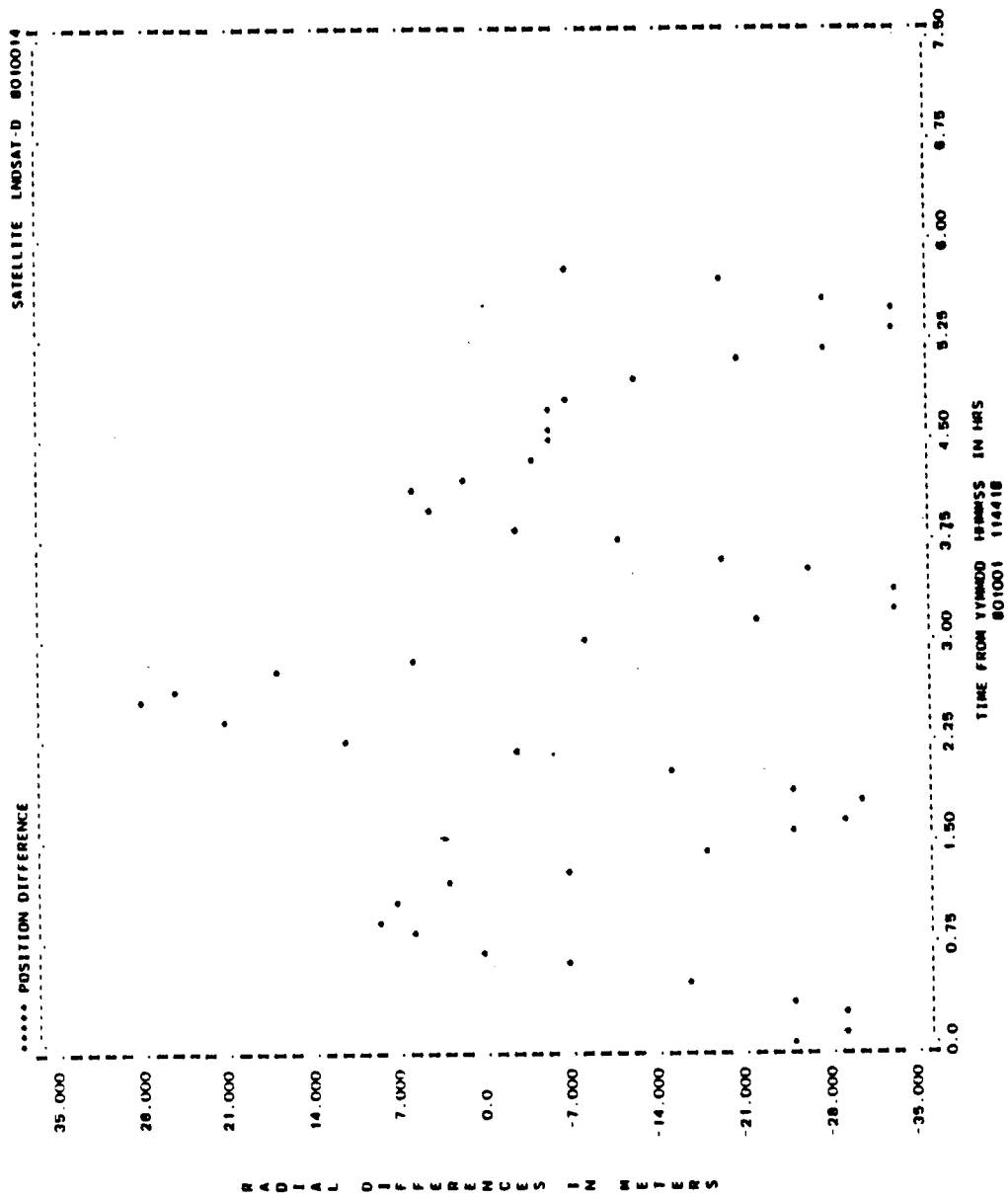


Figure A-49. Radial Differences for Run L22 (2 of 2)

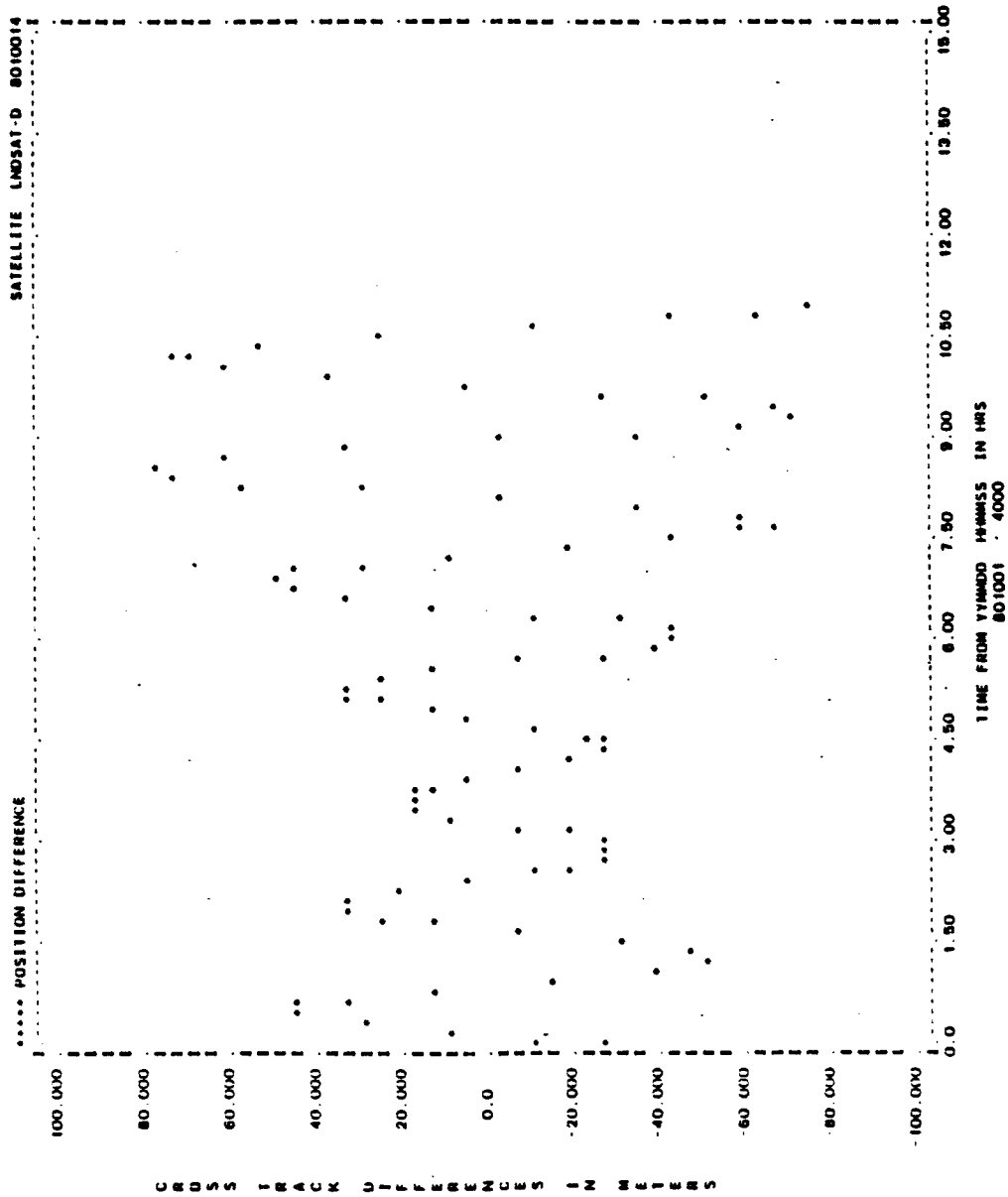


Figure A-50. Cross-Track Differences for Run L22 (1 of 2)

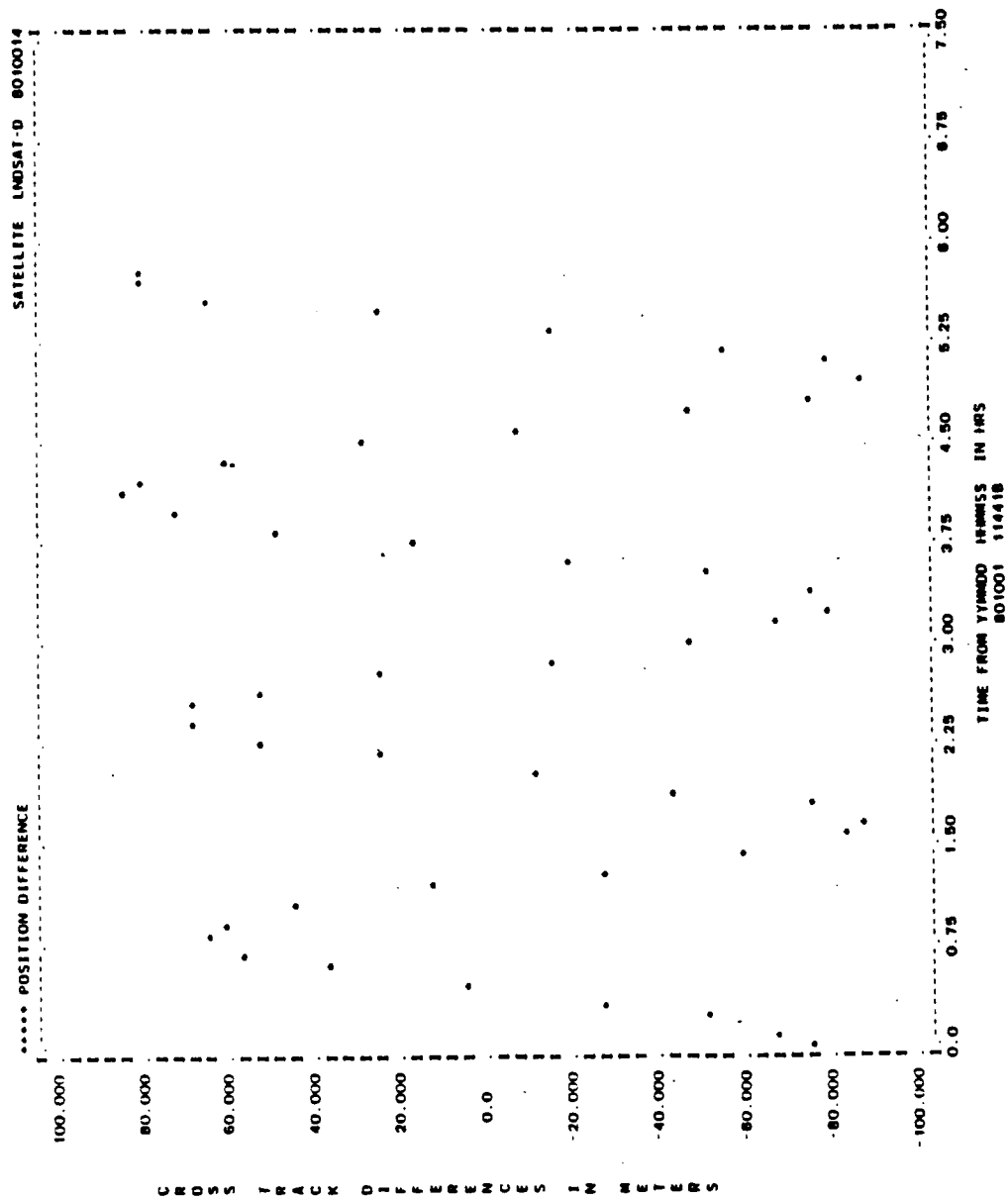


Figure A-50. Cross-Track Differences for Run L22 (2 of 2)

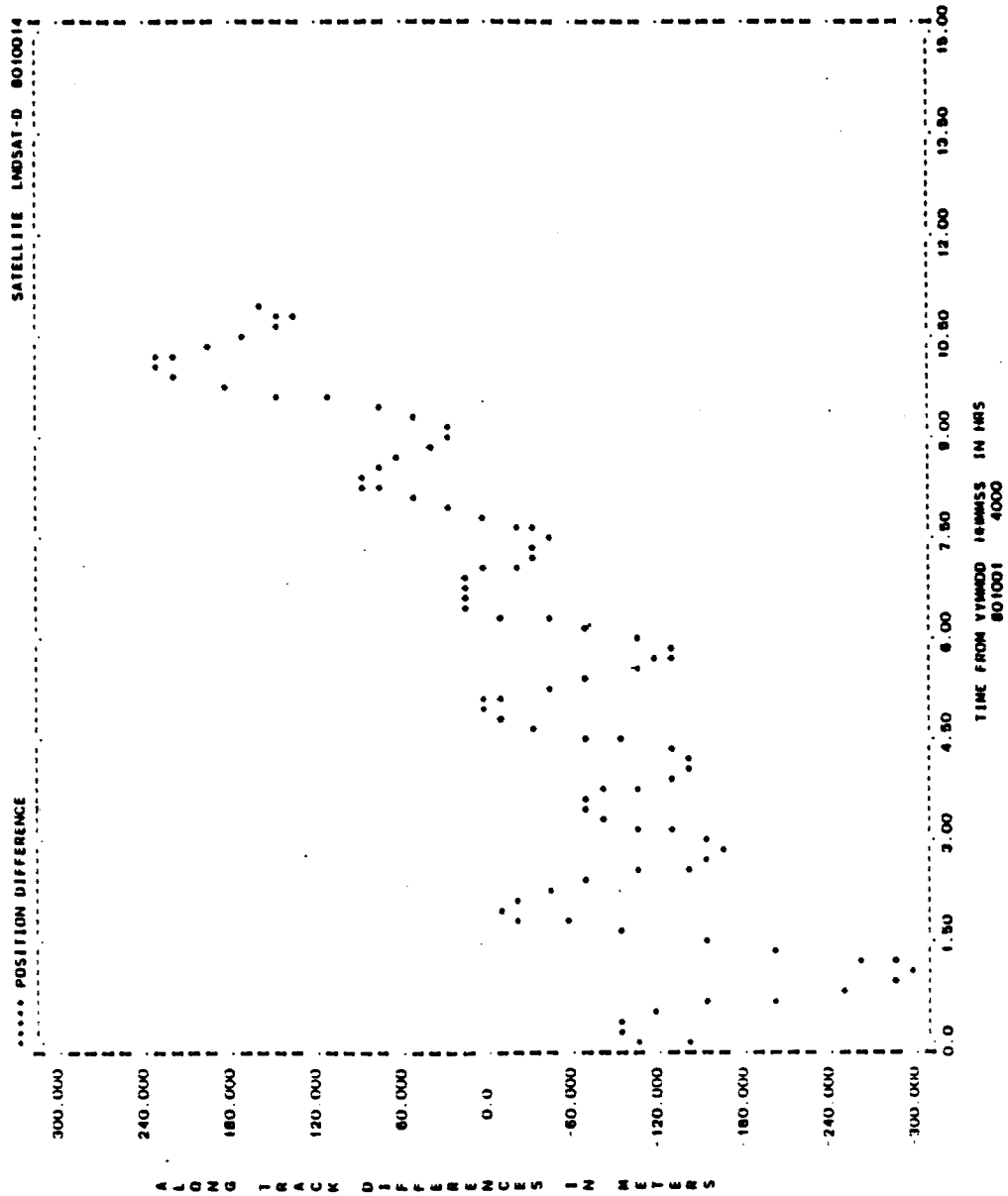


Figure A-51. Along-Track Differences for Run L22 (1 of 2)

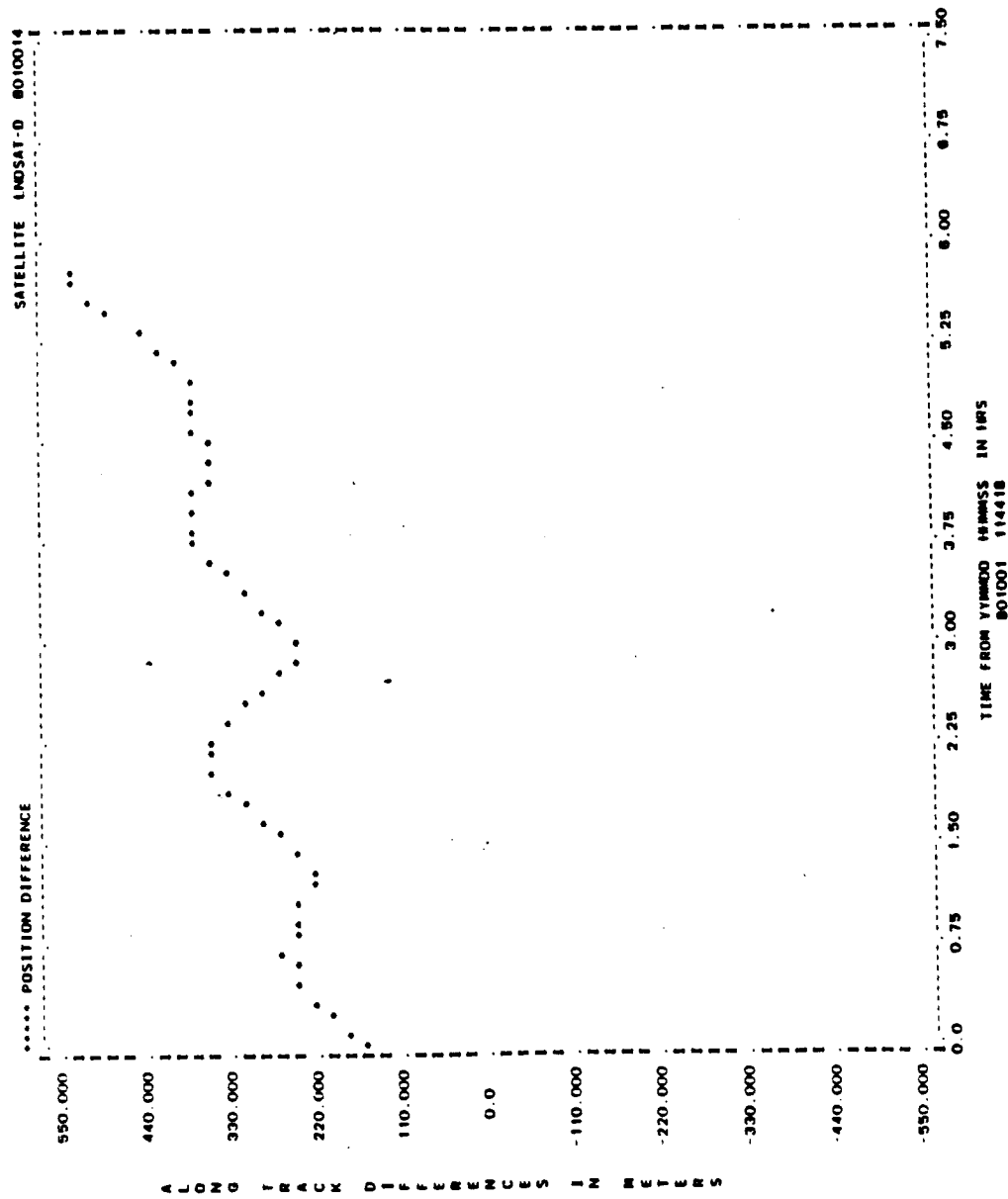


Figure A-51. Along-Track Differences for Run L22 (2 of 2)

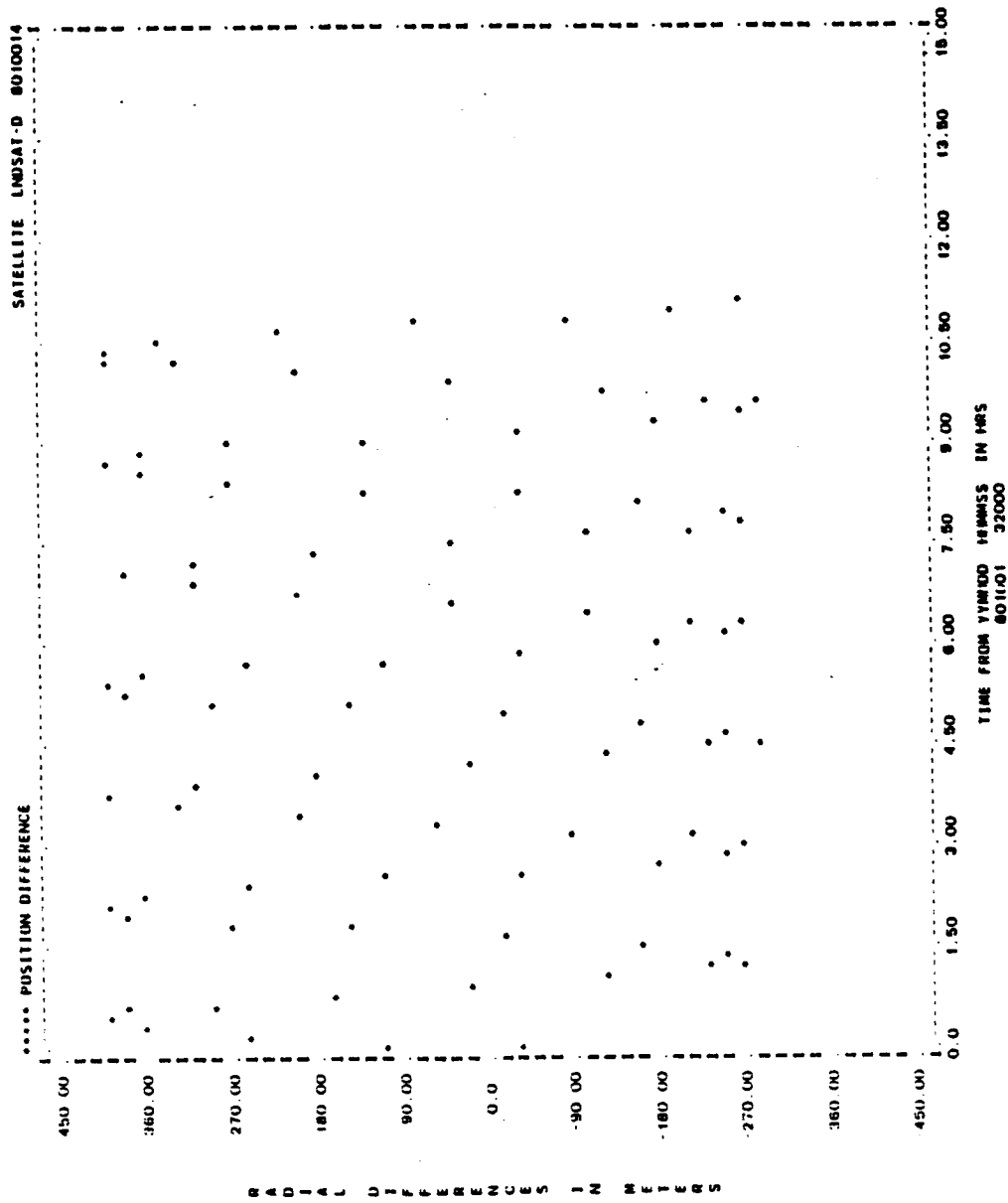
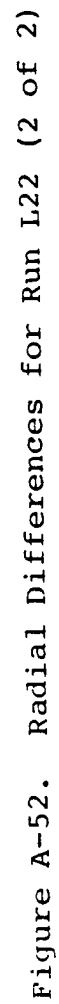


Figure A-52. Radial Differences for Run L22 (1 of 2)



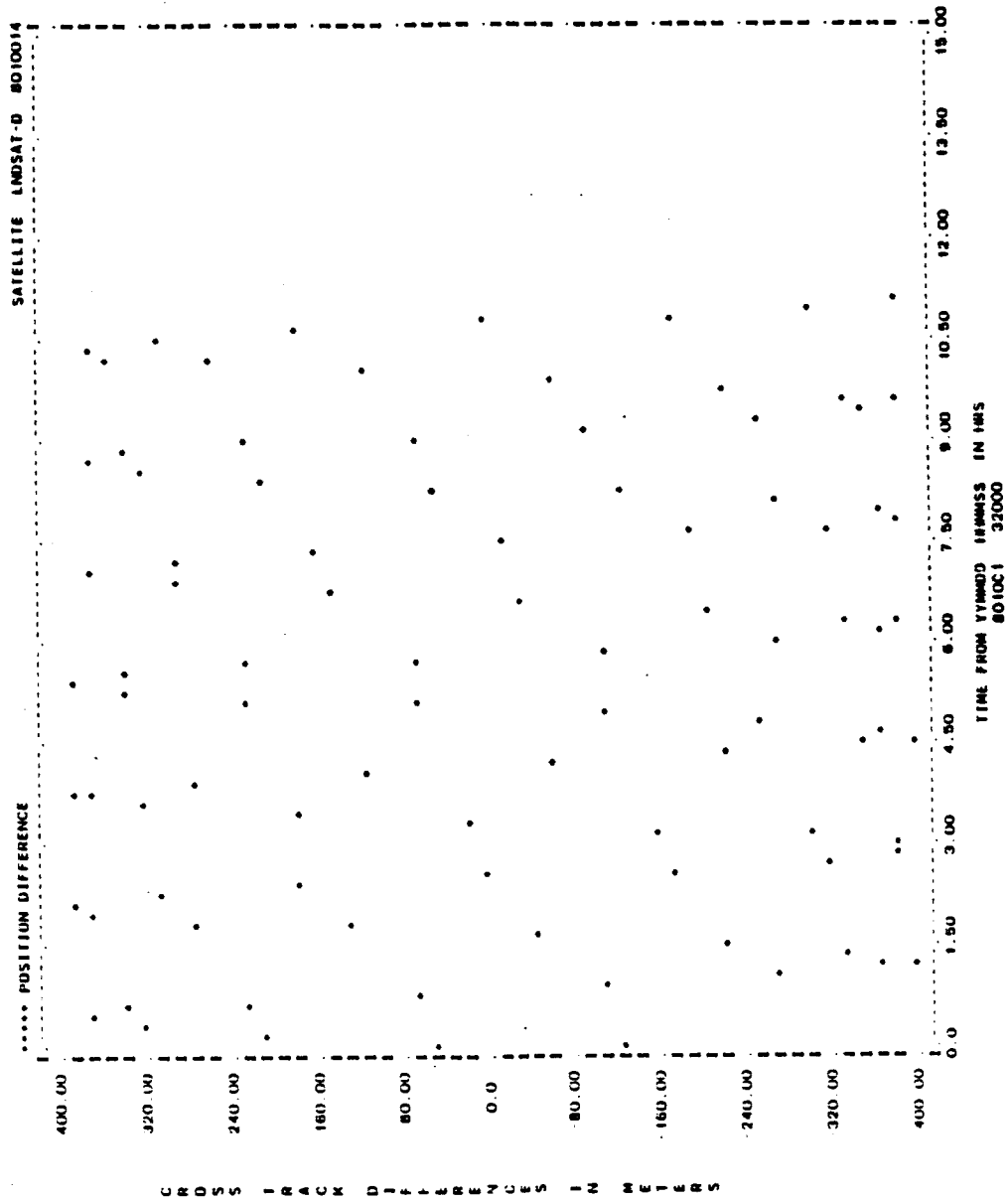


Figure A-53. Cross-Track Differences for Run L22 (1 of 2)

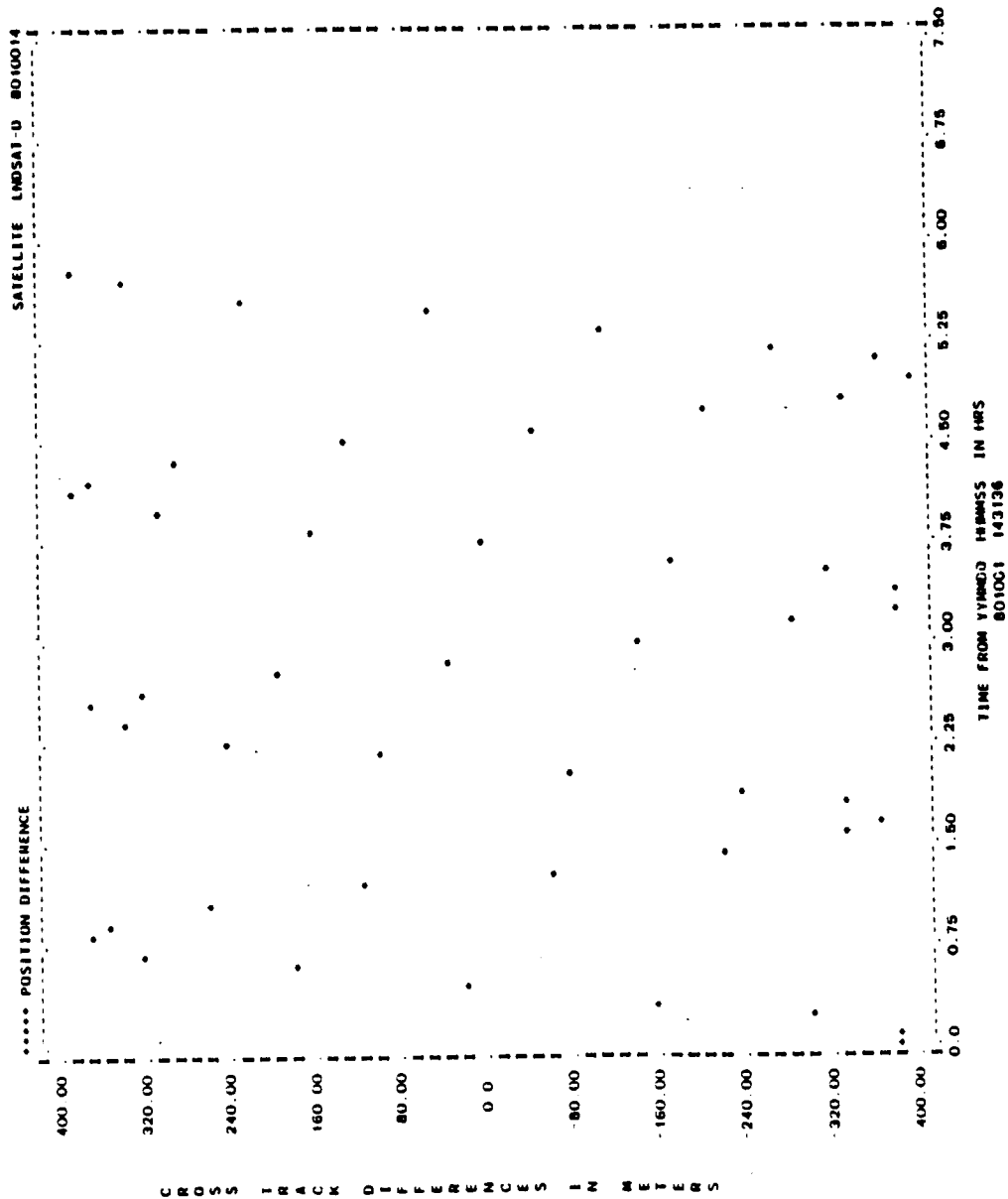


Figure A-53. Cross-Track Differences for Run L22 (2 of 2)

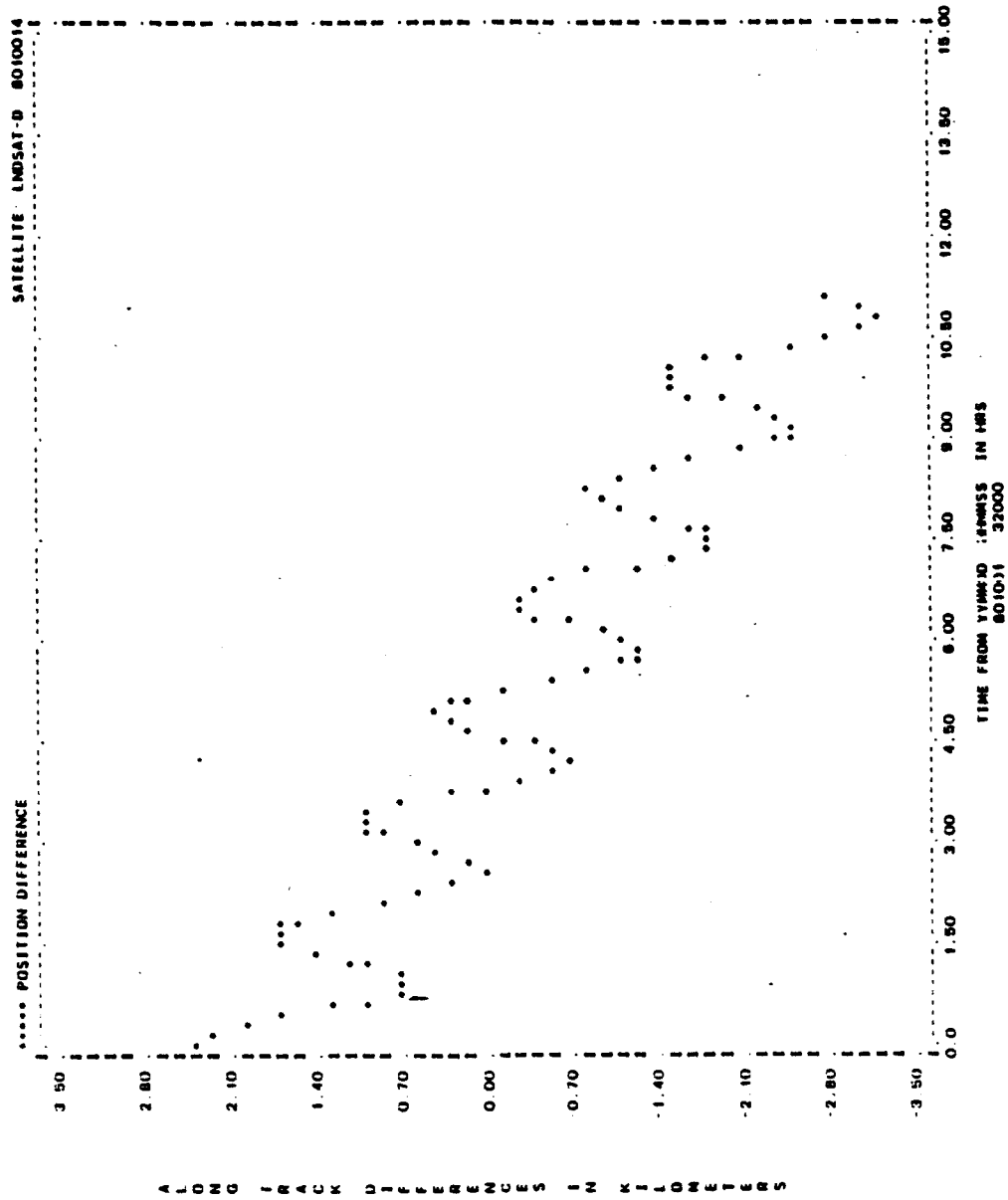


Figure A-54. Along-Track Differences for Run L22 (1 of 2)

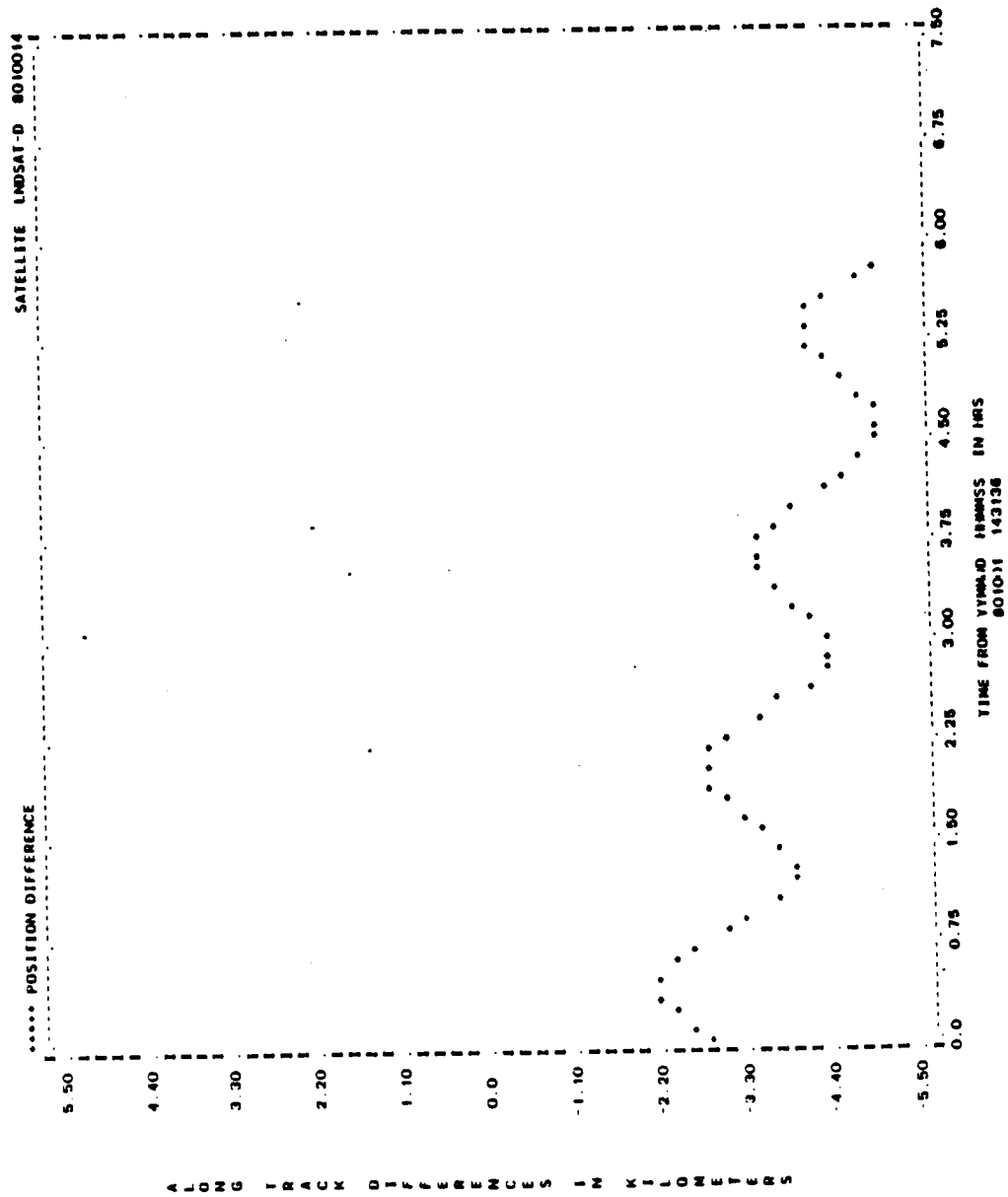


Figure A-54. Along-Track Differences for Run L22 (2 of 2)

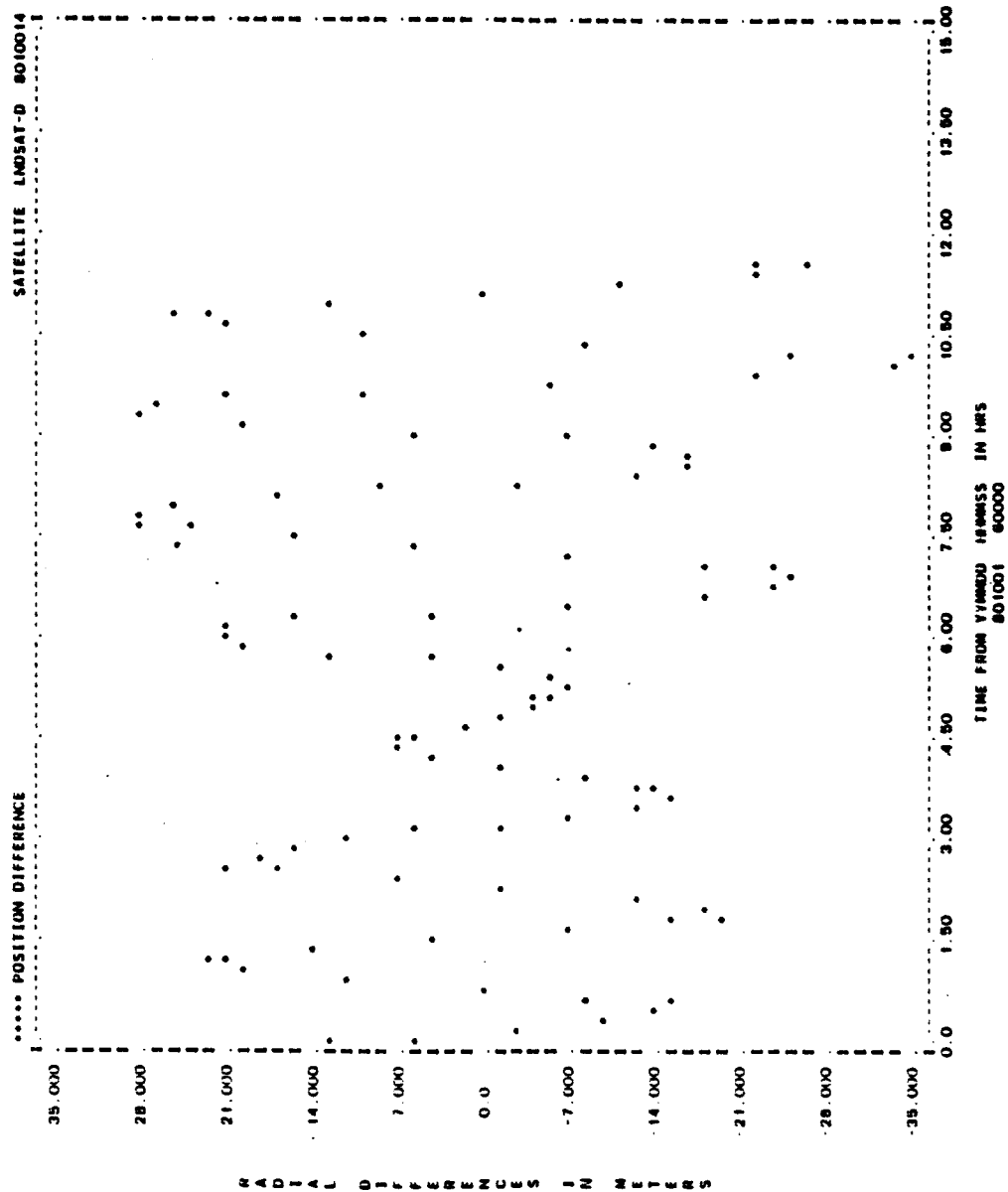


Figure A-55. Radial Differences for Run L22 (1 of 2)

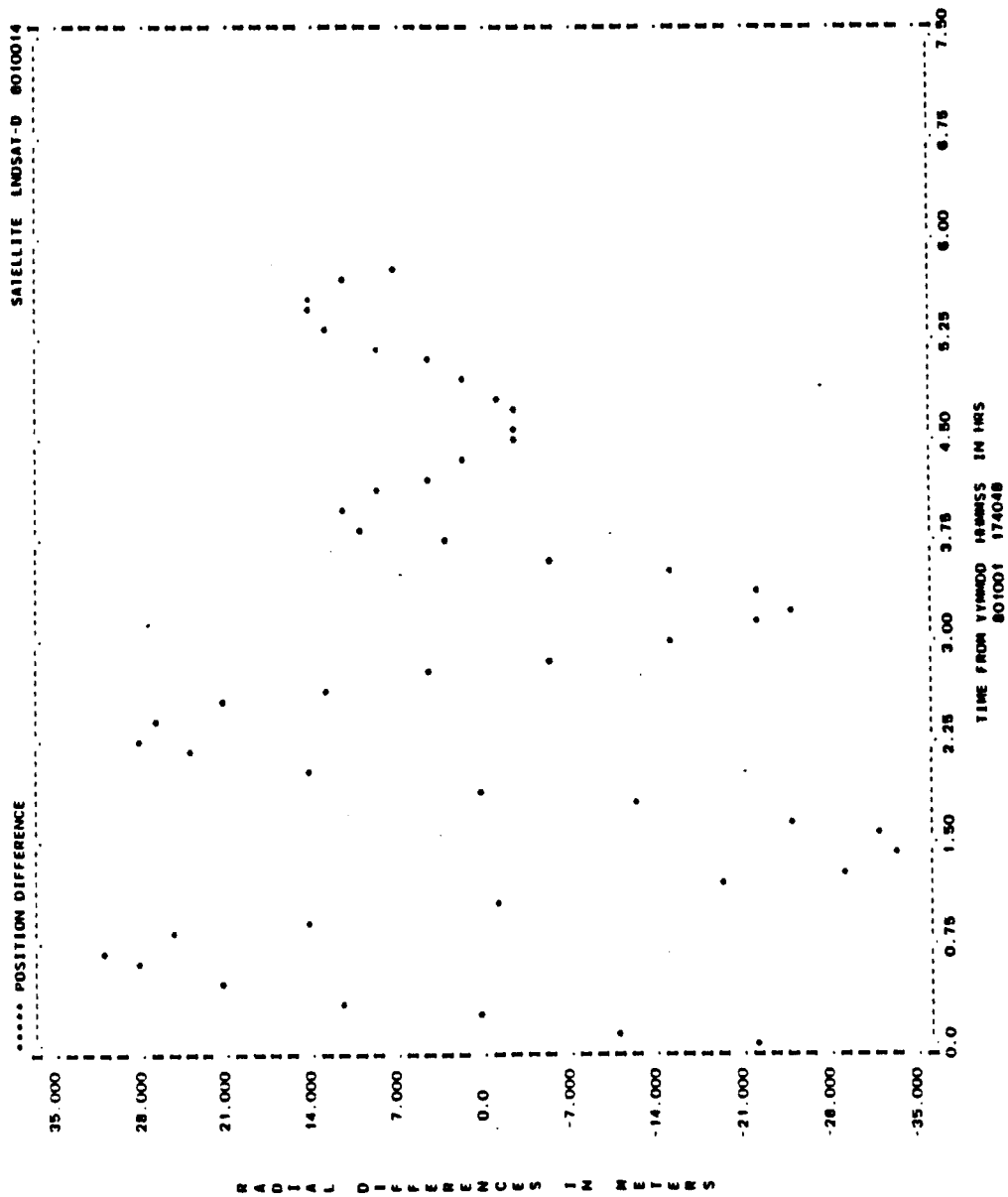


Figure A-55. Radial Differences for Run L22 (2 of 2)

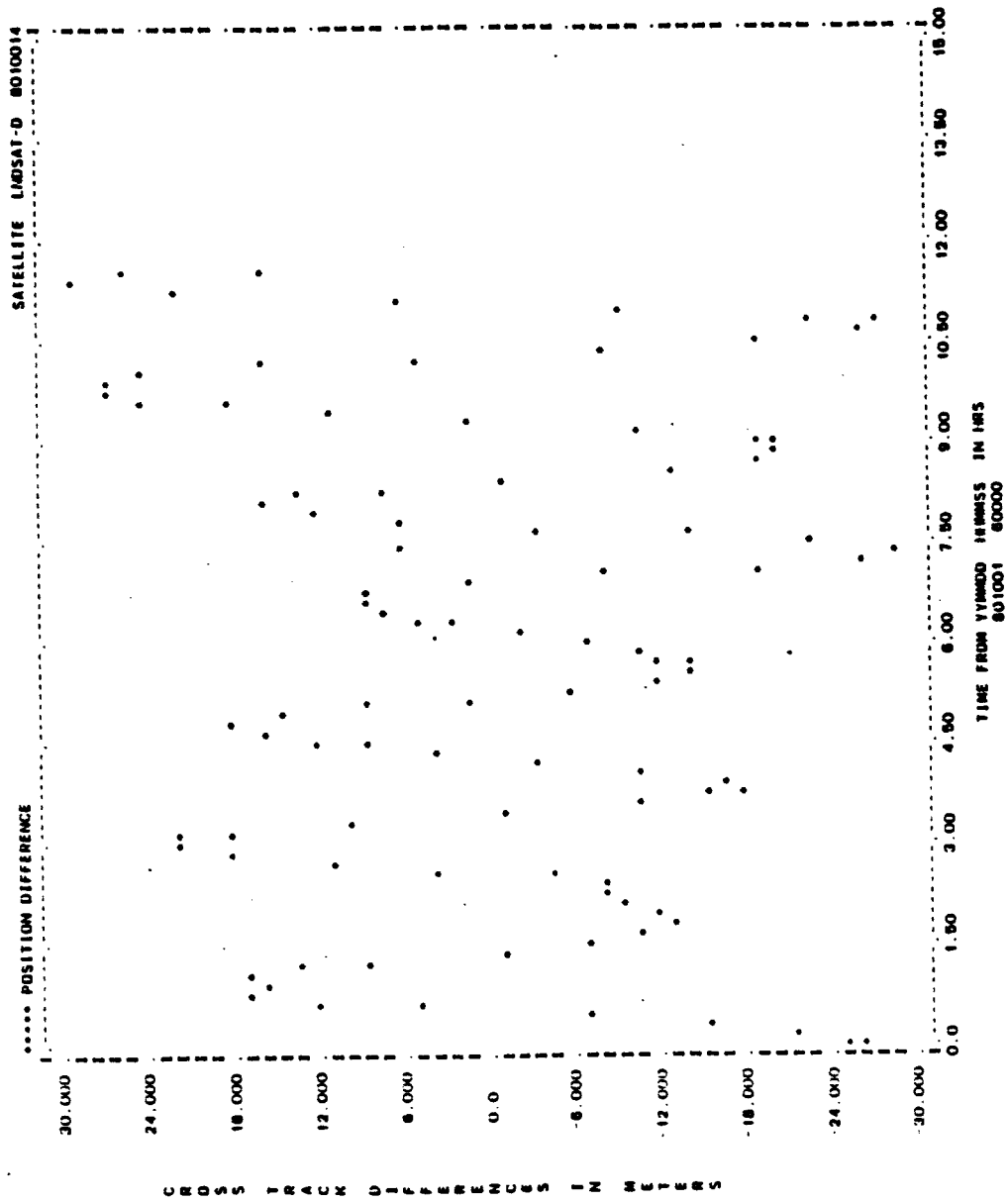


Figure A-56. Cross-Track Differences for Run L22 (1 of 2)

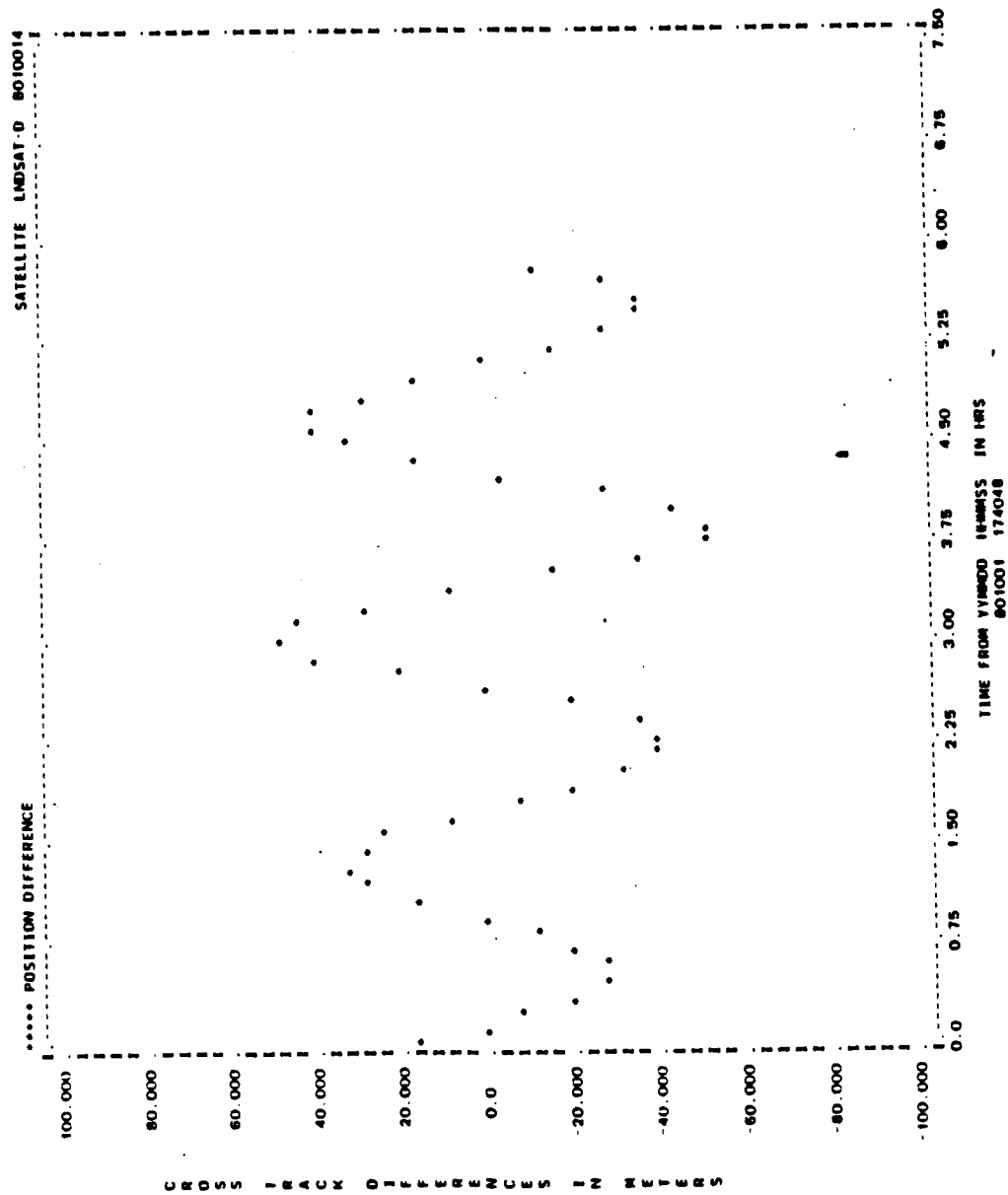


Figure A-56. Cross-Track Differences for Run L22 (2 of 2)

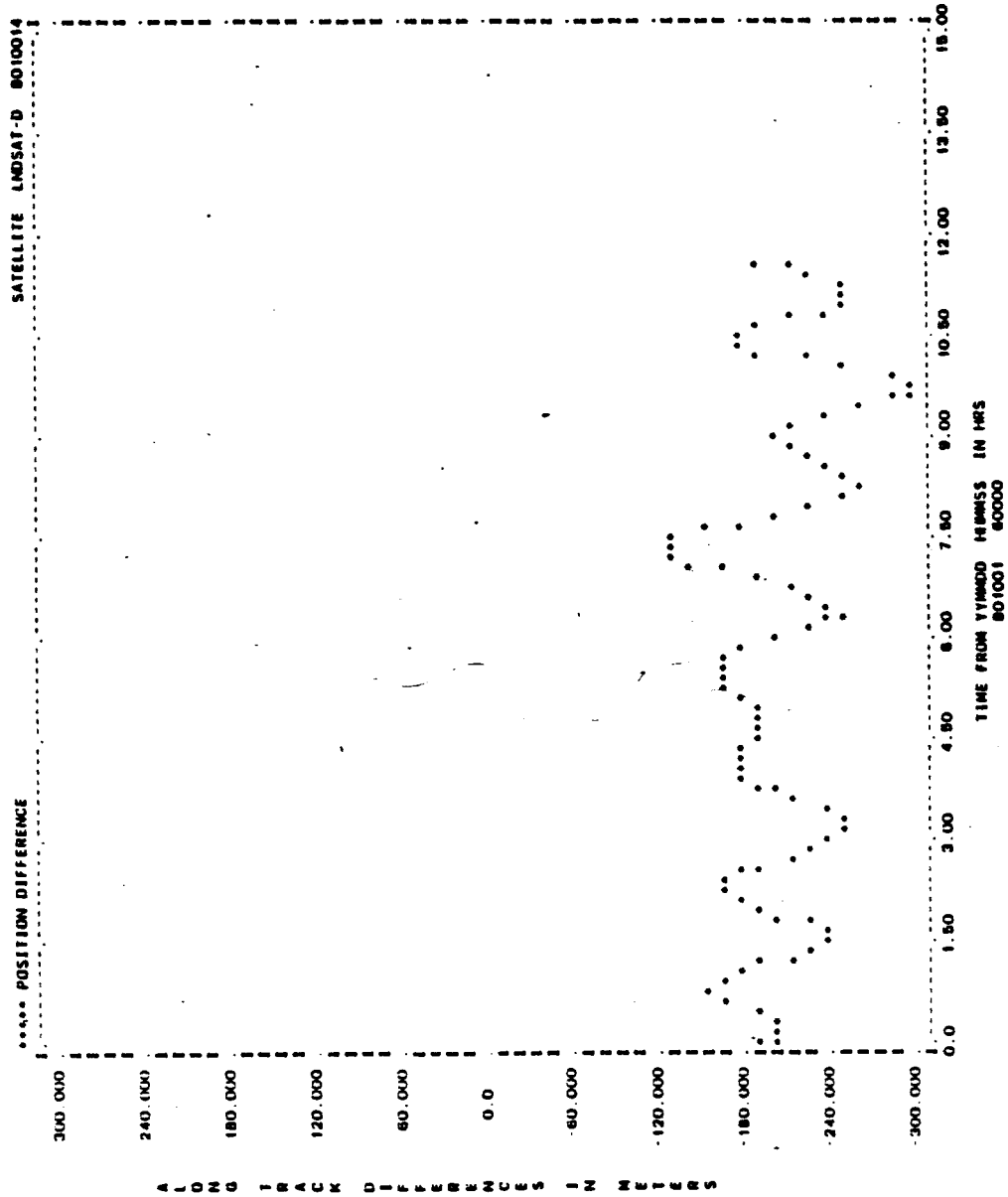


Figure A-57. Along-Track Differences for Run L22 (1 of 2)

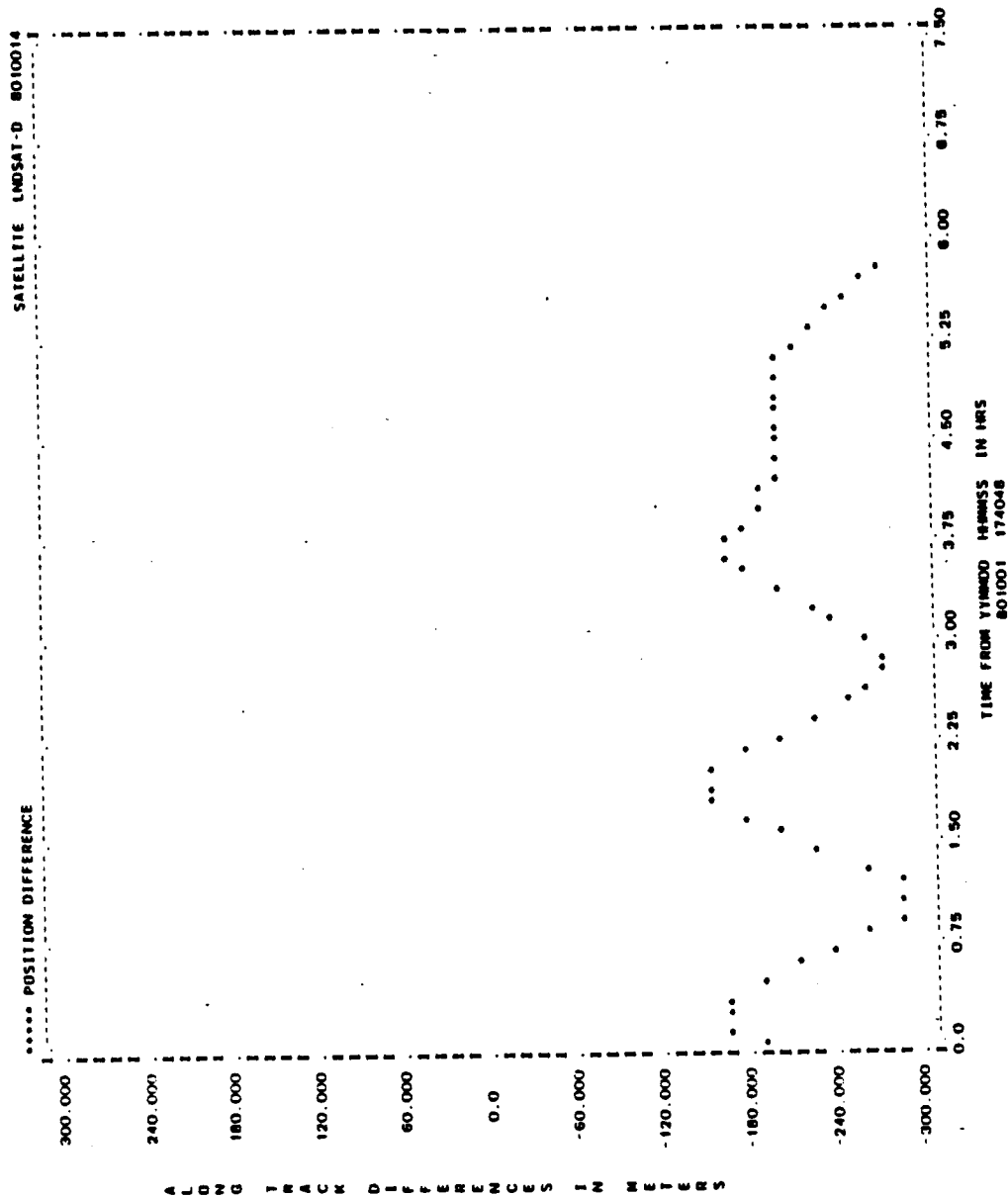


Figure A-57. Along-Track Differences for Run L22 (2 of 2)

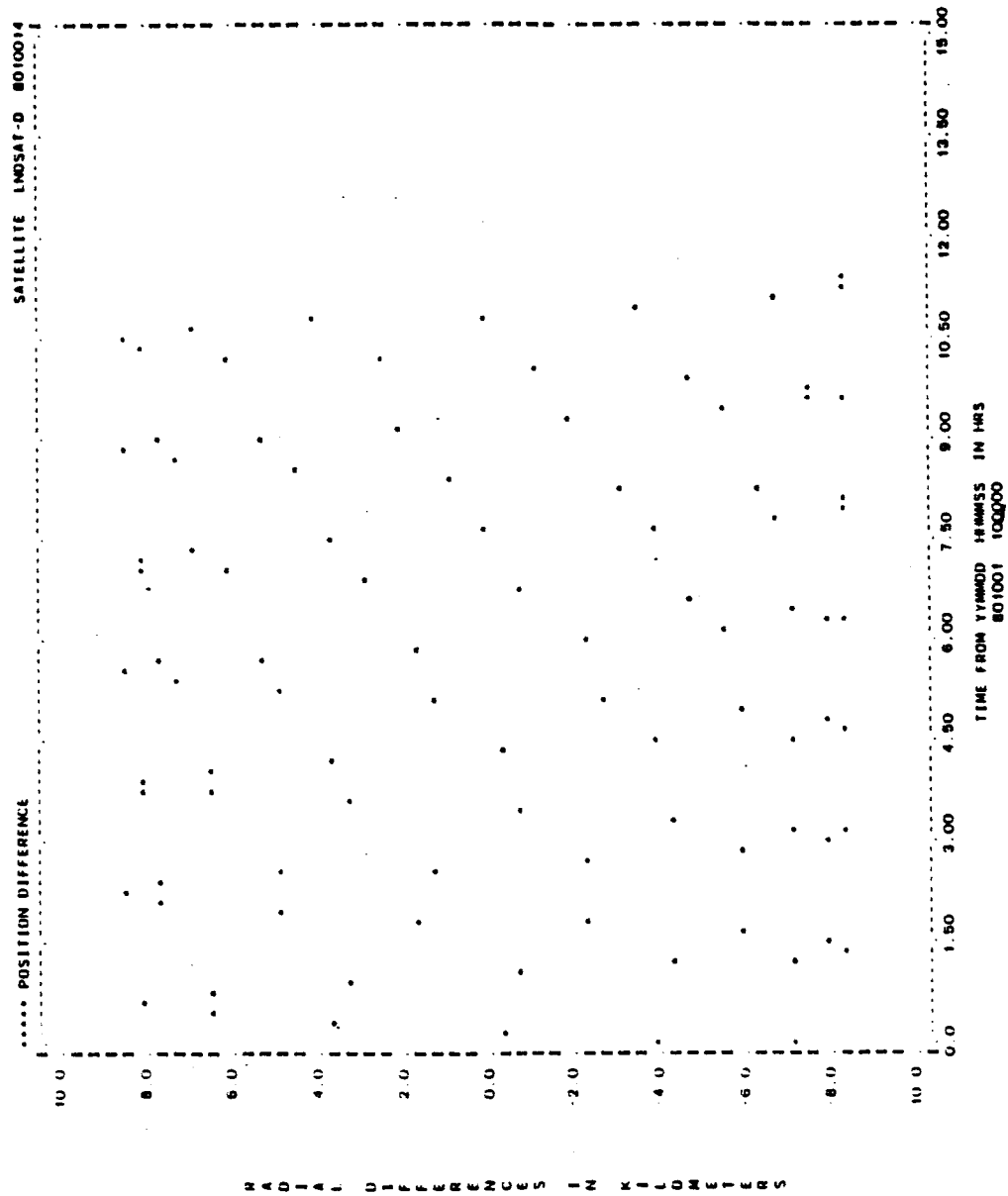


Figure A-58. Radial Differences for Run L22 (1 of 2)

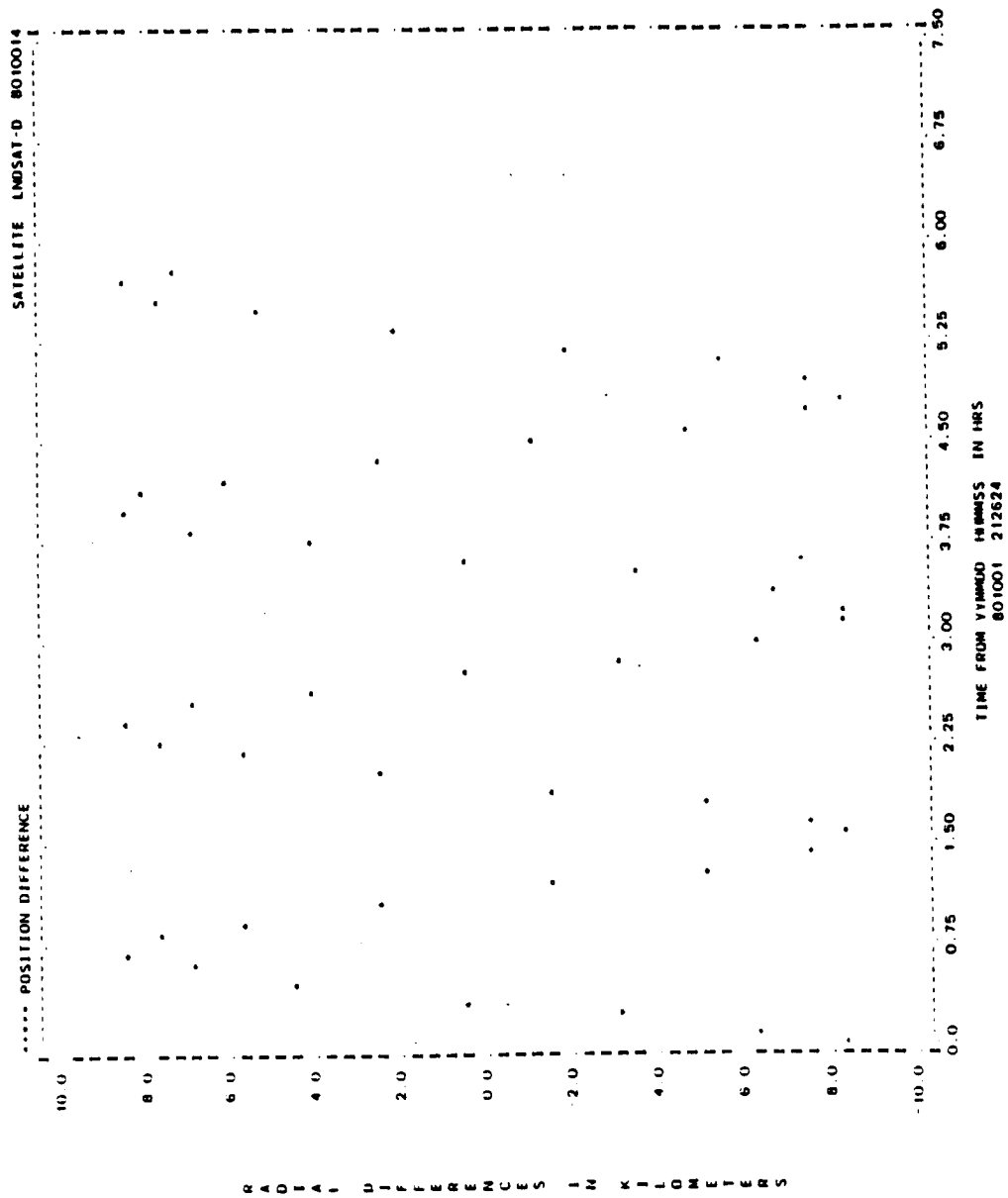


Figure A-58. Radial Differences for Run L22 (2 of 2)

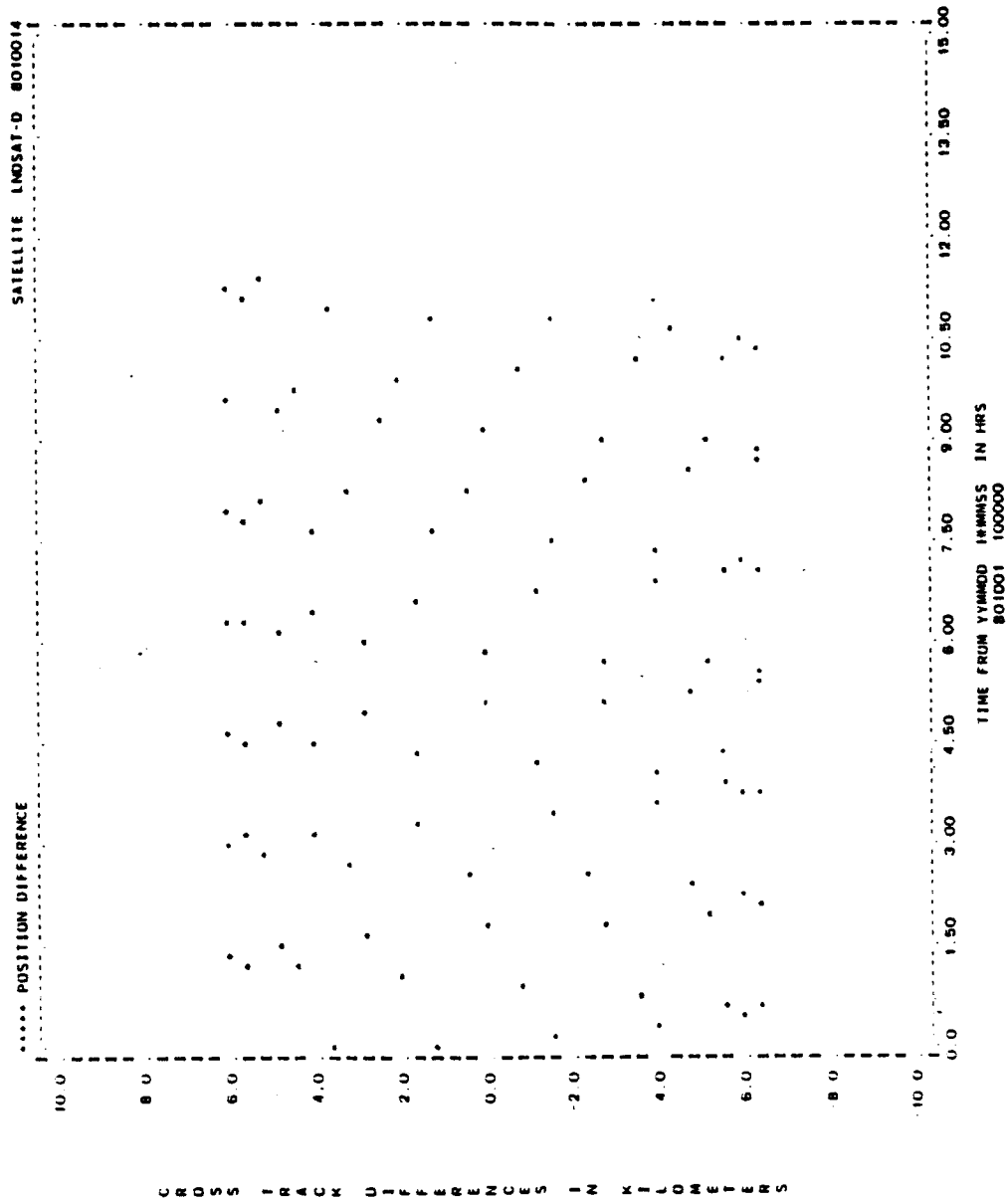


Figure A-59. Cross-Track Differences for Run L22 (1 of 2)

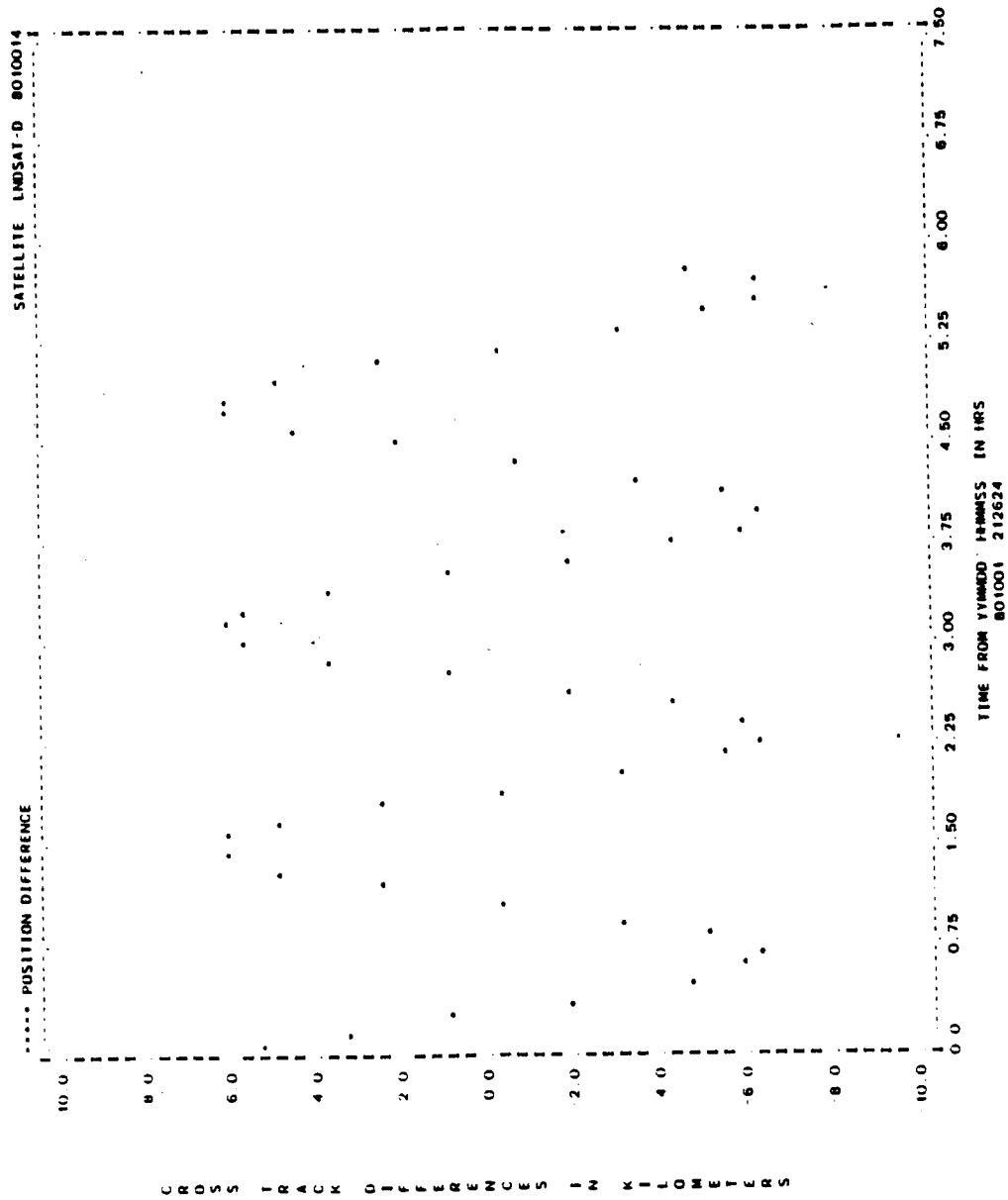


Figure A-59. Cross-Track Differences for Run L22 (2 of 2)

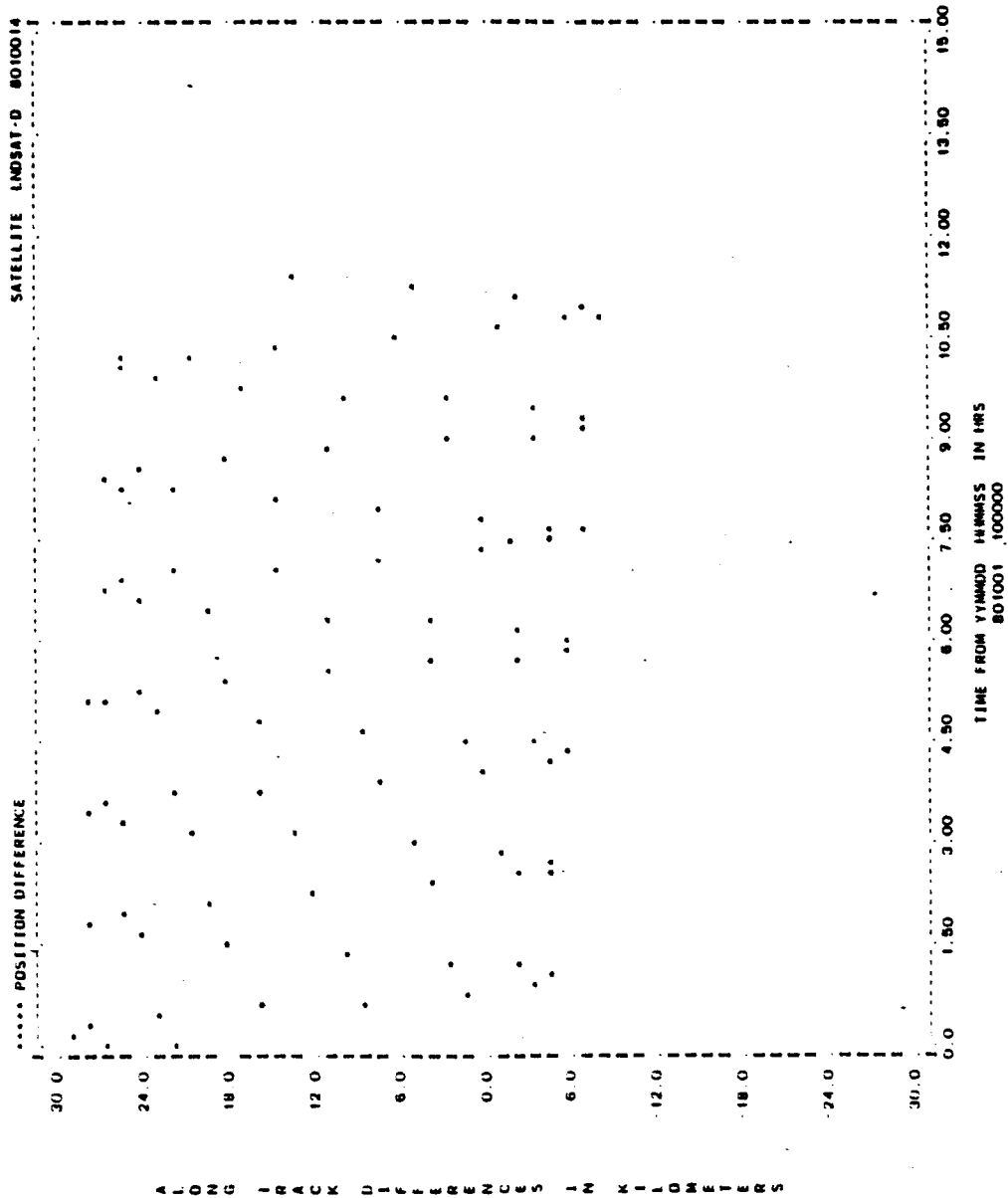


Figure A-60. Along-Track Differences for Run L22 (1 of 2)

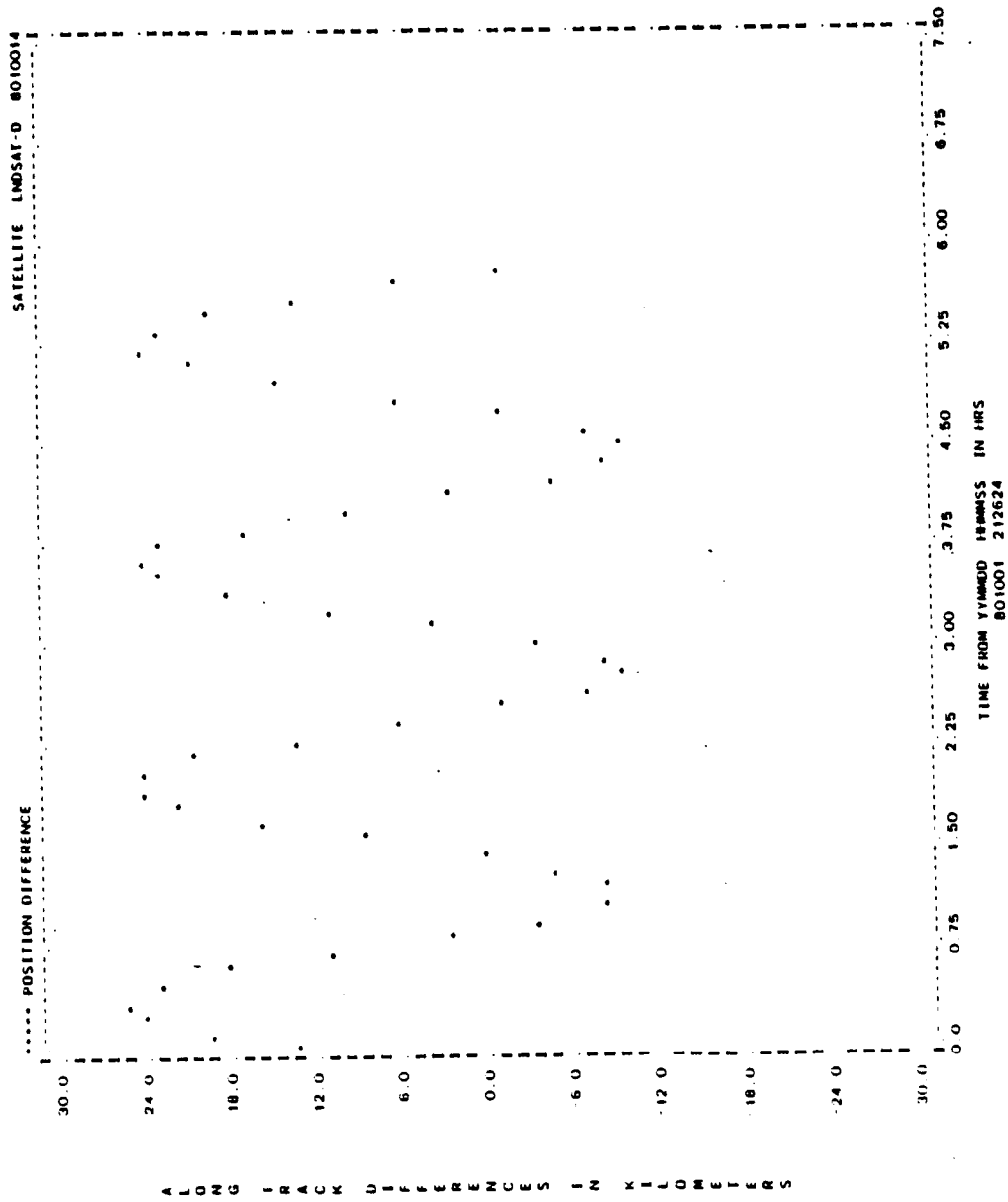


Figure A-60. Along-Track Differences for Run L22 (2 of 2)

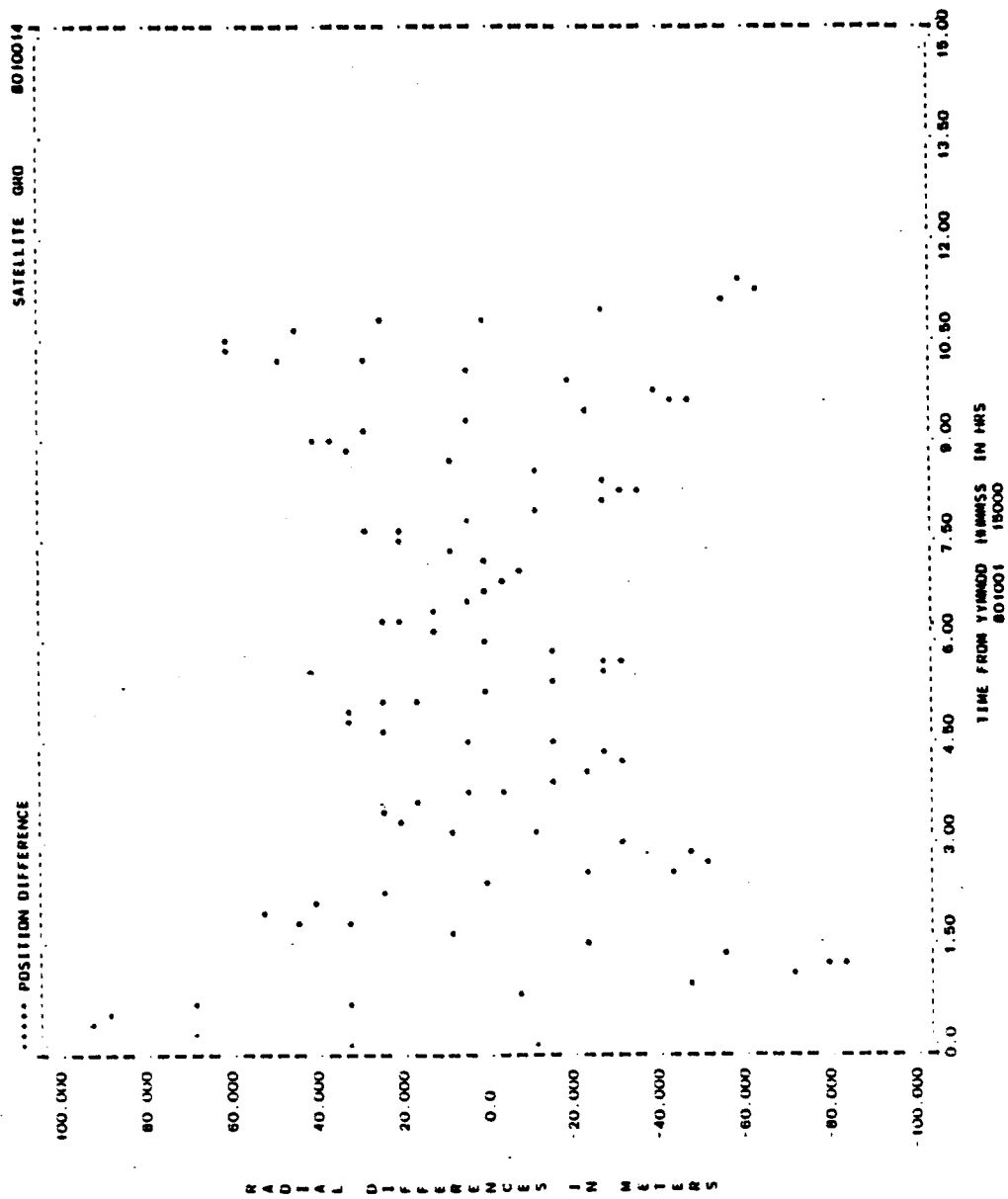


Figure A-61. Radial Differences for Run G01 (1 of 2)

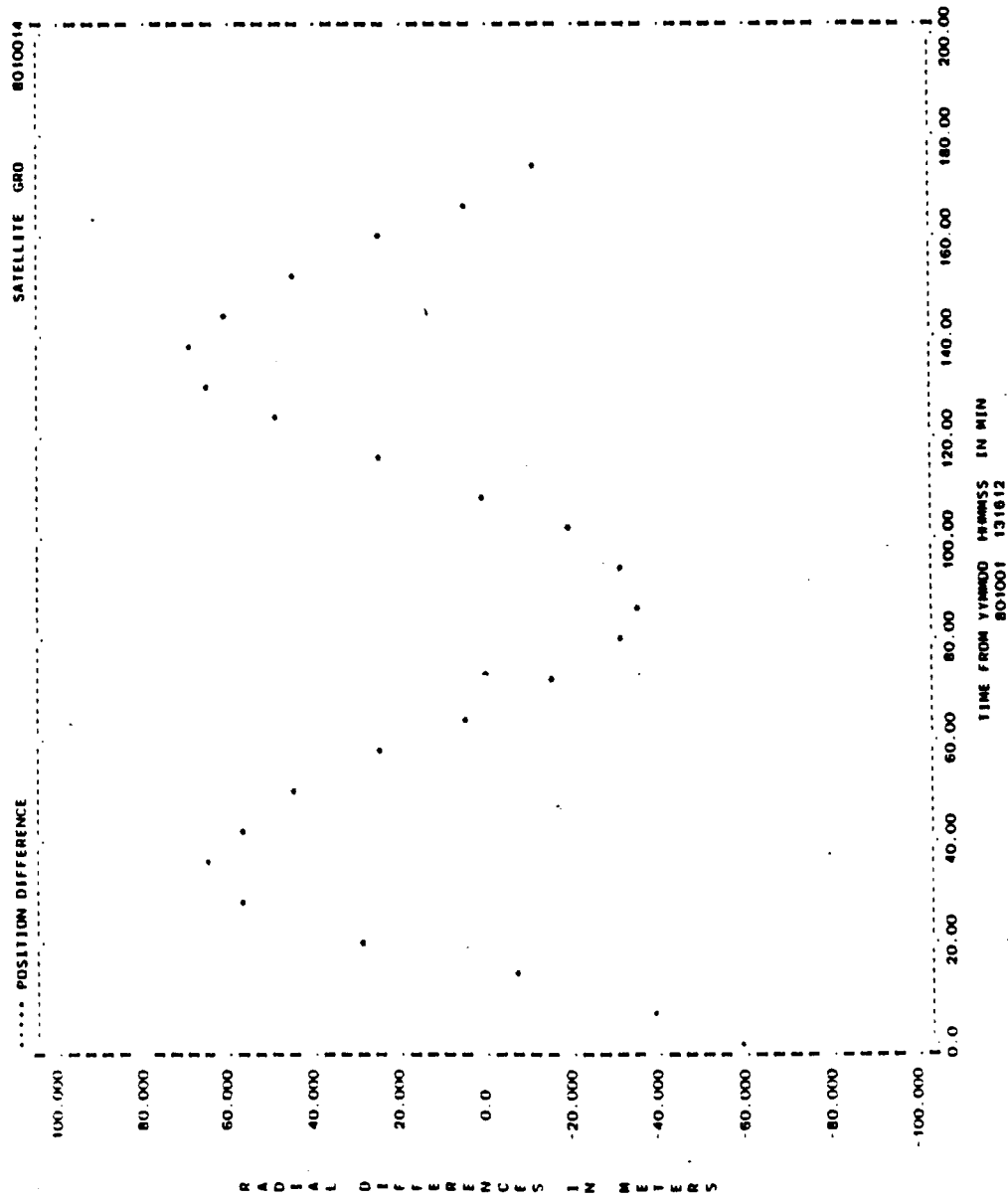


Figure A-61. Radial Differences for Run G01 (2 of 2)

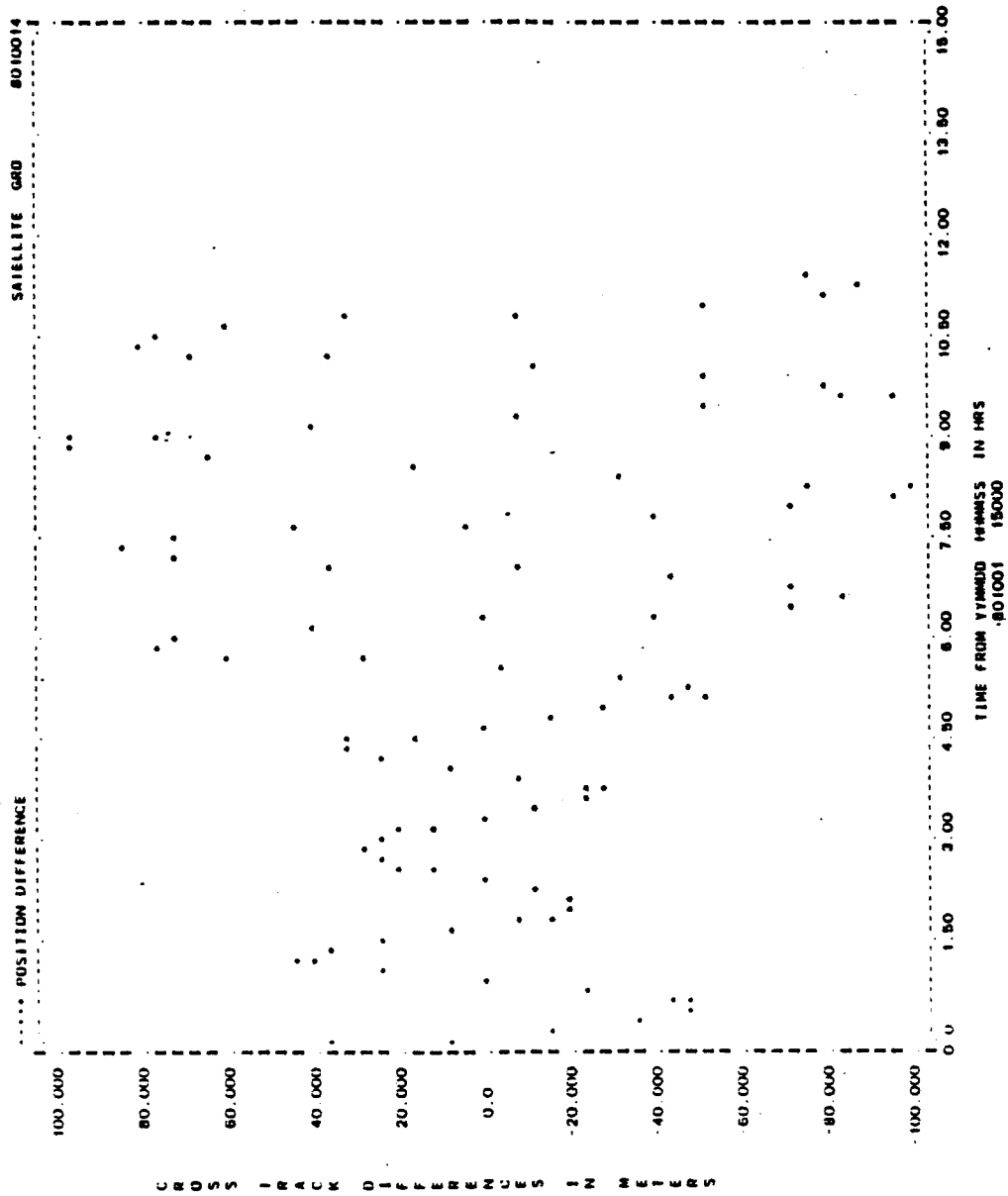


Figure A-62. Cross-Track Differences for Run G01 (1 of 2)

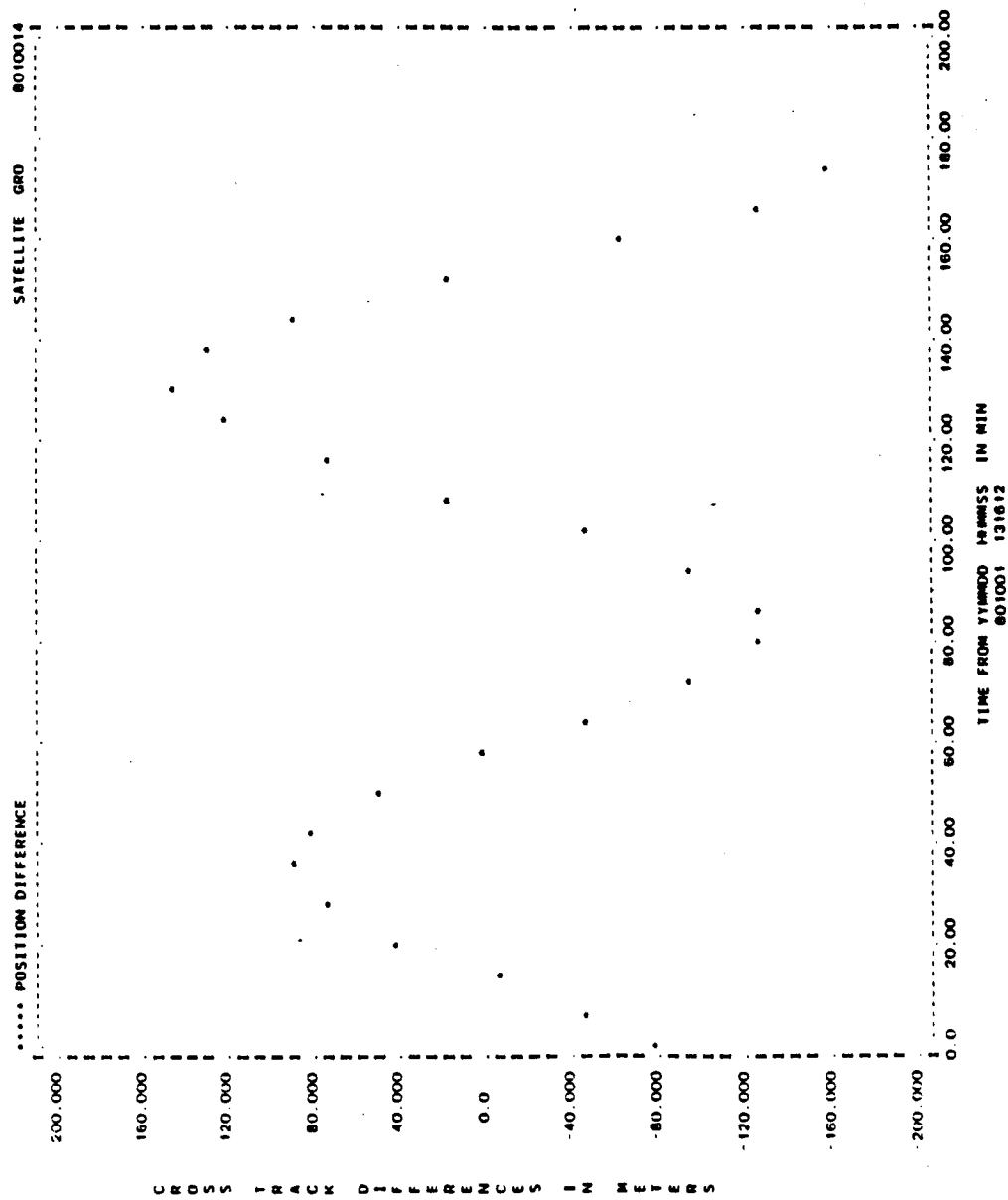


Figure A-62. Cross-Track Differences for Run G01 (2 of 2)

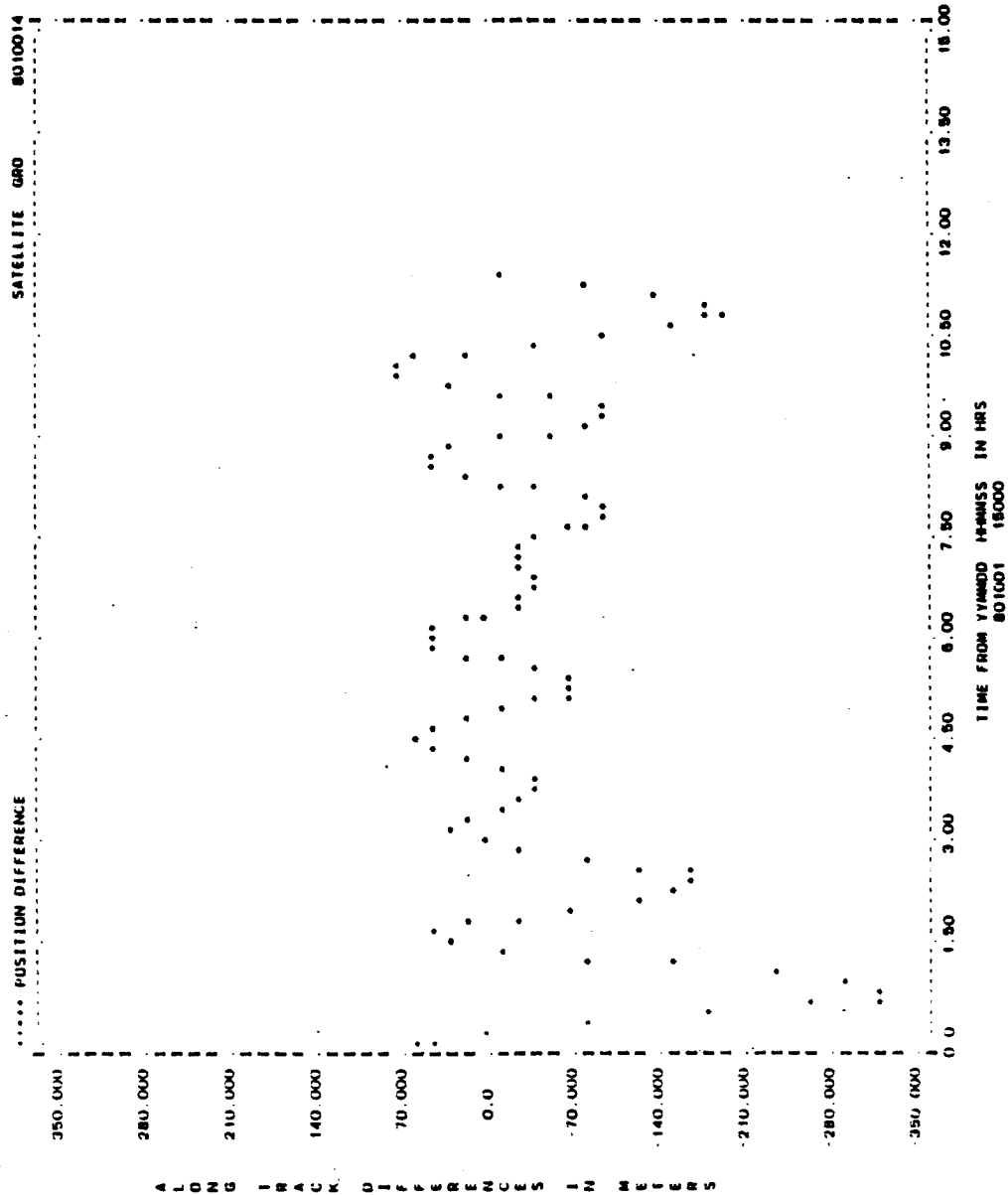


Figure A-63. Along-Track Differences for Run G01 (1 of 2)

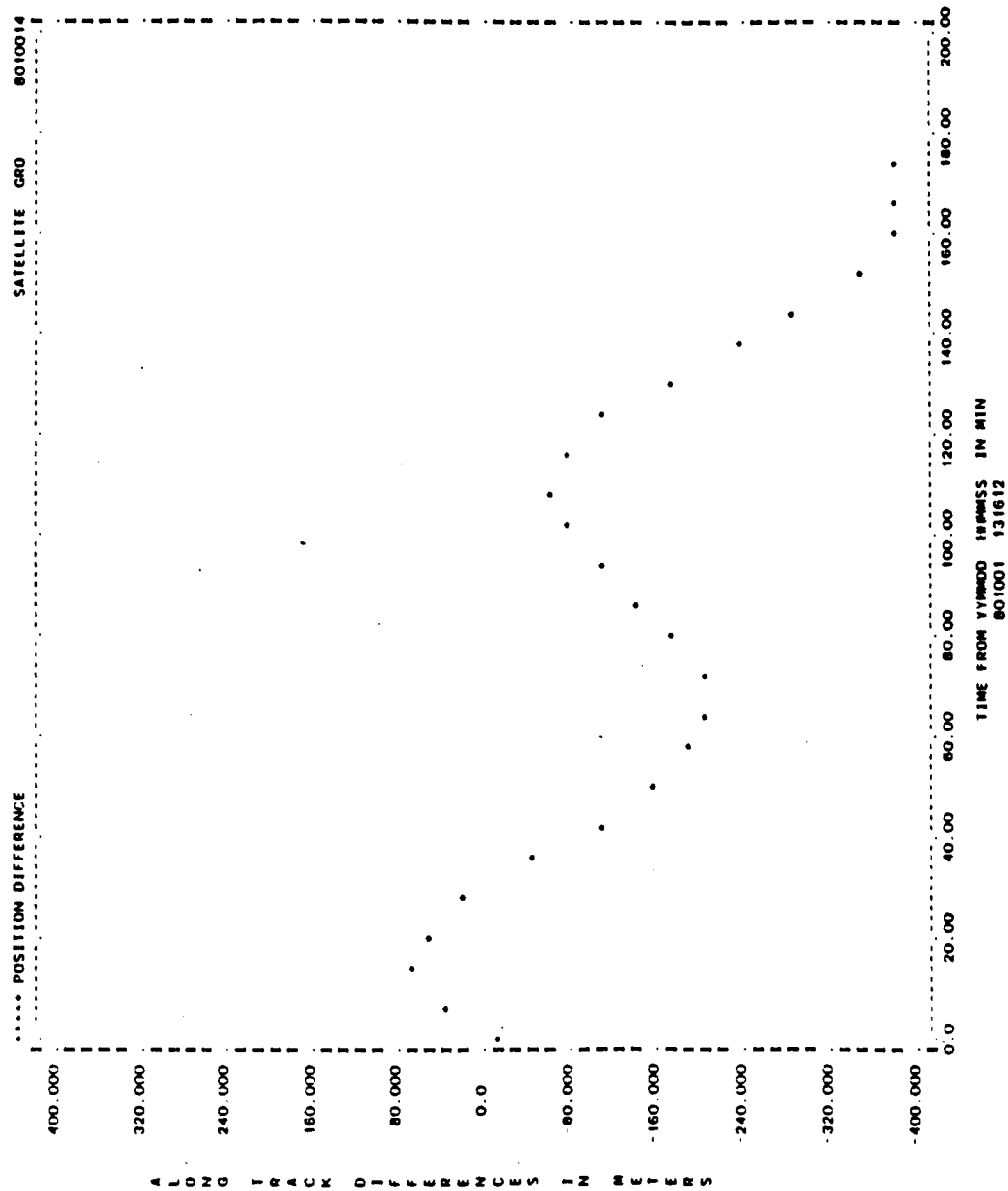


Figure A-63. Along-Track Differences for Run G01 (2 of 2)

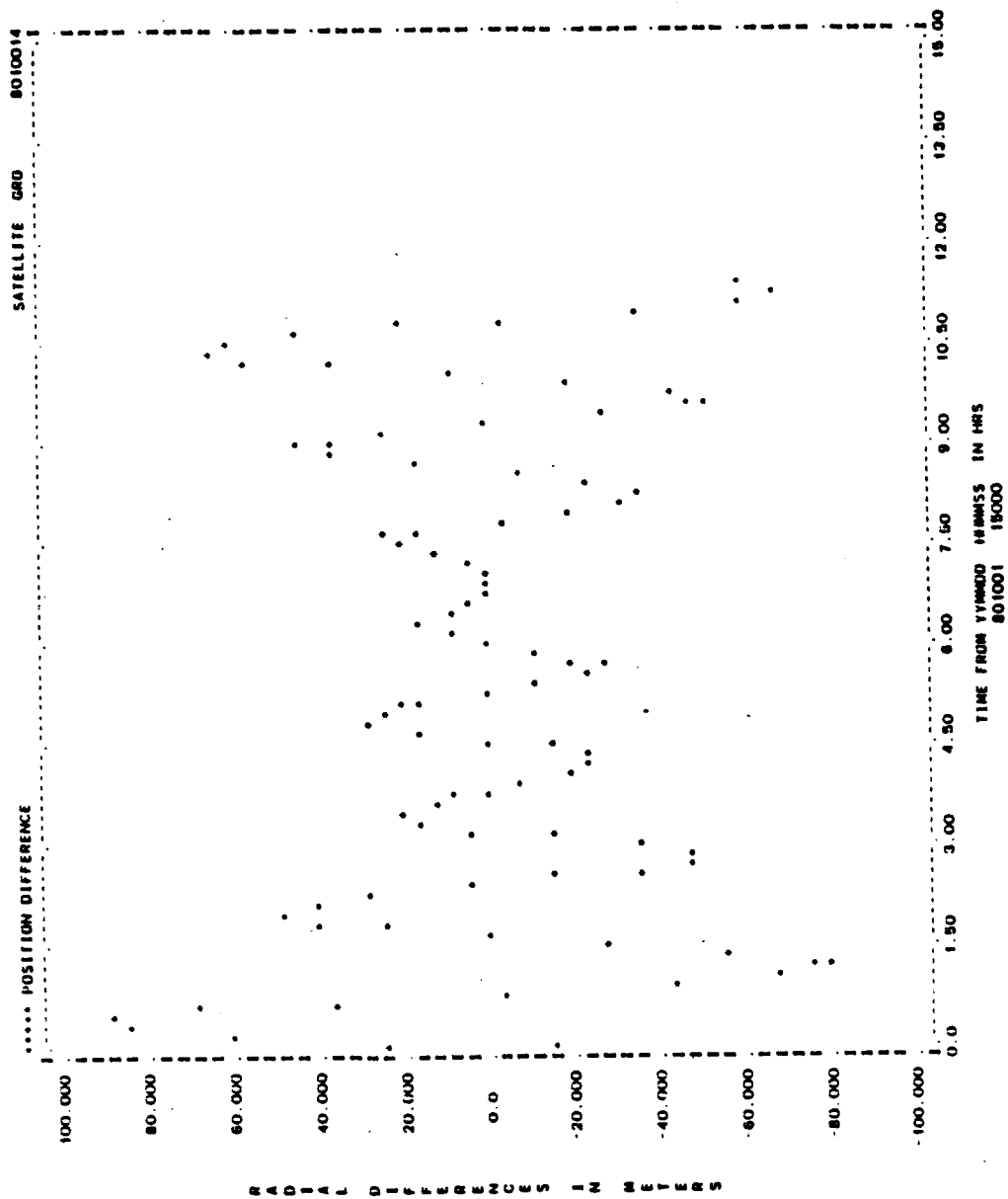


Figure A-64. Radial Differences for Run G04 (1 of 2)

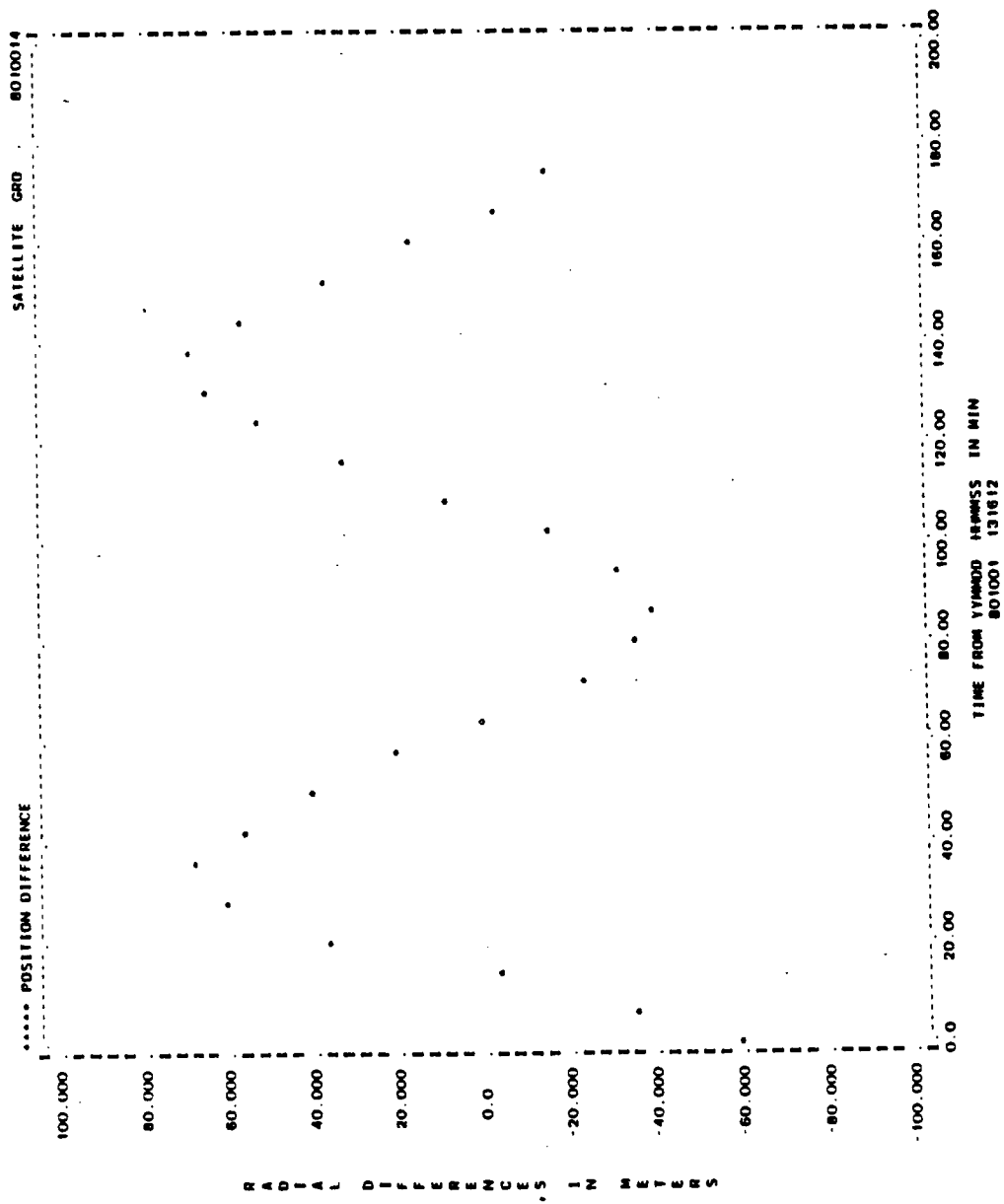


Figure A-64. Radial Differences for Run G04 (2 of 2)

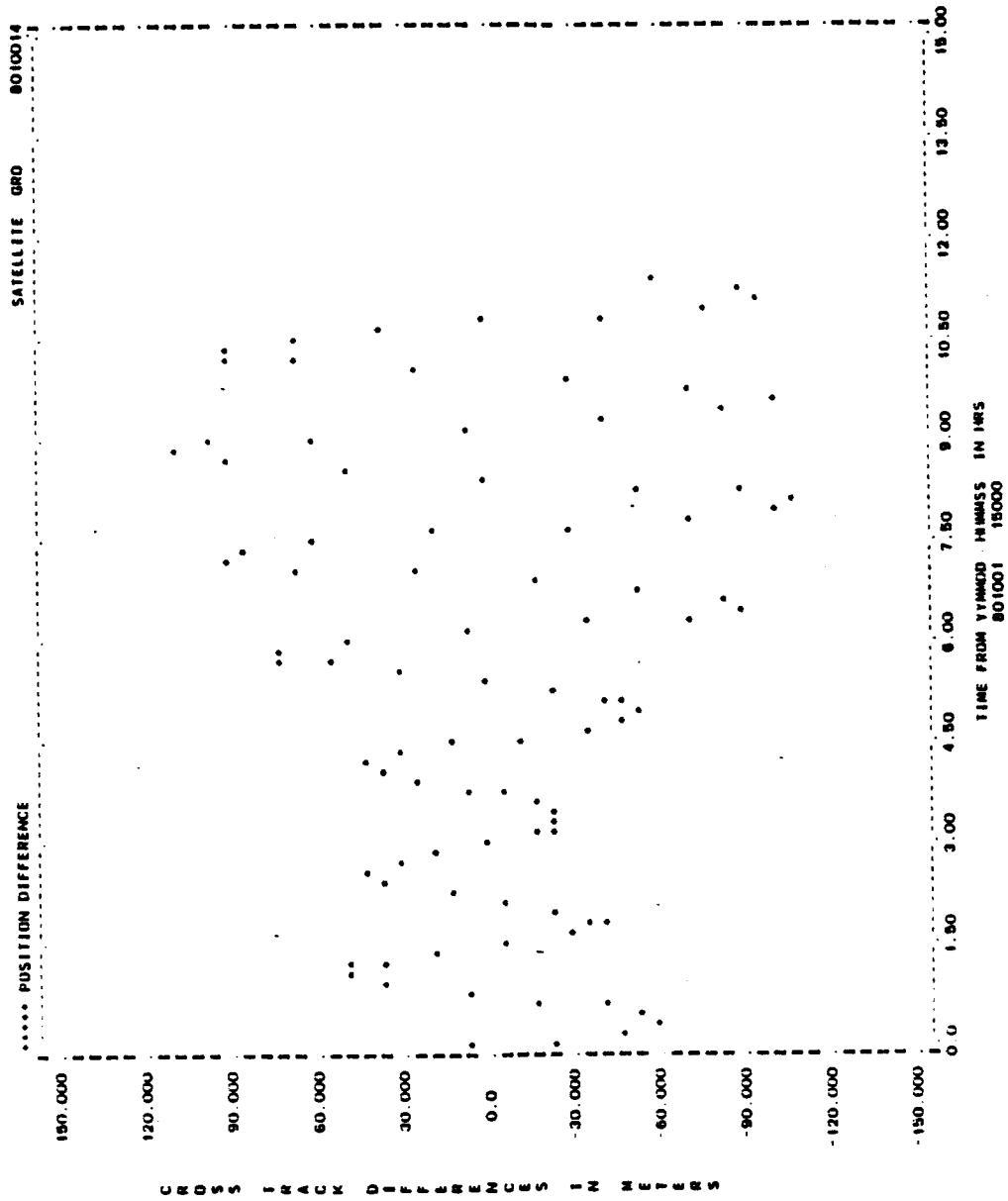


Figure A-65. Cross-Track Differences for Run G04 (1 of 2)

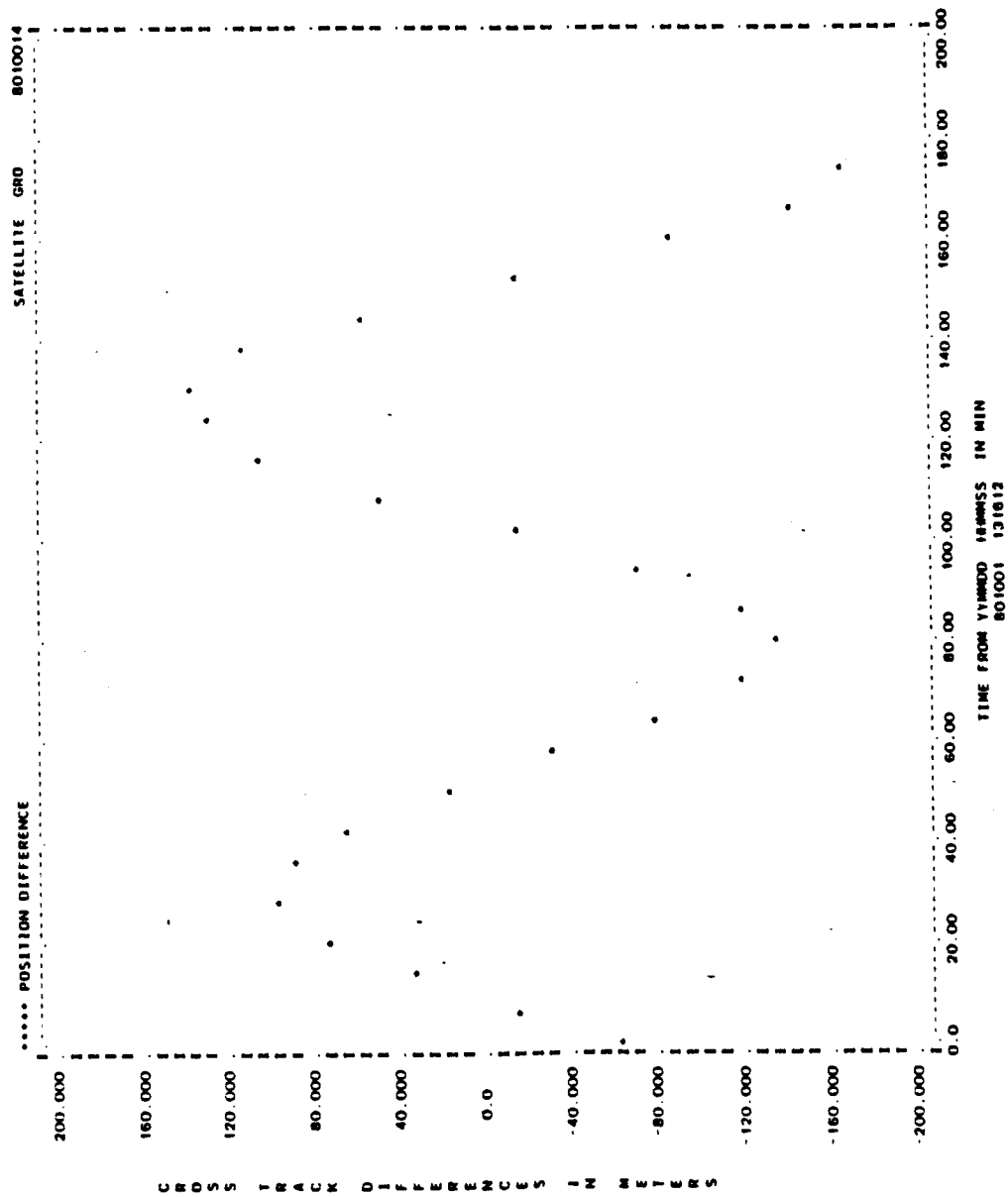


Figure A-65. Cross-Track Differences for Run G04 (2 of 2)

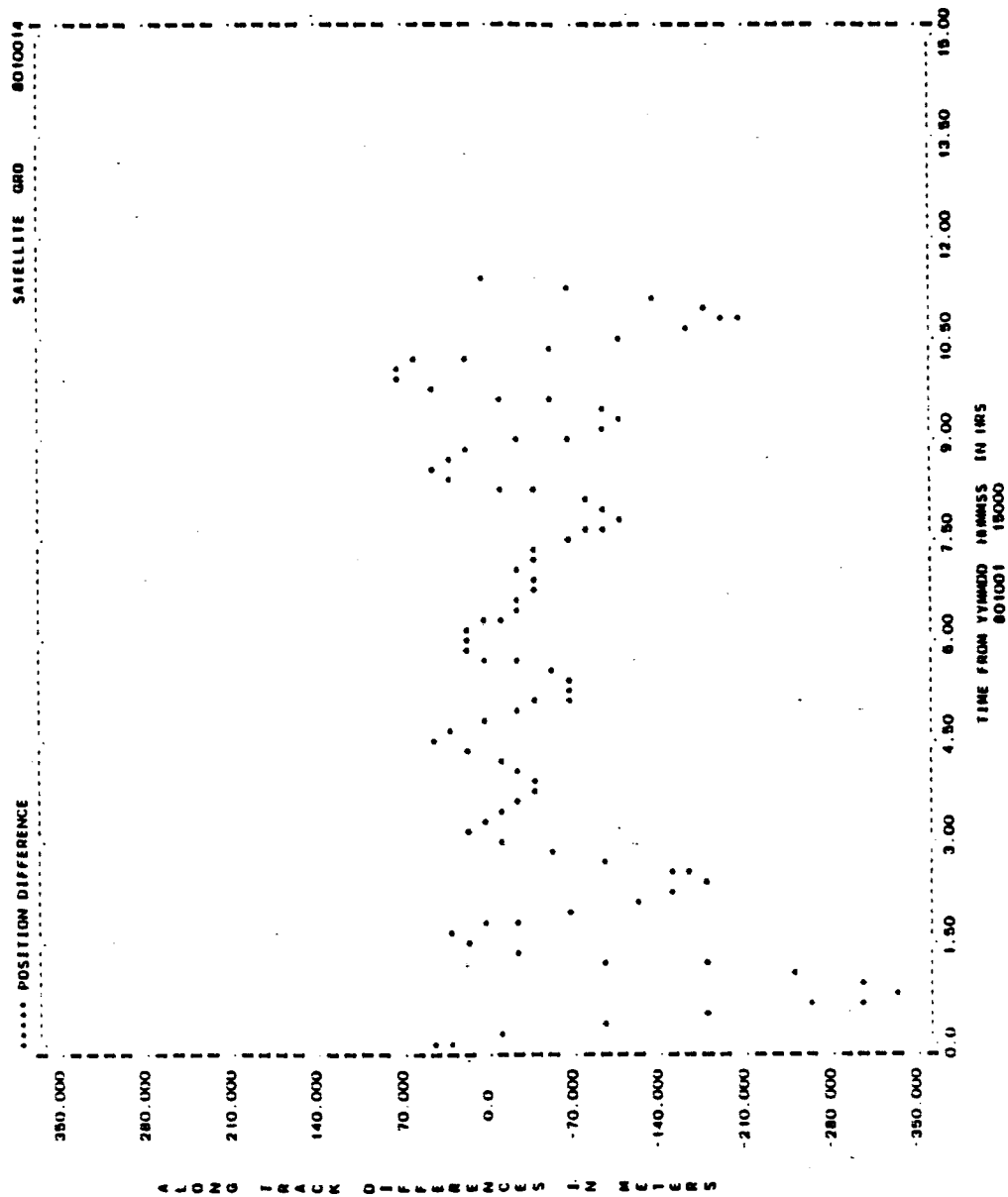


Figure A-66. Along-Track Differences for Run G04 (1 of 2)

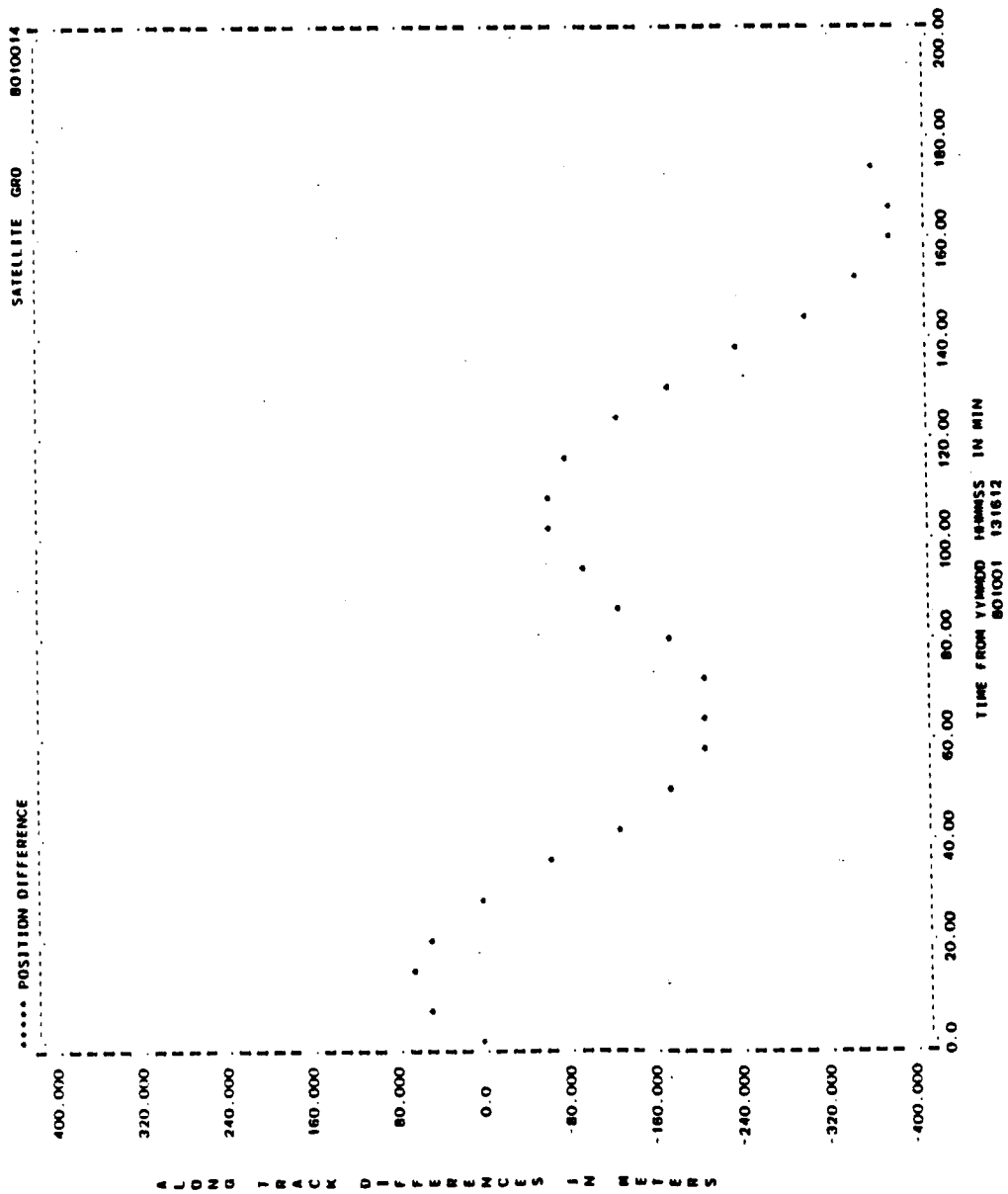


Figure A-66. Along-Track Differences for Run G04 (2 of 2)

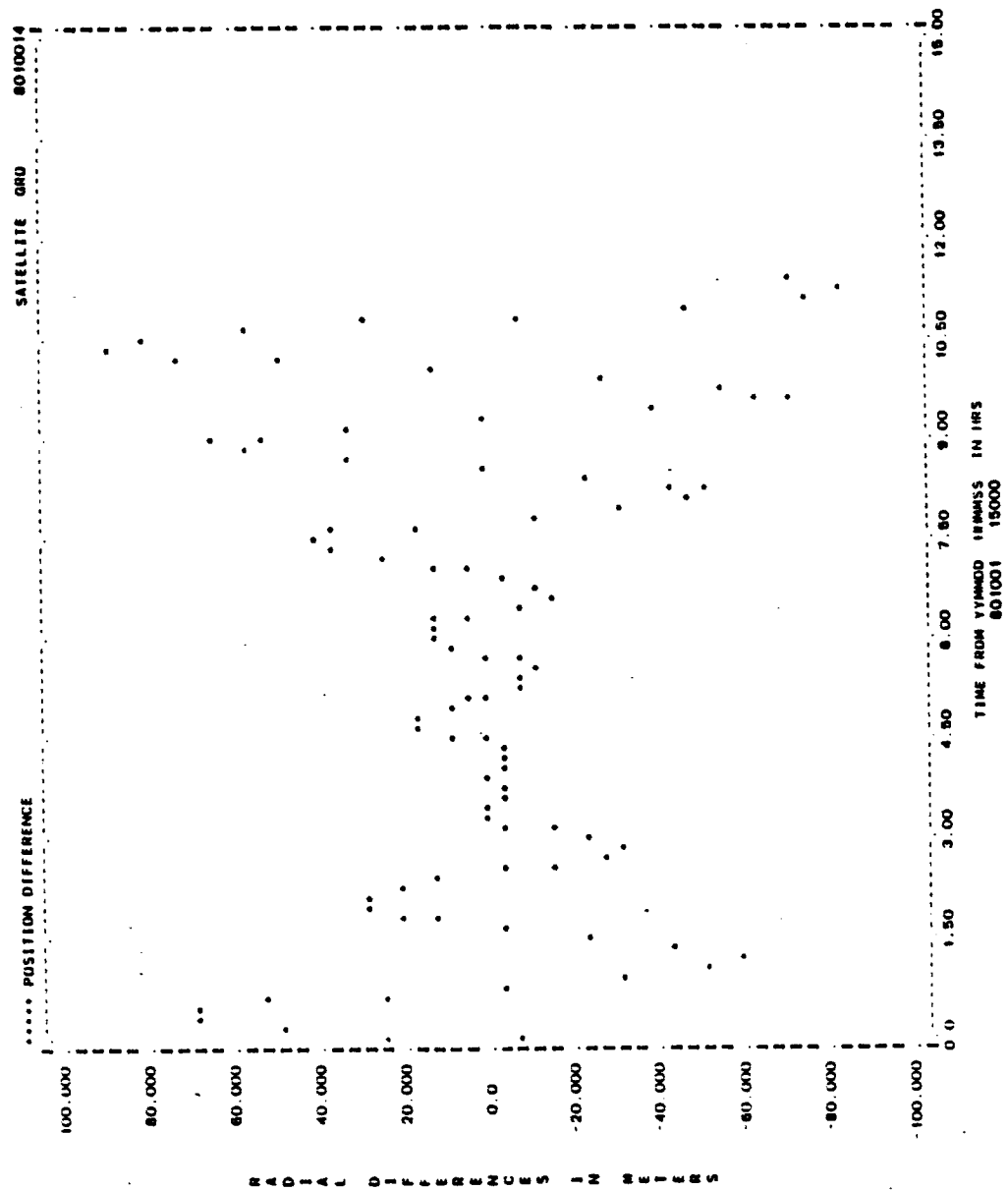


Figure A-67. Radial Differences for Run G05 (1 of 2)

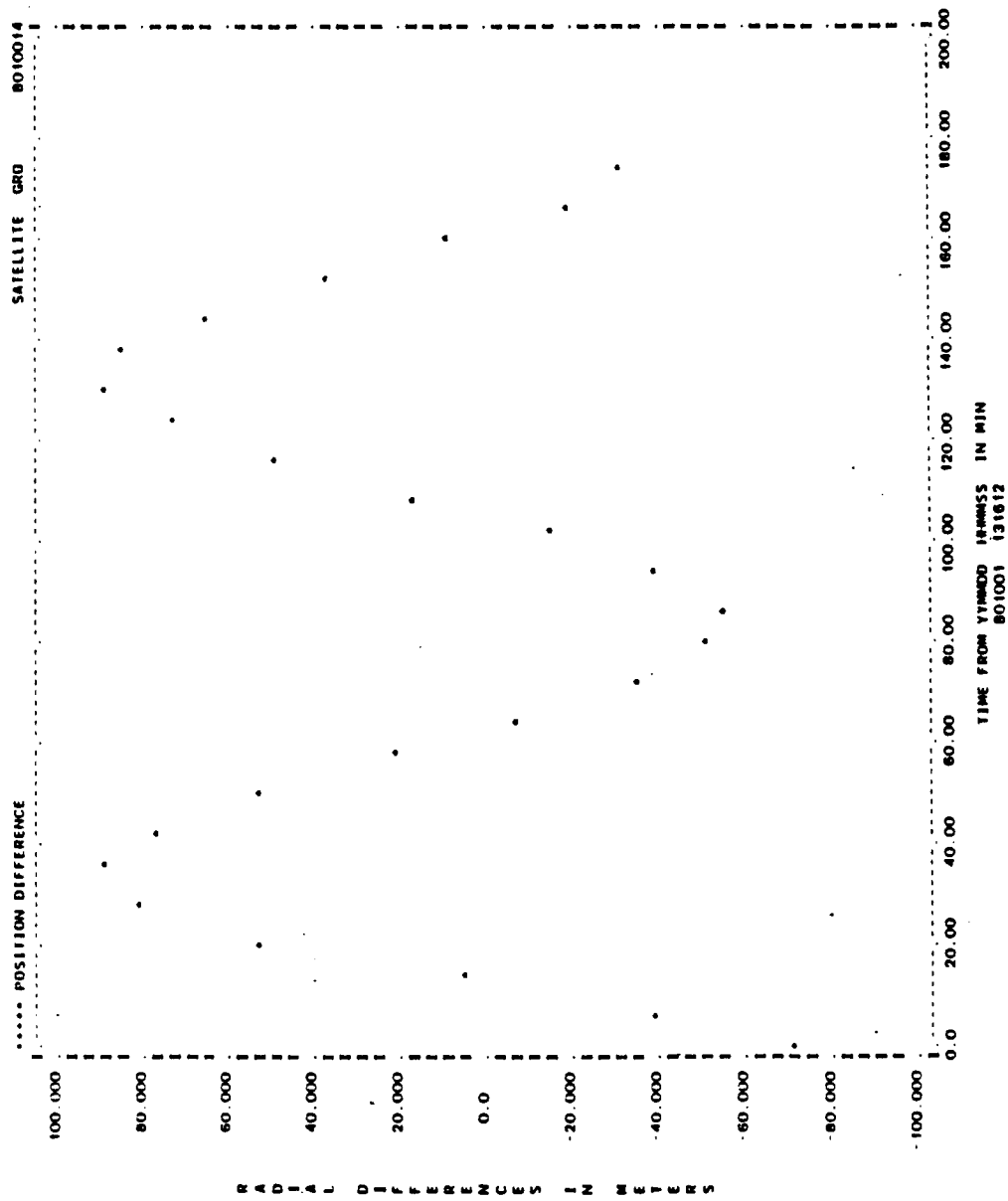


Figure A-67. Radial Differences for Run G05 (2 of 2)

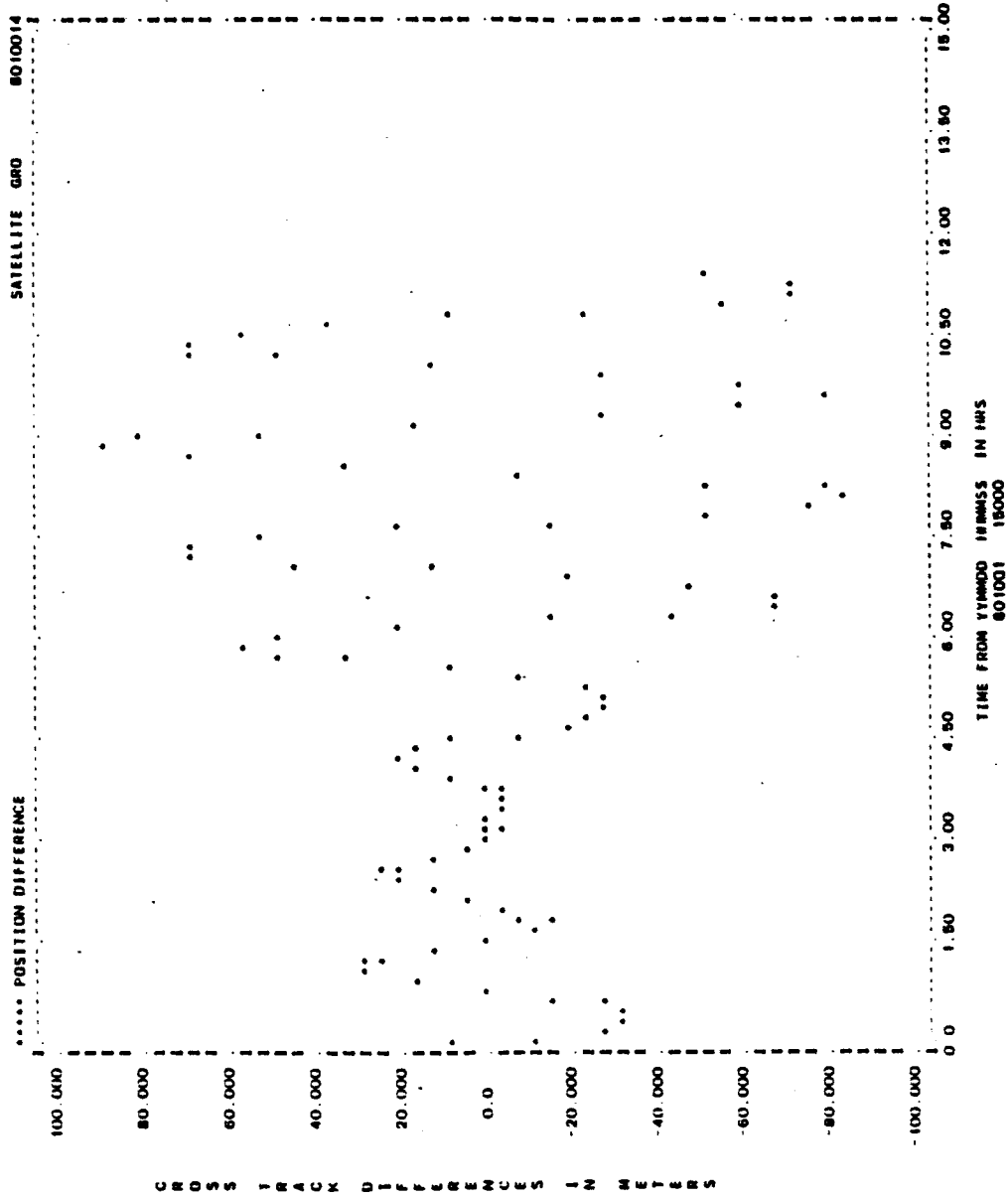


Figure A-68. Cross-Track Differences for Run G05 (1 of 2)

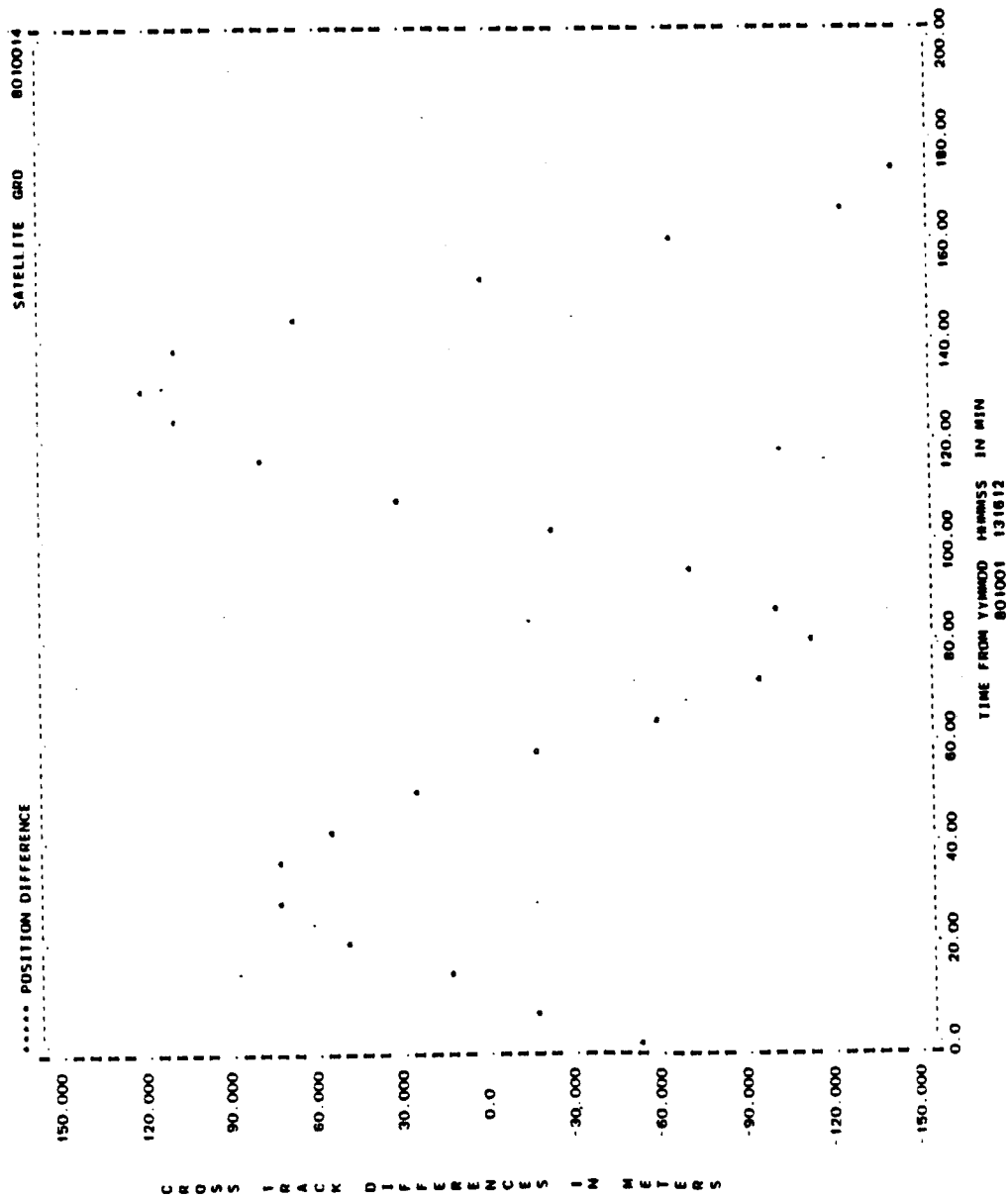


Figure A-68. Cross-Track Differences for Run G05 (2 of 2)

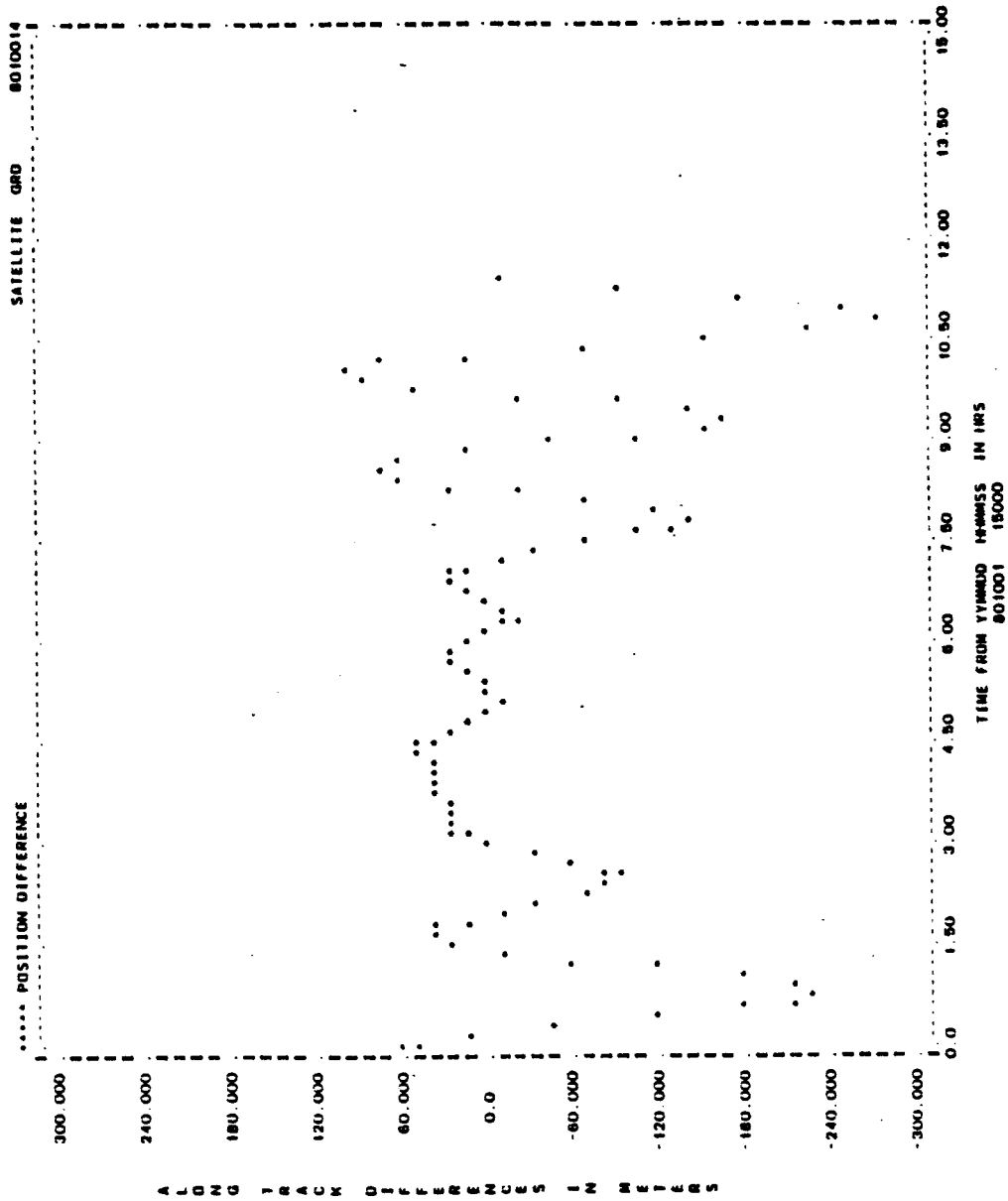


Figure A-69. Along-Track Differences for Run G05 (1 of 2)

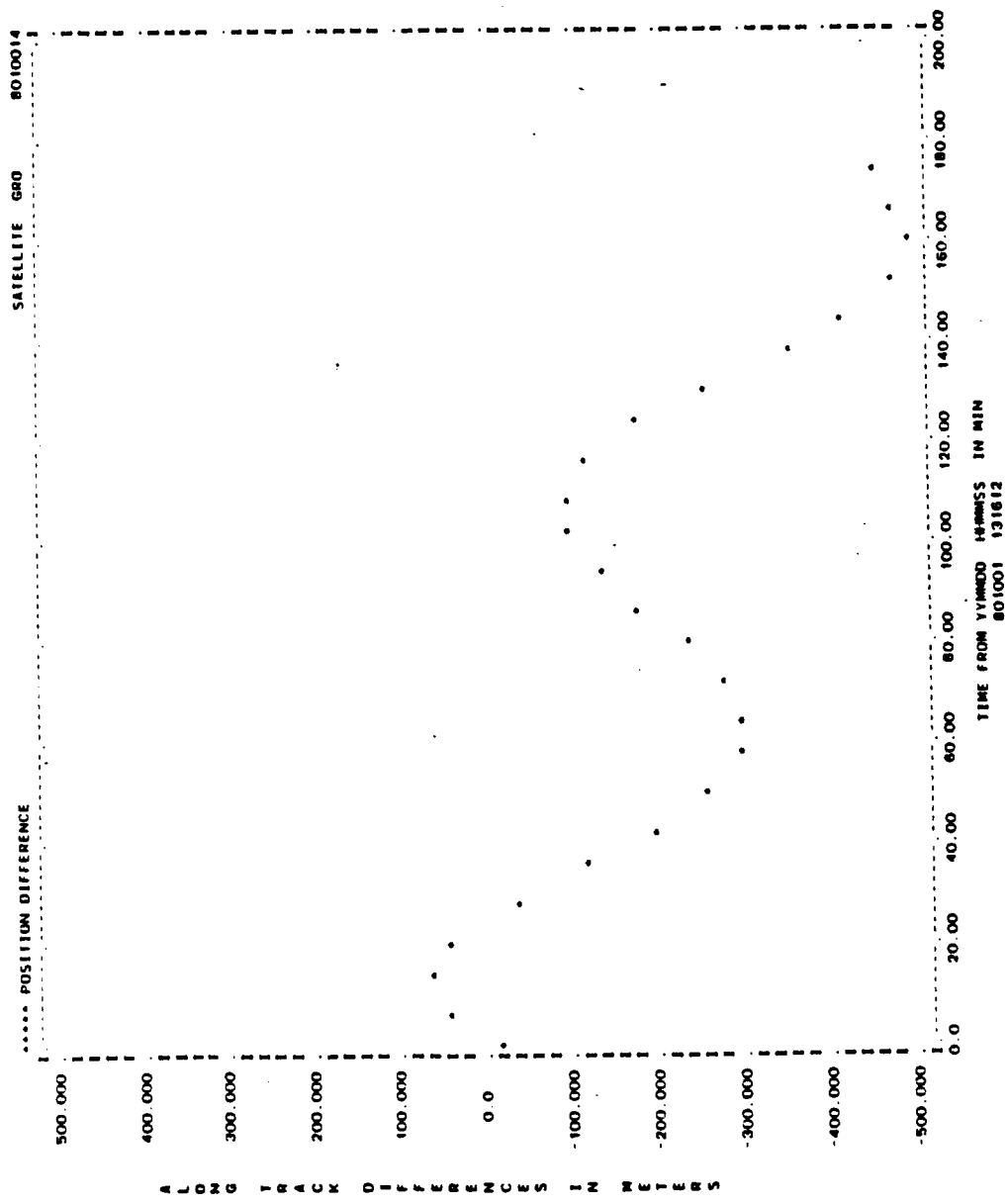


Figure A-69. Along-Track Differences for Run G05 (2 of 2)

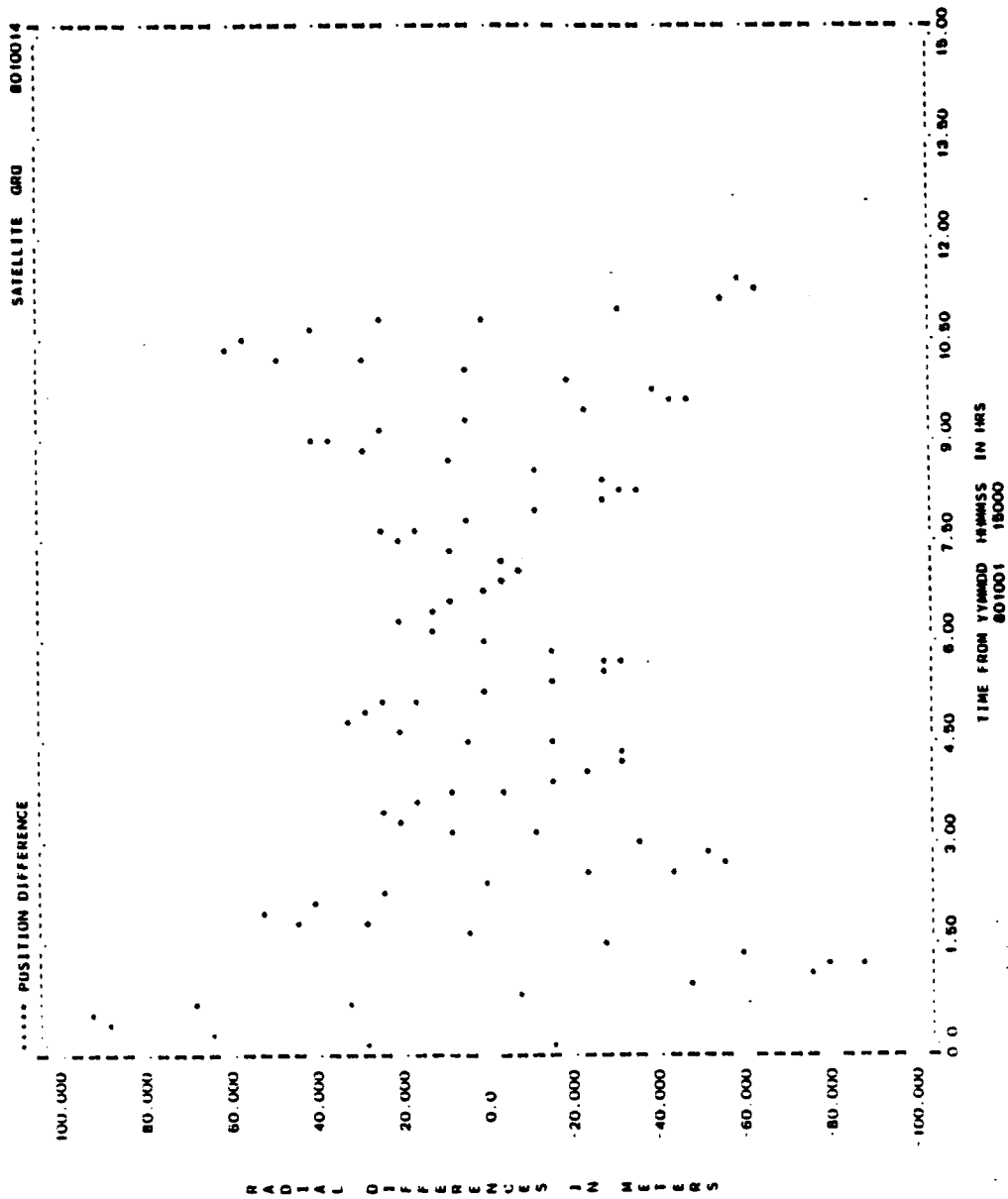


Figure A-70. Radial Differences for Run G06 (1 of 2)

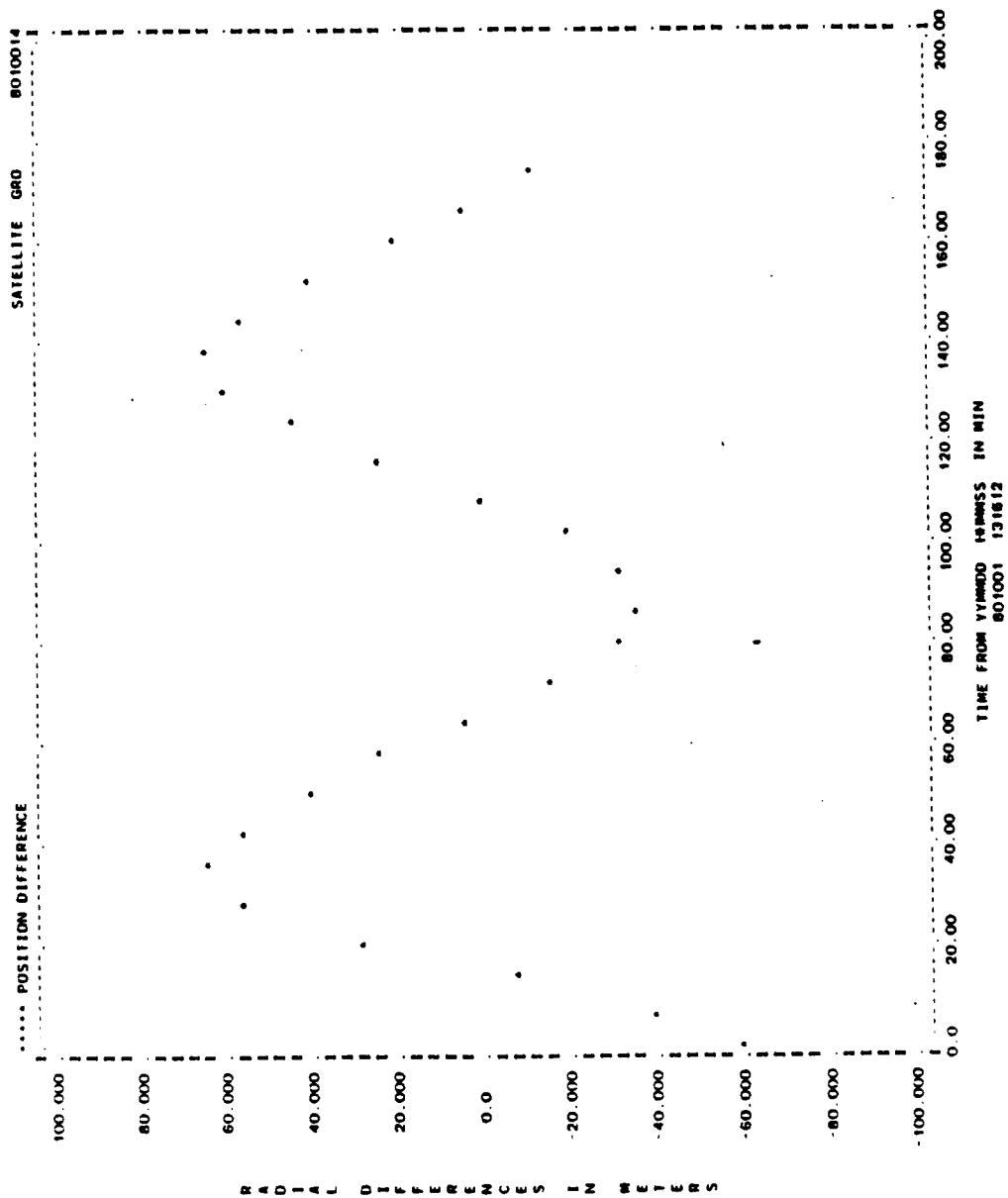


Figure A-70. Radial Differences for Run G05 (2 of 2)

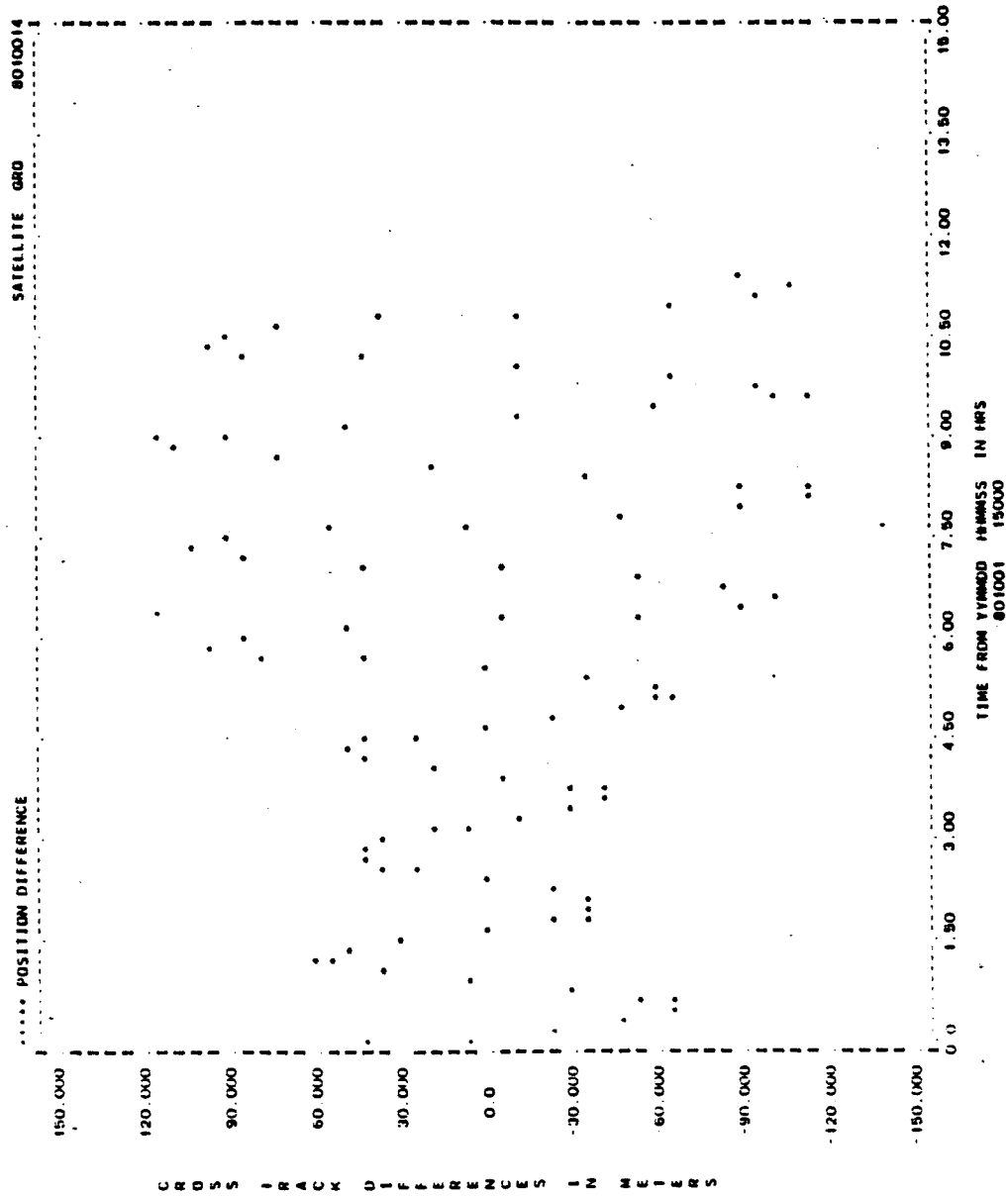


Figure A-71. Cross-Track Differences for Run G06 (1 of 2)

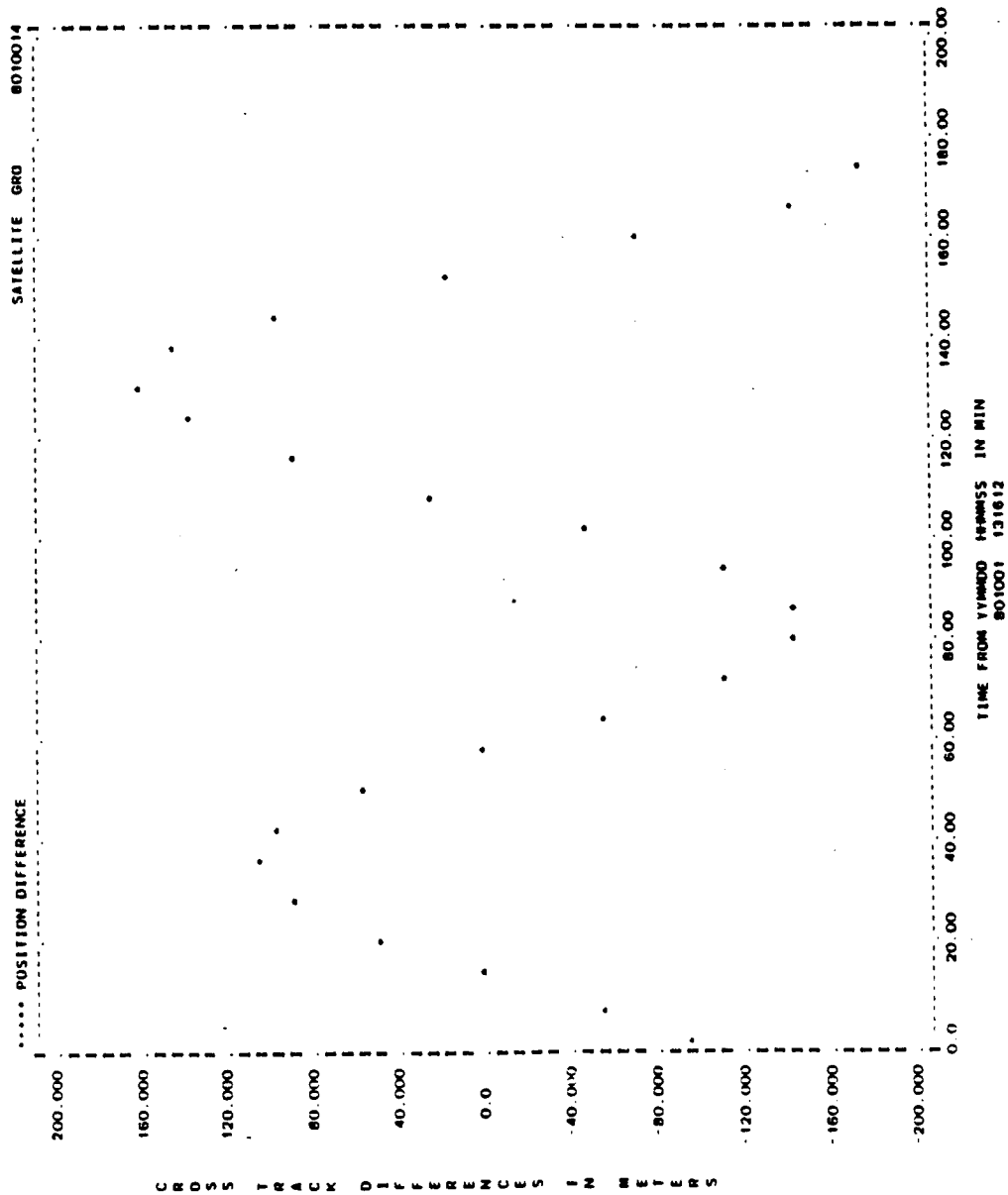


Figure A-71. Cross-Track Differences for Run G05 (2 of 2)

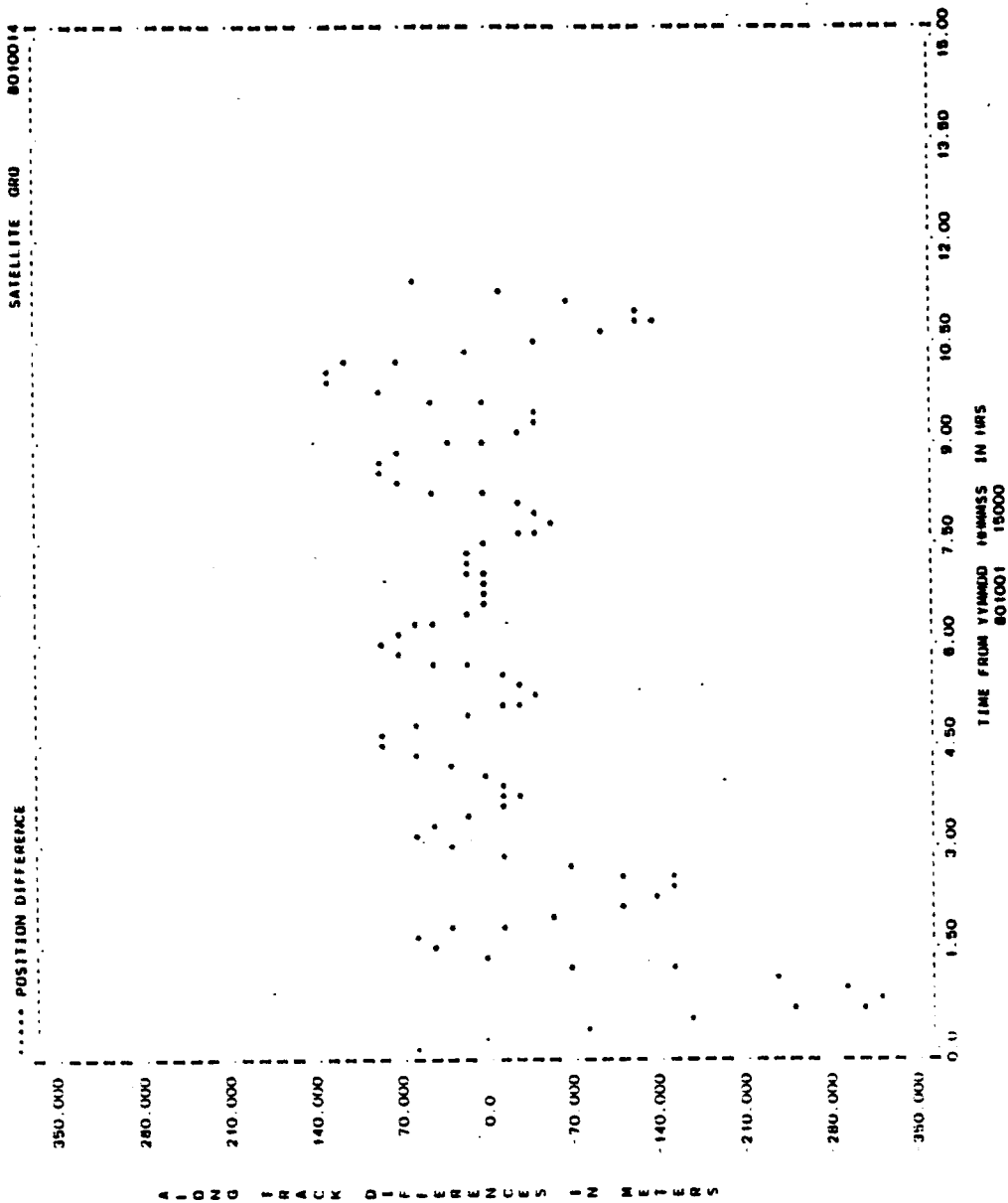


Figure A-72. Along-Track Differences for Run G06 (1 of 2)

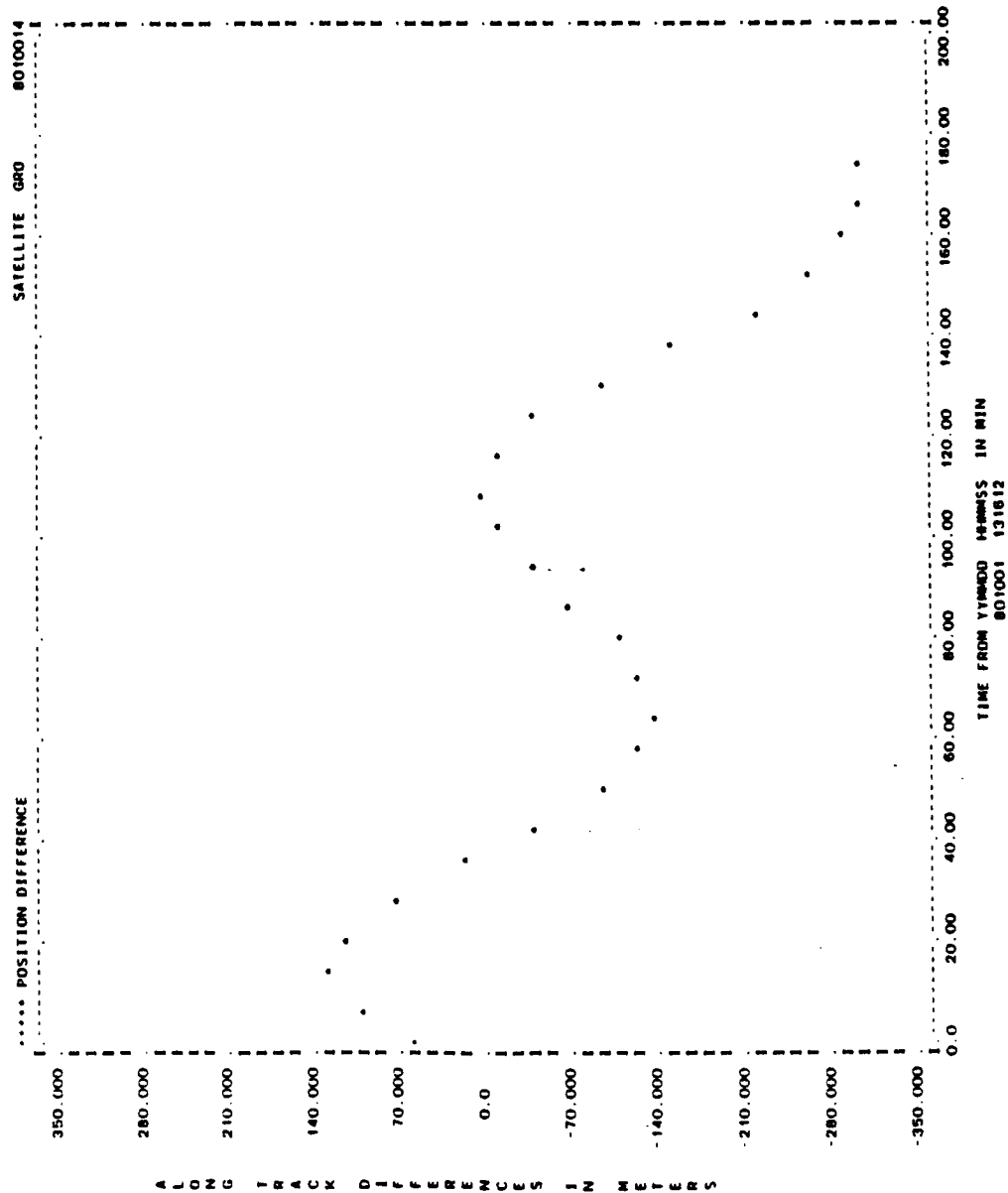


Figure A-72. Along-Track Differences for Run G05 (2 of 2)

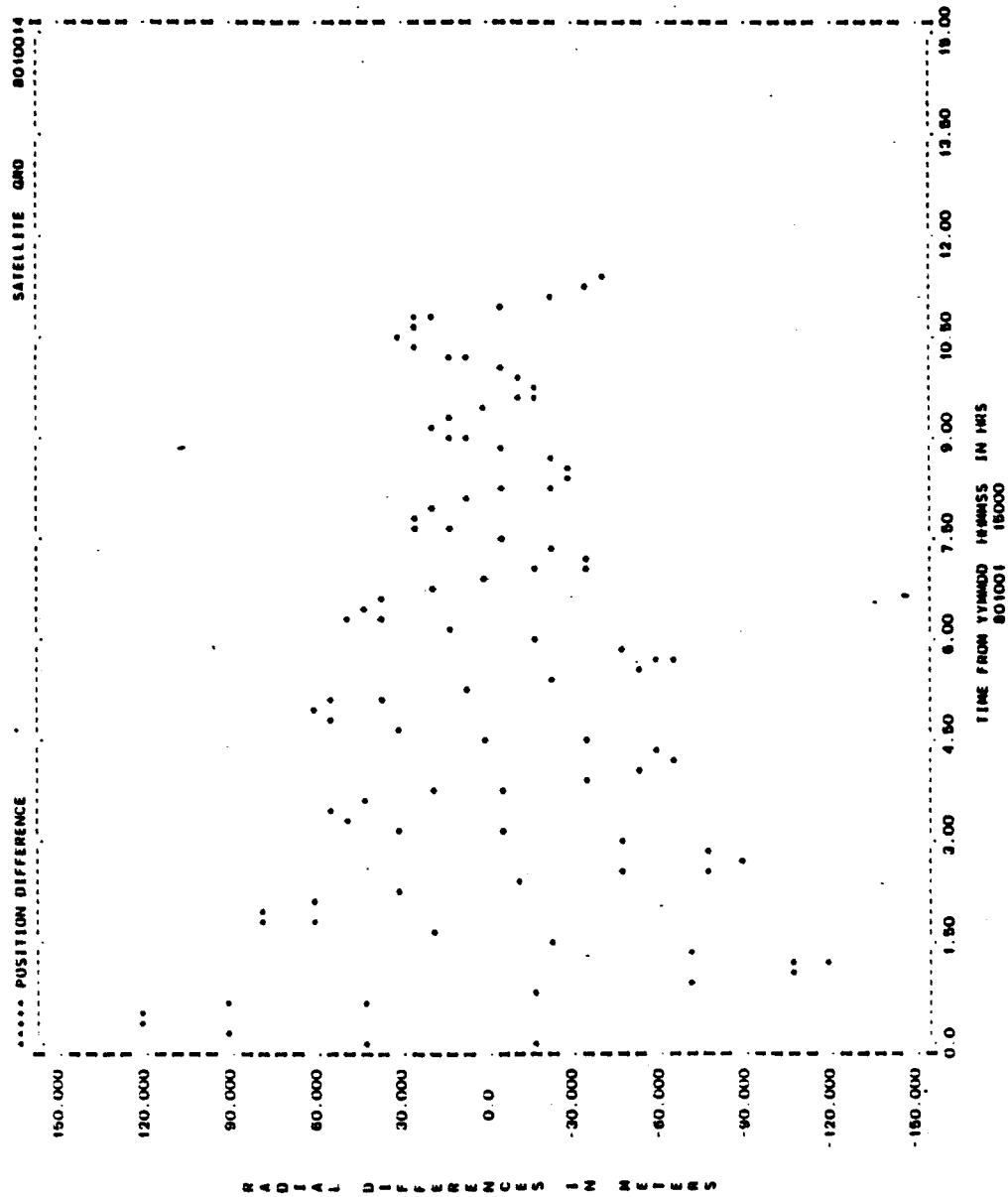


Figure A-73. Radial Differences for Run GL5 (1 of 2)

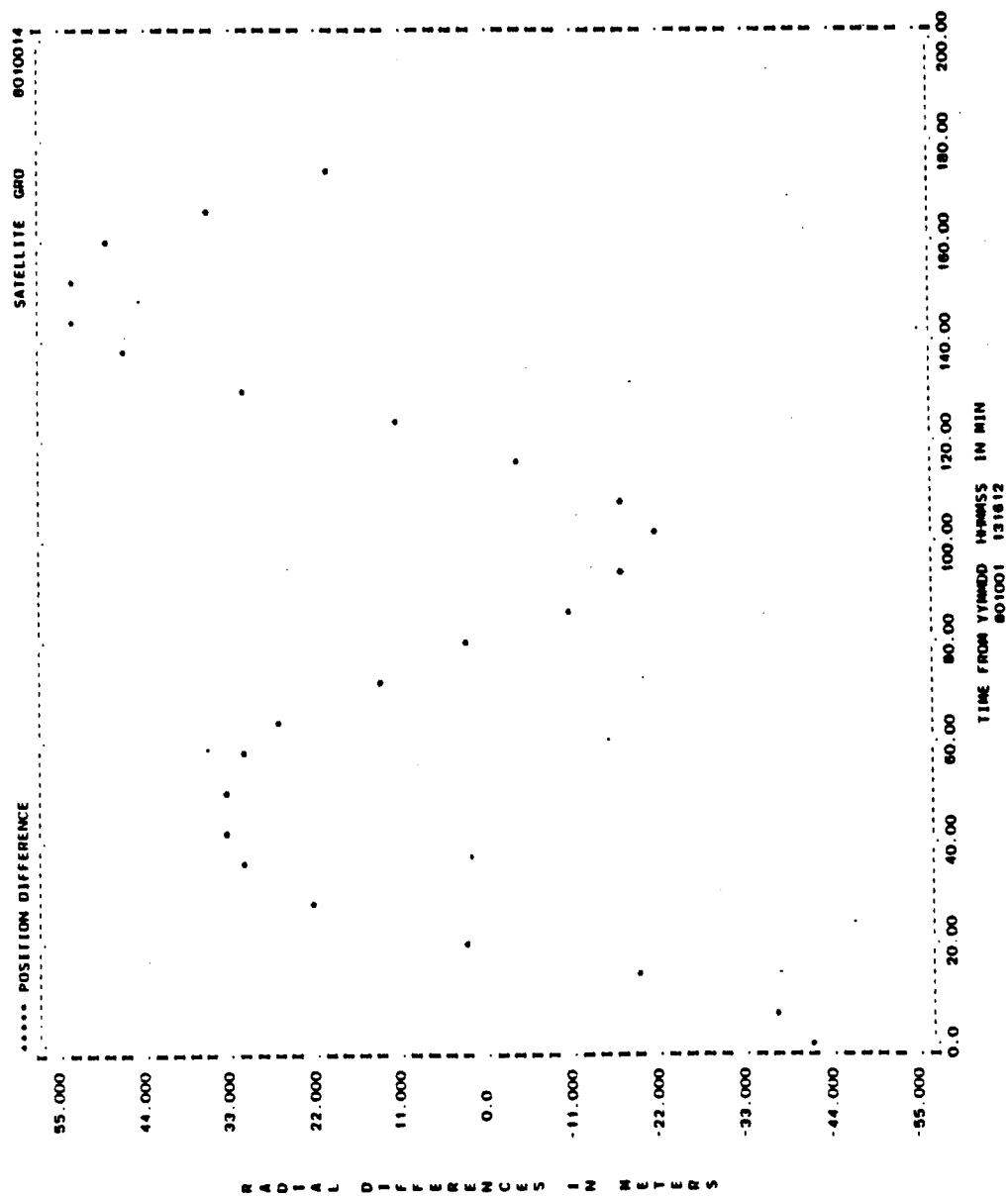


Figure A-73. Radial Differences for Run G15 (2 of 2)

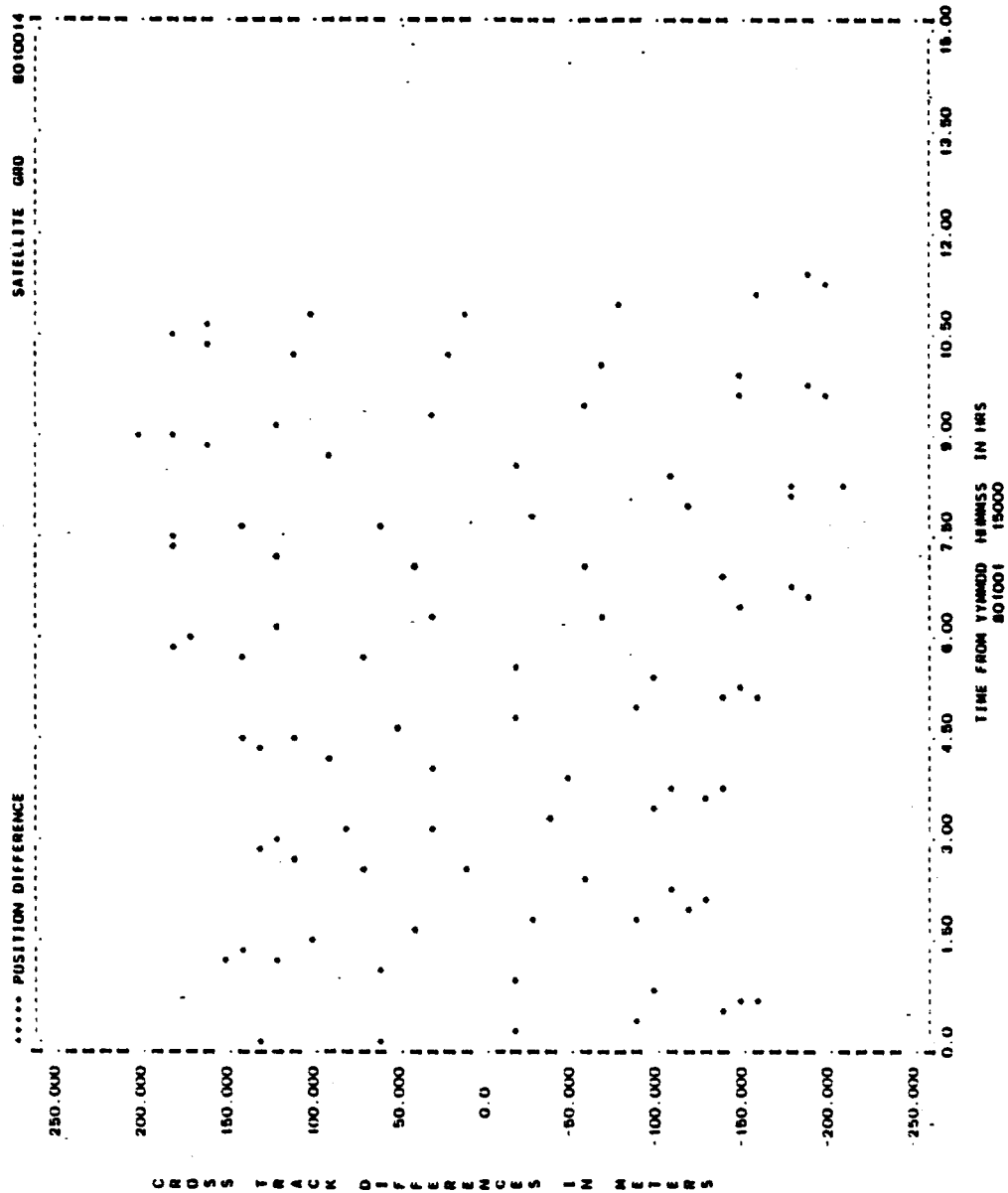


Figure A-74. Cross-Track Differences for Run G15 (1 of 2)

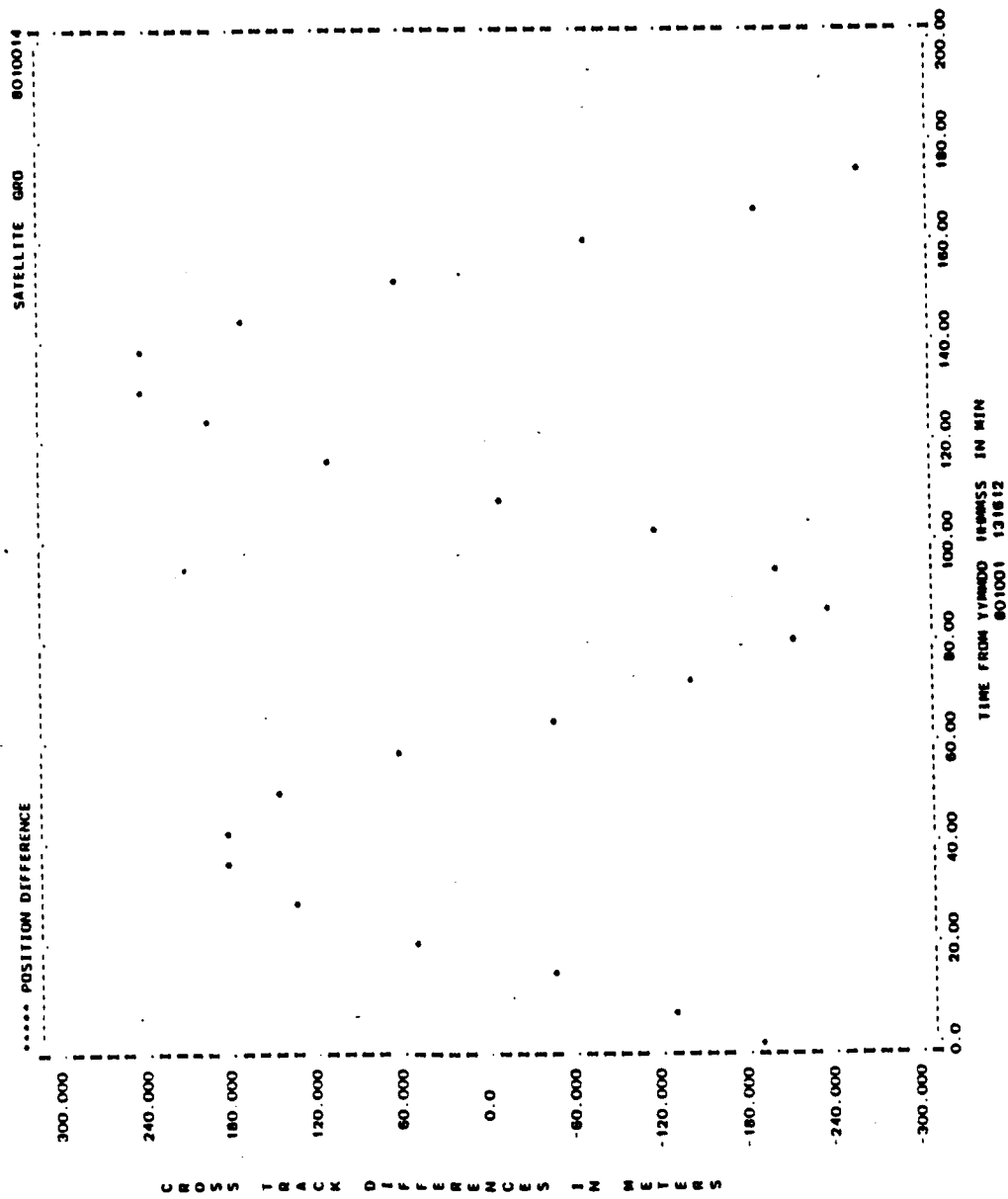


Figure A-74. Cross-Track Differences for Run G15 (2 of 2)

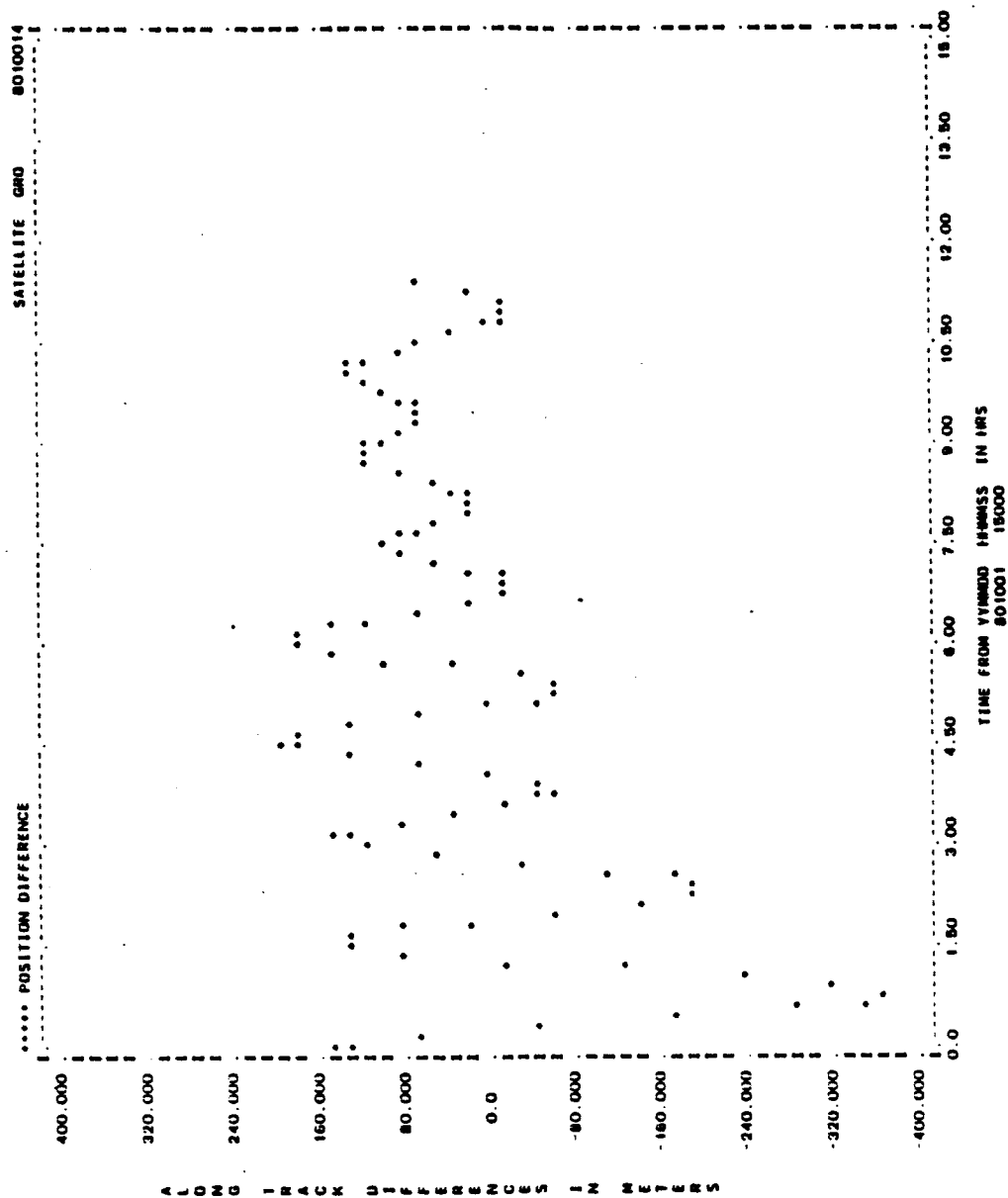


Figure A-75. Along-Track Differences for Run G15 (1 of 2)

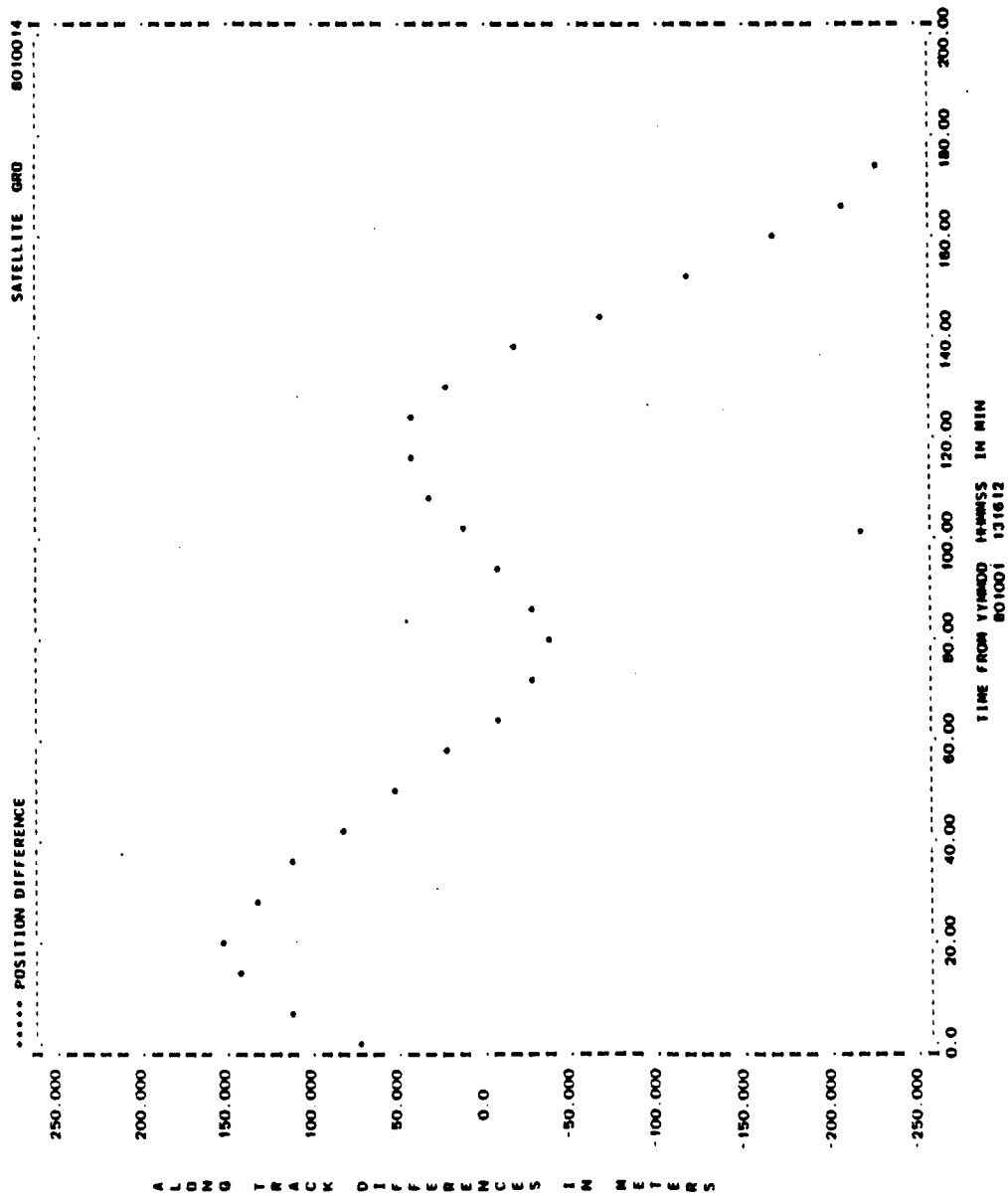


Figure A-75. Along-Track Differences for Run G15 (2 of 2)

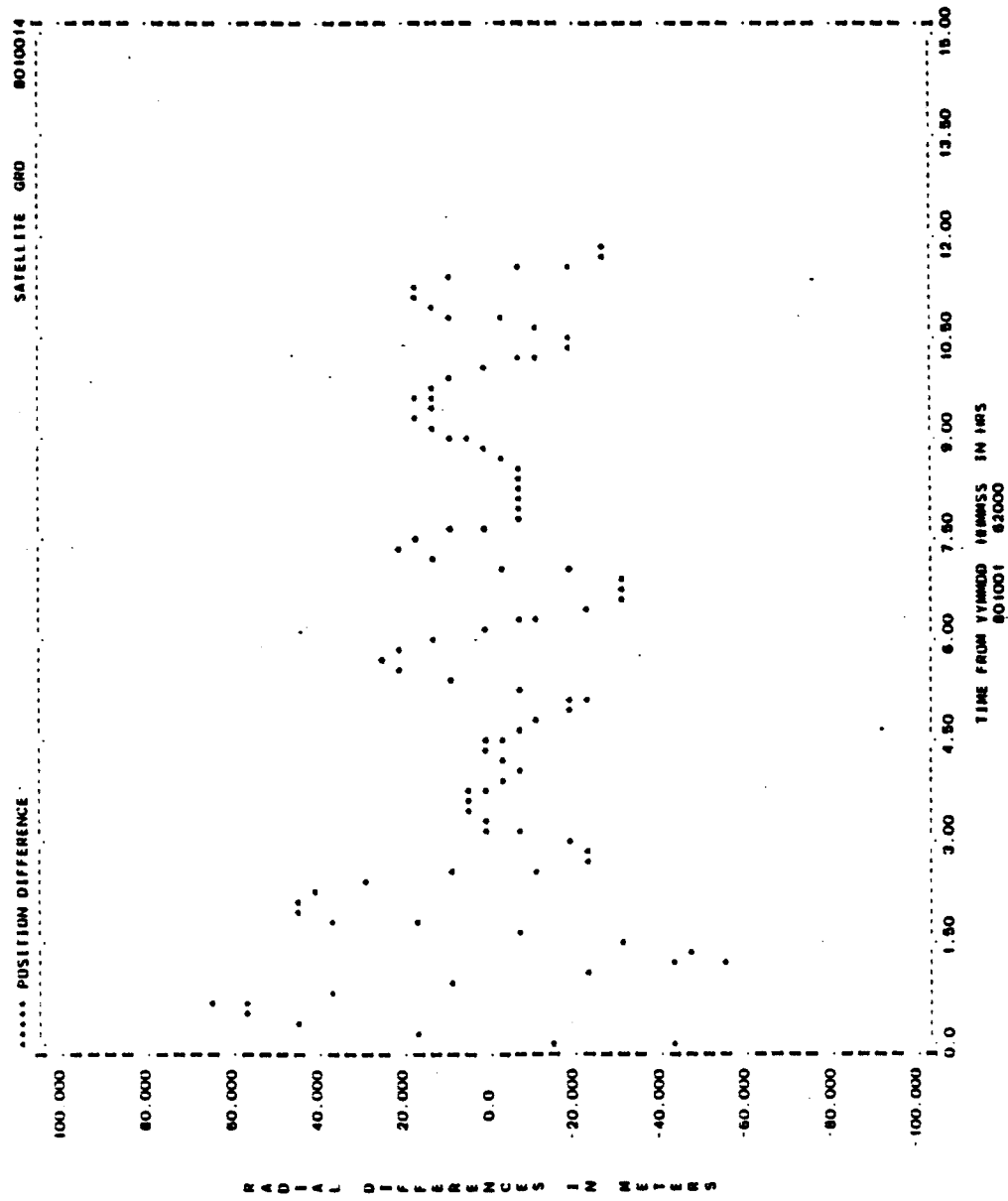


Figure A-76. Radial Differences for Run G15 (1 of 2)

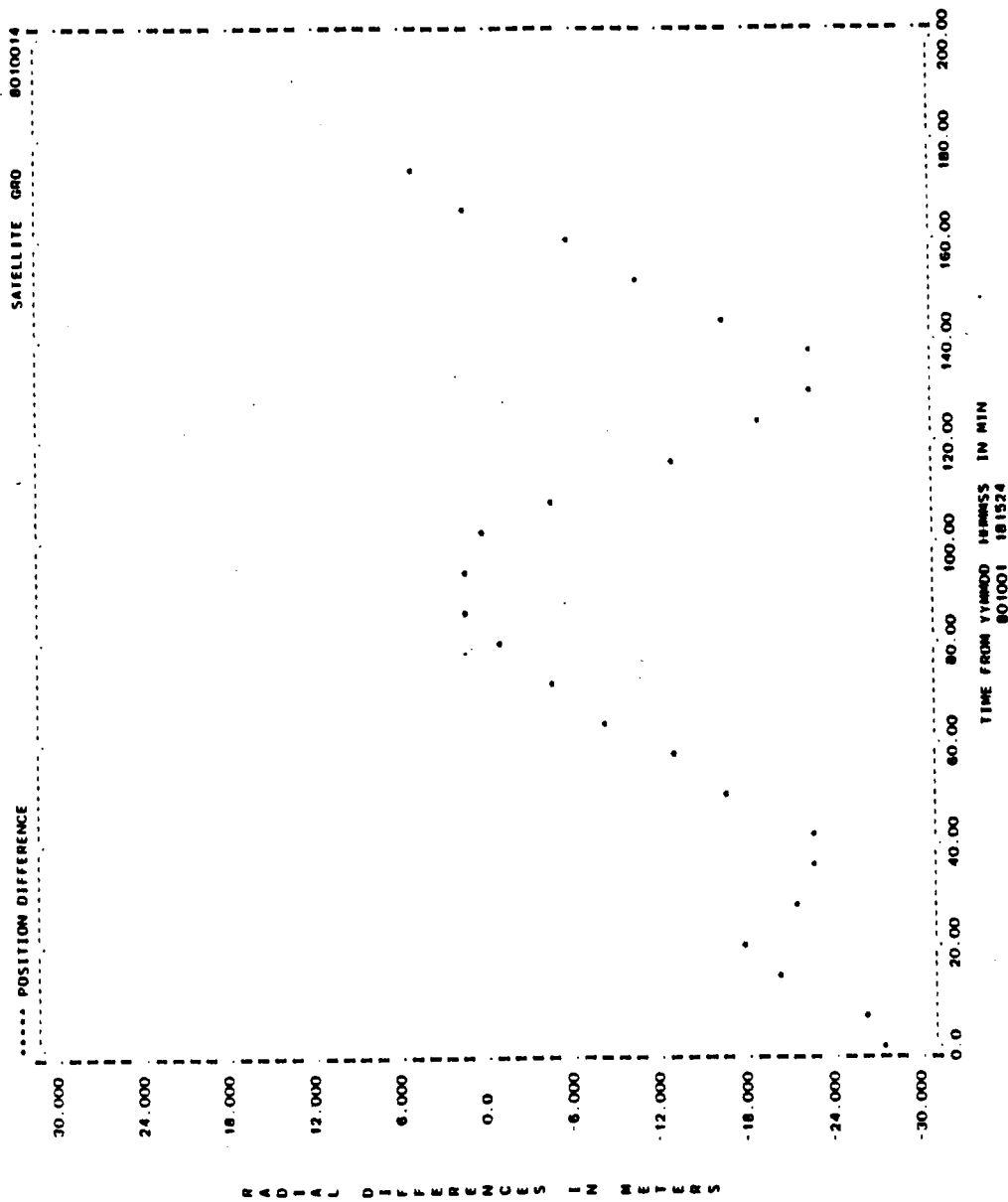


Figure A-76. Radial Differences for Run G15 (2 of 2)

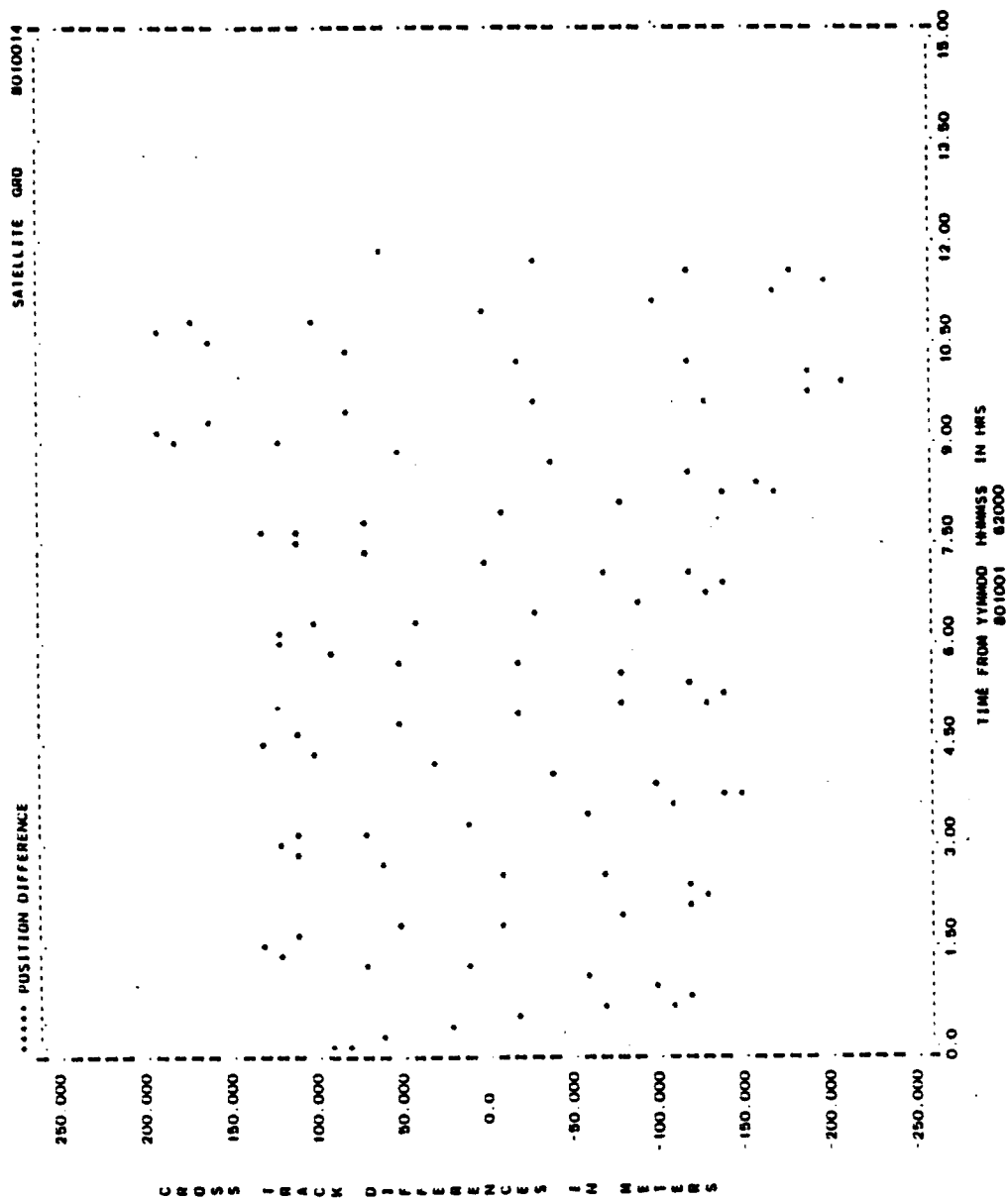


Figure A-77. Cross-Track Differences for Run G15 (1 of 2)

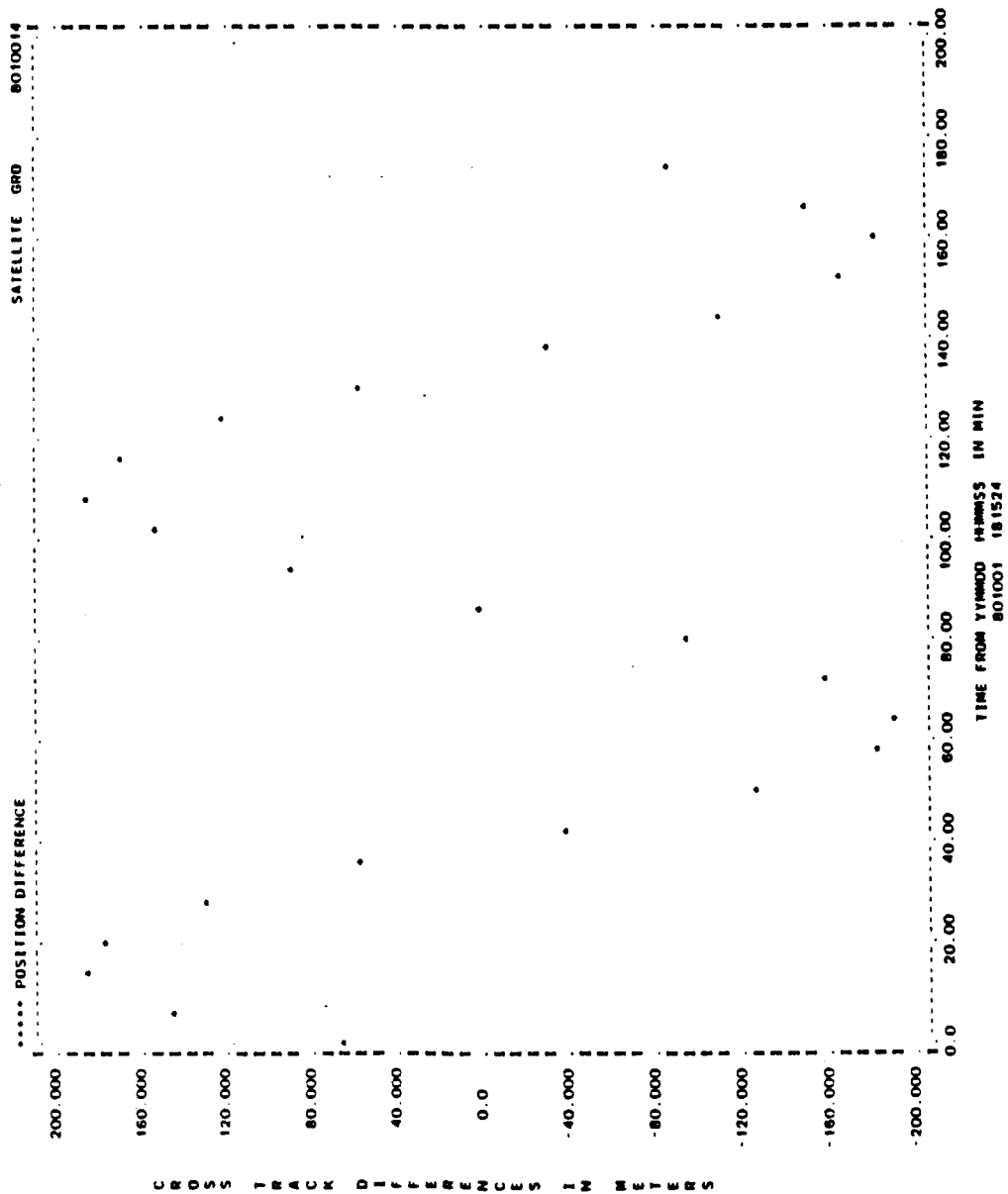


Figure A-77. Cross-Track Differences for Run G15 (2 of 2)

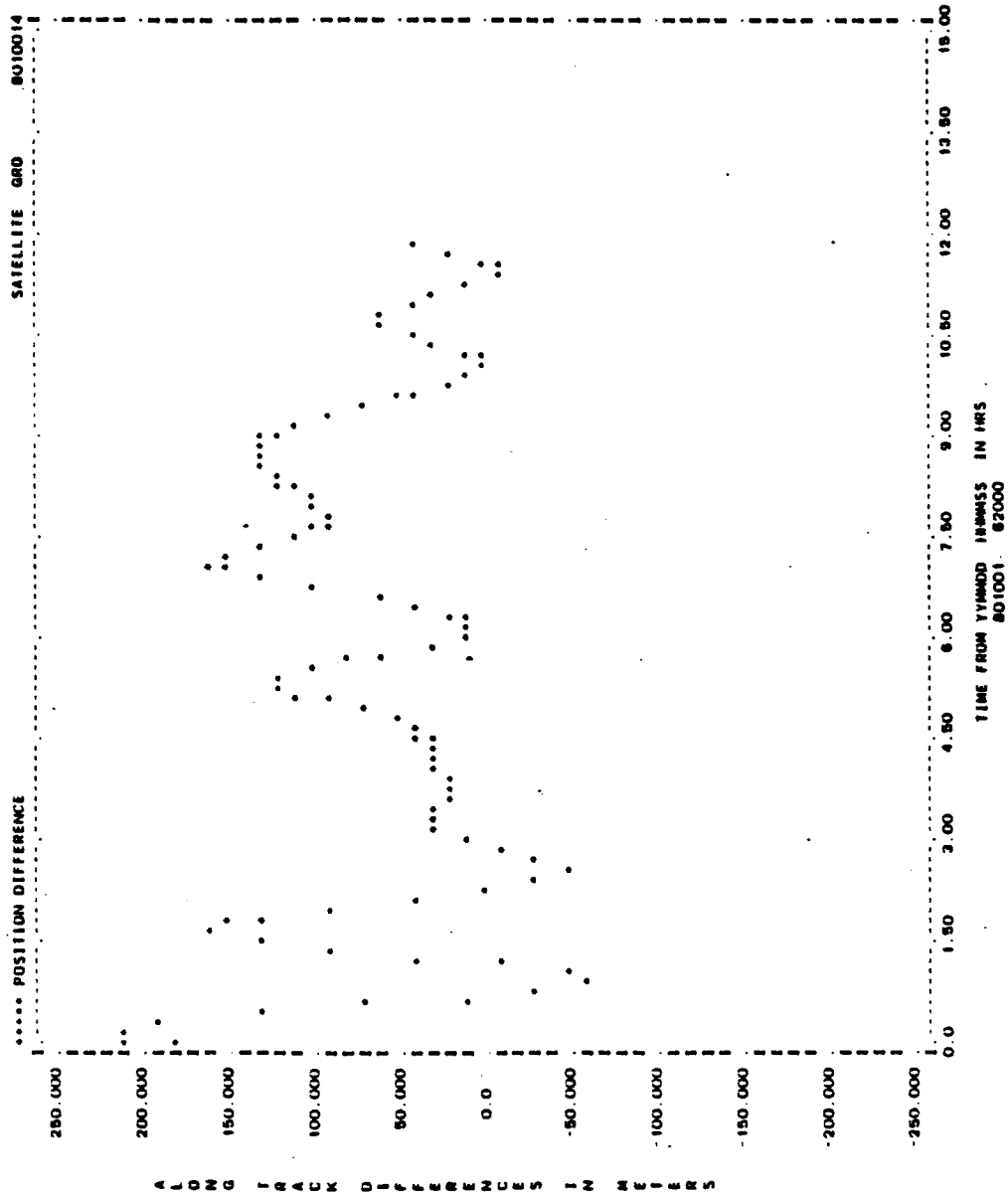


Figure A-78. Along-Track Differences for Run G15 (1 of 2)

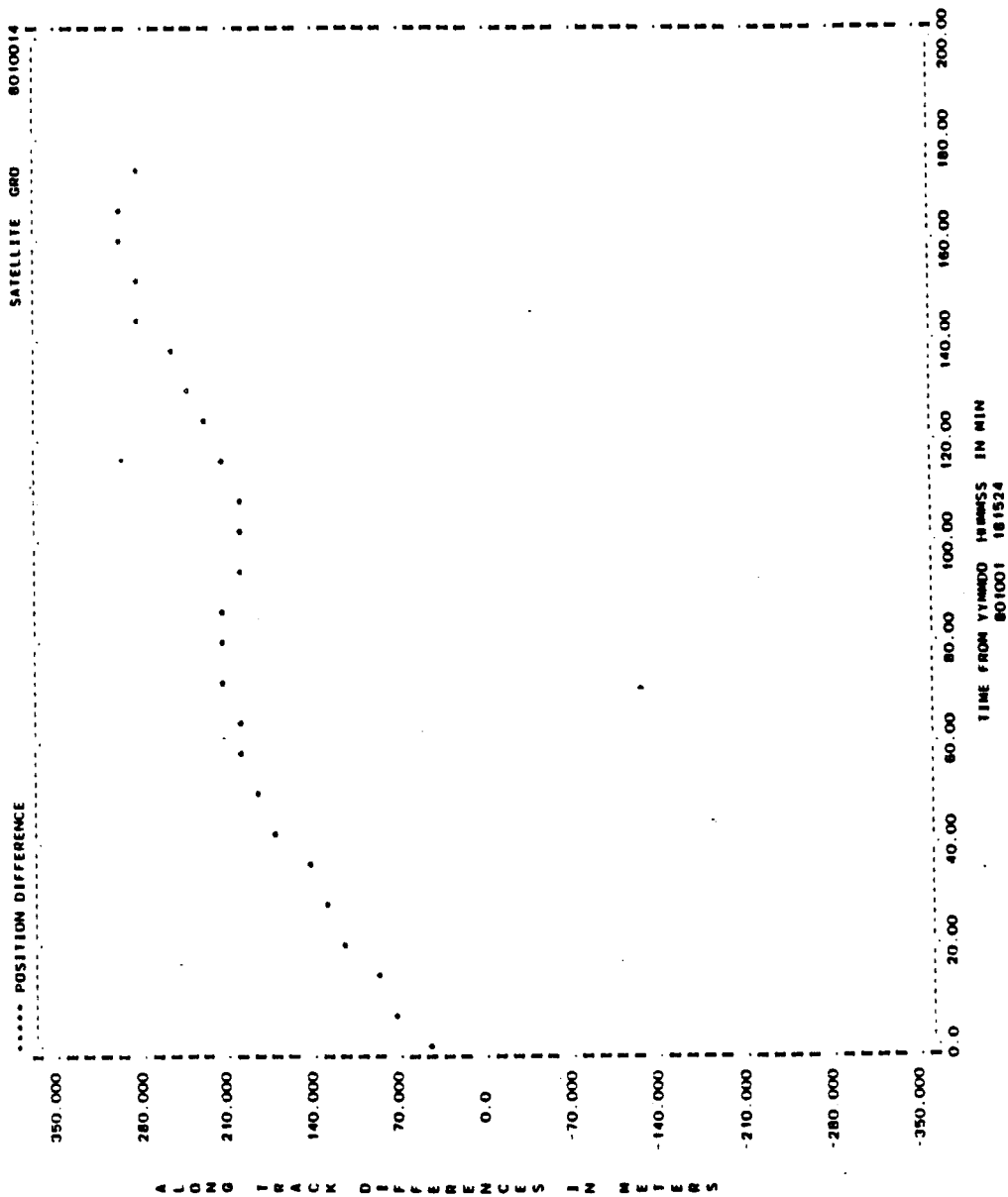


Figure A-78. Along-Track Differences for Run G15 (2 of 2)

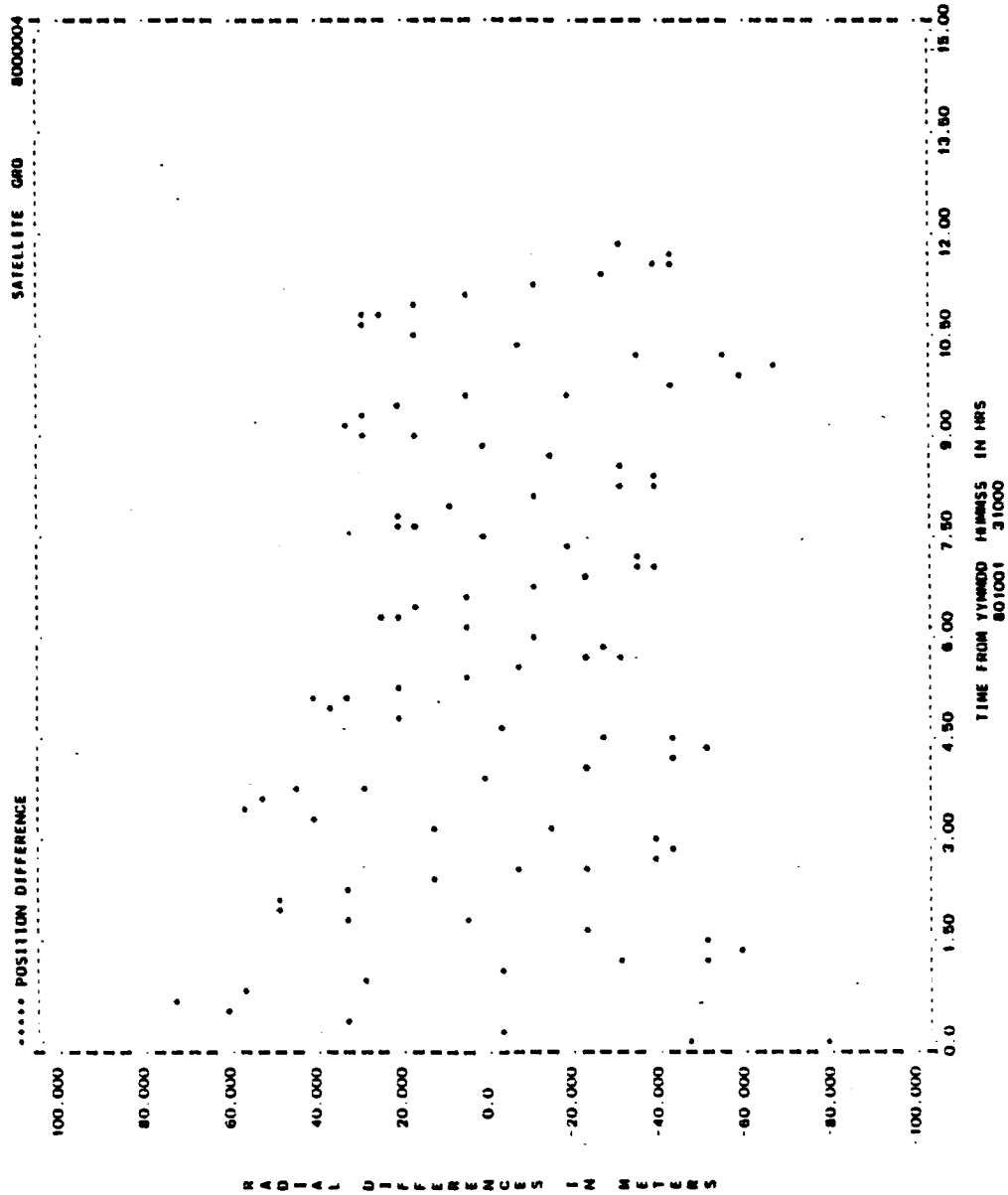


Figure A-79. Radial Differences for Run G11 (1 of 2)

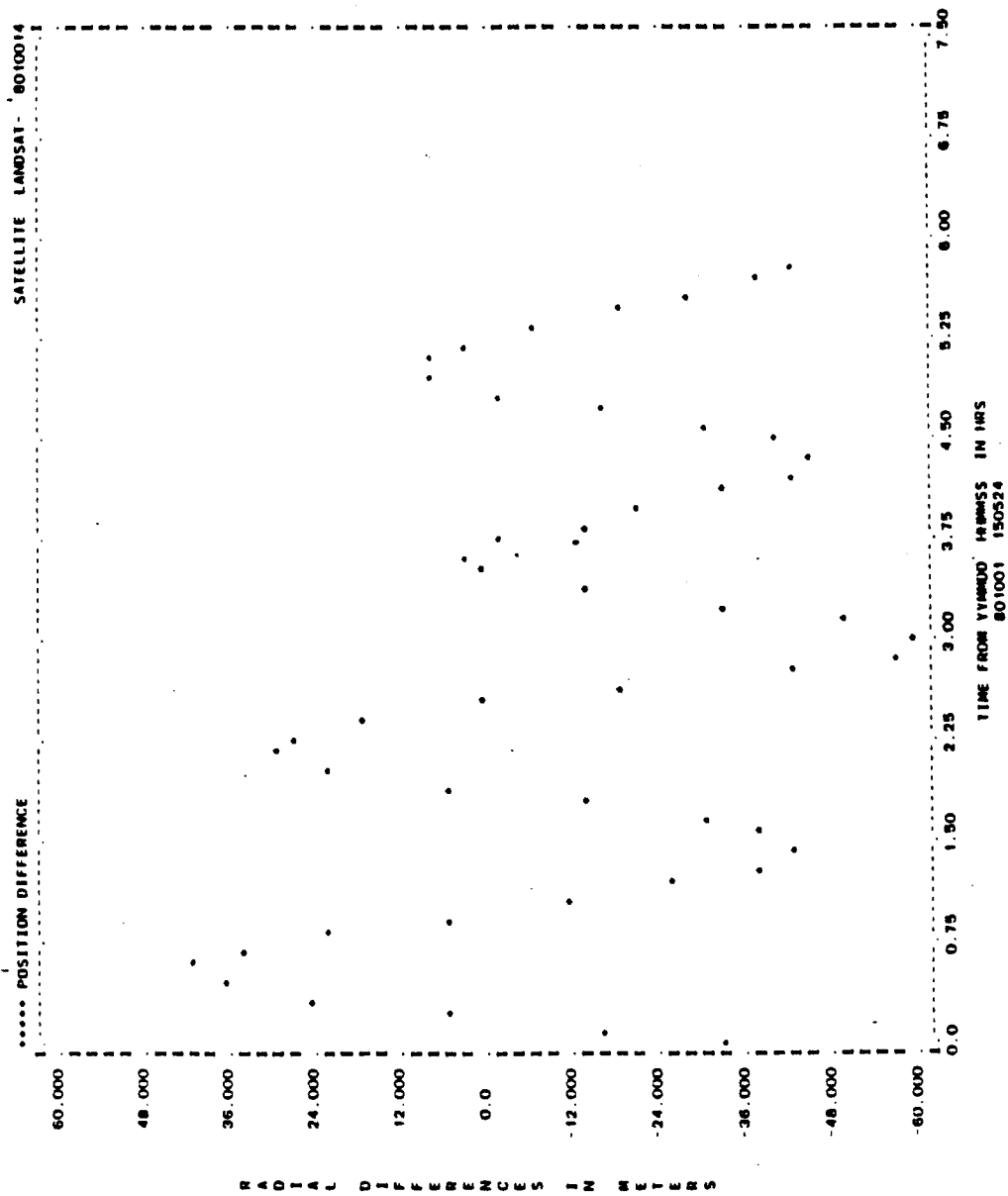


Figure A-79. Radial Differences for Run Gll (2 of 2)

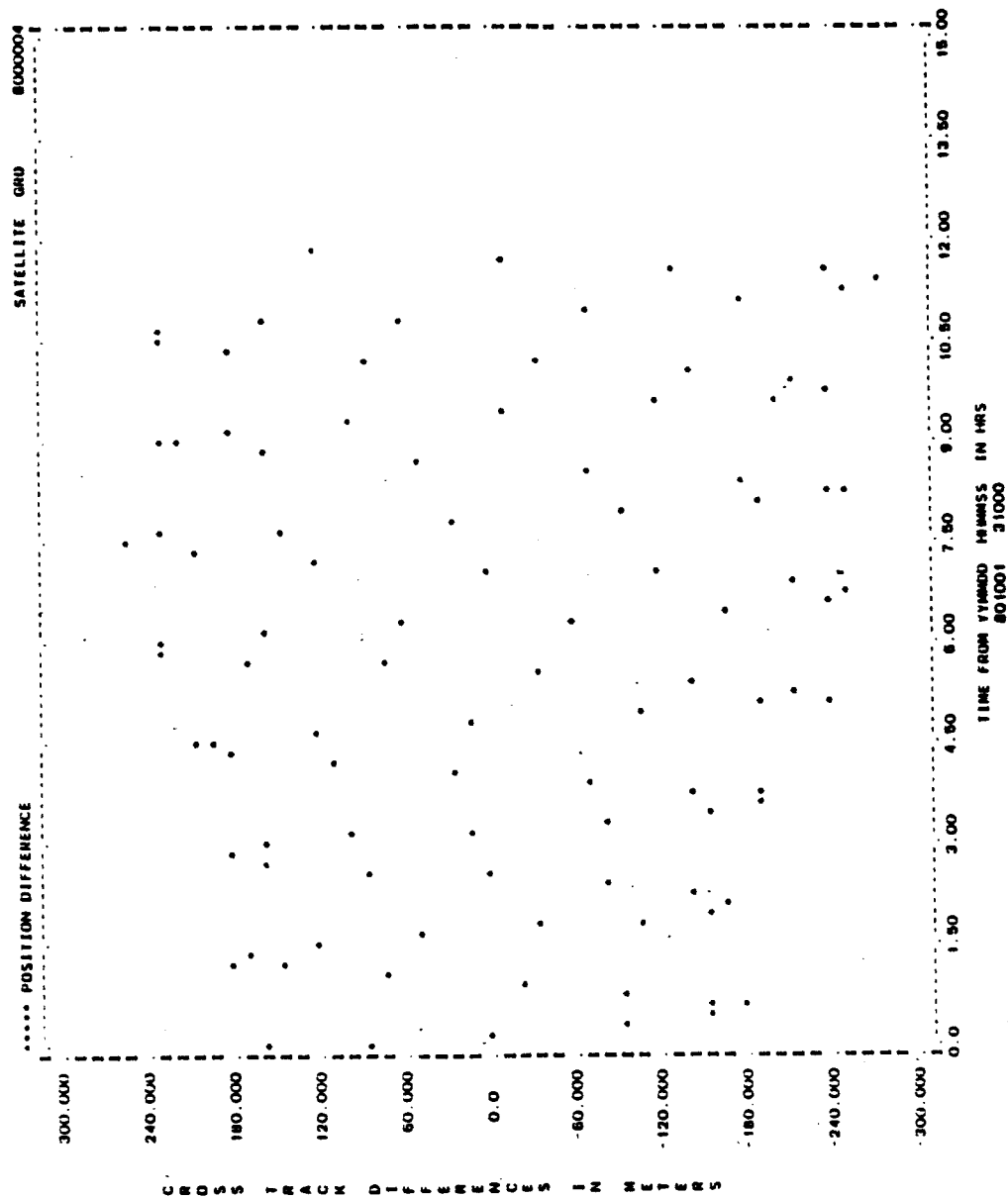


Figure A-80. Cross-Track Differences for Run G11 (1 of 2)



TIME FROM YEMMED H-AMSS IN HRS  
801001 150524

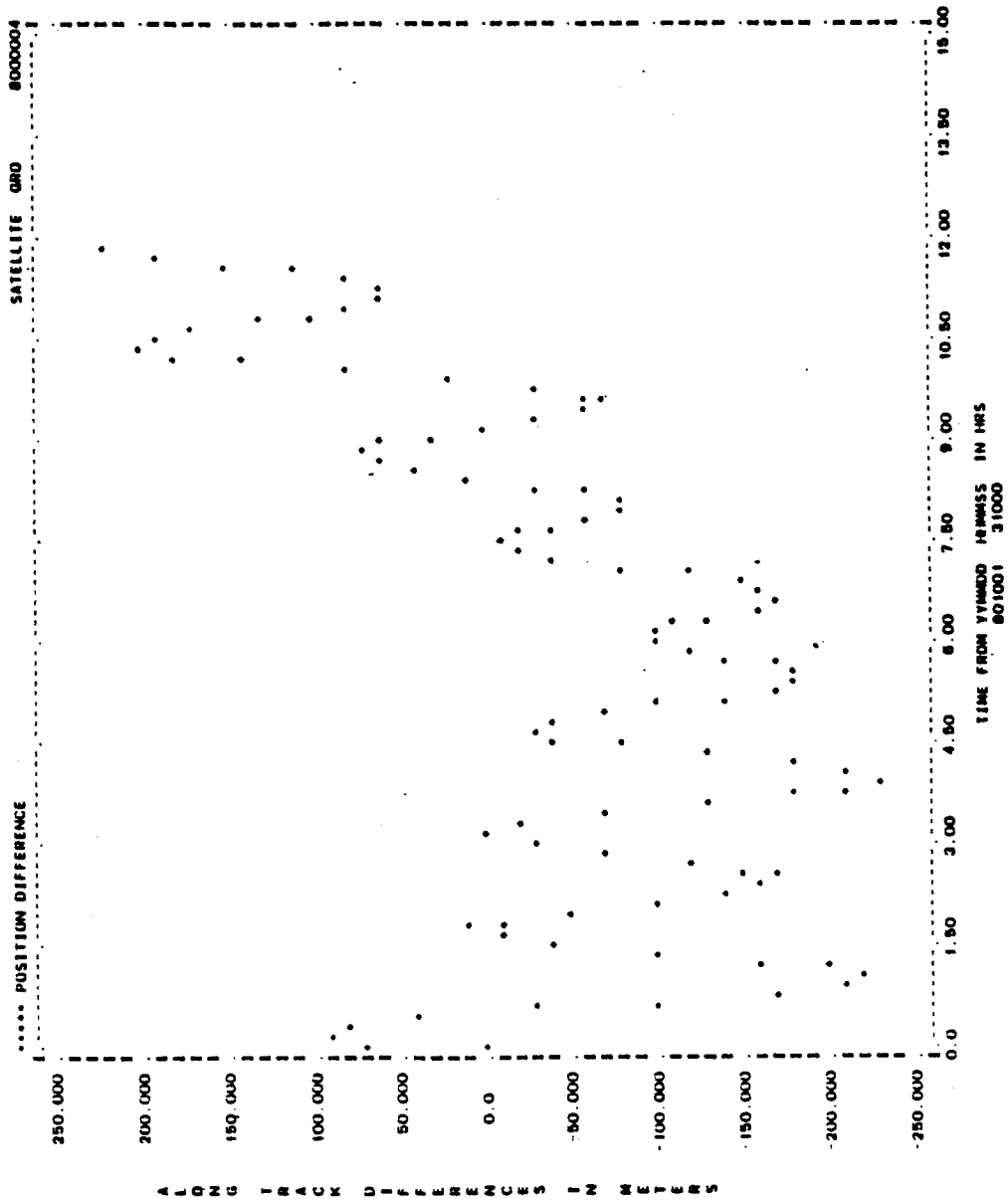


Figure A-81. Along-Track Differences for Run G11 (1 of 2)

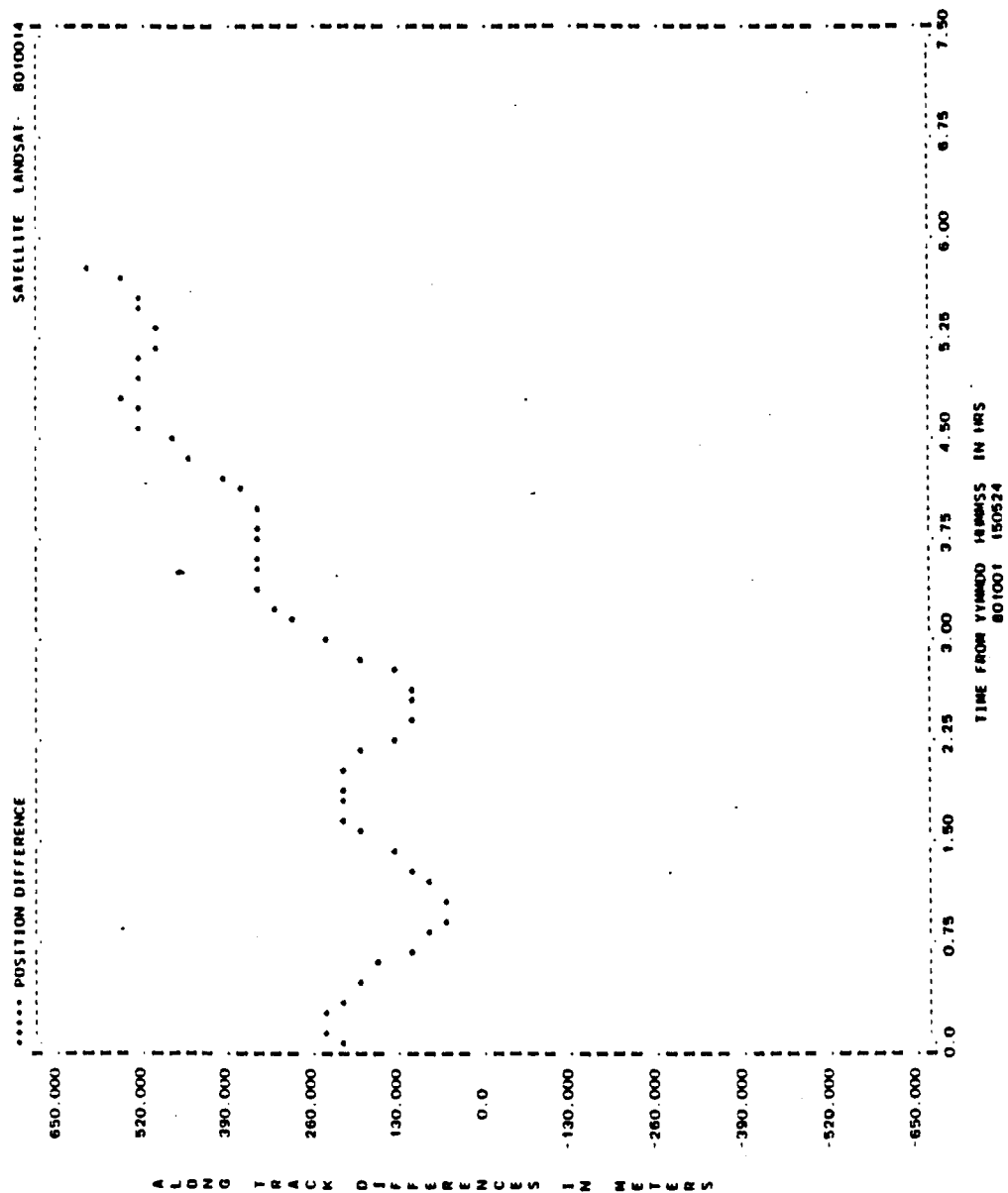


Figure A-81. Along-Track Differences for Run G11 (2 of 2)

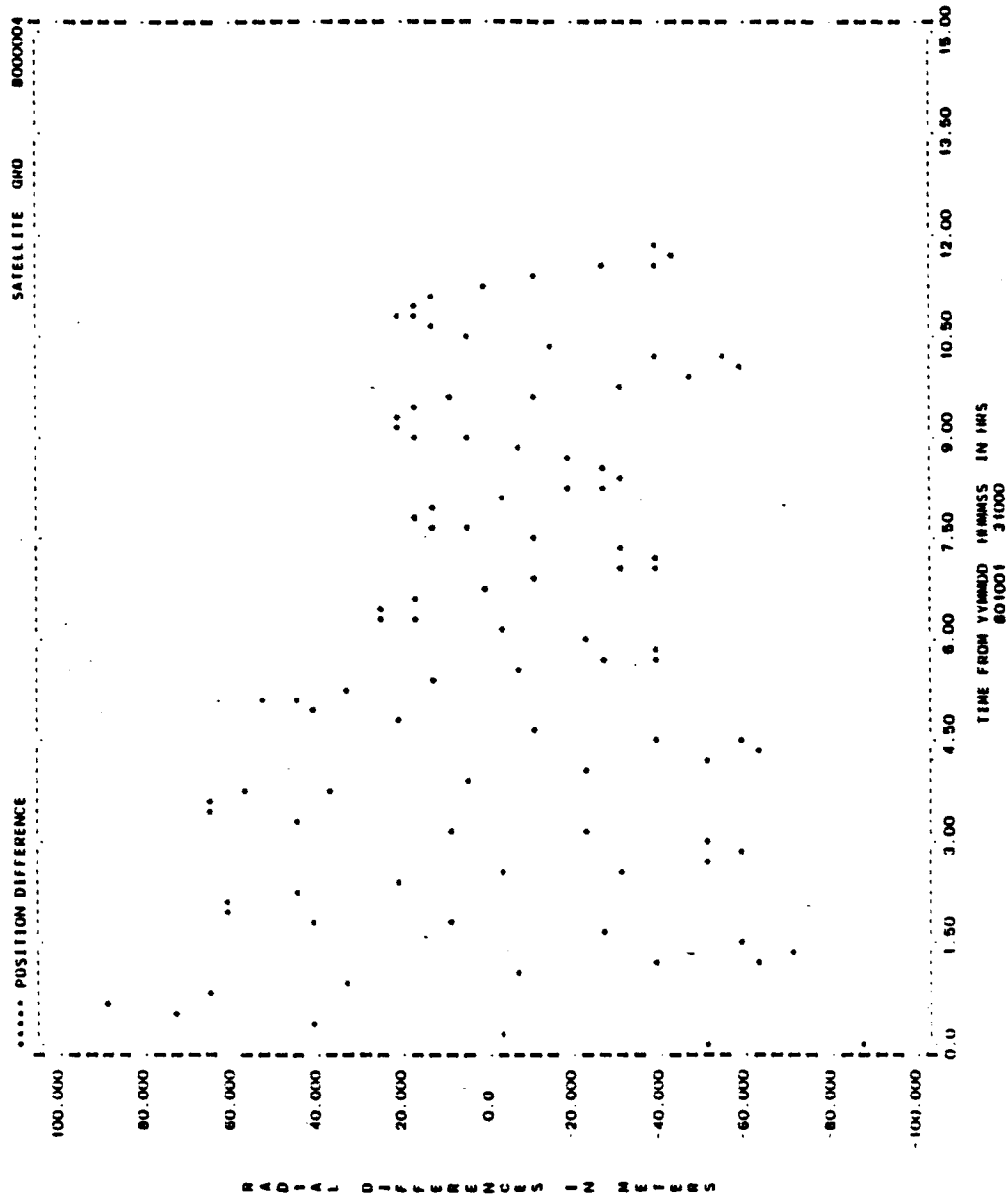


Figure A-82. Radial Differences for Run G14 (1 of 2)

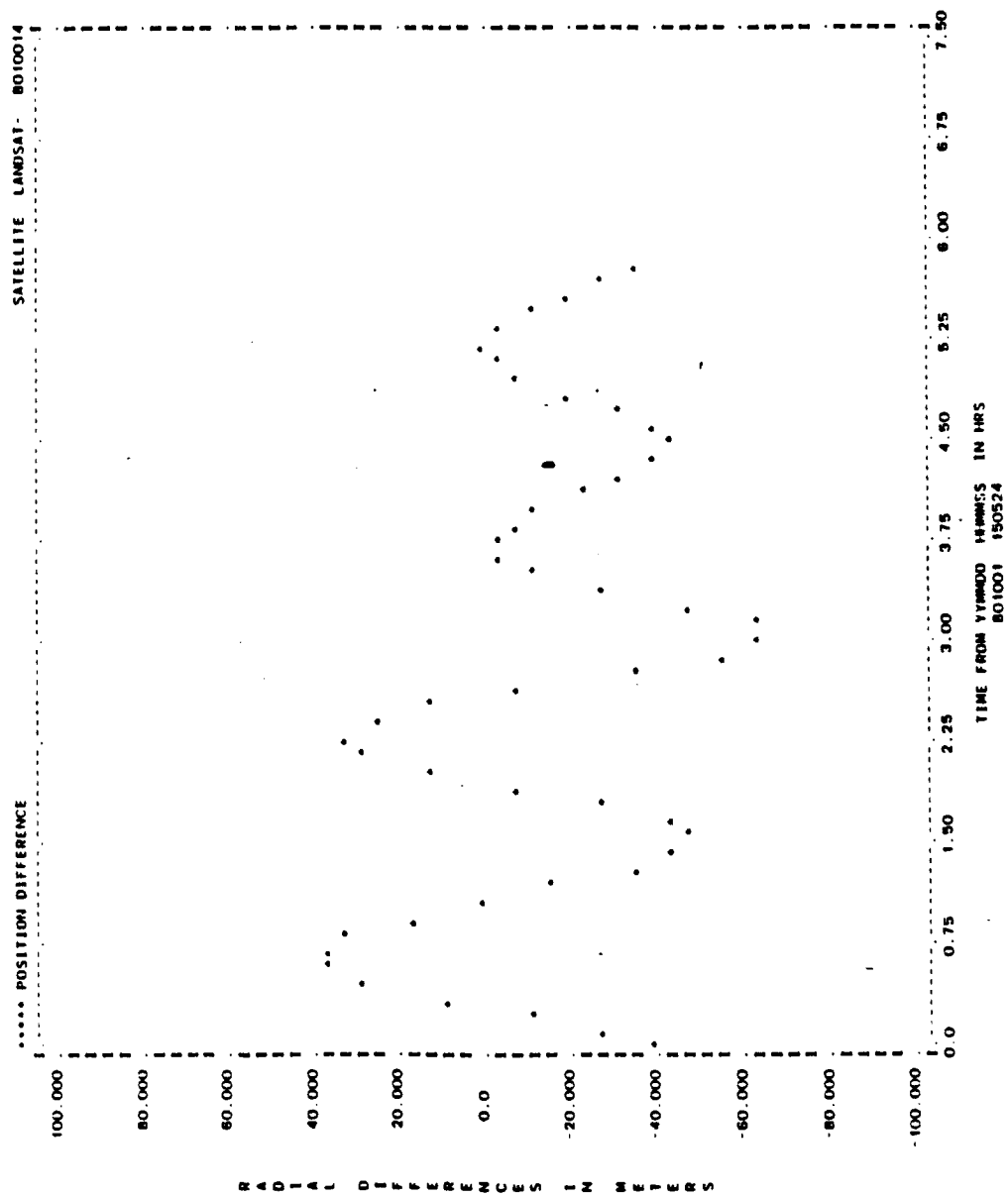


Figure A-82. Radial Differences for Run G14 (2 of 2)

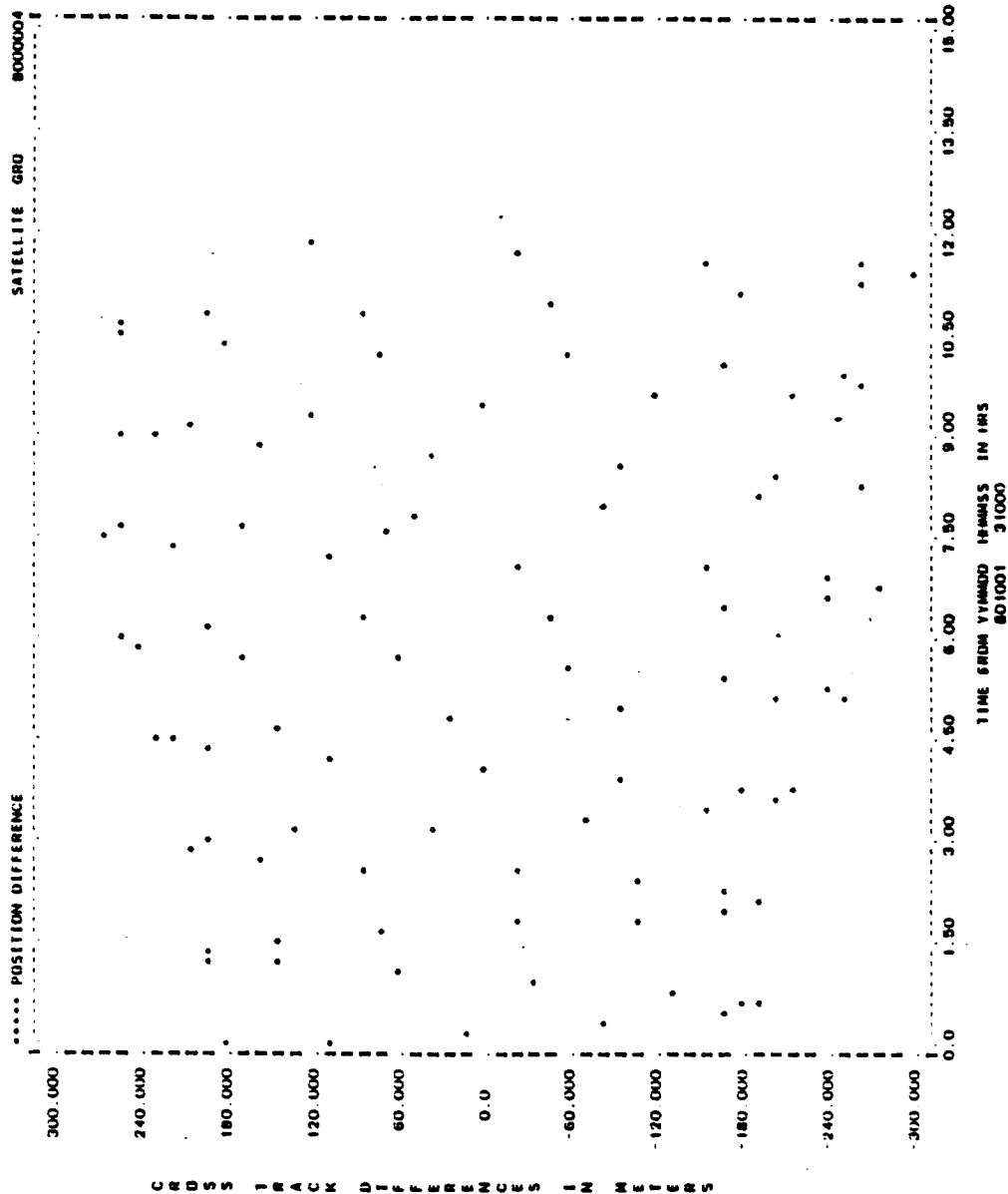


Figure A-83. Cross-Track Differences for Run G14 (1 of 2)

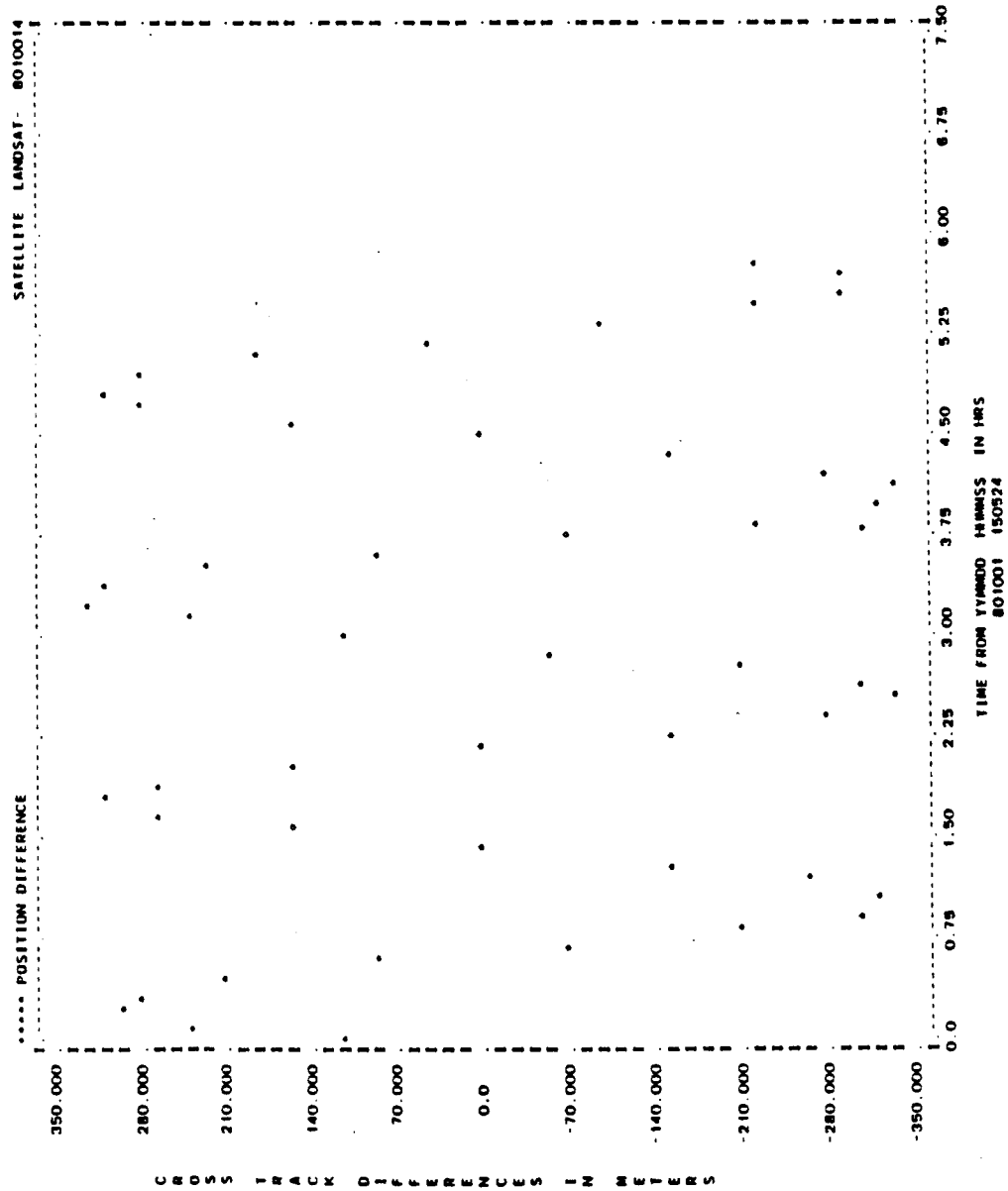


Figure A-83. Cross-Track Differences for Run GL4 (2 of 2)

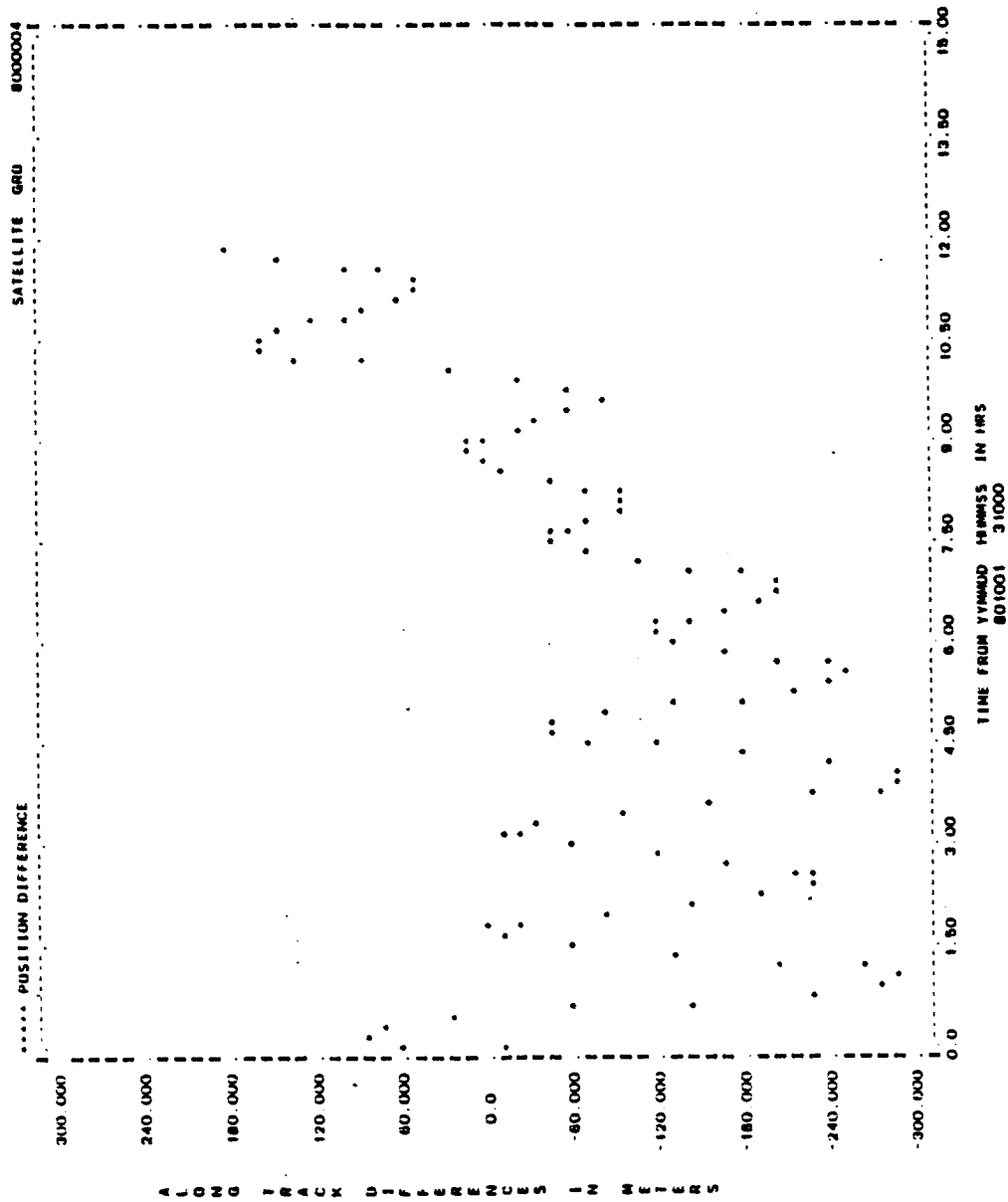


Figure A-84. Along-Track Differences for Run G14 (1 of 2)

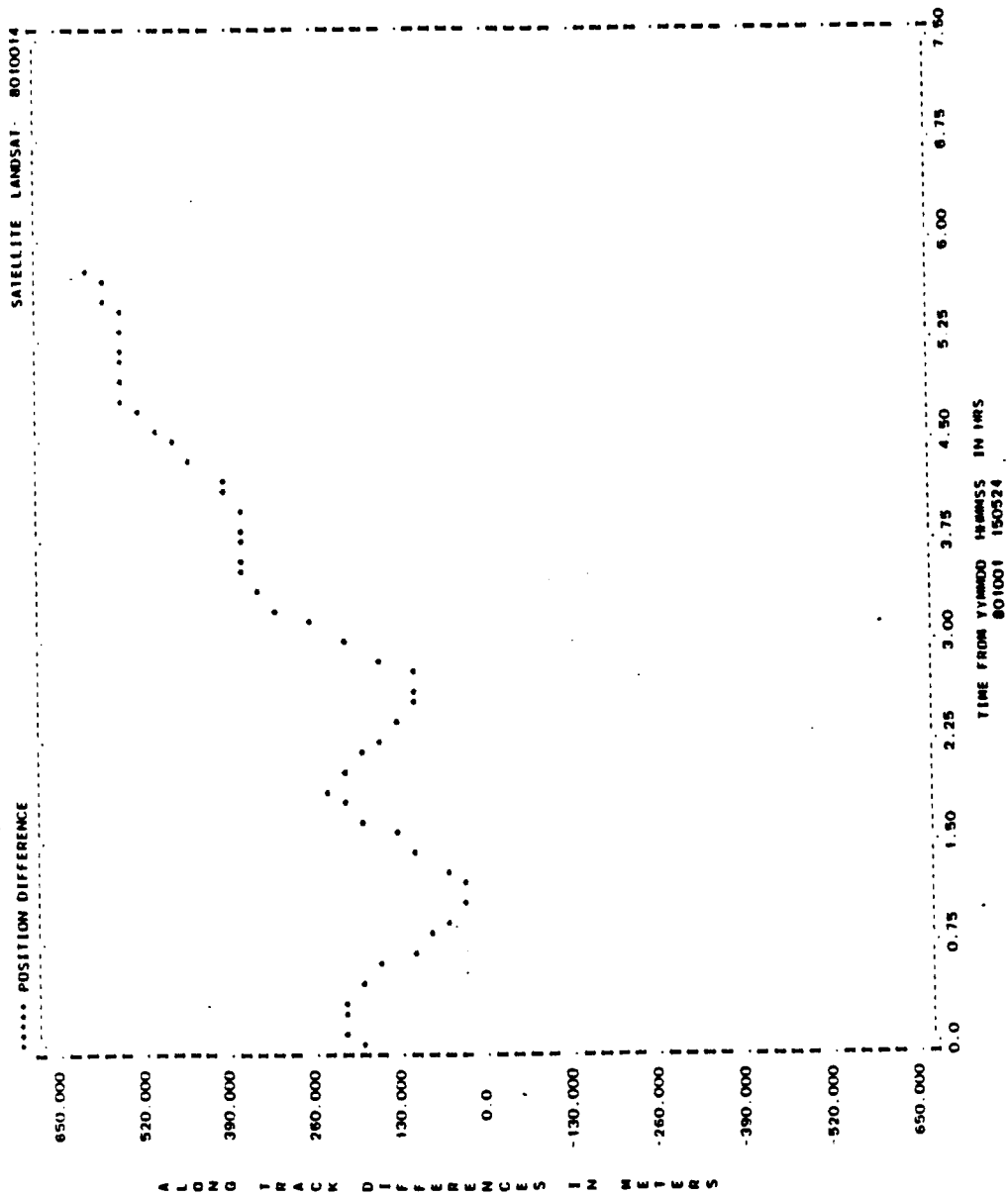


Figure A-84. Along-Track Differences for Run G14 (2 of 2)

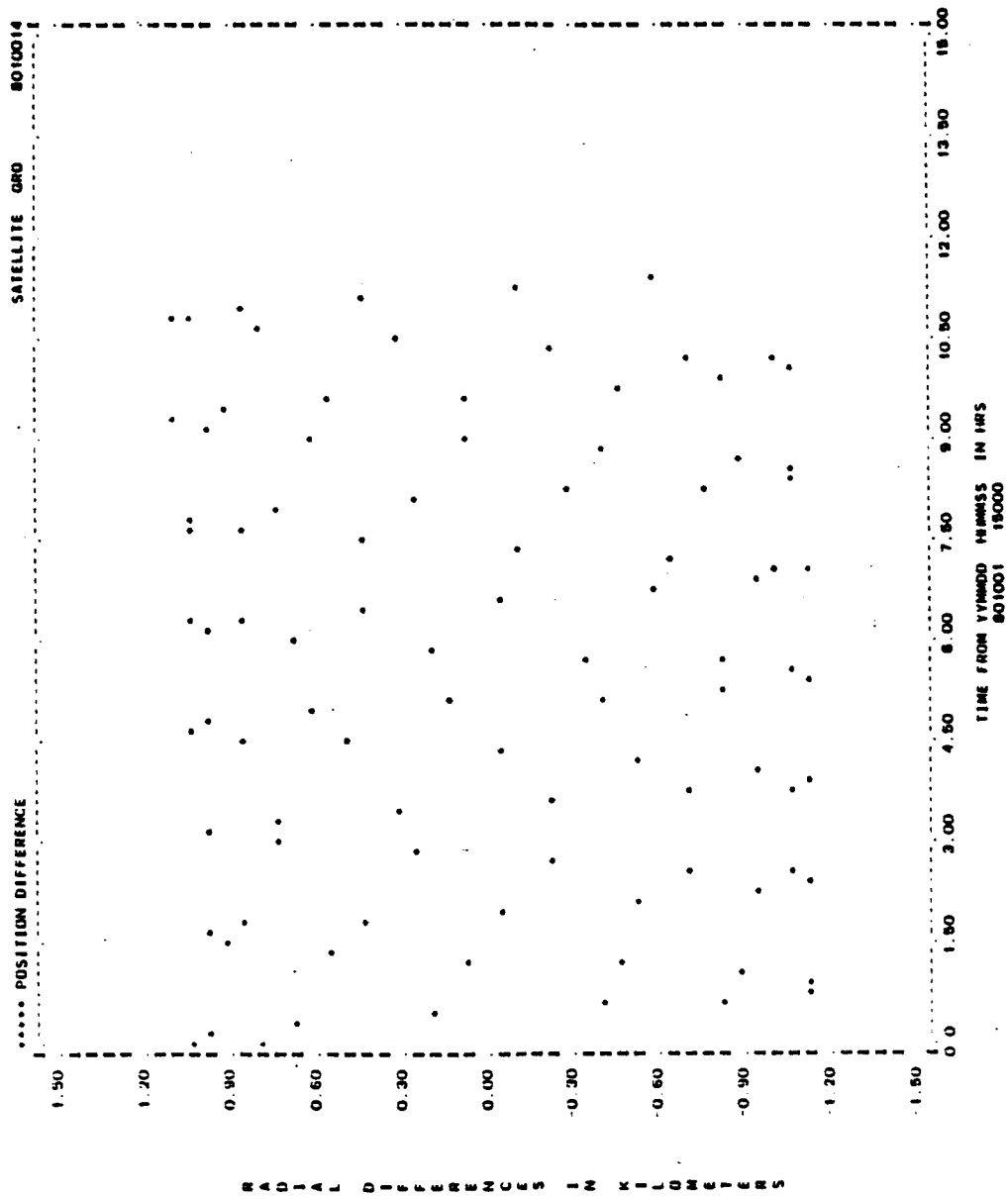


Figure A-85. Radial Differences for Run GL7 (1 of 2)

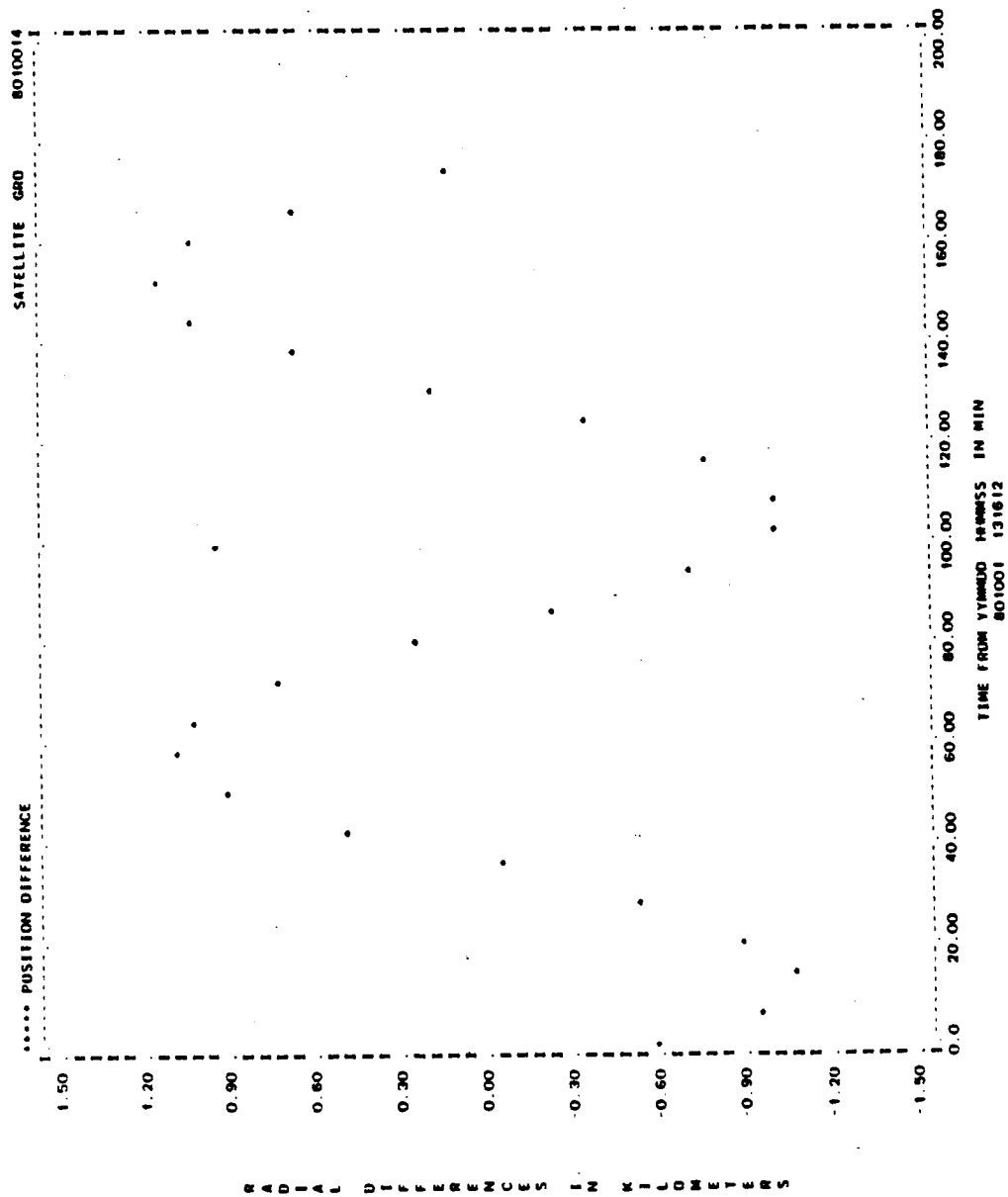


Figure A-85. Radial Differences for Run GL7 (2 of 2)

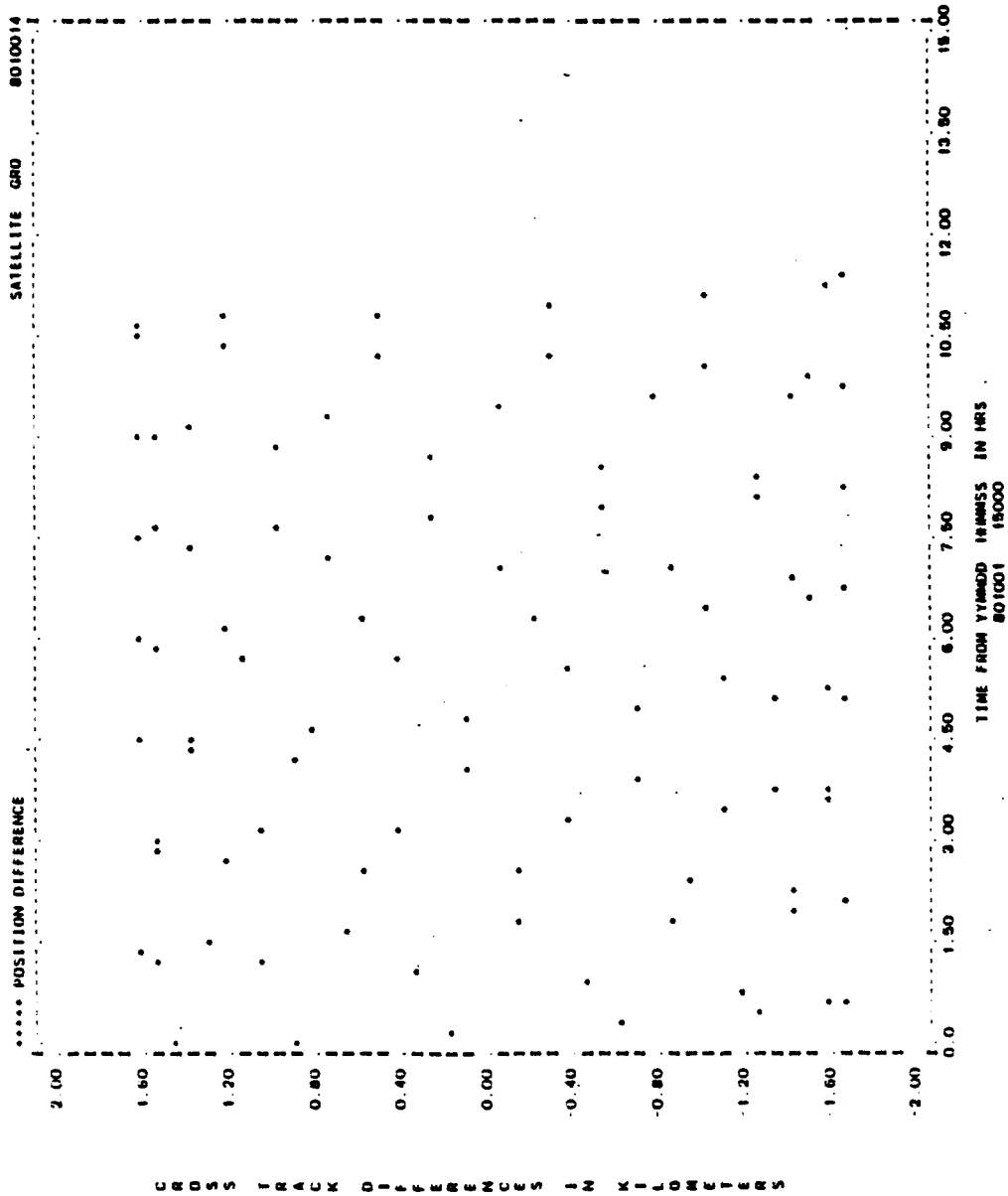


Figure A-86. Cross-Track Differences for Run GL7 (1 of 2)

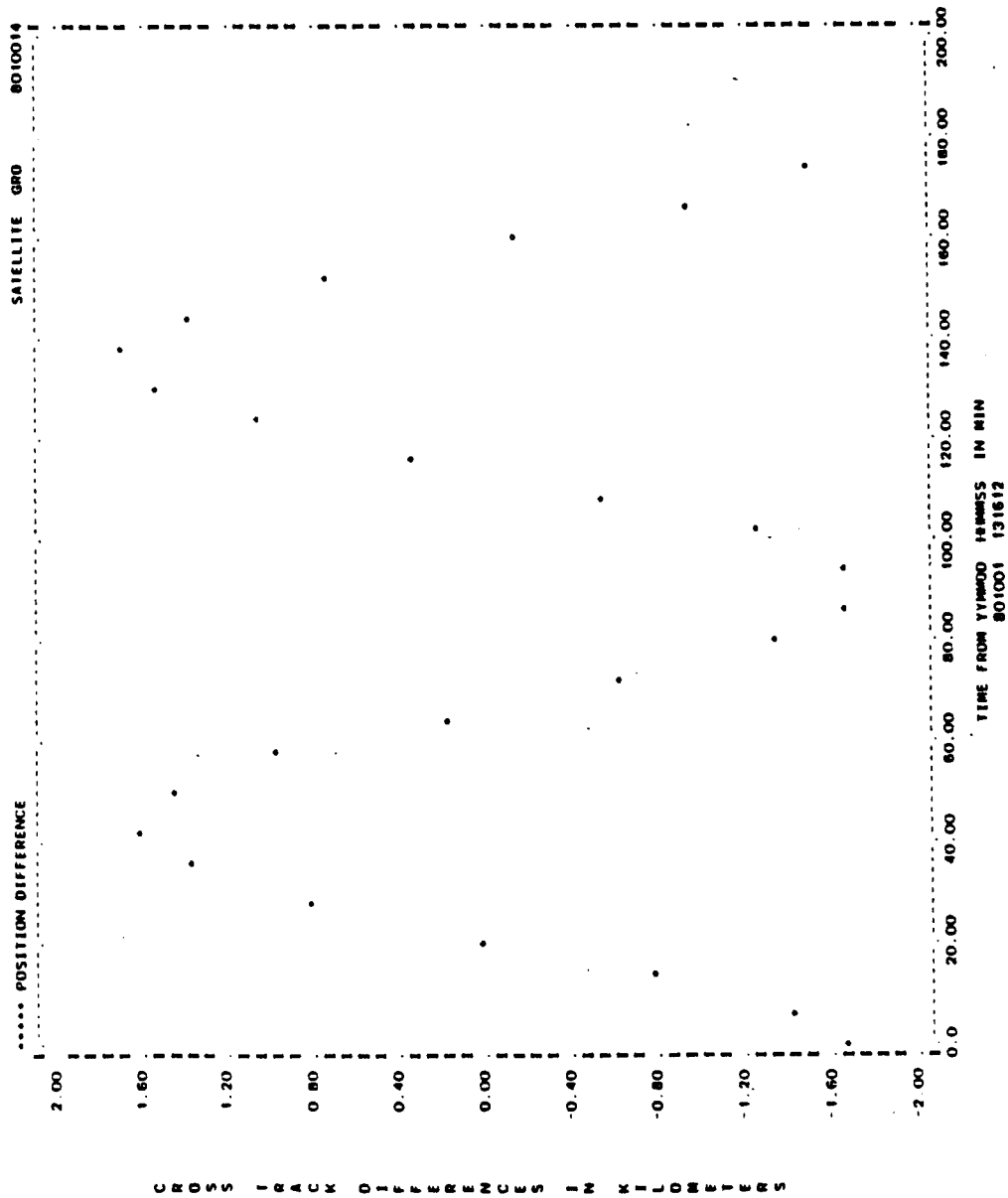


Figure A-86. Cross-Track Differences for Run GL7 (2 of 2)

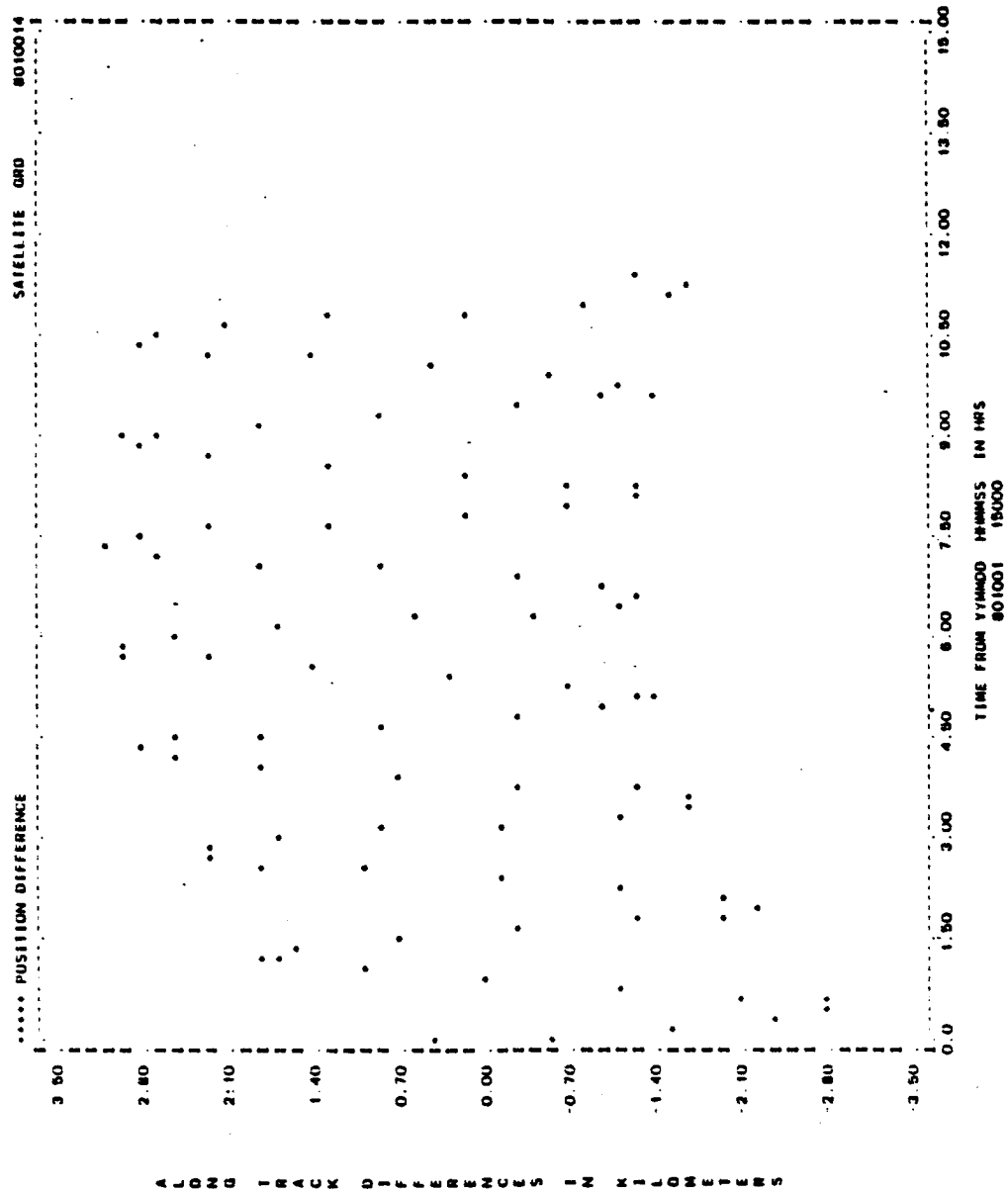


Figure A-87. Along-Track Differences for Run G17 (1 of 2)

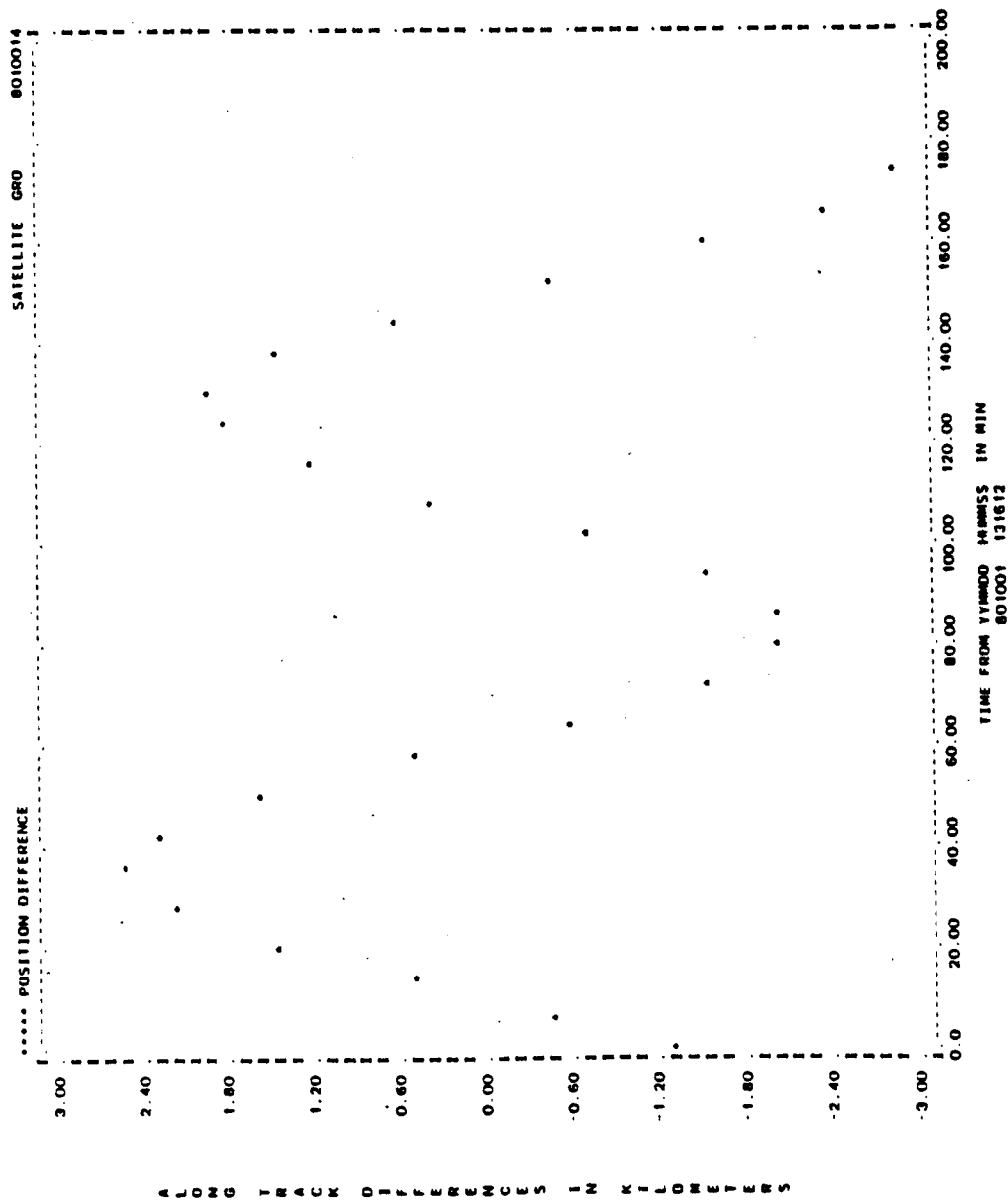


Figure A-87. Along-Track Differences for Run GL7 (2 of 2)

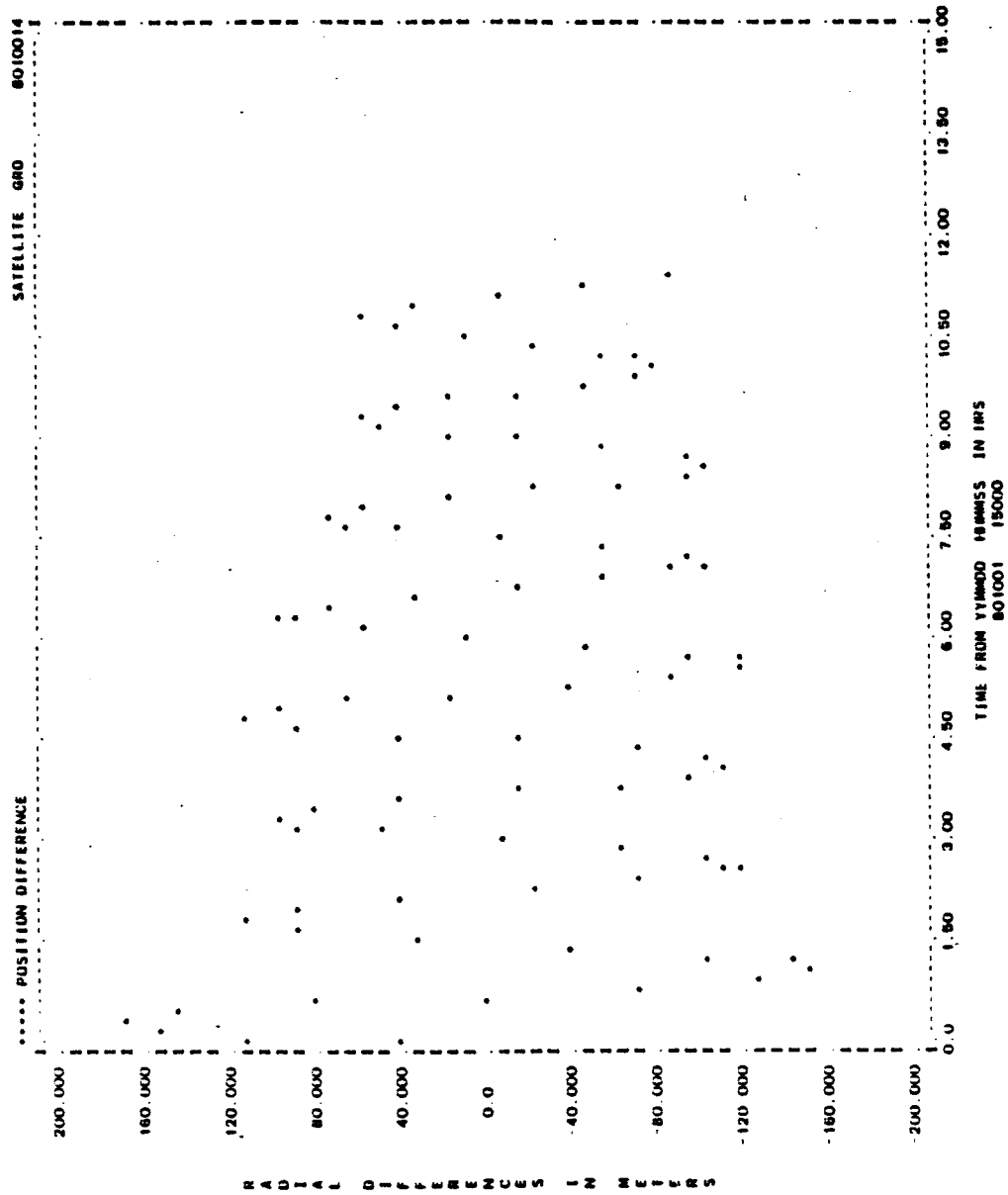


Figure A-88. Radial Differences for Run G19 (1 of 2)

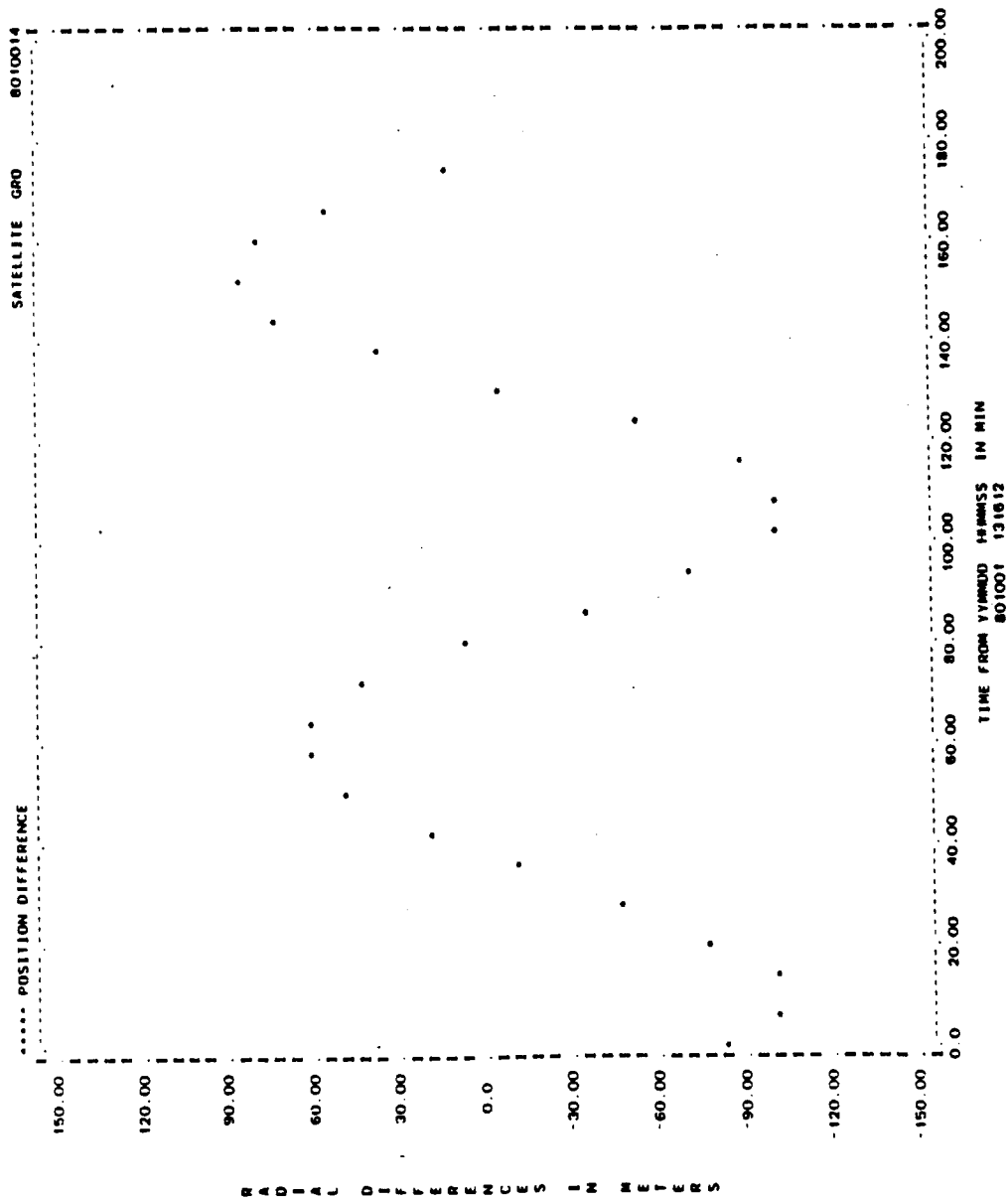


Figure A-88. Radial Differences for Run G19 (2 of 2)

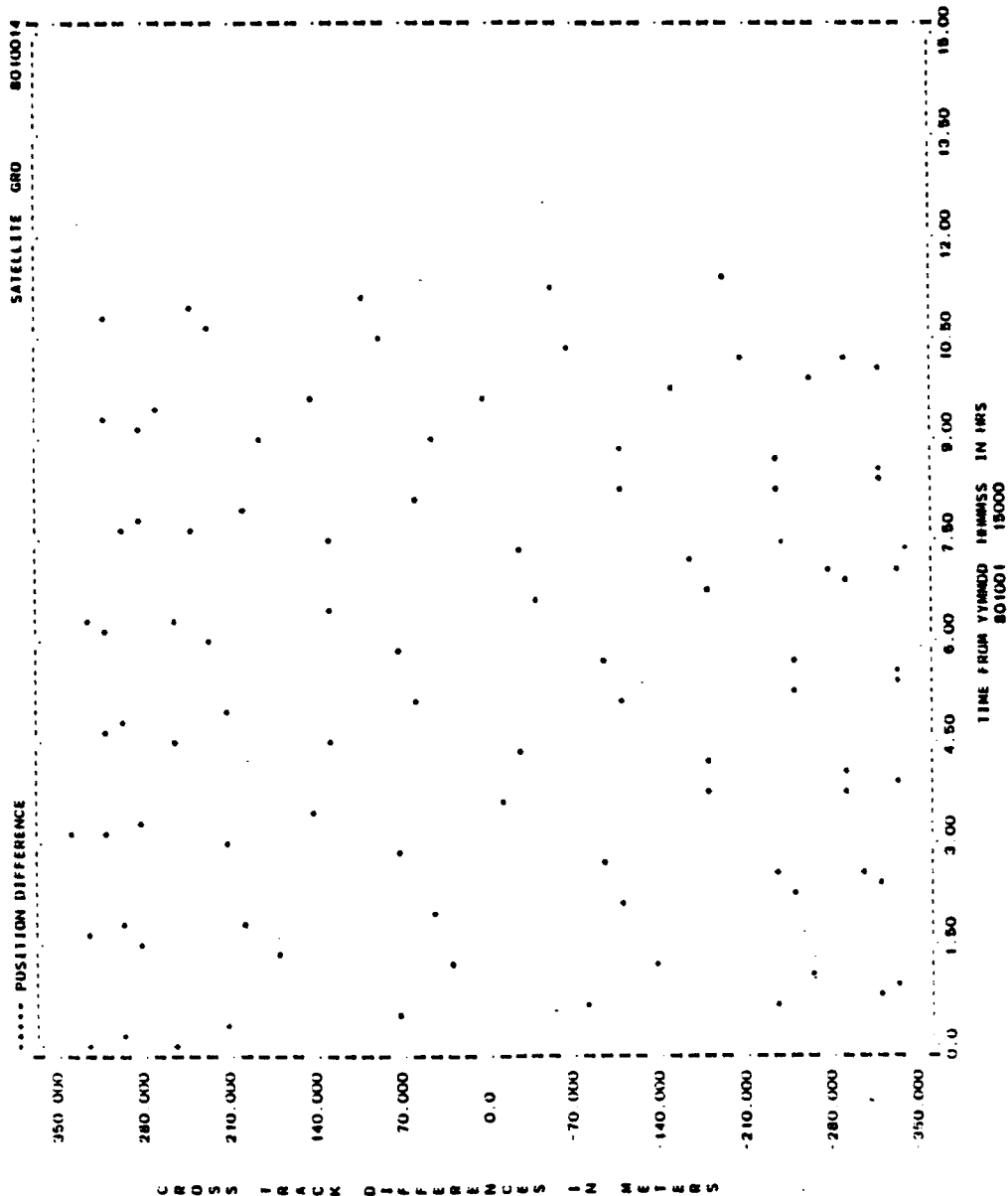


Figure A-89. Cross-Track Differences for Run G19 (1 of 2)

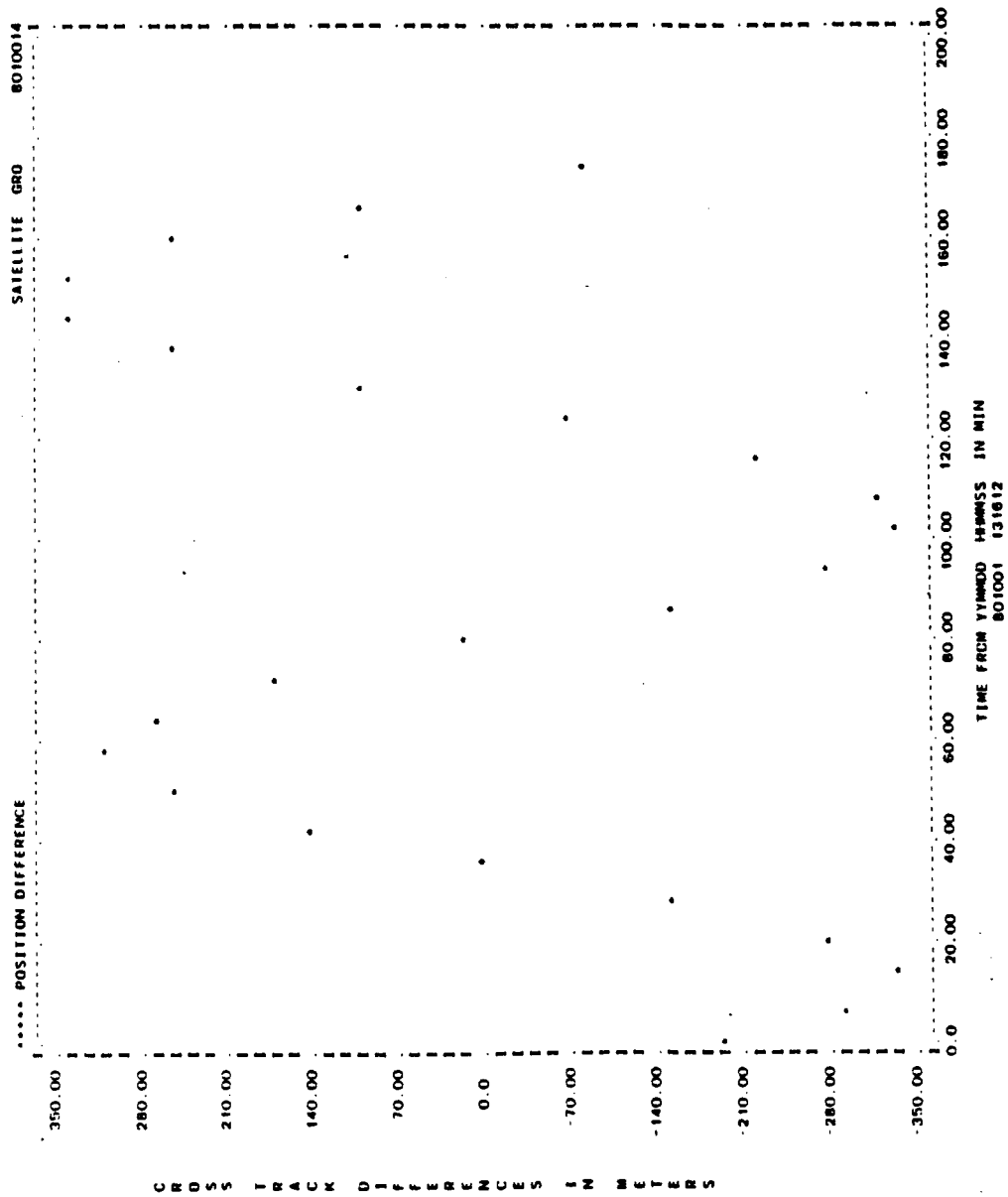


Figure A-89. Cross-Track Differences for Run G19 (2 of 2)

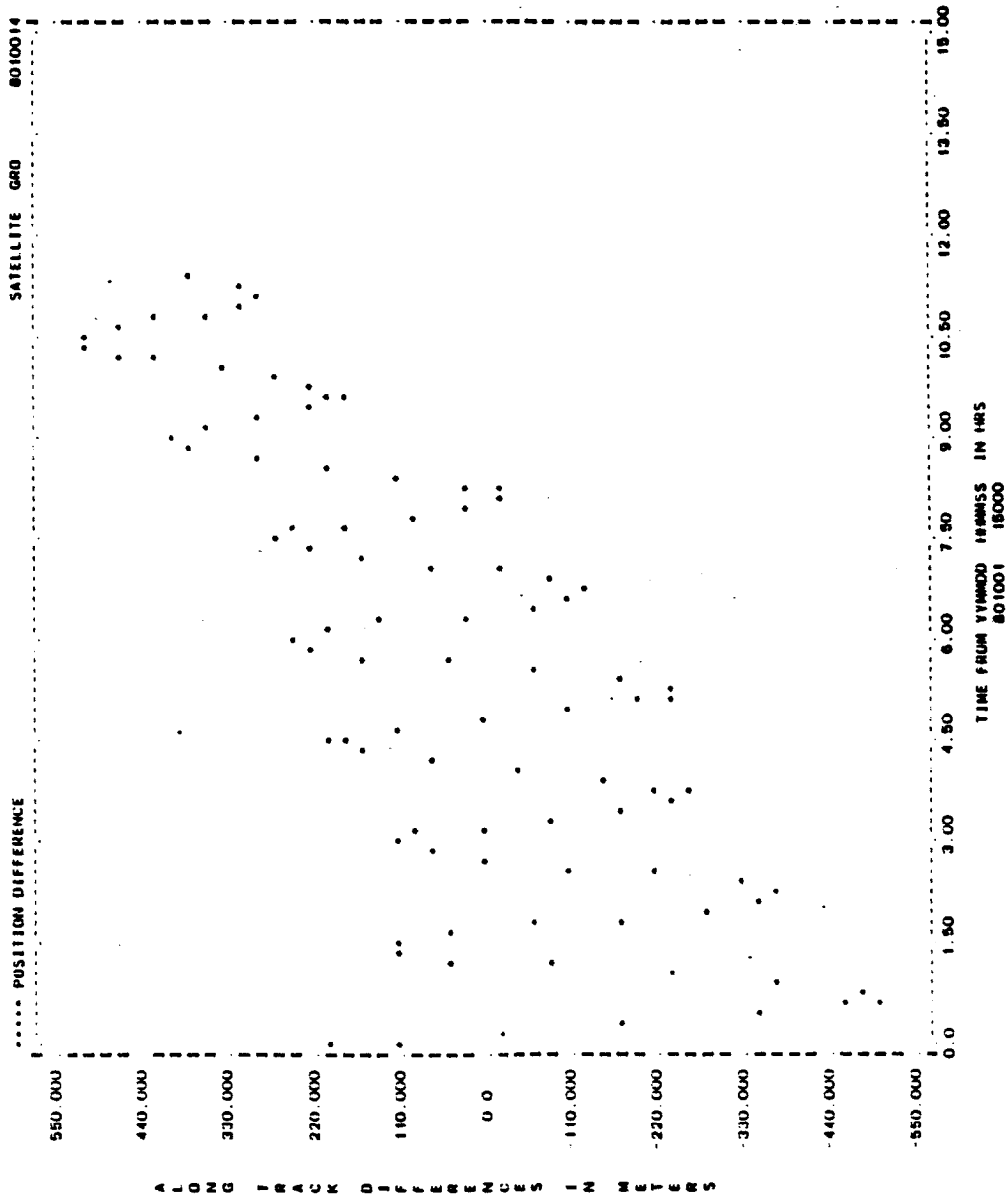


Figure A-90. Along-Track Differences for Run G19 (1 of 2)

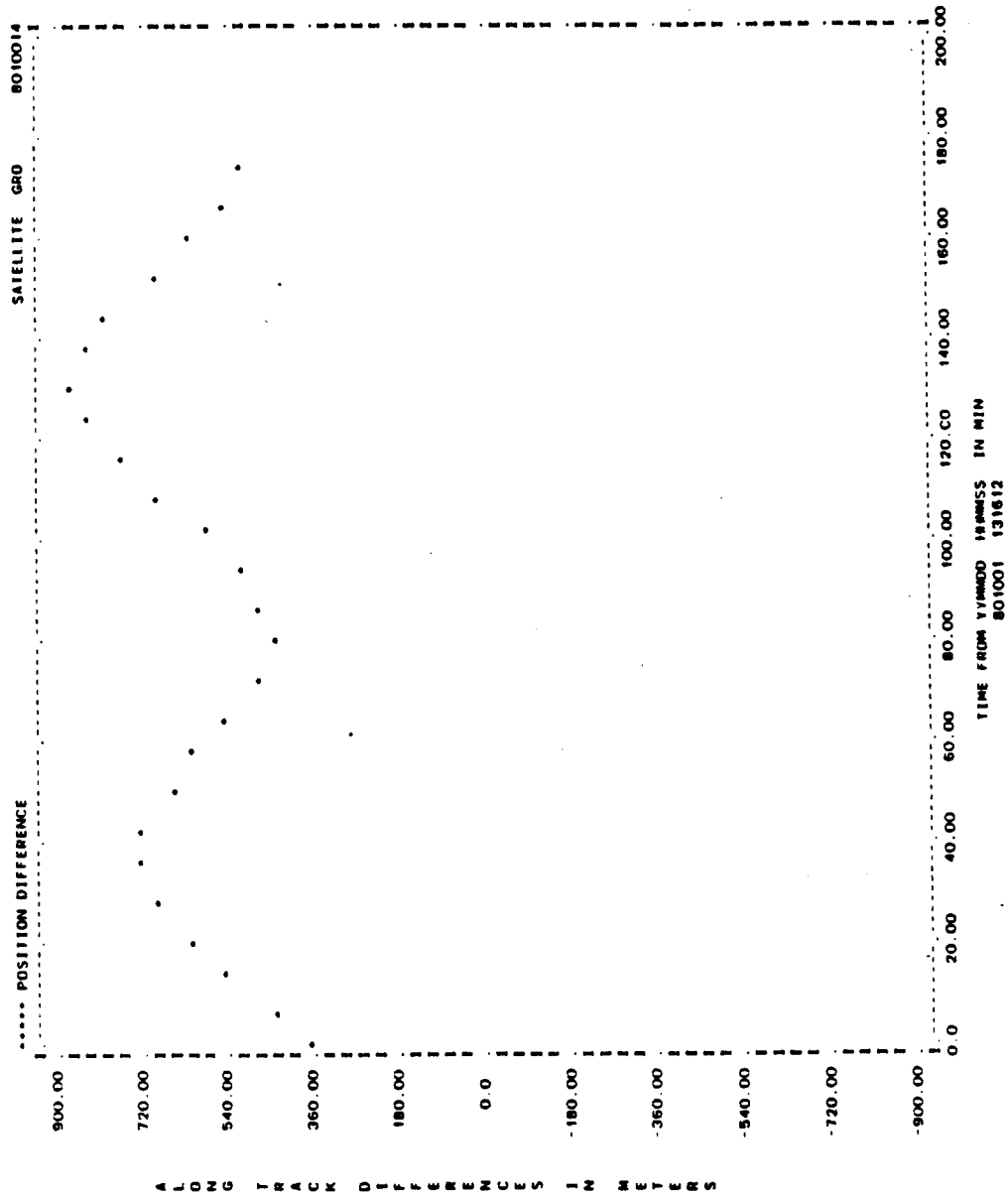


Figure A-90. Along-Track Differences for Run G19 (2 of 2)

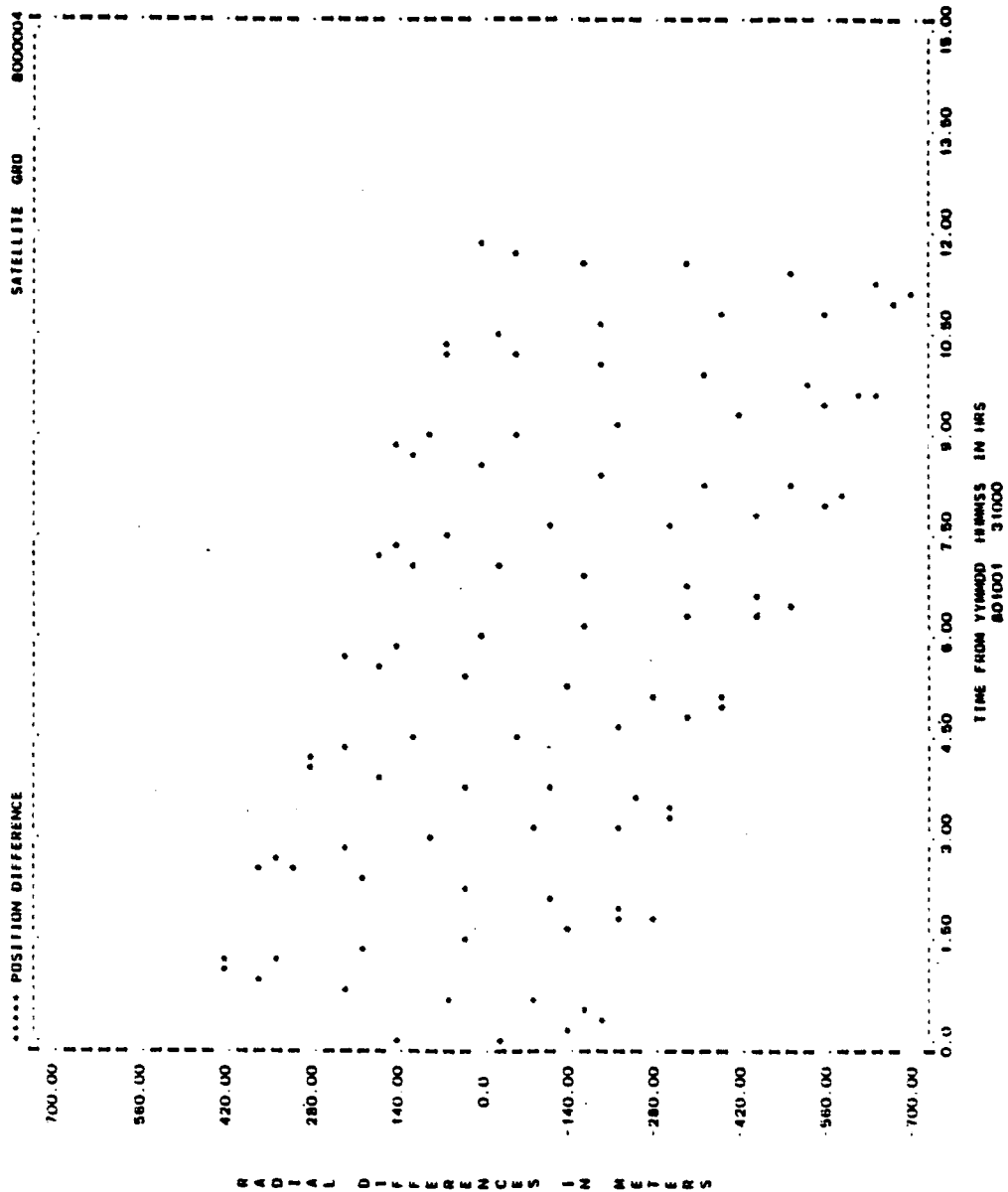


Figure A-91. Radial Differences for Run G20 (1 of 2)

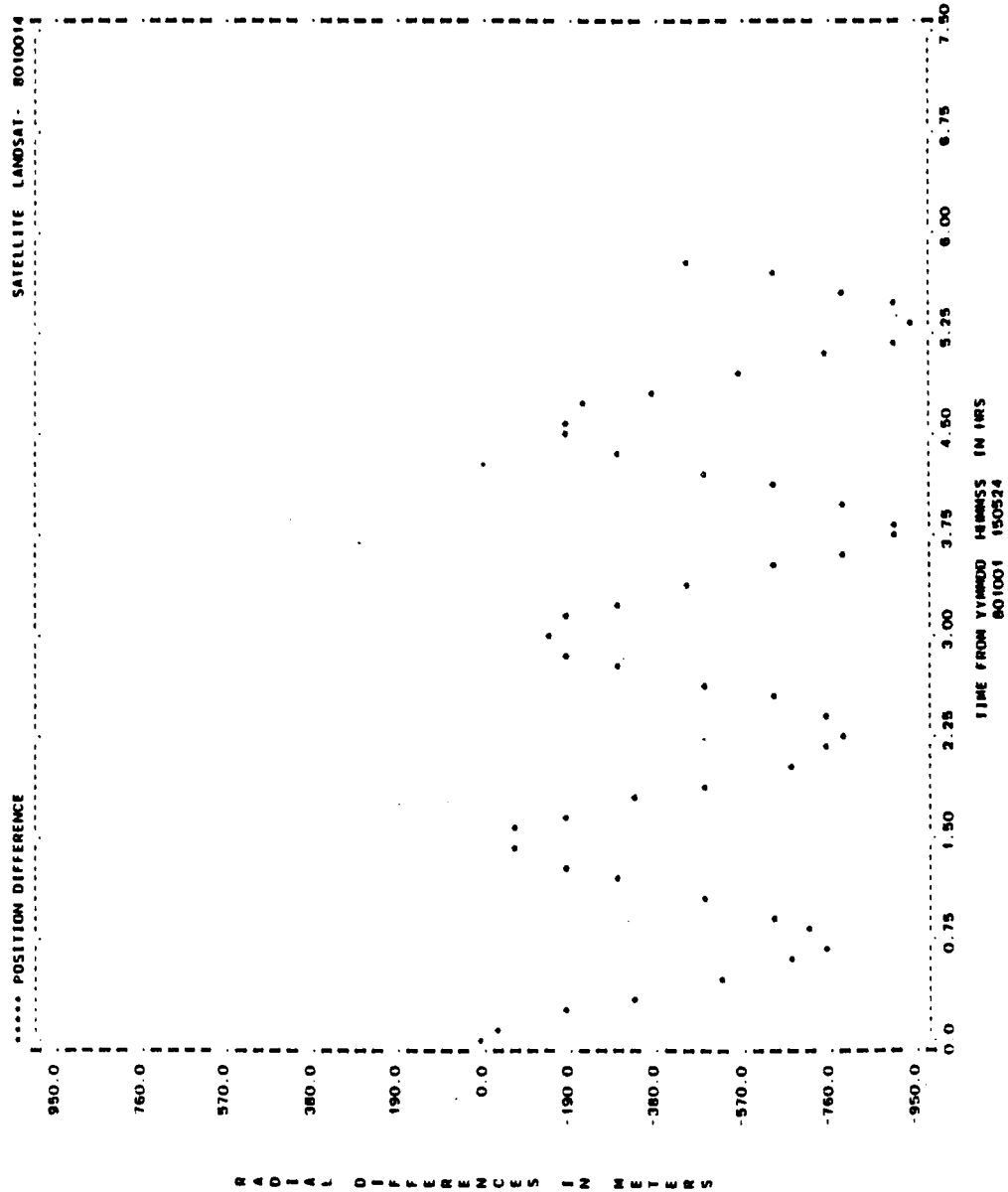


Figure A-91. Radial Differences for Run G20 (2 of 2)

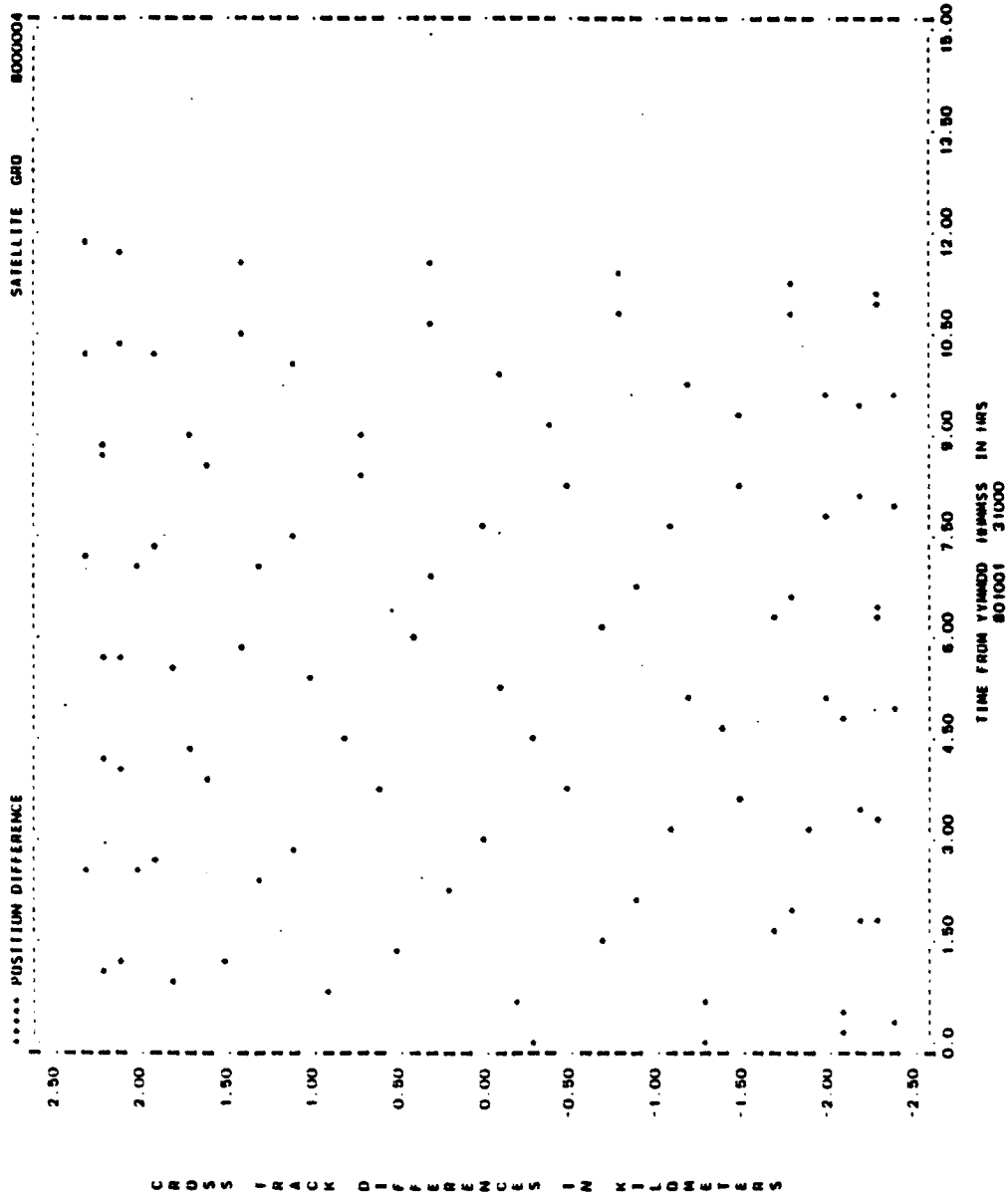


Figure A-92. Cross-Track Differences for Run G20 (1 of 2)

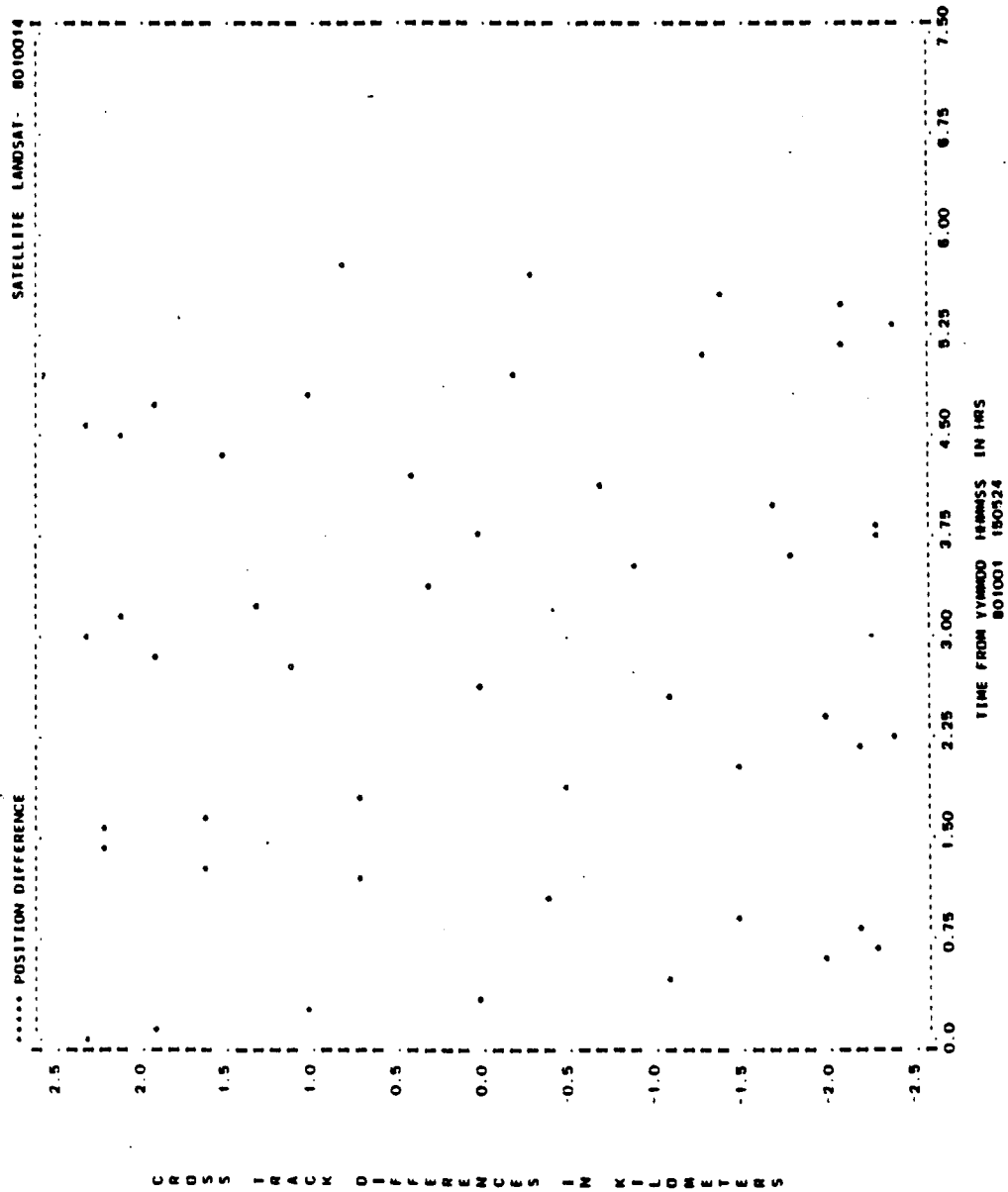


Figure A-92. Cross-Track Differences for Run G20 (2 of 2)

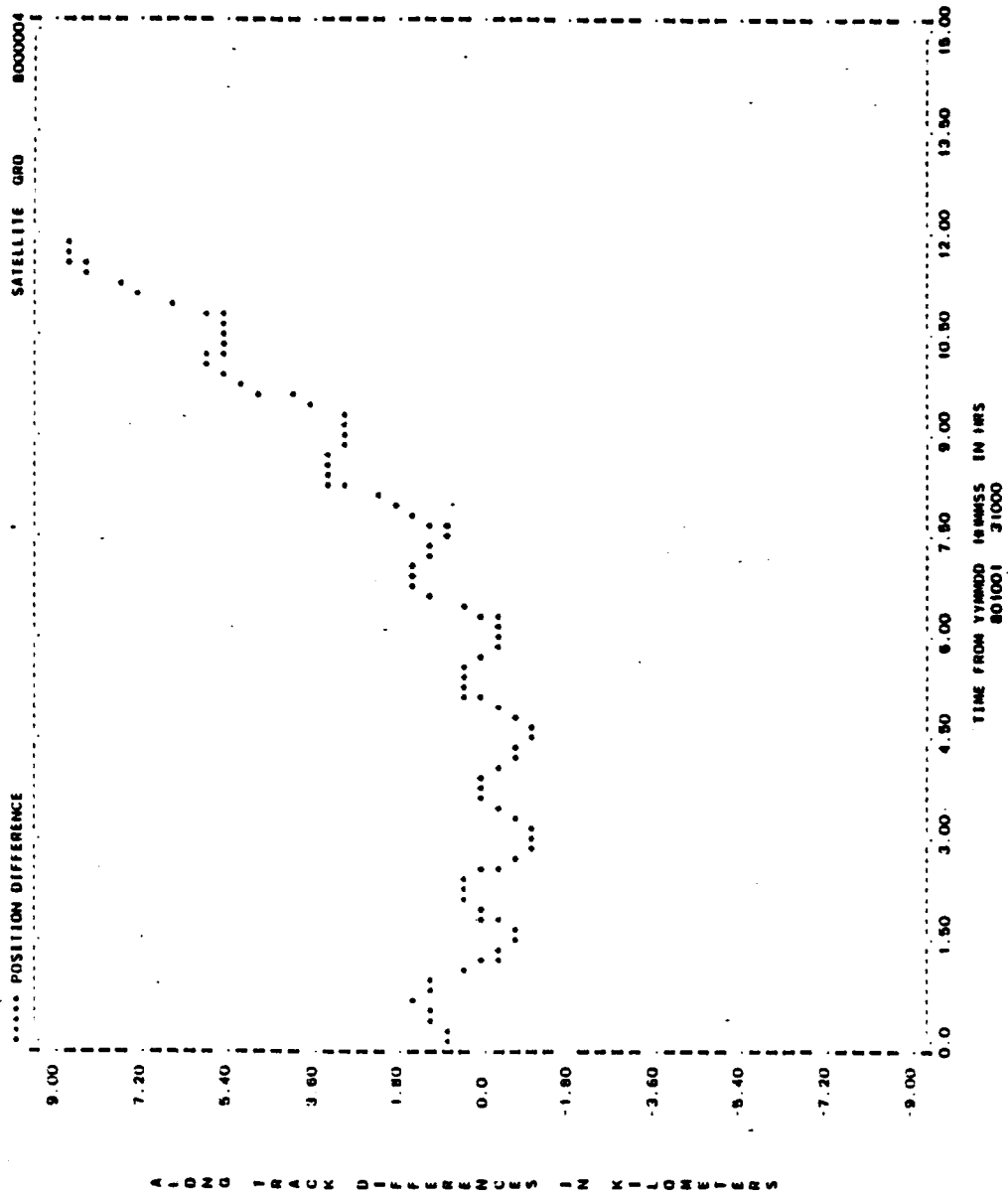


Figure A-93. Along-Track Differences for Run G20 (1 of 2)

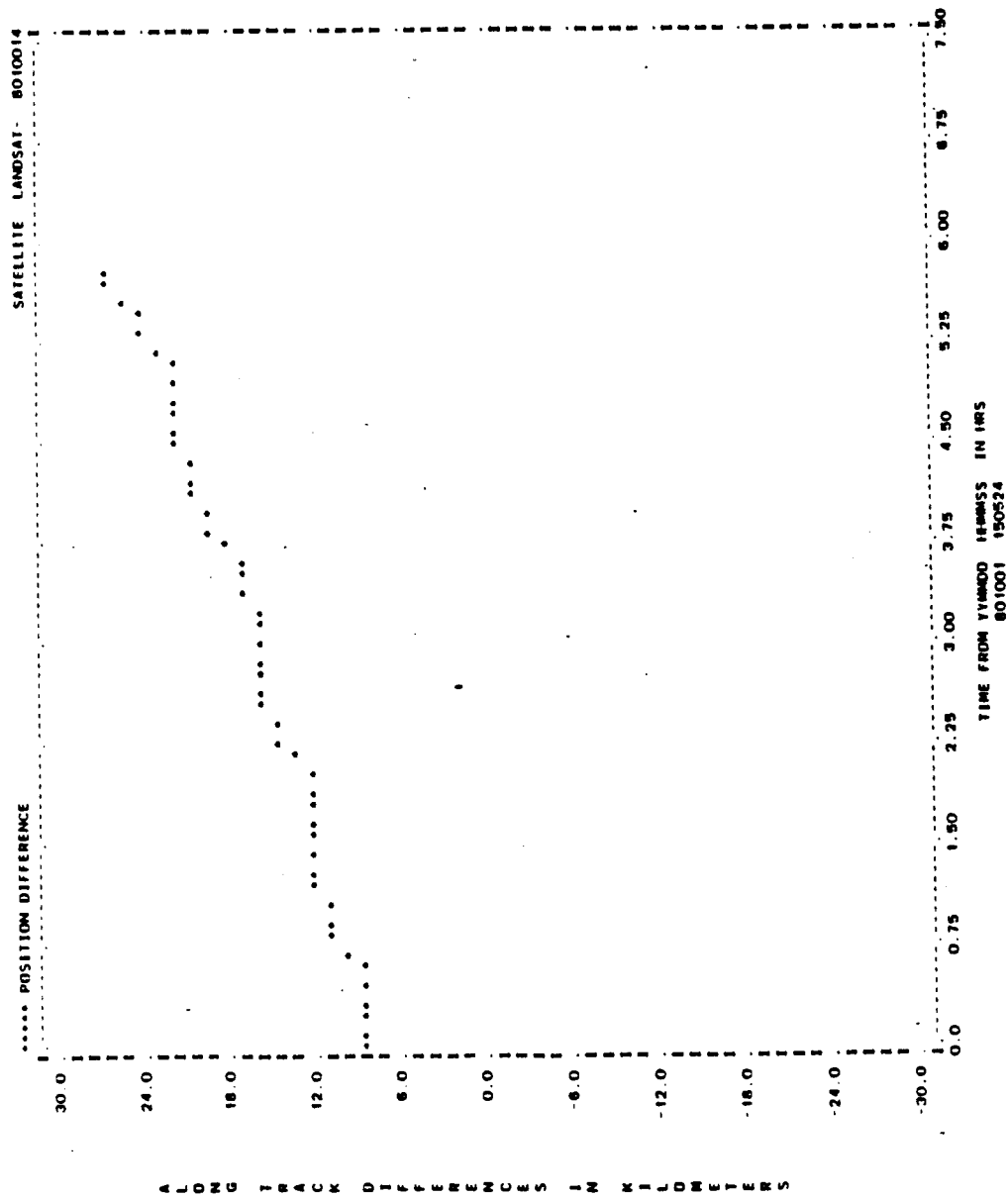


Figure A-93. Along-Track Differences for Run G20 (2 of 2)

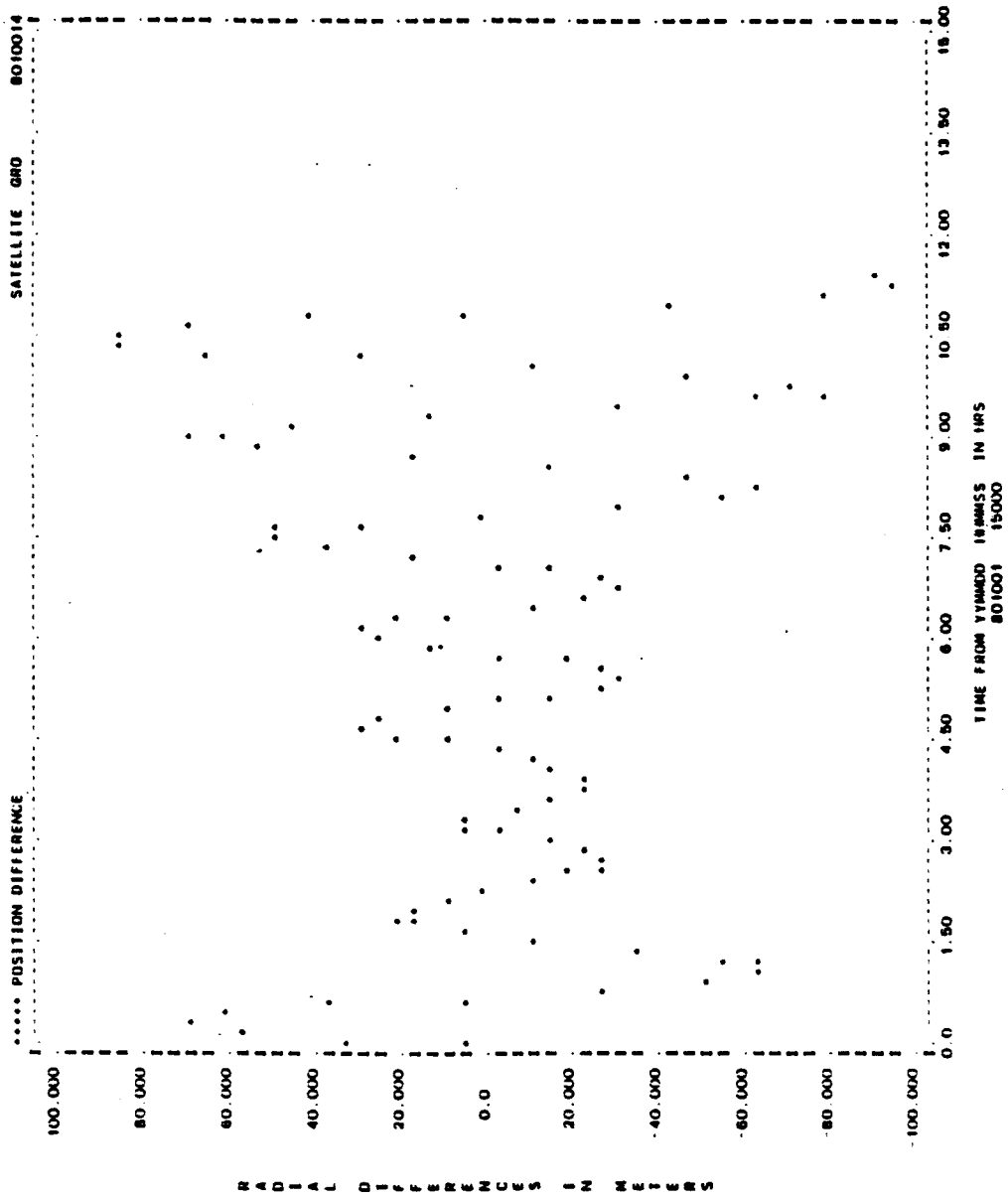


Figure A-94. Radial Differences for Run G08 (1 of 2)

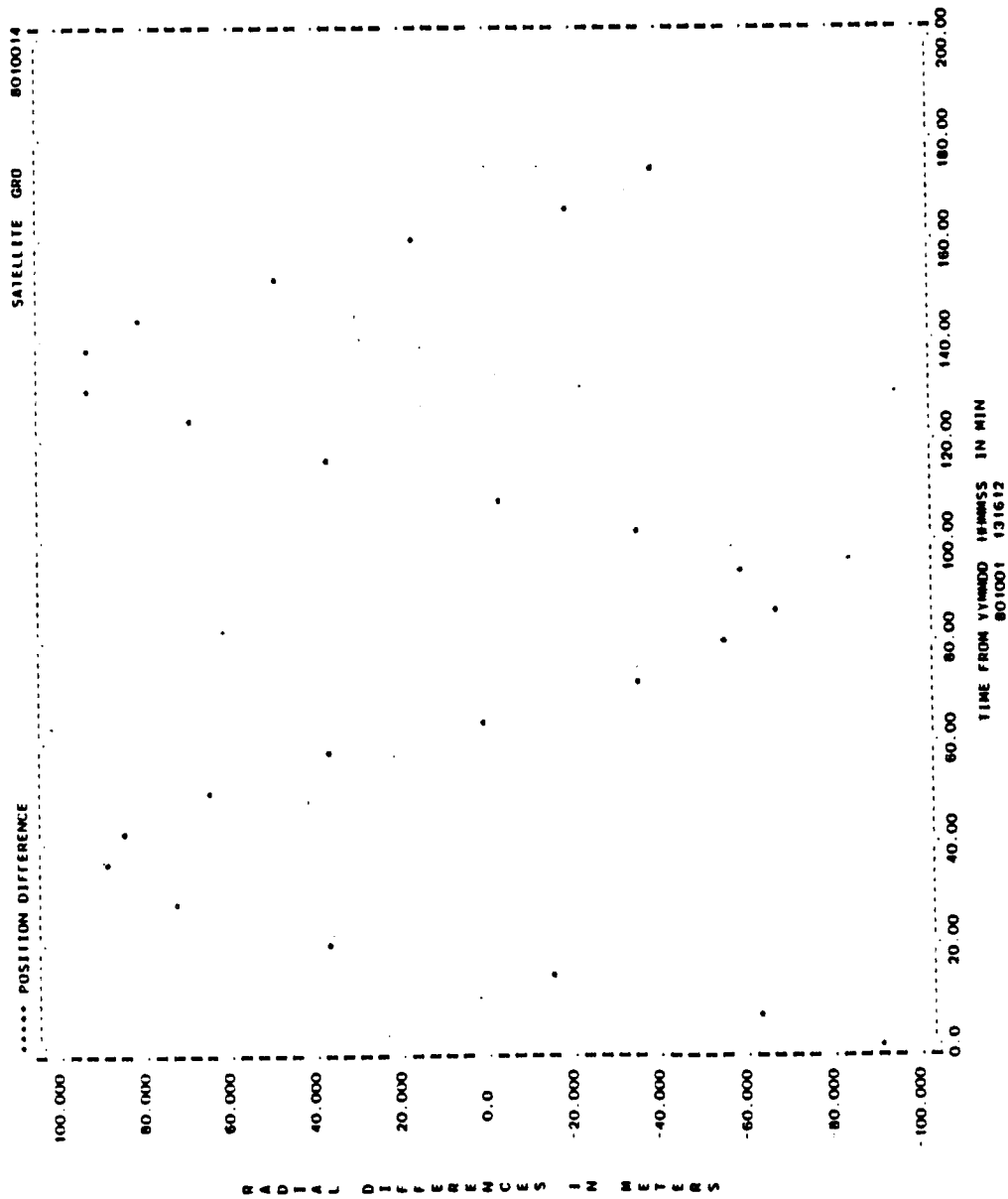


Figure A-94. Radial Differences for Run G08 (2 of 2)

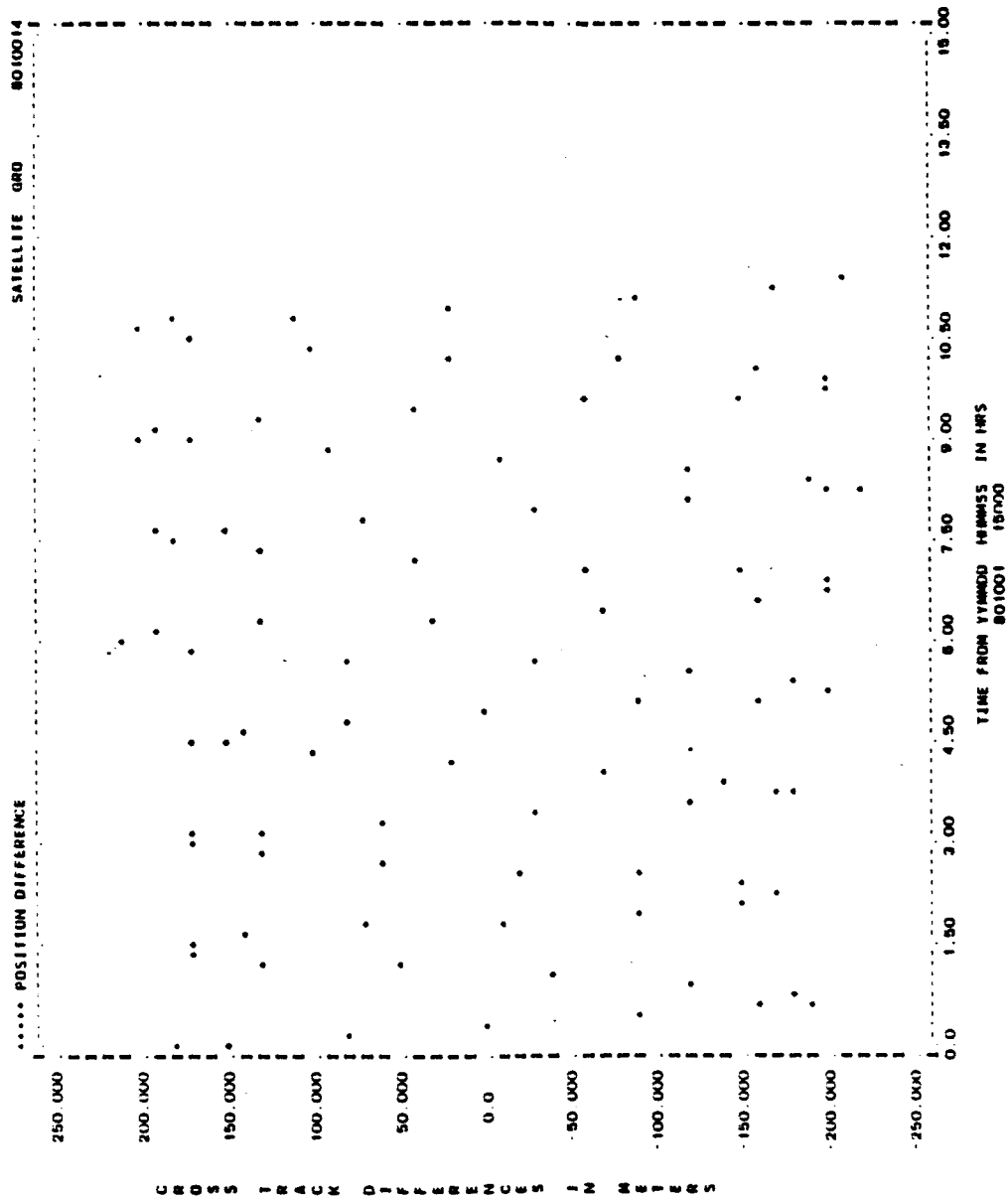


Figure A-95. Cross-Track Differences for Run G08 (1 of 2)

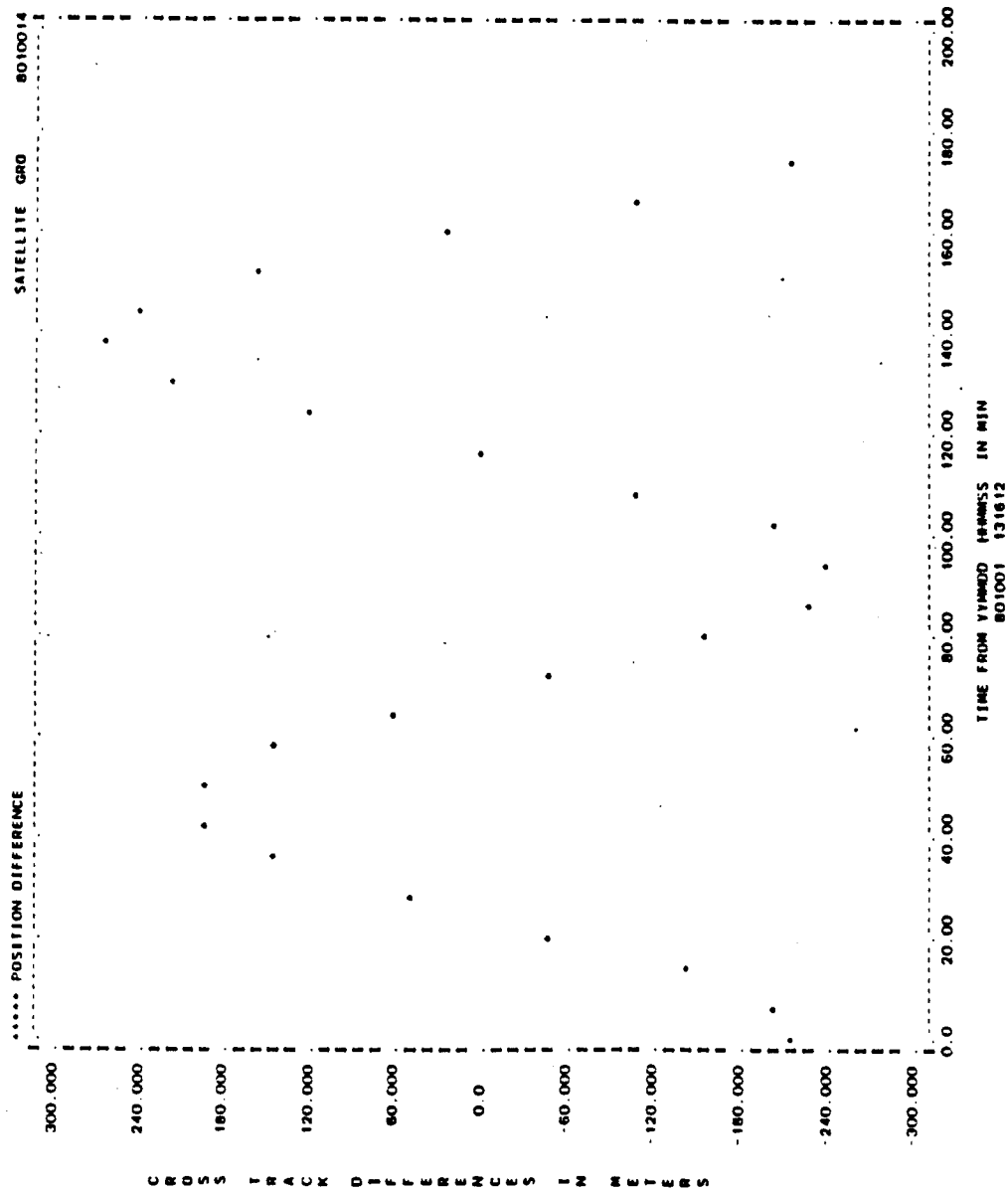


Figure A-95. Cross-Track Differences for Run G08 (2 of 2)

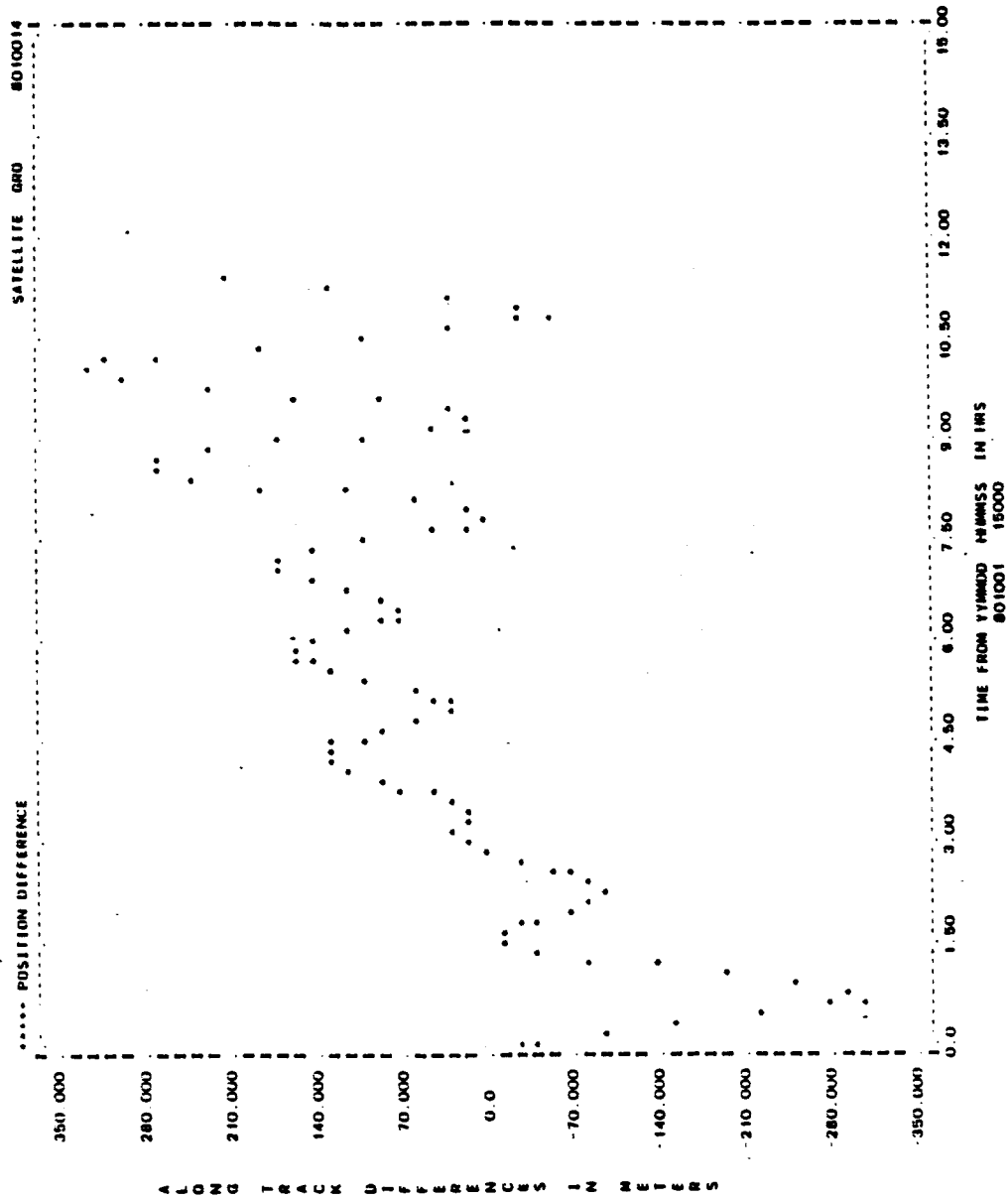


Figure A-96. Along-Track Differences for Run G08 (1 of 2)

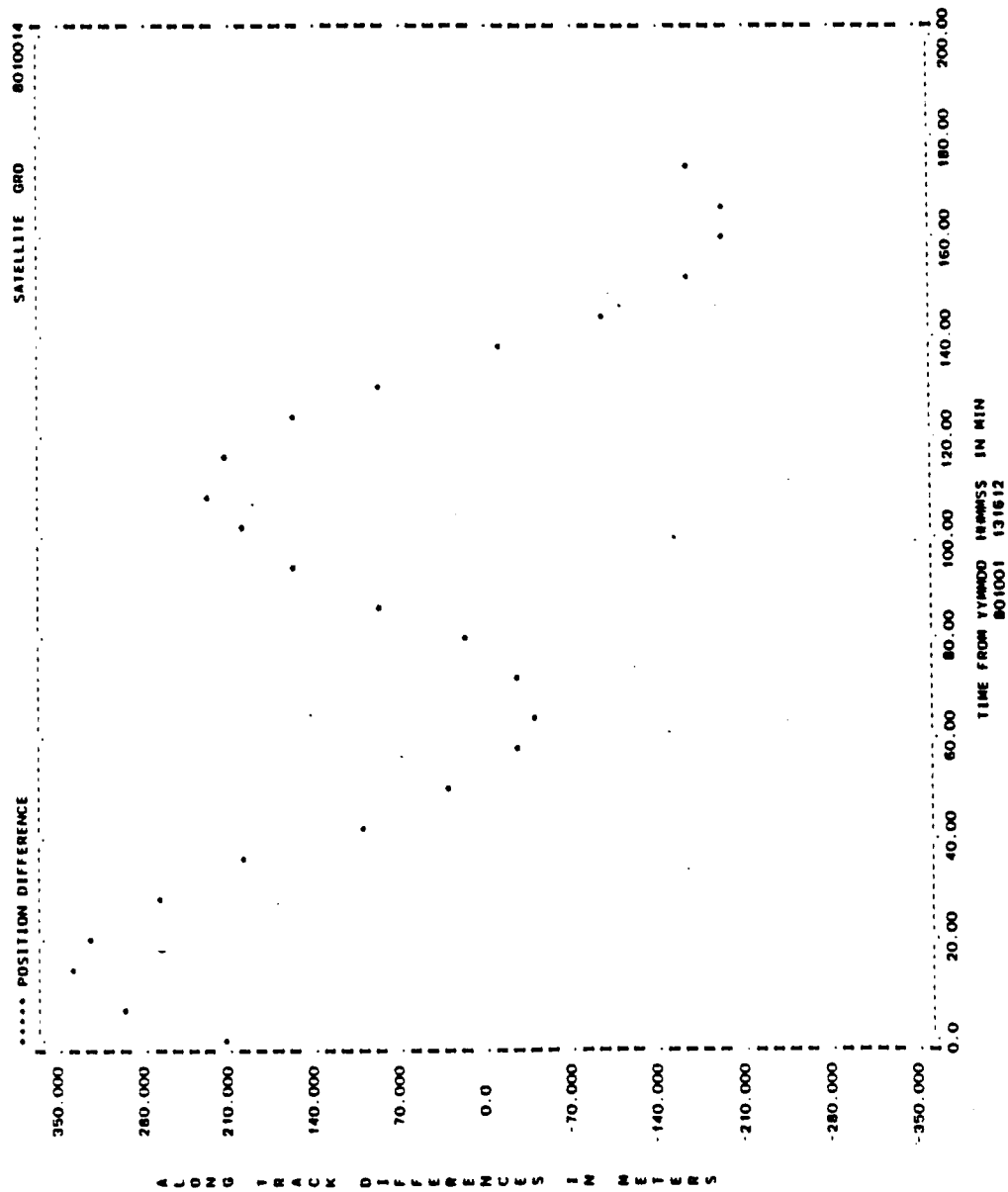


Figure A-96. Along-Track Differences for Run G08 (2 of 2)

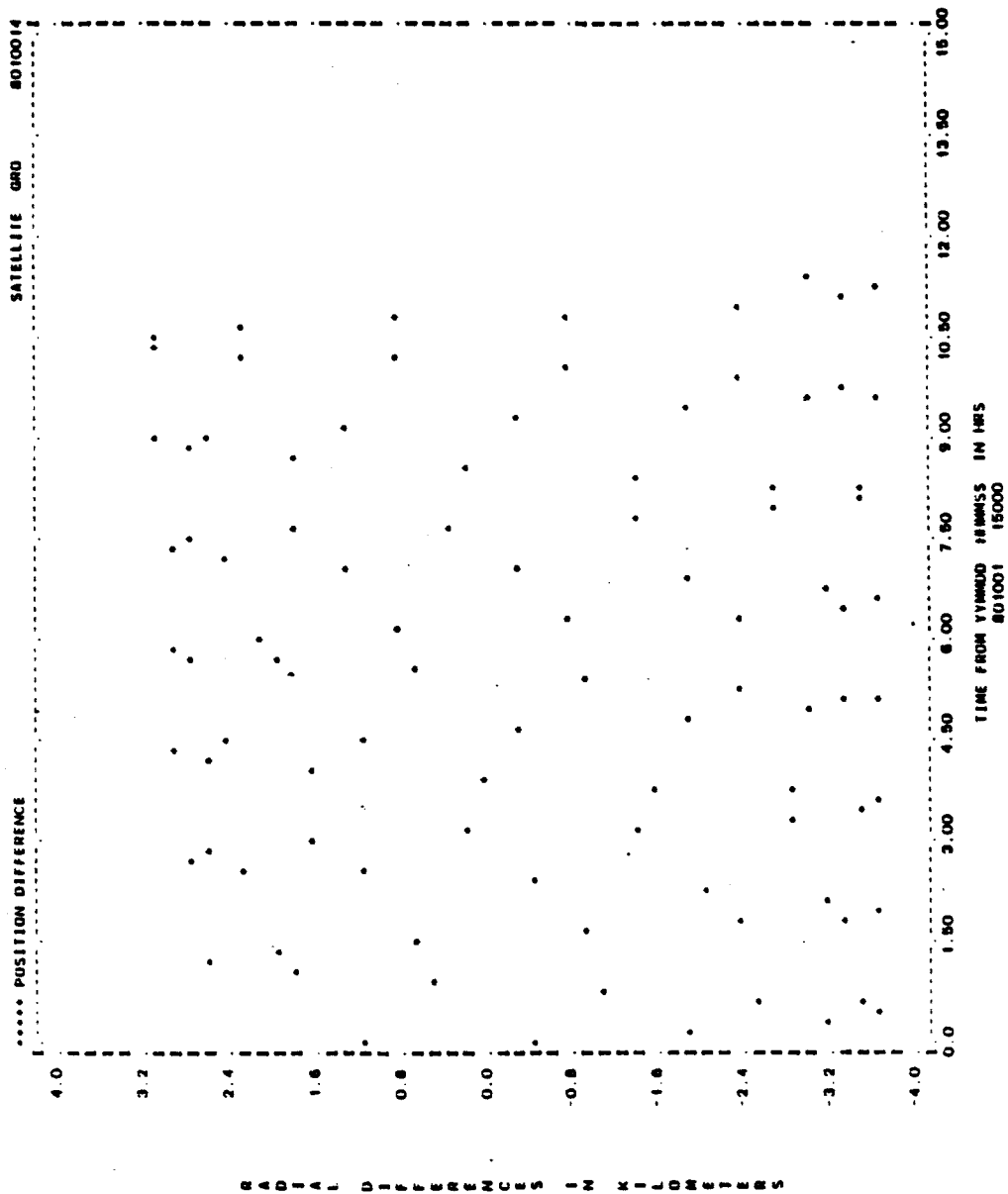


Figure A-97. Radial Differences for Run G09 (1 of 2)

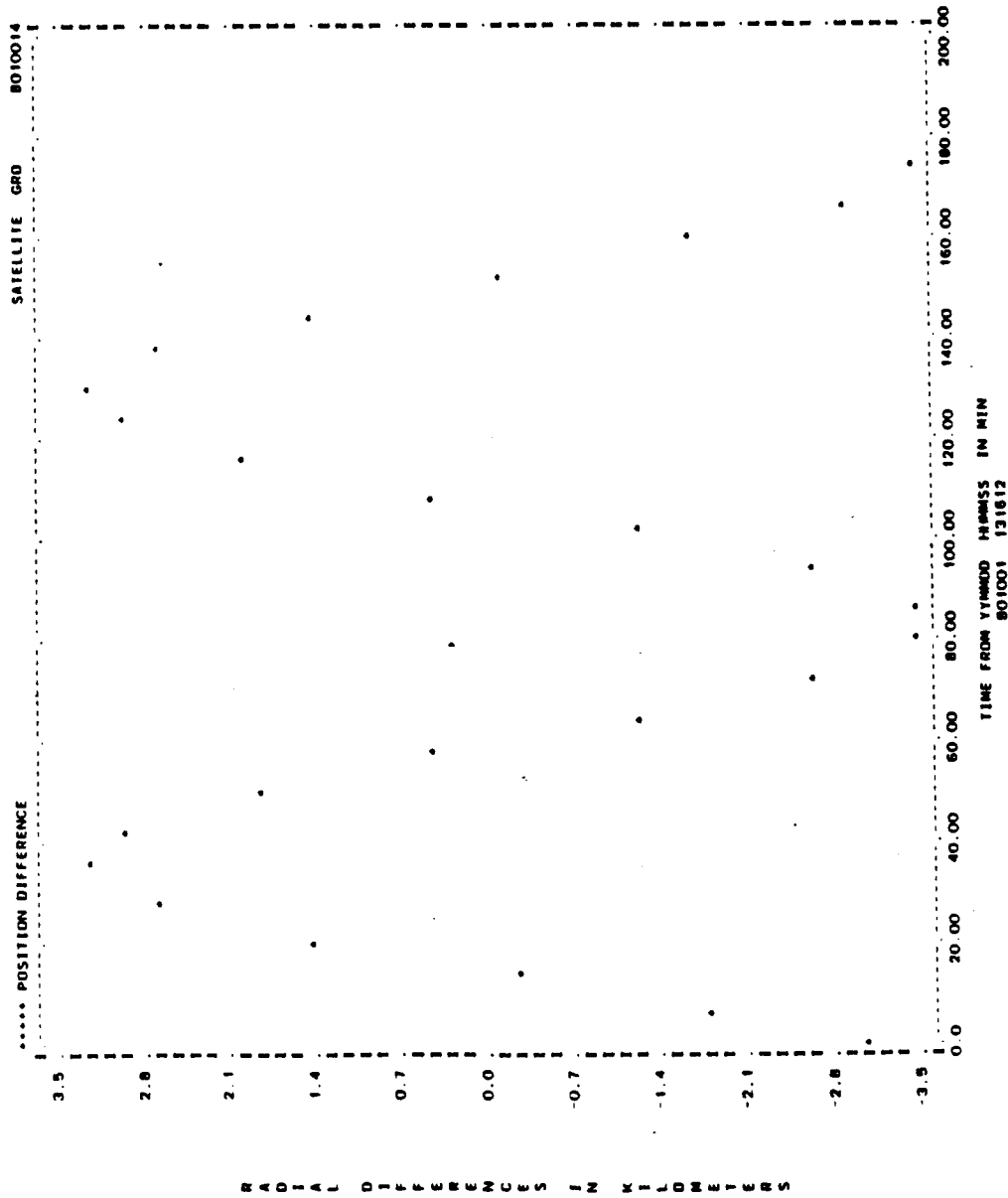


Figure A-97. Radial Differences for Run G09 (2 of 2)

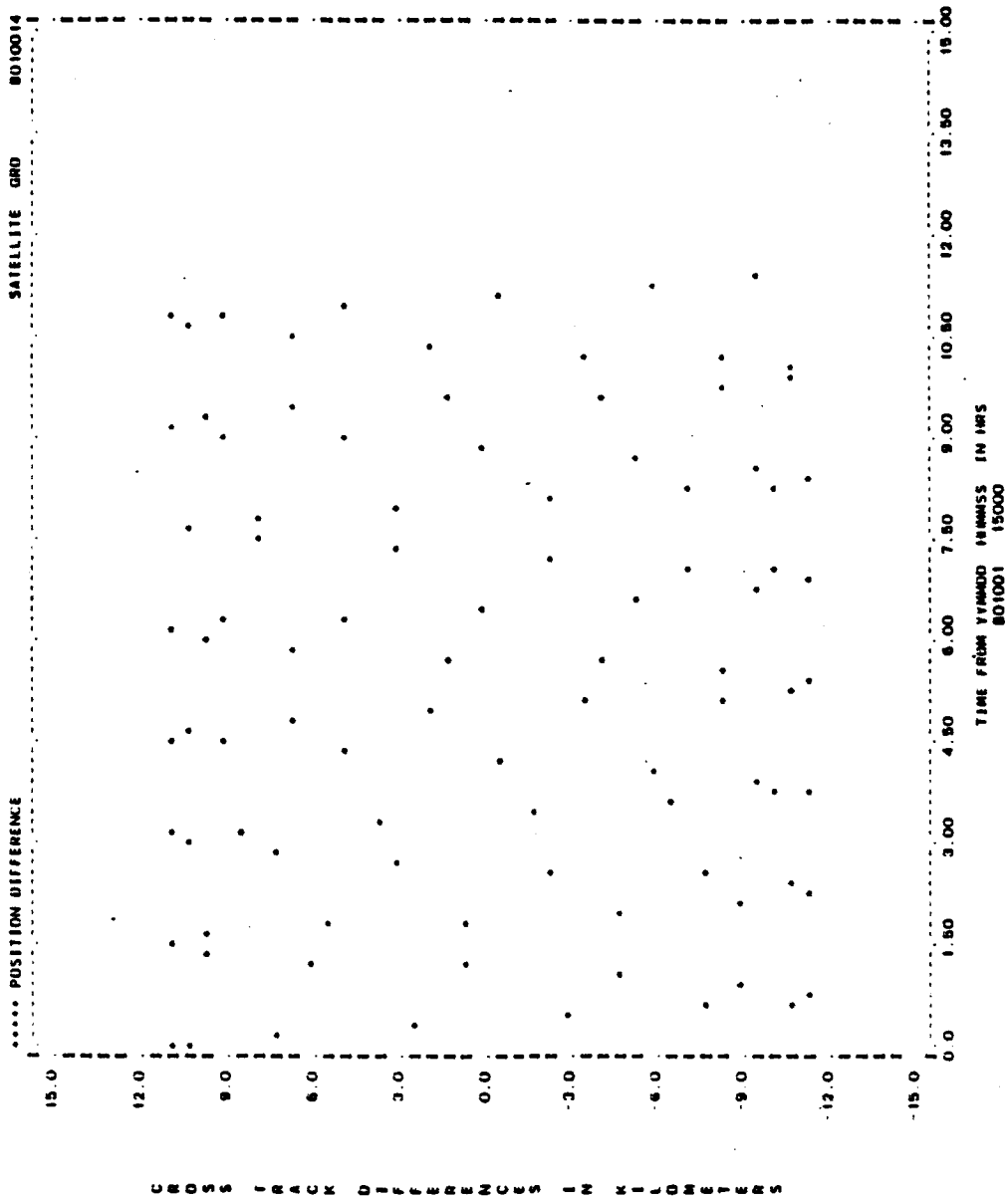


Figure A-98. Cross-Track Differences for Run G09 (1 of 2)

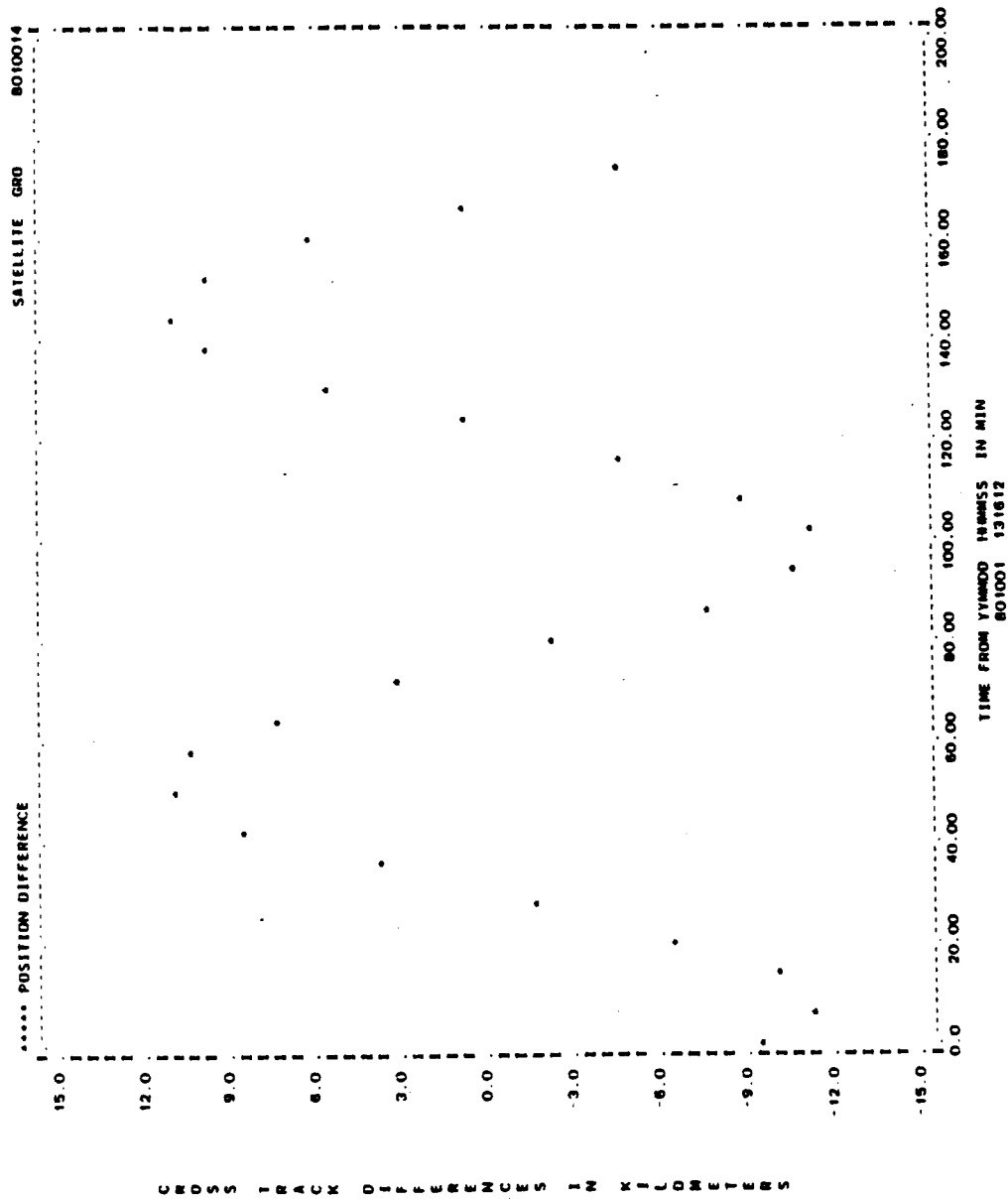


Figure A-98. Cross-Track Differences for Run G09 (2 of 2)

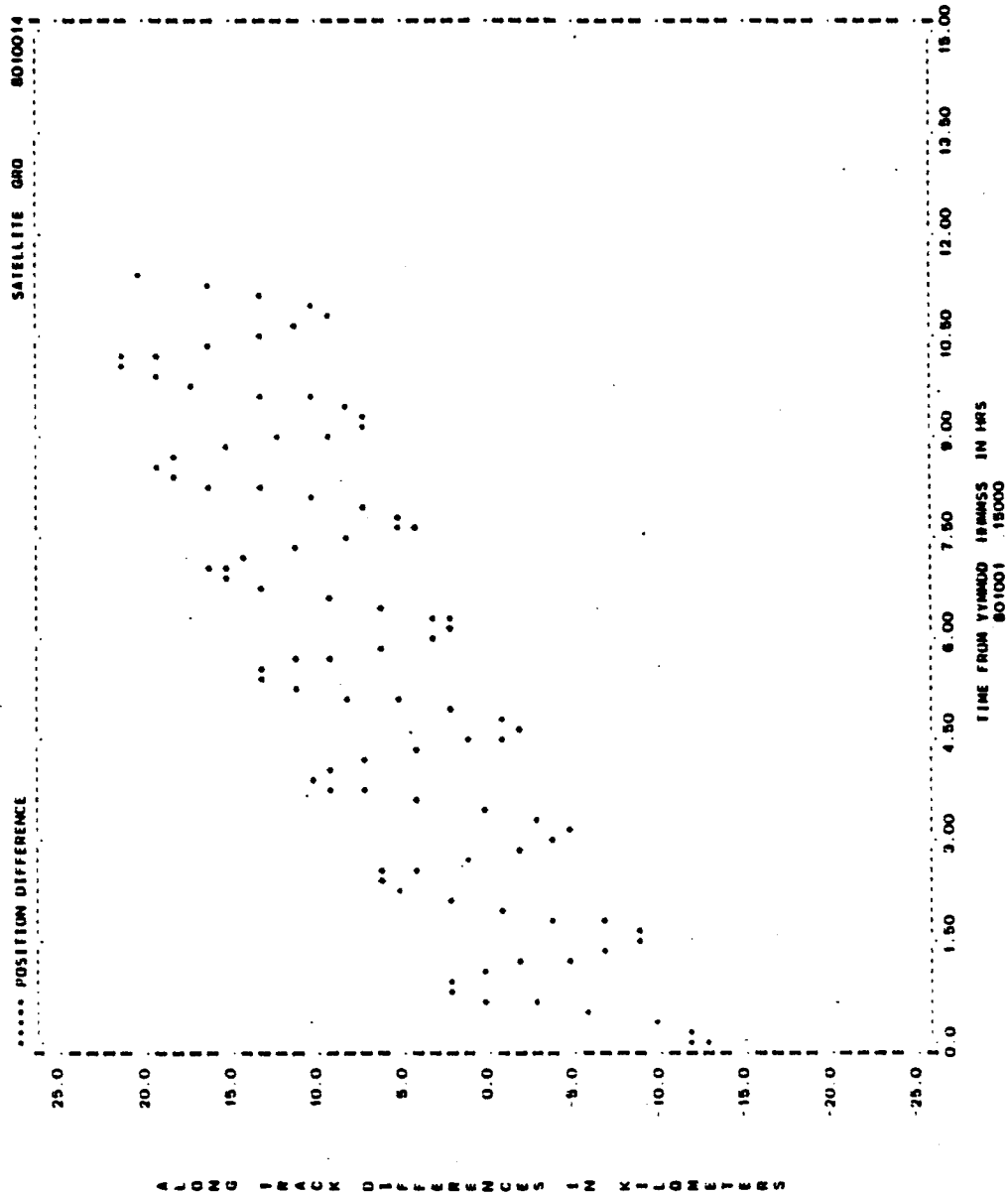


Figure A-99. Along-Track Differences for Run G09 (1 of 2)

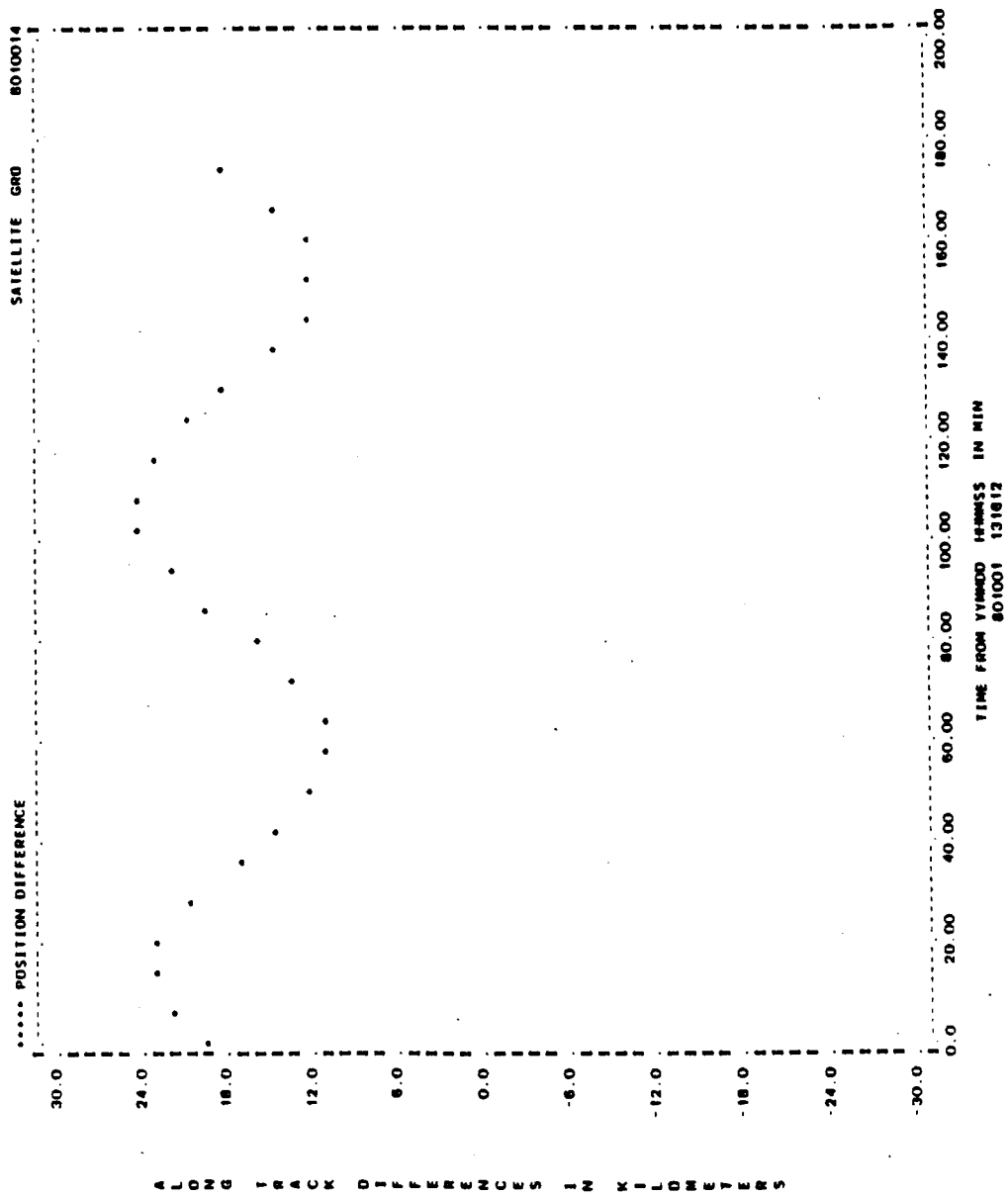


Figure A-99. Along-Track Differences for Run G09 (2 of 2)

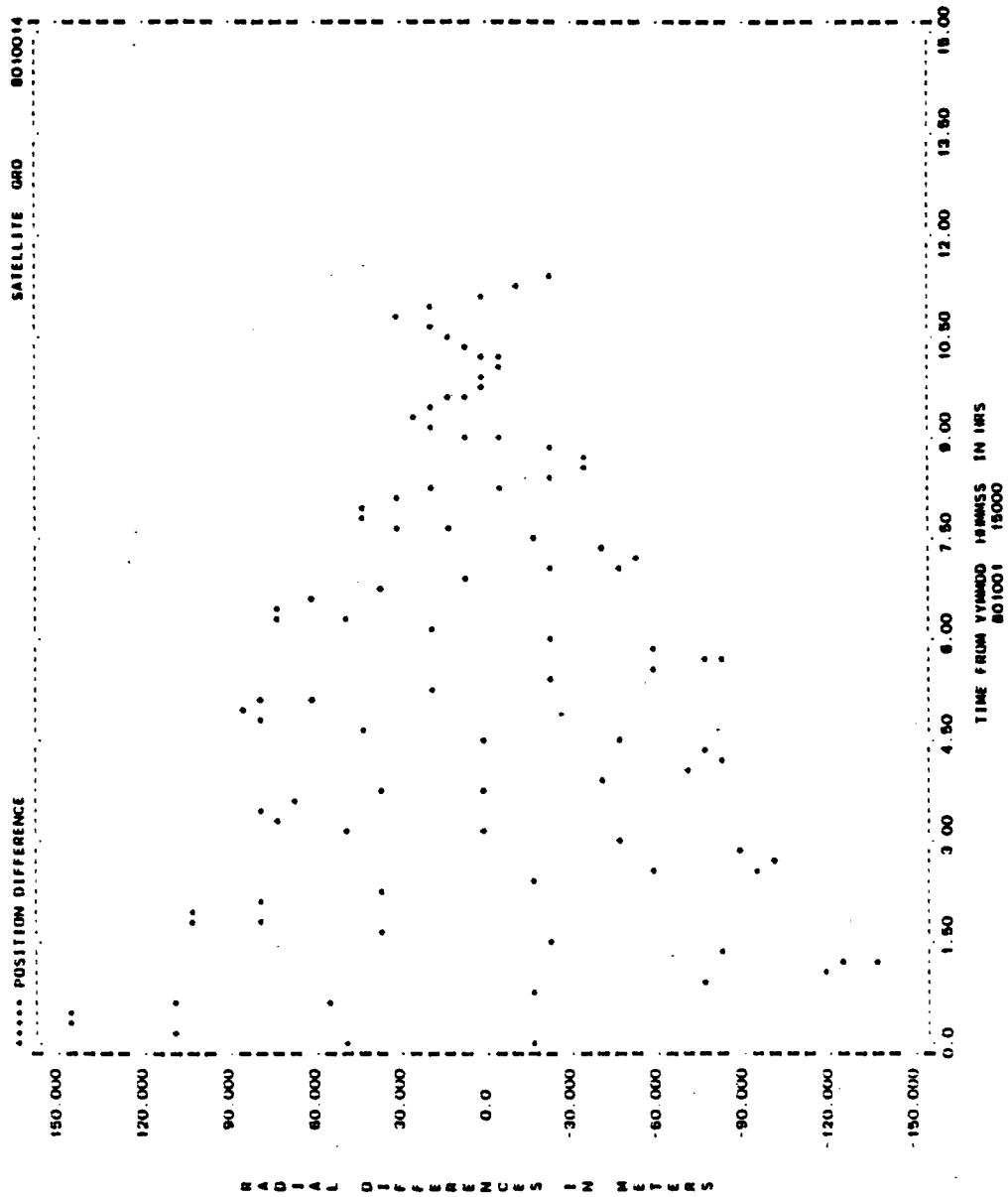


Figure A-100. Radial Differences for Run G10 (1 of 2)

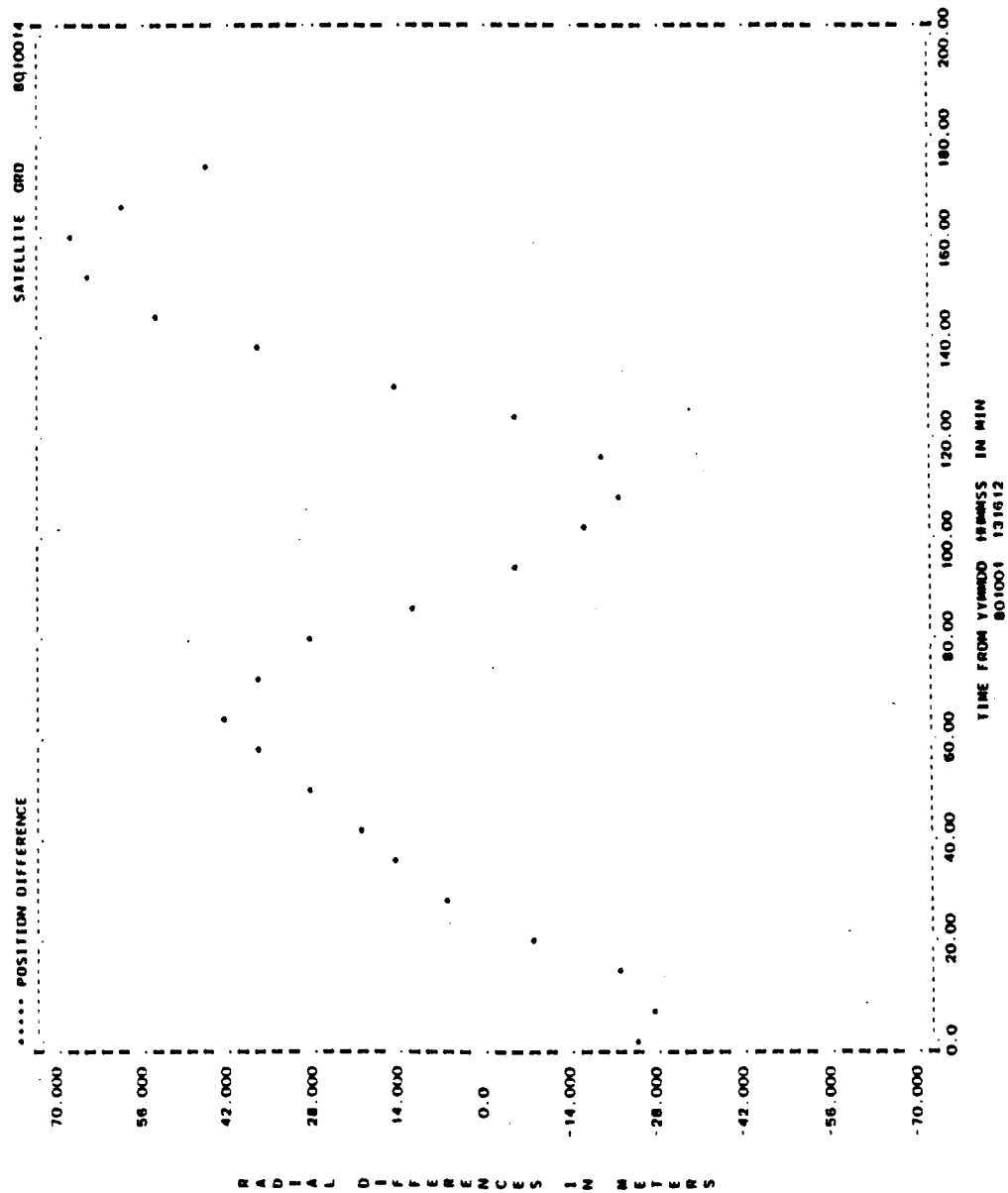


Figure A-100. Radial Differences for Run G10 (2 of 2)

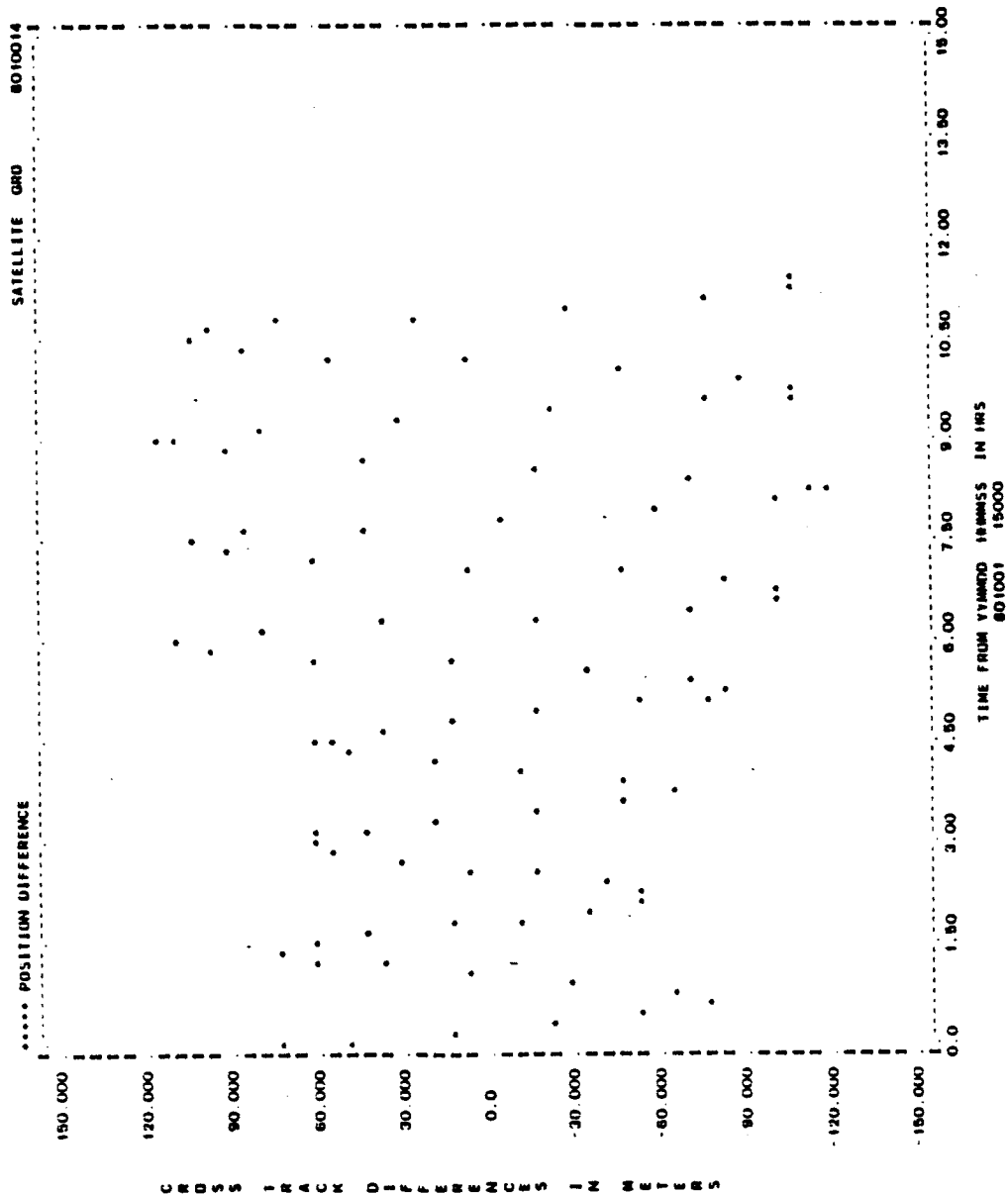


Figure A-101. Cross-Track Differences for Run G10 (1 of 2)

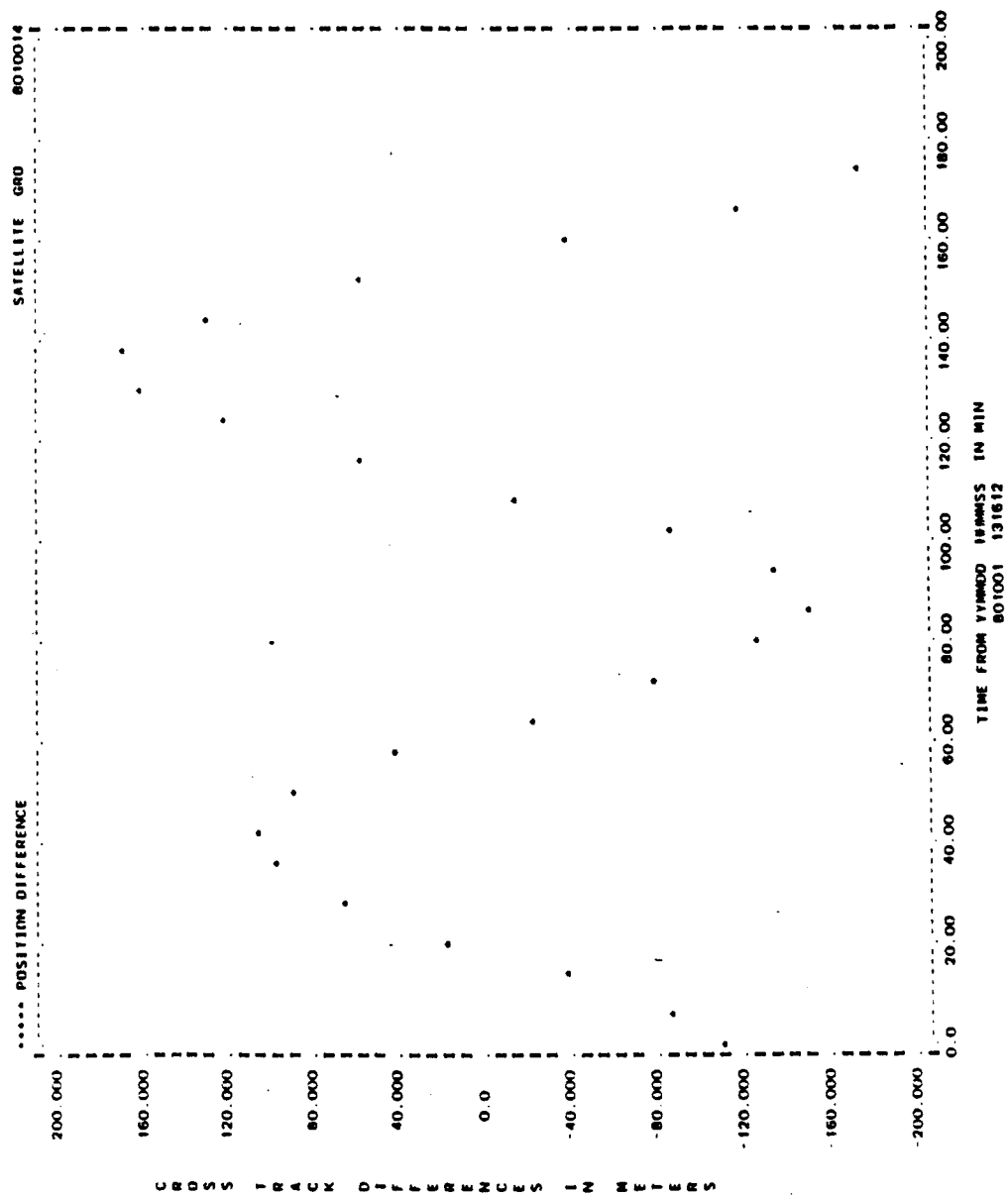


Figure A-101. Cross-Track Differences for Run G10 (2 of 2)

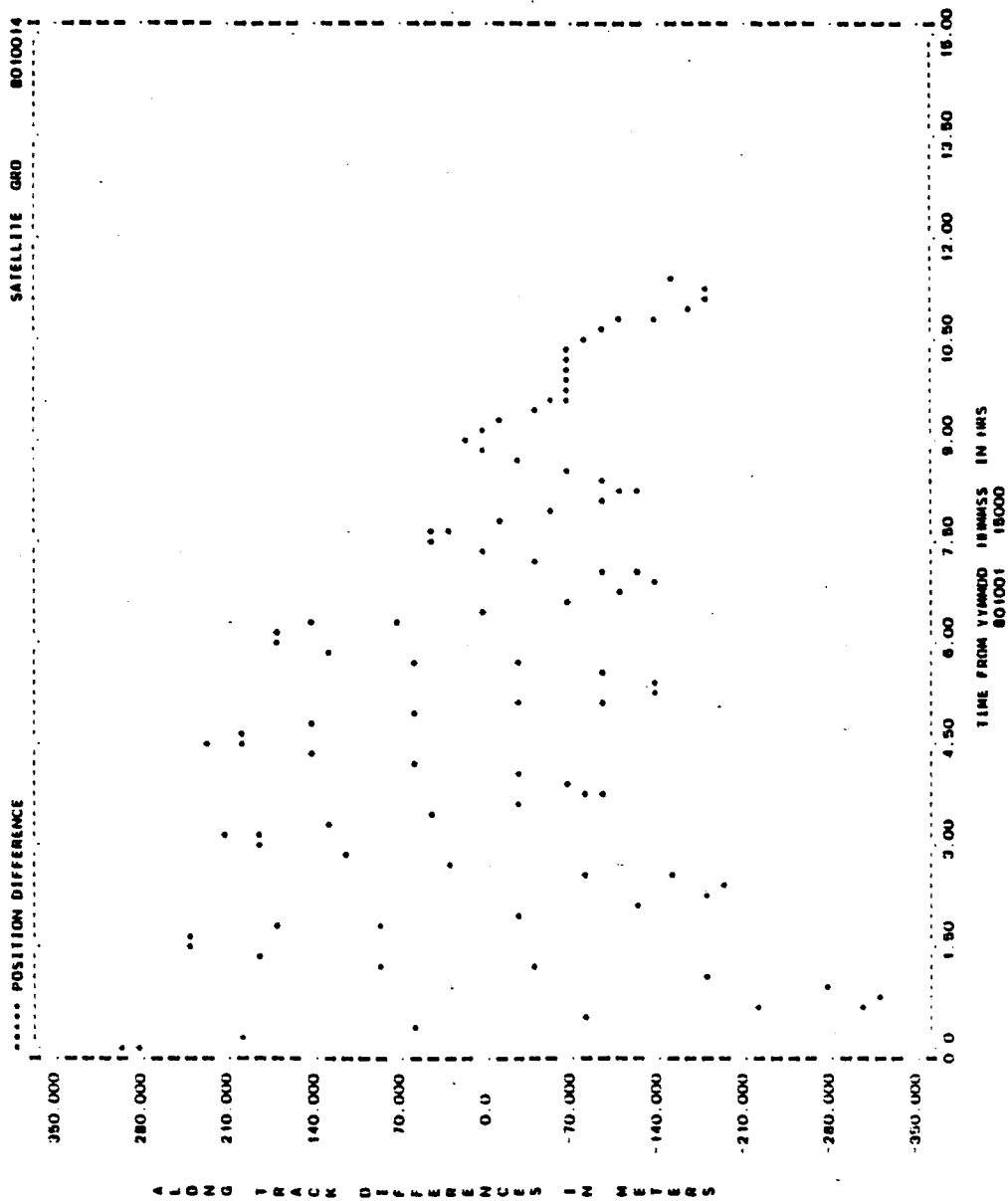


Figure A-102. Along-Track Differences for Run G10 (1 of 2)

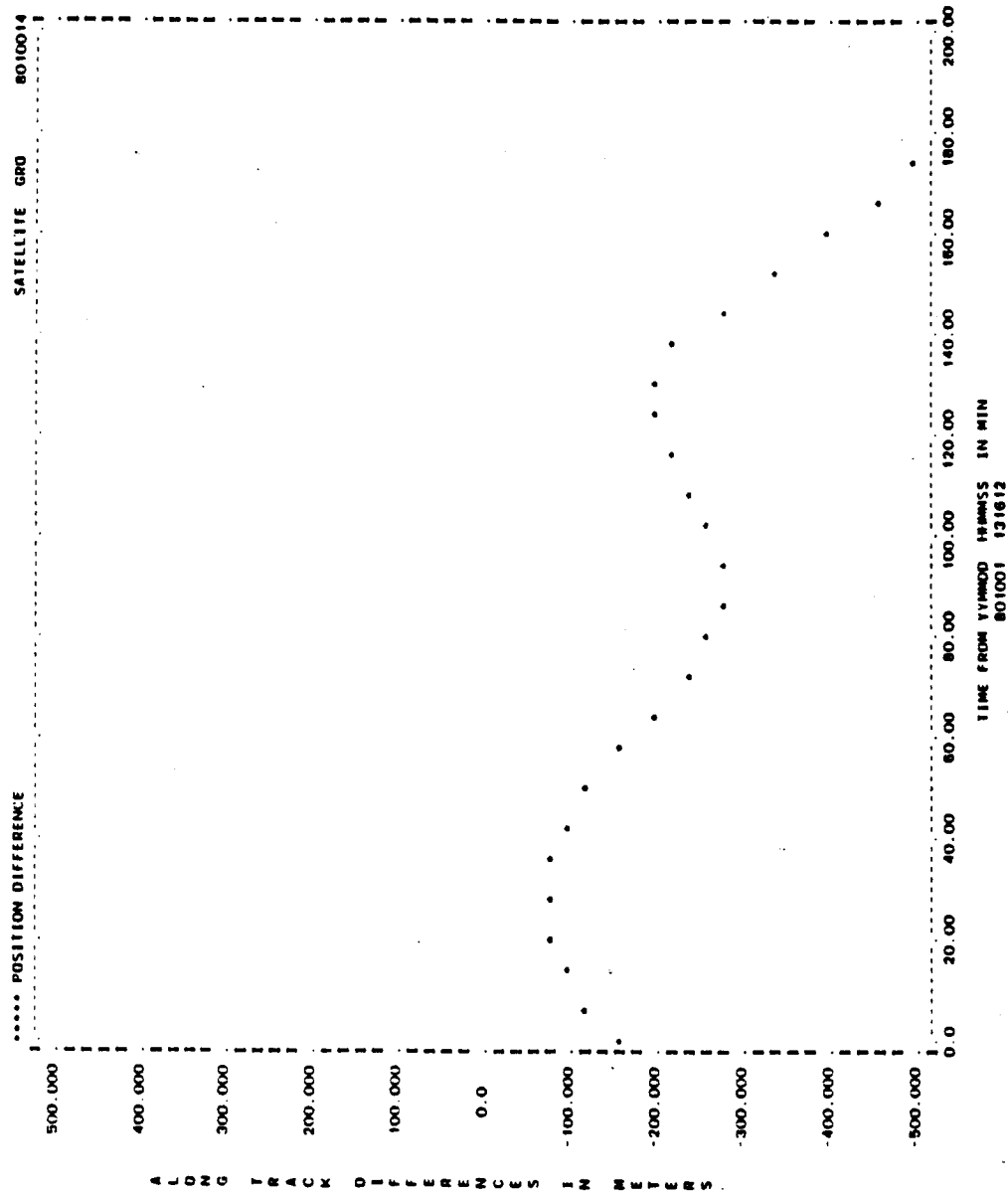


Figure A-102. Along-Track Differences for Run G10 (2 of 2)

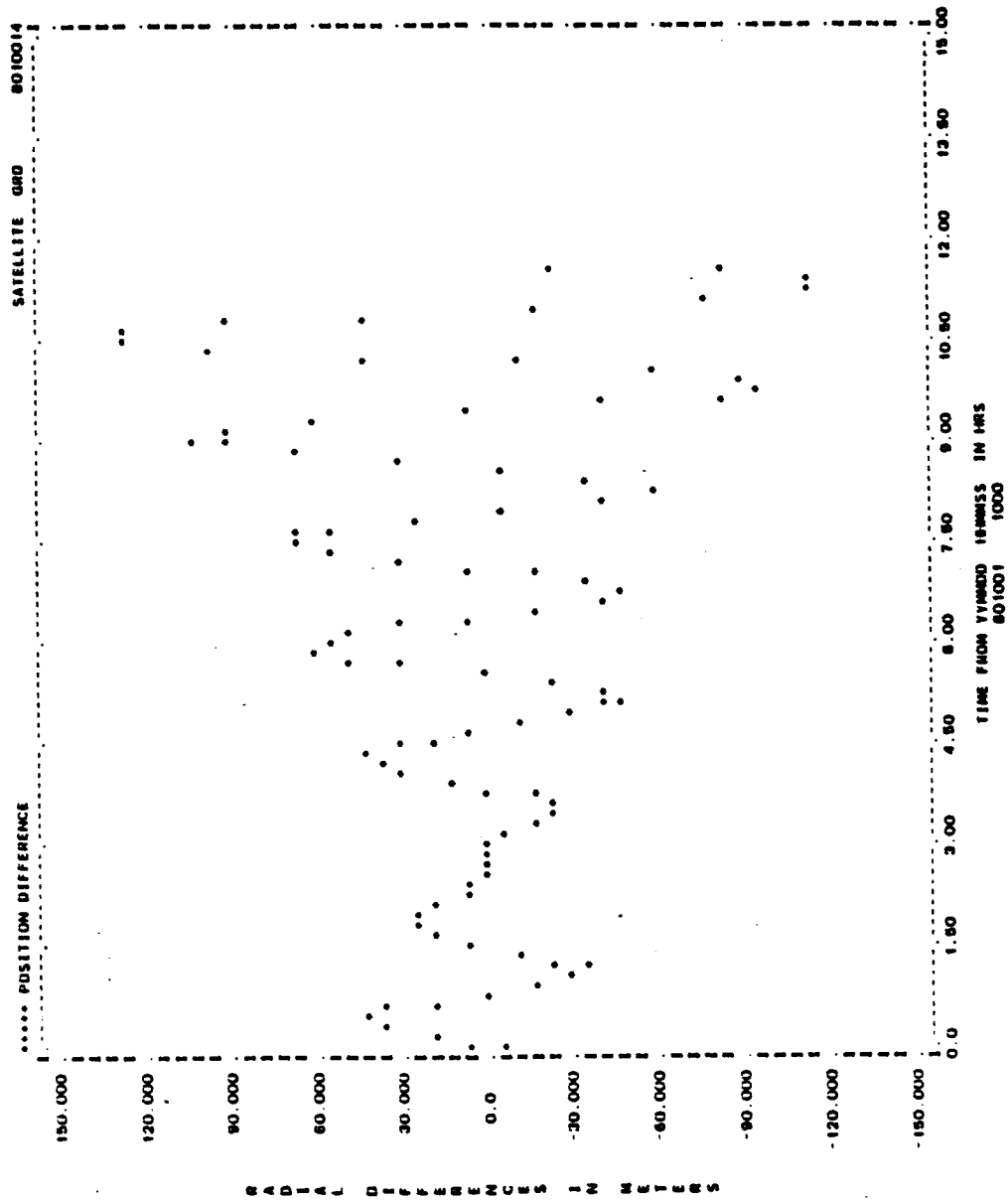


Figure A-103. Radial Differences for Run G22 (1 of 2)

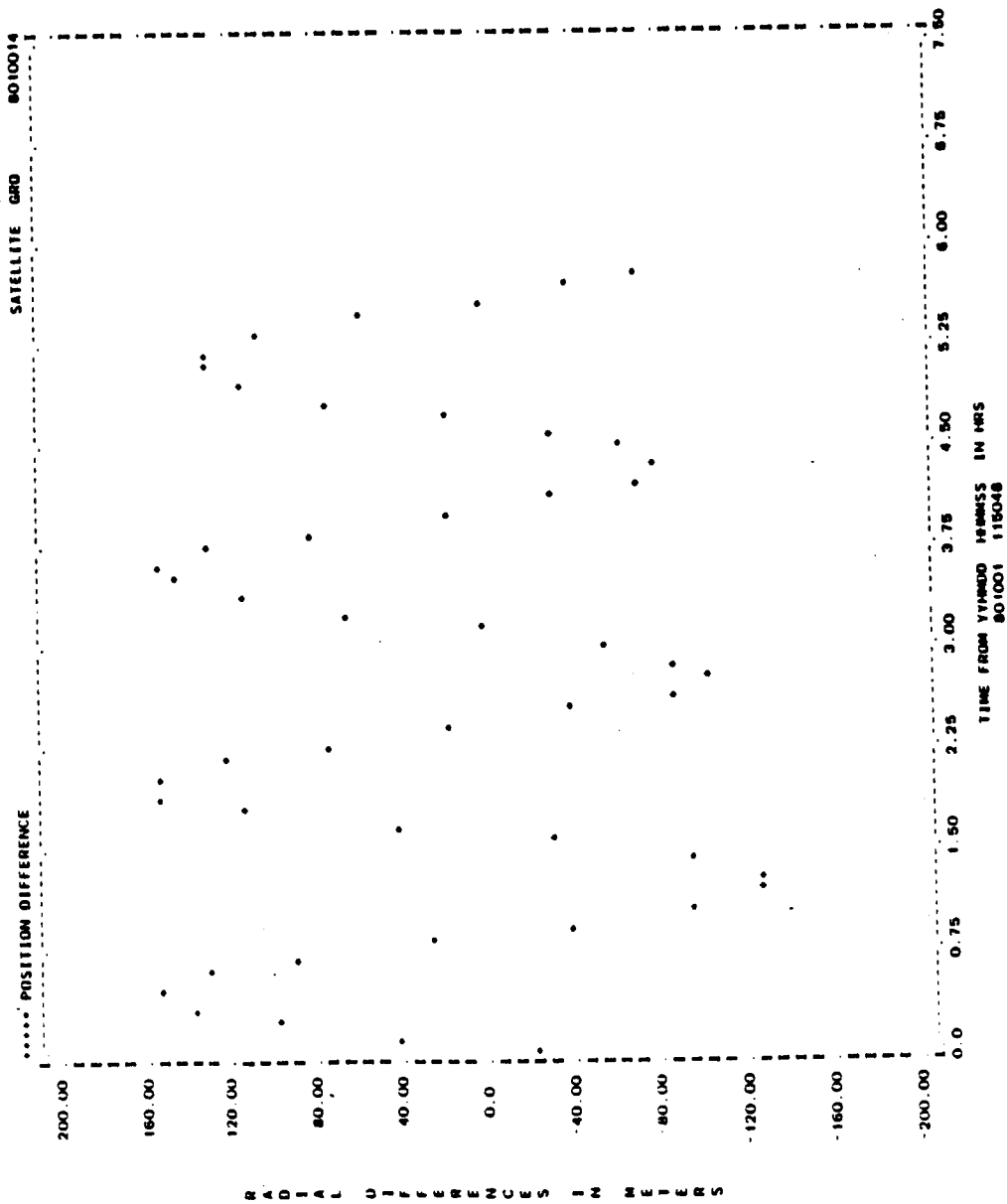


Figure A-103. Radial Differences for Run G22 (2 of 2)

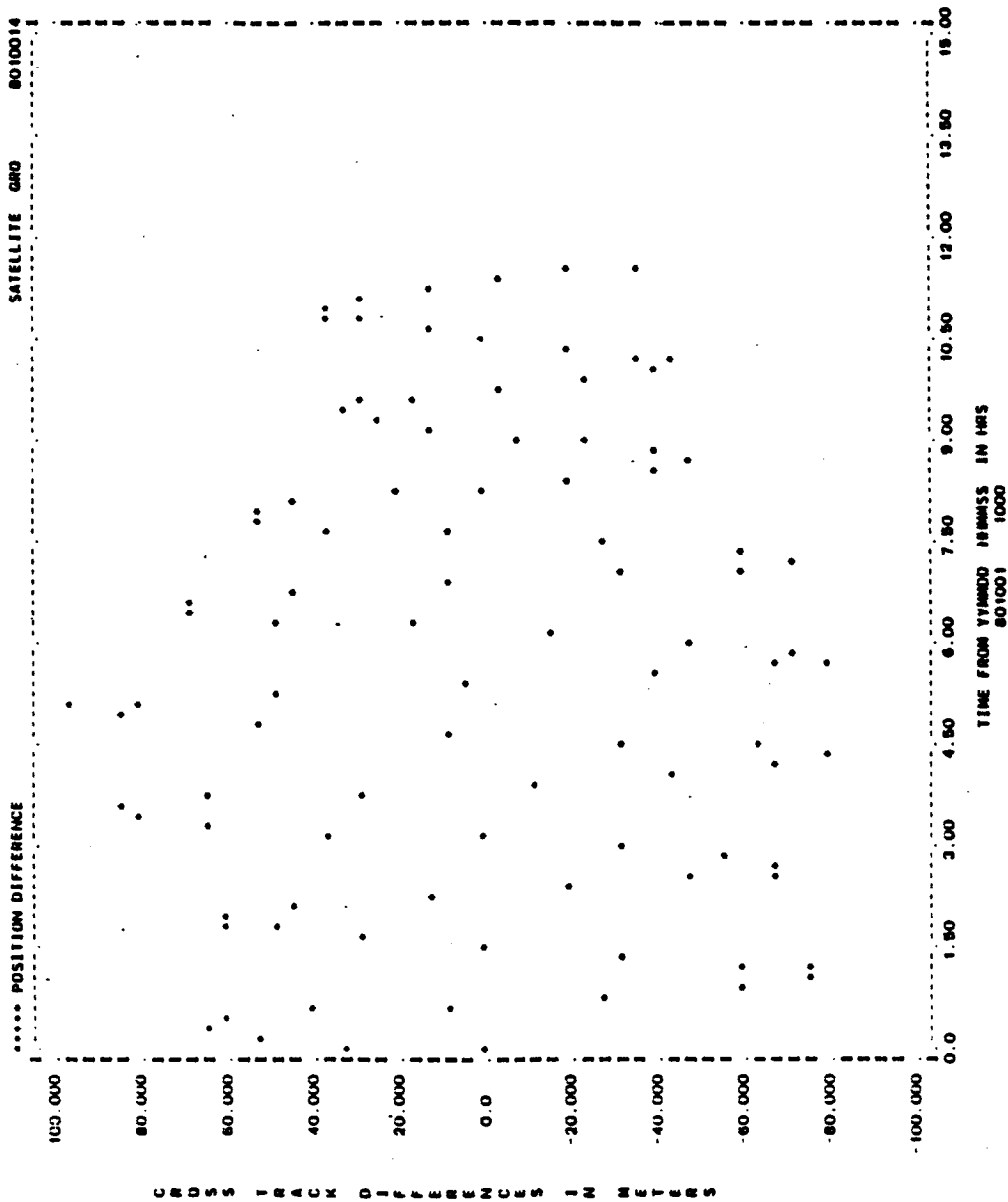


Figure A-104. Cross-Track Differences for Run G22 (1 of 2)

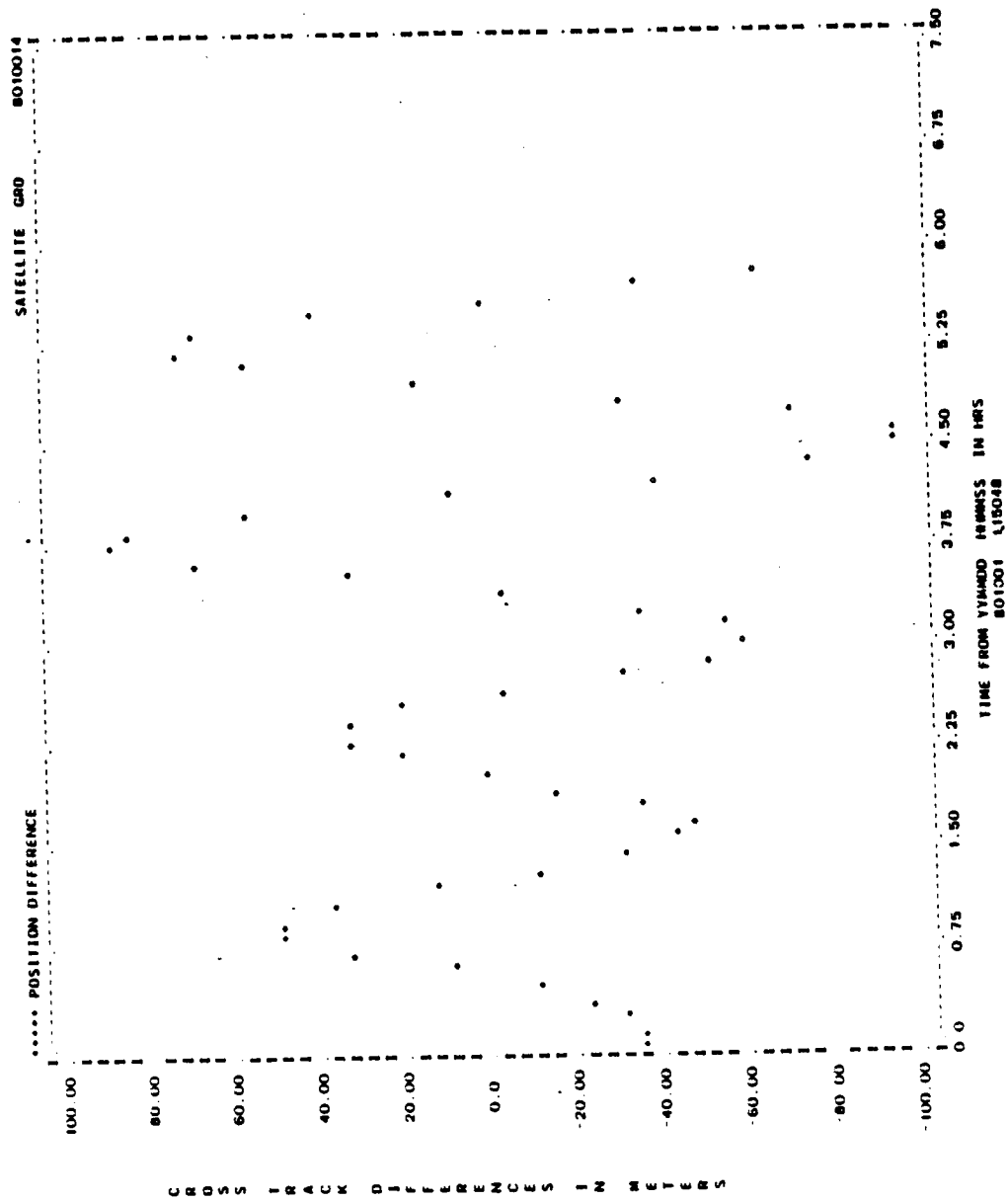


Figure A-104. Cross-Track Differences for Run G22 (2 of 2)

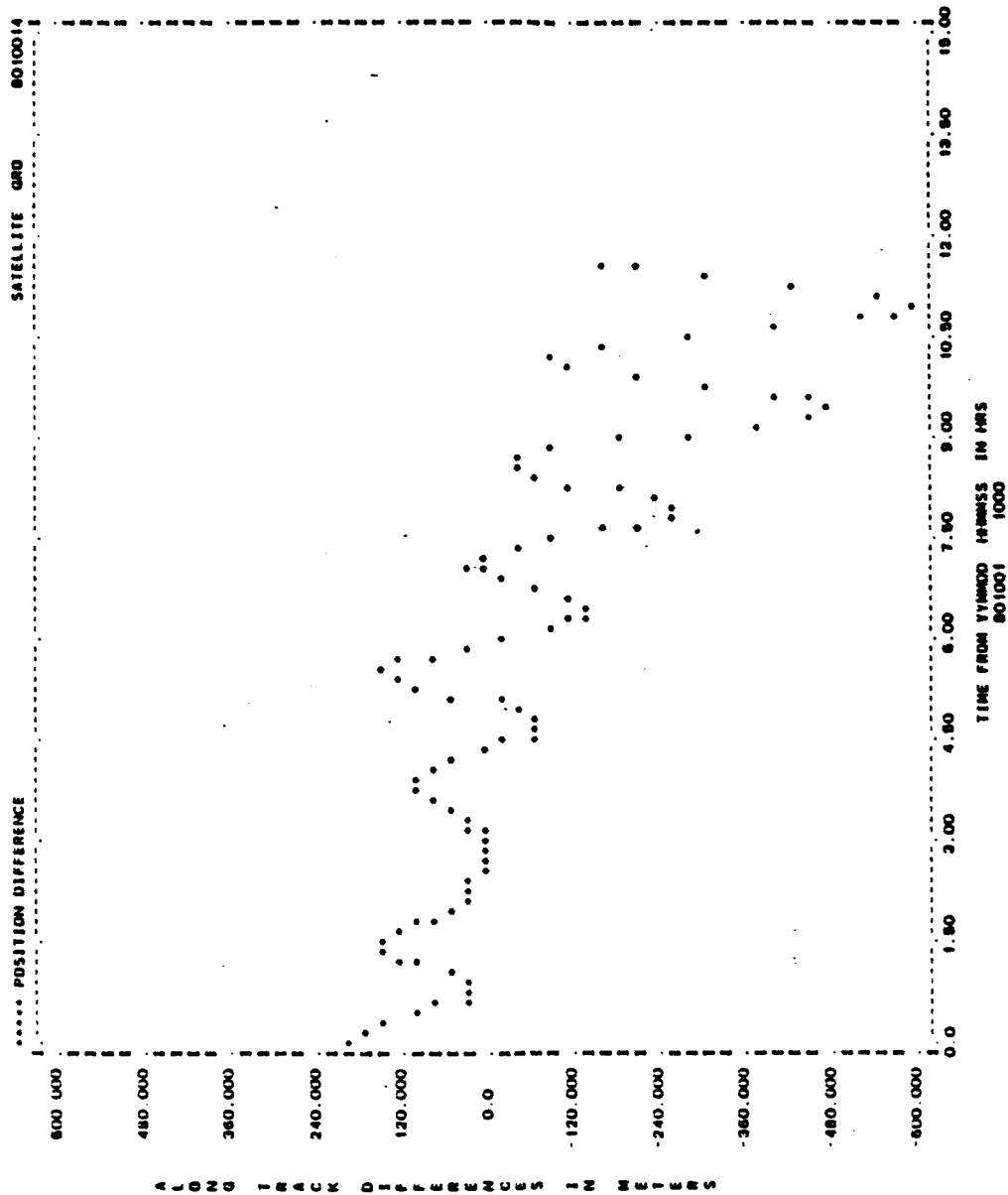


Figure A-105. Along-Track Differences for Run G22 (1 of 2)

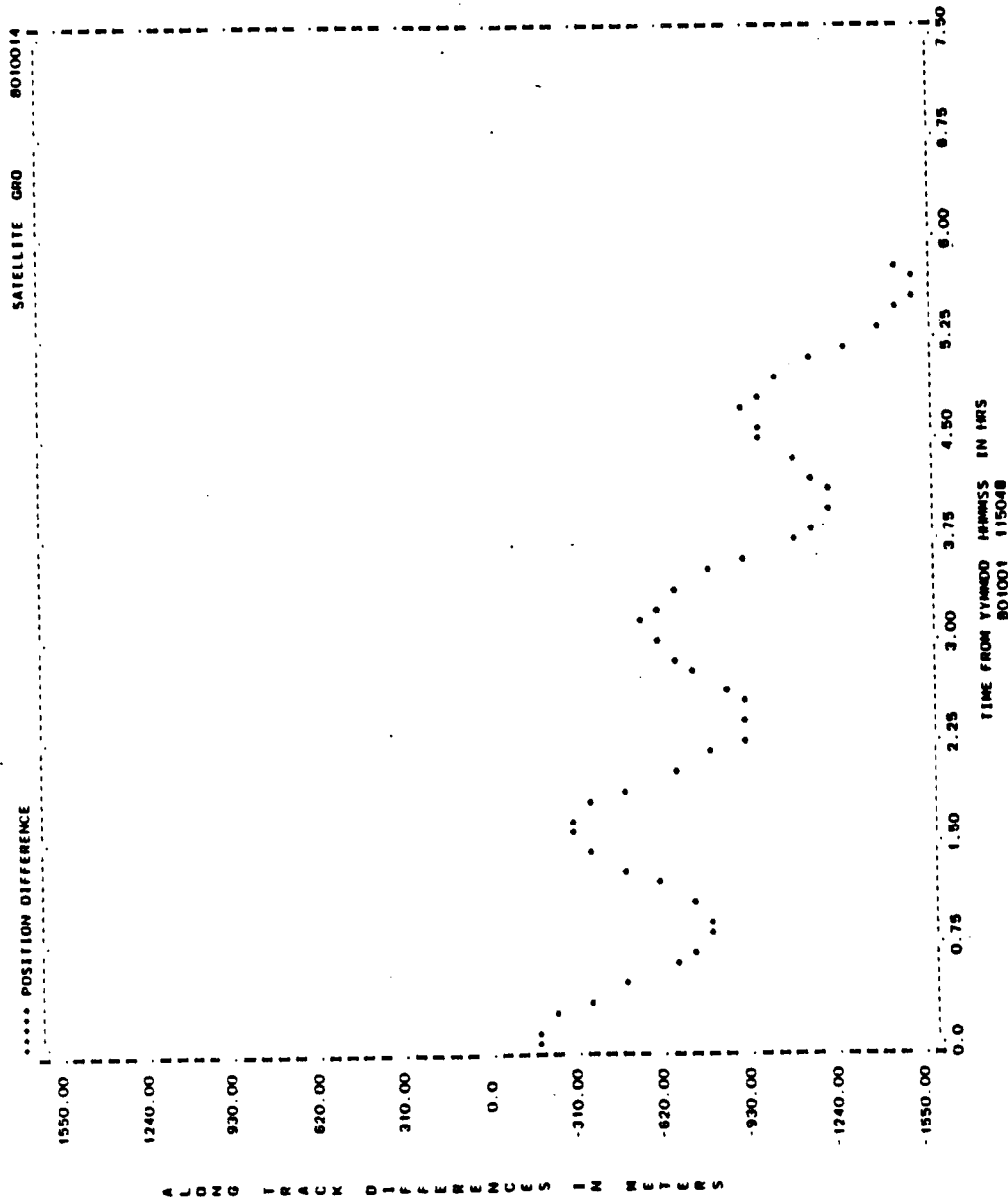


Figure A-105. Along-Track Differences for Run G22 (2 of 2)

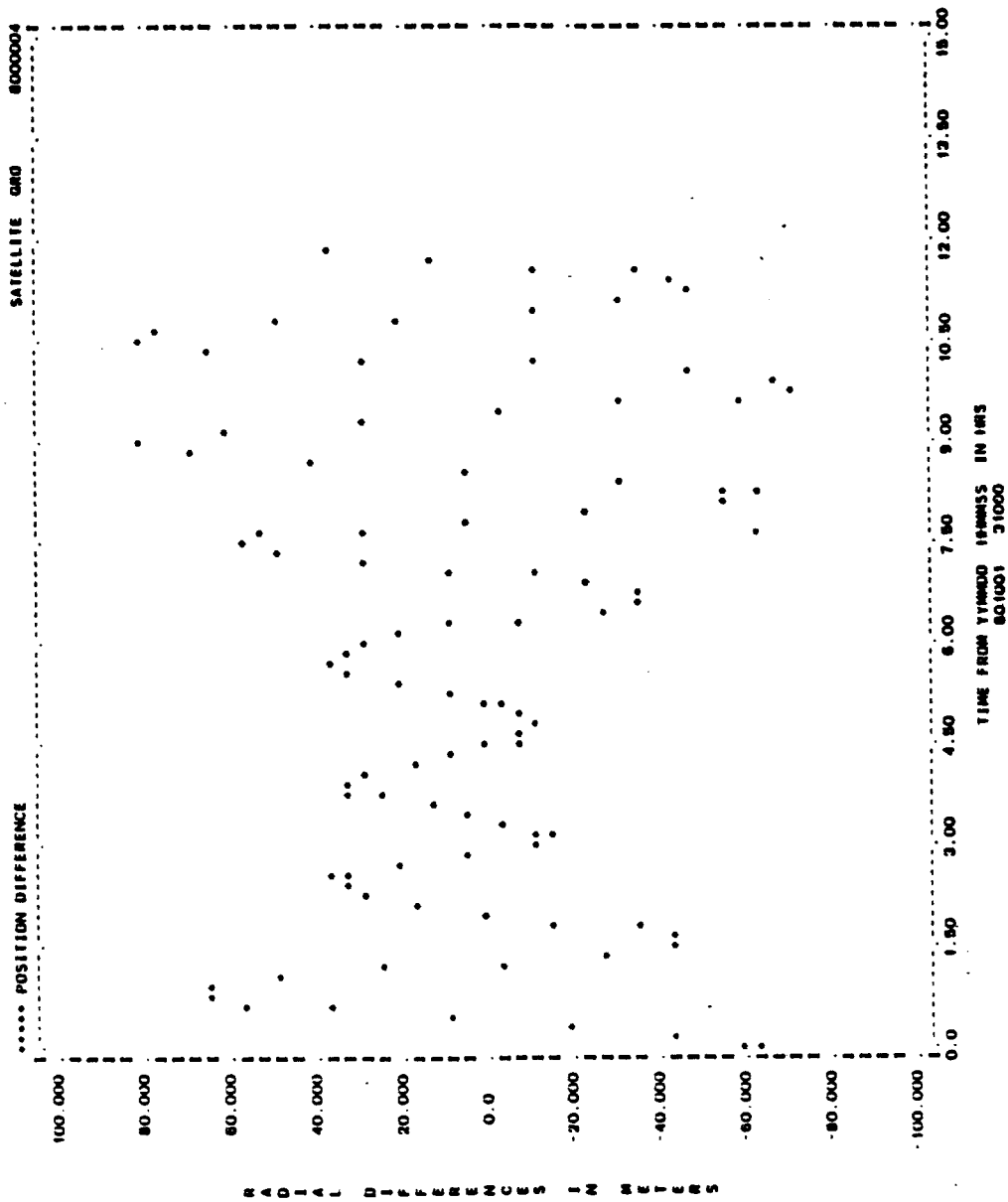
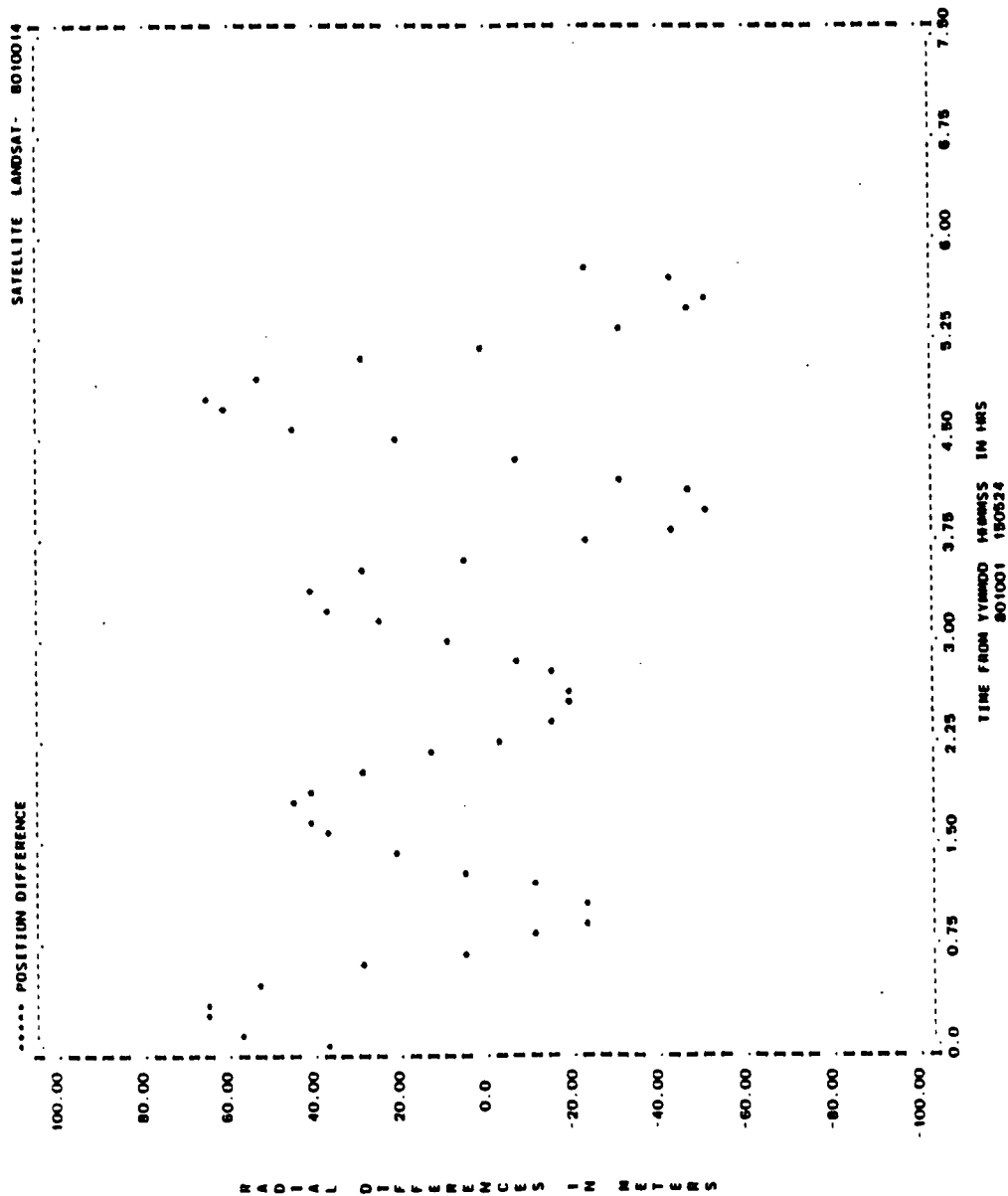


Figure A-106. Radial Differences for Run G22 (1 of 2)



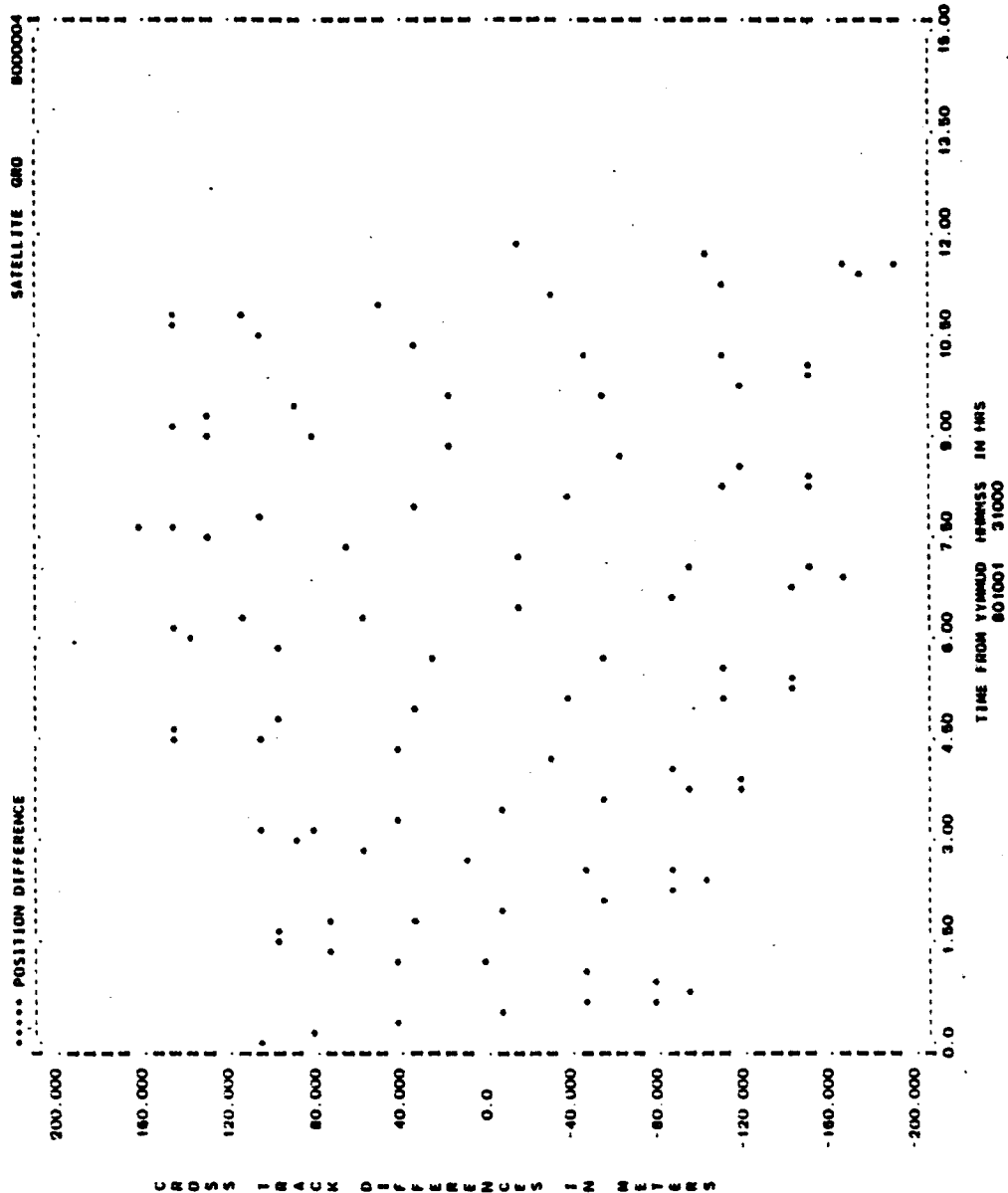


Figure A-107. Cross-Track Differences for Run G22 (1 of 2)

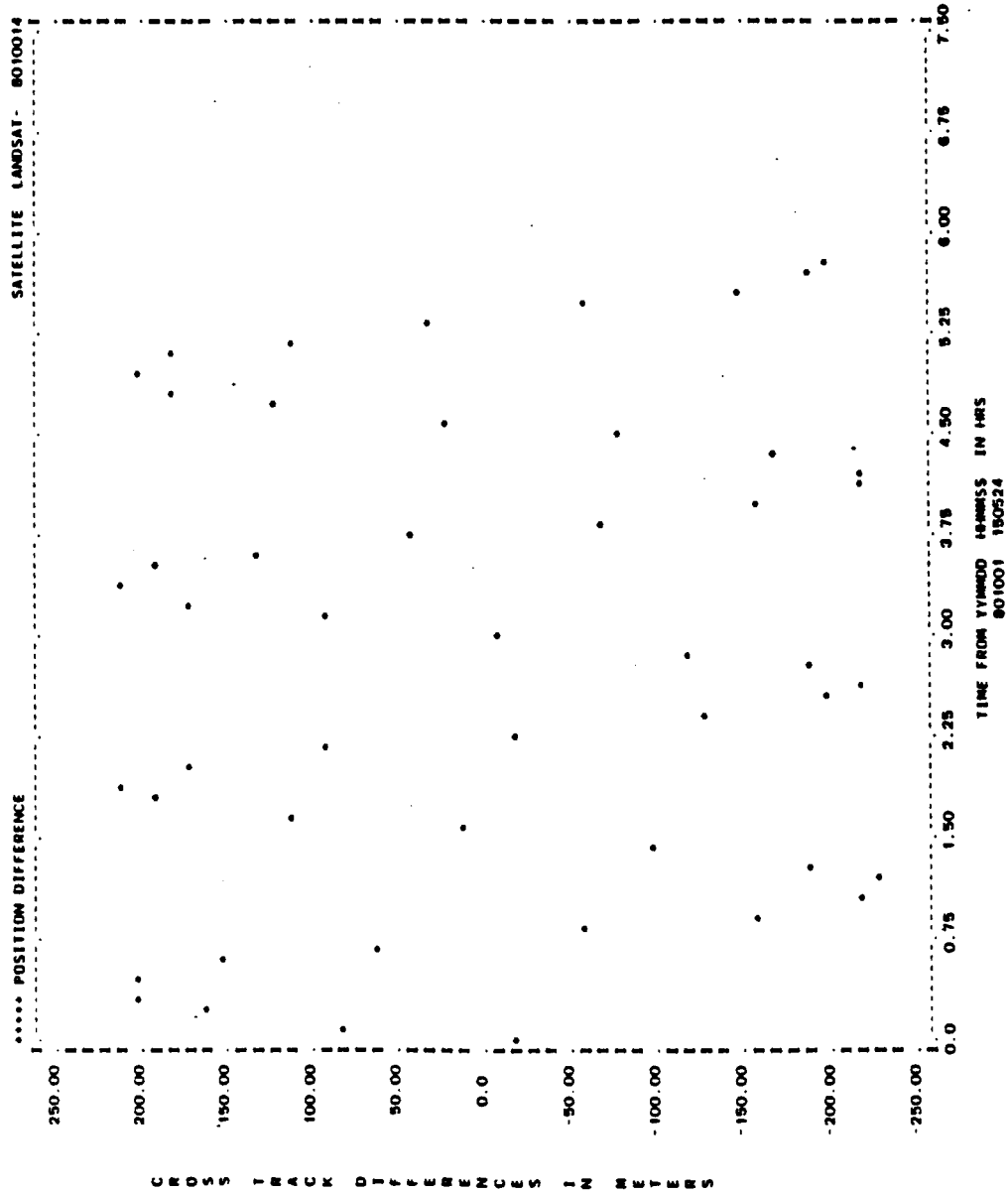


Figure A-107. Cross-Track Differences for Run G22 (2 of 2)

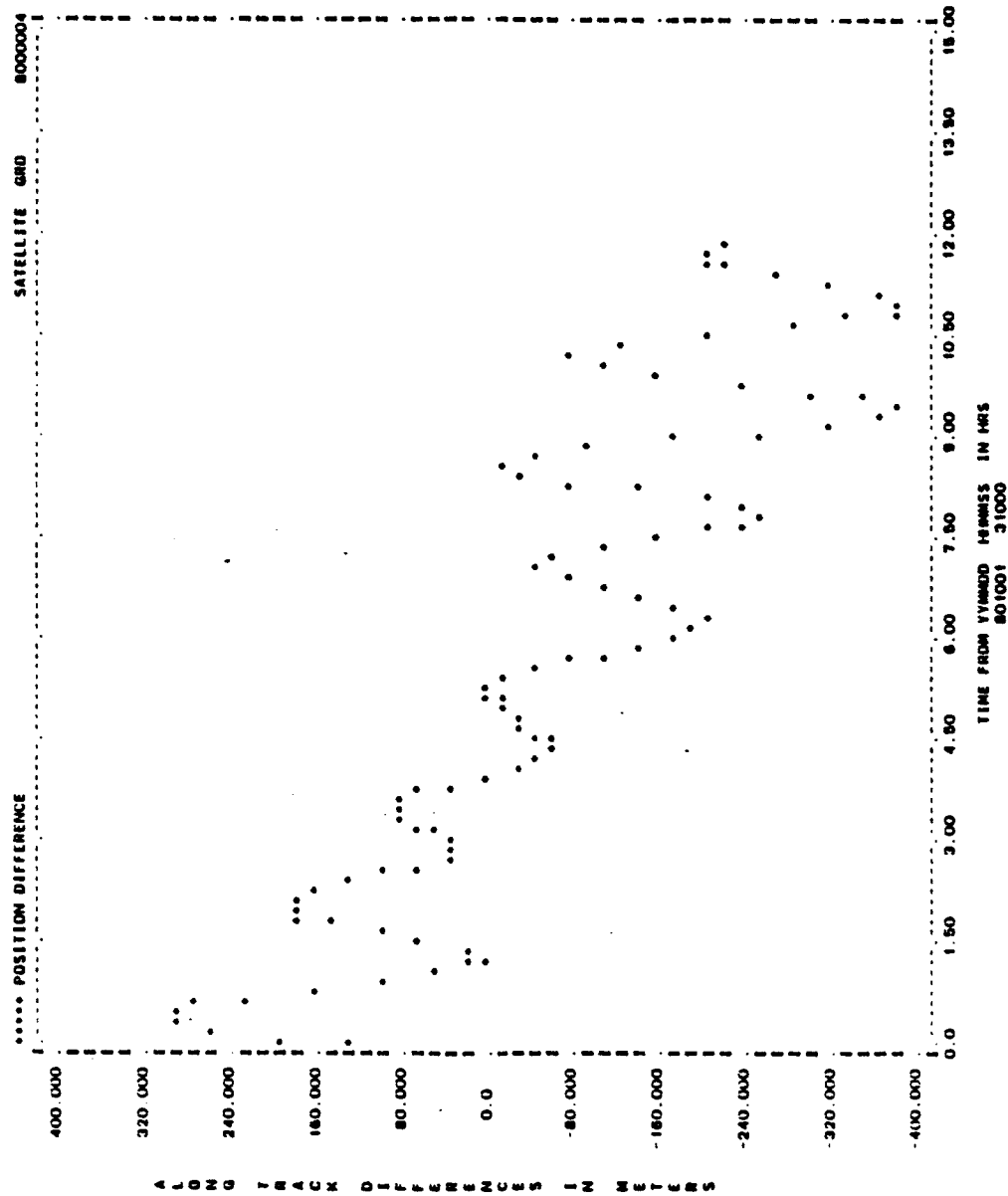


Figure A-108. Along-Track Differences for Run G22 (1 of 2)

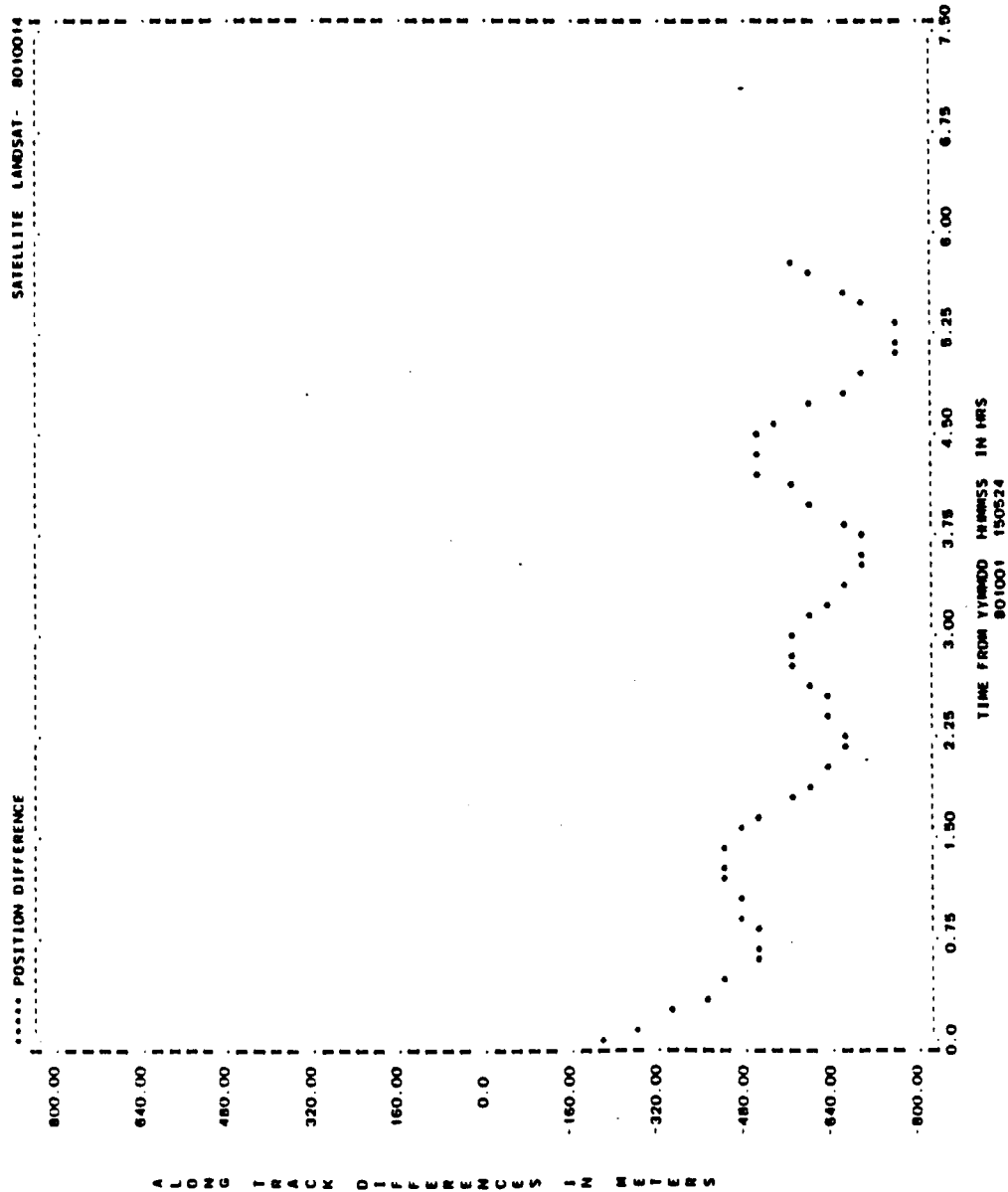


Figure A-108. Along-Track Differences for Run G22 (2 of 2)

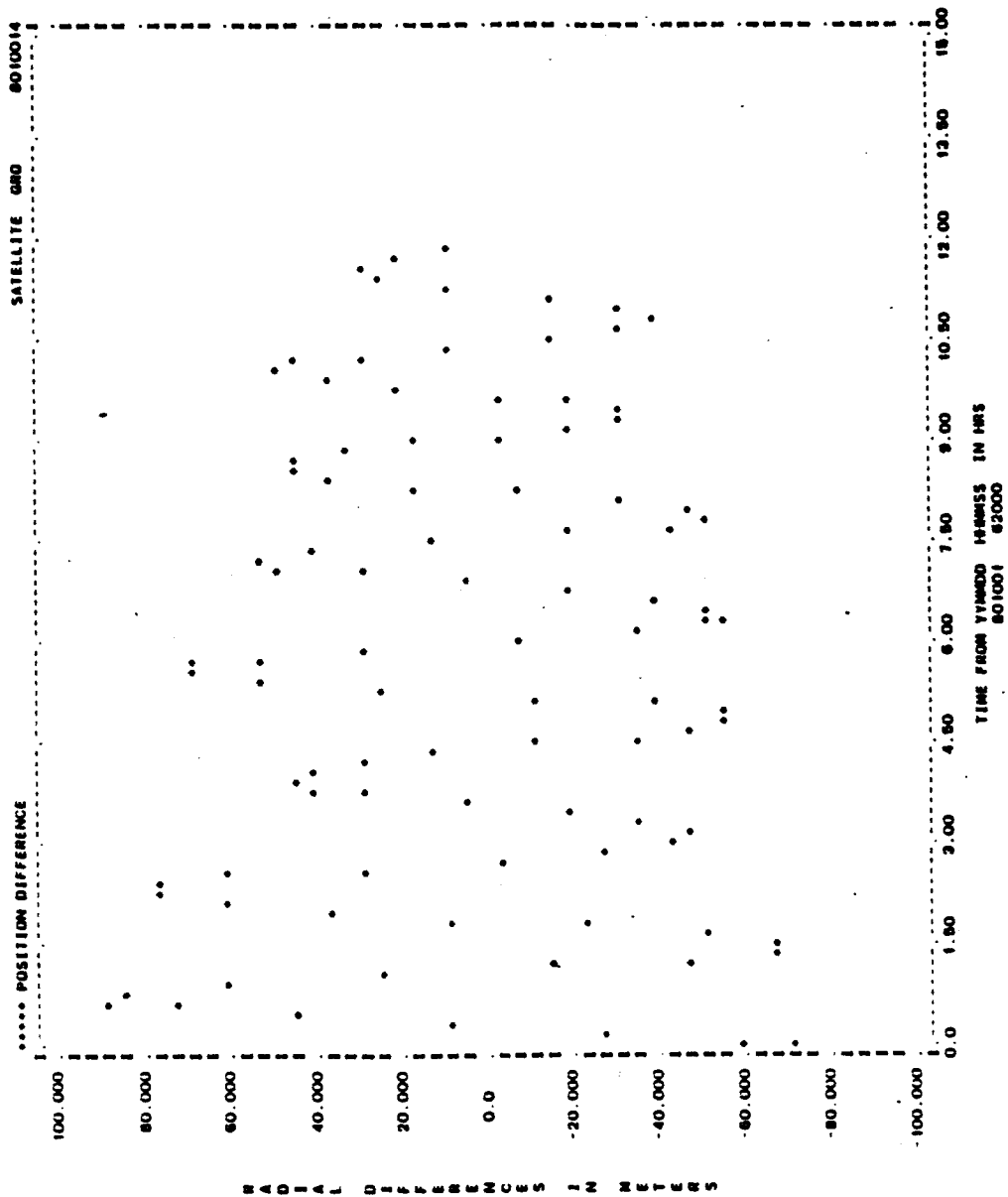


Figure A-109. Radial Differences for Run G22 (1 of 2)

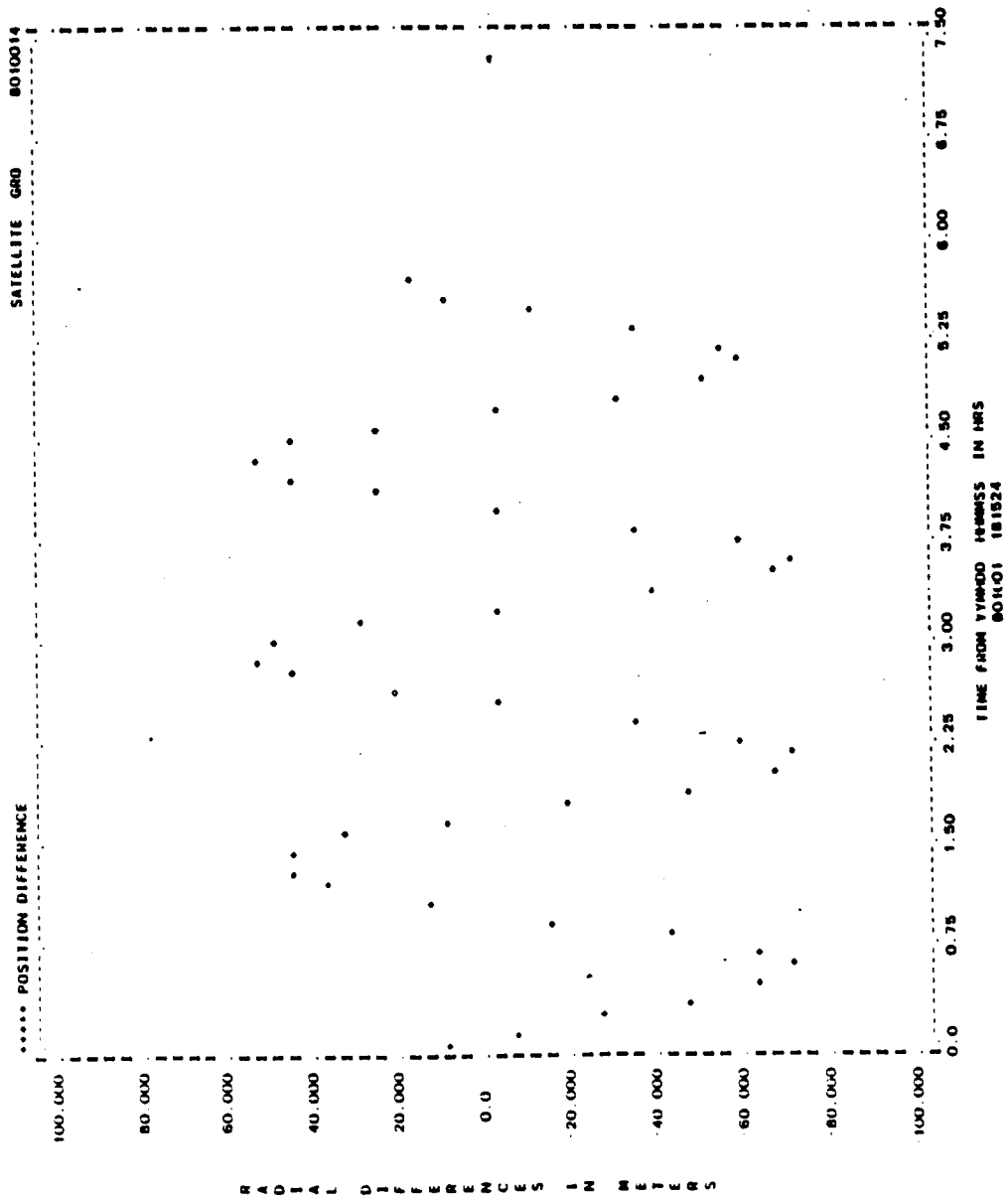


Figure A-109. Radial Differences for Run G22 (2 of 2)

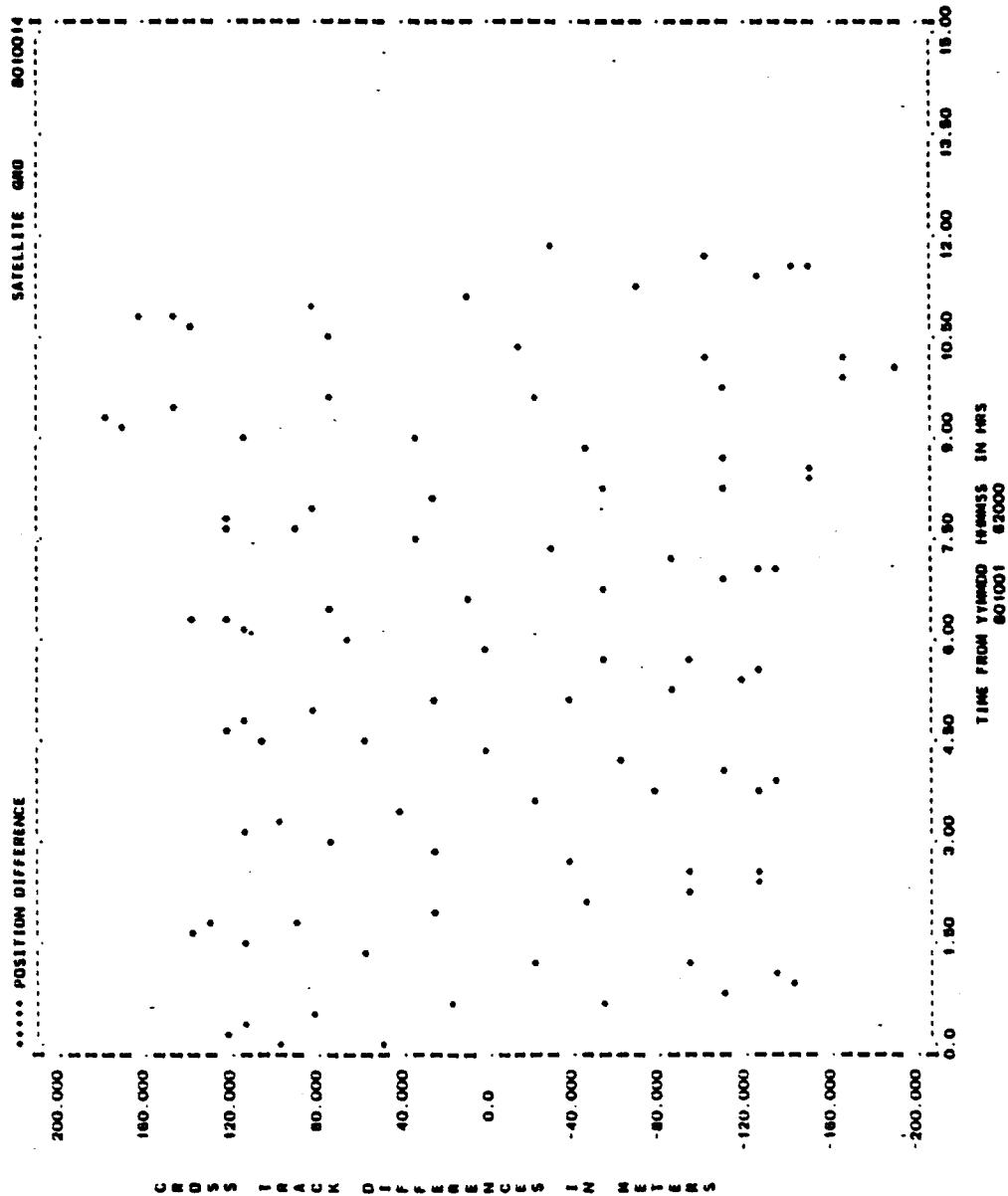


Figure A-110. Cross-Track Differences for Run G22 (1 of 2)

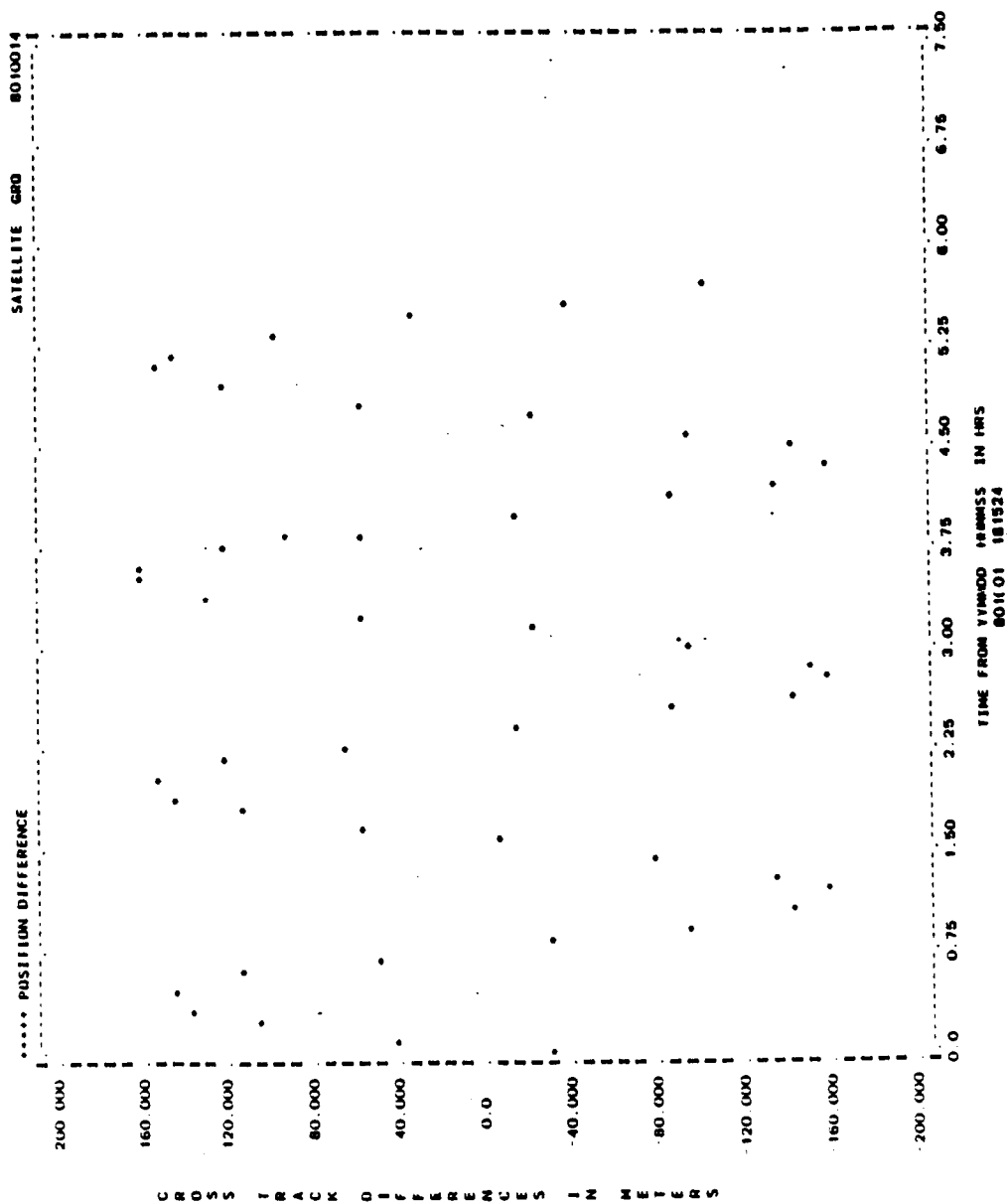


Figure A-110. Cross-Track Differences for Run G22 (2 of 2)

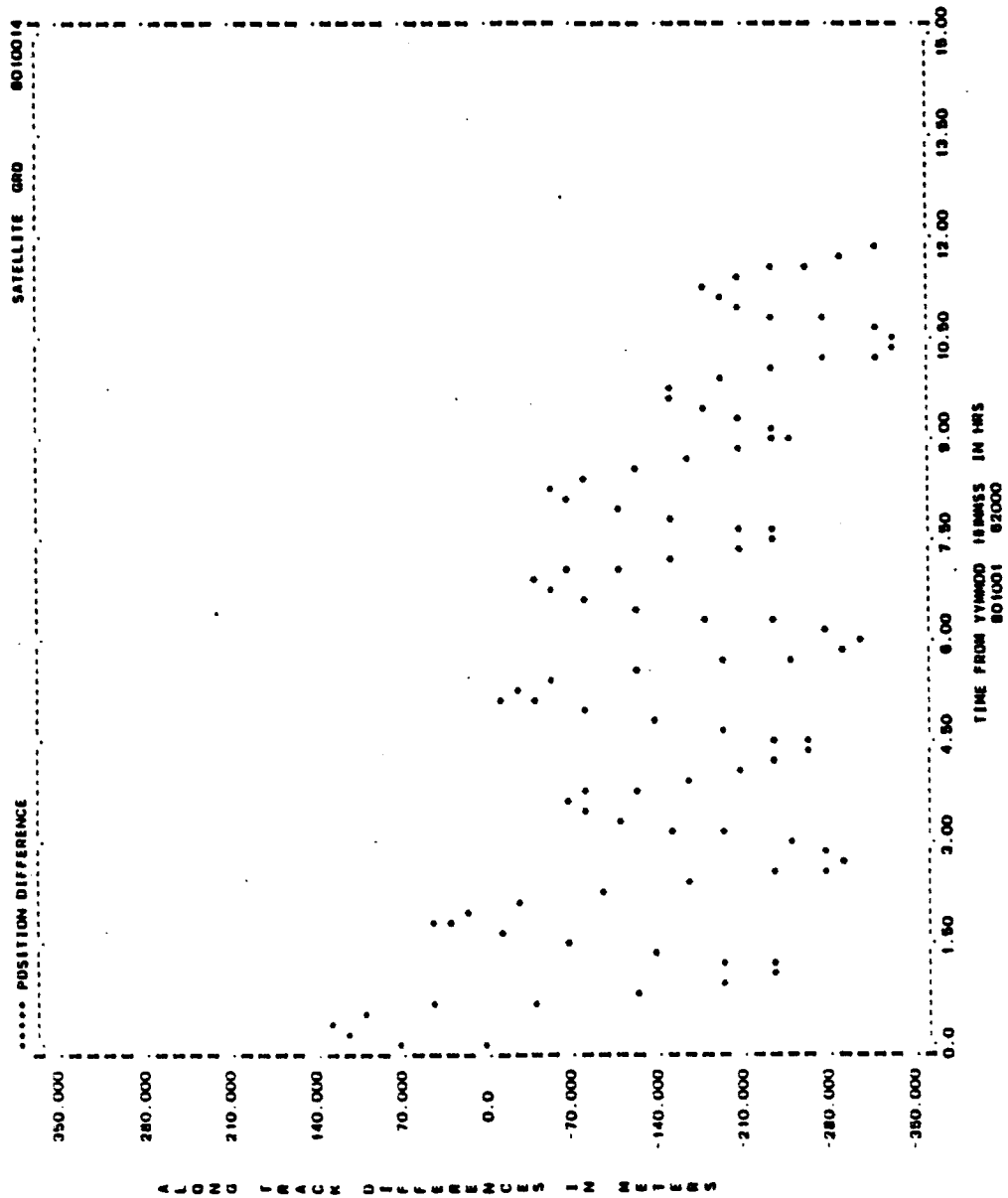


Figure A-111. Along-Track Differences for Run G22 (1 of 2)

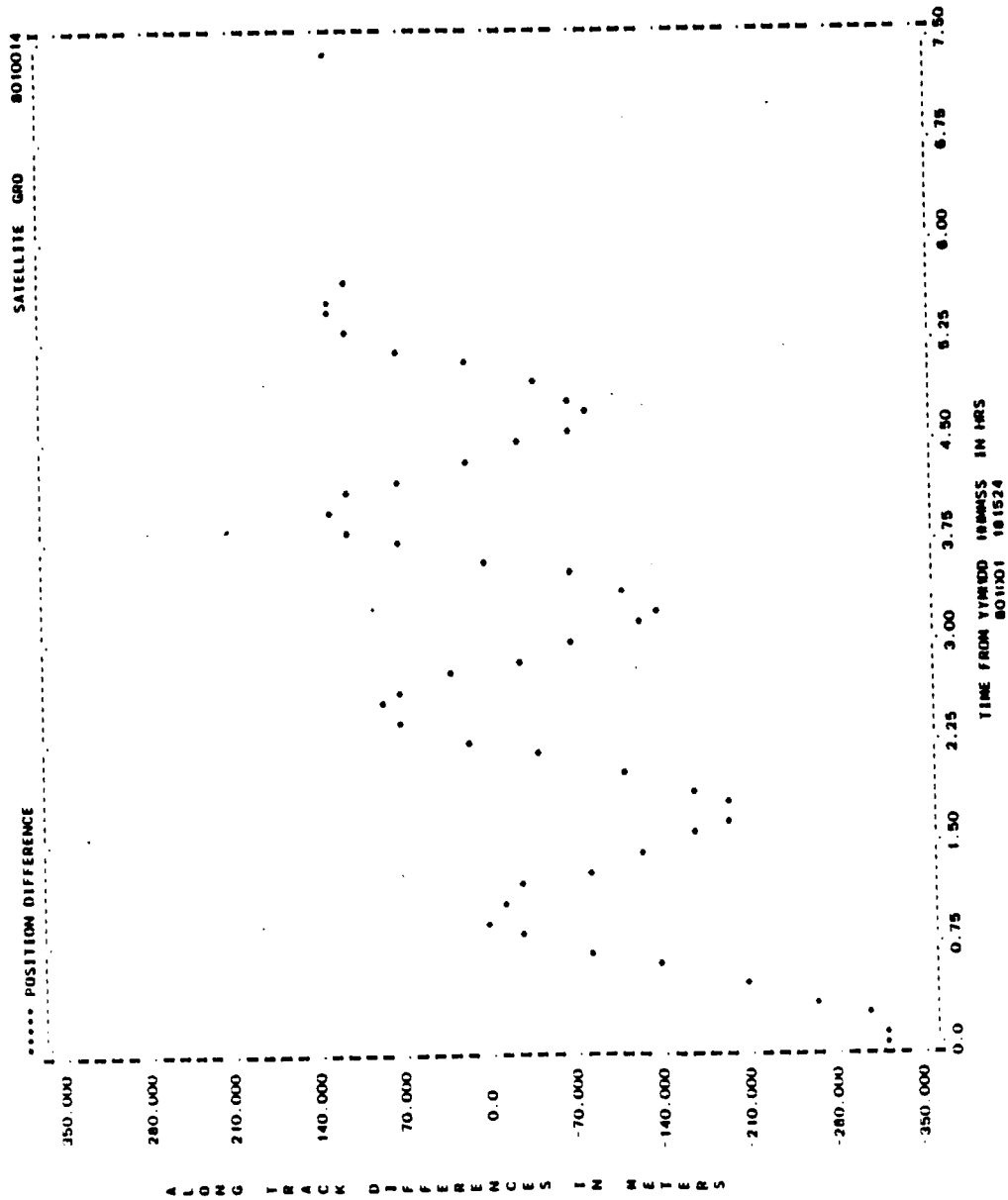


Figure A-111. Along-Track Differences for Run G22 (2 of 2)

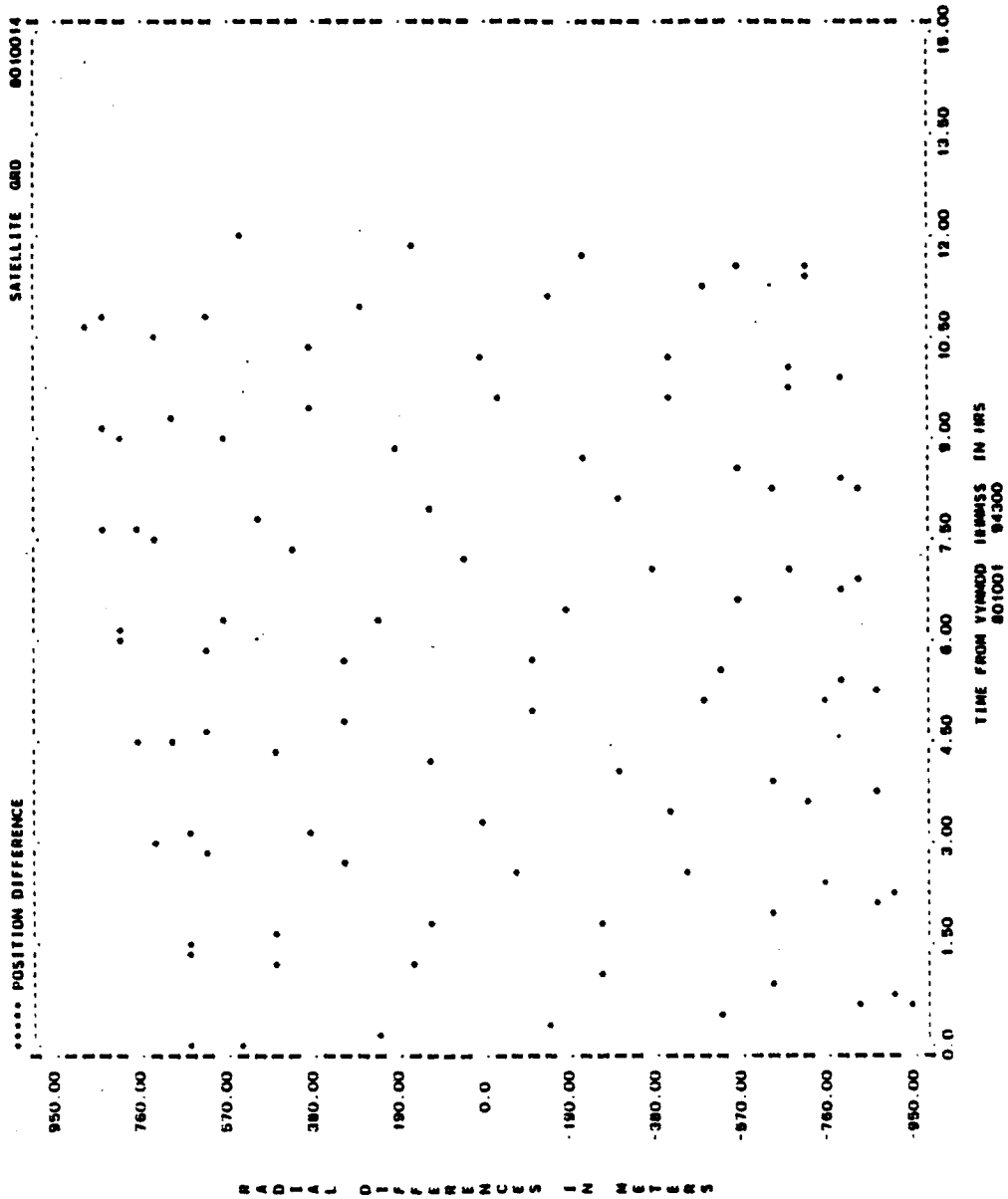


Figure A-112. Radial Differences for Run G22 (1 of 2)

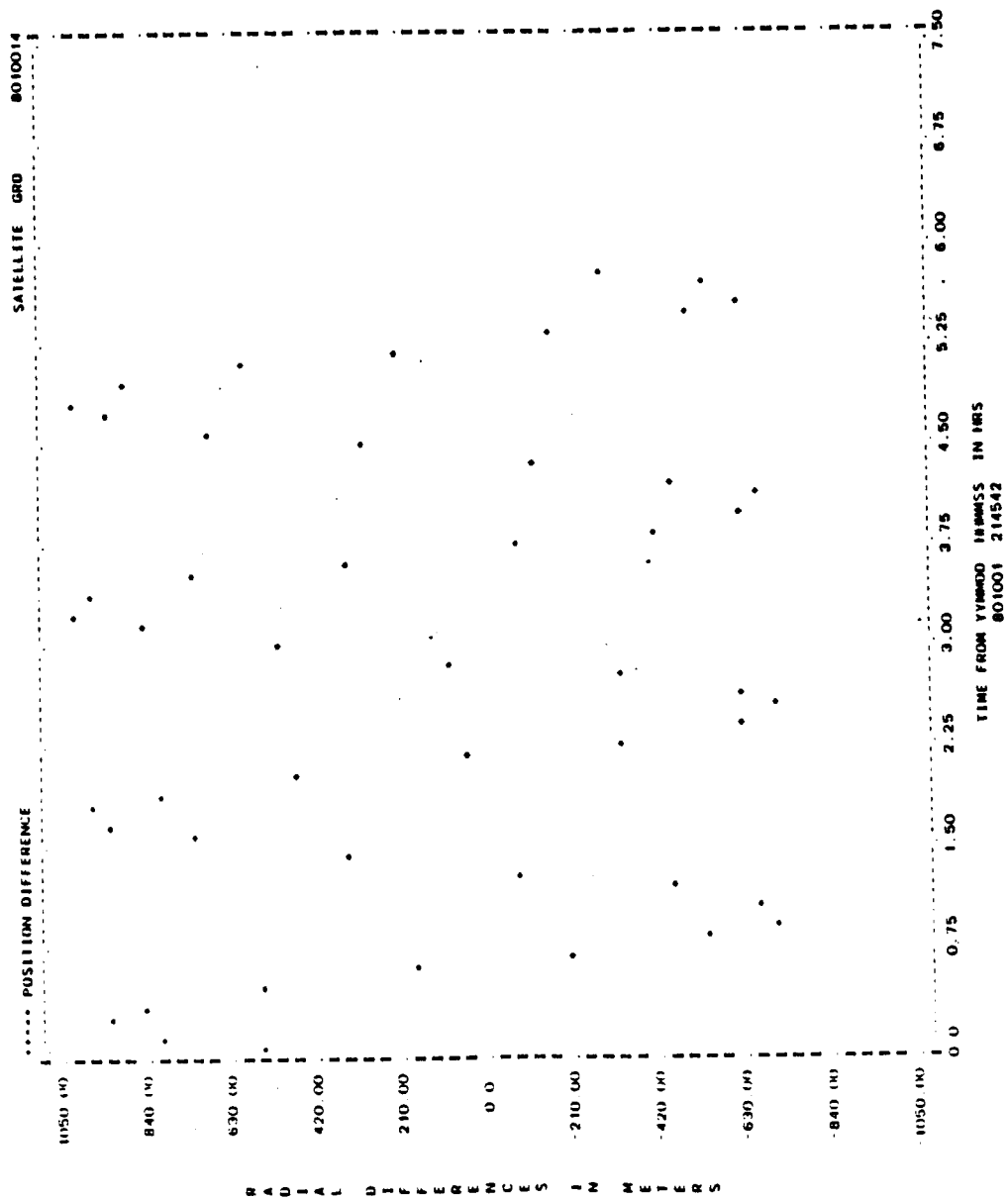


Figure A-112. Radial Differences for Run G22 (2 of 2)

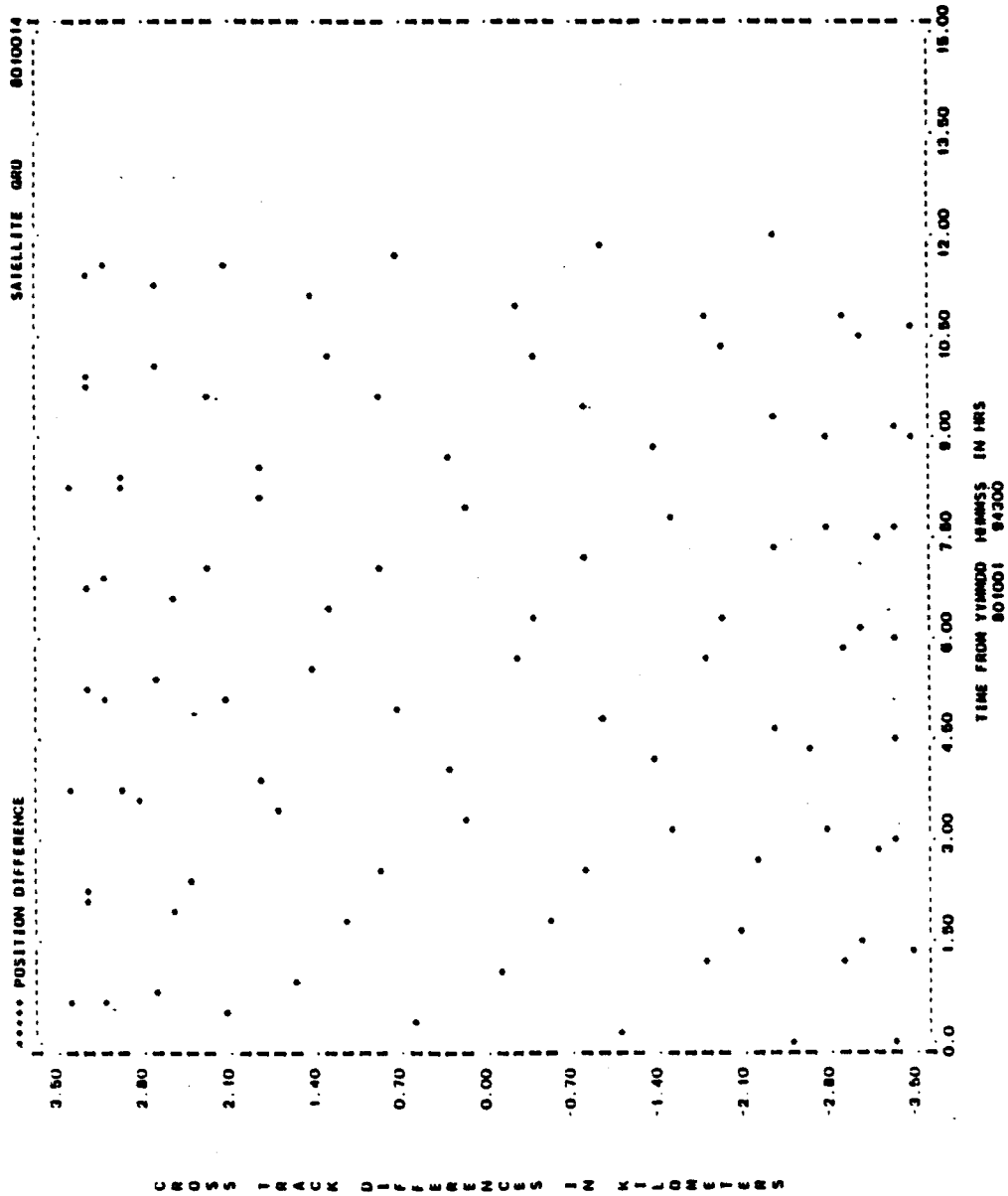


Figure A-113. Cross-Track Differences for Run G22 (1 of 2)

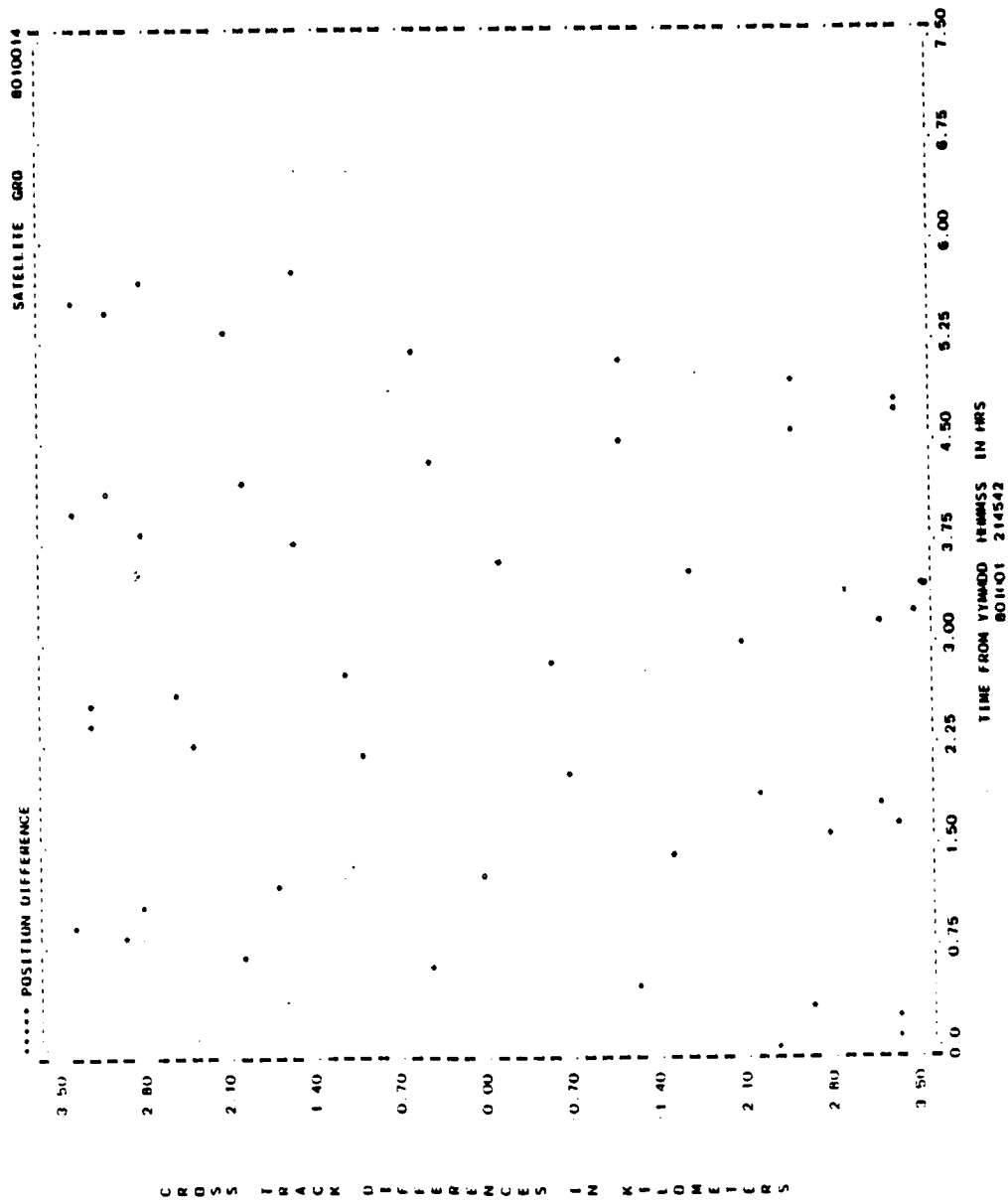


Figure A-113. Cross-Track Differences for Run G22 (2 of 2)

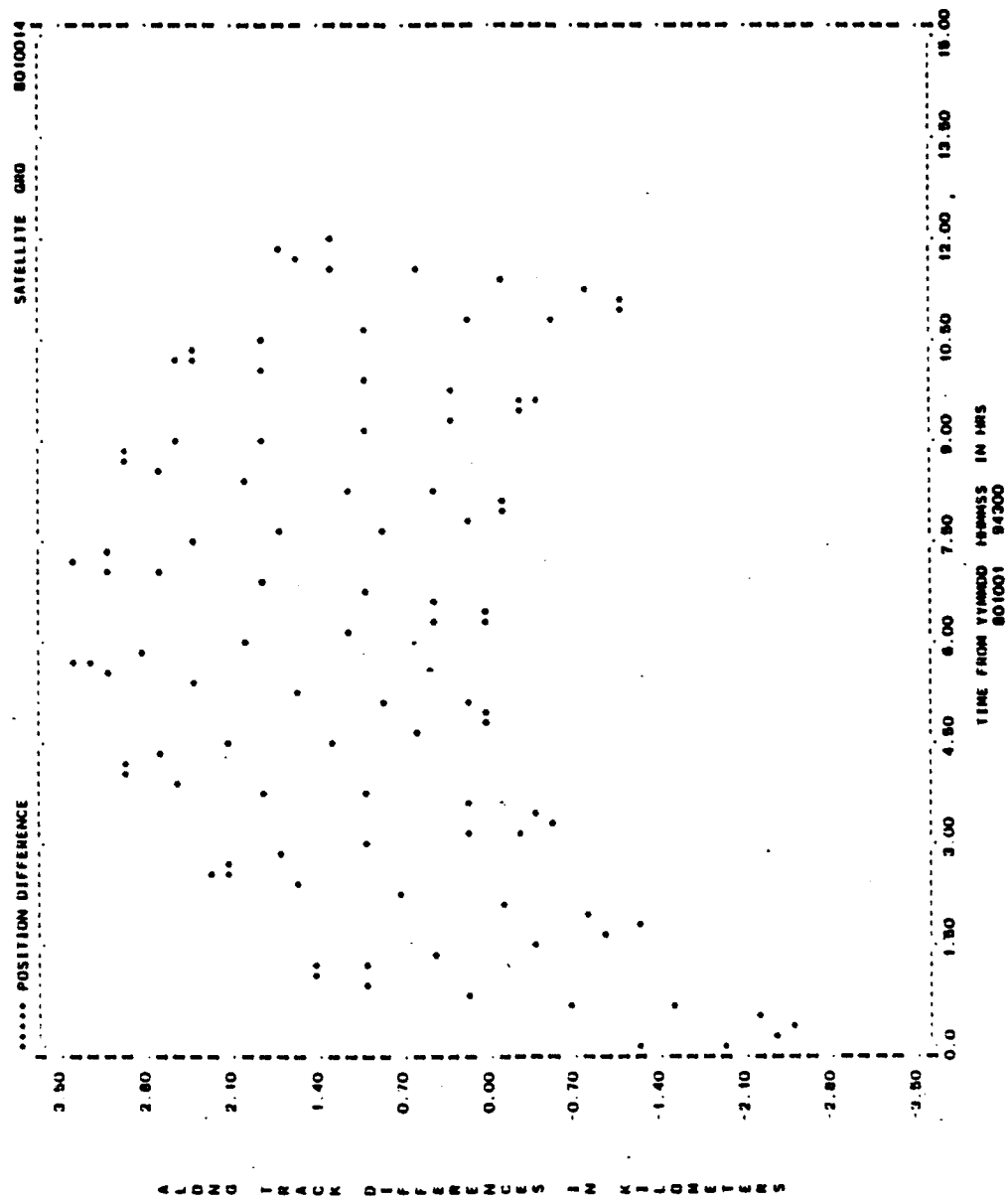


Figure A-114. Along-Track Differences for Run G22 (1 of 2)

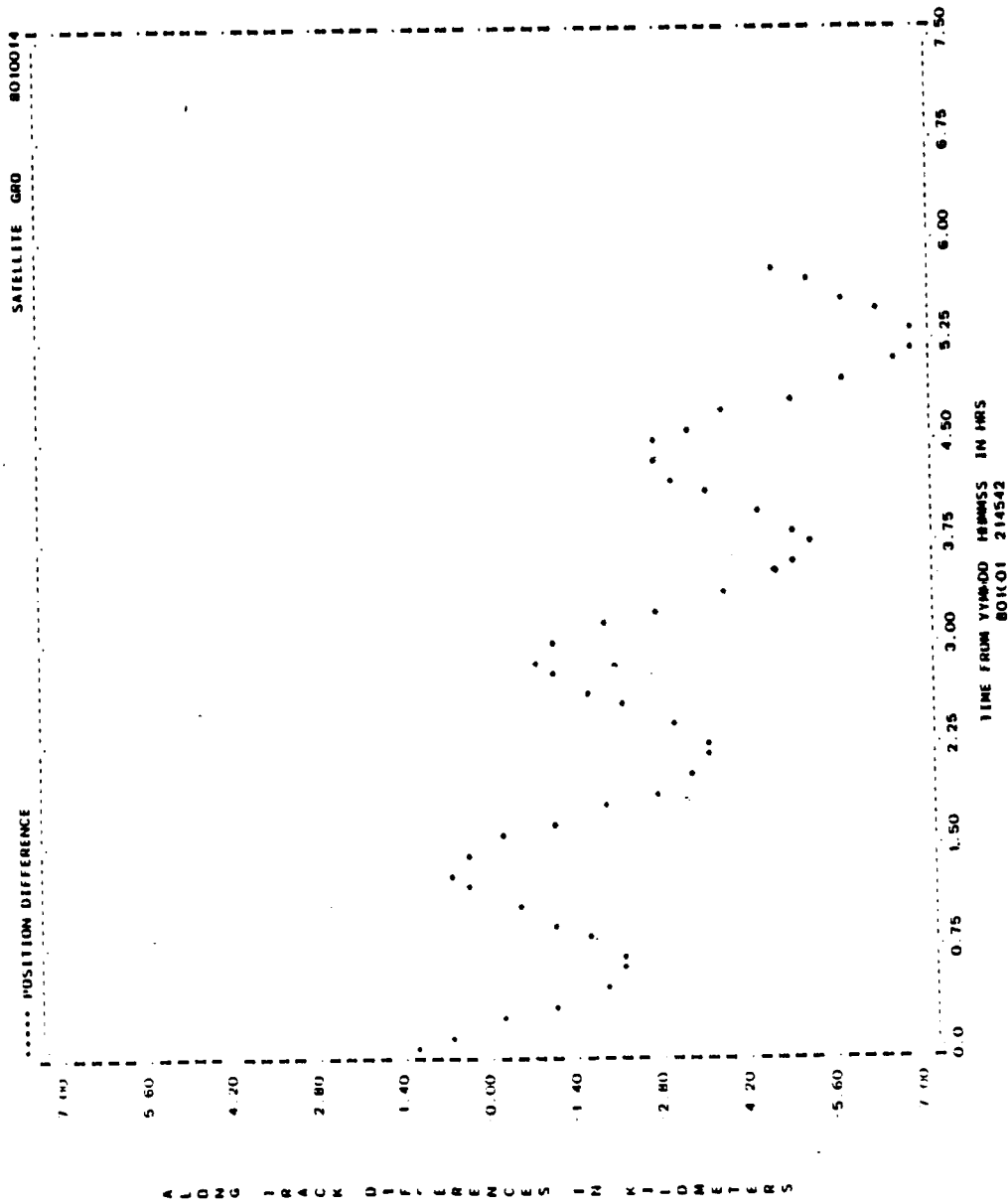


Figure A-114. Along-Track Differences for Run G22 (2 of 2)

## APPENDIX B - ACCURACY OF SBDC FORCE MODEL

To assess the accuracy of the force model used in the SBDC, Landsat-D and GRO runs were made using a 12th-order Cowell integrator with the "truth" force model and the force model used by the SBDC. Each case used the same initial satellite state and was run for a period of 24 hours. (The differences in the force models are specified in Table 4-7.) Ephemerides for each satellite were compared, and radial, long-track, and cross-track differences were plotted. Table B-1 specifies the maximum values for these ephemeris errors and denotes the figure numbers of the  $\Delta H$ ,  $\Delta C$ , and  $\Delta L$  plots that follow.

Table B-1. Ephemeris Error Maximum Values

SATELLITE	MAXIMUM POSITION DIFFERENCE (m)				FIGURE NUMBERS (B- )
	$\Delta H$	$\Delta C$	$\Delta L$	$\Delta R$	
LANDSAT-D	45	94	1,232	1,235	1, 2, 3
GRO	367	103	26,573	26,575	4, 5, 6

7651/80

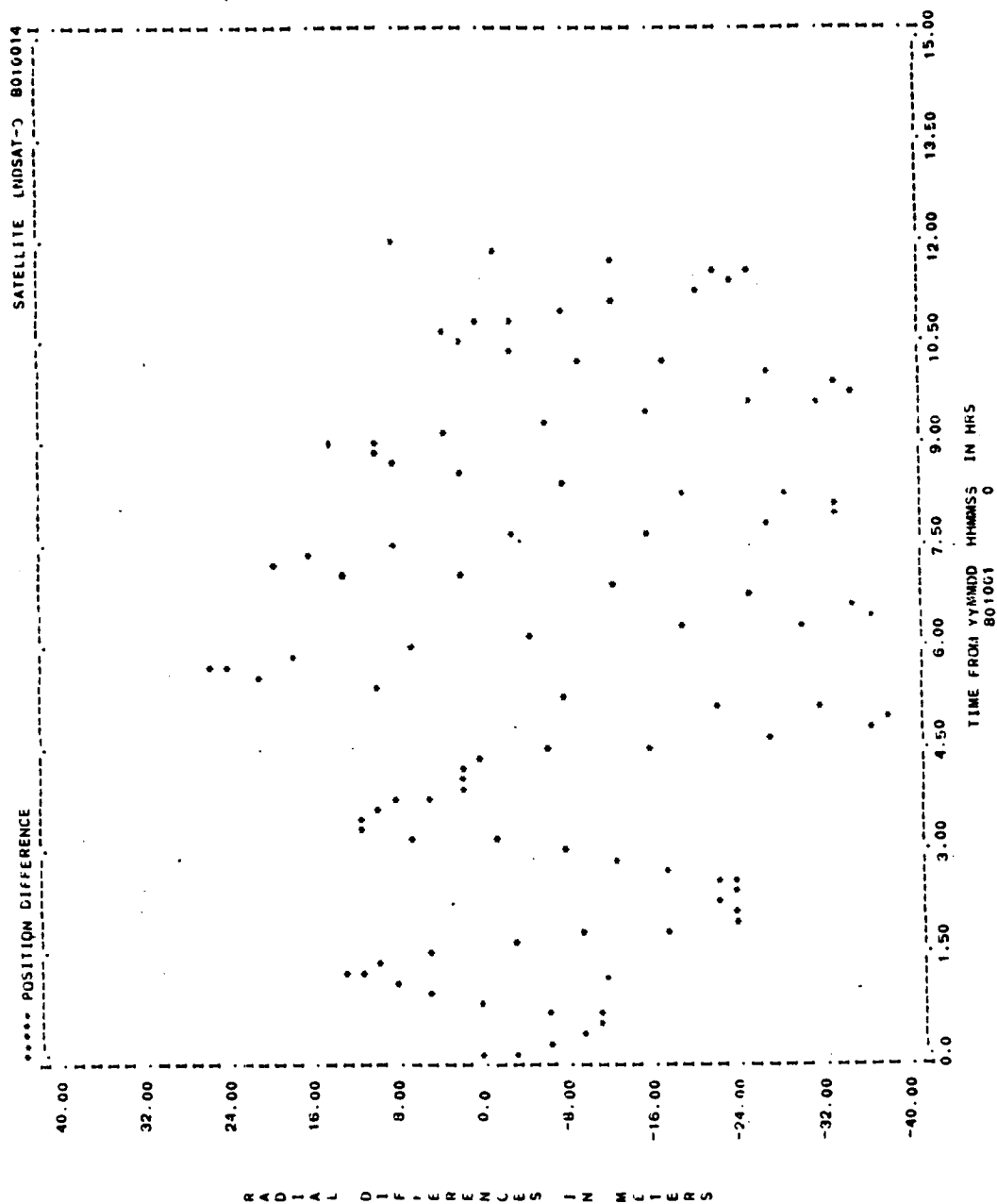


Figure B-1. Error Growth Over 12 Hours for Landsat-D (1 of 3)

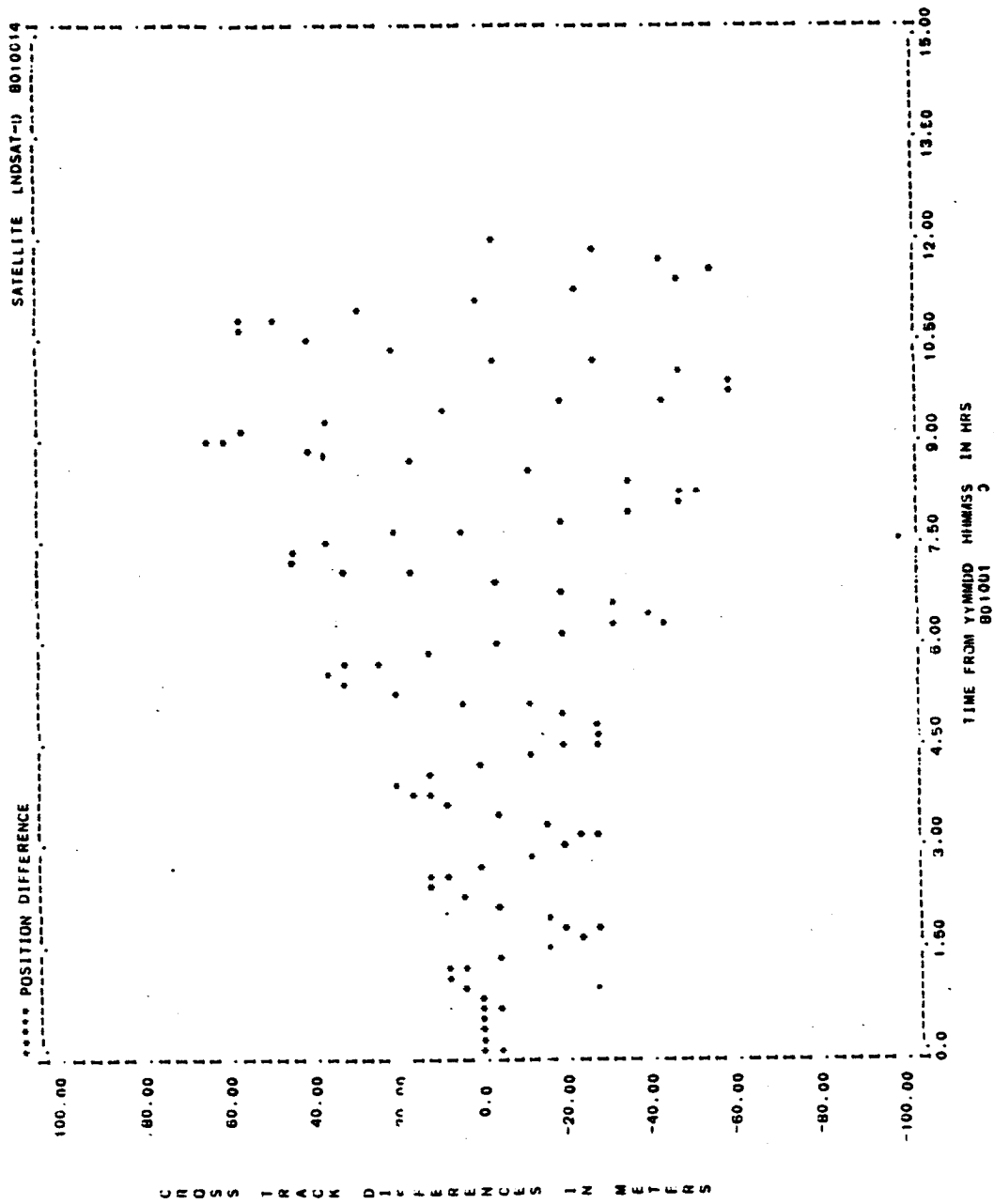


Figure B-1. Error Growth Over 12 Hours for Landsat-D (2 of 3)

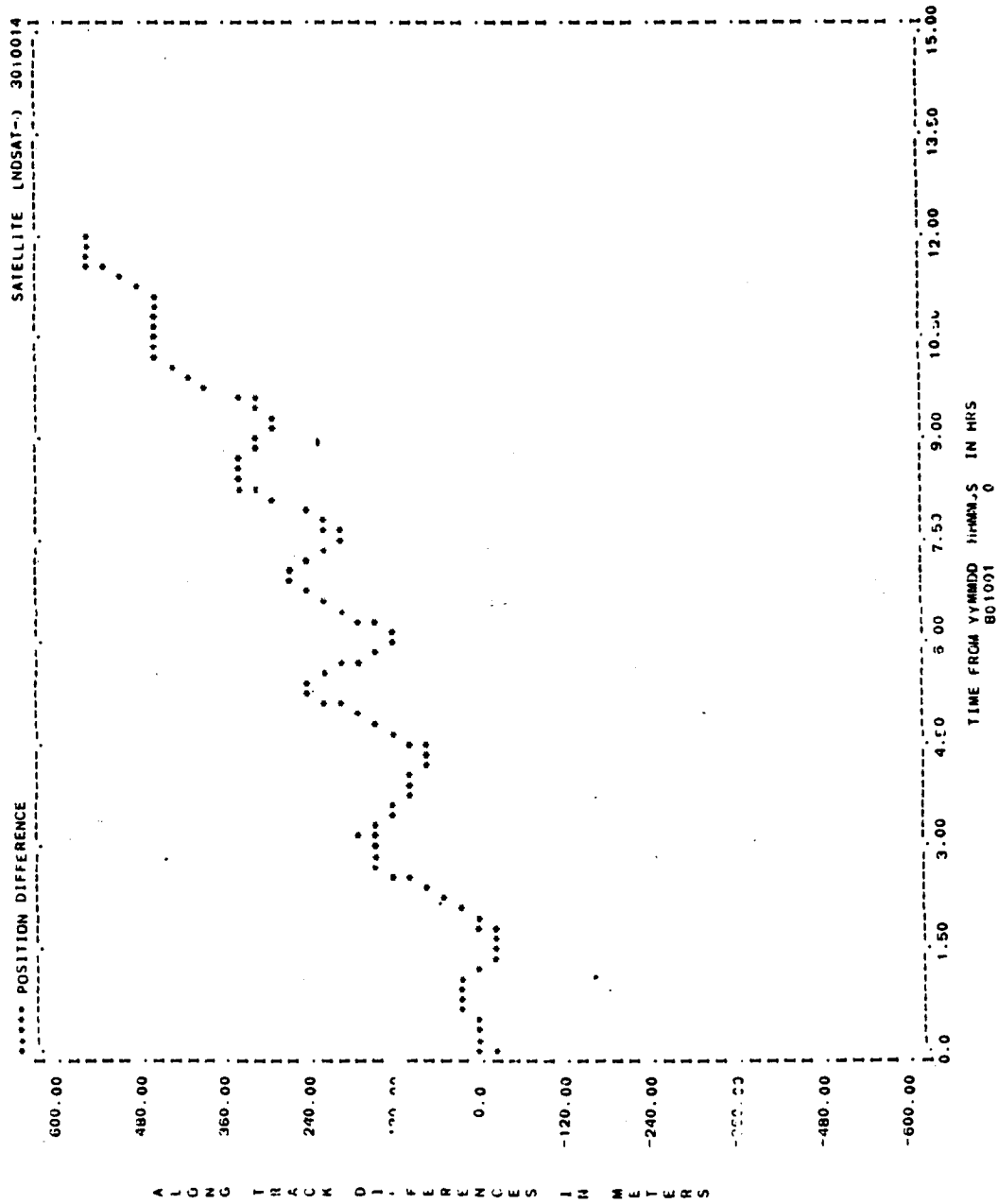


Figure B-1. Error Growth Over 12 Hours of Landsat-D (3 of 3)

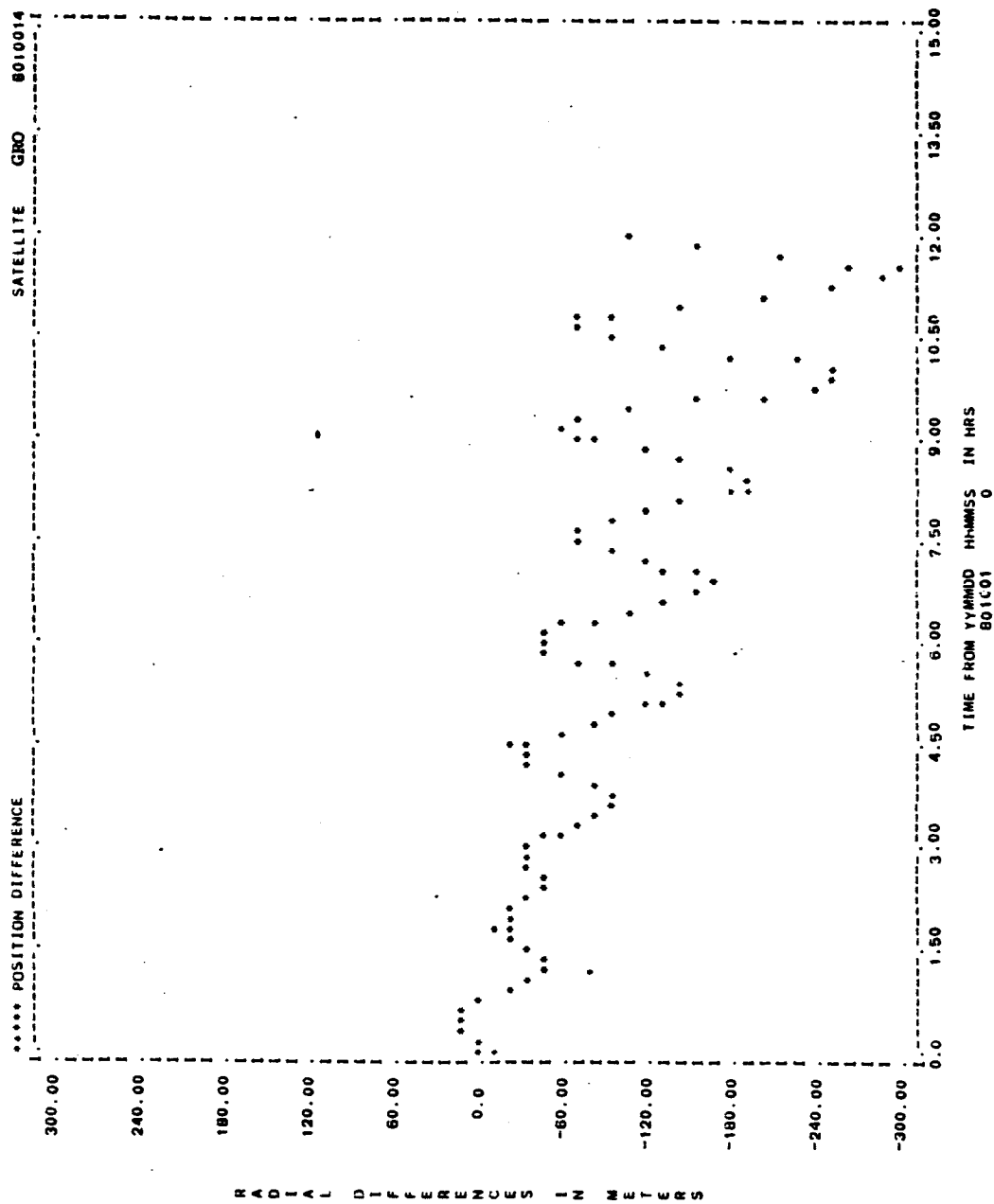


Figure B-2. Error Growth Over 12 Hours for GRO (1 of 3)

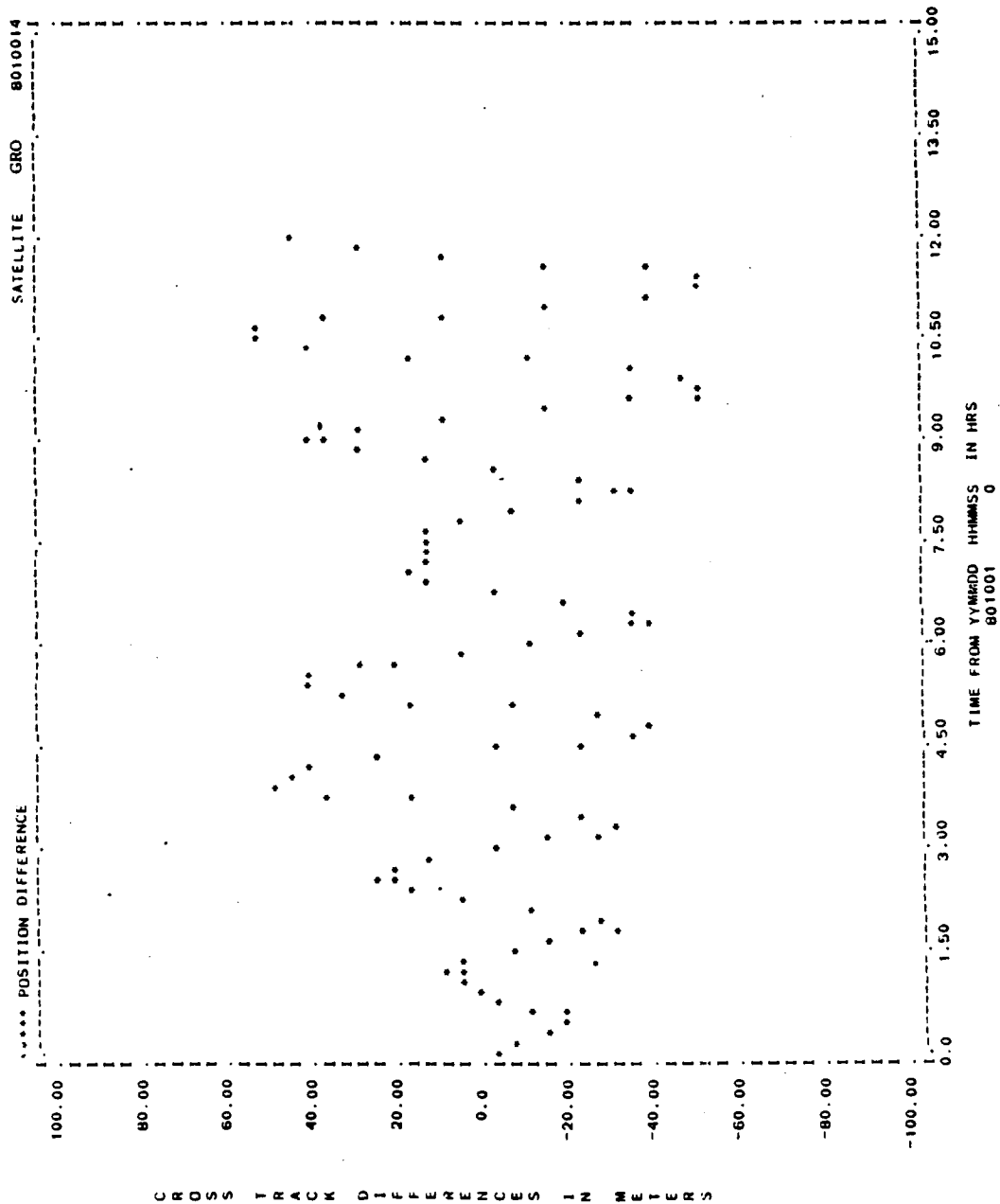


Figure B-2. Error Growth Over 12 Hours for GRO (2 of 3)

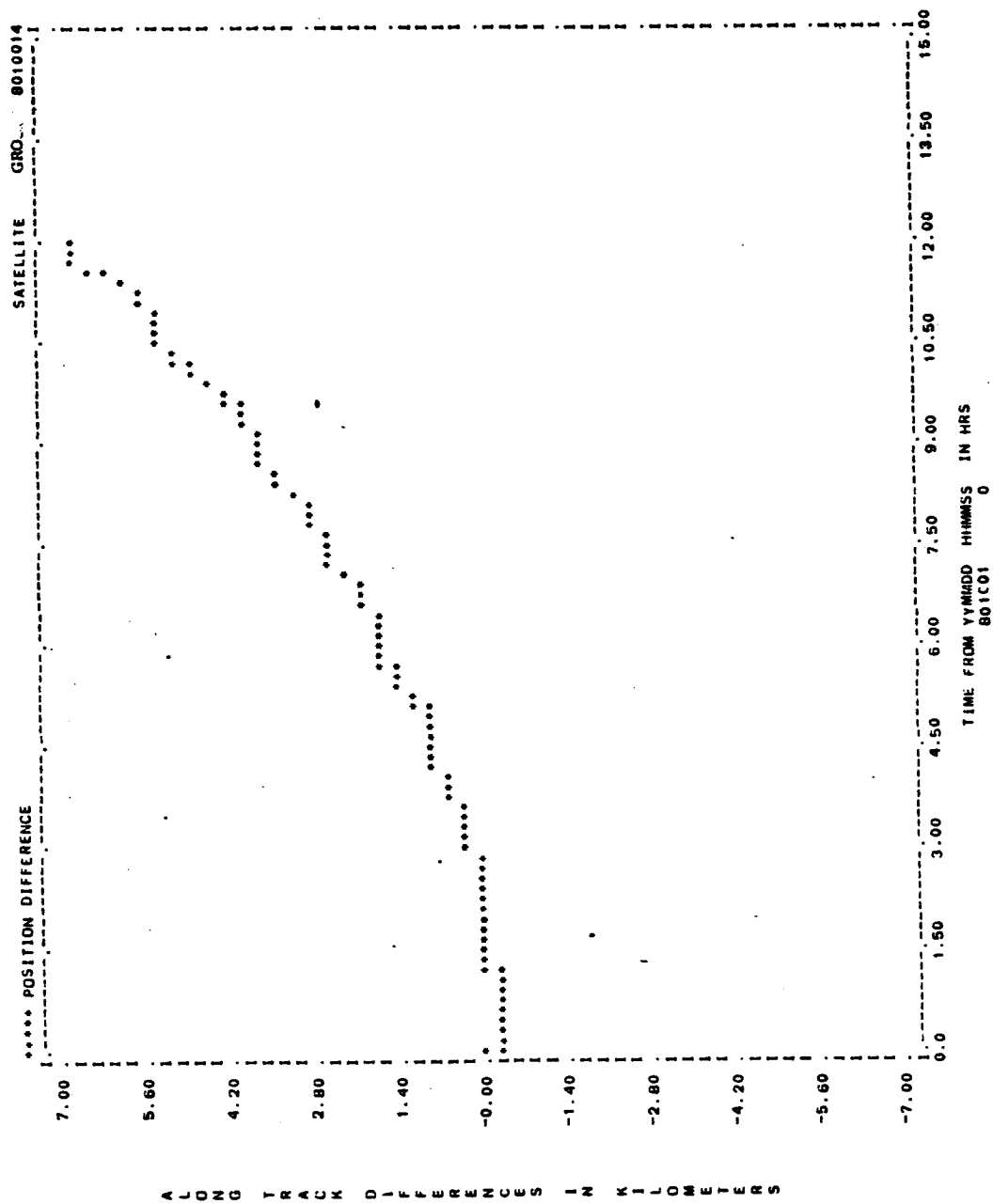


Figure B-2. Error Growth Over 12 Hours for GRO (3 of 3)

## APPENDIX C - PSEUDO-TDRSS OBSERVATIONS FILE DESCRIPTION

The pseudo-TDRSS observations for the R&D GTDS DC program can be read in from tape or disk with a 7200-byte record. The first record in the pseudo-TDRSS observations file is a 7200-byte header record; the following 50 records are 144-byte data records. Tables C-1 and C-2 describe the header and data record formats, respectively. The data format used is a slight modification of the Goddard Trajectory Determination System (GTDS) observation data format. Therefore, some portions of the data records are not used for the pseudo-TDRSS data. They are retained, however, to allow use of the same input/output routines in R&D GTDS.

Table C-1. Pseudo-TDRSS R&D Header Record Format

BYTES	WORD	CONTENTS
1-480	1-60	NOT USED
481-486	61	TIME TAG OF FIRST OBSERVATION IN FILE (YYMMDD.)
489-496	62	TIME TAG OF FIRST OBSERVATION IN FILE (HHMMSS.SS)
497-504	63	TIME TAG OF LAST OBSERVATION IN FILE (YYMMDD.)
505-512	64	TIME TAG OF LAST OBSERVATION IN FILE (HHMMSS.SS)
513-520	65	SATELLITE NAME IN A8 FORMAT
521-524	66 (FIRST HALF)	SATELLITE ID IN INTERGER*4 FORMAT
525-528	66 (LAST HALF)	NUMBER OF OBSERVATION IN FILE (INTEGER)
529-536	67	TIME TAG OF EPOCH OF DATA SIMULATION (YYMMDD.)
537-544	68	TIME TAG OF EPOCH OF DATA SIMULATION (HHMMSS.SS)
545-552	69	NOT USED
553-1672	70-209	NOT USED
1673-1832	210-229	NOT USED
1833-2072	230-259	NOT USED
2073-2080	260	DAY0, JULIAN DATE OF JANUARY 1, 0 HOURS, 0 MINUTES, 0 SECONDS, OF EPOCH YEAR
2081-2088	261	EDAY, ELAPSED TIME IN A.1 SECONDS FROM DAY0 TO EPOCH DATE
2089-2092	262 (FIRST HALF)	'1'
2093-2160	262 (LAST HALF) -270	NOT USED
2161-7200	271-900	NOT USED

7651/80

Table C-2. Pseudo-TDRSS R&D GTDS Data Record Format

BYTES	WORD	CONTENTS
1-8	1	OBSERVATION TIME TAG (YYMMDD.)
9-16	2	OBSERVATION TIME TAG (HHMMSS.SSS)
17-24	3	PSEUDO-RANGE OBSERVATION OR DELTA PSEUDO-RANGE OBSERVATION (KILOMETERS)
25-32	4	INTEGRATION TIME FOR DELTA-RANGE MEASUREMENT IN UNIVERSAL CLOCK TIME SECONDS (ZERO FOR RANGE MEASUREMENT)
33-40	5	NOT USED
41-48	6	TDRS X POSITION COORDINATE (KILOMETERS)
49-56	7	TDRS Y POSITION COORDINATE (KILOMETERS)
57-64	8	TDRS Z POSITION COORDINATE (KILOMETERS)
65-72	9	OBSERVATION TIME IN A.1 SECONDS FROM EPOCH
73-80	10	TDRS X VELOCITY COORDINATE (KILOMETERS PER SECOND)
81-88	11	TDRS Y VELOCITY COORDINATE (KILOMETERS PER SECOND)
89-96	12	TDRS Z VELOCITY COORDINATE (KILOMETERS PER SECOND)
97-100	13 (FIRST HALF)	OBSERVATION NUMBER
101-104	13 (LAST HALF)	NOT USED
105-108	14 (FIRST HALF)	OBSERVATION TYPE (RANGE OR DELTA-RANGE)
109-112	14 (LAST HALF)	'0'
113-116	15 (FIRST HALF)	'0'
117-120	15 (LAST HALF)	NOT USED
121-124	16 (FIRST HALF)	'1'
125-128	16 (LAST HALF)	TDRS IDENTIFICATION NUMBER (1, 2, OR 3)
129-144	17-18	NOT USED

7651/80

#### APPENDIX D - SAMPLE SBDC DECK SETUPS

Figure D-1 shows the GTDS R&D deck setup used to run the SBDC for the baseline case using delta-range data only. Figure D-2 shows the deck setup (fifth slide) used to propagate and compare the estimated output states from this SBDC run.

# INPUT CARD IMAGES

COLUMN 1	CONTROL	EPHEM				LND SAT-D	8010014
	ELEMENT1	2 2 1	7086.901	0.001		98.181	
	ELEMENT2		354.878	180.0		0.0	
	EPOCH		801001.0	0.0			
	ORBTYP	2 1 2	45.				
	OUTPUT	1 3 1	801001.0	240000.0		86400.	
	DMOPT						
	WORKATM	5					
	END						
	OGOPT						
	MAXORDEQ	1	15.0				
	MAXDEGEO	1	15.0				
	POTFIELD	1 5					
	SOLRAD	1	2.0				
	STATEPAR	1					
	STATETAB	1 2 3	4.	5.		6.	
	OUTPART	1	1.				
	OUTOPT	0 1 1	800930235500.0	801001240050.0		60.0	
	DRAG	1	1.0				
	DRAGPAR	3 0	2.0				
	SCPARAM		0.000020	1700.0			
	END						
	FIN						
	CONTROL	ANALYSIS				LND SAT-D	8010014
	DMOPT						
	TDRID	1 2					
	/GPSDATA1	1					
	OBSDEV	82 83	1.	1.			
	END						
	DCOPT						
	TDRSSCH	1 1	801001004000.0	801001004959.0			
	TDRSSCH	2 1	801001022500.0	801001023459.0			
	TDRSSCH	1 2	801001032000.0	801001032959.0			
	TDRSSCH	1 3	801001044500.0	801001045459.0			
	TDRSSCH	2 2	801001060000.0	801001060959.0			
	TDRSSCH	2 3	801001071000.0	801001071959.0			
	TDRSSCH	1 4	801001081800.0	801001082759.0			
	TDRSSCH	2 4	801001100000.0	801001100959.0			
	TDRSSCH	1 5	801001113000.0	801001113959.0			
	TDRSSCH	2 5	801001130000.0	801001130959.0			
	TDRSSCH	1 6	801001142000.0	801001142959.			
	TDRSSCH	2 6	801001162000.0	801001162959.			
	TDRSSCH	1 7	801001173000.	801001173959.0			
	TDRSSCH	2 7	801001192500.	801001193459.0			
	TDRSSCH	2 8	801001211500.0	801001212459.0			
	DSPEA1	6	801001.	0.0			
	DSPEA2	19 1 1	801001.0	240000.0			
	DSPEA3	0 1 1					
	GPSANGLE		0.0	100.0		29.	
	GPSBIAS	1 1 1	23.3				
	GPSCONF	6					
	GPSPOSER	1	35.	35.		80.	
	GPSVELER	1	0.5	0.5		0.28935	
	GPSSEE	1 1 3	10.0	10.0			
	GPSSIM1	0 1 1	10.0	29.		0.0	
	GPSSIM2	0 0 1	86400.				
	USERBIAS	1 1 1					
	GPSSIM4						

Figure D-1. Deck Setup for SBDC Delta-Range Data Baseline Case Run (1 of 2)

```

CONVERG
END
FIN
CONTROL      DC
ELEMENT1     2  1  1  -7051.84      831.96      LNDSAT-D  8010014
ELEMENT2     2  1  1   .095      1.064      0.101
EPOCH        2  1  1  801001.0      0.0      -7.43
OBSINPUT    14.      801001004000.0  801001120000.00
ORBTYP      2  1  2  45.
DMOPT
WORKATM      7
TORID        1  2
/GPSSDATA1   1
OBSDEV      82 83      -40.      1.
END
DCOPT
CONVERG      4      .01
EDIT         3.
TDRSSCH     1  1      801001004000.0  801001004959.0
TDRSSCH     2  1      801001022500.0  801001023459.0
TDRSSCH     1  2      801001032000.0  801001032959.0
TDRSSCH     1  3      801001044500.0  801001045459.0
TDRSSCH     2  2      801001060000.0  801001060959.0
TDRSSCH     2  3      801001071000.0  801001071959.0
TDRSSCH     1  4      801001081800.0  801001082759.0
TDRSSCH     2  4      801001100000.0  801001100959.0
TDRSSCH     1  5      801001113000.0  801001113959.0
TDRSSCH     2  5      801001130000.0  801001130959.0
TDRSSCH     1  6      801001142000.0  801001142959.0
TDRSSCH     2  6      801001162000.0  801001162959.0
TDRSSCH     1  7      801001173000.0  801001173959.0
TDRSSCH     2  7      801001192500.0  801001193459.0
TDRSSCH     2  8      801001211500.0  801001212459.0
USERBIAS    1  1  1      0.0
GPSSIM4
DCSLIDE     5  1  9      43800.
END
OGOPT
MAXDEGEO    1      8.
MAXORDEO    1      9.
NCBODY      1  0  0
POTFIELD    1  4
SOLRAD      1      2.0
STATEPAR    1  1
STATETAB    1  2  3  4.      5.      6.
DRAG        1      1.0
DRAGPAR     3  0      2.2
SCPARAM     3  0      0.000020      1700.0
END
FIN

```

Figure D-1. Deck Setup for SBDC Delta-Range  
Data Baseline Case Run (2 of 2)

# INPUT CARD IMAGES

COLUMN 1	CONTROL	EPHEM				LNDSAT-D	8010014
	ELEMENT1	2 2 1	7086.901	0.001		98.181	
	ELEMENT2		354.878	180.0		0.0	
	EPOCH		801001.0	0.0			
	ORBTYP	2 1 2	45.				
	OUTPUT	1 3 1	801001.0	240000.0		86400.	
	DMOPT						
	WORKATM	5					
	END						
	OGOPT						
	MAXDEGEO	1	15.0				
	MAXORDEQ	1	15.0				
	POTFIELD	1 5					
	SOLRAD	1	2.0				
	OUTOPT	3 1 2	801001060000.0	801001240000.		438.0	
	DRAG	1	1.0				
	DRAGPAR	3 0	2.0				
	SCPARAM		0.000020	1700.0			
	END						
	FIN						
	CONTROL	EPHEM				LNDSAT-D	8010014
	ELEMENT1	2 1	14414.530519210147	-1158.877920717160		5417.964599665298	
	ELEMENT2		-5.832948837862171	-1811820205015269		4.705821636140901	
	EPOCH		801001.0	60000.0			
	ORBTYP	2 1 2	45.				
	OUTPUT	1 3 1	801001.0	240000.0		86400.	
	DMOPT						
	WORKATM	7					
	END						
	OGOPT						
	MAXORDEQ	1	8.				
	MAXDEGEO	1	8.				
	NCBODY	1 0 0					
	POTFIELD	1 4					
	SOLRAD	1	2.0				
	OUTOPT	23 1 2	801001060000.0	801001240000.		438.0	
	DRAG	1	1.0				
	DRAGPAR	3 0	2.2				
	SCPARAM		0.000020	1700.0			
	END						
	FIN						
	CONTROL	COMPARE				LNDSAT-D	8010014
	COMPOPT						
	CMPPLOT	15					
	CMPEPHEM	2202202	801001060000.0	801001174048.0		7.3	
	END						
	FIN						
	CONTROL	COMPARE				LNDSAT-D	8010014
	COMPOPT						
	CMPPLOT	15					
	CMPEPHEM	2202202	801001174048.0	801001203600.0		7.3	
	END						
	FIN						

Figure D-2. Deck Setup for Propagation and Comparison of SBDC Run Estimated Output States

## APPENDIX E - R&D GTDS SBDC Updates

Figure E-1 shows the updates required to run the SBDC. These are updates to the version of R&D GTDS available as of November 1, 1980.

```

//ZBKAPSLD JOB (GC0021311H,T,600405,006018),FFF,MSGLEVEL=(1,1)
//**MAIN CLASS=OVERWRITE
//**FORMAT PU,ODNAME=,DEST=ANYLOCAL
//**FORMAT PR,ODNAME=,DEST=ANYLOCAL
// EXEC ROUCLEG,PARM=LINK=LET,OVLY,SIZE=(550K,30K)',
// REGION,LINK=550K,REGION.GO=550K
//PDSUP.DATAS DD *
$OBSWF
-162 CALL DUMWF
SDC
-101 COMMON/WEICHG/WEINW(10),WTNUM(10)
EQUIVALENCE (IDUMX(3),MTYPE)
195 EDIT OBSERVATION IF NOISE STD DEV. LESS THAN ZERO (OBSDEV PARAMETERS)
DO 3 I=1,10
MTNUM=WTNUM(I)
IF(MTYPE.EQ.MTNUM) GO TO 4
3 CONTINUE
4 IF(WEINW(I).LT.0.00) IEDIT=4
$SETDC
-113
*****
ALL CODE MODIFICATIONS USED FOR THE SLIDING BATCH DC WILL BE ENCLOSED
IN ASTERISKS
*****
COMMONS USED---SLIDE
COMMON/SLIDE/STMAX,PASST*(2,30),NBTORS(30),NUMSLD,NUMPAS,
NPSMAX,NPPSLD
STMAX = MAXIMUM TIME INTERVAL PER SPAN (IN SECONDS)
PASSTM = PASSING TIMES MATRIX
NBTORS = TORS NUMBERS FOR EACH PASS
NUMSLD = TOTAL NUMBER OF SLIDES
NUMPAS = TOTAL NUMBER OF PASSES INPUT
NPSMAX = MAXIMUM NUMBER OF PASSES PER SPAN
NPPSLD = NUMBER OF PASSES TO SLIDE EACH TIME
DATA NUMBER/0/
-398,398 'GPSSIM2 ','DCSLIDE ','GPSSIM4 ','USERBIAS','USERFRQ ',
-760
*****
IF(NUMBER.EQ.0) NUMPAS=0
NUMBER=NUMBER+1
*****
-1119
*****
NUMPAS = NUMPAS + 1
NBTORS(NUMPAS) = I1
PASSTM(1,NUMPAS) = P1
PASSTM(2,NUMPAS) = R2
*****
1274,1278 -----DCSLIDE -----
1279
*****
NUMSLD=I1
NPPSLD = I2
NPSMAX = I3
STMAX=I1
*****
$OBSEXEC
-94
*****
ALL CODE MODIFICATIONS USED FOR THE SLIDING BATCH DC WILL BE ENCLOSED
IN ASTERISKS

```

Figure E-1. Updates Required to Run SBDC ( 1 of 3)

```

COMMONS USED -- EDIT,SATPOS,SLIDE,SWITCH,DCINPT,DCINT,FRC
COMMON EDIT CONTAINS THE START AND END TIMES FOR THE D C SPAN
COMMON/EDIT/RBEDIT(74),R4EDIT(20),I4EDIT(107),I2EDIT(40),
  L1EDIT(221)
  REAL*4 R4EDIT
  INTEGER*2 I2EDIT
  LOGICAL*1 L1EDIT
  DIMENSION STIME(2),ETIME(2),STORB1(2),ETORB1(2)
  EQUIVALENCE (STIME(1),RBEDIT(1)),
    (ETIME(1),RBEDIT(3))
  NAMELIST/SLDDEB/STMAX,PASSTM,NBTORS,NUMSLD,NUMPAS,STIME,
    ETIME,YMDNEW,HMSNEW,REFDA4,POSI,VELI,PVINT,INSW,
    STRTIM,JSAVE1,JSAVE2,NPSMAX,NPPSLD,ICOUNT
COMMON/SLIDE/STMAX,PASSTM(2,30),NBTORS(30),NUMSLD,NUMPAS,
  NPSMAX,NPPSLD
  STMAX = MAXIMUM TIME INTERVAL PER SPAN (IN SECONDS)
  PASSTM = PASSING TIMES MATRIX
  NBTORS = TORS NUMBERS FOR EACH PASS
  NUMSLD = TOTAL NUMBER OF SLIDES
  NUMPAS = TOTAL NUMBER OF PASSES INPUT
  NPPSLD = NUMBER OF PASSES TO SLIDE EACH TIME
  NPSMAX = MAXIMUM NUMBER OF PASSES PER SPAN
COMMON SATPOS CONTAINS EPOCH STATE INFORMATION WHICH MUST BE
BE PASSED DURING A D C SLIDE FROM ONE SPAN TO THE NEXT
COMMON SATPOS EQUIVALENCES
  DIMENSION POSI(3),VELI(3),ELEWS(6),SPHCR(6),BMELS(6)
  EQUIVALENCE (DPSTP(3),POSI(1)), (DPSTP(6),VELI(1)),
    (DPSTP(11),ELEWS(1)), (DPSTP(17),SPHCR(1)),
    (DPSTP(32),STORB1(1)), (DPSTP(34),ETORB1(1)),
    (DPSTP(36),ETORB1),
    (DPSTP(64),YMDIC), (DPSTP(65),HMSIC),
    (DPSTP(66),YMDOUT), (DPSTP(67),HMSOUT),
    (DPSTP(68),YMDFN), (DPSTP(69),HMSFN),
    (DPSTP(70),DELTAT), (DPSTP(71),YMDREF),
    (DPSTP(72),REFJUL), (DPSTP(73),SATNAM),
    (DPSTP(95),BMELS(1)),
    (INTSTP(1),ISODT), (INTSTP(2),ICORD),
    (INTSTP(4),ICTYPE), (INTSTP(5),IDSAT),
    (INTSTP(6),IAIREF)
  EQUIVALENCE (DPDCP(135),YMDNEW),
    (DPDCP(136),HMSNEW),
  EQUIVALENCE (DPFRC(1274),REFDA4)
  EQUIVALENCE (DPDCI(251),PVINT(1))
  DIMENSION PVINT(6),PASJUL(2,30)
*****
228,238
*****
  THE SLIDING BATCH
  120 CONTINUE
  +-----+ CONVERT PASS TIME INTERVALS FROM GREGORIAN TO JULIAN DATES
  DO 1 I=1,2
    DO 1 J=1,NUMPAS
      RTM1 = DFLOAT(IDINT(PASSTM(I,J)/1.06))
      RTM2 = PASSTM(I,J) - RTM1*1.06
      CALL DELTIM(1,RTM1,RTM2,TTTIME,REFJUL,DT)
      PASJUL(I,J) = TTTIME
    1 CONTINUE
  +-----+ CONVERT MAX TIME SPAN FROM SECONDS TO DAYS +-----+
  STMAX = STMAX/86400.00
  +-----+ SLIDING BATCH LOOP +-----+
  DO 15 ICOUNT = 1,NUMSLD
    IF (ICOUNT.NE.1) GO TO 4
  +-----+ COMPUTE START & END TIMES FOR THE FIRST SPAN +-----+
    STRTIM = PASJUL(1,1)
    ENDTIM = STRTIM + STMAX
    DO 2 J = 1,NUMPAS
      JSAVE2 = J - 1
      IF (PASJUL(1,J).GE.ENDTIM) GO TO 3
    2 CONTINUE
    GO TO 16
    3 CONTINUE
    ENDTIM = PASJUL(2,JSAVE2)
    GO TO 8

```

Figure E-1. Updates Required to Run SBDC (2 of 3)

```

      +---+ COMPUTE START & END TIMES FOR SUBSEQUENT SPANS +---+
      4 CONTINUE
      +---+ SLIDE END TIME DOWN NPPSLD PASSES +---+
      JSAVE2 = JSAVE2 + NPPSLD
      IF (JSAVE2.GT.NUMPAS) GO TO 16
      ENDTIM = PASJUL(2,JSAVE2)
      STRTIM = ENDTIM - STMAX
      +---+ COMPUTE START TIME SUBJECT TO MAX CONDITIONS +---+
      DO 5 J = 1,NUMPAS
      JSAVE1 = J
      IF (PASJUL(1,J).GE.STRTIM) GO TO 6
      5 CONTINUE
      6 CONTINUE
      IF ((JSAVE2-JSAVE1+1).GT.NPSMAX) GO TO 7
      STRTIM = PASJUL(1,JSAVE1)
      GO TO 8
      7 CONTINUE
      JSAVE1 = JSAVE2 - NPSMAX + 1
      STRTIM = PASJUL(1,JSAVE1)
      +---+ CONVERT START & END TIMES FROM JULIAN TO GREGORIAN DATES +---+
      8 CONTINUE
      CALL COATE(STRTIM,Y,XM,D,HR,TM,SEC,IERR)
      STIME(1) = Y*1.04 + XM*1.02 + D
      STIME(2) = HR*1.04 + TM*1.02 + SEC
      CALL COATE(ENDTIM,Y,XM,D,HR,TM,SEC,IERR)
      ETIME(1) = Y*1.04 + XM*1.02 + D
      ETIME(2) = HR*1.04 + TM*1.02 + SEC
      +---+ SET UP EPOCH ADVANCE TIMES FOR THE D C +---+
      YMONNEW = STIME(1)
      HMSNEW = STIME(2)
      +---+ SET NECESSARY SWITCHES +---+
      INSW(52) = 1
      INSW(51) = 1
      INSW(88) = 1
      +---+ REWIND OBS. WORKING FILE AND OBS.FILE +---+
      REWIND 17
      REWIND 29
      WRITE(6,SLDDE3)
      +---+ CALL WFCONT TO SET UP THE NEW OBSERVATIONS WORKING FILE
      CALL WFCONT
      +---+ RUN THE D C +---+
      CALL DC(8920)
      IF (ICNTL(1).NE.0) CALL EPHOLT
      +---+ SET NECESSARY SWITCHES AND TRANSFER OUTPUT STATE
      INSW(95) = 3
      INSW(101) = ICTYPE
      ICTYPE = 1
      ICORD = INTERC(2)
      IBODY = INTERC(1)
      POST(1) = PVINT(1)
      POST(2) = PVINT(2)
      POST(3) = PVINT(3)
      VELT(1) = PVINT(4)
      VELT(2) = PVINT(5)
      VELT(3) = PVINT(6)
      15 CONTINUE
      GO TO 200
      16 CONTINUE
      WRITE(6,1011)
      1011 FORMAT('***** ERROR *****',/' NOT ENOUGH PASS',
      'ES OF DATA FOR THE CORRESPONDING BATCH INTERVAL')
      GO TO 230
      EGPSSSE
      -196.196
      IVPAR=1
      /*

```

Figure E-1. Updates Required to Run SBDC (3 of 3)

## APPENDIX F - MERGE ROUTINE SOURCE CODE

Figure F-1 shows the source listing for the SBDC MERGE routine.

```

//      EXEC FORTRANH,PARM=XREF
//SYSIN DD *
C(1)  THIS Q & D ROUTINE MERGES TWO OBSERVATION DATA SETS
C(2)
C(3)      IMPLICIT REAL*8(A-H,O-Z)
C(4)      NAMELIST/TIMES/TIME1,TIME2
C(5)      DIMENSION AOBS(18,50),BOBS(18,50),COBS(18,50)
C(6)      READ(5,TIMES)
C(7)      WRITE(6,TIMES)
C(8)
C(9)  SET THE TIME IN SECONDS FROM EPOCH OF THE MERGE POINT (DEFAULT=12HRS)
C(10)
C(11)      TIME=TIME1
C(12)
C(13)  REWIND ALL FILES
C(14)
C(15)      REWIND 1
C(16)      REWIND 2
C(17)      REWIND 3
C(18)
C(19)  TRANSFER HEADER INFORMATION (WRITE OUT INFO FOR DEBUG)
C(20)
C(21)      READ(1)AOBS
C(22)      READ(2)BOBS
C(23)      WRITE(3)AOBS
C(24)
C(25)  TRANSFER DATA RECORDS FROM FILE1 TO FILE2 UNTIL THE MERGE TIME
C(26)
C(27)  10 READ(1)AOBS
C(28)     READ(2)BOBS
C(29)
C(30)     IF(AOBS(9,50).GE.TIME) GO TO 20
C(31)     WRITE(3)AOBS
C(32)     GO TO 10
C(33)
C(34)  WHEN MERGE TIME IS ENCOUNTERED COPY FILE 1 ONTO FILE 3 ONE
C(35)  OBSERVATION AT A TIME UNTIL MERGE TIME IS MET, THEN SWITCH TO FILE 2
C(36)
C(37)  20 CONTINUE
C(38)     I=1
C(39)  21 CONTINUE
C(40)     IF (AOBS(9,I).GE.TIME) GO TO 30
C(41)         DO 22 J=1,18
C(42)             COBS(J,I) = AOBS(J,I)
C(43)  22     CONTINUE
C(44)         I=I+1
C(45)         GO TO 21
C(46)  30 DO 31 K=1,50
C(47)         DO 31 J = 1,18
C(48)             COBS(J,K) = BOBS(J,K)
C(49)  31 CONTINUE
C(50)     WRITE(3)COBS
C(51)
C(52)  TRANSFER ALL RECORDS AFTER THE MERGE TIME FROM FILE 2 ONTO FILE 3
C(53)
C(54)  40 READ(2,END=500)BOBS
C(55)     WRITE(3)BOBS
C(56)     GOTO 40
C(57)  500 CONTINUE
C(58)     TIME=TIME2

```

Figure F-1. SBDC MERGE Routine Source Listing (1 of 2)



#### REFERENCES

1. Computer Sciences Corporation, CSC/TM-80/6176, Onboard Orbit Determination With Tracking and Data Relay Satellite System (TDRSS) Data, Volume I, The Extended Kalman Filter (EKF), A. C. Long and P. S. Gural (October 1980)
2. --, Goddard Trajectory Determination System Research and Development (GTDS R&D) User's Guide (draft), August 1978
3. National Aeronautics and Space Administration, Goddard Space Flight Center, X-582-76-77, Mathematical Theory of the Goddard Trajectory Determination System, J. O. Cappellari, C. E. Velez, and A. J. Fuchs (editors), April 1976
4. --, STDN Report No. 101.2, Tracking and Data Relay Satellite System User's Guide, Revision 3, January 1978
5. SBDC comparison graphs, available from K. A. Preiss or A. C. Long (Computer Sciences Corporation)